Detection of Faults on Rotary Screen Printed Fabrics using Machine Vision

ANDREW BLOWERS BSC, PHD

A thesis submitted in partial fulfilment of the requirements of De Montfort University for the degree of Doctor of Philosophy

December 1995

Department of Textiles and Fashion
De Montfort University

Abstract

A project was sponsored by the SERC for research into the design of a colour vision system for the detection of print faults in rotary screen printed fabrics. The research was carried out at De Montfort University (formerly named Leicester Polytechnic), which has previous experience with Image Processing in relation to Textiles. The proposed system was required to identify, process and correct the common print faults which can occur during rotary screen printing. These can be divided into two main categories, systematic and random faults.

This thesis covers the work undertaken in the development of a laboratory-based inspection system and the subsequent development and testing of methodologies to facilitate factory-based on-line inspection. Initial investigation identified the requirement for colour segmentation algorithms and the research into and analysis of suitable methodologies for segmentation forms a fundamental part of this thesis.

Important, new colour segmentation algorithms were developed from first principles by the author. These new methods offer improvements (in most cases significant) over the current 'state-of-the-art' colour segmentation technology, and are applicable to a wide-range of computer vision tasks.

These proposed methodologies have been rigorously tested and the findings of the investigation are presented as part of this thesis.

Acknowledgements

First, I thank my project supervisors, Dr. Ray Harwood and Dr. Len Norton-Wayne, without whose continuing help and advice this thesis would not have been possible.

I would also like to express my gratitude to all those have aided me, both academically, and amicably, during this PhD research. In particular, I thank Dr. Rosemary Campbell for her forbearance of my frequently ungracious nature, and her excellent proofreading.

This thesis was generated on a 486-IBM PC-Clone using WordPerfect, Excel, and CorelDraw. The thesis was printed on a DEClaser-1152 Postscript Printer and a Tektronix Phaser 340 Colour Wax Printer. My thanks to the Department of Textiles and Fashion, whose resources were used during the research.

Additional thanks go to those people who stopped me from "giving it all up" at several points over the years, especially my family, and Ms. Catherine Farrer.

... and finally, I would like to thank Mr. Hugh Morley a great friend who knew the importance of balancing work with relaxation, and saved me from myself many times. I dedicate this work to his memory.

Glossary of Terms

ΔE. Delta-E unit used to describe the minimum sufficient tonal difference of two pigments.

A/D converter - Analogue to Digital Converter. Generic term for any device that changes continuous wave (analogue) activity to binary (digital) code, or vice versa.

Additive Colour. Colour produced by the combination of red, green and blue.

Algorithm. Prescribed set of mathematical steps that is used to solve a problem or conduct an operation.

Ambient Illumination. Light which is present in the environment surrounding the machine vision system.

Blanket. A rubber matting in an endless conveyor belt.

Buffer. Device or allocated memory space used for temporary storage.

Bus. Signal path or line shared by many circuits or devices.

CAM - Computer Aided Manufacturing.

CIM - Computer Integrated Manufacturing.

CCD - Charge-Coupled Device. A type of digital camera technology in which the image is focussed on an array of sensing pixels. The small size of the array and high resolution has greatly enhanced "image acquisition".

CIE - Commission International de l'Éclairage. The international commission on illumination, Developer of colour matching systems.

Chroma. The colourfulness judged with reference to white or the general level of surrounding illumination.

Chromaticity. A function of the ratios between the primary colours.

Dark Spike. Pixels that retain a higher brightness value than the surrounding darkened image.

Dithering. Simulating tones by altering the size, shape, or arrangement of background dots.

DORMA. A subsidiary company of Coats Viyella PLC.

Frame Grabber. A device that changes a video picture into a digital computer graphics language.

FFT - Fast Fourier Transform. A commonly used image processing technique used to transform an image into it power distribution.

Grey Scale. The spectrum, or range, or shades of black in an image.

Histogram. A bar graph showing the distribution of intensity levels in an image.

Host. Computer in which an application or database resides, or to which a user is connected.

HSI - Hue Saturation Intensity. A model for colour definition, where colours are defined in terms of their hue (pigment); saturation (the amount of pigment); and intensity (the amount of white included).

Intaglio. Engraved copper rollers.

JND - Just Noticeable Difference. Corresponds to colour differences at the threshold of perceptibility (5 jnd = 1ΔE).

JPEG. Proposed standard for still image compression. Devised by the Joint Photographic Experts Group, sanctioned by the International Standards Organization (ISO) and the CCITT.

LUT - Look-Up Tables. Look up tables are arrays which control the assignment of raw data values.

Pixel. A sort-of acronym for Picture Element. Also called a Pel. When an image is defined by many tiny dots, those dots are referred to as pixels.

PMS - Pantone Matching System. A means of describing colours by assigning them numbers.

Region Growing. Algorithm that attempts to link neighbouring pixels of the same colour/type into a homogenous area.

Quantizing. The second stage of pulse code modulation (PCM). When the waveform samples are measured to find their precise amplitude, they are quantized. These measurements are then converted to binary code or "digitized".

Quantizing Noise. The inability of an analogue signal to be exactly replicated in digital form.

Selvedge. The edges of the fabric which are not printed on.

SERC. The Science and Education Research Council, now called the EPSRC.

Snapshot. A single video frame of data, which can be acquired every 40ms.

Squeegee. A flexible rubber blade that forces the print paste through the open areas of the screen.

Stentering. Stentering is a process whereby fabric is distorted to skew the weft respective to the warp, usually by about 22½°. This allows correct printing of horizontal lines on the fabric which must be printed at the same angle as the out of true fabric. After the fabric is washed and finished they appear in their intended form.

Threshold. A predefined level used to determine whether a pixel will be represented as black or white.

1 Introduction

1.1 Introduction and Definition of the Problem

The purpose of this PhD thesis is to disseminate the academic products of research that was primarily supported by an SERC (ACME) funded project. The project title was the *Automated Inspection and Process Monitoring of Fabric Printing.* Its objective was to research into the feasibility of a digital colour vision system that would enable the online detection and correction of print faults [Dodkin, 1992]. The project was a collaboration between DORMA[1], IBM, and De Montfort University – with later collaboration of Rank Taylor Hobson, who are manufacturers of high quality measuring equipment, and specialize in Research and Development.

The general objective of this research was defined as;

'To develop proposals and the technology for a workstation for automated on-line inspection of printed fabric, using opto-electronic sensing and computer signal processing, including machine vision.'

Two major categories of faults exist for the inspection of printed fabrics. They are *Systematic Faults*, and *Random Faults*. A random fault, by definition, can occur anytime, and at any place on the fabric. This contrasts with the systematic faults, which occur at regular intervals, based on the repeat of the print screen. Readers should understand that this research concentrated on faults in *Rotary Screen Printed* fabrics. Several possible approaches were considered, in increasing order of cost and complexity, and the experimental results regarding their feasibility are included in this thesis.

---

1 *A subsidiary company of Coats Viyella PLC..*

Miles [1994] reports that rotary screen printing is currently the most commonly used method for printing textiles, with a 59% market share. At present any print faults that occur need to be detected visually by the machine operators. As the faults may be as small as 0.5 mm (for systematic faults) and 0.25 mm (for random faults) detection can be difficult. Both kinds of faults cause considerable quantities of materials to be wasted, i.e. to be scrapped or sold as 'seconds'[2] at a greatly reduced price. The difficulty in fault detection and the amount of waste produced makes some form of automatic inspection desirable. The proposed system would need to detect the occurrence of fault conditions and then initiate corrective feedback (whether manual or mechanical). To make the process economically viable it is important that the proposed system is inexpensive, as it is the main objective of any manufacturing business to produce the 'right goods' at the 'right price'.

Understanding the mechanical principles behind rotary screen printing is important in comprehending fully how and when faults appear (refer to Sections 1.5 and 1.6 for more details). On transferring this knowledge to an 'expert' inspection system a level of preemptive detection becomes possible. In succeeding sections of this thesis rotary screen printing and its faults will be discussed from a historical perspective to gain an insight into fault occurrence.

1.2 Thesis Organization

This section describes the organization of this thesis, indicating how material has been arranged into groups of similar information that follow each other logically building towards the research conclusions.

Chapter 1 (Introduction) introduces the main aims and objectives of the research covered by this thesis, identifying the reason for the research and the research methods to be used.

---

2 *Fabric is classified as being of seconds quality if its print standard falls outside the acceptable design tolerances.*

Chapters 2, 3, 4 present essential information for the understanding of the research, which is analysed in later chapters.

Chapter 2 (Machine Vision) establishes the fundamental concepts of Machine Vision systems, identifying their relevance to this research.

Chapter 3 (Concepts of Colour Vision for Humans and Computers) presents the concepts of colour vision (identified as critical to the research in Section 1.2), first in terms of human visual perception, then expanded to cover computer colour perception with particular emphasis on colour image processing, and computer colour interchange spaces.

Chapter 4 (Signal Acquisition and Properties) describes the process of data measurement, identifying relevant methods for machine vision systems and analysing these to establish the best approach for the automatic inspection of printed fabrics.

Chapter 5 (Preliminary Research) builds on the information presented in the preceding chapters to propose a solution to the research problem. A comprehensive literature survey is given, supplying evidence and support for the proposed solution.

Chapter 6 (Methods for RGB Colour Space Segmentation) focuses on colour segmentation, a critical area for this research, that would facilitate the faster processing requirement for on-line inspection by a colour machine vision system.

Chapter 7 (Evaluation of Colour Segmentation Methodologies) evaluates the colour segmentation methodologies identified in Chapter 5 and proposed in Chapter 6. The experimental results given demonstrate the importance of the colour segmentation algorithms for this research.

Chapter 8 (Proposal for an On-line Fault Detection System for Rotary Screen Printed Fabrics) builds on the research presented in earlier chapters to propose a laboratory-based method for the inspection of rotary screen printed fabrics using colour machine vision.

Chapter 9 (Conclusions) defines the conclusions of this research and recommendations to further the research. This chapter examines the implications of the research, defined by the main body of the thesis.

References this section provides clear reference to texts that constitute supporting evidence for arguments presented within this thesis.

Appendices several appendices are attached to this thesis. These offer supporting information and data to the arguments presented within the thesis. In particular they contain; information that is referred to continuously in the thesis, tabular and complex data resulting from the evaluation of methods (too detailed for the main body of the thesis), and general supporting information that has been used during this research.

1.3 The Inspection Task

Inspection at DORMA is currently carried out after the fabric has left the print table, been through a drying and fixing process, and is being collected for further processing. Between the inspection point and print table as much as 90 – 120 metres of fabric can have been produced. Even if inspectors detect the fault as soon as it occurs up-to 120 metres of fabric can be affected. The chances of first time detection, however, are very low. Defects can be very small, and may only occur once. This difficulty in fault detection is the main reason for the investigation into an automated 100% inspection system.

Following discussion with DORMA agreement on a formal requirement for target inspection performance was made. This requires detection of all defects on pigment printed furnishing

fabrics containing up-to twenty colours (the maximum number of screens on DORMA's rotary screen printing machines). Pigments are presumed to be opaque [Hawkyard, 1994], principally due to their particulate nature. Consequently, no more than twenty-one colours (twenty pigments + background) should be present. Nevertheless, in practice some mixing does occur. Pattern designers intentionally exploit this, so more than twenty discrete colours could be present in any one design.

Instrumentation needs to deal with fabric widths from 1.2 to 3 metres. The printing speed is up-to 1 metre per second, with a maximum pattern repeat distance of 640 mm set by screen circumference. To monitor systematic faults, the position of each overlay must be measured to better than 0.5 mm, requiring a maximum spatial resolution of 0.2 mm. Random faults as small as 0.25 mm must be detected, requiring a spatial resolution of 0.1 mm.

1.3.1 100% Inspection

To inspect one pattern repeat across the full width of fabric, at a low resolution of just 1 mm, requires the processing of up-to 3,000 × 640 (1,920,000) points of data. As the data must be colour (preferably 24 bit) for pigment discrimination, this infers a total processing cost of 3 (R, G, B) × 3,000 × 640 (5,760,000) bytes of image data, or 5.76 MBytes every repeat. Because rotary screen machines can print the fabric at up-to a metre per second, this give a processing requirement of 9 MBytes per second. This is only for a fault resolution of 1 mm. In fact, to satisfy DORMA's inspection requirements the inspection system requires a processing speed of 90 MByte per second. Even for modern machine vision systems this is very demanding.

This means that within one second of real-time the inspection system must process a large amount of data (90 MB) to detect, verify, and classify any fault present. The size and complexity of these tasks prevent the real-time inspection of the fabric using a standard PC-based system. Some form of dedicated high speed, multi-processor system could be used to handle this process in real-time. Although, the development of a system was outside the

financial and academic boundaries of this research, still the development of suitable methodologies, to allow such a system to be achieved, remains critical.

To carry out 100% inspection on a PC-based system requires a significant reduction in data processing. Two areas for data reduction are available: decreased spatial resolution; decreased colour resolution. Spatial resolution cannot be reduced as a minimum fault resolution is required. Colour resolution, however, is more flexible. Definition between similar colours is essential. To achieve this, a high resolution (24-bit colour) system must be used. Still, as typically, only twenty colours need to be uniquely identified, a form of adaptive colour quantization may be appropriate. Preprocessing of the data to perform **colour segmentation**, therefore, became a prerequisite of the PC-based fault detection system. It was the data reduction by colour segmentation that the main research attention was focussed. In the event of a multi-processor system being used the colour segmentation is still desirable as a means of colour discrimination.

1.3.2 Pseudo 100% Inspection

The earliest detection of a fault on the printing system currently employed by DORMA, using a human inspector is 90 – 120 metres after the fault occurs. At a maximum fabric throughput of a metre a second, detection is a minimum of two minutes after fault occurrence. If a method of automated inspection could meaningfully reduce this detection time, and accurately flag errors, then a significant saving in fabric would be made. Therefore, it is necessary that the machine vision inspection point occurs before the current inspection point; inspecting the fabric whilst it is still attached to the blanket allows this, and has the additional benefit of dimensional stability. This would be a pseudo 'real-time' inspection process as fault identification is at least as quick as the existing method, as it reduces time between fault creation and detection.

Yet, this form of inspection precludes true 100% inspection as the extra processing time would require skipping of image frames. The result is that some random faults may not be immediately

detected. Due to the occasional and generally non serious nature of random faults (in that they do not always cause second quality goods to be produced) the inspection process can be seen as pseudo 100%. This process of inspection is more feasible for PC-based systems. Later, the transferal of detection algorithms developed using this approach onto a faster processor is then possible. In the laboratory, detection algorithms, for use in a true 100% inspection system, were created and assessed using a pseudo 100% inspection system.

1.4 A History of Screen Printing

Section 1.4 introduces the concepts of screen printing through a historical perspective, focusing in particular on the development of rotary screen printing.

Hand screen printing, and its various mechanical derivatives, is arguably the most significant contribution of the twentieth century to textile printing developments [Storey, 1992] [Hawkyard, 1994]. Screen printing can be considered as an extension of the stencilling process. As children, most of us, will have experimented with stencils by cutting holes in card and transferring the pattern by brushing paint or ink through the holes to the underlying paper. Commercially, stencils are available for numbering and lettering and are usually made from waxed card, metal, or plastic. From these stencils it is seen that 'ties' are used to hold solid areas together, and to retain letters such as O or P (Figure 1.1). These large 'ties' make 'free' shapes impossible [Storey, 1992].

It was at the end of the eighth century that the Japanese introduced the stencil plate, for patterning fabrics. They overcame the difficulty of the unsightly tie lines by using human hair or fine untwisted silk as ties. By using such fine ties it enabled the colour to spread underneath them or for the tie lines to be so slight as to be negligible. This technique for printing fabrics was in worldwide use by the nineteenth century [Storey, 1992][Hawkyard, 1994].

In the late nineteenth and early twentieth centuries, France was leading the way in stencil printing processes, and it was there that metal stencils, or *pochoirs*, were first made. First, they traced a pattern on to varnished zinc or copper plate. Then, after using a sharp tool to engrave the outline, and mastic to protect the edges, the plates were deeply acid etched, enabling the removal of the unwanted parts of the stencil [Storey, 1992][Miles, 1994].

Figure 1.1 : Stencil showing Ties

The first recorded use of a silk gauze stencil for printing, was at Lyon, in 1850, where woven silk fabric was used for continuously supporting the stencil. It was found that by stretching this supporting fabric across a frame they achieved the best results. This combination of fabric and frame became known as a *screen*. The silk gauze provided the ties for the stencil and the

amount of colour paste applied could be controlled. The use of durable paint on the screen fabric soon replaced the traditional paper stencil. Nevertheless, it was not until 1907 that a patent for a screen printing process was first taken out (by a Manchester man). In fact, this method printed the American Stars and Stripes banners used during the First World War, but it was only after 1926 that screen printing in Europe started to form an industry [Hawkyard, 1994].

Earlier in the twentieth century engraved roller printing was still the preferred approach and, provided large quantities of a particular design were required, it was much cheaper. Fashion houses were the first to appreciate the advantages of screen printing. Principally, this was because of the ease of transfer of design to screen and the fact that the frame size of the screen was freely variable. Also the cost of setting up a design was less, the whole process was quicker, and changing the colour set was easier than engraved roller printing. An additional factor that influenced the fashion houses was that screen printing offered an improved 'bloom' or colour strength, as they did not apply the colour with as much pressure as roller printing. This also meant that they did not crush textured surfaces. The advantages, for exclusive design production, were obvious to the fashion houses [Storey, 1992][Hawkyard, 1994].

Fashion houses, with their increased interest in screen printing, encouraged development of the screen printing industry. Designers started seeing screens as an important media for the realization of their designs, rather than as a cost-effective solution. With the increased interest in designs, in particular complex multicolored patterns, an implicit requirement for improved screen stability was needed. Existing screen fabrics are mostly made from hydrophilic yarns, such as silk, cotton, viscose rayon, or cellulose diacetate. When these screens were used with water-based print pastes, sagging, which caused deformation of the design, would occur. By using hydrophobic fibres[3], manufacturing screens that remained stable when used with water-based pigments was possible. A useful by-product of this development was the improved tensile strength of the screen that allowed them to be stretched more tightly over the frame, giving

---

3 *Hydrophobic fibres are synthetics, such as nylon and polyester, which repel water.*

better accuracy. Replacing the wooden frames, which were susceptible to warping, with metal ones gave further improvement in the overall print quality [Storey, 1992][Hawkyard, 1994].

The construction of robust screens was a precursor to the automation of the screen printing process. One of the first developments, which is still in use today, was where fabric is glued onto a long table and one colour is printed at a time. The screen, being printed, is held in a moveable carriage that is slid along the length of the table. The paste was then forced through the screen by a motor-driven squeegee[4]. This is similar to modern hand-printing techniques, with one colour being printed at a time [Hawkyard, 1994].

It was not until the 1950s, however, that the first fully automated screen printing machines were produced — Buser, Stork, and Johannes Zimmer were the primary manufacturers. Printing was achieved using the same principle as for single screens, but instead of the screens being in movable carriages, the fabric moved under the screens. Gluing the fabric to a print *blanket*[5] achieved this. The blanket moves the fabric under the screens where it is then held stationary while printing occurs, the screens are then raised and the fabric moved on to the next screen. As fabric movement is intermittent, this puts limits on the speed and efficiency of production. Continuous movement of the fabric on flat-screen machines has been achieved by moving the screens along the fabric while printing (e.g. the American Precision Midas machine). Still, this is mechanically inefficient and requires a long print bed [Hawkyard, 1994].

1.4.1 Development of Rotary Screen Printing

To achieve a simpler and more economical method for fully continuous printing it was realized that cylindrical (rotary) screens would be needed. In rotary screen printing continuous rotation of a cylindrical screen while in contact with fabric ensure genuinely continuous printing. Early

---

4 *A flexible rubber blade that forces the print paste through the open areas of the screen.*

5 *A rubber matting in an endless conveyor belt.*

attempts were made to produce a cylindrical screen from flat *wire-mesh* screens, but this required a soldered seam. This seam, unless hidden by the design, was visible, on each rotation of the screen, as a line across the width of the fabric. In fact, this was the approach used, by A J C de O Barros, for manufacturing screens on the very first rotary screen printing machine, built by Aljaba and first introduced in 1954 [de O Barros, 1966].

Aljaba realized that wire-mesh screens were unsuitable for rotary printing due to their open structure, so on Aljaba's early machines the screens were plated with copper by electrolysis to fill the holes partially. Later this process was abandoned and woven, seamless, nylon tubes were used. It was not until after the closure of the Aljaba company that W W Sword introduced a new version of the wire-mesh screen, known as the *Durascreen* [Hawkyard, 1994]. The Durascreen uses an electrophoretic coating process to fill the pores in the screen with a flexible polymer. This process is also used to reduce the risk of creasing of electroformed nickel screens.

One of Aljaba's major contributions towards screen printing was the invention of the *duplex* machine, which allowed both sides of a fabric to be printed concurrently. They achieved this by running the fabric vertically between a pair of screens. The paste was applied to the fabric by means of metal rollers that acted as squeegees.

What made rotary screen printing the dominant method of producing printed textiles, with a 59% market share (Figure 1.2) [Miles, 1994], were the invention, and introduction in the early sixties, of the seamless screen formed by electrodeposited nickel [Cormack, 1993][Hawkyard, Miah, 1987][Kool, 1993]. Within a short period rotary screen printing had substantially replaced *intaglio*[6] and flatbed printing. Two main types of nickel plated screens were introduced: the *galvano* screen by Peter Zimmer (Austria) in 1961; and the *lacquer* screen by Stork (Holland) in 1963. It was mainly due to the superiority of these screens, to those produced by Aljaba, that Zimmer and Stork are the principal manufacturers of rotary screen

---

6 *Engraved copper rollers.*

printing machines today [Kool, 1993]. The key factors for the success of rotary screen printing lie in its ability to combine good printing quality, flexible screen manufacturing and competitive overall printing costs.

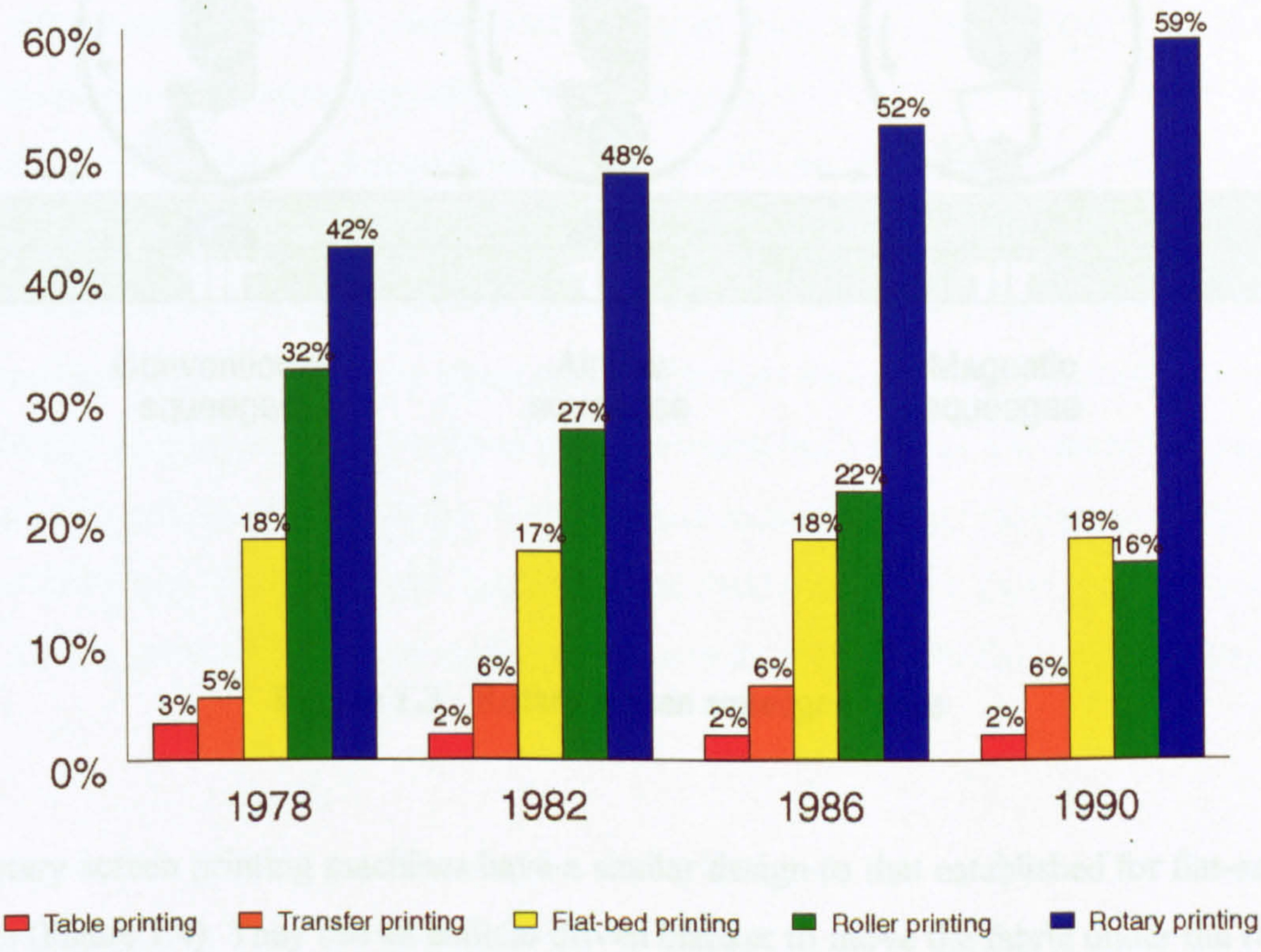

Figure 1.2 : Chart of market share of various textile printing methods [Miles, 1994]

1.5 Mechanics of Rotary Screen Printing

In rotary screen printing, print paste, which is fed to the inside of the screen, is forced out through design areas with the aid of a stationary squeegee. Several different squeegee types are used in rotary screen printing (Figure 1.3). The blade squeegee systems use a flexible-blade. This blade applies pressure to the base of the screen, to force the print paste on to the substrate by the build up in pressure due to screen rotation. Rod or roller squeegee machines, such as those manufactured by Zimmer and Mitter, are successful for printing on wider substrates, as they apply an even pressure across the screen [Ferber, Hilden, 1989].

1 Introduction

1.1 Introduction and Definition of the Problem

The purpose of this PhD thesis is to disseminate the academic products of research that was primarily supported by an SERC (ACME) funded project. The project title was the *Automated Inspection and Process Monitoring of Fabric Printing.* Its objective was to research into the feasibility of a digital colour vision system that would enable the online detection and correction of print faults [Dodkin, 1992]. The project was a collaboration between DORMA[1], IBM, and De Montfort University – with later collaboration of Rank Taylor Hobson, who are manufacturers of high quality measuring equipment, and specialize in Research and Development.

The general objective of this research was defined as;

'To develop proposals and the technology for a workstation for automated on-line inspection of printed fabric, using opto-electronic sensing and computer signal processing, including machine vision.'

Two major categories of faults exist for the inspection of printed fabrics. They are *Systematic Faults*, and *Random Faults*. A random fault, by definition, can occur anytime, and at any place on the fabric. This contrasts with the systematic faults, which occur at regular intervals, based on the repeat of the print screen. Readers should understand that this research concentrated on faults in *Rotary Screen Printed* fabrics. Several possible approaches were considered, in increasing order of cost and complexity, and the experimental results regarding their feasibility are included in this thesis.

---

1 *A subsidiary company of Coats Viyella PLC..*

Miles [1994] reports that rotary screen printing is currently the most commonly used method for printing textiles, with a 59% market share. At present any print faults that occur need to be detected visually by the machine operators. As the faults may be as small as 0.5 mm (for systematic faults) and 0.25 mm (for random faults) detection can be difficult. Both kinds of faults cause considerable quantities of materials to be wasted, i.e. to be scrapped or sold as 'seconds'[2] at a greatly reduced price. The difficulty in fault detection and the amount of waste produced makes some form of automatic inspection desirable. The proposed system would need to detect the occurrence of fault conditions and then initiate corrective feedback (whether manual or mechanical). To make the process economically viable it is important that the proposed system is inexpensive, as it is the main objective of any manufacturing business to produce the 'right goods' at the 'right price'.

Understanding the mechanical principles behind rotary screen printing is important in comprehending fully how and when faults appear (refer to Sections 1.5 and 1.6 for more details). On transferring this knowledge to an 'expert' inspection system a level of preemptive detection becomes possible. In succeeding sections of this thesis rotary screen printing and its faults will be discussed from a historical perspective to gain an insight into fault occurrence.

1.2 Thesis Organization

This section describes the organization of this thesis, indicating how material has been arranged into groups of similar information that follow each other logically building towards the research conclusions.

Chapter 1 (Introduction) introduces the main aims and objectives of the research covered by this thesis, identifying the reason for the research and the research methods to be used.

---

2 *Fabric is classified as being of seconds quality if its print standard falls outside the acceptable design tolerances.*

Chapters 2, 3, 4 present essential information for the understanding of the research, which is analysed in later chapters.

Chapter 2 (Machine Vision) establishes the fundamental concepts of Machine Vision systems, identifying their relevance to this research.

Chapter 3 (Concepts of Colour Vision for Humans and Computers) presents the concepts of colour vision (identified as critical to the research in Section 1.2), first in terms of human visual perception, then expanded to cover computer colour perception with particular emphasis on colour image processing, and computer colour interchange spaces.

Chapter 4 (Signal Acquisition and Properties) describes the process of data measurement, identifying relevant methods for machine vision systems and analysing these to establish the best approach for the automatic inspection of printed fabrics.

Chapter 5 (Preliminary Research) builds on the information presented in the preceding chapters to propose a solution to the research problem. A comprehensive literature survey is given, supplying evidence and support for the proposed solution.

Chapter 6 (Methods for RGB Colour Space Segmentation) focuses on colour segmentation, a critical area for this research, that would facilitate the faster processing requirement for on-line inspection by a colour machine vision system.

Chapter 7 (Evaluation of Colour Segmentation Methodologies) evaluates the colour segmentation methodologies identified in Chapter 5 and proposed in Chapter 6. The experimental results given demonstrate the importance of the colour segmentation algorithms for this research.

Chapter 8 (Proposal for an On-line Fault Detection System for Rotary Screen Printed Fabrics) builds on the research presented in earlier chapters to propose a laboratory-based method for the inspection of rotary screen printed fabrics using colour machine vision.

Chapter 9 (Conclusions) defines the conclusions of this research and recommendations to further the research. This chapter examines the implications of the research, defined by the main body of the thesis.

References this section provides clear reference to texts that constitute supporting evidence for arguments presented within this thesis.

Appendices several appendices are attached to this thesis. These offer supporting information and data to the arguments presented within the thesis. In particular they contain; information that is referred to continuously in the thesis, tabular and complex data resulting from the evaluation of methods (too detailed for the main body of the thesis), and general supporting information that has been used during this research.

1.3 The Inspection Task

Inspection at DORMA is currently carried out after the fabric has left the print table, been through a drying and fixing process, and is being collected for further processing. Between the inspection point and print table as much as 90 – 120 metres of fabric can have been produced. Even if inspectors detect the fault as soon as it occurs up-to 120 metres of fabric can be affected. The chances of first time detection, however, are very low. Defects can be very small, and may only occur once. This difficulty in fault detection is the main reason for the investigation into an automated 100% inspection system.

Following discussion with DORMA agreement on a formal requirement for target inspection performance was made. This requires detection of all defects on pigment printed furnishing

fabrics containing up-to twenty colours (the maximum number of screens on DORMA's rotary screen printing machines). Pigments are presumed to be opaque [Hawkyard, 1994], principally due to their particulate nature. Consequently, no more than twenty-one colours (twenty pigments + background) should be present. Nevertheless, in practice some mixing does occur. Pattern designers intentionally exploit this, so more than twenty discrete colours could be present in any one design.

Instrumentation needs to deal with fabric widths from 1.2 to 3 metres. The printing speed is up-to 1 metre per second, with a maximum pattern repeat distance of 640 mm set by screen circumference. To monitor systematic faults, the position of each overlay must be measured to better than 0.5 mm, requiring a maximum spatial resolution of 0.2 mm. Random faults as small as 0.25 mm must be detected, requiring a spatial resolution of 0.1 mm.

1.3.1 100% Inspection

To inspect one pattern repeat across the full width of fabric, at a low resolution of just 1 mm, requires the processing of up-to 3,000 × 640 (1,920,000) points of data. As the data must be colour (preferably 24 bit) for pigment discrimination, this infers a total processing cost of 3 (R, G, B) × 3,000 × 640 (5,760,000) bytes of image data, or 5.76 MBytes every repeat. Because rotary screen machines can print the fabric at up-to a metre per second, this give a processing requirement of 9 MBytes per second. This is only for a fault resolution of 1 mm. In fact, to satisfy DORMA's inspection requirements the inspection system requires a processing speed of 90 MByte per second. Even for modern machine vision systems this is very demanding.

This means that within one second of real-time the inspection system must process a large amount of data (90 MB) to detect, verify, and classify any fault present. The size and complexity of these tasks prevent the real-time inspection of the fabric using a standard PC-based system. Some form of dedicated high speed, multi-processor system could be used to handle this process in real-time. Although, the development of a system was outside the

financial and academic boundaries of this research, still the development of suitable methodologies, to allow such a system to be achieved, remains critical.

To carry out 100% inspection on a PC-based system requires a significant reduction in data processing. Two areas for data reduction are available: decreased spatial resolution; decreased colour resolution. Spatial resolution cannot be reduced as a minimum fault resolution is required. Colour resolution, however, is more flexible. Definition between similar colours is essential. To achieve this, a high resolution (24-bit colour) system must be used. Still, as typically, only twenty colours need to be uniquely identified, a form of adaptive colour quantization may be appropriate. Preprocessing of the data to perform **colour segmentation**, therefore, became a prerequisite of the PC-based fault detection system. It was the data reduction by colour segmentation that the main research attention was focussed. In the event of a multi-processor system being used the colour segmentation is still desirable as a means of colour discrimination.

1.3.2 Pseudo 100% Inspection

The earliest detection of a fault on the printing system currently employed by DORMA, using a human inspector is 90 – 120 metres after the fault occurs. At a maximum fabric throughput of a metre a second, detection is a minimum of two minutes after fault occurrence. If a method of automated inspection could meaningfully reduce this detection time, and accurately flag errors, then a significant saving in fabric would be made. Therefore, it is necessary that the machine vision inspection point occurs before the current inspection point; inspecting the fabric whilst it is still attached to the blanket allows this, and has the additional benefit of dimensional stability. This would be a pseudo 'real-time' inspection process as fault identification is at least as quick as the existing method, as it reduces time between fault creation and detection.

Yet, this form of inspection precludes true 100% inspection as the extra processing time would require skipping of image frames. The result is that some random faults may not be immediately

detected. Due to the occasional and generally non serious nature of random faults (in that they do not always cause second quality goods to be produced) the inspection process can be seen as pseudo 100%. This process of inspection is more feasible for PC-based systems. Later, the transferal of detection algorithms developed using this approach onto a faster processor is then possible. In the laboratory, detection algorithms, for use in a true 100% inspection system, were created and assessed using a pseudo 100% inspection system.

1.4 A History of Screen Printing

Section 1.4 introduces the concepts of screen printing through a historical perspective, focusing in particular on the development of rotary screen printing.

Hand screen printing, and its various mechanical derivatives, is arguably the most significant contribution of the twentieth century to textile printing developments [Storey, 1992] [Hawkyard, 1994]. Screen printing can be considered as an extension of the stencilling process. As children, most of us, will have experimented with stencils by cutting holes in card and transferring the pattern by brushing paint or ink through the holes to the underlying paper. Commercially, stencils are available for numbering and lettering and are usually made from waxed card, metal, or plastic. From these stencils it is seen that 'ties' are used to hold solid areas together, and to retain letters such as O or P (Figure 1.1). These large 'ties' make 'free' shapes impossible [Storey, 1992].

It was at the end of the eighth century that the Japanese introduced the stencil plate, for patterning fabrics. They overcame the difficulty of the unsightly tie lines by using human hair or fine untwisted silk as ties. By using such fine ties it enabled the colour to spread underneath them or for the tie lines to be so slight as to be negligible. This technique for printing fabrics was in worldwide use by the nineteenth century [Storey, 1992][Hawkyard, 1994].

In the late nineteenth and early twentieth centuries, France was leading the way in stencil printing processes, and it was there that metal stencils, or *pochoirs*, were first made. First, they traced a pattern on to varnished zinc or copper plate. Then, after using a sharp tool to engrave the outline, and mastic to protect the edges, the plates were deeply acid etched, enabling the removal of the unwanted parts of the stencil [Storey, 1992][Miles, 1994].

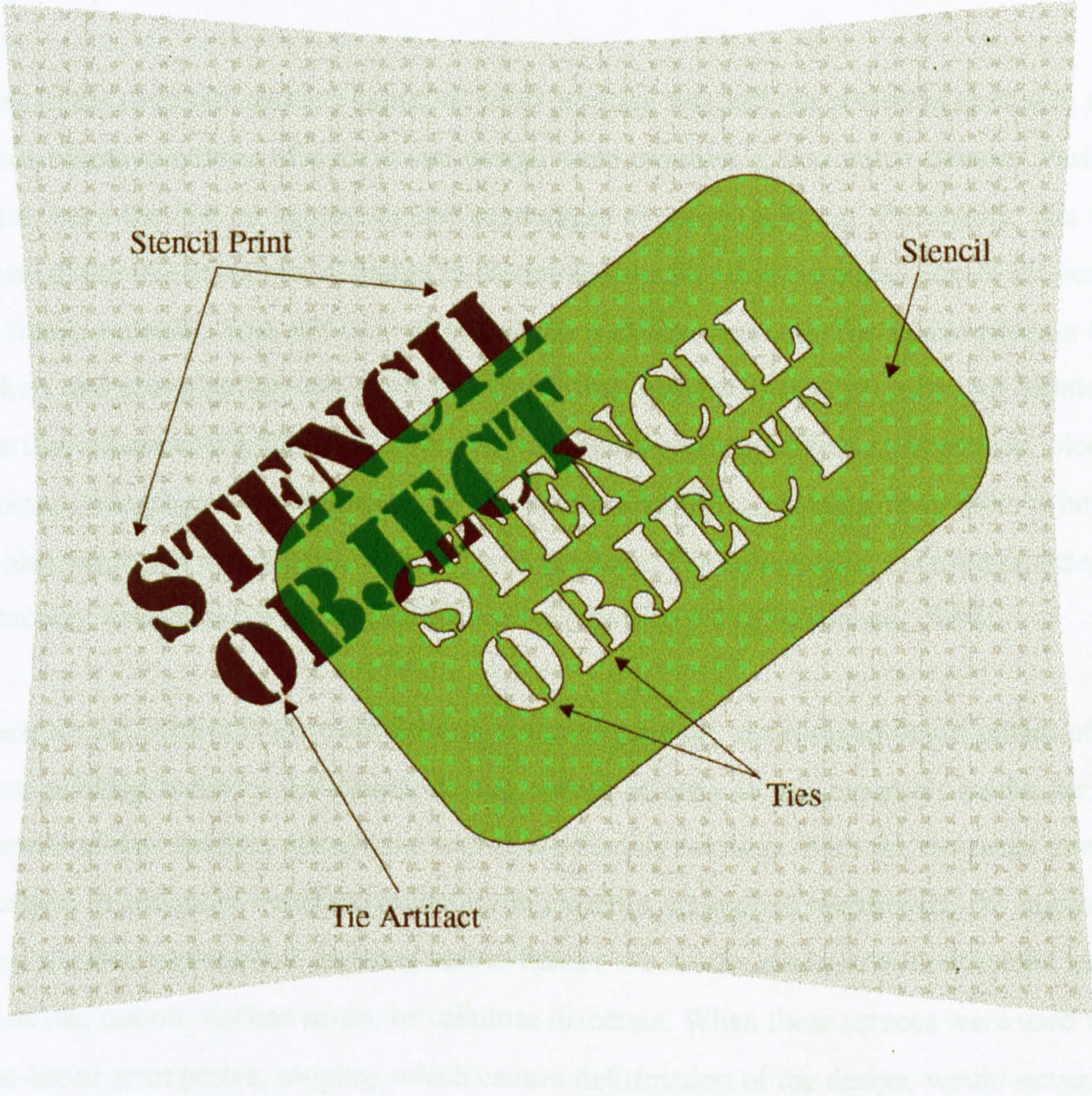

Figure 1.1 : Stencil showing Ties

The first recorded use of a silk gauze stencil for printing, was at Lyon, in 1850, where woven silk fabric was used for continuously supporting the stencil. It was found that by stretching this supporting fabric across a frame they achieved the best results. This combination of fabric and frame became known as a *screen*. The silk gauze provided the ties for the stencil and the

amount of colour paste applied could be controlled. The use of durable paint on the screen fabric soon replaced the traditional paper stencil. Nevertheless, it was not until 1907 that a patent for a screen printing process was first taken out (by a Manchester man). In fact, this method printed the American Stars and Stripes banners used during the First World War, but it was only after 1926 that screen printing in Europe started to form an industry [Hawkyard, 1994].

Earlier in the twentieth century engraved roller printing was still the preferred approach and, provided large quantities of a particular design were required, it was much cheaper. Fashion houses were the first to appreciate the advantages of screen printing. Principally, this was because of the ease of transfer of design to screen and the fact that the frame size of the screen was freely variable. Also the cost of setting up a design was less, the whole process was quicker, and changing the colour set was easier than engraved roller printing. An additional factor that influenced the fashion houses was that screen printing offered an improved 'bloom' or colour strength, as they did not apply the colour with as much pressure as roller printing. This also meant that they did not crush textured surfaces. The advantages, for exclusive design production, were obvious to the fashion houses [Storey, 1992][Hawkyard, 1994].

Fashion houses, with their increased interest in screen printing, encouraged development of the screen printing industry. Designers started seeing screens as an important media for the realization of their designs, rather than as a cost-effective solution. With the increased interest in designs, in particular complex multicolored patterns, an implicit requirement for improved screen stability was needed. Existing screen fabrics are mostly made from hydrophilic yarns, such as silk, cotton, viscose rayon, or cellulose diacetate. When these screens were used with water-based print pastes, sagging, which caused deformation of the design, would occur. By using hydrophobic fibres[3], manufacturing screens that remained stable when used with water-based pigments was possible. A useful by-product of this development was the improved tensile strength of the screen that allowed them to be stretched more tightly over the frame, giving

---

3 *Hydrophobic fibres are synthetics, such as nylon and polyester, which repel water.*

better accuracy. Replacing the wooden frames, which were susceptible to warping, with metal ones gave further improvement in the overall print quality [Storey, 1992][Hawkyard, 1994].

The construction of robust screens was a precursor to the automation of the screen printing process. One of the first developments, which is still in use today, was where fabric is glued onto a long table and one colour is printed at a time. The screen, being printed, is held in a moveable carriage that is slid along the length of the table. The paste was then forced through the screen by a motor-driven squeegee[4]. This is similar to modern hand-printing techniques, with one colour being printed at a time [Hawkyard, 1994].

It was not until the 1950s, however, that the first fully automated screen printing machines were produced — Buser, Stork, and Johannes Zimmer were the primary manufacturers. Printing was achieved using the same principle as for single screens, but instead of the screens being in movable carriages, the fabric moved under the screens. Gluing the fabric to a print *blanket*[5] achieved this. The blanket moves the fabric under the screens where it is then held stationary while printing occurs, the screens are then raised and the fabric moved on to the next screen. As fabric movement is intermittent, this puts limits on the speed and efficiency of production. Continuous movement of the fabric on flat-screen machines has been achieved by moving the screens along the fabric while printing (e.g. the American Precision Midas machine). Still, this is mechanically inefficient and requires a long print bed [Hawkyard, 1994].

1.4.1 Development of Rotary Screen Printing

To achieve a simpler and more economical method for fully continuous printing it was realized that cylindrical (rotary) screens would be needed. In rotary screen printing continuous rotation of a cylindrical screen while in contact with fabric ensure genuinely continuous printing. Early

---

4 *A flexible rubber blade that forces the print paste through the open areas of the screen.*

5 *A rubber matting in an endless conveyor belt.*

attempts were made to produce a cylindrical screen from flat *wire-mesh* screens, but this required a soldered seam. This seam, unless hidden by the design, was visible, on each rotation of the screen, as a line across the width of the fabric. In fact, this was the approach used, by A J C de O Barros, for manufacturing screens on the very first rotary screen printing machine, built by Aljaba and first introduced in 1954 [de O Barros, 1966].

Aljaba realized that wire-mesh screens were unsuitable for rotary printing due to their open structure, so on Aljaba's early machines the screens were plated with copper by electrolysis to fill the holes partially. Later this process was abandoned and woven, seamless, nylon tubes were used. It was not until after the closure of the Aljaba company that W W Sword introduced a new version of the wire-mesh screen, known as the *Durascreen* [Hawkyard, 1994]. The Durascreen uses an electrophoretic coating process to fill the pores in the screen with a flexible polymer. This process is also used to reduce the risk of creasing of electroformed nickel screens.

One of Aljaba's major contributions towards screen printing was the invention of the *duplex* machine, which allowed both sides of a fabric to be printed concurrently. They achieved this by running the fabric vertically between a pair of screens. The paste was applied to the fabric by means of metal rollers that acted as squeegees.

What made rotary screen printing the dominant method of producing printed textiles, with a 59% market share (Figure 1.2) [Miles, 1994], were the invention, and introduction in the early sixties, of the seamless screen formed by electrodeposited nickel [Cormack, 1993][Hawkyard, Miah, 1987][Kool, 1993]. Within a short period rotary screen printing had substantially replaced *intaglio*[6] and flatbed printing. Two main types of nickel plated screens were introduced: the *galvano* screen by Peter Zimmer (Austria) in 1961; and the *lacquer* screen by Stork (Holland) in 1963. It was mainly due to the superiority of these screens, to those produced by Aljaba, that Zimmer and Stork are the principal manufacturers of rotary screen

---

6 *Engraved copper rollers.*

printing machines today [Kool, 1993]. The key factors for the success of rotary screen printing lie in its ability to combine good printing quality, flexible screen manufacturing and competitive overall printing costs.

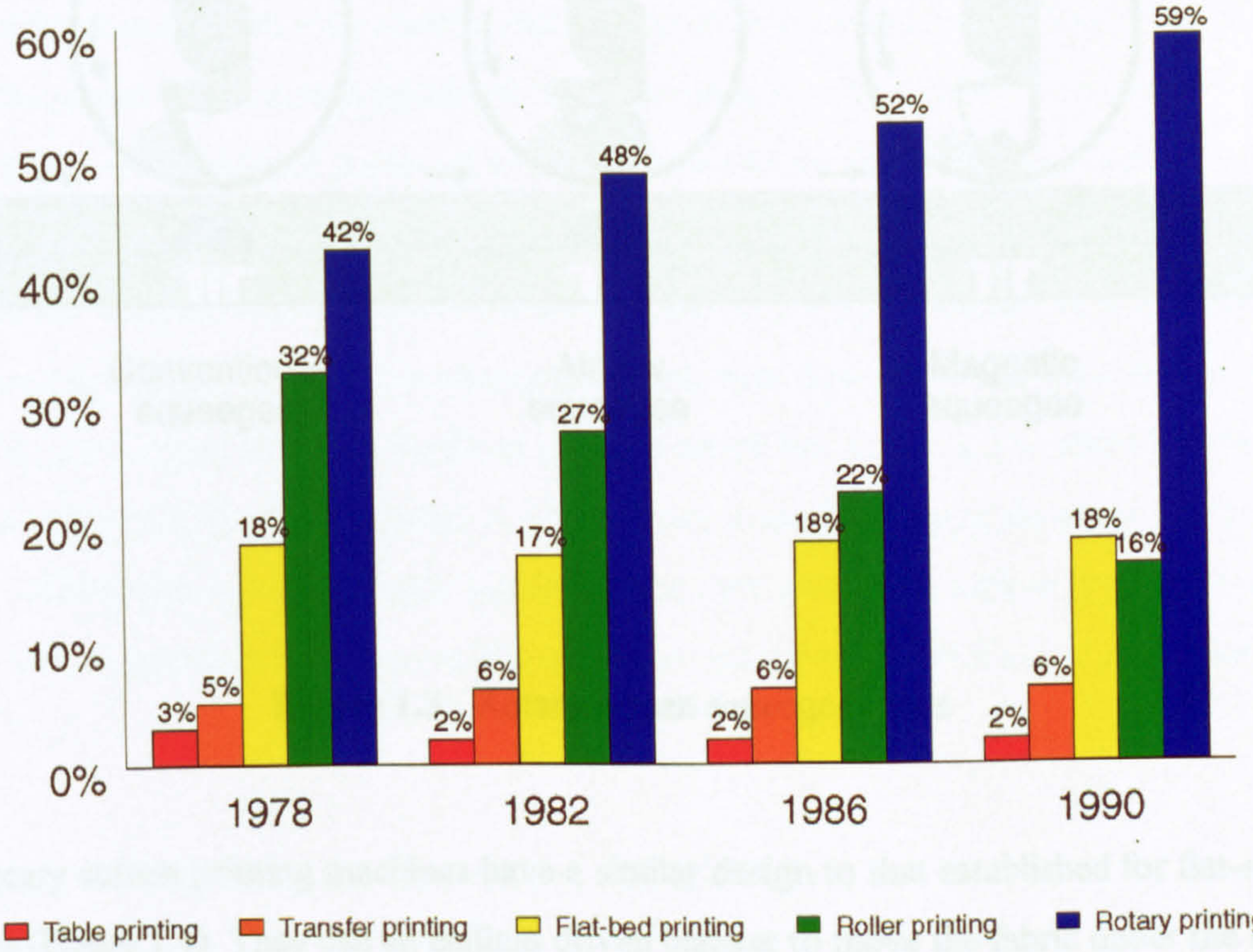

Figure 1.2 : Chart of market share of various textile printing methods [Miles, 1994]

1.5 Mechanics of Rotary Screen Printing

In rotary screen printing, print paste, which is fed to the inside of the screen, is forced out through design areas with the aid of a stationary squeegee. Several different squeegee types are used in rotary screen printing (Figure 1.3). The blade squeegee systems use a flexible-blade. This blade applies pressure to the base of the screen, to force the print paste on to the substrate by the build up in pressure due to screen rotation. Rod or roller squeegee machines, such as those manufactured by Zimmer and Mitter, are successful for printing on wider substrates, as they apply an even pressure across the screen [Ferber, Hilden, 1989].

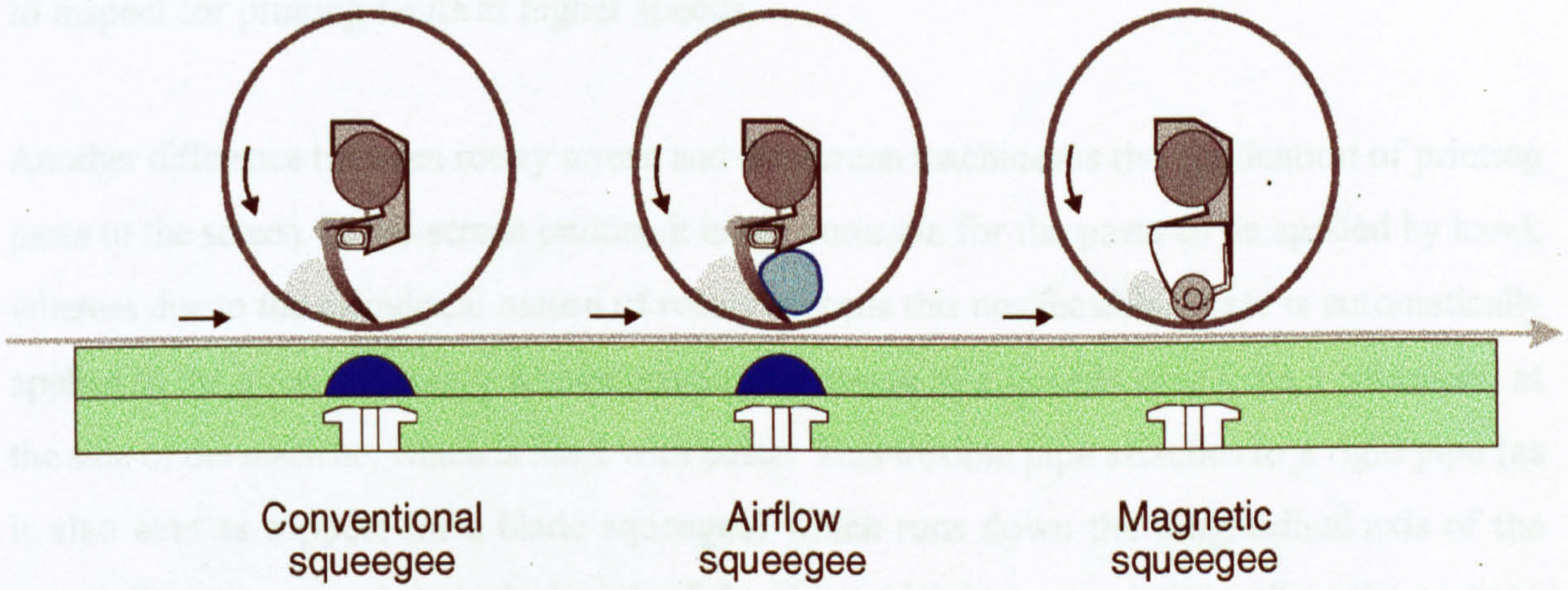

Figure 1.3 : Rotary screen squeegee types

Most rotary screen printing machines have a similar design to that established for flat-screen machines (Figure 1.4). They use an endless driven blanket to move the fabric under the rotary screens, which are positioned along the top. Blanket washing and drying are carried out during the blanket return under the print table. After drying it is common for a thermoplastic adhesive[7] to be applied to the blanket, the fabric is then preheated to facilitate adhesion. This secures the fabric to the blanket for printing, preventing stretching, thus giving the dimensional stability required for print alignment.

With rotary screen printing the cylindrical screens can be placed much closer together than is possible in flat-screen printing. This means that the length of the print table is shorter, for a given number of colours. However, this is balanced to an extent by the need for a longer fabric dryer to ensure adequate drying of the fabric at faster printing speeds. Depending on design and

---

7 *Thermoplastic adhesives become 'tacky' when heated.*

fabric quality, speeds of 30-70 m min^{-1} are typically used. Rotary screen machines will run faster than this but the limitations are imposed by the length and efficiency of the dryers and the ability to inspect for printing faults at higher speeds.

Another difference between rotary screen and flat-screen machines is the application of printing paste to the screen. In flat-screen printing it is still common for the paste to be applied by hand, whereas due to the cylindrical nature of rotary screens this not feasible. Paste is automatically applied to the screens in rotary screen printing by means of a flexible pipe from a container, at the side of the machine, which is filled with paste. This flexible pipe attaches to a rigid pipe (as it also acts as support for a blade squeegee) which runs down the longitudinal axis of the screen. Paste is pumped along the length of the pipe which has pores in it to allow the paste to run down to the bottom of the screens. A level sensor is used to trigger the paste pump when the paste falls below a preset height. Increasing the pore size in the pipe in proportion to the distance from the pump is necessary, as this enables a more even distribution of paste along the screen.

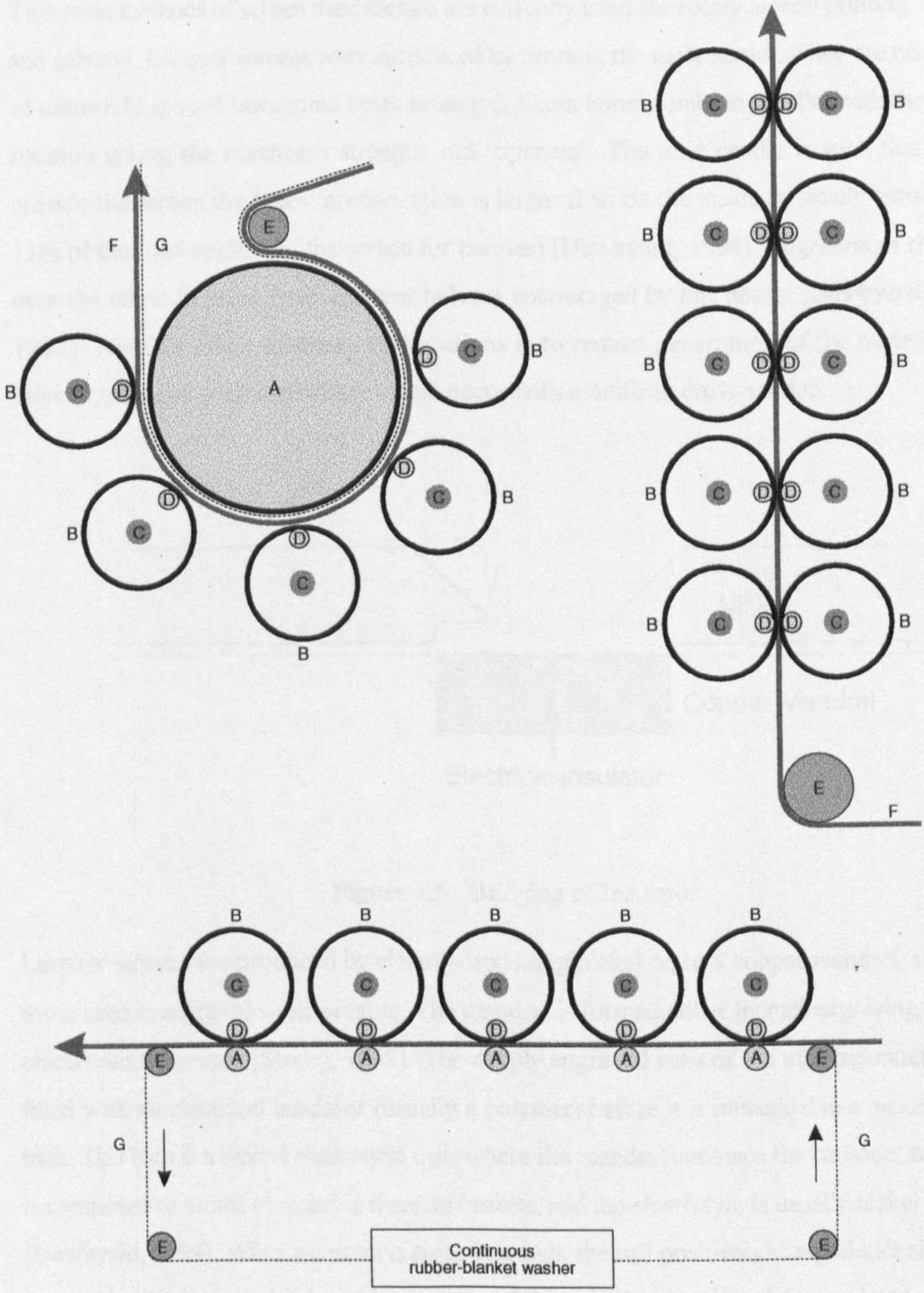

Figure 1.4 : Types of rotary printing machines

1.5.1 Screen Manufacture

Two main methods of screen manufacture are currently used for rotary screen printing: lacquer and galvano. Lacquer screens were introduced by Stork in the early sixties. They are composed of uniformly spaced hexagonal holes arranged, like a honeycomb, in parallel with the axis of rotation giving the maximum strength and 'openess'. The hole profile is such that on the outside the screen the holes' cross-section is larger than on the inside (typically between 9 – 13% of the total surface of the screen for textiles) [Hawkyard, 1994]. Migration of the paste over the fabric to paste from adjacent holes is encouraged by this design [Hawkyard, *et. al.*, 1987]. Another effect of these cross-sections is to reduce penetration of the paste into the fabric, compared with that which would occur with a uniform cross-section.

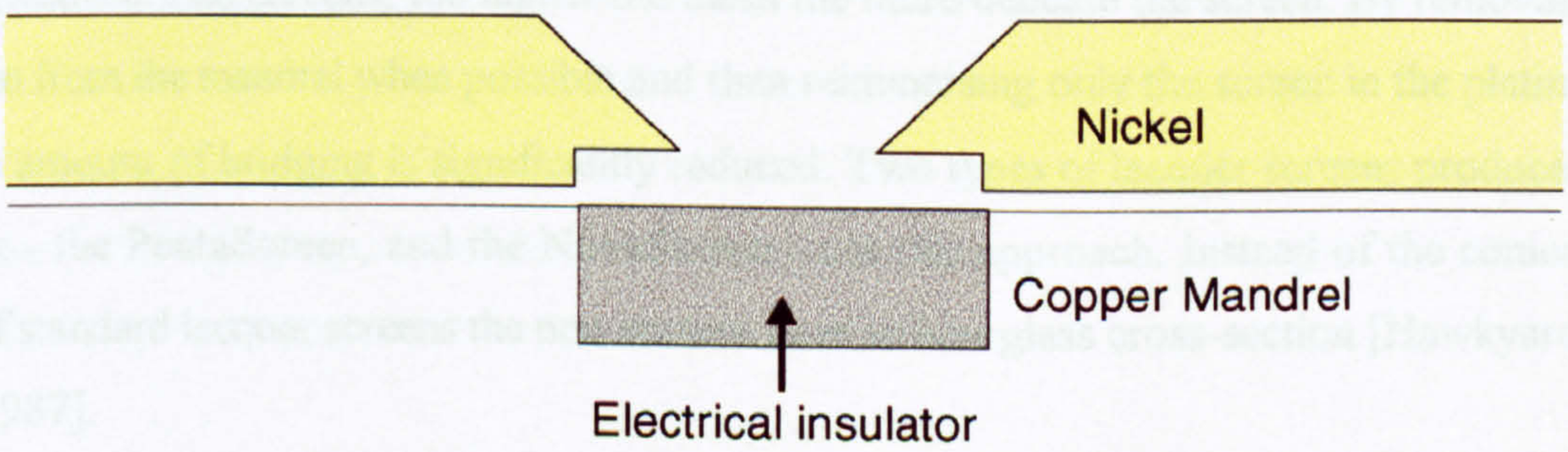

Figure 1.5 : Bridging of Insulator

Lacquer screens are produced by electro-depositing nickel on to a copper mandrel, similar to those used in engraved roller printing. The mandrel is formed either by mill engraving or by an electronic technique [Storey, 1992]. The deeply engraved cells of the mandrel must then be filled with an electrical insulator (usually a polymer) before it is immersed in a nickel-plating bath. This bath is a typical electrolytic cell, where the mandrel becomes the cathode, the anode is composed of lumps of nickel in titanium baskets, and the electrolyte is usually nickel sulphate [Hawkyard, 1994]. When a current is passed through the cell positively charged nickel ions are attracted to the negatively charged mandrel and deposited on the 'land' (uninsulated area). As

plating of the mandrel progresses the layer of nickel not only thickens but spreads sideways producing the conical cross-section (Figure 1.5). This means that producing screens finer than 100 mesh (pores per linear inch) is not possible using this method, and the finer the mesh the thinner the screen. When the nickel layer is approximately 0.1 mm thick (rotary screens are usually between 0.08 and 0.19 mm thick) the mandrel is removed from the bath, cleaned, and the newly formed nickel screen detached.

Rotary screens produced by this method have screen meshes of about 60 mesh for blotches and motifs, and 80 mesh for outlines and synthetic fabrics. When compared to flat screens it is seen that flat screens have a much finer mesh than rotary screens. Therefore, flat screens have better edge definition and can print finer lines. Stork realized that to produce screens with higher meshes, thus higher definition, it was important to stop the bridging of the insulator as this directly affected the numbers of pores possible in a given area. The problem had always been that for electroformed screens, the higher the mesh the more delicate the screen. By removing the screen from the mandrel when possible and then reimmersing only the screen in the plating bath, the amount of bridging is significantly reduced. Two types of lacquer screens produced by Stork - the PentaScreen, and the NovaScreen - use this approach. Instead of the conical profile of standard lacquer screens the new screens have an hourglass cross-section [Hawkyard, *et. al.*, 1987].

Once the screens have been manufactured, the next step is to introduce the design. Screen designs are transferred from a positive using a photochemical process. A similar approach is used for design transfer on flat screens. First, the screen must be thoroughly cleaned and degreased. This is usually achieved by applying chromic acid with a nylon brush [Storey, 1992]. The screen is then coated with photosensitive polymer solution and lacquer (containing other polymers) which promotes adhesion to nickel, then dried. Polymers such as poly(vinyl alcohol) and poly(vinyl acetate), which have been sensitized with a dichromate salt, are commonly used. These polymers will crosslink when exposed to blue, or ultraviolet, light and become insoluble [Hawkyard, 1994]. The polymer is applied to the screen using either an annular squeegee

(designed by Stork) or a modified doctor blade. Several coats of the polymer are applied with a brief drying period between coats – the screen is then ready to be exposed.

Prepared screens are then transferred to a copying machine where they are placed on an inflatable rubber tube to maintain their shape. A full-size (full-out) positive of the design is then wrapped around the screen. The shutter of the copying machine is then opened, exposing the screen that is then rotated for a set time. It is important that the temperature is regulated during exposure as the polymer is also thermosensitive (becoming insoluble at temperature) and to prevent the film sticking to the emulsion. After exposure the screen is removed from the copying machine and immersed in a water bath for approximately fifteen minutes, this dissolves out any unexposed parts of the screen. The screen is then dried and finished (if necessary), after which it is ready for use.

As lacquer screens use a thin uniform mesh filled with a layer of lacquer, they can be susceptible to pinholes in the non-design area. The other major type of nickel screen design, the galvano screen, first introduced by Zimmer in 1961, combines the design and the screen during electrodepositing. Resulting screens have solid areas of nickel in the non-design areas and are therefore stronger and less prone to pinholes than lacquer screens.

The principle behind galvano screen manufacture is the use of a thin nickel tube, known as an *elastic matrix*, which is placed on an inflatable rubber screen/mandrel [Storey, 1992]. The rubber screen is first inflated and the elastic matrix is coated with a photosensitive lacquer and the tube slightly deflated. Next, a full-size negative of the design is wrapped around the matrix with a second negative on which the required grid pattern is reproduced. When the rubber tube is reinflated close contact between the films, matrix, and mandrel is ensured (Figure 1.6). The screen is then exposed and washed similarly to lacquer screens, which frees the non-design and supporting mesh in the design from the polymer. As well as defining the design areas, the polymer also acts as a dielectric resist [Hawkyard, 1994]. The rubber is again deflated, and the patterned nickel sleeve is removed then plated in the nickel-plating bath. On completion of the plating the screen is replaced on the rubber mandrel, which is then inflated to stretch the nickel

tube slightly. It is then immediately deflated releasing the galvano screen from the elastic matrix.

Comparison of these two main types of screen manufacture shows each method has areas in which they operate better than the other. A major problems of galvano screens, more so than with lacquer screens, is the bridging of the insulator. The finest mesh that can be reliably manufactured using galvano screen production is about 80 mesh [Hawkyard, 1994]. It is reasoned that for narrow fabrics with fine pattern detail the lacquer screen type is more suitable. Yet, for wider fabrics, due to their additional strength and resistance to pin-holing, galvano screens are more appropriate. This is especially true in the adverse environment of carpet printing, where the galvano screens have a coarser mesh and an increased wall thickness (0.35-0.4 mm), instead of the standard thickness of 0.08-0.1 mm for textiles.

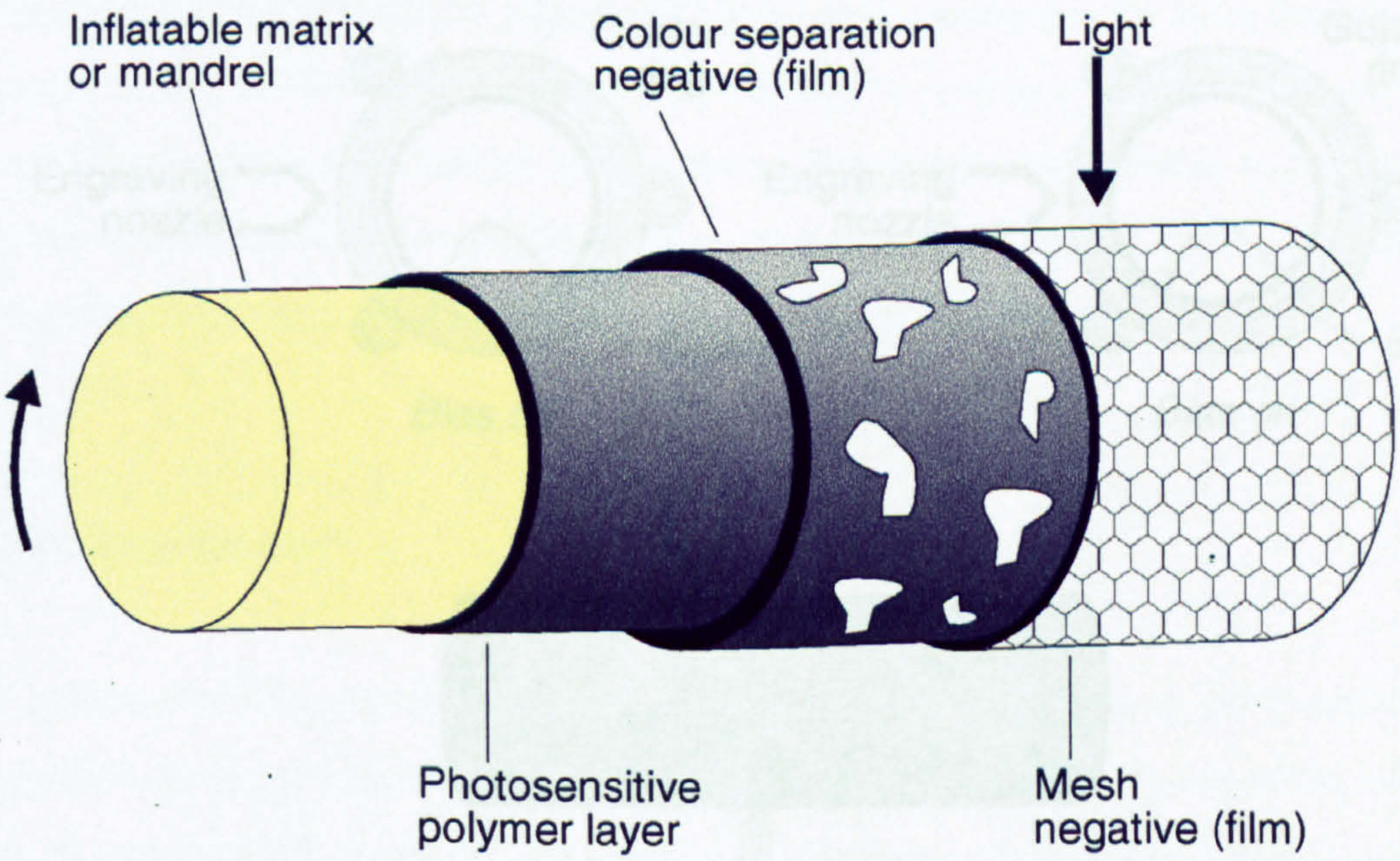

Figure 1.6 : Galvano screen manufacture

Another method for screen manufacture has recently come into use – laser engraving. This approach, developed from flexographic (used for transfer prints) print screen production, uses laser light to engrave a polymer-coated screen. The laser used, has to be sufficiently powerful (1 kW) to strip the lacquer from the screen, this allows used screens to be recycled. A powerful suction and filter unit is employed to avoid contamination of the optical system by degraded lacquer.

When engraving the screen it is important that it is held precisely in position. ZED Instruments have developed a system that uses a moving hardened steel guide ring that is just larger than the screen, to hold the screen in place. When a screen is being loaded or unloaded, from the engraver, the guide ring is concentric with the screen. During engraving, the guide ring is moved away from the engraver lens, this brings the ring into gentle contact with the screen. The guide ring and screen are then rotated at the same speed. This produces enough friction to hold the screen securely in position for engraving (Figure 1.7).

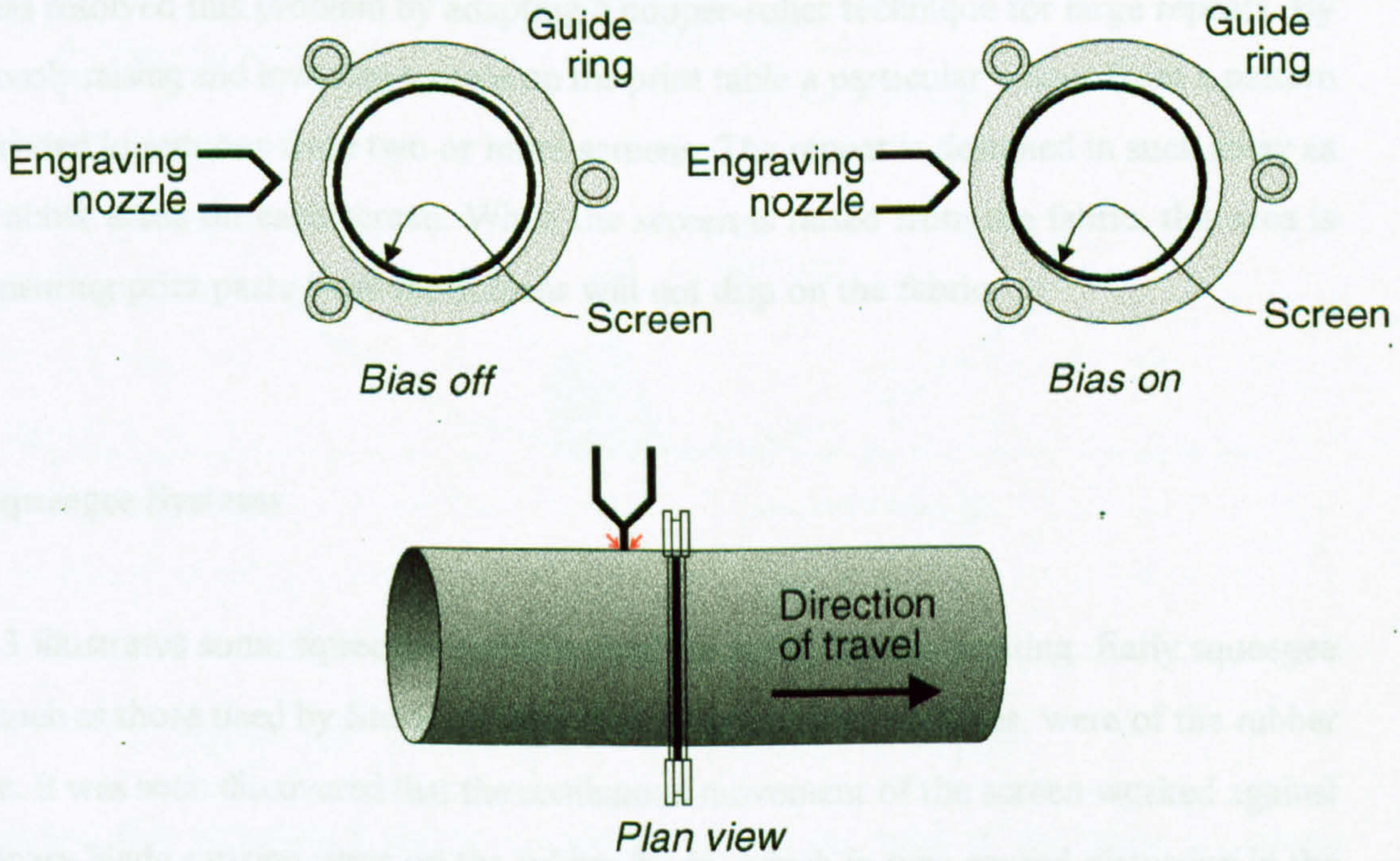

Figure 1.7 : ZED Instrument guide ring system

Laser engraving of screens has led to a computer integrated approach to rotary screen manufacture. Designs can now be realized on CAD (computer aided design) systems, colour separations, repeats, and scaling can also be generated by the computer. Finalized screen designs are then down loaded, via a network or storage media, to the laser engraver, thus reducing the need for costly (in time and money) intermediary stages.

1.5.2 Screen Dimensions and Repeats

A wide range of screen sizes of cylindrical nickel screens (dependant on the size of the mandrel on which they are electrodeposited) is available for rotary screen printing. For printing fabrics, screens with an internal circumference of 640.0-640.1 mm are most frequently used [Hawkyard, 1994]. Screens with circumferences of 518, 637, 640, 668, 725, 801, 819, 914 (the most common of larger screens) and 1018 mm may be obtained as standard. Even the largest rotary screens manufactured do not provide as large a repeat as the flat-screen approach. Zimmer has resolved this problem by adapting a copper-roller technique for large repeats. By synchronously raising and lowering screens on the print table a particular colour from a pattern may be printed in sections from two or more screens. The repeat is designed in such away as to leave blank areas on each screen. When the screen is raised from the fabric, this area is lowest, ensuring print paste from the screens will not drip on the fabric.

1.5.3 Squeegee Systems

Figure 1.3 illustrates some squeegee systems used for rotary screen printing. Early squeegee systems, such as those used by Stork on their first rotary screen machines, were of the rubber blade type. It was soon discovered that the continuous movement of the screen worked against the stationary blade causing wear on the rubber blade, which in turn caused distortion in the screen [Storey, 1992]. This led to the replacement of rubber squeegees with flexible stainless steel blades which Ferber[*et. al.*, 1989] refers to as 'doctor' blades . Squeegee systems are

called 'doctor' blades when the geometry of the compression zone is formed by a stationary blade and the screen.

The dynamics of the squeegee system are such that the curvature of the blade, which directs the angle of the contact between the blade and screen, can be controlled by applied pressure. Doctor blade squeegee systems are designed with bearings at both ends of the squeegee assembly to control this factor. These same bearings also allow lateral adjustment of the blade so that it is not necessarily at the lowest point of the screen. This has benefit of increasing the paste wedge's (indirect) contact with the fabric.

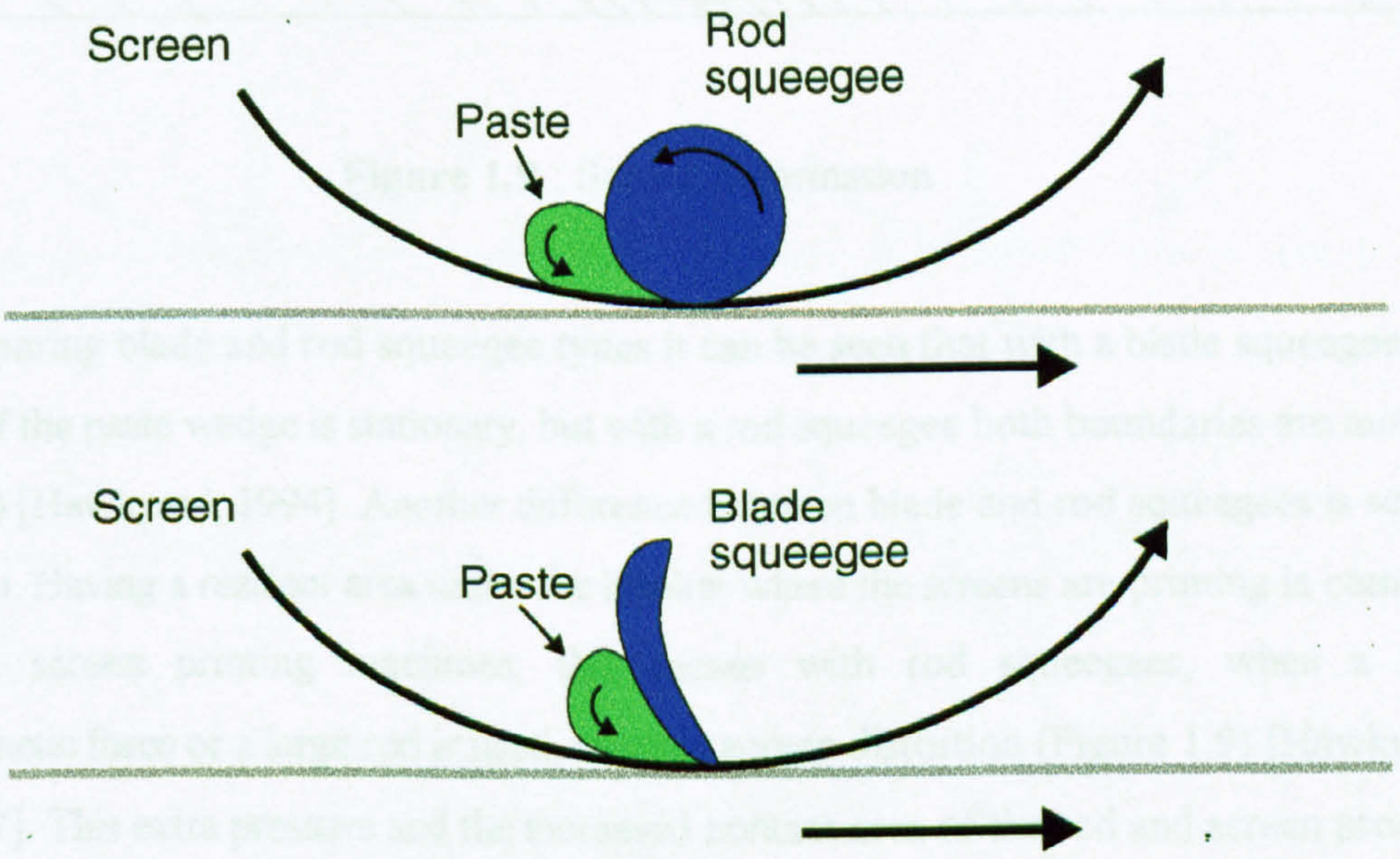

Figure 1.8 : Comparison of rod and blade squeegees

It is important that squeegee pressure is constant across the width of the fabric as uneven pressure can result in an unlevel appearance of the final print. This problem becomes especially critical when printing wide fabrics. Several manufacturers have developed special systems to

deal with it. The most common approach, which was first introduced by Zimmer and Mitter [Hawkyard, 1994], is the use of a rod or roller squeegee system, which uses an electromagnet to apply even pressure across the length of the squeegee. Another approach is that of the Reggiani Airflow squeegee (see Figure 1.3), which consists of a phosphor-bronze doctor blade against which a rod is forced, ensuring an even pressure, by an inflatable tube running behind the blade under the feed pipe.

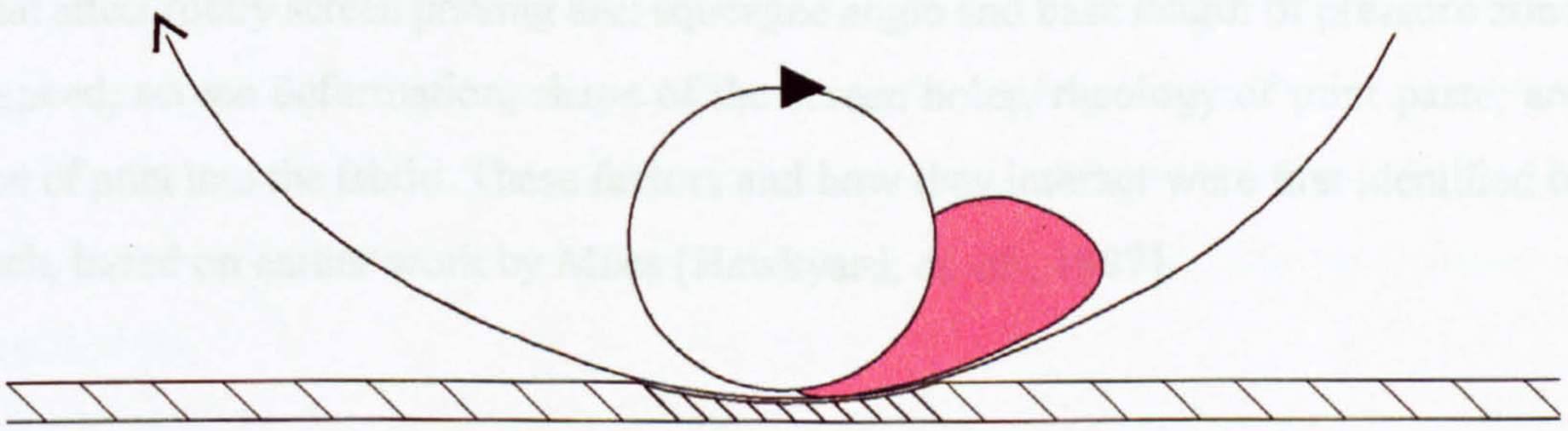

Figure 1.9 : Screen deformation

When comparing blade and rod squeegee types it can be seen that with a blade squeegee one boundary of the paste wedge is stationary, but with a rod squeegee both boundaries are moving (Figure 1.8) [Hawkyard, 1994]. Another difference between blade and rod squeegees is screen deformation. Having a resilient area under the blanket where the screens are printing is common for rotary screen printing machines, this means with rod squeegees, when a high electromagnetic force or a large rod is used, there is screen distortion (Figure 1.9) [Hawkyard, *et. al.*, 1987]. This extra pressure and the increased contact area of the rod and screen produce a higher minimum of paste being forced through the screen than in doctor blade techniques. Blade systems are used instead of rods on lightweight synthetic fabrics or paper as they require less paste and therefore a lower minimum paste application is desirable.

1.5.4 Parameters of Rotary Screen Printing

Many variables affect the quality of print in rotary screen printing. A requirement of any system designed to detect and correct print faults is a knowledge of when and why faults occur. To understand fault occurrence it is important to comprehend the fundamental mechanisms of machine printing.

Factors that affect rotary screen printing are; squeegee angle and base length of pressure zone, printing speed, screen deformation, shape of the screen holes, rheology of print paste, and penetration of print into the fabric. These factors and how they interact were first identified by Kassenbach, based on earlier work by Miles [Hawkyard, *et. al.*, 1987].

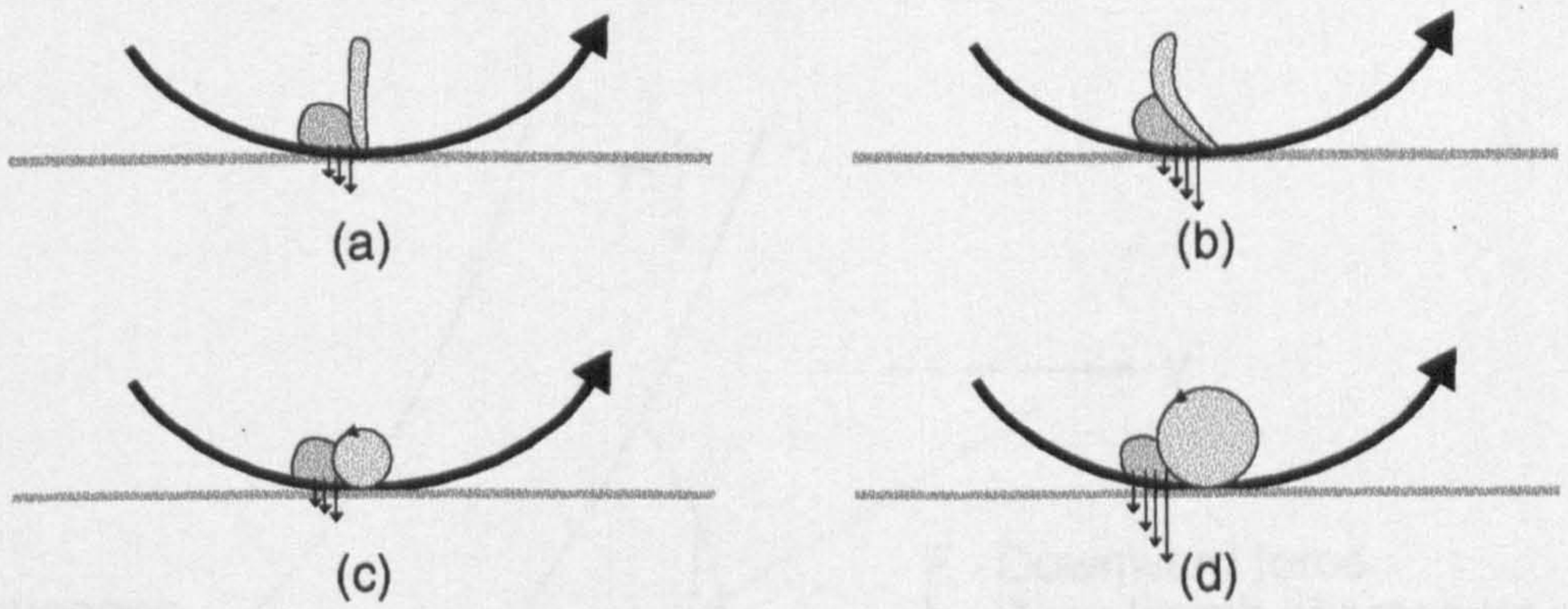

(a) Blade, large squeegee angle
(b) Blade, small squeegee angle
(c) Rod, small diameter
(d) Rod, large diameter

Figure 1.10 : Pressure profiles for rod and blade squeegees

Squeegee angle and 'base' length are critical elements of rotary screen printing as they are constituents of the hydrodynamic processes that is present in all screen printing; the distance

within the paste wedge where significant hydrodynamic pressure exists, is called the base length. When using rod or roller systems, the two surfaces, which are moving, bring their boundary layers of paste into the wedge (see Figure 1.8) giving a higher hydrodynamic pressure compared with that induced by a stationary blade (Figure 1.10). It was estimated by Dowds that this hydrodynamic pressure could be larger by a factor of five for roller or rod squeegees at a constant printing speed [Dowds, 1970]. The quantity of paste finally being applied is dependant on restrictions due to the screen holes and uptake of paste by the fabric, and not just the amount of paste pressure. In a blade squeegee system, the hydrodynamic forces are affected by several factors (Figure 1.11), the downward force F on the squeegee is necessary to produce the required angle α and to prevent the blade lifting off the screen. F has minimal effect on the hydrodynamic pressure, but when combined with screen distortion there may be an effect on the squeegee angle.

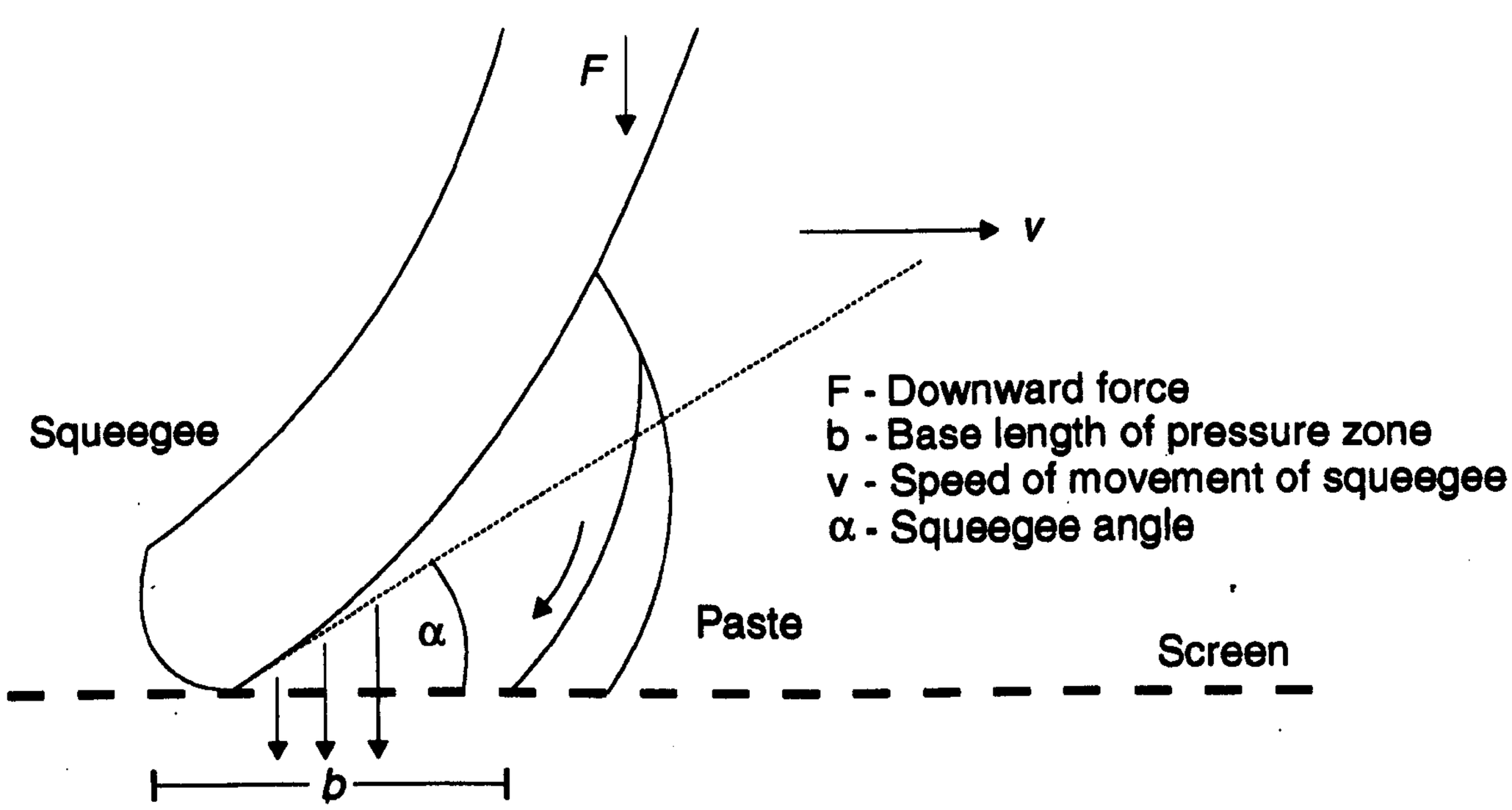

Figure 1.11 : Pressure profile of the paste wedge

Printing speed is also an important consideration as a factor of printing quality. Varying the printing speed has three main effects. Principally, it alters the contact time between screen and fabric, the faster the printing speed the lower the contact time. A secondary effect is the increase of paste shearing with print speed by the screen and (particular with rod squeegees) the squeegee. The increased shear on the paste will affect the paste according to its rheological properties, but usually print pastes are 'shear thinning' so the viscosity of paste will be reduced [Hawkyard, *et. al.*, 1987]. The final effect of printing speed is that hydrodynamic pressure increases with speed. It can be seen that the first two factors work against one another, as shorter amount of contact time will reduce the amount of paste applied, whereas lower viscosity will allow more paste to flow through the screen — this relationship is therefore dependant on the paste rheology.

Because the nickel electrodeposited screens are only approximately 0.1 mm thick they are easily deformed. This property can be used to the printer's advantage — it allows the screens to run over thicker areas of fabrics and seams between pieces without becoming damaged. But, it also means that screens will be deformed by excess squeegee pressure — although rod squeegees with diameters as large as 80 mm are available, those above 25 mm could not be used due to the increased risk of screen damage. Screen deformation has two main effects. It reduces the effective squeegee angle and it compresses the fabric, thus reducing the volume of fabric interstices (see Figure 1.9) [Hawkyard, *et. al.*, 1987].

It is usual when calculating the passage of paste through the screens to assume a cylindrical cross-section for the screen holes. Notwithstanding that the screen holes are rarely cylindrical, typically having a conical cross-section (see section 1.4.1). Simple flow through the holes in screens can be approximated using the Poiseuille relationship (Equation 1.1); where Q is the quantity of paste flowing through a hole of length l and average radius r, P is the pressure drop across the hole, and η is the paste viscosity [Hawkyard, 1994].

$$Q = \frac{Pr^4}{8\eta l} \qquad 1.1$$

It is seen that the instantaneous viscosity of the print paste is an important factor in determining the amount of paste that passes through the screen under shear. Hawkyard and Miah have shown that highly pseudo plastic pastes will be more susceptible to changes in printing speed, as at high speeds the viscosity falls off markedly [Hawkyard, *et. al.*, 1987]. Yet, another important factor that concerns viscosity is the amount of paste that drips through the screens when they are lifted out of contact with the fabric during machine stops or multiple screen repeats. Viscosity also affects the amount of paste threading which occurs when the rotary screen lifts of the print zone (Figure 1.12). These threads can lead to irregular accumulations of printing paste on the fabric substrate, thus producing faults [Ferber, *et. al.*, 1989]. The more paste applied to the substrate and not taken-up by the fabric the longer are the threads formed. Therefore, the faster the printing paste penetrates the fabric the better the print uniformity will be.

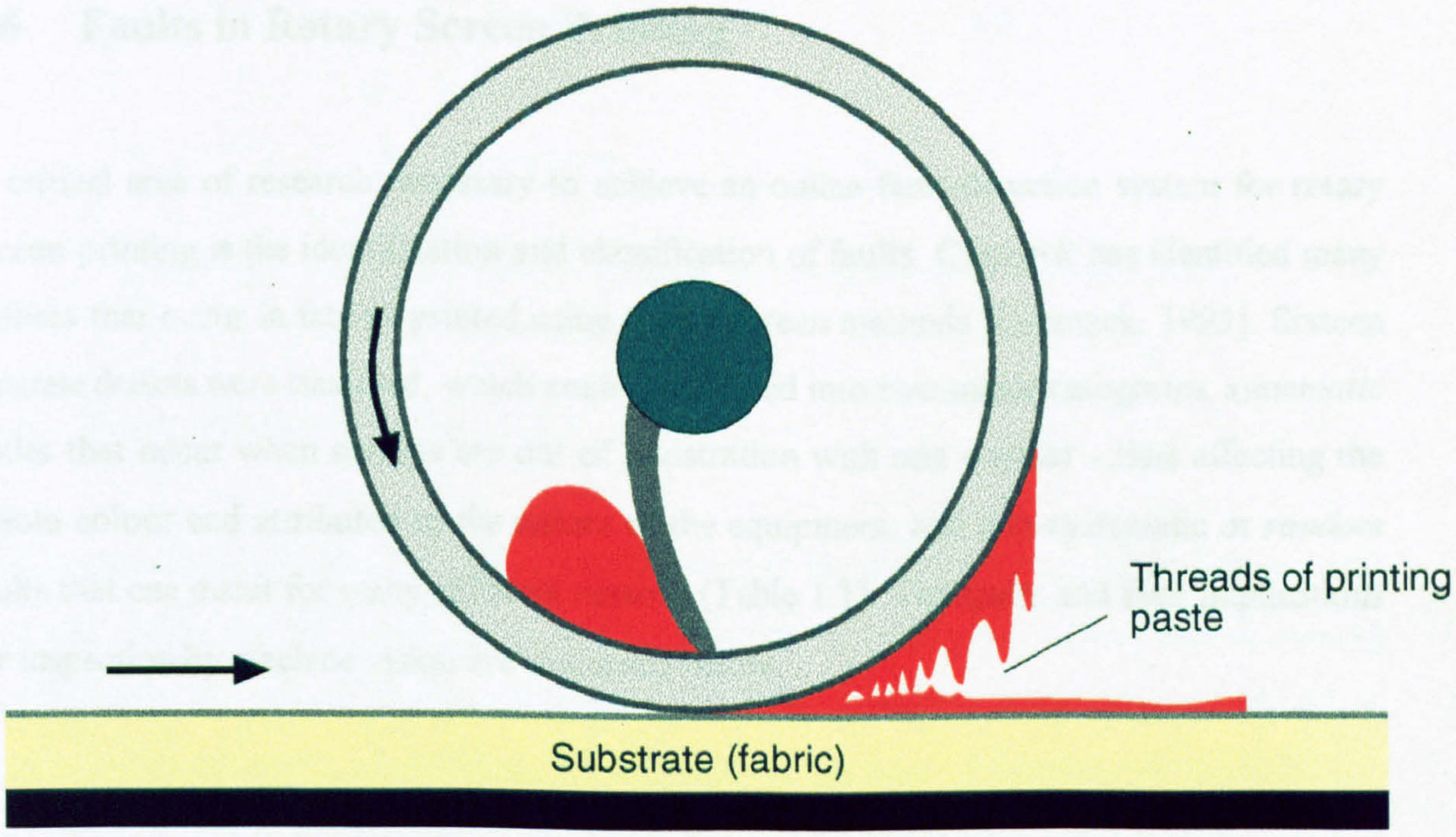

Figure 1.12 : Paste threading

The maximum penetration of paste possible is determined by the fabric substrate. However, the degree of penetration achieved depends on the rheology of the printing paste. Penetration can be determined objectively by taking reflectance measures on the underside of the fabric [Ferber, *et. al.*, 1989]. As already mentioned fabric compression and paste viscosity are the two principal factors affecting paste penetration. Other elements of the fabric that affect paste uptake are its three-dimensional form (the amount of free space between yarns and fibres), the absorbency of the fibres and penetration between yarns. Penetration through the fabric is mainly due to hydrodynamic pressure and the kinetic energy with which the paste leaves the screen pores. Yet, under low shear conditions' sideways spreading of pseudo plastic pastes is restricted due to its high viscosity. In addition fabric preparation is important to ensure satisfactory paste penetration. A water-based pigment will not be absorbed into a badly prepared polyester/cotton fabric due to surface tension.

1.6 Faults in Rotary Screen Printing

A critical area of research necessary to achieve an online fault-detection system for rotary screen printing is the identification and classification of faults. Cormack has identified many defects that occur in fabrics printed using rotary screen methods [Cormack, 1993]. Sixteen separate defects were classified, which could be divided into two major categories; *systematic* faults that occur when screens are out of registration with one another - thus affecting the whole colour and attributed to the nature of the equipment, and non-systematic or *random* faults that can occur for many different reasons (Table 1.1). The faults and their implications for inspection by machine vision are discussed below.

	Defect	Occurrence (%)
1.	Misfit	14.4
2.	Off straight	3.2
3.	Stop marks	10.3
4.	Off shade	9.0
5.	Other print	7.9
6.	Colour missing	6.7
7.	Other prep/fin	6.5
8.	Screen block	6.2
9.	Screen leak	5.7
10.	Creases	4.0
11.	Stains	2.6
12.	Oil spots	0.96
13.	Streaks	0.28
14.	Cloth defect	9.5
15.	Fabric width	5.1
16.	Miscellaneous	8.2

Table 1.1 : Defect prevalence in rotary screen printing [Cormack, 1993]

1.6.1 Registration/Systematic Faults

Clearly, screens require considerable care in alignment at the start of the print run. The patterns from each screen must be synchronized to create the desired final print. Rotary screen printing machines allow screens to be adjusted along their lateral, horizontal and rotational axis. Often there is a requirement to skew the screens slightly, at the start of printing, to adjust for any alignment errors that may have occurred when the screens were manufactured. Still, during a print run a screen may become further skewed due to some movement along the lateral axis. Also the design may be advanced/retarded due to some alteration in the screen's respective

rotational position (mainly due to lunging or seizing of the screen). It is also known for some screens to oscillate around a fixed position.

Any misfitting of a screen will cause its colour to overlap (or be overlapped by, depending on print order) another colour on one side and leave an area uncoloured on the opposing side. It is, therefore, critical that the screens are in perfect register and their circumference, and speed of rotation, identical to prevent misfitting. If the misfitting is due to the screen engraving then a new screen is required. Misprinting can also occur if the fabric is not properly fixed to the print blanket [Cormack, 1993]. Depending on the type of fibre and the fabric quality, different adhesive formulation and concentrations are required to ensure secure fixing of the fabric to the blanket.

While sometimes these systematic errors fall within design tolerances (dependant on the type of design, customer, colour, and current market preferences) there will be periods when the error falls outside these acceptable limits. A requirement of the fault detection system is to detect and correct these faults before they drift out of tolerance. The detection of errors should always be to the highest available accuracy — whether or not to take corrective action is then dependent on the individual design's tolerances.

In total, systematic faults only account for approximately 18% of the total faults in rotary screen printing (Table 1.1, Faults 1 & 2) [Cormack, 1993]. This is a misleading figure as they account for two-thirds of the 'seconds' quality fabric produced. Principally, this is due to fault detection time. In a typical rotary screen printing setup, the fabric is only inspected after the dye has been 'fixed' and dried — usually 90 metres after the fault occurrence. Due to the consistent and repetitive nature of systematic faults all 90 metres of fabric have to be classified as seconds.

Refer to Sections 1.6.1, 1.6.2, and 1.6.3 for more detailed information on defects.

1.6.2 Screen Bowing

Another common type of fault is that of bowing, this occurs when a screen flexes along its lateral axis, and is particularly prevalent in wide fabric printing. This, however, is not a truly systematic error (which occur across the full width of the fabric), but an error that falls between the two major categories of systematic and random faults. Confirmation of this can be seen when bowing occurs, due to screen flexing, the centre of the design can be significantly misaligned, while the edges may still be within design tolerance. There is nevertheless a degree of misfitting in width and length.

Screen deformation due to bowing is thought to be influenced by a complex interaction of several variables that includes factors such as;

- *The mass of the colour (print-paste) in the screen* – bowing may occur due to the varying amount of paste within the cylinder. If the screen contains a large amount of colour, they will reflect this in a general increase in the mass of the screen. This in turn means there is an increased frictional loading of the screen onto the print media. As this media is travelling under the screen at, usually in the order of, 1 ms^{-1}, to assume that some level of dragging of the screen by the media occurs seems valid. Inversely, if there is less than an average mass of colour in the screen the more firmly clamped ends may remain in position, whereas the lighter middle section can oscillate due to the decreased friction.

This factor with the others causes bowing, although this is probably the principal cause. An obvious solution would be to maintain a constant mass of print-paste in the screen. Currently they feed print-paste into the screen using a min/max switching probe – when the print-paste reaches a minimum level they insert more into the cylinder until the maximum level is reached. This can mean a major change in mass of the screen, which a constant flow device would eliminate.

- *The basic screen construction and length* – a screen is made out of a thin lightweight mesh and is comparatively long, and will be prone to flexing due to the natural weakness inherent in its structure.

  Changes in the structural design of the screen may be possible to alleviate the problem of flexing. They could make screens thicker, reducing their flexibility. This would infer a slight weight increase, but nothing as drastic as the current changes in mass due to the print-paste insertion technique. The extra costs of the screens may be a factor for consideration, but with their intrinsic recyclability, it should not be. Different alloys/amalgams could be used in screen manufacturing — ones that are less flexible. Nevertheless, a balance needs to be found between inherent strength, brittleness, lightness, flexibility, and cost. Despite these factors, the key point is that thicker screens are less flexible (cf. screen manufacture).

- *Printing speed* – in relation to the previous point, the higher the speed of the media under the screen the more pronounced the bowing of a screen is likely to be. This would mean that the printer has to measure the pros and cons of increasing the throughput of the system and the increased likelihood of fabric with bowing related faults – a difficult decision to make.

- *Squeegee design and pressure* – this factor is difficult to detect. However, some indication of how bowing may occur in this area is when there is uneven pressure over the longitudinal length of the squeegee. In the rubber bladed type, this may happen if wear occurs on a section of the squeegee, which can cause an uneven amount of friction over the screen length. Perceiving the same sort of problem occurring with an electromagnetic squeegee design is hard, but there are two major ways in which it could occur. A warped rod would apply pressure unevenly to the fabric, and a fluctuating electromagnet may cause uneven frictional loading on the screen, therefore bowing.

These are the major areas liable to cause bowing. There is some speculation whether print design may be a causative factor. The rationale behind this is because print screens that have a larger block of colour towards the centre than the edge, may drag due to the cohesive forces of the print paste (cf. random faults – colour drag). This is best shown when printing straight on to the print blanket. When applying paste directly to the fabric puckering of the design occurs due to the viscosity of the paste. When printing on fabrics observation of this factor is difficult, as fabrics absorb the paste and therefore reduce the puckering effect. Still, the fact that there is puckering suggests a certain level of adhesiveness of the paste, but this would be difficult to eliminate without the development of some new printing pigments.

1.6.3 Random/Non-Systematic Faults

Random defects are faults that can occur anywhere and at any time during rotary screen printing. Therefore, this defines them as nontemporal and nonspatial defects. Examples of random faults are screen blockage, fabric faults, and faults due to poor maintenance. They account for approximately 82% (see Table 1.1) of the total printing faults, but only one-third of fabric wastage as seconds (cf. systematic faults). Cormack[1993] identified fourteen fault types classified as random faults.

- *Screen block* – if the screen pores become blocked, from either inside or outside the screen, they prevent colour from being printed on the fabric leaving an uncoloured area. In areas of contrasting colours this form of the fault is particularly noticeable. The fault will occur regularly (every rotation) until corrected, yet it is not a systematic fault as it does not affect the full width of the fabric.

Causes for screen blockages are usually due to a build up of thread or lint from the fabric that become attached to the screen. Neps (small balls of tangled fibre) may also become attached to the screen, leaving pinhead sized areas of unprinted fabric, but fall off after printing. Improved fabric preparation would reduce this problem, along with

regular cleaning of the thermo-adhesive rollers at the end of the print table. Another factor contributing to screen blockages is dried paste in the pores if the screen is not properly cleaned between print runs.

- *Screen leak* – due to the nature of rotary screens manufacture which produces thin walled, therefore intrinsically weak screens (cf. screen manufacture), they are easily damaged. This is especially true of screens with large design areas, or screens with a high mesh (pores per linear inch). When a screen becomes worn out either due to mishandling or excessive use, cracks and holes can appear in the screen. These flaws allow an excess of print paste through the screen onto the fabric which can lead to pinholing and colour drag. Regular inspection of the screens and their replacement before undue wear occurs reduces the problem of screen leak.

- *Missing colour or dry screen* – this fault can be awkward to detect, especially if the colour has been missing throughout the print run. There are two major causes for missing colour. First the screen may be dry — the screen is not filled with paste, this is probably due to either an empty paste barrel, a blocked feeder pipe, or faulty colour level probe. The second possible cause is a missing screen. The screen has not been set up on the print table.

Classification of this fault is difficult as it is not truly random or systematic. If the fault occurs due to a missing screen, then it affects the full width of the fabric and as such is systematic, but unlike other systematic faults it does not gradually move out of tolerance, so cannot be predicted. However, if the fault is due to a paste barrel running dry, a faulty level probe, or inconsistent feed then initially it is of a more random nature. The fault will first show itself as uneven colour, or missing patches and these can occur anywhere across the design.

- *Uneven colour or print definition* – many factors affect the application of print paste to the fabric (cf. parameters of rotary screen printing). It is important that the colour

is uniformly printed throughout the print run to avoid variations in intensity and streaking. If screens apply excessive paste to the fabric, it is expensive, and this might also adversely affect its handling, especially when printing with pigments.

There are several reasons why poor print definition or uneven colour may occur. If the print paste in the screen is running out, this may result in the colour becoming fainter or uneven (cf. missing colour or dry screen). Variations in paint viscosity and squeegee pressure may also cause uneven colour. If they have not properly pretreated the fabric, then the interaction of the paste with the fabric can be affected, causing an uneven uptake of colour. Also, if the screen is, unduly, worn there may be problems with print definition. Other problems may occur during machine stops and when seams pass under the screen.

- *Watermarks* – in the factory environment, where they carry out rotary screen printing, hot and humid conditions are common, especially due to excessive steam release during fixing. These conditions encourage the build up of condensation — water droplets maybe formed over the print table, where they can drop randomly onto the print. Watermarks are circular in appearance and cause a lessening of colour intensity within them. An adequately ventilated print room virtually eliminates this problem.

- *Oil stains* – if oil used to lubricate the printing machines is allowed to contaminate the fabric, oil stains will occur. Contamination by oil can occur anytime during the fabrics' life cycle, so special care is needed when transporting and handling fabrics. Oil stains affect the uptake of pigments by the fabric, with dark dye stuffs they affect the intensity, whereas the yellow colour of the oil alters lighter pigments.

- *Slubs* – slubs occur when a yarn thickens over a short distance. When a yarn containing slubs is woven into a fabric these slubs can produce an uneven surface. When printing onto a fabric comprising some large slubs, the slub raises the screen away from the fabric in the immediate area. This results in an uncoloured area surrounding the slub.

- *Stop marks* – stop marks are common in fabric production, especially when the fabric is being dried after bleaching and stentering[8]. If they stop the fabric without extinguishing the burners, it can become singed, producing brown stripes across the fabric. This is not directly a fault of rotary screen printing, but fabric is often taken immediately from the dryer to the print table without inspection.

  The other form of a stop mark is caused if the printing machine is stopped without raising the screens. Excess paste seeps through the screen and appears as strips of increased intensity when they resume the print run. Both forms of stop marks can be eliminated if machine stops are avoided.

- *Creases* – if the fabric is folded or creased then it will not be properly printed, with unexposed areas inside the fold remaining uncoloured. Creases vary in width and length and are usually self-correcting. Typically, they appear at the beginning and end of a fabric roll, at the seams, due to the fabric not being uniformly fed into the sewing machine.

- *Colour drag* – this fault can occur when an intense (thick rather than bright) horizontal line of colourant is printed. Due to the cohesive force of the paste the screen may seize briefly, causing an excess of print paste to reach the fabric. The screen then drags this paste (acting as a squeegee) and threading occurs and colour drag appears partially or completely across the fabric width. After a colour bar the screen can either snap back into position, or remains out of register giving a systematic fault. Colour drag may also be a factor for screen bowing.

---

[8] *Stentering is a process whereby fabric is distorted to skew the weft respective to the warp, usually by about 22½ °. This allows correct printing of horizontal lines on the fabric which must be printed at the same angle as the out of true fabric. After the fabric is washed and finished they appear in their intended form [Storey, 1992] p. 90.*

Manual intervention is commonly required to eliminate colour drag. Unlubricated, or stiff bearings are possibly the major cause for colour drag, along with build up of debris in the system. Frequent maintenance is the best solution to this fault.

- *Screen wipe* – if a screen becomes blocked it is usually wiped to remove the blockage. This wiping action smears the paste on the screen across the screen surface from which it is then transferred to the fabric. Cormack classifies it as a secondary defect as it is formed by the removal of the primary blockage defect, and appears at uniform intervals becoming fainter with each rotation [Cormack, 1993].

- *Incorrect colour* – this fault occurs when there is a deviation from the customer approved colour schemes. Both manufacturer and customer keep reference swatches to ensure they do not introduce new colours without the customer's consent. Incorrectly prepared paste, wrong paste selection, or inaccurately labelled paste barrels are the most common causes for this error.

- *Dye stains* – when handling dyes and pigments care needs to be taken to ensure they do not splash onto critical areas, such as the fabrics or screens. If a particularly heavy splash falls on the fabric it may be taken-up by the screen and printed on each rotation until exhausted (cf. screen wipe), therefore it is self-correcting.

From this information it can be seen that the occurrence of random faults can be greatly reduced with frequent maintenance. Given that 82% of faults are due to random defects it is surprising that little action is being taken to reduce them.

2 Machine Vision

2.1 Introduction

The following chapter introduces the concepts of machine vision and identifies its relevance to this research. Machine vision is an extremely broad discipline. It blends traditional engineering with computer science. In the manufacturing industry tasks that require visual inspection have always in the past been carried out by human operators. The upshot of this was a restriction on the spread of automation (especially to repetitive mechanical tasks) [Hollingum, 1984].

2.2 An Overview of Machine Vision

Over the last three decades vision technology has only been used intermittently. Principally, the space industry and the military were the major users, with only limited industrial applications. Nevertheless, the continuing development of machine vision, so that it now provides a competitively priced robust solution, to inspection problems, is initiating a change from human to machine vision for inspection. In the next decade we can expect to see a large increase in the development of machine vision systems for industrial tasks. The supporting technologies for machine vision are now sufficiently advanced to be viable. Reliable hardware is now available at a reasonable cost. A greater pool of expertise in machine vision exists — more individuals have the hardware and programming knowledge necessary to apply the technology. Most importantly, problems exist that require a vision technology solution [Galbiati, 1990].

Machine vision has both advantages and disadvantages when compared with human vision for industrial inspection. Humans have integrated vision systems that are interdependent on various sensors, using adaptive coupling with the brain and other sensory organs. In addition, the level of fatigue, previous training, and knowledge all affect the performance of the human visual

system in quantifiable ways. Comparisons can only be made, therefore, between the two visual systems on a functional basis (summarized in Table 2.1).

High-volume manufacturing using human inspectors seldom simplifies complete product inspection. Still, automated visual inspection techniques may make full inspection possible; this is dependent on the complexity of the inspection task and the throughput required from the manufacturing system. This factor is important if inspection is to be on-line (inspecting during manufacture) [Vernon, 1991].

Machine vision can be much faster than human vision in certain circumstances. It does not tire, or lose concentration, and is therefore consistent. Also machine vision has the advantage of being able to work in hostile conditions, which would be either unpleasant or impossible for a human operator. Another factor where machine vision is better is in measurement, it can give accurate dimensional measurement (assuming proper calibrations) whereas humans can only make estimates. Important to this research is the ability of machine vision to measure other variables objectively such as colour, which a human operator could only classify subjectively. Usually, all the human vision capabilities can be performed by machine vision systems. The level of performance of machine vision is superior to that of human vision for reliability and precision.

	Human	Machine
Flexibility	Very adaptable and flexible as to task and type of input.	Rigid as to task; requires quantized data (pixels).
Ability	Can make relatively accurate *estimates* on subjective matters.	Can make dimensional measurements based on predetermined data inputs.
Colour	Subjective in colour	Measures the magnitude of the chromatic parameter (R, G, B).
Sensitivity	Adaptive to lighting conditions, physical characteristics of item's surface and distance to object. Limited in the ability to distinguish between shades of grey. Varies as function of individual as from day to day. Can identify about 7 to 10 levels of grey.	Sensitive to level and frequency of illumination as well as physical nature of surface and distance to object. Ability to quantize is relatively high and fixed by sensor, environment and system characteristics. Can easily identify 256 levels of grey.
Response	Speed of response is slow and on the order of 1/10 second at best.	Speed of response is very high and dependent on system computation and bandwidth. Speeds of response on the order of 1/1000 of second and higher are technically achievable.
2-D and 3-D	Can handle 3-D tasks and multi wavelength (colour wavelengths) easily.	Can handle 2-D tasks easily but limited on 3-D tasks. Requires 2 cameras and is very slow in 3-D. Can perform mathematical operations on data, enhance data and use pixels for calculating areas, controls, and the like.
Data Output	Can manually supply secondary discrete data input. Cost is high and data subject to high error rate.	Can automatically supply precise discrete data input to manufacturer's data base on a continuous basis at relatively low incremented cost basis.
Perception	Perceives brightness on logarithmic scale. Affected by surrounding area (background).	Can perceive brightness in either linear or logarithmic scale.
Spectrum	Limited to visual spectrum 380 to 700 millimicrons	Can make measurements in entire spectrum from X-rays to IR.

Table 2.1 : Comparison of Human and Machine Vision [Galbiati, 1990]

2.3 Typical System Architecture

A machine vision system comprises all the elements necessary to obtain a digital representation of the visual image, to process the data, and to output this data to provide feedback. Image acquisition is usually performed by a camera, connected to a frame grabber[9]. The image must be properly illuminated, so there is a requirement for some form of lighting system. After acquisition processing of the data is then necessary. Typically, processing equipment combines both hardware and software in a vision processing unit. Once data has been processed, it is output via some form of an electronic interface, such as feedback via a process control unit, an alarm, or another form of information display. Figure 2.1 shows the functional architecture of a standard vision-manufacturing system and their interrelation.

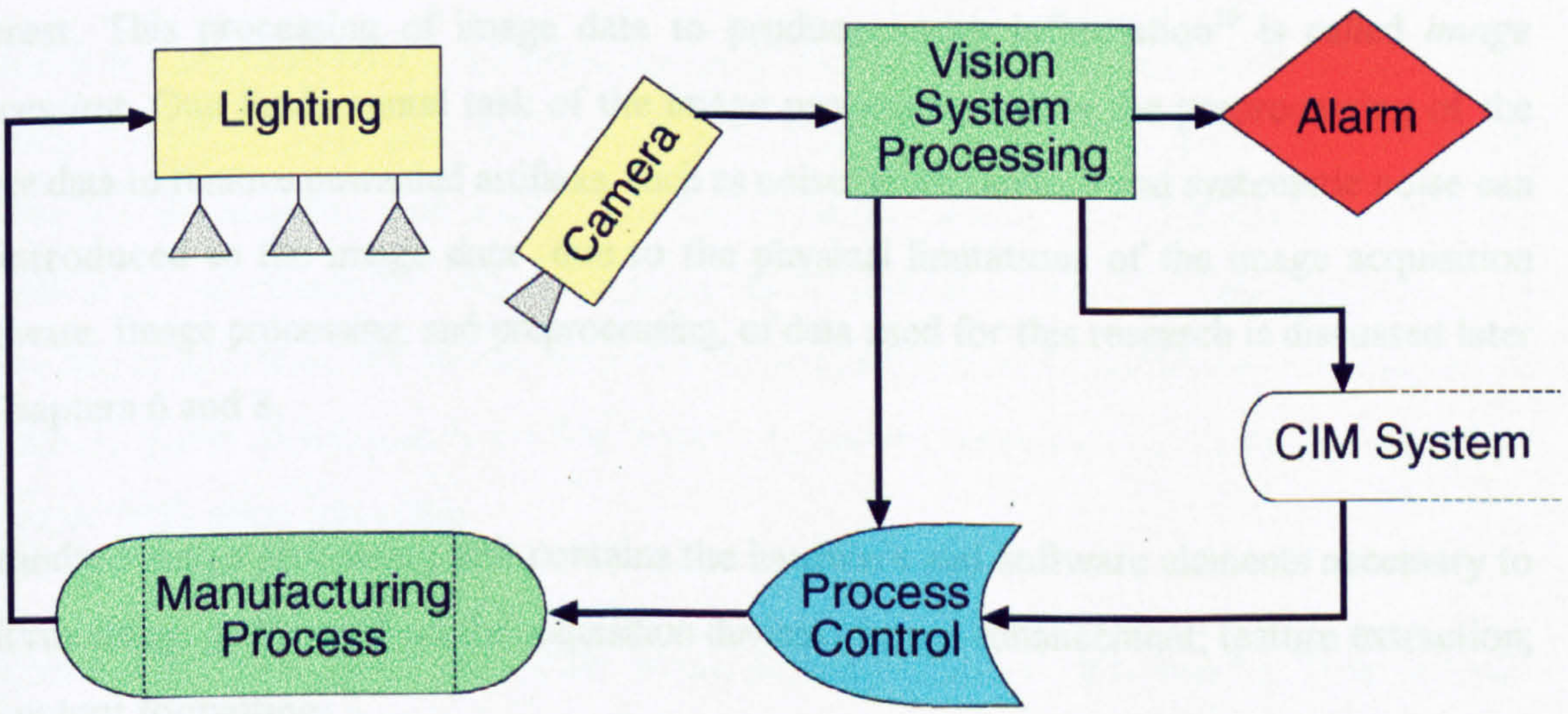

Figure 2.1 : Vision system function in manufacturing cell

---

9 *A frame grabber is a hardware device which converts the analogue image signal from the camera into a digital signal for processing by the computer. It usually comprises one or more frame buffers (memory areas for digital image storage).*

2.3.1 Image Acquisition

Galbiati [1990] defines image acquisition as — *'the transformation of the visual image of a physical object and its* ***intrinsic characteristics*** *into a set of digitized data which can be used on the processing unit of a system'*. Image acquisition is subdivided into four separate phases: illumination; image formation or focusing; image detection or sensing; and formatting camera output signals. Discussion of these phases in relation to this research is presented later in the thesis (Chapter 4).

2.3.2 Image Processing

After image acquisition, the data needs to be altered in a way that enhances the features of interest. This processing of image data to produce image information[10] is called *image processing*. One fundamental task of the image processing unit is the preprocessing of the image data to remove unwanted artifacts, such as noise. Both random and systematic noise can be introduced to the image data due to the physical limitations of the image acquisition hardware. Image processing, and preprocessing, of data used for this research is discussed later in Chapters 6 and 8.

A standard image processing unit contains the hardware and software elements necessary to perform: image grabbing (from the acquisition devices); image enhancement; feature extraction; and output formatting.

Either hardware or software can perform data processing. The use of hardware for processing results in a faster system, but offers less flexibility, and has a higher initial cost than software. For research a software-based image processing system is desirable — requiring integration of a hardware solution at the development stage.

---

10 *Processed data is referred to as* ***Information***.

2.3.3 Output or Display

Standard vision systems usually have the capability of outputting, or acting on, the processed data via data printout (hardcopy), data display (usually via a VDU), and control signals (used for feedback). Depending on the application the vision system is being used for this output can be highly customized. For example, a pass/fail system that visually inspects parts against a good/bad criterion may only need to generate a control signal to eject the faulty part, and maybe some form of display identifying number of parts accepted or rejected for production management information.

2.4 Machine Vision and Textiles

Advances in Computer Integrated Manufacture (CIM) methods have improved the efficiency of many industrial processes. Yet, Convery, Lunney, *et. al.* [1994], state that the textile industry overall (including both knitted and woven fabric manufacture) is still labour intensive in production, and especially in inspection processes. The textile industry is well-established and mature and as such there is a certain resistance to computerization. In particular, the integration of machine vision techniques to on-line textile or garment manufacture has been slow, when compared with other industries.

Munden and Norton-Wayne [1988] offer several explanation to why this may be. They propose that visual inspection of fabric (whether knitted or woven) for irregularities is complicated. They suggest that the 'natural' structural variations (e.g. slubs or knops) that give the fabric its 'character' could cause false triggering in a visual inspection system. Since the publishing of Munden and Norton-Wayne's paper there has been an increasing amount of research into this area.

Norton-Wayne, Bradshaw, *et. al.* [1993] discuss signal processing for the detection of defects in automated inspection of unprinted web materials using machine vision. They present a generalized methodology that they claim is applicable to a wide range of inspection tasks. A universal scheme for detecting surface defects in the presence of noise, is suggested, based on published methodology. This allows the design of a system to achieve quantitative performance requirements through probability of defect detection versus probability of false alarms.

Bradshaw [1994] goes on to propose a monochrome line scan-based system for the detection of faults in plain woven fabrics. Also working on defects in plain fabrics (in this case knitted) Convery, *et. al.* [1994] developed a prototype machine vision system for automatic fabric inspection. Their system uses a standard CCD camera for detection of knitted fabric faults, such as drop-stitches, and needle lines. Nevertheless, they emphasize that currently this is only a prototype system for algorithm development, and to show the feasibility of automated fabric inspection.

Campbell [1995], looked at the use of machine vision as method for inspecting for faults in patterned woven Axminster carpets. The paper evaluates methodologies for automatic inspection and offers some theoretical proposals for a fault detection system. This system would make quality assessments against *a priori* known design specifications. Campbell identifies some fundamental problems with patterned carpet inspection. In particular, specifying the difficulties of automatically inspecting highly structured surfaces that produce 'noisy' signals from any image capture device. Also mentioned were the problems due to the physical dimensions of the carpet and the difficulties this invokes with capture, lighting, and processing. This factor is also common to rotary screen printed fabric inspection.

Schicktanz [1993] has also done some work into the possibilities of fault detection on nonwoven fabrics using laser scanners. Tsai, Shentu, Lin, *et. al.* [1993], designed a system for pattern recognition of fabric structures in woven structures. Similar to Bradshaw [1994], Tsai, *et. al.* [1993], use line scan cameras to capture the image, the system obtains a complete identification of fabric structure within a minimum time.

A related use of machine vision in the textile field is not for fault detection in woven and knitted fabrics, but for contactless thread density measurement. Such a system is outlined by Dusek [1991] and uses a CCD area camera for image acquisition. The image processing system developed can accurately evaluate dimensional changes in woven and knitted fabrics. Processing takes a few minutes, but the results produced can statistically differentiate between fabrics of 1% and more thread density variation.

Kaasjager [1990] suggested that machine vision could be used to monitor the effectiveness of other textile processes such as calendering and stentering. He argues that web monitoring via machine vision based on texture parameters can be used for processes that change the fabric surface, such as shrinkage, factors affecting gloss and hairiness. Determination of the fabric properties does not require continuous, full-width inspection. Regular sampling will suffice, and as processing speed is not critical, relatively, unsophisticated equipment can be used. Hinze and Viertel [1991] have also been conducting research in this area.

Another problem with machine inspection for textiles, is that they are flexible and distort easily. In fact the EC codename for textiles is flexible materials [Munden, Norton-Wayne 1988]. Due to their flexible nature, the dimensions of textiles are difficult to define. This leads to problems when developing a machine inspection system. For accurate fabric characterization and fault detection it is critical that the vision system has a workable model. For machine vision to compete against the human eye will require a great deal of further research and will certainly be complex. For instance, one of the simplest faults in textiles detectable by a human operator is that of colour variation. The development of a machine vision system to adequately detect colour faults is just one example of the complexity of this research area.

In 1989, Leicester Polytechnic (now De Montfort University, Leicester) opened the first CIM centre in the world that concentrated on the use of computers in the textile and clothing industry. This centre became known as CIM*TEX* (for Computer Integrated Manufacture in Textiles). It was recognized that a vital part of the automated manufacturing process in textiles was for continuous inspection throughout the process. This naturally progressed into the

development of a vision research group at De Montfort University, under the guidance of Dr. Norton-Wayne. A great deal of textile related image processing work has been carried out by this group — including this research. Areas covered include plain fabric inspection, lace inspection, measurement of thread spacing, various levels of garment inspection, printed fabric inspection, and other related areas of textiles. The cross-fertilization of ideas that occur in this group has shown the importance of collaboration between research establishments working in related fields. Dr. Norton-Wayne has done much to ensure that this collaboration exists with regular meetings between machine vision groups from other British universities (Brunel, Hull, Bristol, Bradford, and others).

Currently the use of machine vision in textiles is still limited. Nevertheless, the important initial developments have been made, and the necessary components are now (or soon will be) available. It is a critical stage for further development of machine vision in textiles, where the onus is now on the textiles system user to try new innovative ideas. In the highly competitive textile market the advantages of consistent high-quality inspection methods are clear. However new technology requires funding, and without a significant investment from the textile industry, automatic inspection remains something for the future.

3 Concepts of Colour Vision for Humans and Computers

3.1 Introduction

Section 1.2 (The Inspection Task) identifies why colour is critical for the rotary screen printed fabric inspection process and highlights the principal difficulty of integrating a high resolution colour system with an on-line inspection strategy. This chapter presents the concepts of colour vision, first from a human visual perception standpoint, where the basics of light, colour, and perception are explained. These ideas are then expanded to cover computer colour perception with particular emphasis on colour image processing. Finally, several computer colour interchange spaces are analysed to decide their suitability for clustering and other relevant processes.

3.2 Colour Vision

3.2.1 Human Vision

Colour is the perceptual response to one or more wavelengths of light in the visible region of the electromagnetic spectrum. The normal human visual system is sensitive to light wavelengths in the region of 380 nm (nanometres) to 700 nm. A *spectral power distribution* (SPD) is used to express the *radiance* (physical power) of the individual wavelengths that when combined are perceived as colour. The SPD is typically subdivided into 32 ten-nanometre bands. In fact, colour exists only due to the human eye/brain perception. In the physical world a colour is expressed as an SPD [Chamberlin, Chamberlin, 1982].

Humans perceive colour due to electromagnetic radiation (in the visible light wavelengths) falling on a light sensitive surface in the eye (the *retina)*. The human retina has three types of

colour photoreceptor *cone* cells that respond to incident radiation with different spectral response curves. A fourth type of photoreceptor cell, the *rod*, is also present in the retina. Rods are effective only at low light levels, and although important for vision, play no part in colour perception. The three types of colour photoreceptors each have differing sensitivity to the visual wavelengths. When the signal strengths from each receptor are combined by the brain they are interpreted as a colour, therefore they are responsible for colour discrimination. Although the spectral sensitivities of the receptors overlap, each type is particularly sensitive in one area of the spectrum, nominally red, green, and blue wavelengths. These are classified as ρ cones (sensitive to a red stimulus), γ cones (sensitive to a green stimulus), and β cones (sensitive to a blue stimulus) [Hunt, 1992].

Because three types of colour photoreceptor are used by the human visual system, three numerical components are needed to describe a colour. This is usually sufficient if appropriate spectral weighting functions are used. The science of *colorimetry* is concerned with this. In 1931, the Commission Internationale de L'Éclairage (CIE) adopted standard curves for a hypothetical *Standard Photometric Observer*. Later, in 1964 these curves were updated with the standard photometric observer's field of view being increased from 2° to 10°. These curves specify how an SPD can be transformed into a set of three numbers that uniquely specify a colour [Hunt, 1992][Poynton, 1995].

If the observed colour is from a self-luminous source (such as a display) then the CIE system is immediately and almost universally applicable. Typically, however, the colours produced by reflective systems such as photography, *printing* or paints are a function not only of the colourants but also of the SPD of the ambient illumination. In which case using spectral matching is not an important issue in *this* application as the perceived colour is also dependant upon the spectrum of the illuminant.

A common term used when referring to colour is *intensity*. Intensity is a measure, over an interval of the electromagnetic spectrum, of the flow of power radiated from, or incident on, a surface. It can be termed a *linear-light* measure, which is typically expressed in units such as

watts per square metre. NB. The voltages presented to a cathode-ray tube (CRT) monitor control the intensities of the RGB colour components, but this is nonlinear. Therefore, CRT voltages are not directly proportional to intensity.

A term that is often confused with intensity is *brightness*. The CIE defines brightness as "*the attribute of a visual sensation according to which an area appears to emit more or less light*". Brightness perception is a very complex area, because of this, the CIE defines a more usable quantity called *luminance*. This is expressed as radiant power weighted by a spectral sensitivity function that is characteristic of vision. The luminous efficiency of the Standard Photometric Observer is defined numerically, peaking at approximately 555 nm. When an SPD is integrated using this curve as a weighting function, the result is CIE *luminance*, denoted *Y* [Poynton, 1995].

Like intensity, the magnitude of luminance is proportional to physical power. However, the spectral composition of luminance is related to the brightness sensitivity of human vision. Luminance should be expressed in a unit such as candela[11] per metre squared (cd/m^2). However, it is often normalized to 1 or 100 units with respect to the luminance of a specified or implied *white reference*. One example is where $Y = 1$ after normalizing against a specified white reference of luminance 80 cd/m^2 (typical luminance value of a studio monitor) [Poynton, 1995].

It has been established that humans have a nonlinear perceptual response to brightness [*Retinex theory*, Land, M°Cann, 1971, cited Hunt, 1992][Land, 1977]. For instance, a source that has a luminance of only 18% of a reference luminance appears about half as bright. The perceptual response to luminance is called *Lightness*. (Again, this term is often confused with brightness,

---

11 *Unit of luminous intensity. The candela is the luminous intensity, in a given direction, of a source emitting a monochromatic radiation of frequency 540×10^{12} hertz, the radiant intensity of which in that direction is 1/683 watt per steradian*†.

† *Unit of solid angle defined as: the solid angle that, having its vertex in the middle of a sphere, cuts of an area on the surface of the sphere equal to that of a square with sides of length equal to that of the radius of the sphere, [Hunt, 1992].*

intensity, and luminance.) It is denoted by L^* and is defined by the CIE as a modified cube root of luminance (Equation 3.1):

$$L^* = 116\sqrt[3]{\left(\frac{Y}{Y_n}\right)} - 16; \qquad 0.008856 < \frac{Y}{Y_n} \tag{3.1}$$

where Y_n is the luminance of the white reference. If the luminance is normalized to a reference white, the fraction does not need to be computed. L^* has a range of 0 to 100, and a ΔL^* of unity is taken to be roughly the threshold of visibility. This means lightness perception is roughly logarithmic. An observer can detect an intensity difference between two patches when their intensities differ by more than one about percent. CCD camera systems approximate the lightness response of human vision using RGB signals that are each subject to a 0.45 power function. This is comparable to the ⅓ power function defined by L^* (in Equation 3.1).

Often colours are expressed as hue, saturation, and lightness (or brightness). According to the CIE "*hue is the attribute of a visual sensation according to which an area appears to be similar to one of the perceived colours, red, yellow, green and blue, or a combination of two of them*". This implies that if the dominant wavelength of an SPD alters, the hue of the associated colour will alter.

Saturation is defined by the CIE as, "*the colourfulness of an area judged in proportion to its brightness*". Saturation runs from neutral gray through pastel to saturated colours. This can be translated as the more an SPD is concentrated at one wavelength, the more saturated the associated colour will be. A colour can be unsaturated by additive blending of the SPD with light that contains power at all wavelengths.

Direct acquisition of luminance requires use of specific spectral weighting. However, luminance can also be computed as a weighted sum of red, green and blue components. If three sources appear red, green and blue, and have the same radiance in the visible spectrum, then the green

will appear the brightest of the three. This is because the luminous efficiency function peaks in the green region of the spectrum. The red will appear less bright, and the blue will be the darkest of the three. Because of the luminous efficiency function, all saturated blue colours are quite dark and all saturated yellows are quite light. When computing luminance from red, green and blue, the coefficients will depend on the particular red, green and blue spectral weighting functions employed, but the green coefficient will be quite large, the red will have an intermediate value. The blue coefficient will be the smallest of the three. The weights to compute true CIE luminance from **linear** red, green and blue (shown without prime symbols), according to Rec. 709 (ITU-R Recommendation BT.709, *Basic parameter values for the HDTV standard for the studio and for international programme exchange*, [formerly CCIR Rec. 709]), are these:

$$Y_{709} = 0.2125R + 0.7154G + 0.0721B \qquad 3.2$$

This computation assumes that the luminance spectral weighting can be formed as a linear combination of the scanner curves, and assumes that the component signals represent linear-light. Either or both conditions can be relaxed to some extent depending on the application [M^{ac}Donald, Luo, *et. al.*, 1989].

This has implications for computer colour image representation, because the blue component has a small contribution to the brightness sensation. Therefore the blue element of the colour signal can be assigned fewer bits than the red and green. However, human vision has good colour discrimination capability in the blue region. This suggests that giving the blue component fewer bits than red or green, will introduce noticeable contouring in the colour images.

3.2.2 Expressing Colour for Computers

Several systems for expressing colour exist, the CIE system defines how to map an SPD to a triple of numerical components that are the mathematical coordinates of a three-dimensional colour space. Common colour specifications include CIE XYZ, CIE xyY, CIE L*u*v* and CIE L*a*b*.

Originally, HSB and HLS were developed to specify numerical Hue, Saturation and Brightness (or Hue, Lightness and Saturation). The usual formulations of HSB and HLS are flawed with respect to the properties of colour vision. Numerical values of hue and saturation are not very useful for colour specification, since, now users can choose colours visually, or via related media (such as PANTONE™), or even use perceptually-based systems like L*u*v* and L*a*b*. Therefore, machine vision systems based on HSB or HLS colour spaces are now considered inappropriate for colour work [Farhoosh, Schrack, 1986].

The principal reason for not using the HSB or HLS space is that they have been superseded by perceptually-based systems. However, other considerations need to be taken into account. When using the "lightness" factor for colour selection, (usually running from 0 to 100), a lightness of 50 may be half as bright as a lightness of 100. Yet the usual formulations of HSB and HLS do not allude to the linearity or non-linearity of the underlying RGB, and do not refer to the lightness perception of human vision. The usual formulation of HSB and HLS compute "lightness" or "brightness" as (R+G+B)/3. This computation conflicts badly with the properties of colour vision, as it computes yellow to be about six times more intense than blue with the same "lightness" value (say L=50).

Also, HSB and HSL are not suitable for image computation because of the discontinuity of the hue at 360°. This means that arithmetic mixtures of colours expressed in polar coordinates cannot be easily performed. Nearly all formulations of HSB and HLS involve different computations around 60° segments of the hue circle. These calculations introduce visible discontinuities in colour space. Although the claim is made that HSB and HLS are "device

independent", the conventional formulations are based on RGB components whose chromaticities and white point are unspecified. Consequently, HSB and HLS cannot convey accurate colour information [Poynton, 1995].

It is important that a colour specification system can represent any colour with high precision. Since few colours are handled at a time, a specification system can be computationally complex. Any system for colour specification must be intimately related to the CIE specifications. A single "spot" of colour can be specified using a *colour order system* such as the Munsell Colour System (MCS) first proposed in 1905 (Figure 3.1). Colour specification systems such as PANTONE, the MCS, and Colour Dimensions© (***Dulux*** *TRADE*) come with colour sample (swatch) books for visual colour matching, and have documented methods of transforming between coordinates in the system and CIE values. However, these systems are unsuitable for image data representation due to the computational overheads of the transformations.

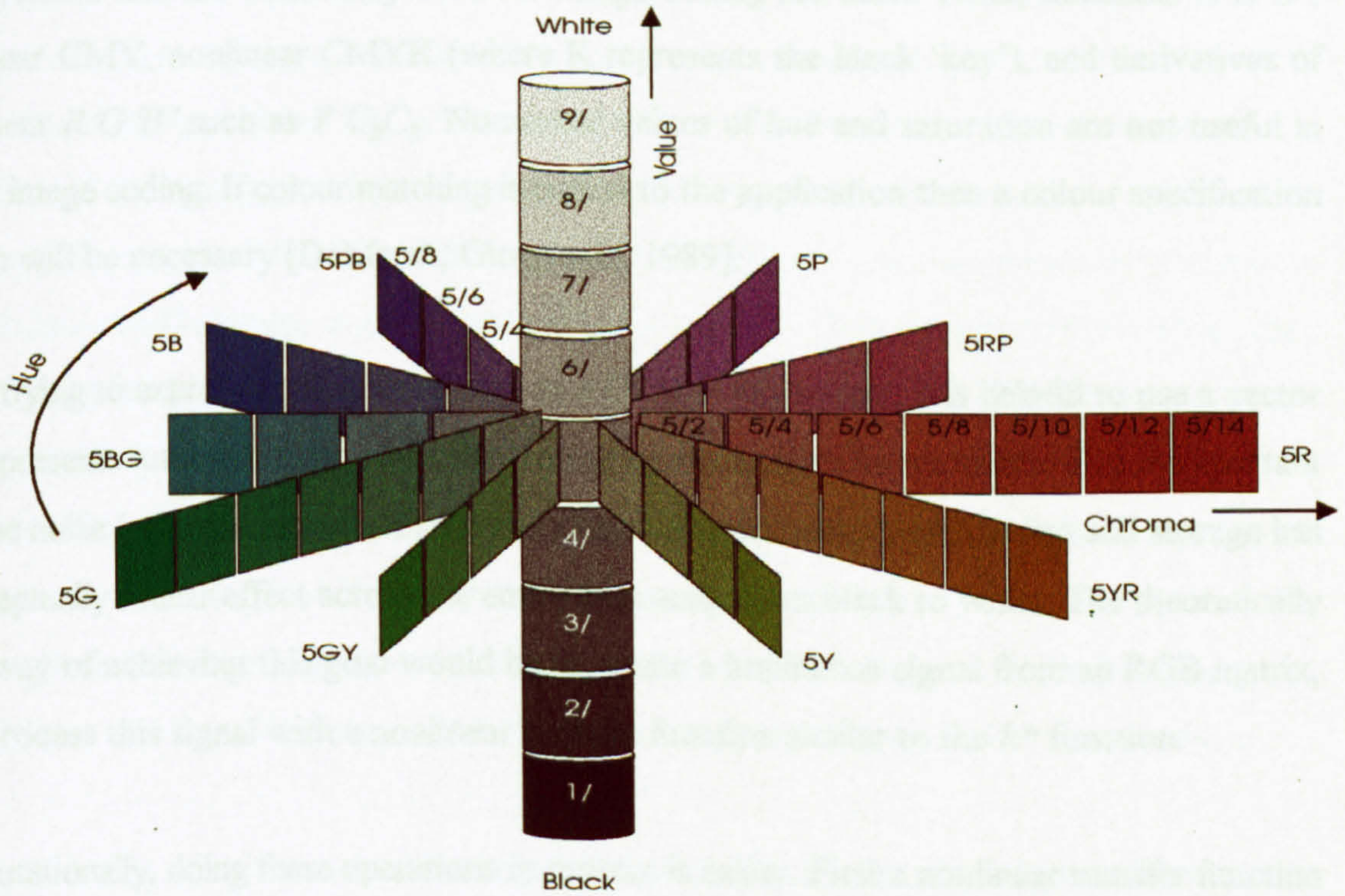

Figure 3.1 : Munsell Colour System

A digitized colour image is represented as an array of pixels, where each pixel contains numerical components that define a colour. Three components are necessary and sufficient for this purpose, although in printing using a fourth component (black) is convenient. This is comparable to inkjet technology where a separate black is used because of the absorption problems of additive mixing. Mixing cyan, magenta and yellow does not produce an economic/good black, hence the need for a separate black component.

In theory, the three numerical values for image coding could be provided by a colour specification system. Nevertheless, a practical image coding system needs to be computationally efficient, and as such cannot afford unlimited precision. There is no inherent need for such a system to be related to a CIE system. Typically, such a system needs only a wide range of colours and not necessarily all the colours.

The systems that are commonly used for image coding are linear RGB, nonlinear $R'G'B'$, nonlinear CMY, nonlinear CMYK (where K represents the black 'key'), and derivatives of nonlinear $R'G'B'$ such as $Y'C_BC_R$. Numerical values of hue and saturation are **not** useful in colour image coding. If colour matching is critical to the application then a colour specification system will be necessary [DeMarsh, Giorgianni, 1989].

When trying to express a colour in relation to a CCD video system, it is helpful to use a vector that represents luminance and two other colour representative components. This is important because noise (or quantization artifacts) introduced in transmission, processing and storage has a perceptually similar effect across the entire tone scale from black to white. The theoretically ideal way of achieving this goal would be to create a luminance signal from an RGB matrix, then process this signal with a nonlinear transfer function similar to the L^* function.

Computationally, doing these operations in reverse is easier. First a nonlinear transfer function – *gamma correction* – is applied to each of the linear R, G and B. Then a weighted sum of the nonlinear components is computed to form a signal representative of luminance. The resulting

component is related to brightness but is **not** CIE luminance and is typically called *luma* and given the symbol Y'. As such, it is commonly confused with luminance Y.

Equation 3.3 computes nonlinear video luma from nonlinear red, green and blue as standardized by the ITU-R Recommendation BT. 601-2 (formerly CCIR Rec. 601-2). The prime symbol(′), in this and following equations in this chapter, denote nonlinear components.

$$Y'_{601} = 0.299R' + 0.587G' + 0.114B' \qquad 3.3$$

3.2.3 Illumination

Another important aspect when dealing with colour is the idea of what is meant by white. In additive image reproduction, the *white point* is the chromaticity of the colour reproduced by equal red, green and blue components. Therefore, the white point depends on the ratio (or *balance*) of power among the primaries. In subtractive reproduction, white is the SPD of the illumination, multiplied by the SPD of the media. NB. No unique physical or perceptual definition of white exists, so to achieve accurate colour interchange the characteristics of the white must be specified. Defining white as a uniform SPD is often convenient for purposes of calculation. An Illuminant has a defined SPD light source, hence a physical source of light. This white reference is known as the *equal-energy illuminant*, or the CIE *Illuminant E*.

A more realistic reference that approximates daylight has been specified numerically by the CIE as *Illuminant* D_{65}. The print industry commonly uses D_{50} and photography commonly uses D_{55}. These various illuminants represent compromises between the conditions of indoor (tungsten) and daylight viewing. This is a principally due to a feature known as colour temperature.

SPDs radiated by a hot object are known as *black-body radiators* or *Planckian radiators* (after Max Planck, who originated a formula for deriving the power at each wavelength from a knowledge of the temperature of the source). Many sources of illumination are from heated objects, so characterizing an illuminant by specifying the temperature is often useful (in units

of Kelvin, K) of a black-body radiator that appears to have the same hue. Although an illuminant can be specified informally by its colour temperature, a more thorough specification is provided by the chromaticity coordinates of the SPD of the source [Hunt, 1992].

An image viewed in isolation – such as a slide projected in a dark room – creates its own white reference as human vision adapts to white in the viewing environment. Therefore a viewer can tolerate errors in the white point, but if the same image is viewed in the presence of an external white reference or a second image, then differences in white point can be unacceptable.

Complete adaptation is confined to the range 5000 K to 5500 K. For most people, D_{65} has a little hint of blue. While, tungsten illumination, at 3200 K, appears to have a yellow colour cast.

3.2.4 Additive and Subtractive Colour Systems

Additive reproduction is based on physical devices that produce all-positive SPDs for each primary. Physically and mathematically, the spectra add. The largest range of colours will be produced with primaries that appear red, green and blue. Human colour vision obeys the principle of superposition, so the colour produced by any additive mixture of three primary spectra can be predicted by adding the corresponding fractions of the XYZ components of the primaries: the colours that can be mixed from a particular set of RGB primaries are completely determined by the colours of the primaries by themselves. Subtractive reproduction is much more complicated: the colours of mixtures are determined by the primaries and by the colours of their combinations.

Subtractive systems involve coloured dyes or filters that absorb power from selected regions of the spectrum. The three filters are in tandem. A dye that appears cyan absorbs long-wave (red) light. Therefore, by controlling the how much cyan dye (or ink) is used, the amount of red in the image is modulated.

In physical terms the spectral transmission curves of the colourants multiply, so this method of colour reproduction should really be called "multiplicative". Photographers and printers measure transmission in base-10 logarithmic *density* units, where transmission of unity corresponds to a density of 0, transmission of 0.1 corresponds to a density of 1, transmission of 0.01 corresponds to a density of 2 and so on. When a printer or photographer computes the effect of filters in tandem, they subtract density values instead of multiplying transmission values, therefore the system is *subtractive*.

To achieve a wide range of colours in a subtractive system requires filters that appear coloured cyan, yellow and magenta (CMY). Cyan in tandem with magenta produces blue, cyan with yellow produces green, and magenta with yellow produces red [Schettini, Della Ventura, *et. al.*, 1992].

For a wide range of colours in an additive system, the primaries must appear red, green and blue (RGB). In a subtractive system the primaries must appear yellow, cyan and magenta (CMY). It is complicated to predict the colours produced when mixing paints, but roughly speaking, paints mix additively to the extent that they are opaque (like oil paints, cf. pigments), and are subtractive to the extent that they are transparent (like watercolours, cf. dyes).

In an ideal subtractive system, CMY filters would have spectral absorption curves with no overlap. The colour reproduction of the system would correspond exactly to additive colour reproduction using the red, green and blue primaries that resulted from pairs of filters in combination [Haase, Meyer, 1992].

However, practical photographic dyes and offset printing inks have spectral absorption curves that overlap significantly. For example, most magenta dyes absorb medium-wave (green) light as expected, but also absorb about half that amount of shortwave (blue) light. If reproduction of a colour, say brown, requires absorption of all shortwave light then the incidental absorption from the magenta dye is not noticed. Nevertheless, for other colours, the "one minus RGB" formula produces mixtures with much less blue than expected, and therefore produce pictures

that have a yellow cast in the mid tones. Similar but less severe interaction is evident for the other pairs of practical inks and dyes. Due to the spectral overlap among the colourants, converting CMY using the "one-minus-RGB" method works for applications where accurate colour need not be preserved, but the method fails to produce acceptable colour images [Haase, *et. al.*, 1992].

Multiplicative mixture in a CMY system is mathematically nonlinear, and the effect of the unwanted absorptions cannot be easily analysed or compensated. The colours that can be mixed from a particular set of CMY primaries cannot be determined from the colours of the primaries themselves, but also depend on the colours of the sets of combinations of the primaries.

Print and photographic reproduction is also complicated by non-linearities in the response of the three (or four) channels. In offset printing, the physical and optical processes of *dot gain* introduce non-linearity that is roughly comparable to gamma correction in video. In a typical system used for print, a black code of 128 (on a scale of 0 to 255) produces a reflectance of about 0.26, not the 0.5 that would be expected from a linear system. Therefore, computations cannot be meaningfully performed on CMY components without considering non-linearity.

An additive RGB system is specified by the chromaticities of its primaries and its white point. The extent (*gamut*) of the colours that can be mixed from a given set of RGB primaries is given in the (x, y) chromaticity diagram by a triangle whose vertices are the chromaticities of the primaries (Figure 3.2). However, in computing there are no standard primaries or white points. An RGB image must have information about its chromaticities, for accurate image reproduction.

The NTSC in 1953 specified a set of primaries that represented phosphors used in colour CRTs of that era. Yet phosphors changed over the years, primarily in response to market pressures for brighter receivers, and by the time of the first the videotape recorder the primaries in use were quite different from those specified. Contemporary studio monitors have different standards in North America, Europe and Japan. Yet, international agreement has been reached

for high definition television (HDTV) primaries. These primaries are closely representative of contemporary monitors in studio video, computing and computer graphics. The primaries and the D_{65} white point of Rec. 709 [ITU-R, 1990] are as follows (Table 3.1):

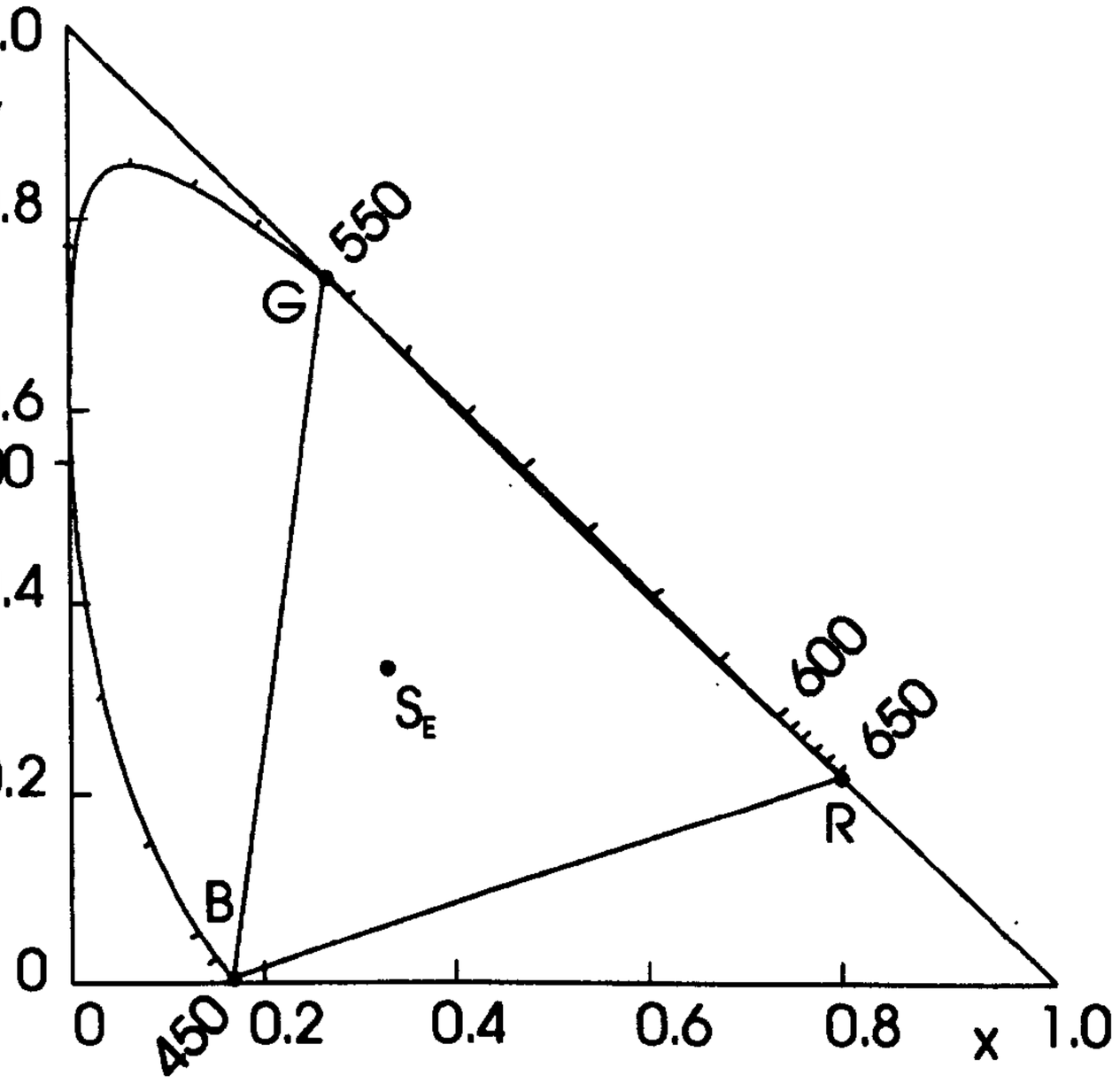

Figure 3.2 : Chromaticity Triangle

	R	G	B	White
x	0.640	0.300	0.150	0.3127
y	0.330	0.600	0.060	0.3290
z	0.030	0.100	0.790	0.3528

Table 3.1 : Primaries and White Point for Rec. 709

Yet another ambiguous term often used in colour science is that of *colour difference*. This term can be interpreted in two different ways. In its first sense, colour difference refers to numerical differences between colour specifications. The perception of colour differences in XYZ or RGB is highly nonuniform. The study of *perceptual uniformity* concerns numerical differences that correspond to colour differences at the threshold of perceptibility (*just noticeable differences*, or JNDs).

The second interpretation of colour difference refers to colour components where brightness is "removed". Vision has poor response to spatial detail in coloured areas of the same luminance, compared with its response to luminance spatial detail. If data capacity is at a premium, transmitting luminance with full detail is advantageous, forming two *colour difference* components each having no contribution from luminance. The two colour components can then have spatial detail removed by filtering, and can be transmitted with much less information capacity than luminance. Instead of using a true luminance component to represent brightness, using a non-linearly computed luma signal is customary for practical reasons (as previously stated).

The easiest way to "remove" brightness information to form two colour channels is to subtract it. The luma component already contains a large fraction of the green information from the image, so forming the other two components by subtracting luma from nonlinear blue is standard (to form $B'-Y'$) and by subtracting luma from nonlinear red (to form $R'-Y'$). These are called *chroma*. Figure 3.3 shows a block diagram for luma/colour difference encoding and decoding.

Various scale factors are applied to $(B'-Y')$ and $(R'-Y')$ for different applications. The $Y'P_BP_R$ scale factors are optimized for component analog video, whereas the $Y'C_BC_R$ scaling is appropriate for component digital video such as studio video, JPEG and MPEG. Kodak's PhotoYCC™ uses scale factors optimized for the gamut of film colours. $Y'UV$ scaling is

appropriate as an intermediate step in the formation of composite NTSC or PAL video signals, but is not appropriate when the components are kept separate. The $Y'UV$ space is ambiguous, as it is sometimes used to denote any scaling of $(B'-Y')$ and $(R'-Y')$. NB. $Y'IQ$ coding has now become redundant.

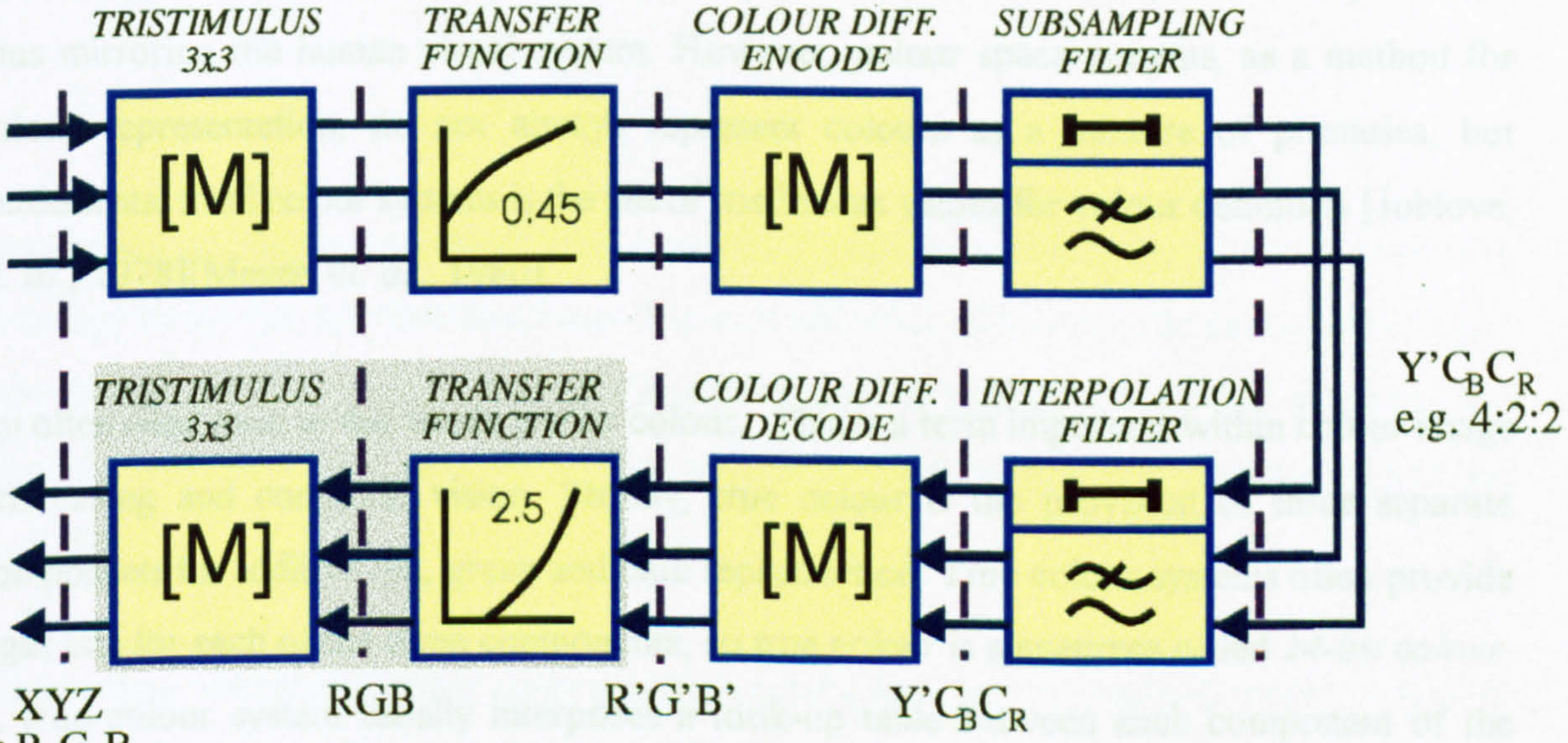

Figure 3.3 : Luma/colour difference encoding and decoding

Section 3.2 has identified the pertinent issues of colour physics in relation to this research. It is important that these factors are well understood before developing a computer-based colour vision system.

3.3 Colour Analysis by Computer

3.3.1 Colour Spaces

As previously stated normal human colour perception is a product of three independent sensory systems (the cones). A computer display creates colours as a mixture of the three primaries, thus mirroring the human visual system. However, colour space systems, as a method for colour representation, do not always represent colours as a mixture of primaries, but fundamental to all colour systems is the use of tristimulus values for colour definition [Joblove, *et. al.*, 1978][Meyer, *et. al.*, 1980].

An often cited term in this thesis is *true* colour. This is a term important within colour image processing and computer vision. Strictly, true colour is the provision of three separate components for additive red, green and blue reproduction. True colour systems often provide eight bits for each of the three components, so true colour is sometimes called *24-bit colour*. A true colour system usually interposes a look-up table between each component of the framestore and each channel to the display. This makes it possible to use a true colour system with either linear or nonlinear coding.

The CIE system is based on the description of colour as a luminance component Y, and two additional components' X and Z. The spectral weighting curves of X and Z have been standardized by the CIE based on statistics from experiments involving human observers. XYZ *tristimulus* values can describe any colour. The magnitudes of the XYZ components are proportional to physical energy, but their spectral composition corresponds to the colour matching characteristics of human vision [Hunt, 1992, p. 52].

It is often convenient to discuss "pure" colour without brightness. The CIE defines a normalization process to compute "little" x and y *chromaticity coordinates* (Equation 3.4). A

colour can be specified by its chromaticity and luminance, as a *xyY* triplet. The transform matrix back to X and Z from chromaticities and luminance is expressed by Equation 3.5.

$$x = \frac{X}{X+Y+Z} \qquad y = \frac{Y}{X+Y+Z} \tag{3.4}$$

$$X = \frac{x}{y}Y \qquad Z = \frac{1-x-y}{y}Y \tag{3.5}$$

To represent an image either the RGB, or the XYZ systems can be used. In fact, once light is on its way to the eye, any *tristimulus-based* system will work. However, the interaction of light and objects involves spectra, not tristimulus values. In synthetic computer graphics, the calculations are simulating sampled SPDs, even if only three components are used [Meyer, *et. al.*, 1980].

It is common when using colour space systems to refer to its *perceptual uniformity*. A system is perceptually uniform if a small change to a component value is equally perceptible across the range of that value. Volume control on a hi-fi is an example of a perceptual uniform system. Rotating the knob ten degrees produces approximately the same perceptual increment in volume anywhere across the range of the control. If the control were physically linear, the logarithmic nature of human loudness perception would place all of the perceptual "action" of the control at the bottom of its range. In fact, on the more expensive amplifiers the volume control is often labelled with a logarithmic scale (decibels). This use of a logarithmic scale for perceptual uniformity for loudness perception is also applicable to vision (human visual perception is logarithmic).

However, the XYZ and RGB systems are not perceptually uniform. The CIE standardized two systems, $L^*u^*v^*$ and $L^*a^*b^*$, sometimes written CIELUV and CIELAB. It took the CIE over a decade to figure out the transformation from XYZ into these perceptually-uniform spaces. This emphasizes their complexity. $L^*u^*v^*$ and $L^*a^*b^*$ both improve the approximately 80:1

perceptual non-uniformity of the XYZ to about 6:1. Nevertheless, both demand too much computation to allow for useful real-time processing.

Computation of CIE $L^*u^*v^*$ involves intermediate u' and v' quantities, where the prime denotes the successor to the obsolete 1960 CIE u and v system. Equation 3.6 denotes the conversion from XYZ to u' and v'.

$$u' = \frac{4X}{X+15Y+3Z}, \qquad v' = \frac{9Y}{X+15Y+3Z} \tag{3.6}$$

The first stage of the conversion is to compute u_n' and v_n' for the reference white X_n, Y_n and Z_n. Then u', v' and L^* are computed for the other colours. Equation 3.7 shows the final computations for u^* and v^* (L^* computation has already been expressed, see Equation 3.1).

$$u^* = 13L^*(u'-u_n'), \qquad v^* = 13L^*(v'-v_n') \tag{3.7}$$

$L^*a^*b^*$ is computed as follows (Equation 3.8), for $(X/X_n, Y/Y_n, Z/Z_n) > 0.01$:

$$a^* = 500\left[\sqrt[3]{\frac{X}{X_n}} - \sqrt[3]{\frac{Y}{Y_n}}\right], \qquad b^* = 200\left[\sqrt[3]{\frac{Y}{Y_n}} - \sqrt[3]{\frac{Z}{Z_n}}\right] \tag{3.8}$$

It can be seen that these equations are not suited to real-time computational encoding. Although it was not specifically optimized for this purpose, the nonlinear $R'G'B'$ coding used by video is perceptually uniform, having the advantage of being fast enough for interactive applications.

3.3.2 Interchange Systems

RGB ↔ CIE XYZ

RGB values in a particular set of primaries can be transformed to and from CIE XYZ by a three-by-three matrix transform. These transforms involve *tristimulus values*, that is, sets of three linear-light components that conform to the CIE colour matching functions. CIE XYZ is a special case of tristimulus values. In XYZ, any colour is represented by a positive set of values [SMPTE, 1993], [Kasson, Plouffe, 1992].

To transform from CIE XYZ into Rec. 709 RGB (with D_{65} as the white point), the following transform is used (Equation 3.9):

$$\begin{bmatrix} R_{709} \\ G_{709} \\ B_{709} \end{bmatrix} = \begin{bmatrix} 3.240479 & -1.537150 & -0.498535 \\ -0.969256 & 1.875992 & 0.041556 \\ 0.055648 & -0.204043 & 1.057311 \end{bmatrix} \cdot \begin{bmatrix} X \\ Y \\ Z \end{bmatrix} \qquad 3.9$$

This matrix has some negative coefficients: XYZ colours that are *out of gamut* for a particular RGB transform to XYZ where one or more RGB components are negative or greater than unity. The inverse transform for Equation 3.9 is shown in Equation 3.10, where because white is normalized to unity, the middle row sums to unity. To recover primary chromaticities from such a matrix, compute little x and y for each RGB column vector. To recover the white point, transform RGB=[1, 1, 1] to XYZ, then compute x and y.

$$\begin{bmatrix} X \\ Y \\ Z \end{bmatrix} = \begin{bmatrix} 0.412453 & 0.357580 & 0.180423 \\ 0.212671 & 0.715160 & 0.072169 \\ 0.019334 & 0.119193 & 0.950227 \end{bmatrix} \cdot \begin{bmatrix} R_{709} \\ G_{709} \\ B_{709} \end{bmatrix} \qquad 3.10$$

Colour difference components are obtained from tristimulus values (ref. Figure 3.3) using the following procedure. From linear XYZ – or linear $R_lG_lB_l$ whose chromaticity coordinates are

different from the interchange standard – apply a 3×3-matrix transform to obtain linear RGB according to the interchange primaries. Apply a nonlinear transfer function ("*gamma correction*") to each component to get nonlinear $R'G'B'$. Apply a 3×3-matrix to obtain colour difference components such as $Y'P_BP_R$, $Y'C_BC_R$ or PhotoYCC. If necessary, apply a colour sub-sampling filter to obtain sub-sampled colour difference components. For decoding, the above procedure is reversed, i.e. run through the block diagram right-to-left using the inverse operations. (Refer to Appendix A for other relevant colour space transforms.)

4 Signal Acquisition and Properties

4.1 Introduction

Applying machine vision to the automatic inspection of printed fabric is dependent on the types of signals obtainable. Research was carried out to identify how best to capture the essential image data. For detecting systematic faults it was theoretically established that the fabric would have to be inspected at a minimum of three different points across its width, requiring local optical sensors at these points [Blowers, Dodkin, 1994].

Four possible approaches of signal acquisition for systematic faults were identified. The most simplistic approach would be the use of a *monochrome point sensor* linked with registration marks. For inspection inside the printed design area, *colour point sensors*, at key points across the design, would be needed. Point sensors, however, are position critical and have theoretical limitations with certain print designs. The other identified approaches would be to use *colour line scan cameras* or *colour area cameras* for data capture. Each of these options has been thoroughly investigated to identify the best approach for this research.

For random fault detection, due to the nature of the faults, carrying out full-width inspection of the fabric is necessary. Research identified two approaches for full-width inspection: *colour line scan cameras*; *colour area cameras*. The required resolution for random fault detection of 0.5 mm introduces additional problems. First, commercial availability of high-resolution colour cameras (be it line scan or area) is limited. Also, if a camera has sufficient resolution this can cause other problems, concerning optics, lighting, and physical environment. To give full coverage, with least optical distortion, the camera would need to be some distance from the fabric. If lower resolution cameras are used, connecting several cameras in parallel to provide coverage of the full width of the fabric would be necessary. This is costly both financially and computationally.

Random fault detection was simulated in the laboratory using a single colour area camera. This camera provided a maximum fault coverage width of;

$$FC_{\max} = R_h \times E_{\min}$$
$$0.256m = 512 \times 0.5\times10^{-3}m \qquad 4.1$$

where $FC_{\max}$ is the maximum fault coverage, R_h is the horizontal resolution of the camera (pixels), and $E_{\min}$ is the minimum size of error (fault). From this equation it can be seen that to inspect the width of the fabric completely (up-to 3 metres) would require twelve standard colour area cameras. This is an unrealistic solution — colour line scan cameras, with their higher resolution offer the only practical alternative.

4.2 Image Acquisition Devices

The various image acquisition devices evaluated during this research are discussed in more detail in this following section. Each device is examined for its suitability for achieving the research goals. It was found that no one device, currently available, could achieve the final research requirement of incorporation into an on-line inspection system. Yet, each acquisition device was essential for identifying and carrying out fundamental research into the problem.

4.2.1 Point Sensing Devices

Monochrome Point Sensors

Pointscan sensors are optoelectronic devices that examine a small (0.2 mm^2 diameter) region of the inspected surface. They are attractive for economy and simplicity. A monochrome point sensor theoretically provides the simplest method for detection and quantifying of systematic

defects when used with a system of registration marks. It is common practice in printing to use registration marks on the selvedge[12]. However, DORMA print across the full width of the fabric, therefore any registration marks would have to be printed on the blanket. This is unacceptable due to pigment smearing on the blanket (refer to Chapter 1). If the fabric selvedge is available for printing, then the design of marks for optical registration analysis becomes important. Standard registration marks (bomb-sites) are inappropriate for image analysis using point sensors as they are insensitive to lateral shifts, compared with vertical shifts in printing (see Figure 4.1).

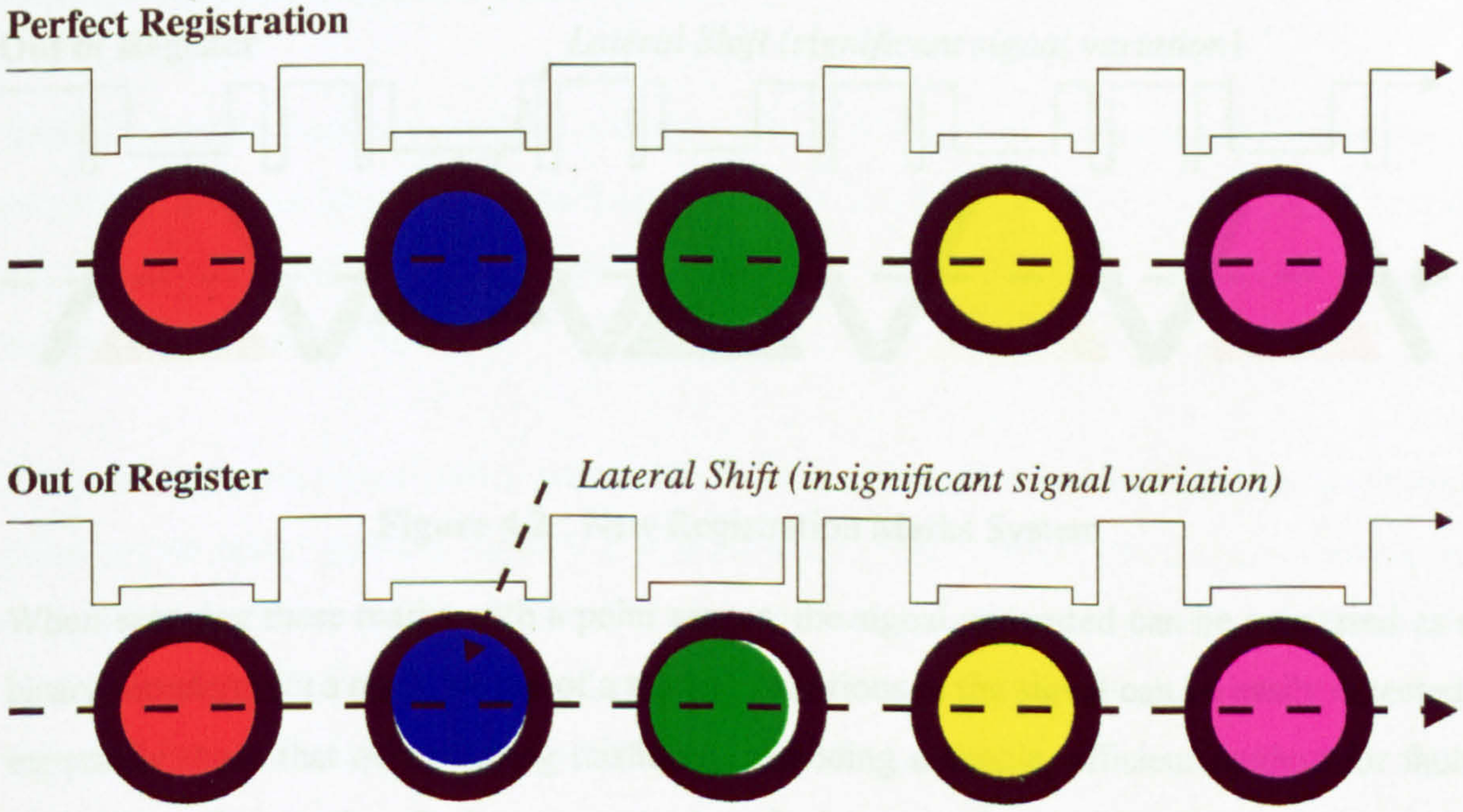

Figure 4.1 : Traditional System of Registration Marks

Research to create registration marks that would provide independent information on lateral and vertical alignment for each colour, when analysed by a single monochrome point sensor was carried out (see Figure 4.2). Although this approach assumes selvedge printing is available

---

12 *The edges of the fabric which are not printed on.*

it is still useful to this research as it introduces auto-correlation — this has wider implications for later research [Blowers, Dodkin, 1994].

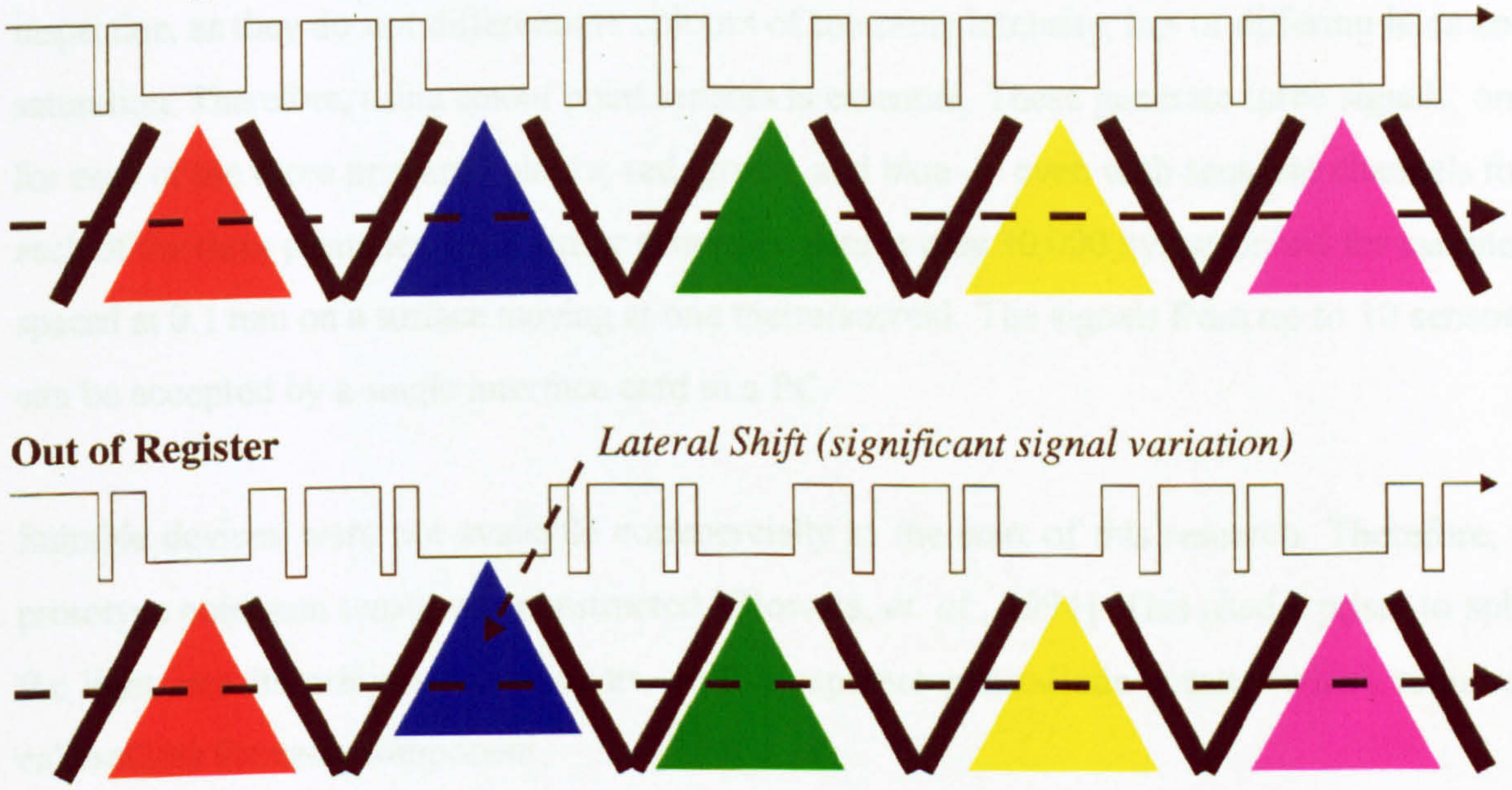

Figure 4.2 : New Registration Marks System

When scanning these marks with a point sensor, the signal generated can be expressed as a binary waveform (*in* a mark, or *out* of a mark). Variations in the signal can be easily detected, especially those that occur during misfitting, providing a simple, efficient method for fault evaluation and correction. Such systems give benefits in terms of cost, ease of manufacture, and high processing speed. However the method does not deal with bowing related faults (see Chapter 1), and is dependent on the ability to print on the selvedge. Therefore, registration markers are not an option in this particular instance and an approach based on them is of limited value.

Colour Point Sensors

As selvedge-based inspection is unsuitable, inspection inside the printed area of the fabric is necessary. Once inside the fabric, monochrome point sensors would be unsuitable for inspection, as they do not differentiate colours of the same intensity, but of differing hues and saturation. Therefore, using colour point sensors is essential. These generate three signals, one for each of the three primary colours; red, green, and blue — even with separate channels for each of the three primaries, each sensor generates data at only 30,000 bytes/second for samples spaced at 0.1 mm on a surface moving at one metre/second. The signals from up to 10 sensors can be accepted by a single interface card in a PC.

Suitable devices were not available commercially at the start of this research. Therefore, a prototype pointscan sensor was constructed [Blowers, *et. al.*, 1994]. This used a prism to split the light into its primary components, with a separate photodiode sensor (which required calibration) for each component.

The prototype point sensor system specification was that it could monitor the colour at a single point on an object passing beneath it continuously (here, printed fabric). The associated software would then notify an operator of any deviations, of the colour, from a previously scanned "perfect" pattern. Software should only report errors that fall outside previously defined tolerance limits for the particular pattern being scanned.

This prototype point sensor consisted of a circuit board with three amplifying circuits connected to individual photodiodes, one for each of the primary colour groups (red, green, and blue). The circuit board was mounted in a large metal box in a position so that light entering the box is passed through a simple prism to split into its spectrum of constituent wavelengths. This light was then focused, by a system of lenses, onto the three photodiodes arranged to intercept the three primary colour sections of the visible light spectrum. The output from the circuit board was three analogue signals that could then be fed into an "Analogue to

Digital" convertor board. However, due to the required lengths of the optical paths the sensor was too large for practical purposes, as can be seen in Figure 4.3.

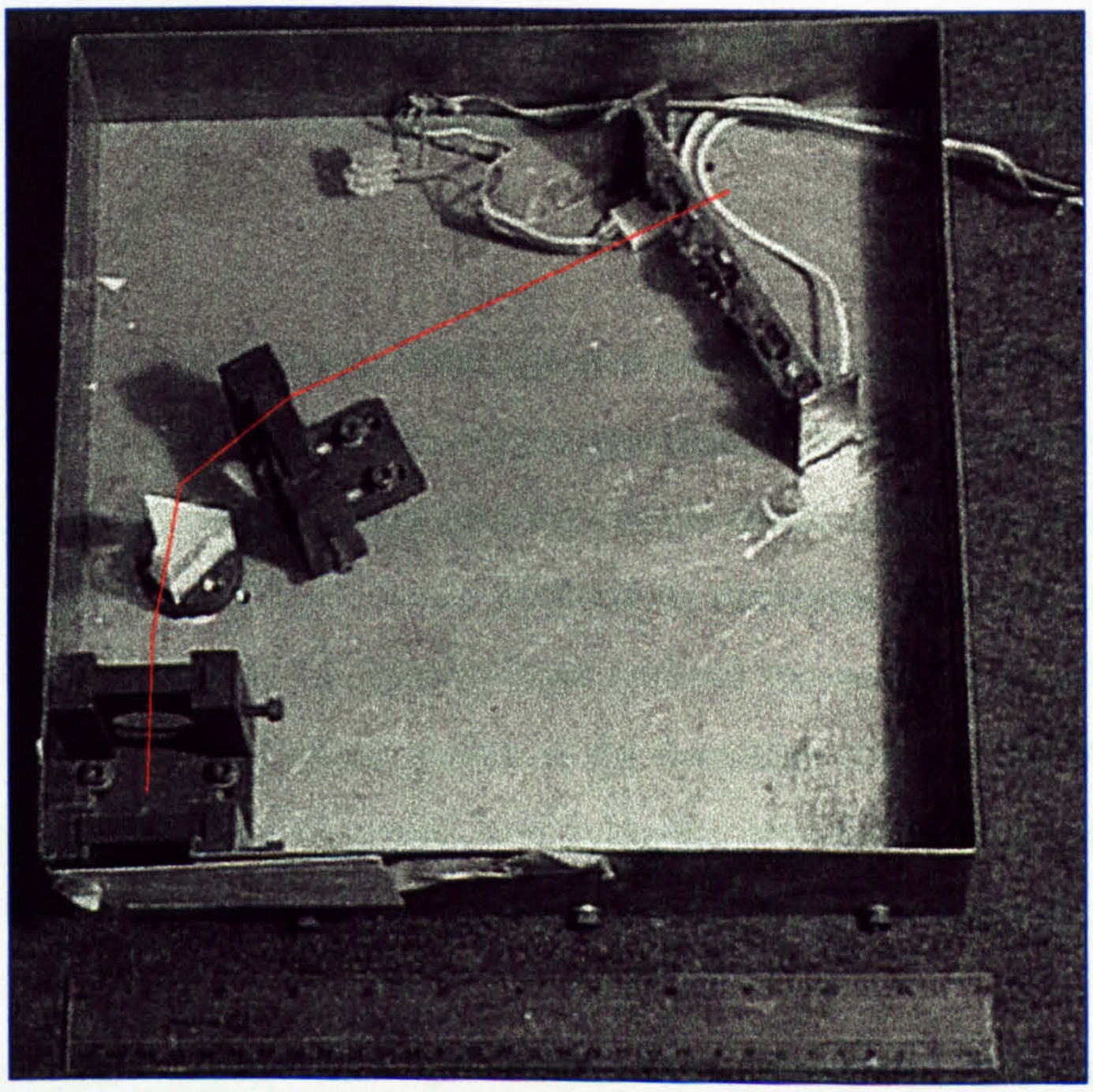

Figure 4.3 : Prototype Optical Point Sensor

To resolve this problem a colour point sensor was developed using fibre optics to give a compact and robust construction. Fibre-optics can be used to collect the light reflected from the object being inspected. A possible approach would employ a trifurcated fibre-optic bundle with a lens system at the single end. This is to focus the light being reflected from the object under inspection. At each of the triple ends, a filter is attached that only transmits light within a specific waveband (Kodak Gel filters, one for each primary). Therefore, light from the object, is focussed by the lens system, transmitted along the fibre (where it is split), passing through a filter directly onto the appropriate photo-diode.

The circuit board of the original point sensor was modified so that the amplifier circuits could be easily adjusted (by means of variable resistors) to equalize the output levels on all three

channels. Also, the fibre-optic approach allowed the photo-diodes to be positioned well apart and away from other components. This simplified the mounting of the filters in suitable positions, with enough free space around them to make the circuit board less cluttered. The use of fibre-optics also meant that the circuit board would not need to be mounted in a large box or positioned close to the object being inspected. This simplifies the positioning of the light sensor "head".

However due to the lighting requirements of the system it was determined that a quadrifurcated system was required. This would have to be designed specifically for the point sensor, with one of the four fibre bundles being used as a light path for sample illumination. The remaining three bundles would pass reflected light back to the photodiode detectors. A benefit of this system is that light is supplied directly to the sensing head without the need for accurately aligned optics. This is useful for a factory-based system as the detection circuitry can be mounted in a protected environment, with only the sensing head in the factory environment. Also, a flexible fibre-optics system helps alignment of the sensing head over the desired sample path.

However, inherent problems with a fibre-optic system exist, principally, light loss. If the light is being produced from a bundle with a given area (assuming that the bundle is non-coherent and equally split) 25% of the reflected light will be lost due to the non-receptive light emitting fibres in the bundle. This implies that each colour receptive bundle will only receive 25% of the reflected light. Also, the light is filtered into one of the three primary colours wavebands. Therefore, each photodiode would receive a maximum of 8% of reflected light. NB. This is for achromatic light, if the light is "coloured" this figure will vary. Also, this reflected light will only be a fraction of the original emitted light.

A possible solution to this problem is to use one photodiode that can sense colour. In 1987, Yamaba proposed such a device. It was initially designed for sensing the positions of laser beams. The colour photo-diode consists of four individual photo-diodes with optical colour filters, arranged in three layers: PIN photo-diode array; colour filters; and infrared cut filters. Three of the photo-diodes are filtered for the R, G, B primaries. The fourth photo-diode is a

complemental non-filtered diode. (The filters are Eastman Kodak gelatin filters, cf. original fibre-optic point sensor construction.) By inserting each photo-diode into the same metal can the whole unit can then be treated as an individual photo-diode [Yamaba, 1987]. The benefit of this system over the quadrifurcated fibre-optic approach is that the sensor will receive 75% of the reflected light rather than 25%. Figure 4.4 shows the proposed fibre-optic point sensor using the Yamaba Photo-diode.

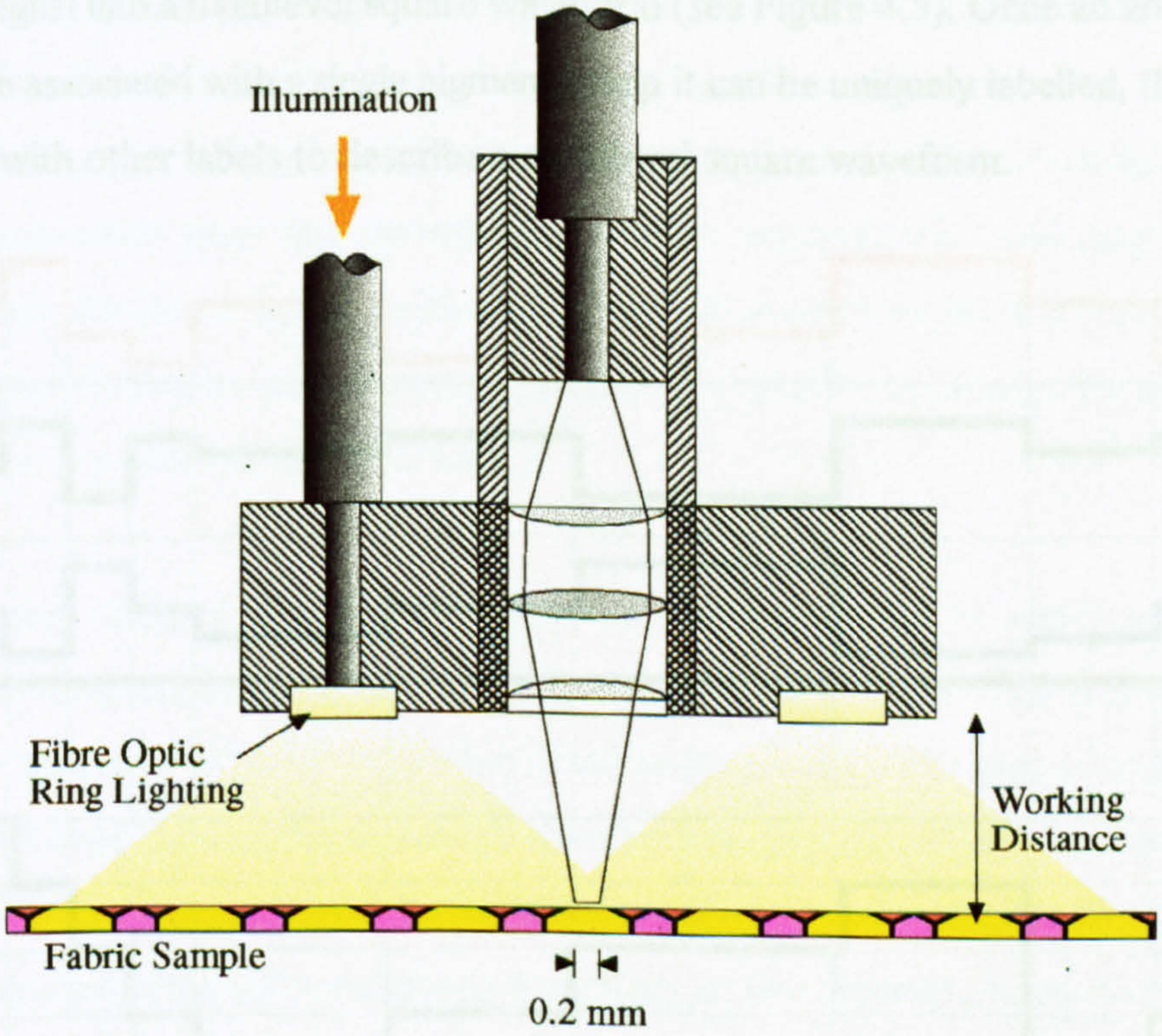

Figure 4.4 : Proposed Fibre Optic Point Sensor

Another approach was to adapt a miniature colour camera to simulate a point sensor. This was satisfactory in all respects except the resolution that at 0.5 mm was not really adequate.

The rationale for using colour point sensors was that from the three input signals individual pigments can be expressed as their ratios in red, green, and blue. Therefore, an individual element of the input signal can be expressed as a pigment (k) in relation to its instantaneous amplitudes — R, G, B and the coefficients $C_{k,r}$, $C_{k,g}$, and $C_{k,b}$, which specify the location of

pigment k in the colour space – giving $C_{k,r}.R$, $C_{k,g}.G$, and $C_{k,b}.B$. From this it can be shown that pigments occupy a finite space, rather than discrete points. (When the coefficients, describing a pigment, are plotted in colour space, it is seen that the area they define is non-discrete.) Also, the centroid (mean) value of the pigment can be expressed through its coefficients. Forced segmentation of the signal can then simplify this three-dimensional signal. Attaching unique identifiers to each pigment region can realise this, enabling the translation of the trivector signal into a multilevel square waveform (see Figure 4.5). Once an area of colour space has been associated with a single pigment group it can be uniquely labelled, this label can then be used with other labels to describe a multilevel square waveform.

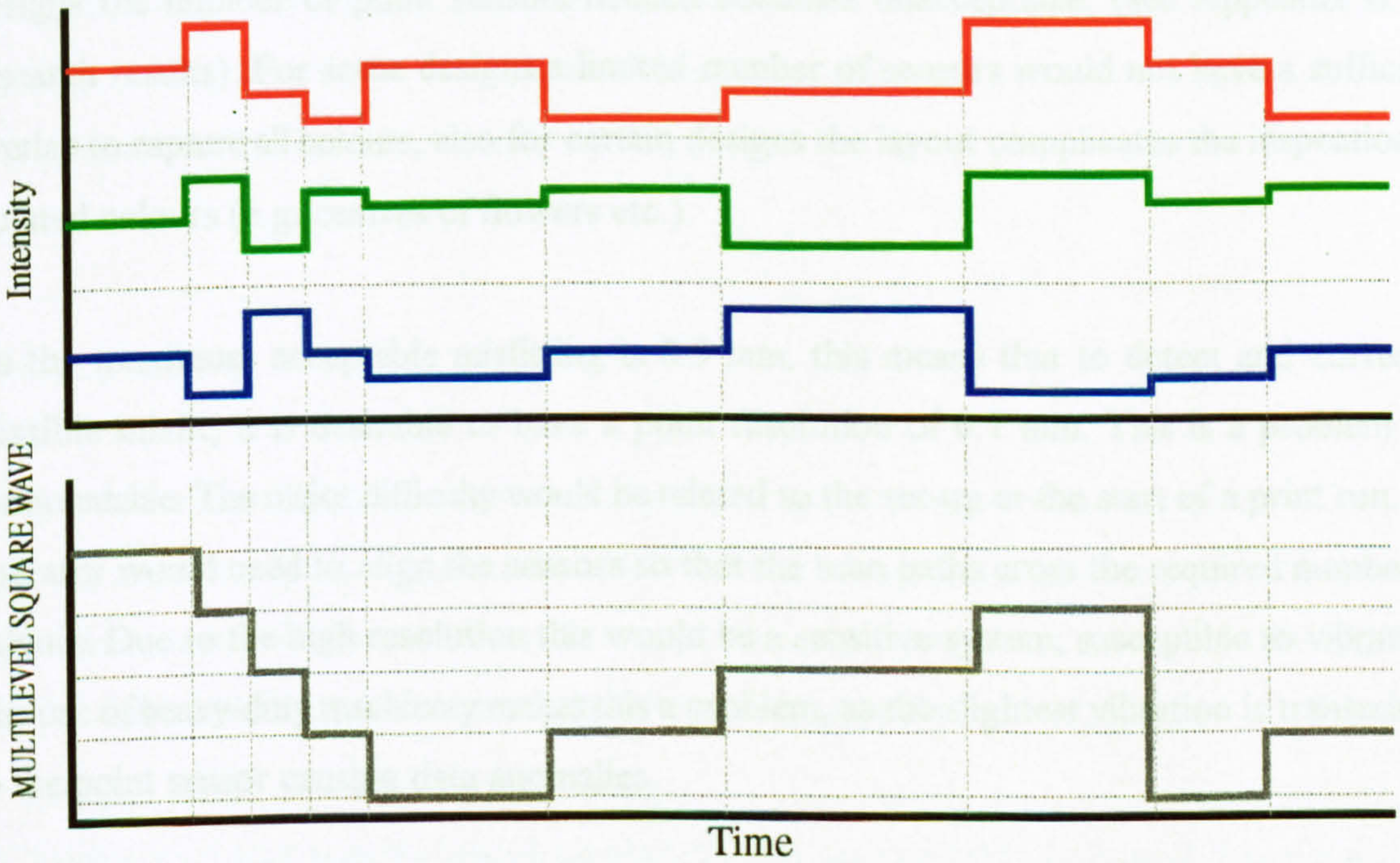

Figure 4.5 : Multilevel Square Wave Signal

This multilevel waveform could then be processed directly or disassembled into the component binary pigment signals, giving a vast reduction in signal processing. For any given design of N pigments, theoretically $N+1$ binary signals should exist, as the background can also be registered as a distinct pigment. (Pigments do not mix in a truly additive or subtractive manner,

and generally due to their opaque nature the topmost pigment, at any point, defines the colour of that point). Only one binary signal should be *high* at a time, showing the presence of a specific pigment at that point.

Registration analysis can be done by means of *binary fingerprint* matching, where the ideal registration information obtained at the print setup is used to verify succeeding print repeats. Optimum positioning of the colour point sensors would be towards the edge of the fabric, with the middle of the fabric also being inspected for bowing. Though, as previously stated, point sensors are position critical, and positioning is extremely dependent on the design. For some designs the number of point sensors needed becomes unacceptable, (see Appendix B for research results). For some designs a limited number of sensors would not have a sufficient overlap to capture all colours, also for certain designs the layout complicates the inspection of isolated colours (e.g. centres of flowers etc.).

As the maximum acceptable misfitting is 0.5 mm, this means that to detect and correct a possible misfit, it is desirable to have a point resolution of 0.1 mm. This is a problem but surmountable. The major difficulty would be related to the set-up at the start of a print run. An operator would need to align the sensors so that the scan paths cross the required number of colours. Due to the high resolution this would be a sensitive system, susceptible to vibration. The use of heavy-duty machinery makes this a problem, as the slightest vibration is transmitted to the point sensor causing data anomalies.

4.2.2 Line Scan

Monochrome Line Scan Sensors

As previously stated, once inspection moves inside the printed area of the fabric, monochrome sensors are unsuitable as they cannot sufficiently resolve colours of similar intensities. A benefit

of monochrome line scan cameras, when compared to colour line scan cameras, is their greater commercial availability.

Creation of a colour sensor from a monochrome sensor is possible using a colour wheel system. A colour image of a scene could be obtained by taking three successive 'snapshots' through different primary filters. This can affect the useful sampling speed of the sensor because of mechanical constraints, but for some situations, due to its lower costs, it is still usable. In research carried out by Dodkin [1994] a monochrome colour wheel camera was designed and constructed. A stepper motor was used to move the separate filters in front of the lens. Dodkin concluded that these timing limitations would make a colour wheel camera unsuitable for viewing moving objects. As such, due to the high throughput of rotary screen printing, it is not a practical solution for this research.

Colour Line Scan Sensors

Use of colour line scan cameras instead of point sensors would give more positional flexibility to the system. A colour line scan camera can be treated as an array of colour point sensors, with a minimum inter-cell distance. Methods for selecting the *key areas* of colour boundaries, from the line scan data, have been researched and are discussed later in this thesis.

CCD linescan colour sensors having resolutions exceeding 8,000 pixels were found described in literature from several manufacturers (e.g. Kodak, Primagraphics, Dalsa). The Primagraphics system was impressive; it has a resolution of 5,000 pixels and costs only about £8,000. Unfortunately operation is possible at only one rate - 100 lines/second, which is insufficient for the research requirements.

Recent improvements in the resolution, accuracy, cost, and commercial availability of colour line scan cameras mean that they are now becoming a feasible sensing option. An ideal system for sensing systematic faults would be composed of two (or three) colour line scan cameras,

placed at the sides (and the middle to inspect for bowing) of the fabric. Data is generated at too high a rate for easy capture, and the stimuli for the colour components are generated by different (though adjacent) pixels so a fidelity problem exists when detail is monitored. Data processing from such a system can be shown to be initially very high, but by using the key areas methodologies this can be greatly reduced to the equivalent of a point sensor system.

Recently, a team of Russian scientists, from Moscow Technical State University, working in collaboration with the Department of Textiles and Fashion at De Montfort University, have developed a theoretical design for a colour line scan camera. The system proposed by Vetskous, Shavirin, *et. al.* [1994], would be ideal for rotary screen inspection as its registration is speed invariant, unlike existing colour line scan cameras (see Figure 4.6).

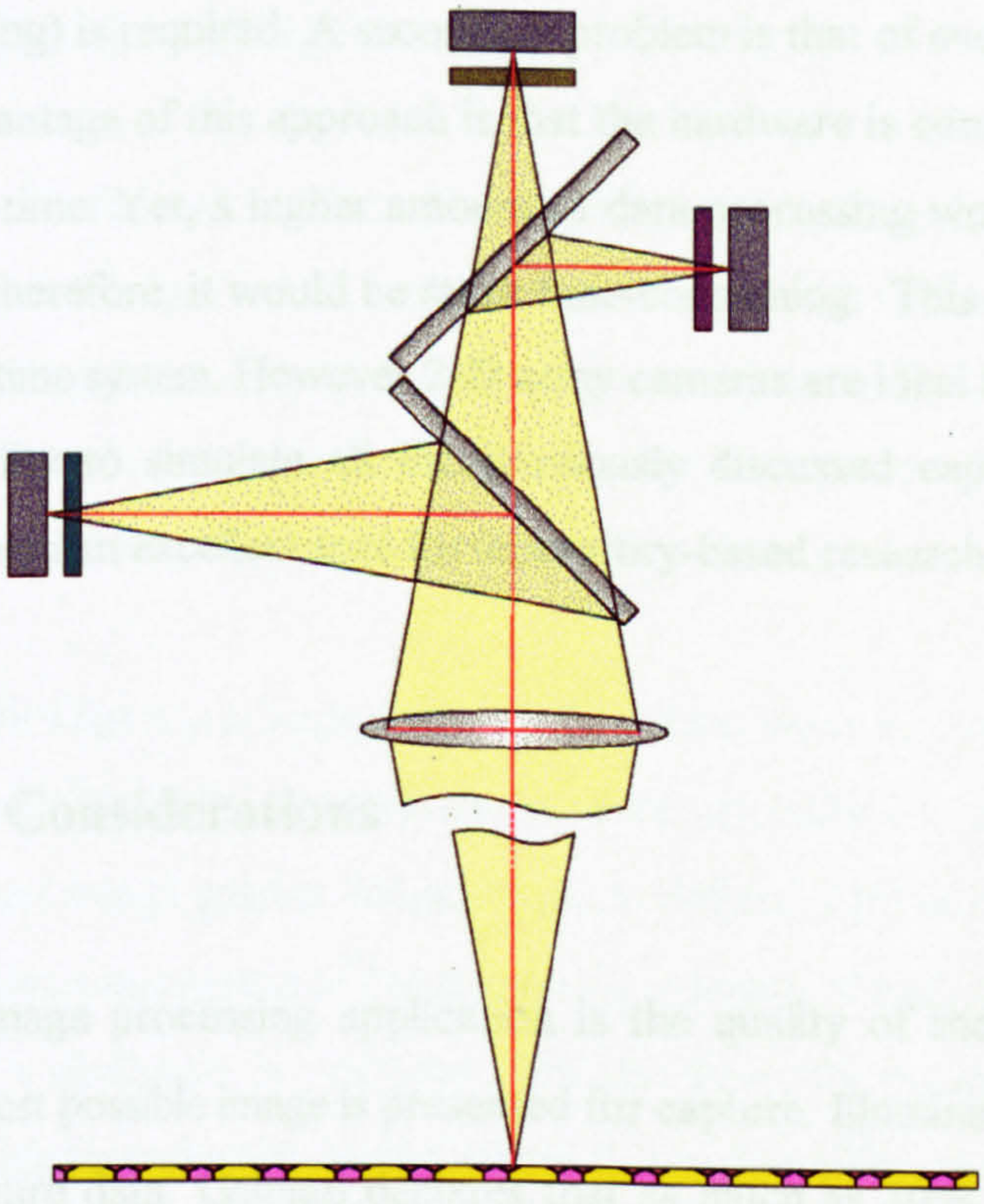

Figure 4.6 : Speed invariant Colour Line Scan Camera

Achievement of registration is simple. By placing the three linear arrays in the image plane, but dispersing them spatially using semi-reflecting surfaces, speed invariant registration is assured. Each linear array has an appropriate colour filter placed before it. Problems arising due to

overall intensity variation at each sensor can be reduced by: use of semi-reflecting surfaces with different ratios of reflection and transmission; filters of differing density; and varying the spectral sensitivity of the linear arrays [Vetskous, *et. al.*, 1994].

4.2.3 Colour Area Cameras

Colour area cameras could be used instead of colour line scan cameras. This is not really an alternative, because although colour area cameras are readily available, their comparative cost is too high for the required resolution. If colour area cameras are used, fast shuttering, or strobing, to stop the motion blur on the captured image of the moving fabric (line scan cameras do not need shuttering) is required. A secondary problem is that of even illumination over the image. A major advantage of this approach is that the hardware is commercially available and has been for some time. Yet, a higher amount of data processing would be needed than for other approaches; therefore, it would be more time-consuming. This can causes problems in the design of a real-time system. However 2-D array cameras are ideal for many aspects of the research, their ability to simulate all the previously discussed capture devices and their availability make them an excellent tool for laboratory-based research.

4.3 Lighting Considerations

Essential to any image processing application is the quality of the acquired image. It is important that the best possible image is presented for capture. Illumination directly affects the quality of the capture data. Galbiati declares that as much as 30% of application effort is directed at creating the best illumination environment [Galbiati, 1990].

For any machine vision application illumination needs to be customized, as currently generic solutions are unavailable. Historically, industrial machine vision systems have used visual light

sources. Primarily, this is because the machine vision application is an automation of an already existing human visual inspection system. As such, the inspection is based on the human visual perception system, which works only within the visible portion of the spectrum. Nowadays, more machine inspection work is being carried out using non-visible light sources such as, infrared (IR), ultraviolet (UV) and X-rays. These illumination methods make previously difficult inspection more accessible. This is because they judge the product on the visible appearance and conformity of the pattern.

Four major categories of lighting setups exist for machine vision systems: *back lighting*, *front lighting*, *structured lighting*, and *strobe lighting*. The following subsection classifies these lighting types. Each lighting approach is investigated to establish which form is the most advantageous for the required image acquisition.

Ambient illumination[13] affects all machine vision systems. This 'background' light can alter the total level of illumination of an object, and is evident as noise in the image data. Reducing the effect of the ambient lighting using light shields that act as baffles for the lens is possible, thus reducing the amount of stray light radiation entering the system. This may not always be practical, especially when the system is in a restrictive environment.

Realizing that standard lighting is inappropriate for machine vision is important. Several reasons exist for this statement. Primarily, conventional incandescent bulbs are not always stable enough to ensure a consistent image quality. Degradation in emitted light intensity is common due to operating characteristics and ageing of the lamp. For example, standard fluorescent tubes have as much as a 15% decrease in emission over the first 100 hours [Galbiati, 1990]. The environment, in which incandescent lamps are used, can also affect their emission. Light-level irregularities can occur due to voltage fluctuations. This can be a particular problem in factory environments where temperature variations and the activation of nearby machinery are common. Furthermore, incandescent bulbs emit considerable IR radiation. While this is not a

---

13 *Light which is present in the environment surrounding the machine vision system.*

hindrance for human inspectors (as the human visual system is not sensitive to IR) it can be problematic for some camera sensors. CCD cameras are sensitive to IR radiation and reflected IR rays can affect the quality of the visual image data captured.

Therefore, constant performance monitoring of the image acquisition system (to ensure the system is within operating tolerances) is essential. For accurate image representation avoidance of 'auto-iris' systems[14], when used with machine vision, is necessary. Auto-irises work by altering the lens aperture, so that the average amount of light passing through the lens is constant. This is inappropriate for machine vision as the grey-tone of a particular feature would vary, depending on the intensity of the ambient lighting [Vernon, 1991]. Section 4.5.1 discusses the lighting and camera conformance testing carried out as part of this research to develop an appropriate machine vision system.

4.3.1 Back Lighting

Illuminated of an object from behind is called back lighting. The use of frosted glass over the

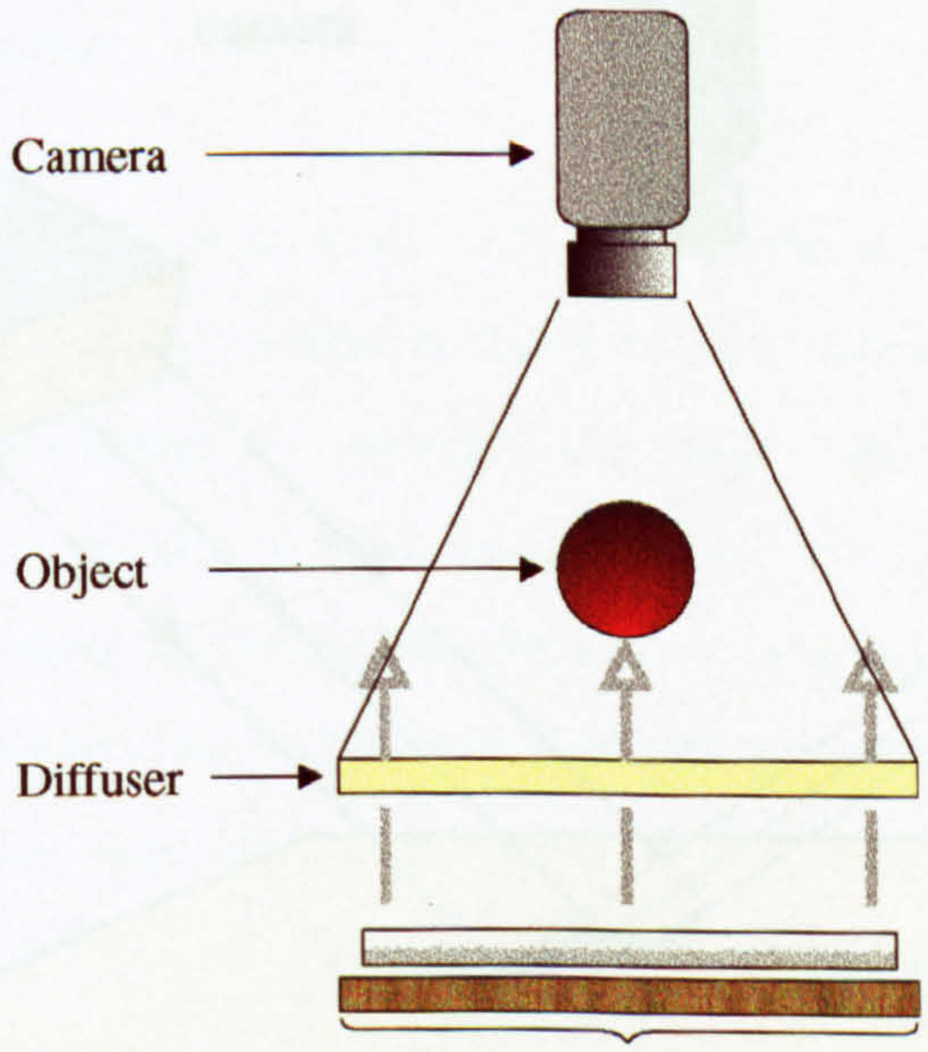

Figure 4.7 : Back Lighting System

14 *Electronically controlled aperture lenses.*

light source to produce a diffuse area emitter is common. Back lighting is particularly useful for creating high-contrast silhouettes, if the object is opaque. This greatly reduces the additional amount of image processing required, e.g. object isolation or segmentation. Figure 4.7 shows a typical back lighting setup.

Due to the nature of object presentation for this research (fabric glued to an opaque blanket) and the fact that surface information is required (i.e. pattern detail), back lighting is an unsuitable approach. Even if the blanket was translucent, the only pertinent information that is acquirable using back lighting, would be fabric width and although this maybe useful for production management it is irrelevant for printing defects.

4.3.2 Front Lighting

When the camera and light source are positioned on the same side of the object for inspection,

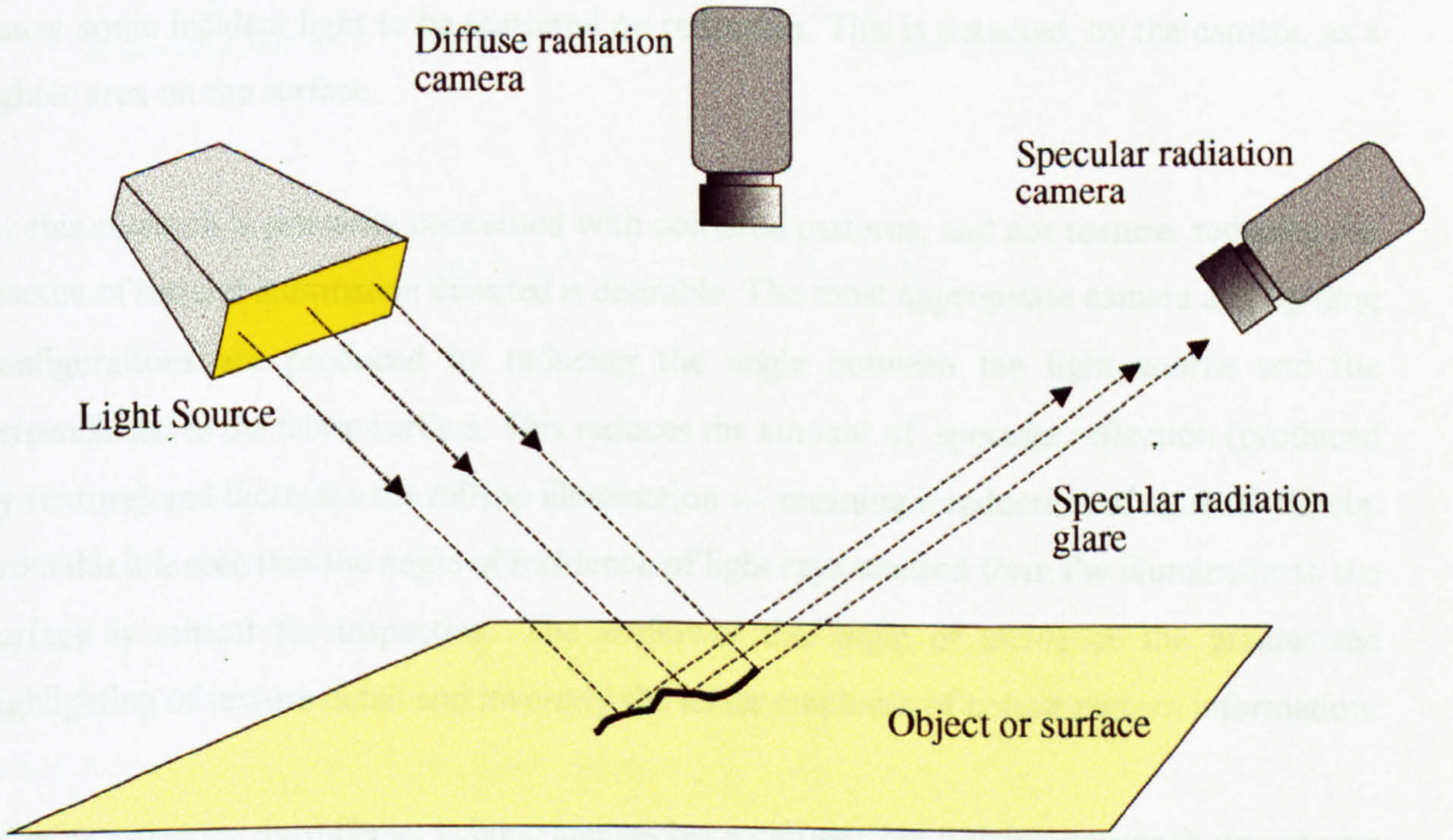

Figure 4.8 : Front Lighting System

it is known as front lighting. The camera captures light reflected from the object, which, dependant on the camera position, can be either *specular* or *diffuse* illumination (see Figure 4.8). This form of illumination is used to emphasize surface information, such as surface *texture* or features (patterns, colours, etc.). Dimensional information can still be found using the front lighting approach, although the image is of lower contrast.

Specular illumination measurement techniques are known as *bright field illumination*; a smooth surface appears bright, as the light rays from the illuminator are reflected directly from the object to the camera. Ideally, for specular reflection measurement the camera position is at the same angular displacement to the perpendicular vector as the light source (ref. Figure 4.8). The reflected light intensity is very sensitive to changes in the surface angle of the object. This method is best suited to textural inspection.

Conversely, diffuse lighting measurement techniques are called *dark field illumination*. The camera is perpendicular to the surface (ref. Figure 4.8). Therefore, a smooth surface will appear dark as there is least scattering of light. Whereas, any surface aberration, such as a scratch, will cause some incident light to be scattered on reflection. This is detected, by the camera, as a lighter area on the surface.

As this research is primarily concerned with coloured patterns, and not texture, reducing the amount of textural information detected is desirable. The most appropriate camera and lighting configurations are produced by reducing the angle between the light source and the perpendicular to the fabric surface. This reduces the amount of specular reflection (produced by texture) and increases the diffuse illumination — meaning a reduction of textural effects. From this it is seen that the angle of incidence of light rays emitted from the illuminator to the surface is critical for inspection. The shallower the angle of incidence the greater the highlighting of texture detail and inversely the lesser emphasis of colour pattern information.

After investigating the different lighting approaches a diffuse front lighting approach was shown to be the best solution. The requirement for the prototype lighting rig was to give a high angle

of incidence of omnidirectional lighting to reduce texture effects (see Figure 4.9). Nevertheless, with a highly textured surface, such as woven fabrics, removing all the texture artifacts by lighting methods is impossible. These artifacts, and their effects on image analysis are discussed in more detail later in the thesis (Chapter 6).

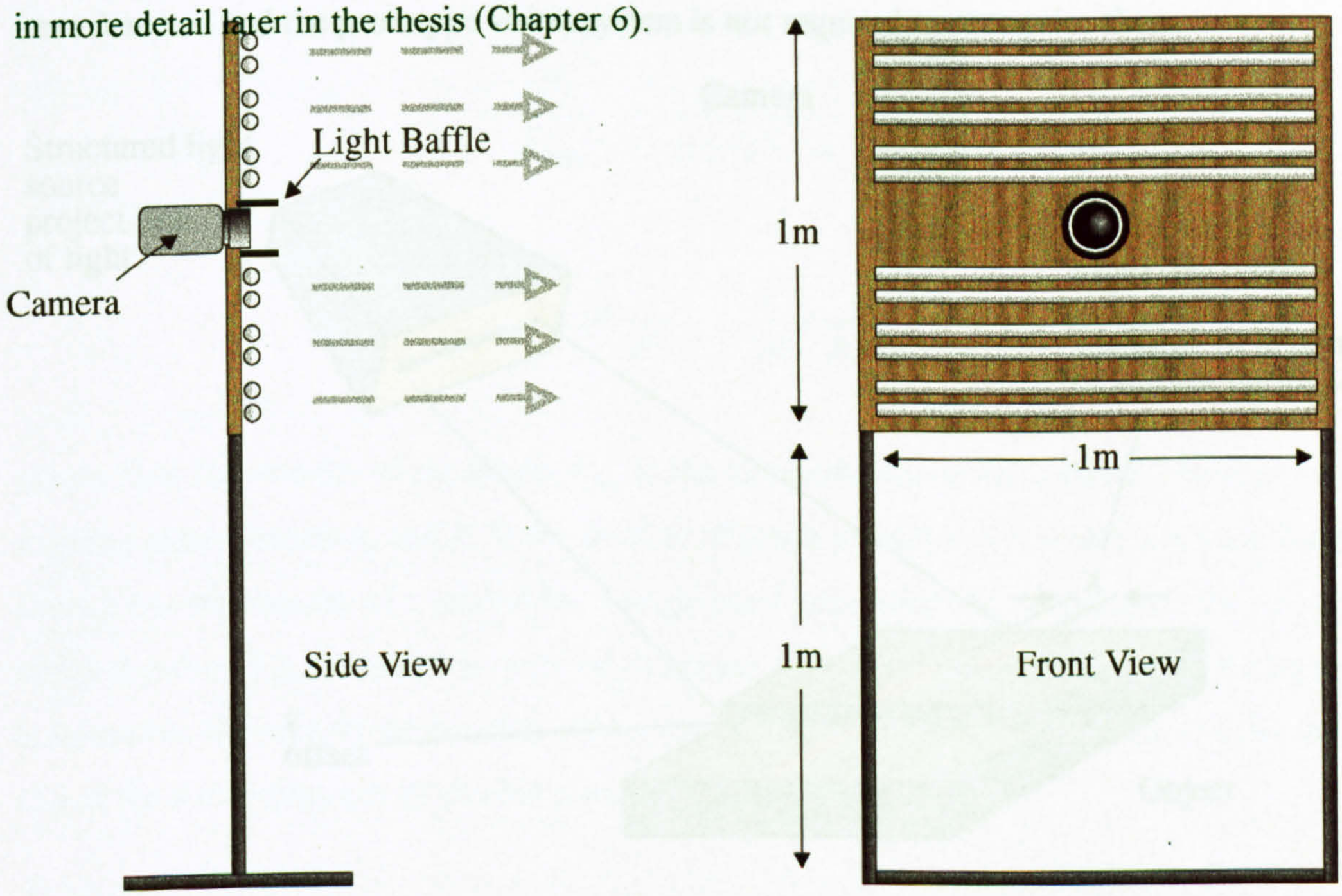

Figure 4.9 : Proposed Lighting Rig

4.3.3 Structured Lighting

If illumination of the object is done with a special pattern or grid, this is known as structured lighting. The intersection of the object and the projected illumination give a unique pattern, dependant on the dimensions of the object and illumination grid. An example of structured lighting for object analysis is shown in Figure 4.10. The use of structured lighting for inspection is only beneficial for three-dimensional objects.

However, for this research due to the nature of the object inspection (fabric glued to a flat blanket) structured lighting is not appropriate. For research purposes the object can be considered two-dimensional. Any variations in the surface due to slubs etc., should have already been detected and the prototype vision system is not required to recognize them.

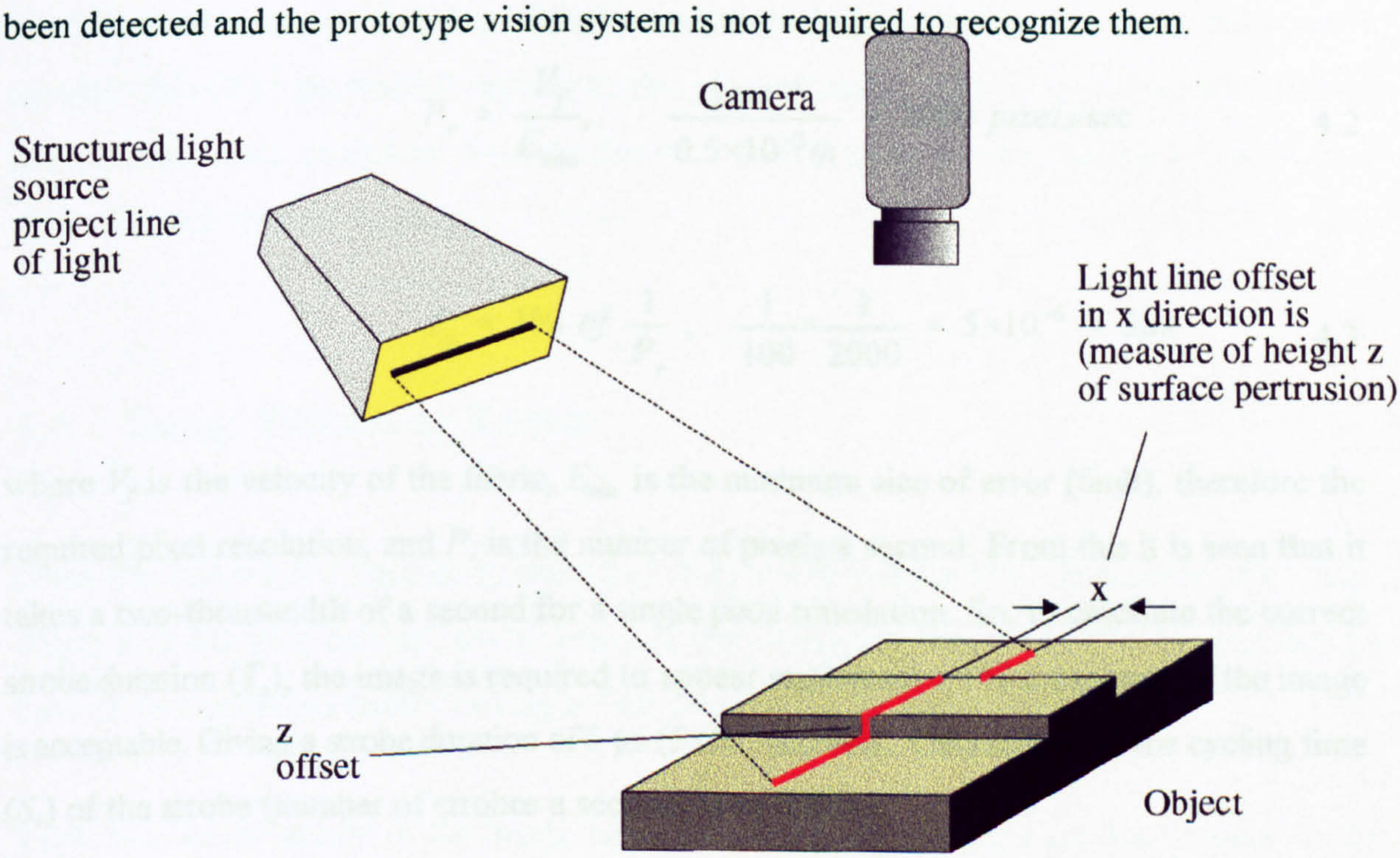

Figure 4.10 : Structured Lighting System

4.3.4 Strobe Lighting

We refer to illumination of the object by a short pulse (5 - 50 μs) of high-intensity light as strobe lighting [Galbiati, 1990]. Strobe lighting is used to freeze the motion of a moving object and to eliminate the effect of ambient lighting. It is important that the light source and camera are synchronized due to the short duration of the pulse. The pulse duration directly affects the amount of perceived motion of the object — the longer the pulse the greater the likelihood of blurring due to motion being measured.

For the prototype system the strobe duration would have to freeze the fabric motion that is travelling at up-to a metre a second. Given a required fault resolution of 0.5 mm and assuming the use of a standard CCD camera and framestore, calculation of the pulse duration as follows;

$$P_r = \frac{V_f}{E_{\min}}, \quad \frac{1 ms^{-1}}{0.5\times10^{-3} m} = 2000 \; pixels/\text{sec} \qquad 4.2$$

$$T_s = 1\% \; of \; \frac{1}{P_r}, \quad \frac{1}{100}\times\frac{1}{2000} = 5\times10^{-6} = 5\mu s \qquad 4.3$$

where V_f is the velocity of the fabric, $E_{\min}$ is the minimum size of error (fault), therefore the required pixel resolution, and P_r is the number of pixels a second. From this it is seen that it takes a two-thousandth of a second for a single pixel translation. So, to calculate the correct strobe duration (T_s), the image is required to appear stationary, a 1% movement of the image is acceptable. Giving a strobe duration of 5 µs (5×10^{-6} seconds). Calculation of the cycling time (S_v) of the strobe (number of strobes a second) is as follows;

$$S_v = R_v \times E_{\min}, \quad 0.256m = 512 \times 0.5\times10^{-3} m \qquad 4.4$$

$$T_s = \frac{V_f}{S_v}, \quad \frac{1 ms^{-1}}{0.256m} = 3.90625 \approx 4 \; per \; second \qquad 4.5$$

where S_v is the vertical sample length for an image system with a vertical camera resolution (R_v) with a minimum error resolution $E_{\min}$. To calculate the number of strobes a second (T_s) the velocity of the fabric and the vertical sample length is needed. For this research the cycling time is approximately four flashes a second.

It was decided that strobe lighting was inappropriate for a factory-based system. The primary reason for this was due to the effect of strobing on the environment. For strobing to be used,

in a work space where humans are present, enclosure of the strobed light is essential as it is considered a health hazard (especially at the projected rate of four flashes a second). Enclosure of the strobe unit is unrealistic for the rotary screen fault detection system due to the physical limitations of system positioning. Also, it was determined that strobing is not necessary as a standard 2-D CCD system (that requires strobing or shuttering to freeze motion) does not have sufficient horizontal resolution. A colour line scan system (with a higher horizontal resolution) does not need strobed lighting.

4.4 Image Processing System

Once the camera and lighting systems (ref. Figure 4.9) required by this research for image acquisition has been defined, specification of the processing unit is possible. Several factors have to be considered before making a final decision on the best system.

First, due to the nature of the image to be processed, the system must have colour image processing capabilities. Another requirement of the system, is that it interfaces with the existing computer system in operation in the laboratory. This means that the frame grabber must connect into either a MCA (Micro Channel Architecture) bus, as used by the IBM PS/2[15] machines, or it should connect into the AT bus used by the PC[16]. The status of board availability for the MCA bus is limited, this means that the likelihood of finding a suitable colour board is small. Several image processing companies did start making boards for MCA machines, but due to the small number of MCA-based machines being used in the image processing environment, this option became economically unviable. Therefore, using an AT bus-based, colour board was necessary.

---

15 *Personal Systems 2*

16 *Personal Computer*

The next requirement of the processing unit is that it satisfies the technical requirements of this research: that the system can process up-to 24 bit true colour (giving a colour palette of approximately sixteen million colours); have at least a 512 by 512 frame area; have the facility for an overlay plane; and the potential for interfacing with an accelerator (be it another board, or a chip that plugs into the existing board). Also it is important that the board comes supplied with a good software library and that source code for this library is available, preferably written in the C programming language. An optional requirement is that of interfacing to a line scan camera (as colour line scanning is of interest). The other remaining requirement is cost. The overall cost of the vision system cannot exceed the £25,000 equipment budget.

With these requirements in mind several image processing products were inspected. Notably: Data Translations *DT-series* of boards; the *TCS3000* series manufactured by Digital Imaging Systems; Quintek colour boards (that use a parallel architecture); and the *Imaging Technology* range, manufactured by Texas Instruments and supplied by Data Cell (see Table 4.1). After examining and costing each board, the DIS3000 was selected as most suitable to satisfy the research requirements.

Manufacturer	Product	Host system/ bus	Video Source	Function	Memory	Description	Price(£)
Data Translation	DT2871	PC/AT	CCIR RGB	Colour frame grabber	1Mbyte	Colour frame grabber for colour image processing featuring real-time conversion to hue-saturation-intensity (HSI) data	4,295
Digital Imaging Systems (DIS)	TCS3000	PC/AT, Sun, VME, Vax Q-bus	True colour RGB, CCIR, PAL, slow scan	True colour RGB framestore and image processor	768K-1536K standard	Real-time acquisition and processing of true colour 512x512x24-bit resolution images. Concurrent processing of RGA for real-time averaging, arithmetic and logic operations	8,500 11,000
Imaging Technology	Visionplus AT Product Line	PC/AT	CCIR/RS170, PAL, NTSC, 12-bit digital or 8-bit analogue (0 to 15 MHZ)	Mid-range framegrabbers and floating-point accelerator	Variable from 1,024 x 512 x 12-bit to 4Mbytes	Mid-range framegrabbers and floating point accelerators which communicates via the Visionbus. Overlay frame grabber - entry level with 4-overlay planes and 12-bit visionbus. Advanced frame grabber combines flexible input with high resolution display (1,024 x 1,024); Colour frame grabber - 24-bit true colour image processing; and image processing accelerator.	1,900 6,500
Matrox	VIP 1,024	VME, AT/EISA	RS170, CCIR, NTSC, PAL, Linescan, slow scan	Framestore, processor, graphics	1Mbyte 2-8Mbytes	Low cost VME single board framestore. Modular image/ graphics processing system. 32-bit framestore with 4-bit overlay. Colour and monochrome. Real-time processor. 1,280 x 1,024 display. X and MS Windows support. High speed local bus	From 4,000
Quintek	MosaiQ-C	PC/AT	True colour RGB	Graphics, frame grabber, and vector DSP processor	4Mbytes VRAM	Image capture and display in 8 or 24-bit colour supported by an overlay plane and cursor. Optional vector co-processors for floating-point analysis at pixel level, convolution, FFT filtering, interpolation	3,800 6,995
Synoptics	Synergy	VME-bus PC/AT	CCIR, RGB, RS170, slow scan	16-bit framestore with on-board fast processor	6Mbytes	1,024 x 1,024 true colour display and accelerated processing or images. Memory can also be configured to capture video sequences and animate them	5,000 8,000

Table 4.1 : Colour Image Processing Board Survey.

4.5 Image Environment for Research

From the research on methods and approaches to signal acquisition design of a prototype system was possible. With this system simulation, in the laboratory, of an industrial inspection system is achievable.

Sample fabrics are attached to a rigid board and illuminated from the front with an array of twelve daylight fluorescent tubes. (Daylight tubes are commonly used by the department stores that sell the finished fabric.) The lighting rig was designed to give even diffuse lighting over a one metre square area (ref. Figure 4.9). A three-CCD RGB area camera (Panasonic F250) is used for image capture. This data is digitized by a DIS3000 24-bit framestore (8 bit per colour plane). Image processing is carried out in parallel by the framestore, and an interfaced 486/50 MHZ PC. Information is displayed via an SVGA computer screen and a broadcast quality monitor (Sony Trinitron). A schematic of the prototype system is shown in Figure 4.11.

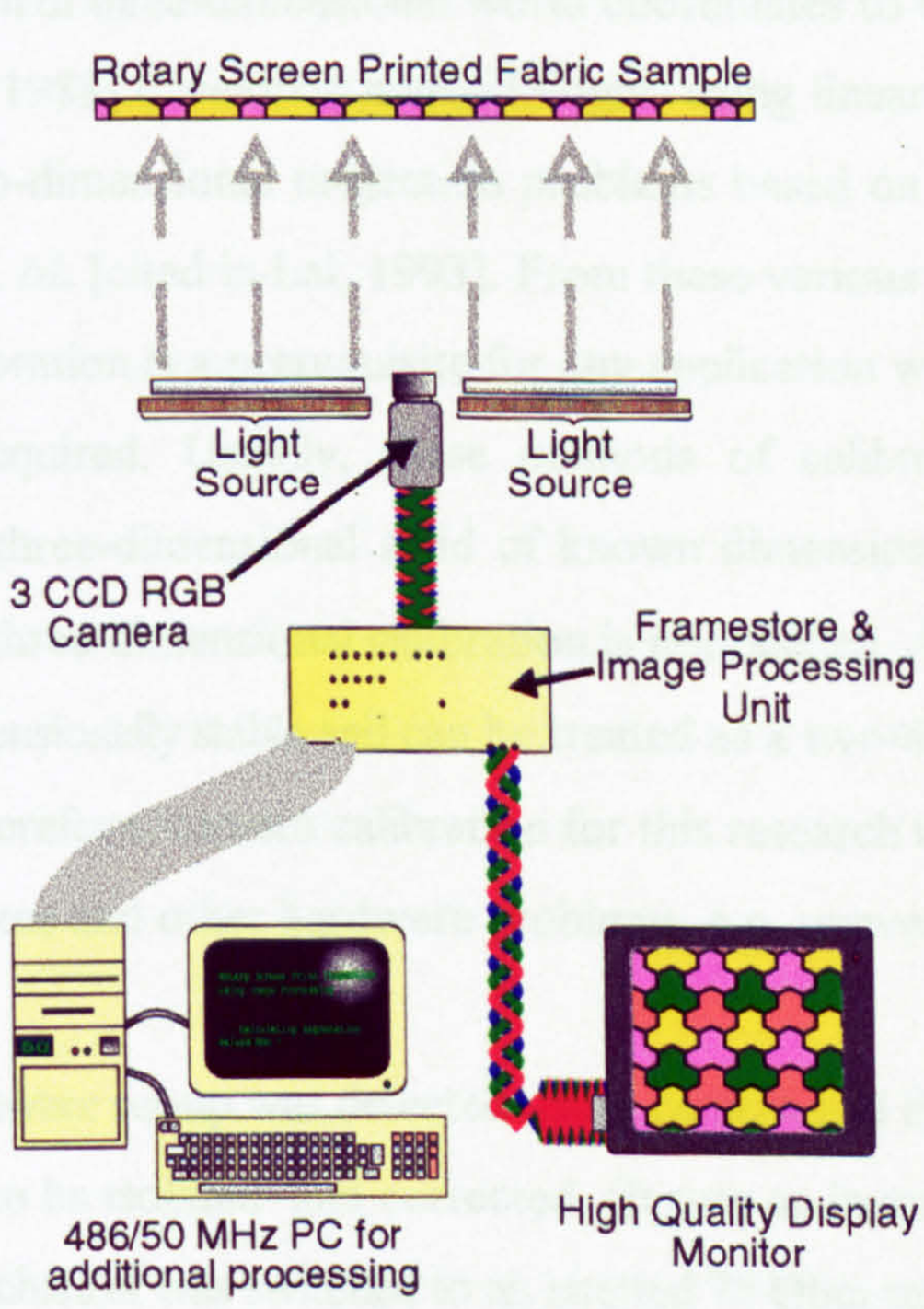

Figure 4.11 : Schematic of Prototype Acquisition System

4.5.1 System Calibration

First it was necessary that the camera and lighting system's performance should be examined. The major reason for this was to try to detect whether the camera and lighting were adversely affecting the colour image signal. Any spatial variations in the system needed to be identified. The results of the testing could then be used to calibrate the system. Temporal variations in the lighting system also needed to be investigated.

Lai [1993] and Fauyeras, Luong, and Maybank [1992] propose solutions to the problem of camera calibration. They recognize that correct camera calibration is an important task for successful computer vision. Fauyeras, *et. al.* [1992] state that the purpose of camera calibration is to establish the projection of three-dimensional world coordinates to two-dimensional image plane. Gremban, *et. al.* [1988] developed methodologies using linear equations to solve the three-dimensional to two-dimensional projection problems based on a two plane approach developed by Martins, *et. al.* [cited in Lai, 1993]. From these various calibration approaches it is seen that camera calibration is a prerequisite for any application where three-dimensional world information is required. Usually, these methods of calibration require complex calculations based on a three-dimensional solid of known dimensions. Fortunately, for the purposes of this research three-dimensional calibration is not needed. As the fabric is glued to the print-blanket, it is dimensionally stable and can be treated as a two-dimensional object, thus simplifying calibration. Therefore, camera calibration for this research is concerned principally with identifying dark-spikes and other hardware problems, e.g. uneven illumination.

A fault in the original hardware set-up was detected using camera and lighting testing. The test results enabled the error to be isolated and corrected. (It was an incorrect dip switch setting. Video output on the blue channel was switched to an internal 75 Ohm termination, OUT, rather

than 75 Ohm termination, IN. The error it produced was similar to a CCD originating error, and without the testing would have been difficult to diagnose.)

The (Panasonic 250-A, 3 chip CCD) camera testing examined the effect of variations in the gain, aperture, and magnification on the mean pixel intensity and standard deviation over a plain, grey image. This indicated the optimum settings for the camera and identified areas of decreased/increased sensitivity over the image plane. This information was vital for research, as the 'auto-iris' system (cf. Section 4.3 Lighting Considerations) affects consistent image acquisition.

It was speculated that the pixels towards the centre of the image would be brighter than the mean and those towards the boundaries of the image would be darker, a 'halo' effect. This, it was thought, would be mostly due to the optical effects of the camera, but it was anticipated that there would be some variation with magnification. At low magnification the 'halo' effect would be more pronounced due to non-uniform illumination ($\cos^4$ illumination law — worst when the lens is zoomed out to give maximum field of view). As magnification increases, the 'halo' effect should decrease, as the lighting becomes more uniform. This needs to be proven before further assumptions about the colour processing are made. It was also anticipated that this 'halo' would be affected by aperture and gain settings.

Another area to investigate was the possible 'Vignetting Effect[17]', which is an optical effect caused by wide aperture settings, which again manifests itself as a 'halo' type effect (with darker areas towards the boundary). Once the test data has been collected, it can be processed to show what the optimum settings are for the camera. These settings will be optimum when the standard deviation is low and the 'halo' effect is reduced.

---

17 *Vignetting occurs when off-axis light rays are refracted so that they are absorbed by the lens mounting. Therefore, the vignetting effect increases as the aperture is opened as more off-axis light is incident on the lens.*

The data was collected using a software-based sampling process. The rationale for this was to provide consistent data sampling and reduce human interaction, where errors can occur. Ten full colour frames are captured, at a rate of one every two seconds, giving a total data sampling period of twenty seconds. The reason for the multiple frame capture was to reduce the chance of errors caused by fluctuations in the lighting. Before sampling the lighting unit is given a half hour warmup time, to allow the colour temperature of the fluorescent tubes to settle.

After data sampling the mean and standard deviation for each of the red, green, and blue channels were calculated. This information was stored in a data file along with information about the gain, magnification and aperture setting of the camera. A mean image is produced from the ten sampled frames and this can then be inspected with respect to the standard deviation and mean pixel values.

Results from this inspection can then be plotted in a graphical form to show the haloing effect with respect to the mean image. The haloing effect can be shown for any multiple of standard deviations from the mean. The preferred multiple of standard deviations from the mean is three. For data that obeys a Normal Gaussian Probability Distribution (based on Tchebychev's theorem[18]), 99.7% of the data should be within three standard deviations of the mean.

The results of these tests are included in Appendix C in tabular and graphical form. The size of each sample is, 10 x 512 x 512 = 2,621,440 pixels, this gives a statistically useful sample distribution.

The basic algorithm used for the sampling was as follows;

---

18 *For any set of data (population or sample) and any constant k greater than 1, the proportion of the data that must lie within k standard deviations on either side of the mean is at least*

$$1-\frac{1}{k^2}$$

```
REPEAT
   Initialise Variables and Data Arrays;
   Initialise Frame Store;
      ⋮
   FOR Number = 1 TO 10
     Capture Frame [Number];
   NEXT Number.
      ⋮
   Calculate Mean and Standard Deviation;
   Calculate Mean Image;
   Add Information to Database;
      ⋮
UNTIL End-Of-Sampling.
```

The mean was calculated using the following formula;

$$\bar{x} = \frac{\sum x}{n} \qquad 4.6$$

where x is a sample element and $\bar{x}$ is the mean of the sample.

The mathematical formula for the standard deviation of a sample is;

$$s = \sqrt{\frac{\sum (x-\bar{x})^2}{n-1}} \qquad 4.7$$

where s is the standard deviation of the sample.

This formula is unsuitable for computational purposes as it requires the mean to have been calculated before the calculation for standard deviation. A more computationally efficient method for calculating standard deviation exists. It is calculated by the difference between the sum of the squares of the sample elements and the sum of the sample elements squared in relation to the sample size. This computing formula is as follows;

$$s = \sqrt{\frac{n(\sum x^2) - (\sum x)^2}{n(n-1)}} \qquad 4.8$$

Gain 0dB, Magnification ×15						
Aperture	Mean G	Std Dev G	Mean R	Std Dev R	Mean B	Std Dev B
16	41	4.959888	23	7.713953	29	5.607186
11	61	6.606017	50	7.333932	52	6.14773
8	88	6.840621	82	7.028469	84	6.781089
5.6	105	0.585308	97	2.114828	103	3.07063
4	111	1.711146	102	1.600441	109	2.153617
2.8	110	1.072266	101	0.982089	108	2.012513
2	109	0.917277	101	0.903171	107	1.929753
1.4	109	0.971007	101	1.050509	107	1.932115

Table 4.2 : Sample of Calibration Test Data

From the results of the camera and light testing (see Appendix C) producing calibration overlays and graphs was possible. Table 4.2 and Figure 4.12 show a sample of test data and its associated graph.

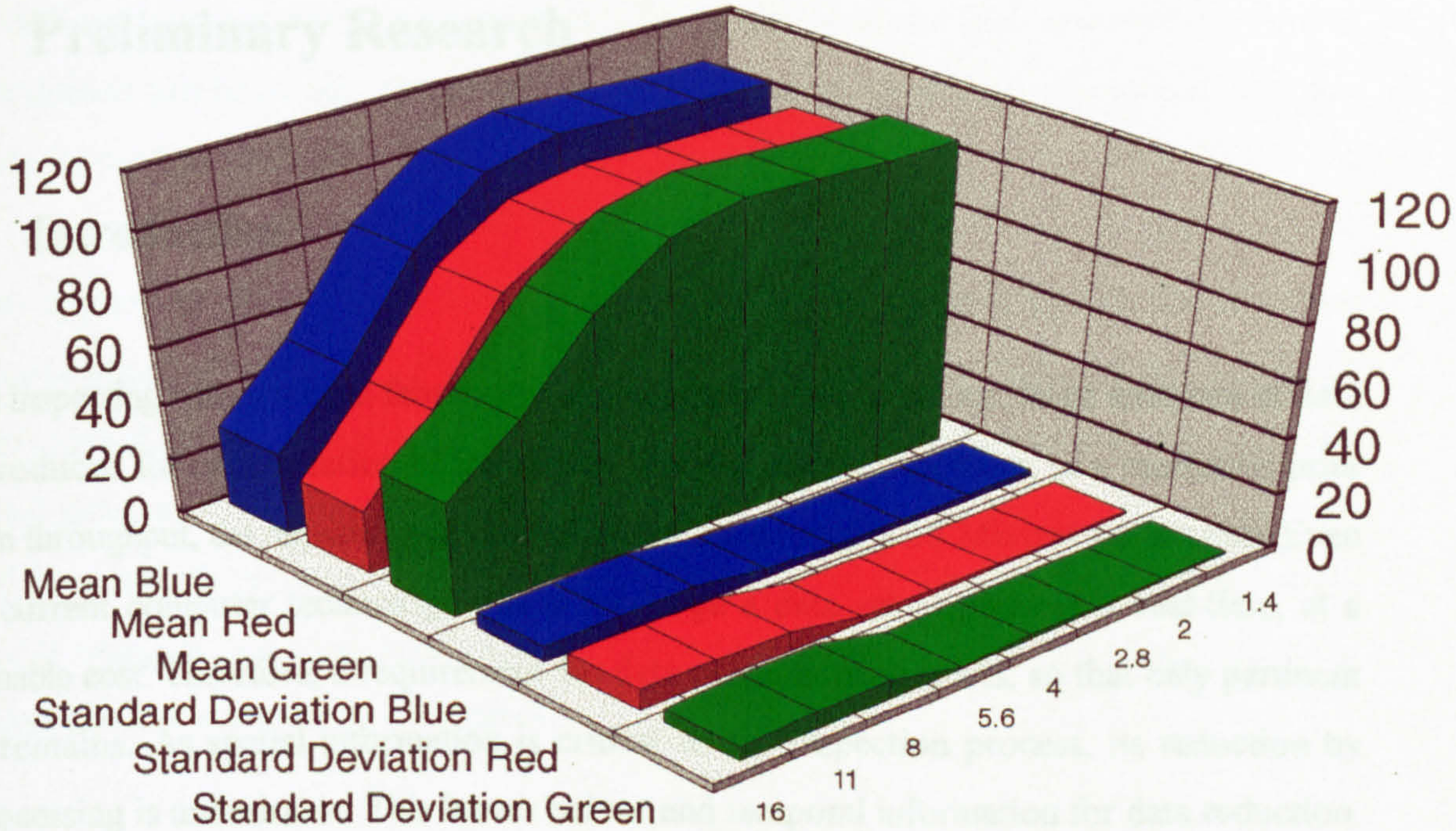

Figure 4.12 : Graph derived from test data in Table 4.2

4.6 Summary

This chapter has identified the main areas that need to be addressed to satisfactorily acquire image data for further processing. It is essential that the system captures the best possible image as all further processing is dependant on its quality. Proposals for a suitable acquisition system have been given in this chapter, and they form the basis of the on-line inspection system advanced in Chapter 8. In Chapter 5 methods for the preliminary analysis of the data are examined (via a comprehensive literature survey). Chapter 6 concentrates on the critical preprocessing of the acquired data through colour segmentation, and these methods are evaluated in Chapter 7.

5 Preliminary Research

5.1 Introduction

When inspecting rotary screen fabrics at high resolution, and in colour, large amounts of data are produced for each rotation of the screen. For full-width inspection, at a maximum print system throughput, the required data processing rates are roughly 36 MBytes per second. Even with current computer technology this is too large a data set to process in real-time, at a reasonable cost. Therefore, a requirement for data preprocessing exists, so that only pertinent data remains. As spatial information is critical to the inspection process, its reduction by preprocessing is undesirable. This leaves colour and temporal information for data reduction.

Certainly, reduction of the temporal data set giving a pseudo 100% inspection approach is possible. For systematic faults the requirement to continuously monitor the fabric is not strictly essential. Systematic faults tend to be predictable, meaning they can be detected before they go out of tolerance. Designing the machine vision system to sample only at the critical colour boundaries is possible. As a percentage of the screen repeat, these boundaries are very rarely more than 5% of the total repeat. Full-width inspection is not required to detect systematic faults, just samples at key points across the fabric. Significant data reduction can be achieved using this spatial/temporal approach, as much as 99% of secondary data can be eliminated. Nevertheless, this method is only suitable for systematic faults. Random faults still require full-width inspection.

The temporal approach is still feasible for random fault inspection, although 100% inspection is impossible. Due to the irregular and infrequent nature of random faults (see Table 1.1) continuous sampling may not be essential. Often random faults can be insignificant or indiscernible (e.g. a pinhole on an already speckled background). As suggested in 1.2.2 Pseudo 100% Inspection, taking samples of repeats at regular intervals may be adequate. By regular,

but non-continuous sampling, random faults of a repetitive nature can be detected, whereas one-off defects may be missed. However, the repeating defects cause most second classification of fabric by random faults.

A better approach to data reduction, while retaining critical fault information, is that of colour quantization (or segmentation). The rotary screen fabrics printed by DORMA are principally pigment printed. Pigments, unlike dyes, are almost opaque to underlying colours, therefore only a limited amount of blending occurs on pigment printed fabrics. Consequently, any pigment printed fabric has, theoretically, only as many colours as screens. Ideally, these colours would appear as compact points in colour space. Unfortunately, due to texture, lighting, and some blending, these points are more dispersed.

One way of reducing the colour information is to use an 8-bit instead of 24-bit colour system. This is not a practical solution. An 8-bit colour system will reduce the amount of image data by two-thirds, but it lowers the colour resolution by a factor of 65 thousand. (An 8-bit system can differentiate 256 colours, whereas 24-bit system can differentiate up-to 16.7 million colours.) It is important that the system can separate colours of similar hues. Systems using 8-bits cannot achieve this. A more adaptive colour quantization method is essential. The following section examines existing colour segmentation methodologies, chronologically, and discusses their suitability for preprocessing the rotary screen image data.

5.2 Literature Survey

This section reports on the principal papers referenced during this research that are not discussed in detail elsewhere in this thesis. It is divided into three sections: the first concentrates on papers related to colour segmentation methodologies (a vital part of this research); the second section covers colour image processing applications that are relevant to this research;

while the final section acts as a 'catchall' for the other important papers that are not referenced elsewhere. The papers are referenced in chronological order.

NB. The following literature survey is not a complete report on all papers examined, but as more than three hundred papers were collected during this research, only the principal papers are reviewed. It is also important to note that this large number of papers does not mean this is a well-researched area, on the contrary there are very few papers in this research field. Most of the papers are referenced to corroborate individual areas of the research.

5.2.1 Colour Segmentation Methodologies

Pre 1985

The earliest useful paper was published in 1982, by Connah and Fishbourne. It proposed two strategies for segmentation by colour, which they first presented at an IERE colloquium on image processing [Connah and Fishbourne, 1983]. This work was based on a paper that was first published in 1981 [Connah and Fishbourne, 1981].

For the first segmentation method they identified that areas in digitized pictures that humans recognize as being of uniform shade actually contain many small variations in shade. For purposes of realistic segmentation these small differences in shade should be ignored. Clearly, in a notional RGB space, colours that vary only slightly in shade will be very close together, thus forming clusters. The algorithm they propose identifies these clusters and assigns any pigment within the same cluster to the same trivector colour value. It is interesting that this segmentation method is similar to the second stage of segmentation used in this research. However, this research uses a more complex clustering algorithm approach for the analysis of rotary screen printed fabrics.

The second segmentation algorithm designed by Connah and Fishbourne [1983] use hue and saturation information for colour quantization. They argue that in a simple application it may, where colour is being used to distinguish between otherwise similar objects, be sufficient to ignore changes in intensity and represent colours as hue (cf. hue space segmentation, Dodkin, 1994).

However, Connah and Fishbourne state that despite the appeal of this simple approach, there exist several problems. Namely, detecting noise points is difficult, and the conversion from RGB to hue and saturation involves floating point numbers, that can never be exactly compared. Also, bright colours generate more hue values than dim colours. Another problem exists when determining whether two adjacent pixels of differing hues should be regarded as the same hue and when one of them should be defined as a noise point.

Nevertheless, the hue saturation approach is better suited to some industrial applications (those involving similar parts of different colour) than the RGB colour space approach. In his thesis Dodkin [1994, p.68] states that Connah and Fishbourne report that the hue saturation segmentation method can discriminate two supposedly identically coloured objects. There is no evidence in the paper to support this statement, in fact Connah and Fishbourne declare that hue saturation segmentation is only suited to rudimentary colour differentiation applications.

Chassery and Garbay [1984], identify an iterative approach to segmentation based on contextual colour and shape criterion. The method was developed for the segmentation of convex coloured objects on a relatively homogenous background. It works by using region detection methods, where a region is defined as a spatially connected set of pixels that satisfy some homogeneity criterion. *A priori* knowledge of the image (such as shape or texture) is needed before iterative processing can begin. The actual region detection is a combination of colour similarity measurements and aggregation criteria. Colour similarity is expressed in terms of a distance over a perceptual colour space (Equations 5.1 – 5.8).

$$A = \frac{1}{3}(\log R + \log G + \log B), \quad 5.1$$

$$C_1 = \frac{\sqrt{3}}{2}(\log R - \log G), \quad 5.2$$

$$C_2 = \log B - \frac{1}{2}(\log R + \log G). \quad 5.3$$

The logarithmic transforms of the R, G, B images are linearly combined giving one achromatic image (A) and two chromatic images (C_1, C_2). These transforms are based on a model of human colour perception [Garbay, Brugal, *et. al.* 1981, cited in Chassery *et. al.*, 1984]. By decorrelating the luminance and chrominance images further characterization of a colour by its luminance (L), saturation (S), and hue (H) is possible.

$$L = A, \quad 5.4$$

$$S = \sqrt{(C_1^2 + C_2^2)}\ , \quad 5.5$$

$$H = \arccos(C_1 / S). \quad 5.6$$

An *Euclidean* metric can be defined over the (A, C_1, C_2) and for (L, S, H) polar coordinates as;

$$D^2 = (\Delta A)^2 + (\Delta C_1)^2 + (\Delta C_2)^2 \quad 5.7$$

or,

$$D^2 = (\Delta L)^2 + (\Delta S)^2 + \left(\frac{S_1 + S_2}{2}\right)^2 (\Delta H)^2. \quad 5.8$$

where S_1 and S_2 are the respective saturations of the pixels under consideration. This is similar in method to the colour cluster determination employed by the current research, which uses an *Euclidean* metric for determining distance. However, due to the requirement for *a priori* knowledge and the slow recursive nature of the algorithm it is of limited use for printed fabric segmentation. Although some assumptions on the texture of the fabric can be made, this is common to the whole image and will not, by itself, differentiate regions. Chassery, *et. al.* 1984, tested their methods subjectively using estimation by a human observer. On a set of samples containing 150 images of bone marrow cells, they state that 79% were classified as good segmentation, 7% badly segmented.

1985 — 1989

Pienkowski and Dennis [1985], recognized that decision processing of colours will require more than the traditional colour science approach to colour machine vision design. They introduce the idea of 'fuzziness' to be used in artificial colour determination. The rationale for fuzzy logic in colour segmentation is that colours are not rigidly defined entities, and the computer model must be 'relaxed' to allow for this. Two reasons are given for using fuzziness in modelling colour: the chromatic noise due to texture, and non-uniform reflection of the colour components; and electrical noise within the colour image data. These factors mean that it is impossible to accurately define what a colour will be when viewed by a machine vision system.

By using fuzzy set theory Pienkowski and Dennis argue that it provides a natural weighted tolerance to any colour definition, so that a form of 'objective subjectivity' can be introduced into the machine vision model. This subjectivity is measurable in machine vision terms and can be used by a machine to view the colour world. The use of fuzzy logic seems to have bearing on analysing the textural effects of the fabric on the pigment, and as such is of help in the research. Pienkowski, *et. al.* [1985], offer no experimental evidence quantifying the success of their colour segmentation method.

A method for segmenting colour images using edge-preserving filters was proposed by Pietikäinen and Harwood [1986]. It uses a colour symmetric nearest neighbour (SNN) filter for edge-preserving and two-pass connected components for regioning. First the image is smoothed using the colour-SNN filter. This smooths homogenous areas and sharpens edges. Further processing is required to ensure that edges at critical points are also enhanced.

After smoothing segmentation is carried out by the connected components (CC) algorithm. Pixels are connected if the magnitudes of their colour differences are small. Nevertheless, this method although performing well when compared to existing techniques [Ohlander, *et. al.*, 1978] still requires a degree of human intervention, such as the thresholding parameter for the connected components algorithm. What Pietikäinen and Harwood recognized was that edges are useful descriptors of colour regions, as they tend to define the colour boundaries. This is comparable to the edge masking technique developed for the segmentation of rotary screen printed fabrics.

Pietikäinen, *et. al.* [1986] use unrelated 8-bit images to test their methods. They state that the experimental results were good, but offer no quantified evidence. It is presumed that the criterion for evaluating the segmentation was via a human observer and therefore subjective. Also, due to the iterative nature of the algorithms they propose for colour segmentation, this method would be too computationally expensive for 24-bit colour images. The filter-based, rather than colour space, segmentation of images is an interesting approach that needs further investigation.

Connolly, Littlewood, and King [1988] offered a solution to image segmentation from colour data. In comparison to existing methods it was not well developed, initially requiring extensive manual intervention. They identify the mean and standard deviation of a colour as being important for segmentation purposes.

A method for assessing the quality of the segmentation is proposed by Connolly, *et. al.* [1988]. It is suggested that segmentation success can be measured by the appearance of the segmented

image (subjective) and quantified by counting the number of correctly and incorrectly 'tagged' pixels. Automated segmentation at two standard deviations gave results in the order of between 62 – 85% of the pixels being successfully assigned. The large variation in the results emphasised the need for a more controlled inspection environment.

A stepwise optimization approach, using hierarchy for picture segmentation was proposed by Beaulieu and Goldberg [1989]. Although this method is not aimed at colour segmentation it does offer solutions to some problems of connecting homogenous areas and could be adapted for a colour image. They approach segmentation by regarding it as a polynomial approximation of a picture. The approximation error is then regarded as a global criterion, and further segmentation is done to reduce this criterion.

Using a hierarchical structure reduces the search space and global optimization can then be replaced by stepwise optimization (which is derived from the global criterion). This method has implications for a fast automated segmentation such as would be needed by an on-line inspection system. The merging of similar areas in this method is dependent on spatial position and textural criterions. However, this could be adapted so that the merging of regions of similar colour but spatial difference could be achieved. This is especially important if the optimization could also resolve lighting variations in disparate areas of the image. (Such a problem is likely to arise when trying to illuminate a three-metre wide piece of fabric.)

<u>1990 — Present Day</u>

Lim and Lee [1990] take a similar approach to Pienkowski and Dennis [1985] for colour image segmentation. They determine that for machine vision segmentation some fuzzy set approach is necessary. In particular they define a segmentation method using thresholding and fuzzy c-means (FCM) techniques. They use a scale-space filter as a tool for analysing the histogram of the colour components. By using a two-pass approach they reduce the computational requirements of the FCM algorithm.

The first pass segments the image coarsely using a thresholding approach. On the second pass any remaining pixels are then assigned to the nearest class using the FCM. Interestingly, the approach to coarse segmentation is very similar to that used by the research, although both were developed independently. The FCM algorithm used for fine segmentation is based on a clustering algorithm, but unlike the clustering algorithm developed by the research the FCM approach requires *a priori* knowledge of the number of classes (regions).

Lim and Lee [1990] was the best paper found on colour segmentation (and not just because of the similarities between their approach and the ones used in this research), it is clearly written and has made good use of existing algorithms. They propose that to evaluate the performance of their proposed algorithms the probability of error between the manually segmented reference image and the automatic segmentation needs to be calculated. The probability of error is defined as follows (Equation 5.9);

$$P(e) = \sum_{j=1}^{c} \sum_{\substack{i=1 \\ i \neq j}}^{c} P(R_i|R_j) \cdot P(R_j) \qquad 5.9$$

where R_i and R_j are the ith and jth regions among the c regions in an image. Their results showed that the XYZ, UVW, and the YIQ colour systems are inappropriate for colour segmentation, with probabilities of error of 0.6519, 0.3552, and 0.6563 respectively. The best results being in the RGB colour space and the Ohta coordinate system, giving probability of error of 0.0287 and 0.0119 respectively. The Ohta coordinate system is a three component system using simple, linear transforms of RGB space as follows;

$$I1 = \frac{(R+G+B)}{3}, \tag{5.10}$$

$$I2 = R-B, \tag{5.11}$$

$$I3 = \frac{(2G-R-B)}{2}. \tag{5.12}$$

The comparison performed by Lim, *et. al.* [1990] on four different segmentation methods suggest that the RGB colour system or a linear derivative, such as Ohta, give the consistently best results (see Table 5.1).

	Ohlander	Bezdek	Rosenfeld	Lim-Lee
RGB		0.0622	0.0139	0.0287
XYZ		0.3718	0.6526	0.6519
YIQ	0.0222	0.0552	0.0164	0.3552
UVW		0.4171	0.3698	0.6563
Ohta's		0.2108	0.0133	0.0119

Table 5.1: The probability of error for four algorithms

Khotanzad and Bouarfa [1990] also developed a method for colour segmentation using a parallel, non-parametric histogram based clustering algorithm. Interestingly, this appeared in the same journal edition as Lim and Lee's [1990] paper. Nonetheless it is sufficiently different to warrant further investigation. Khotanzad and Bouarfa state that this approach is totally automatic. As such, it may be suitable for an on-line inspection system. Clusters are identified by mode analysis of the image in a three-dimensional perceptual colour space (RGB), using an iterative peak-climbing algorithm.

Khotanzad, *et. al.* [1990], recognize that this method is easily parallizable, and developed a parallel processing system based on this. Although their colour segmentation and clustering algorithm are relatively simple, the identification of parallel processing for sharing the segmentation task is important. The benefit of parallel processing for on-line inspection is obvious as it can provide fast multi-streamed processing. Their method requires *a priori* selection of the quantization level, so cannot be fully automated.

No direct evaluation of segmentation is given by Khotanzad, *et. al.* [1990]. They do give a performance evaluation of their two clustering techniques in relation to the number of processors used, but only on two-dimensional data. The best case is for the 'M' clustering method, running on eleven processors, where clustering is completed within 0.74 seconds. Nevertheless, they present no evidence on the quality of clustering or segmentation. This is an interesting theoretical paper, but is of limited value to this research.

Yet another colour clustering solution to image segmentation was proposed by Celenk [1990]. This method operates in the 1976 CIE (L*, a*, b*)-uniform colour coordinate system. It detects image clusters in some circular-cylindrical decision elements of the colour space. This approach allows estimation of the colour distribution of the clusters while maintaining constant lightness and chromaticity loci.

It is reasoned that the use of a uniform colour space such as L*a*b* could improve the performance of colour clustering. This system is obtained from RGB colour space by converting the tri-stimulus R, G, B values into the XYZ colour space (cf. Chapter 3 on colour). The L*, a*, and b* values are obtained by applying a cube-root transform to the X, Y, Z values (Equations 5.13 – 5.18).

$$X = 2.7690R + 1.7518G + 1.1300B \quad 5.13$$

$$Y = 1.0000R + 4.5907G + 0.0601B \quad 5.14$$

$$Z = 0.0000R + 0.0565G + 5.5943B \quad 5.15$$

$$L^* = 116 \sqrt[3]{(Y/Y_0)} - 16, \qquad Y/Y_0 > 0.01 \quad 5.16$$

$$a^* = 500 \left[\sqrt[3]{(X/X_0)} - \sqrt[3]{(Y/Y_0)} \right], \qquad X/X_0 > 0.01 \quad 5.17$$

$$b^* = 200 \left[\sqrt[3]{(Y/Y_0)} - \sqrt[3]{(Z/Z_0)} \right], \qquad Z/Z_0 > 0.01, \quad 5.18$$

Where X_0, Y_0, and Z_0 are the XYZ values for the reference white. It is important to note that the transform matrix for the RGB to XYZ colour space has not been standardized (cf. Chapter 3, Colour Space Transforms for the *de facto* standard). Various sources, Hunt [1991], Poynton [1995], and others all cite different values for the transformation.

As with other papers no quantifiable results are offered. However the use of one-dimensional histograms in the estimating process for detecting three-dimensional colour clusters reduces the computational cost involved in maintaining many derived images and obtaining their three-dimensional distributions [Celenk, 1990]. This could have important implications for real-time segmentation systems. Still, this needs to be balanced against the additional computational costs of converting from the RGB colour space to the L*a*b* colour coordinate system.

Orchard and Bouman [1991] identified that many image display devices allow for only a few colours to be displayed simultaneously. Usually the colours displayed are subsets of available colours from the system colour palette. Standard quantization does not allow for realistic representation of colours in natural scenes, where colours are arbitrarily arranged. Their paper deals with two areas concerning this problem: the selection of an *optimal* colour palette; and the mapping of each image pixel to this palette. They look at hierarchical tree structures

incorporating subjective evaluations as a method for resolving the problem. It is argued that tree structures reduce the computational expense of palette design and mapping as they can handle densely populated areas of colour space.

This paper is applicable to the research as it deals with some of the difficulties in displaying colour images using a restricted palette. A direct comparison can be made between this and the rotary screen analysis problem, as the number of screens can be used to define a restricted palette from a 24 bit (16.7 million) colour system. Previous approaches to this dilemma use an iterative refinement process of an initial palette. Obviously, for on-line inspection, iterative processing is unacceptable as it alters the qualitative analysis, thus the overall consistency. Another problem with existing applications is that pixel mapping is performed locally at display time. This is due to standard approaches use of high correlation values of neighbouring pixels to reduce the transmission bit rate. In a natural scene high correlation between neighbouring pixels is not usually seen.

Existing palette construction techniques have been based, primarily on the Linde-Buzo-Gray (LBG) algorithm for quantizer design. The LBG algorithm attempts to reduce the total squared error (TSE) between the original pixels and colours assigned from the palette. Although the LBG approach reduces the initial TSE, it is affected by the initial palette structure and as such can become very computationally expensive.

The algorithms proposed by Orchard, *et. al.* [1991] attempt to minimize the objective error criteria by using vector quantization linked with a tree hierarchy. This, tree structure significantly reduces the computation requirements of palette design and pixel mapping. They state that empirical evidence shows that methods that reduce the TSE do not necessarily produce the best colour palettes. The rationale is that the TSE approach presumes relational properties on spatially adjacent pixels, which is not always the case in natural scenes. By using a weighted TSE approach (WTSE) that applies a subjective weight to the squared error of each pixel, the perception of small intensity changes as a function of the spatial intensity gradient of each pixel is improved.

Orchard, *et. al.* [1991]'s paper then goes on to suggest the use of dithering approaches to segmentation; by matching the local colour average of the output image to the local colour average of the original. However, this method is only applicable to images that receive further viewing by humans, and is irrelevant for the machine vision approach of this research. Still, as a whole the paper is useful as it identifies flaws in the TSE approach to colour quantization of natural scenes.

A 'merge and box' algorithm that performs colour quantization using a single instruction stream, multiple data stream (SIMD) parallel processor was presented in a paper by Fletcher [1991]. The algorithm finds colour space boxes that cover all colours in the input images. It then uses this box information to produce a colour look-up table of the correct size. Early research in the rotary screen project produced a similar quantization approach. However, this method was abandoned for being too coarse for fine segmentation of the non-cuboid colour clusters of the fabric image.

Fletcher's [1991] 'merge and box' algorithm uses two passes to quantize the image colours. The first pass constructs a representative table of N colours from the original image. From this table the second pass quantizes the image for display. This is achieved by enclosing each of the N colours in the smallest enclosing box possible (for colours in RGB colour space each box will have boundary lengths of one). Therefore, each box is defined by three pairs of values corresponding to the values for each colour axis containable in the box.

To quantize the image there is a requirement to combine boxes by forming a new box from the two most distant corners of a pair of boxes (Figure 5.1). Fletcher states that box merging occurs when N+1 boxes have been allocated. The two closest boxes must be found and merged. No experimental evidence is given in this paper as to quantization success as it only aims to improve the perceived image quality (a subjective process).

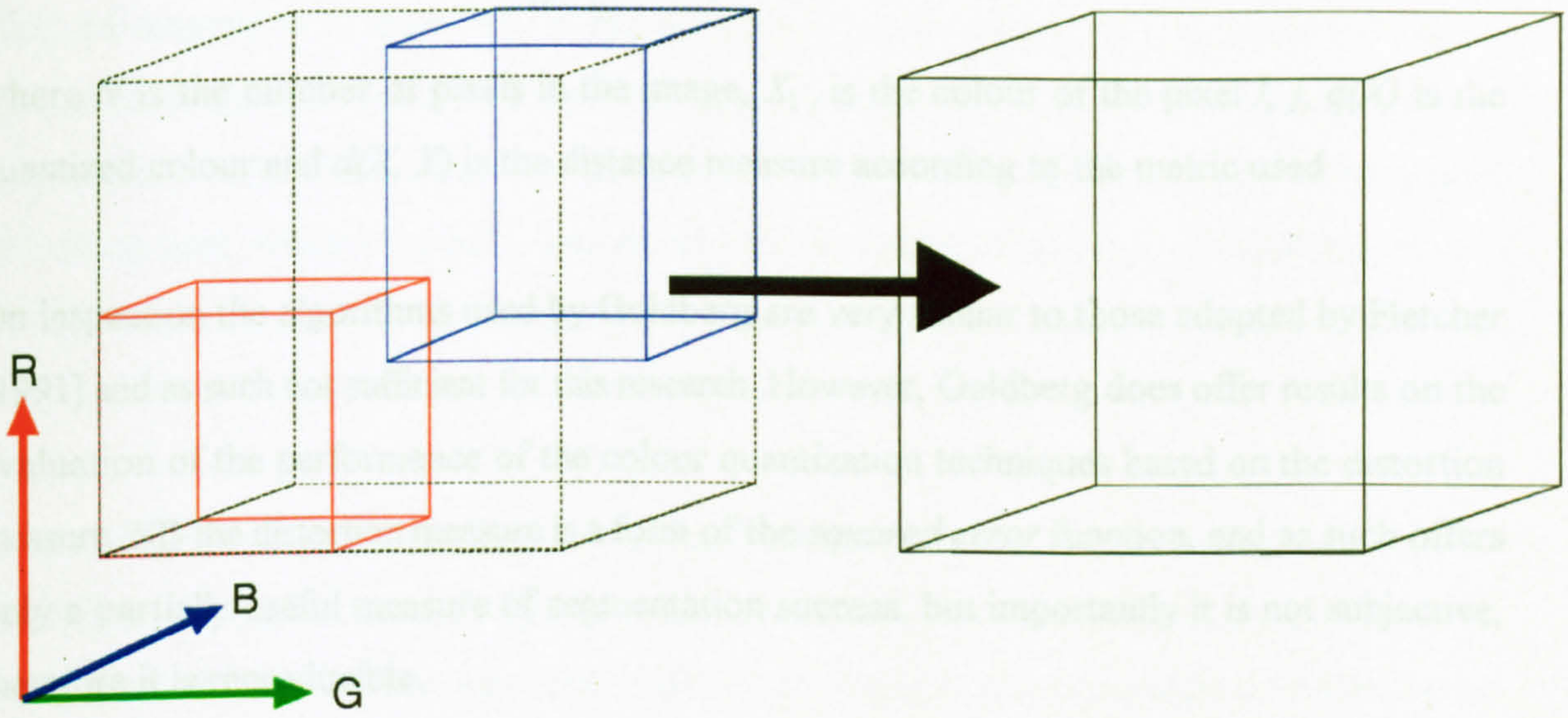

Figure 5.1 : Merge step of merge and box algorithm

Goldberg [1991] developed algorithms for quantizing colour images on high resolution graphics displays. The quantization algorithm proposed is a generalization of the common vector quantization algorithms used for data compression. Goldberg identifies colour metrics as important for determining the distance (difference) between colours. The paper examines two colour metrics for difference determination in the RGB colour space. They are the *Euclidean* metric (Equation 5.7)(cf. Chassery, *et. al.* [1984]) and the *Manhattan* metric (Equation 5.19).

$$d_M(X,Y) = |x_r - y_r| + |x_g - y_g| + |x_b - y_b| \qquad 5.19$$

An important aspect of Goldberg's paper is the suggestion of a method for evaluating the quantization quality using a distortion measure. This measure depends on the difference between the original and quantized images. The average distortion in a quantized image is calculated according to the equation (5.20):

$$D = \frac{1}{N} \sum_{i,j} d(X_{i,j}, q(X_{i,j})) \qquad 5.20$$

where N is the number of pixels in the image, $X_{i,j}$ is the colour of the pixel I, j, $q(X)$ is the quantized colour and $d(X, Y)$ is the distance measure according to the metric used.

On inspection the algorithms used by Goldberg are very similar to those adopted by Fletcher [1991] and as such not sufficient for this research. However, Goldberg does offer results on the evaluation of the performance of the colour quantization techniques based on the distortion measure. NB the distortion measure is a form of the *squared error* function, and as such offers only a partially useful measure of segmentation success, but importantly it is not subjective, therefore it is reproducible.

In a paper by Syeda-Mahmood [1992], colour segmentation methodologies are used to set the likelihood of regions in an image coming from a single object. Syeda-Mahmood uses a method of colour specification by colour categories to design a fast segmentation algorithm to extract perceptual colour regions from the original image. These colour regions are then used for model-driven selection of instances of a model in the image. This approach is comparable to the pattern analysis requirements of the machine vision system for rotary screen fabric inspection. Although, Syeda-Mahmood method is directed towards three-dimensional images (where occlusion, pose, and illumination changes are critical) there is good correlation between it and the primarily two-dimensional fabric inspection.

Colour specification for selection is realized by the partitioning of the RGB colour space into sub-spaces where the perceptual colour is the same (and distinct from other sub-spaces). Syeda-Mahmood [1992] defines these sub-spaces as *perceptual colour categories*. The overall colour of a perceptual colour category is designated as the colour of the majority of pixels, the *dominant colour*. From psychophysical studies of RGB colour space, Syeda-Mahmood states that 220 different colour categories were sufficient to describe the colour space. Once the RGB colour space has been subdivided into these perceptual colour categories image segmentation can be carried out.

The algorithm for colour image segmentation uses a three-pass approach. First, all the image pixels are mapped to their corresponding perceptual colour category. Next, pixels belonging to the same category are grouped. Finally any interleaved groups that are of compatible colour categories are merged. Grouping is achieved by subdividing the image into windows (bins) and processing each window using a connected component algorithm (cf. Pietikäinen, *et. al.* [1986], discussed previously). Similarly the windows approach is used to merge interleaved groups.

This paper offers yet another approach to image segmentation by using a pre-segmented RGB colour space. Syeda-Mahmood argues that this perceptual-based segmentation remains stable under changes in illumination. Also, that since the perceptual categories depend on the colour space they are image independent. This allows preprocessing of the image from more than sixteen million colours to just 220 colours that can then be further segmented in stages 2 and 3 of the algorithm. No experimental proof is presented in the paper to qualify these statements, but pre-partitioning the RGB colour space may have further implications for colour machine vision systems.

Another method for the segmentation of colour images, this time using normalized colour, is suggested by Healey [1992]. Healey examines the suitability of several existing colour segmentation techniques, e.g. the clustering approaches to segmentation. He states that these clustering techniques suffer from several disadvantages, identifying problems in pixel classification in real images, where colour clusters may overlap. Also, Healey implies that surface texture when viewed under different geometric conditions will produce different clusters in colour space, thus causing incorrect colour assignment. This is important to the rotary screen printing research, where by the nature of the fabric presentation (moving blanket) different geometric conditions will occur. However, the textural effects of the fabric are reduced by reducing the angle between the light source and the perpendicular to the fabric surface (cf. Section 4.3.2 on Front Lighting).

Healey [1992] also examines the region splitting method for colour segmentation that involves splitting the image into smaller and smaller pieces until each piece is unique in some property. Generally, he found that the region splitting algorithms he scrutinized were inappropriate for colour segmentation for several reasons. Approaches that used global histogram information tended to miss small image regions because they do not produce strong peaks in the histogram. Another problem is that region splitting does not deal well with scene geometry, i.e. curved surfaces of a single material of a unique colour may be segmented into separate regions due to variations in surface reflection. This is not a problem for the research in rotary screen fabric inspection as it is inspecting a nominally two-dimensional surface.

Healey [1992] identified that for most images, sensor noise and surface texture would cause variations in perceived colour values. He reasoned that these variations need to be characterized accurately. To achieve this he proposed that the image be normalized using Bayes decision theory to reduce the error rate. For segmentation purposes Healey rationalizes that a change in colour in the image (in his case due to a new object) will cause an irradiance discontinuity.

The first step of the segmentation algorithm suggested by Healey performs an edge detection pass on the image. This should identify any irradiance discontinuity, therefore, defining areas of the same colour. The next pass of the segmentation works in a similar manner to region splitting methods, by examining increasingly smaller regions of the image. When processing a region, Healey surmises that regions containing edge pixels from the first pass may correspond to more than one colour in the image. Such regions are split into sub-regions and reprocessed. Conversely, if a region contains no edge pixels, the region is assumed to correspond to a single colour.

After image splitting each region (determined as single colour) is normalized. Accordingly, for a region R, a mean normalized colour vector v_R is computed (Equation 5.21):

$$\hat{v}_R = \frac{\sum_{S \epsilon R} S}{\left\| \sum_{S \epsilon R} S \right\|} \qquad 5.21$$

where each S is a measured sensor vector in R. In equation 5.21, $\|\cdot\|$ is used to denote the L^2 norm. We define the L^2 normalization as follows;

Let $S = (s_0, \ldots, s_{N-1})$ denote the measured sensor vector at a point in the image and let $\hat{S}$ denote the L^2 normalization of the sensor vector (Equation 5.22):

$$\hat{S} = \frac{S}{\sqrt{s_0^2 \cdots + s_{N-1}^2}} = (\hat{s}_0, \cdots, \hat{s}_{N-1}). \qquad 5.22$$

Next the pixels in region R are assigned a label corresponding to the class for which they have a minimum error rate (Bayes Theorem). Once the window size has been reduced to four pixels or less, they are then merged with a spatially adjacent class. This prevents the formation of new classes or formation of isolated regions of an existing class. The final pass of the segmentation, is when the window size is one pixel. The edge data is eliminated and edge pixels are merged with a spatial adjacent class for which they have a minimum error rate. Pixel classification is complete when every pixel has been assigned a label.

Healey [1992] offers experimental results as images before and after segmentation. Although the segmentation appears visually convincing there is no measure of the degree of successful pixel assignment. This approach to colour segmentation offers a reasonable alternative to existing methods, but as Healey states it is only a general segmentation algorithm and is weighted towards three-dimensional colour scene segmentation. As such it is not an ideal strategy for segmenting specific case, in particular rotary screen printed fabrics.

Also in 1992, Huang, Cheng, *et. al.* [1992] presented a new hybrid segmentation method for colour images. This method combines the scale-space filter (SSF), as proposed by Lim, *et. al.* [1990], and the Markov random field (MRF) approach. The SSF is used to find the local extrema of the derivatives of a scale-space image resulting from the Gaussian convolution of the histogram of the original image. This scale-space image is then separated into regions corresponding to peaks and valleys.

SSF is used to perform coarse image segmentation, and then the MRF method is employed to provide fine segmentation. For MRF-based segmentation to work the image needs prior segmentation (provided by the SSF) method so that it can fine segment to the global minimum. The MRF relies on each pixel in an image having some relationship with other pixels (this is a form of connected component processing). The SSF is fundamentally a histogram-based segmentation method (cf. first-pass segmentation used in the rotary screen printed fabric segmentation), while the MRF is a neighbourhood-based segmentation.

The SSF uses *scaled* Gaussian functions for histogram smoothing, and generating the scale-space image. When the *scale* is small minor peaks in the histogram will be apparent. As the *scale* increases, the smaller peaks will disappear, and finally the curve becomes a horizontal line. The histogram can then be determined by $f(x)$ where x is the value of the grey level and $F(x, \sigma)$ the scale-space function (Witkin, [1984], also cited in Huang, *et. al.* [1992]) (Equation 5.23):

$$F(x,\sigma) = f(x) * g(x,\sigma)$$
$$= \int_{-\infty}^{\infty} f(u) \frac{1}{\sigma\sqrt{2\pi}} \exp\left[-\frac{(x-u)^2}{2\sigma^2}\right] du \qquad 5.23$$

where ' * ' denotes the convolution with respect to x. Equation 5.23, shows that the convolution of the image and Gaussian function produces the scale-space image. The scale is defined by the standard deviation σ, and F defines a surface in the (x, σ) plane.

Typical to many papers offering colour segmentation solutions Huang, *et. al.* [1992] give no hard evidence of the quality of segmentation. However, they do suggest that the MRF approach would be inappropriate for an on-line machine vision system as it too slow (typically, 4 hours on a 24 MIPS workstation). As such, it is unsuited to the rotary screen printed fabric research. However, the SSF seems effective and as such warrants further investigation.

Wu [1992] presents a novel colour-space segmentation strategy based on observations that the colours of an image have a significant statistical bias along the major axis of the input data. Wu proposes that a colour space be optimally partitioned in this principal direction, rather than bi-partitioning and orthogonal approaches used by many other colour quantization algorithms. By using dynamic programming, Wu suggests that, the total quantization error, in the principal direction can be reduced, and that it gives a five-fold improvement in the TSE over traditional methods. The algorithm works in all colour spaces and can be generalized to other error measures.

It should, however, be noted that Wu's method is for convincing visual representation, without noticeable loss of colour fidelity, of an image on a computer display, and therefore not a true colour segmentation algorithm. Wu identifies a problem common to bi-partitioning algorithms, namely, intermediate subsets are partitioned one at a time in isolation from one another. This means that intercluster interactions are ignored in an attempt to minimize the TSE. Wu's method corrects this problem by simultaneously optimizing the partitioning along the principal axis.

The results of Wu's method in comparison with two other popular colour quantization methods, cited in his paper, are presented in Table 5.2. It is seen from these results that for the

two test images Wu's approach gives an approximate factor of five improvement in quantization error.

	Median-Cut		Wan *et. al.*		Wu	
Colours	Image 1	Image 2	Image 1	Image 2	Image 1	Image 2
16	1328.9	1076.4	1294.6	1138.3	301.9	211.5
32	1228.1	695.7	581.9	466.6	156.3	103.1
64	713.2	343.2	304.1	252.2	78.7	57.3
256	79.5	68.3	69.6	52.6	24.0	20.4

Table 5.2 : Quantization Error of Different Algorithms on Test Images [Wu, 1992]

In 1993, a unified approach to image segmentation was published by Caelli and Reye in the Pattern Recognition Journal [Caelli, *et. al.*, 1993]. This method displayed how colour, texture and shape can be encoded in a single spatio-chromatic feature space, showing how such features can be used to identify image regions via filtering and correlation methods. They propose a new model for spatio-chromatic information processing (see Figure 5.2).

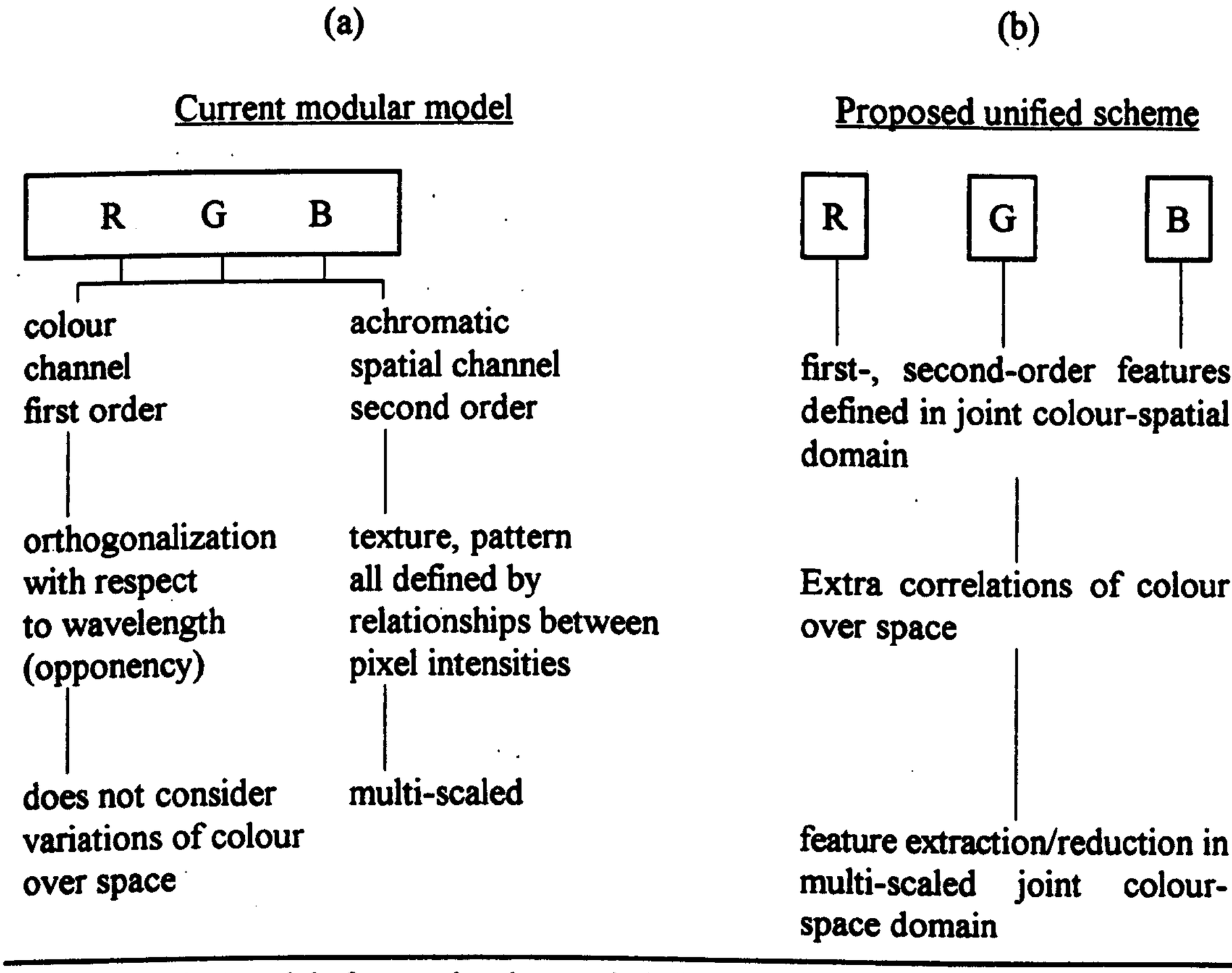

Figure 5.2 : Models for spatio-chromatic information processing (Caelli, *et. al.* [1993])

Caelli, *et. al.* [1993] state that apart from a few cases, the processing of colour covariances (correlations) over space has been ignored, because it has been believed that spatial correlations are sufficiently encoded by the 'texture' or 'pattern' channels. The later normally defined by second-order (relational) statistics computed over the chromatic (intensity) image. They give two examples in their paper why this traditional approach is suspect. However, apart from identifying a possible problem with the usual approaches to segmentation, their methods are unsuited to this research because of the use of shape and textural information for segmentation. Due to the nature of the fabric the texture is concurrent through each colour region (thus cannot be used to differentiate colour areas). Also the shapes of the colour regions are arbitrary and complex, which can cause difficulties in segmentation.

Liu and Yang [1994] present a multi-resolution method for colour image segmentation. Similar to the algorithm proposed by Huang, *et. al.* [1992] it uses the SSF and the MRF algorithms for segmentation. As such it offers little new information and can be viewed as a supporting paper to the work carried out by Huang, *et. al.* [1992]. However, unusually, they do identify the need for consistent evaluation criteria for image segmentation, declaring that most image segmentation results are evaluated visually and qualitatively. Therefore, to evaluate segmentation results scientifically, they developed quantitative methods.

To evaluate segmentation results, both locally and globally, Liu, *et. al.* [1994] define a novel evaluation function F defined as (Equation 5.24):

$$F(I) = \sqrt{R} \times \sum_{i=1}^{R} \frac{e_i^2}{\sqrt{A_i}} \qquad 5.24$$

where I is the image to be segmented, R, the number of regions in the segmented image, A_i, the area, or the number of pixels in the ith region, and e_i, the colour error of the region I. This colour error is the sum of the *Euclidean* distance of the colour vectors between the original and segmented image for each pixel in the region. The term $\sqrt{R}$ is a global measure that penalizes a segmentation that forms too many regions, while the term $e_i^2/\sqrt{A_i}$ is a local measure that penalizes small regions or regions with a large colour error.

Later in 1994, a paper was published by Uchiyama and Arbib [1994] that uses competitive learning strategies to achieve colour segmentation. Like many other colour segmentation approaches the method uses clusters based on the least sum of squares criterion to divide the colour space into segmentation regions.

Uchiyama, *et. al.* [1994] identify the problems with multiple histogram-based thresholding schemes. These schemes divide colour space by thresholding the histograms of each axis.

However, since thresholding is an approach for dividing grey-scale images (i.e. one-dimensional axes) it is not appropriate for multi-dimensional colour images. When applied to colour images it produces rectangular clusters (Figure 5.3a). A method better suited to multi-dimensional clusters is the Voronoi tessellation (Figure 5.3b), in which each position in space belongs to the nearest weighted vector W_i. This is a form of vector quantization by weight vector. If the quantization error is minimum in all possible W_i, this division becomes clustering based on the least sum of squares criterion.

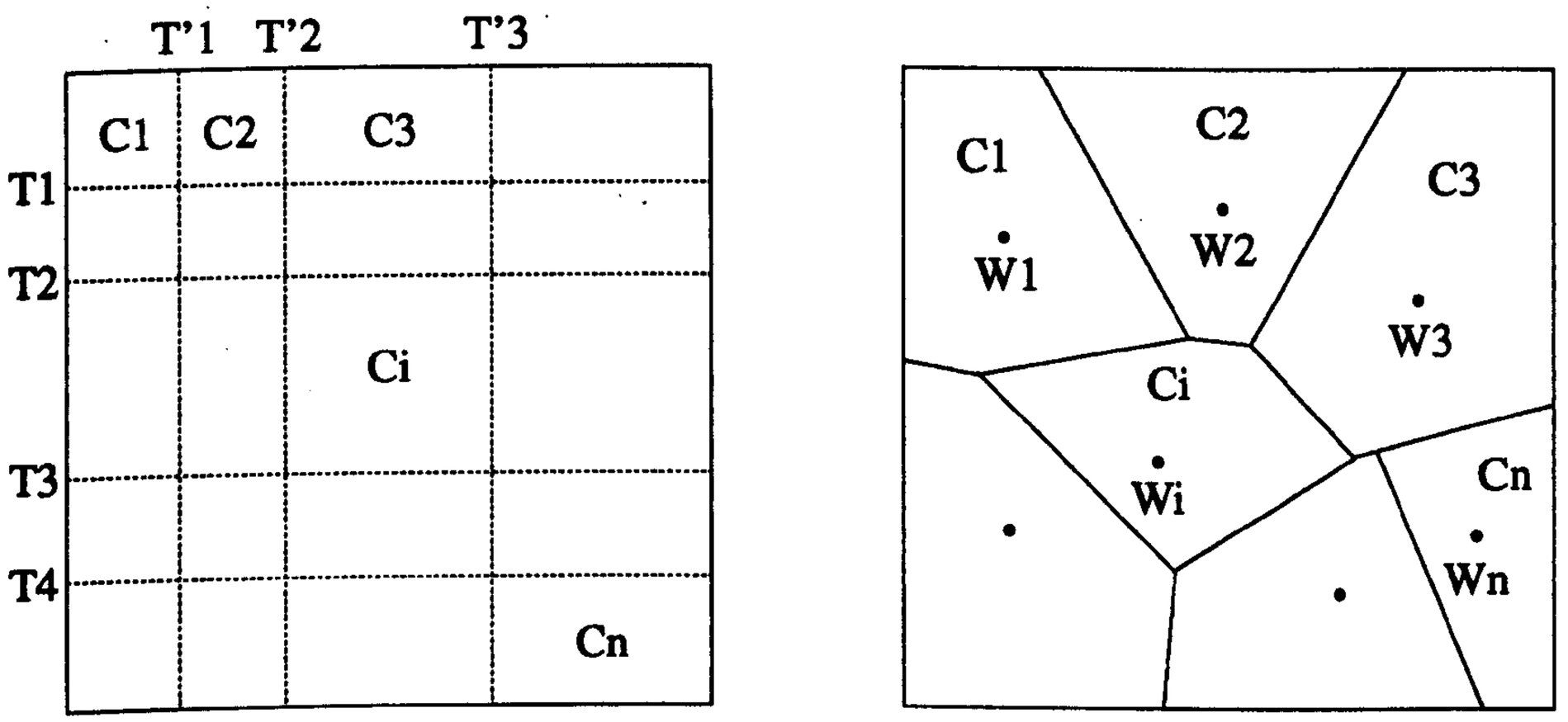

Figure 5.3 : Division of 2-D data

The rationale for using competitive learning for clustering given by Uchiyama, *et. al.* [1994] is that competitive learning converges to an equilibrium regarded as the solution of the vector quantization problem. They show in the paper that clustering can be replaced by vector quantization, hence competitive learning can realize clustering. Their algorithm is summarized as follows:

1) *Initialization*

2) *Competitive learning*

a) Select one input vector X randomly from $\mathcal{X}$ (set of input vectors). Decide a winner derived from input vector X. A unit that is closest to X in the squared *Euclidean* distance $\|X-W_i\|^2$ is chosen as a winner W_{winner}. (If there are several such units one is chosen at random.)

b) Update the weight vector of winner W_{winner} by $\Delta W_{winner} = \tau(X-W_{winner})$

where τ is the learning rate of competitive learning. Add 1 to *wincount* of winner.

c) If a winner's *wincount* = θ_t (and number of units < n), then generate a new unit with the same W as the winner and clear the *wincount* of both to 0. (Where θ_t is the threshold of counts, and n is the maximum number of units).

d) Add 1 to N_R. If ($N_R = N_{max}$), then stop competitive learning, else continue competitive learning from a).

3) Clusters $\mathcal{C}$ are determined by Equation 5.25:

Let X_j ($j = 1, \cdots, m$), C_i ($I = , \cdots, n$), W_i ($I = , \cdots, n$) ($m > n$) be a finite number of input vectors (=$\mathcal{X}$), clusters (=$\mathcal{C}$), and weight vectors (=$\mathcal{W}$), respectively. A partition function $\mathcal{C}_f(\mathcal{W})$, is defined that is a Voronoi tessellation determined by weight vector $\mathcal{W}$ in Figure 5.4 as:

$$X_j \in \text{ iff } \forall\ k(k \neq i)\ \|X_j-W_i\|^2 < \|X_j-W_k\|^2 \qquad 5.25$$

Uchiyama, *et. al.* [1994] theoretically show that competitive learning converges to a local optimum solution of clustering based on the least sum of squares criterion. However, they only show the efficiency of the competitive learning strategy on grey scale images. This is an interesting solution to the colour clustering dilemma.

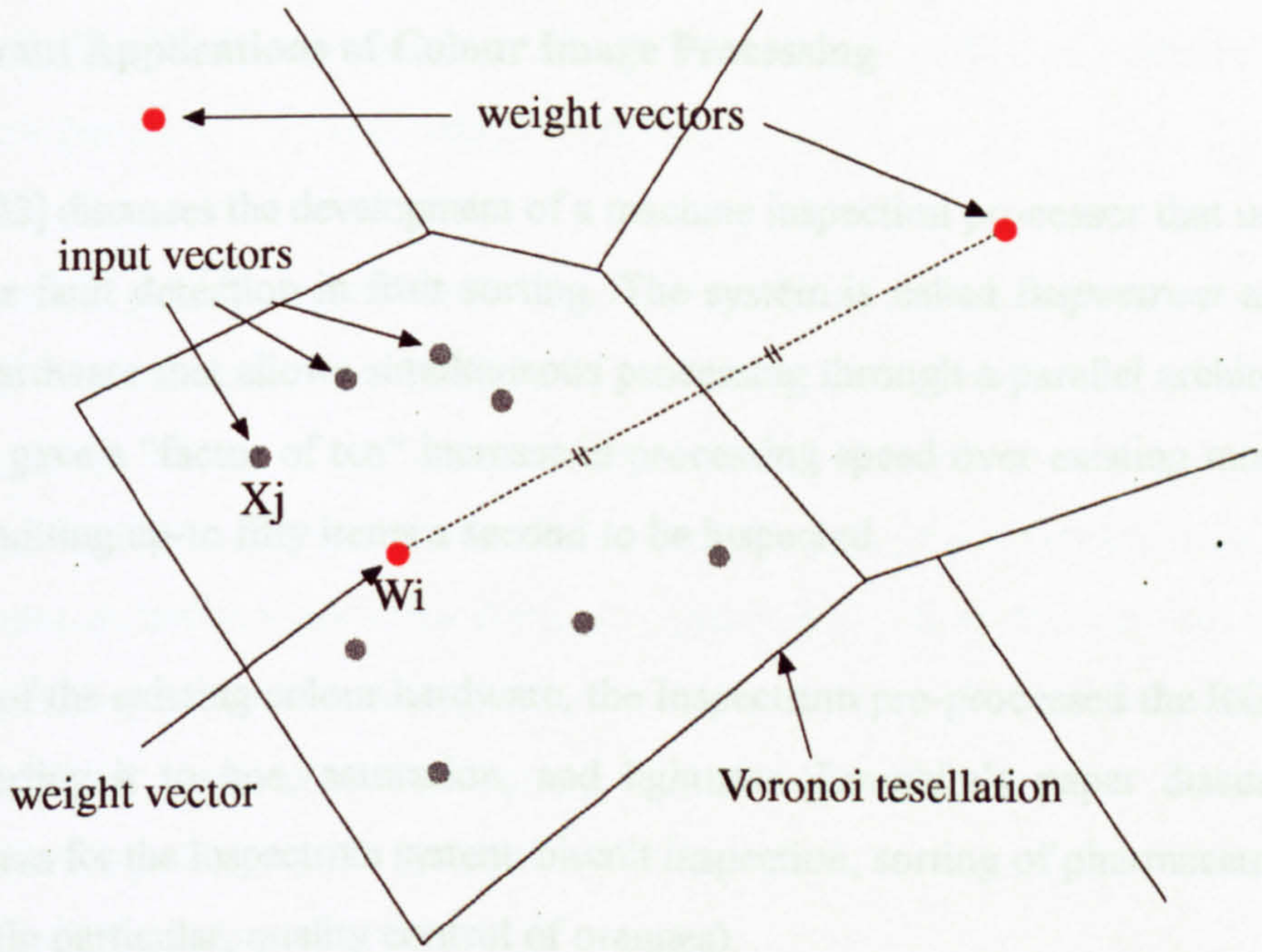

Figure 5.4 : Vector quantization

This section has shown that various approaches to colour segmentation algorithms have been made. However, as can be seen in Chapter 7, these algorithms vary greatly in their performance. Although some come close to the efficiency of the algorithm developed by this research they all suffer from a common problem — they are generic solutions, whereas the research algorithm is specific. In fact, most of the algorithms referenced were designed for generic natural scene analysis, which differ greatly from the colour groupings seen in rotary screen fabric images.

5.2.2 Relevant Applications of Colour Image Processing

Loughlin [1982] discusses the development of a machine inspection processor that uses colour as a basis for fault detection in fruit sorting. The system is called *Inspectrum* and it uses specialized hardware that allows simultaneous processing through a parallel architecture. At the time this gave a "factor of ten" increase in processing speed over existing monochrome systems, permitting up-to fifty items a second to be inspected.

Unlike most of the existing colour hardware, the Inspectrum pre-processed the RGB camera signal converting it to hue, saturation, and lightness. Loughlin's paper discusses three application areas for the Inspectrum system: biscuit inspection; sorting of pharmaceuticals; and fruit sorting (in particular, quality control of oranges).

The application of biscuit inspection used the Inspectrum to examine biscuits for an incomplete covering of chocolate. To facilitate this, the biscuits are presented to the inspection system on a white conveyor belt, simplifying the segmentation of the biscuit from the background. It is assumed that the chocolate covering and biscuit base have a similar hue value. Therefore, this element is discarded. Fault detection is carried out by analysing the saturation and lightness values of each biscuit, finding areas that are outside predefined (set by the operator) tolerances.

The Inspectrum system is also used to determine bake quality of the biscuit before it is coated with chocolate. Again, the hue value is ignored and the biscuit is inspected against predefined tolerance identifying the acceptable level of 'brownness'. The assumption being the lightness and saturation values of the biscuit will alter as the biscuit becomes browner. After processing the fault report is given as a binary image, where faulty biscuits are displayed as white on a black background. Obviously, these results could be connected to an automatic rejection system.

Unlike the biscuit application, the Inspectrum system relies on hue information for pharmaceutical sorting. In this application two types of tablets of different colour (hue) need

to be separated. This is a simple inspection task if the tablets are sufficiently different in colour to allow peak separation in a basic histogram threshold.

Fruit inspection is a popular machine vision application. The Inspectrum system was used for determining whether oranges were ready for picking. Ripeness was determined by a narrow hue specification (only orange oranges should be selected), as well as having lightness and saturation values within preset tolerances. It is critical that the orange should be picked at its optimal ripeness, as unlike many other fruits, oranges stop ripening after picking. Obviously, there are many problems when inspecting the fruit on the tree, due to changes in shading, ambient lighting, and obscuration from foliage, each of which can affect the colour. Loughlin [1982] does not adequately explain how these difficulties were overcome and as such, the paper must be regarded as academically irrelevant.

Krey, Ayache, *et. al.* [1984] proposed a colour-based system for fruit sorting. The system was designed to sort green and red apples on up-to sixteen conveyor-belts at a time. It analysis the whole surface of the fruit, thus avoiding problems with any non-homogeneity in the apples' colour. The system actually uses monochrome cameras with (single) optical filters (maybe a polarizer) and differentiates between apples by examining the grey level histogram of the fruit. The calculated mean variance of the histogram data is then used to categorize the fruit.

Obviously this approach of colour segregation is too simplistic for the inspection of rotary screen printed fabrics. Yet, it suggests that the mean and variance information from this histogram may be used as an aid to colour discrimination. No experimental evidence, is presented in the paper. Although, Krey, *et. al.* [1984] claim that their prototype system can sort five fruit per second on each conveyor-belt with a less than 5% error rate.

A method for segmenting blue-dyed areas from an image, was suggested by Crabtree, Ehrlich, and Prince [1984]. The goal of the segmentation process was to separate blue-dyed pores, from the background information, in thin sections of reservoir rocks. Image acquisition is through a transmitted light petrographic microscope with an attachment for a monochrome camera. By

using three filtering gels (red, green, and blue) of known spectral response a colour image of the 30 μm thick section is composed. They evaluated three existing, and two new segmentation techniques.

First, and simplest, was segmentation using single-dimensional histograms of RGB components. By looking for peaks and troughs in the histograms threshold levels are then set. It was found that for their samples these histograms tended to uni-modal, or where they were poly-modal the troughs were poorly defined. As such, they found this approach unsuitable for their application.

Another technique examined by Crabtree, *et. al.* [1984] was the use of two-dimensional histograms for pore segmentation: The red, green, and blue signals are combined into three different two-dimensional histograms ((red, blue); (red, green); and (blue, green)). Where the *x-y* plane is the axis for the intensity level of the colour component, and the *z* plane is for the frequency of occurrence of the two dimensional colour signal. Plotting of the image data using this method produces an isometric representation of the two-dimensional histograms.

This method was found to offer reasonable segmentation for images with small pores, but was unacceptable in large pore images. Principally, this is due to the 'ghost' colours that occur at boundaries (such as between the pores and the background matrix). Large pores have many edge points, due to their colour blend, these points obscure the separation of pore and background. An important element of this approach is that it identifies problems caused by colour edge boundaries.

Ohlander, *et. al.* [1978, cited in Crabtree, *et. al.*, 1984], advanced a colour segmentation method for natural scene segmentation, that uses 9 components for quantization. This approach was investigated in relation to the reservoir rock segmentation [Crabtree, *et. al.*, 1984]. The nine components used in Ohlander's segmentation technique include RGB histograms, CIE HSI histograms, and histograms of I, Y, and Q. It was quickly determined that this approach was unsuitable for the reservoir rock problems due to the lack of poly-modality in any of the

histograms. Similarly it is unsuited to the rotary screen problem, as it requires conversion between three separate colour spaces and offers little useful information.

It was realized by Crabtree, *et. al.* [1984] that dyed pore segmentation is, for humans, a trivial visual task. Therefore, they decided to develop segmentation strategies that closely simulate the human visual response, rather than using other *ad hoc* segmentation approaches. The other two approaches of colour segmentation examined by Crabtree, *et. al.* [1984] were methods for enhancing the pores, based on human perception, and as such were too specialized for rotary screen segmentation.

The first novel approach uses blue-red thresholding and the ratio (B-R). As there is a requirement only to separate the blue-dyed pores from the image background, it was decided to discard the green input plane from the image data and use it for storing the results of the segmentation. The final result will be a pseudo-colour, but absolute colour reproduction is not critical.

Experimental results show that the blue-dyed pores rarely fell outside a 15% – 50% intensity range, so pixels outside this range can be excluded from the image data. Further segmentation of the pores from the background image data is then carried out using the blue-red ratio. Pixels that are more bluish tend to be pore related. However, this requires human intervention to set the blue-red ratio threshold and as such is subjective and time consuming (one acceptably segmented image per 15 minutes).

Using HSI information for their second approach, Crabtree *et. al.* [1984] feel offers the best solution as it requires the least amount of human intervention. An approach similar to that developed by Dodkin [1994], showing that the HSI method was suitable for automation. This method defines the blue pore pixels as lying within two angles on the hue histogram (181 – 299°). However, this means that pixels within this hue confine may range from very low intensity (black) to very high intensity (white). Therefore, the use of just the hue histogram is inappropriate.

By adapting the Ostwald colour system (Figure 5.5) it is possible to identify a region of 'visual blue pores' that can be used to segment the image. Non-pore pixels usually possess a high intensity and low saturation value. The segmentation approach is as follows. First the image is segmented on hue values (181 – 299°). Next, these 'blue' pixels are processed and any that fall outside the range 7 – 75% intensities are eliminated. It was found that the saturation and intensity of the remaining pore pixels were related as follows: as intensity varies from 10 – 30%, the minimum saturation varies linearly from 3 – 5%; in the intensity range 30 – 75%, the minimum saturation is 5%. Any pixels remaining after this processing are defined as pore pixels. This approach, although good for single colour segmentation, is unsuitable for a multi-colour segmentation method (as need for rotary screen printed fabrics).

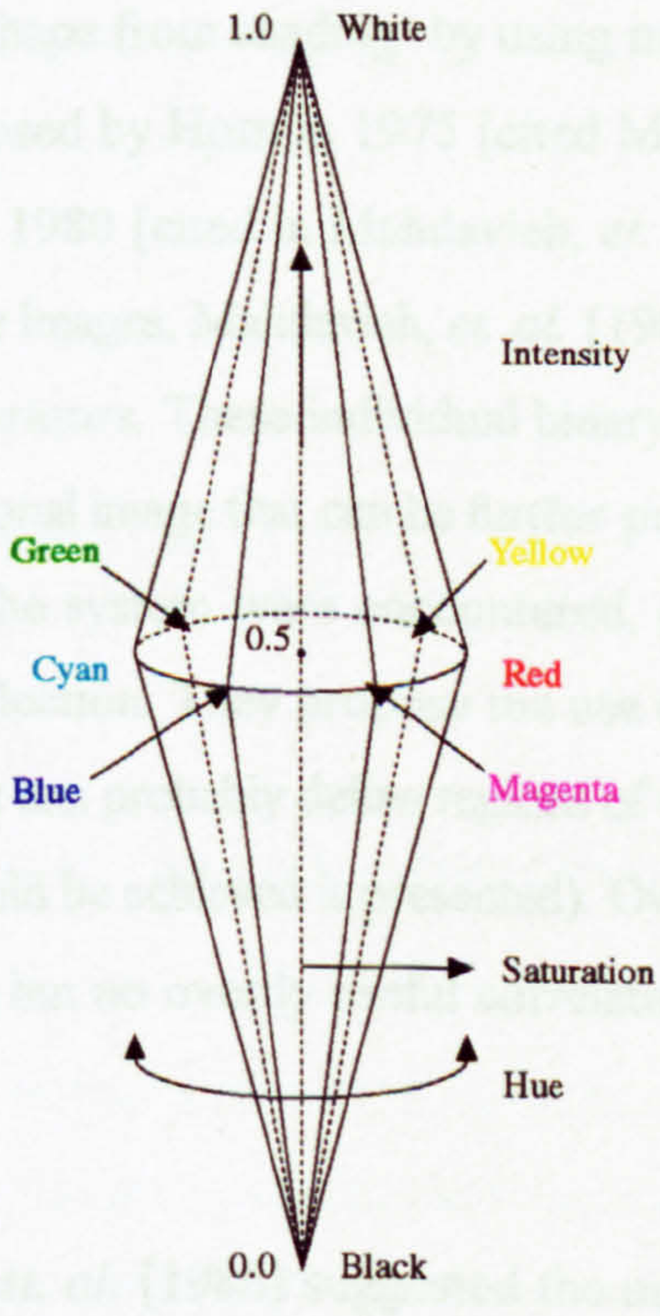

Figure 5.5 : Ostwald Colour System

Verification of the various segmentation approaches examined by Crabtree, *et. al.* [1984], was based on comparisons with visual techniques and as such subjective. Nevertheless, they could

show that the specialized segmentation techniques, that modelled the human visual perception, performed better than the more *ad hoc* techniques.

In 1985, Mahdavieh, Stark, *et. al.* [1985] proposed a colour photometric stereo vision system that enabled fast recognition and inspection of industrial parts. The system that uses a single viewing position could operate in low contrast environments. This meant that grey-level information alone was not sufficient to discriminate between an object and its background. Therefore, a colour system is used. To achieve this multiple colour light sources are used. These produce coloured shadows that allow a discriminatory approach to silhouetting by using height profiles.

The notion of extracting 'shape from shading' by using multi-coloured light sources was not new, originally being proposed by Horn in 1975 [cited Mahdavieh, *et. al.*, 1985] and further expanded by Woodham in 1980 [cited in Mahdavieh, *et. al.*, 1985]. By treating each of the RGB planes as monochrome images, Mahdavieh, *et. al.* [1985], could isolate the shadow areas using standard gradient operators. These individual binary images could then be combined to give a pseudo three-dimensional image that can be further processed to define the object shape. However, problems with the system were encountered, particularly in an environment that exhibits strong specular reflection. They propose the use of a fourth light source to eliminate this problem, implying that it can probably define regions of strong specular reflection (although no evidence of how this would be achieved is presented). Overall, this is an innovative approach to colour image processing but no overtly useful correlation between it and the research area can be discerned.

In 1986, Harms, Gunzer, *et. al.* [1986] suggested the use of local colour and texture as an approach for stained blood cell analysis. They combine colour and texture information to classify areas of the image as *textons* (the smallest texture grains). These textons can then be analysed using common image processing and pattern recognition techniques. Each texton is then colour coded by calculating their average colour coordinate, using a non-linear coding system. The first step is to normalize each pixel in the image compared with the brightest region

in the picture. This procedure reduces the inherent variations due to the dynamic response of the camera. Once normalized the pixels are then converted into the standard CIE colour coordinate system XYZ. Figure 5.6 shows a block diagram of the colour and texture processing used by Harms, *et. al.* [1986]. Their approach offers little benefit to the rotary screen printing research.

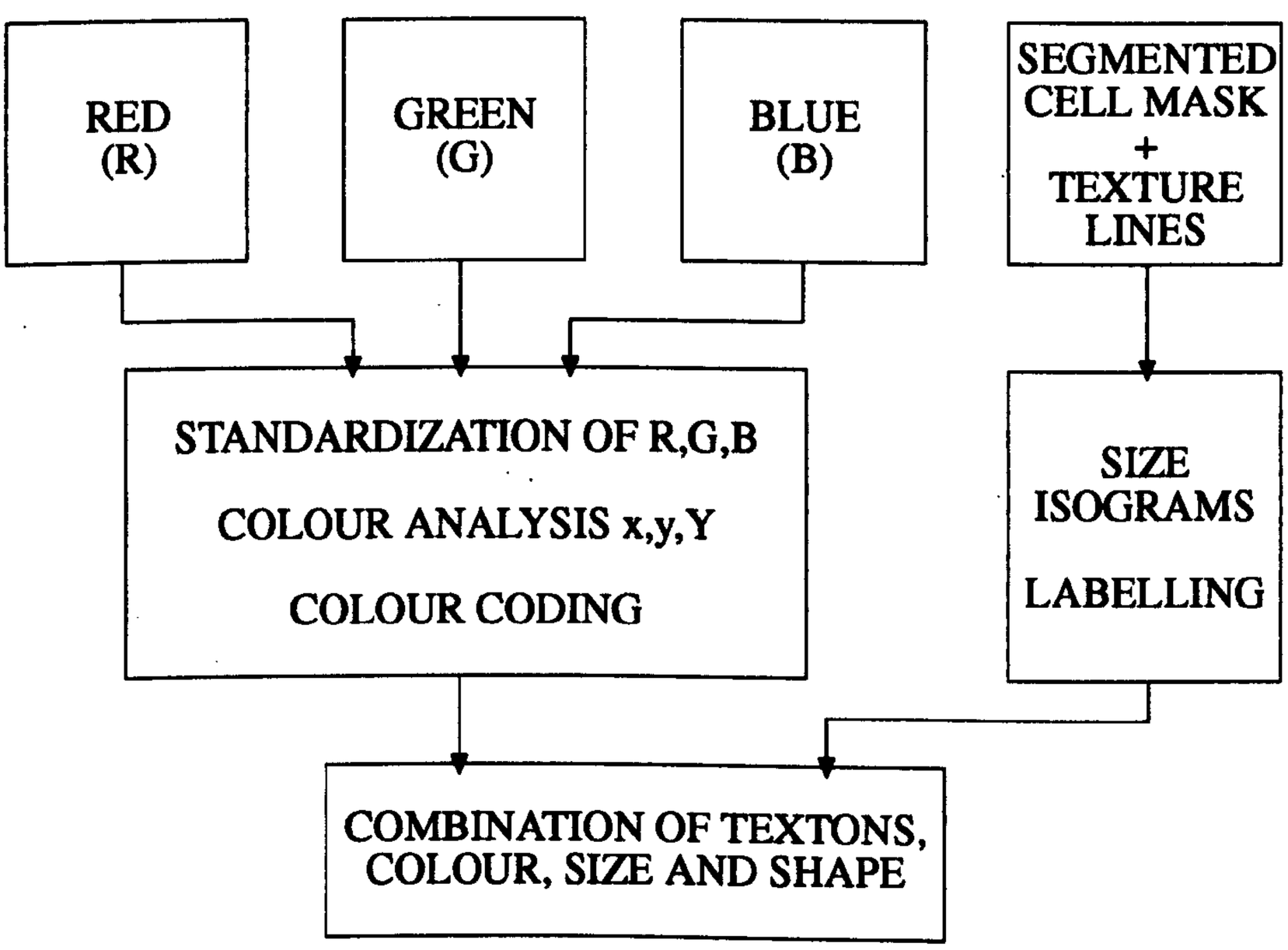

Figure 5.6 : Block diagram of colour and texture processing used by Harms, *et. al.* [1986]

A system with a similar aim to that proposed by Krey, *et. al.* [1984], was advanced in a paper by van Renesse [1990]. This paper examines the feasibility of using colour image processing techniques for the grading and sorting of apples with respect to ripeness and quality, (Apple Quality And Ripeness Inspection System — AQUARIS). Classification of ripeness involves the local detection of colour of apples of different ripening behaviour. Inspection for quality requires the detection and grading of surface defects such as bruising and rot.

The solution submitted by van Renesse [1990] was to compare the spectral responses of apples being inspected against a database of 'perfect' apples. Evaluation of the spectra of apples has shown that quality and ripeness can be characterized using three spectral wavebands. These wavebands are: the chlorophyll band (570 nm); the ripeness band (640 nm); and the near infra-red (beyond 750 nm). By using the reflection ratio of the chlorophyll band and the ripeness band an indication of ripeness can be obtained. This is based on the premise that, during ripening, chlorophyll decomposes while ripeness colour increases.

Detection of defects is done by analysing the spectral response for the near infra-red band. Experimental evidence has shown that defects have a lower spectral response in the near infra-red when compared with a healthy surface. The rationale for this is that the presence of defects is accompanied by the chemical decomposition of the different fruit dyes in the skin. These dyes show reflectance in the near infra-red.

Although, AQUARIS uses colour image processing techniques to characterize the apples, it is a specific optical solution to the problem. As such, it is not suited for adaption to the more generic colour processing requirements of this research. For applications requiring colour differentiation between a small set of, *a priori* known colours, it offers a sensible hardware-directed approach.

In 1991 Gunawardena, Clark, *et. al.* [1991] developed a system that uses colour detection as a method for quality inspection of agricultural produce. The principal aim of the system was to sort and route tomatoes to their appropriate output grades depending on their ripeness and size. This quality control approach is directly comparable to the methods proposed by van Renesse [1990] and by Krey, *et. al.* [1984], for ripeness testing of apples.

They identify that use of uni-dimensional thresholding to define the systems region of colour acceptance in unacceptable. Stating, the high degree of ambiguity between colours detected. Especially if the region occupied by the target colour in colour space is non-rectangular, which is commonly the case. Gunawardena, *et. al.* [1991] propose the use of multi-dimensional look-

up tables to identify spatial areas that contain the target colour. They use conventional colour television primaries (red, green, and blue) to define the three axes of the colour cube. Then by training the system on a known sample colour, a three-dimensional region of arbitrary shape and size can be defined within the look-up table and set to logic 1. The undefined region of the colour space is then set to logic 0. This is a similar approach to the second pass segmentation used by the research, but the research defines multiple regions of colour within the look-up table.

Addressing of the look-up table is achieved using the tri-vector signal from the RGB camera. When a pixel with coordinates within the defined colour region is passed to the colour space a logic 1 is output, (otherwise the output is logic 0). This gives a binary image where only the areas on the input image that matches the trained colour are highlighted. By incorporating the look-up table in hardware real-time image segmentation can be achieved. Again, this is similar to the proposed solution to the research's segmentation application. No information detailing the degree of successful colour segmentation is offered, so although the approach appears logical it cannot directly be assessed in relation to other segmentation techniques.

5.2.3 Other Papers

Equitz [1989], advances a new vector quantization clustering algorithm. Clustering, as can be determined from section 5.2.1, is a commonly used approach to segmentation. This paper is relevant to this research as it offers an alternative to the standard Linde-Buzo-Gray (LBG) algorithm. Equitz defines a Pairwise Nearest Neighbour (PNN) algorithm for vector clustering that derives a vector quantization codebook, which he claims is inherently faster than previous methods (5% of the time taken by existing LBG algorithm); an important consideration when developing an on-line system for colour segmentation. The PNN algorithm can also be used with TSE and WTSE distortion measures.

The PNN is presented as a substitute for the LBG algorithm, although Equitz [1989] then goes on to state that the algorithm can be used as an initializer for the LBG algorithm. As such it providing better performance than either algorithm can achieve separately. The PNN begins with a separate cluster for each vector in the training set and merges two clusters at a time until the desired codebook size is achieved. At the start of the clustering process N clusters, each containing one vector, are merged to the optimal (N - 1) clusters, by merging into a single cluster the two closest training vectors. The cluster is then relabelled as the centroid value of its two component vectors. Clusters are then further combined by merging the two clusters that result in the best tradeoff between merging close clusters and affecting fewer training vectors. These clusters can be calculated as follows (in Equations 5.26 - 5.35) given the following notation:

C_i = ith cluster of training vectors

C_{ij} = cluster formed by merging ith and jth clusters

n_i = number of training vectors in C_i

n_{ij} = number of training vectors in C_{ij}

$\bar{x}_i$ = centroid (mean) of the training vectors C_i

$\bar{x}_{ij}$ = centroid (mean) of the training vectors C_{ij}

S_i^2 = average squared error between $\bar{x}_i$ and the training vectors in C_i

S_{ij}^2 = average squared error between $\bar{x}_{ij}$ and the training vectors in C_{ij}

$\langle x, y \rangle$ = inner product of x and y,

then

$$n_{ij} = n_i + n_j \tag{5.26}$$

$$\bar{x}_{ij} = \frac{n_i \bar{x}_i + n_j \bar{x}_j}{n_i + n_j} \tag{5.27}$$

$$n_{ij} S_{ij}^2 = \sum_{x \in C_{ij}} |x - \bar{x}_{ij}|^2 \tag{5.28}$$

$$= \sum_{x \in C_i} |x - \bar{x}_{ij}|^2 + \sum_{x \in C_j} |x - \bar{x}_{ij}|^2, \tag{5.29}$$

where

$$\sum_{x \in C_i} |x - \bar{x}_{ij}|^2 = \sum_{x \in C_i} \left(|x|^2 - 2 \langle x, \bar{x}_{ij} \rangle + |\bar{x}_{ij}|^2 \right) \tag{5.30}$$

$$= n_i \left(S_i^2 + |\bar{x}_i|^2 \right) - 2 n_i \langle \bar{x}_i, \bar{x}_{ij} \rangle + n_i |\bar{x}_{ij}|^2 \tag{5.31}$$

$$= n_i S_i^2 + n_i |\bar{x}_i - \bar{x}_{ij}|^2 \tag{5.32}$$

$$= n_i S_i^2 + n_i \left| \frac{n_i \bar{x}_i + n_j \bar{x}_i - n_i \bar{x}_i - n_j \bar{x}_j}{n_i + n_j} \right|^2 \tag{5.33}$$

$$= n_i S_i^2 + n_i \left| \frac{n_j \bar{x}_i - n_j \bar{x}_j}{n_i + n_j} \right|^2 \tag{5.34}$$

$$= n_i S_i^2 + \frac{n_i n_j^2}{(n_i + n_j)^2} \cdot |\bar{x}_i - \bar{x}_j|^2. \tag{5.35}$$

Equation 5.35, can be further reduced to give an expression for the squared error introduced by C_i and C_j. For PNN the clusters that minimize the squared error are chosen for merging.

This approach is similar to the one developed independently for the rotary screen fabric inspection research, as it provides a fast, powerful non-iterative way to generate vector quantization codebooks (cf. hashed codebook production for three-dimensional RGB segmentation).

5.3 Conclusions

At the start of this research (early nineties) there were a limited number of papers on colour segmentation. These papers were either purely theoretical, or industrial papers based on specific cases. Colour image processing has only recently developed greater significance in the field of image processing. Early tendencies were to use the well-established rules of colour science and apply them to colour inspection systems. However, it was not until the mid-eighties that Pienkowski and Dennis [1985] identified the need to challenge this traditional view. Since then a more computer-orientated technique to colour analysis has taken form.

The nineties showed a significant increase in the number of colour segmentation papers. As the awareness of the importance of preprocessing image data has risen, so has the number of papers on segmentation methodologies. A noticeable preference for fuzzy logic and clustering algorithms has emerged. Importantly, this supports the decision taken independently during this research to use a fuzzy logic and clustering approach. Although, the field of colour segmentation is still in its infancy, it is expected that the next five years will see it mature into a well researched and developed field.

It should also be emphasized that most of the colour segmentation/quantization algorithms were designed specifically for visual display. As such, their success is based on producing a visually convincing representation of the original image. This is not necessarily the best approach for a computer-based inspection system, although it can be argued that the final product only needs to satisfy inspection by a human observer. Nevertheless, an algorithm that

observes visual perception rules may be overly complex, or limiting, for a machine vision system and this factor needs to be addressed.

Another fact that was obvious on examining the papers relating to colour segmentation methods was the lack of any standardized method of evaluating the qualitative or quantitative success of the algorithms. A *de facto* method that occurs in several papers is based on a form of the *squared error* function: a distortion measure [Fletcher, 1991]; a probability of error function [Lim, *et. al.*, 1990]. This approach is of some use as it is not subjective, therefore it is reproducible.

6 Methods for RGB Colour Space Segmentation

6.1 Introduction

Early in this research it was determined that colour segmentation of the pigment printed fabric was highly desirable as it would facilitate the faster processing requirement for on-line inspection by a colour machine vision system. Pigments, unlike colour dyes, are relatively opaque. This factor is useful for segmenting the printed image into its constituent colours. When two or more dyes are overprinted they produce a tone that is a blend of its constituent colours. However, pigment printed designs are composed of fewer colour blends therefore simplifying the segmentation process. In simple terms, the colour values of darker pigments printed over lighter pigments will approximate to those of the darker pigments (due to their opaque nature). More translucent lighter pigments printed on a dark background will have a constituent of the background colour. This is not problematical as the colour shift from the pigment is usually small [Dodkin, *et. al.*, 1993].

Pigment printed designs use dithering[1] to create the perception of colour blends. Blending of colours is, therefore, primarily due to the accommodative process of the eye-brain mechanism. Typically, a machine vision system has no visual rules for accommodative blending. Therefore, an artificial intelligence approach (to simulate accommodation) is not needed, as the machine vision system is not required to have an appreciation of blending.

With these factors in mind, reducing the image's constituent colours from the possible sixteen million to the unique pigments used in the design is theoretically possible. A segmented image, although containing less colour information, retains the pertinent boundary details. Therefore, the applicability of these segmentation techniques to other images is dependent on the inspection requirement (such as boundary detail or colour fidelity). Factors that have to be

---

1 *A series of dots of different colours in close proximity used to simulate a blend.*

addressed are: the number of levels of colour differentiation required; when do similar colours become sufficiently tonally different ()E) to form a unique colour group [Massen, Volk, 1990][Hunt, 1992][Wyszecki, Styles, 1982].

In fault detection for rotary screen printed fabric the critical information is based upon the intersection of colour groups. If each pigment can be uniquely identified there is no requirement for absolute colour. This factor has lead to the development of colour segmentation algorithms that retain the significant boundary information at the cost of absolute colour fidelity. Even so, the colour fidelity achieved with these methodologies is still excellent, and colours can be uniquely identified within a close tonal range (a few)Es).

Colour segmentation was chosen as it reduces signal processing with minimum loss of pertinent information. For pigment printed rotary screen designs the ideal scenario is the reduction of captured pattern information into its component colours, one for each screen. This method of segmentation would enable the reduction of the image into critical colour groups, while maintaining the significant boundary information.

Software algorithms have been derived for the segmentation of images into distinct colour levels. Two innovative approaches to colour image segmentation have been fully investigated. The first method was an adaption of existing algorithms that use the CIE HSI colour space (see Chapter 3 for further information on colour spaces). The second method uses the RGB colour space to make segmentation decisions. Other colour segmentation approaches were also investigated and are discussed in Chapter 5.2.1 (Colour Segmentation Methodologies).

6.2 The CIE HSI Segmentation Method

It was originally intended to use an adaption of an existing colour segmentation method to achieve colour separation on the screen printed fabric. This approach was proposed by Dodkin, [1994] and uses an orbital search in a modified CIE HSI colour space (that discards the intensity component to produce a two-dimensional colour space) to identify colour groups. Using the cluster information, the image is then segmented into the most commonly occurring colour groups. However, this approach, while successful for correct colour assignment, is computationally expensive due to: the required conversion from RGB to CIE colour space; the intensive cluster finding algorithmic approach. In addition, the discarding of the intensity value is questionable. Also it is now generally accepted that the CIE HSL, HSI, and HSB colour spaces are inappropriate for computational colour work (cf. Chapter 3).

$$R' = \frac{R}{(R+G+B)} \qquad 6.1$$

$$G' = \frac{G}{(R+G+B)} \qquad 6.2$$

$$\theta = \tan^{-1}\left[\frac{(G'-\frac{1}{3})}{(R'-\frac{1}{3})}\right] \qquad 6.3$$

$$S = \sqrt{(G'-\tfrac{1}{3})^2+(R'-\tfrac{1}{3})^2} \qquad 6.4$$

To convert to CIE HSI colour space the R, G, and B components of the video signal from the colour image capture device are first normalised. In an RGB colour system, white occurs when the RGB components are equal (therefore, r=g=⅓) [Asano, Kenwood, *et. al.*, 1986]. The hue (θ) and saturation (S) for each pixel is then calculated using the normalised values (Equation 6.1 – 6.4). These two values give the polar representation of the chromaticity coordinates using white as the origin of the transformation (see Figure 6.1).

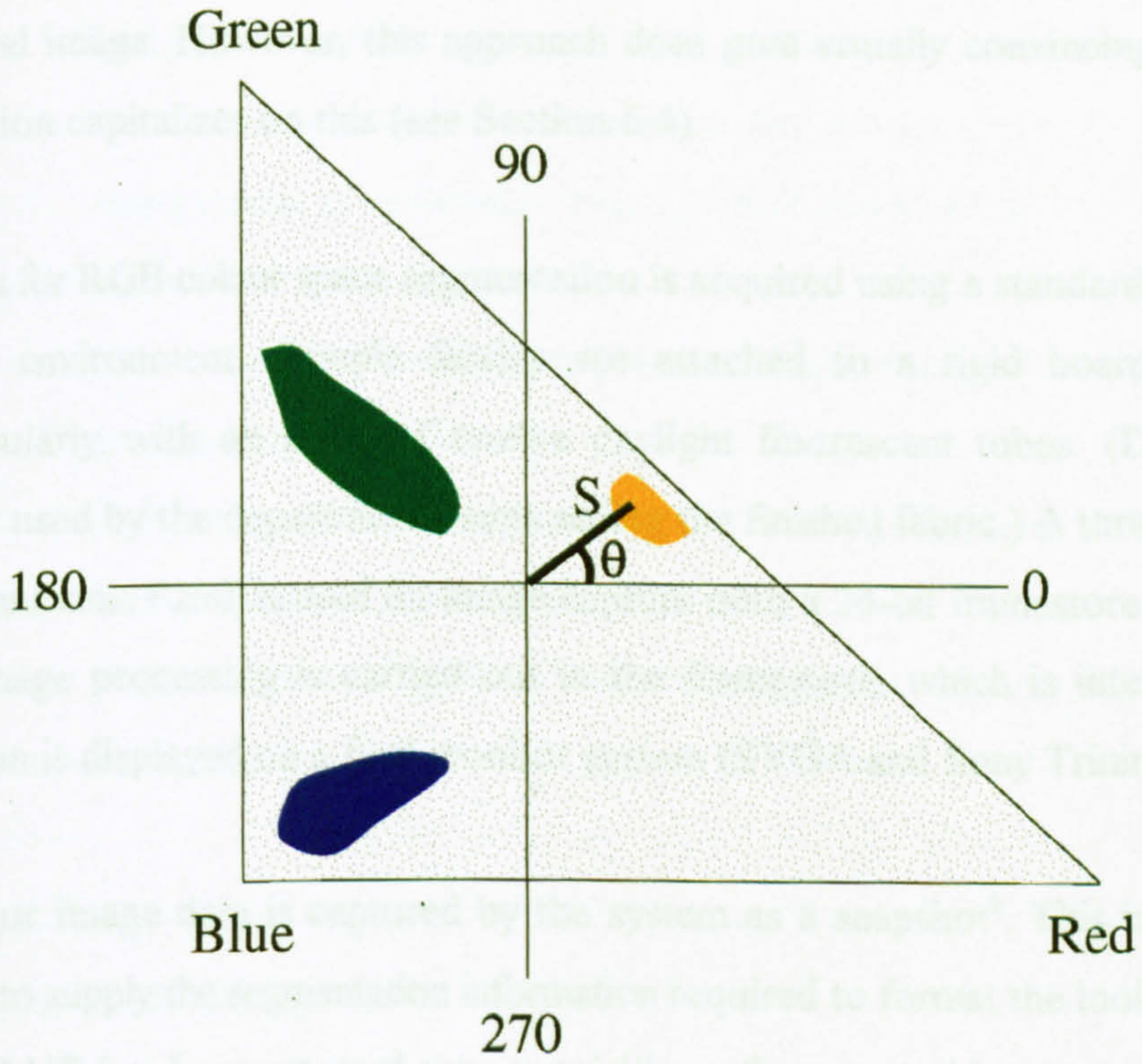

Figure 6.1 : 2D CIE *HSI* Colour Space (intensity ignored)

6.3 Coarse Gaussian-based Segmentation of RGB Colour Space

An alternate method for colour segmentation uses the RGB colour space. This is a more fundamental approach to colour segmentation, unlike most existing methods for segmentation which use some form of transform colour space. As such, this method is tacitly faster as it operates in the RGB colour space (as generated by the camera) instead of a derived colour space, such as the CIE. It was decided that the RGB segmentation approach had a greater likelihood of achieving the requirement of fast on-line segmentation [Blowers, *et. al.*, 1993].

This method can be divided into two sections, coarse and fine segmentation. The coarse segmentation uses a Gaussian-based approach to colour differentiation, but as it is defined by the individual colour planes it can only be described as "coarse". Colour groups resulting from this segmentation are indeterminate, as they do not cross-reference between other planes and

the original image. However, this approach does give visually convincing results. The fine segmentation capitalizes on this (see Section 6.4).

Image data for RGB colour space segmentation is acquired using a standard image processing hardware environment. Sample fabrics are attached to a rigid board and illuminated perpendicularly with an array of twelve daylight fluorescent tubes. (Daylight tubes are commonly used by the department stores selling the finished fabric.) A three-CCD RGB area camera (Panasonic F250) is used for image capture onto a 24-bit framestore (8-bits per colour plane). Image processing is carried out in the framestore, which is interfaced to the PC. Information is displayed on a dual monitor system (SVGA and Sony Trinitron).

Raw colour image data is captured by the system as a snapshot[2]. This information is then processed to supply the segmentation information required to format the look up table (LUT)[3]. Once the LUT has been set *real-time* acquisition of segmented images can take place. The image is simplified with minimum loss of critical boundary information, allowing for the faster processing of registration information.

The stages for segmentation are as follows:

1. Initialisation of image processing system.
2. Capture of a colour image, using RGB CCD camera and image framestore.
3. Determination of critical boundaries for mask production.
4. Application of a boundary mask to the raw colour image.
5. Colour histogram acquisition.
6. *First pass* colour segmentation of the image, using Gaussian derived techniques on the RGB histogram information.

---

2 *A single video frame of data, which can be acquired every 40ms.*

3 *Look up tables are arrays which control the assignment of raw data values.*

7. Initialisation of the *regioned* RGB colour cube, using centroid and standard deviation segmentation values calculated during step 6.
8. Assignment of individual image *picture elements* (pixels) to an RGB colour cube.
9. *Second pass* colour segmentation of the image, using pixel density cube growing algorithms.
10. Assignment of colour *regions* to three-dimensional RGB LUT, allowing unique identification of colour groups.
11. Registration validation of *real-time* segmented images (repeat step 11 until a new pattern).

6.3.1 Initialisation (Stage 1)

The first step of the Gaussian-based segmentation is the initialization of the image processing system. This is essential to ensure realistic segmentation. Ensuring the local buffers of the image processing unit and the RAM cache memory of the computer are reset is important. The system is given a "clean sheet", this is critical for this form of coarse segmentation as the system must not have any preconceptions of what colours to expect. Primarily, this is due to problems that could occur due to inconsistencies between preconceived colours and actual colours as delineated by the environment.

6.3.2 Capture (Stage 2)

After initialization of the image processing system the image information is captured using standard image processing techniques. A single frame from the camera is passed through flash A/D converters and stored as (in this case) a 512×512 8-bit deep pixel image in three separate frame buffers (one for each colour plane). This image data is further processed to derive boundary and colour information as follows.

6.3.3 Boundary Detection (Stage 3)

Once the image is acquired, a copy is made into another framebuffer (this only takes 40ms, a single frame time in a 25 frames/second system). It is this copy of the image that is used for the production of the boundary mask. The elimination of boundary information from the image data (via the mask) before segmentation is important for improving segmentation quality. Principally, this is because of the *'ghost'* colour artifacts that are often found in digitised colour images at colour boundaries.

Ghost colours usually occur when the boundaries of two colours (of varying intensities) fall on the same *photosensitive charge well* on the camera CCD. The camera perceives these two colours to be a blend and thus produces a spurious colour value. Further colour blending at colour boundaries can occur in the framestore when the analogue signal from the camera is digitised. A reduction in the amount of ghost colour production can, therefore, be made by having a direct digital camera link to the framestore. Another reason for ignoring the boundary information when segmenting is that pigment overlapping can occur in these areas naturally during printing. Although pigments are generally opaque, some blending does occur in overlapping areas. However, these blends are extraneous to registration analysis (only the primary pigments need to be segmented, one for each screen). By masking out areas where blending occurs the number of unique colours is reduced, therefore reducing the amount of processing required.

A useful side-effect of the boundary masking is the ability to use the mask information to identify the critical inspection areas for registration. This is an important factor for achieving faster image inspection.

6.3.4 Boundary Implementation (Stage 4)

Boundary mask data is generated from the image information by two 3x3 convolutions followed by *binarisation.* The convolutions first *compress* (Table 6.1) the image intensity information, and then *enhance* (Table 6.2) all remaining boundaries. Compression of the intensity information is used for defining the boundaries that are liable to produce ghost colours (boundaries of high contrast). The boundaries, which are then enhanced, are the areas in which ghost colour are most likely to occur. Binarisation produces an overlay mask that is used with the original image data for colour segmentation [Pietikäinen, Harwood, 1986].

A compression convolution is performed with the following standard averaging convolution linear filter that is then scaled to compress the image intensity range:

1	1	1
1	1	1
1	1	1

Table 6.1: Intensity averaging convolution linear filter.

Enhancement of the compressed image is performed using the following standard *Laplacian* style convolution linear filter:

-1	-1	-1
-1	8	-1
-1	-1	-1

Table 2: Boundary enhancing (Laplacian) convolution linear filter.

Once the image has been compressed and enhanced a standard thresholding algorithm is used to binarize the image. All values above the *cutoff* level (for example, half the maximum

intensities, 127 for a 24 bit colour system) are set to the maximum intensity value (255), while all below the threshold value are assigned to the minimum intensity setting (0).

The mask defined by the convolutions is then overlaid on the raw image data. To carry out this, the mask is first inverted so that edge areas are of minimum intensity value and non-edge information is at maximum intensity. This inverted edge mask is then *logically and*ed to the original raw image and the resultant image stored in a new framebuffer (see Figure 6.2). Further processing can be carried out on the mask before this stage to allow for the *dilation* of the boundaries, which is particular useful in highly textured or pastel designs where the exact boundary point is ambiguous.

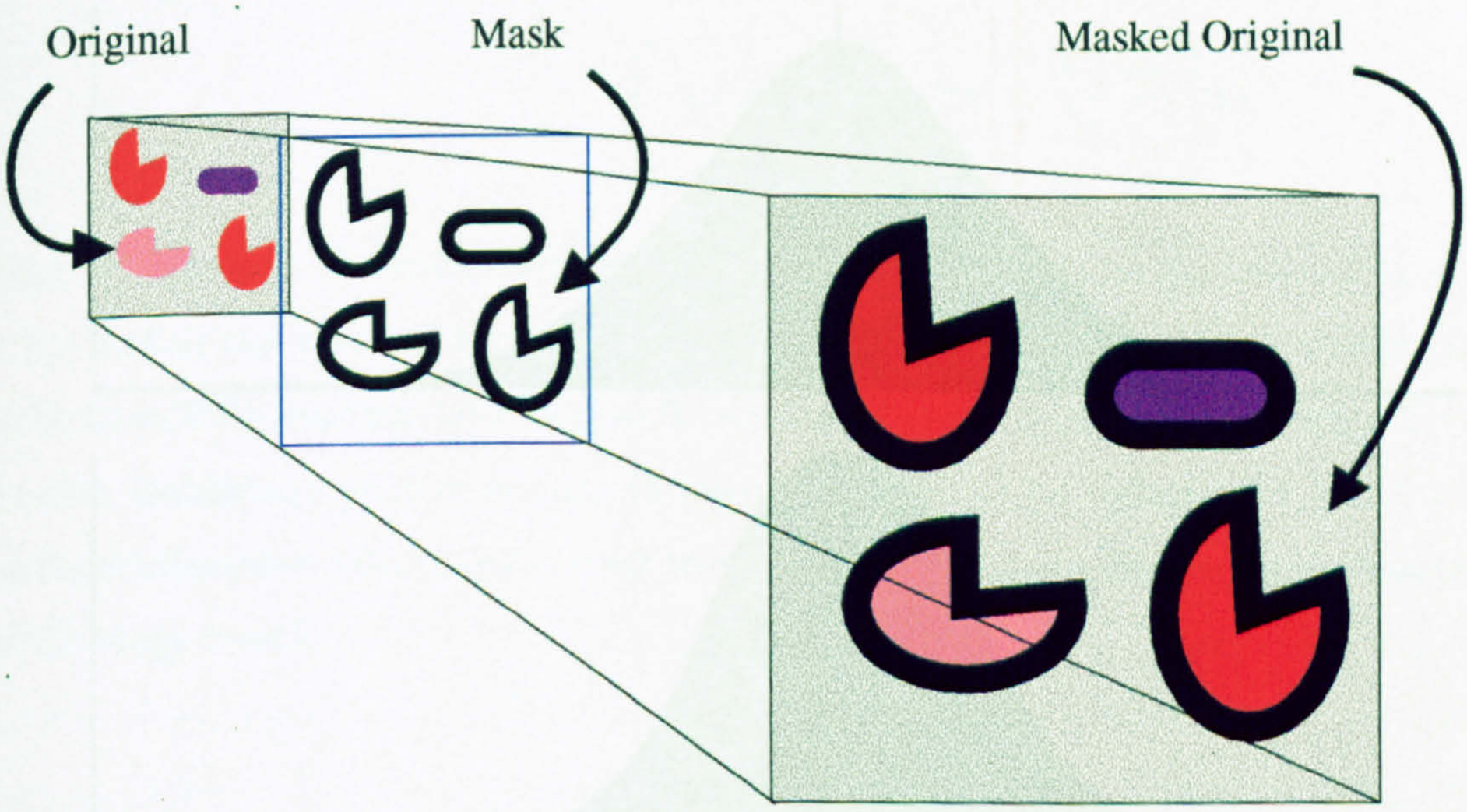

Figure 6.2 : Boundary Masking

NB. *Designs that have a high factor of texture due to fabric structure, or a combination of fabric and design, segment better when the original image is deliberately blurred. Blurring*

is induced by 'knocking' the camera out of focus. This reduces the texture effect while retaining a high degree of pertinent colour information.

If the pigment distribution is inspected after image masking the standard deviation of the normalised spread will have decreased due to elimination of hue variation at pigment overlap areas (see Figure 6.3). A tighter definition on the pigment area increases the pigment density towards the centre of mass of the pigment, therefore increasing the accuracy of the three-dimensional analysis of the RGB colour space at the second pass of segmentation.

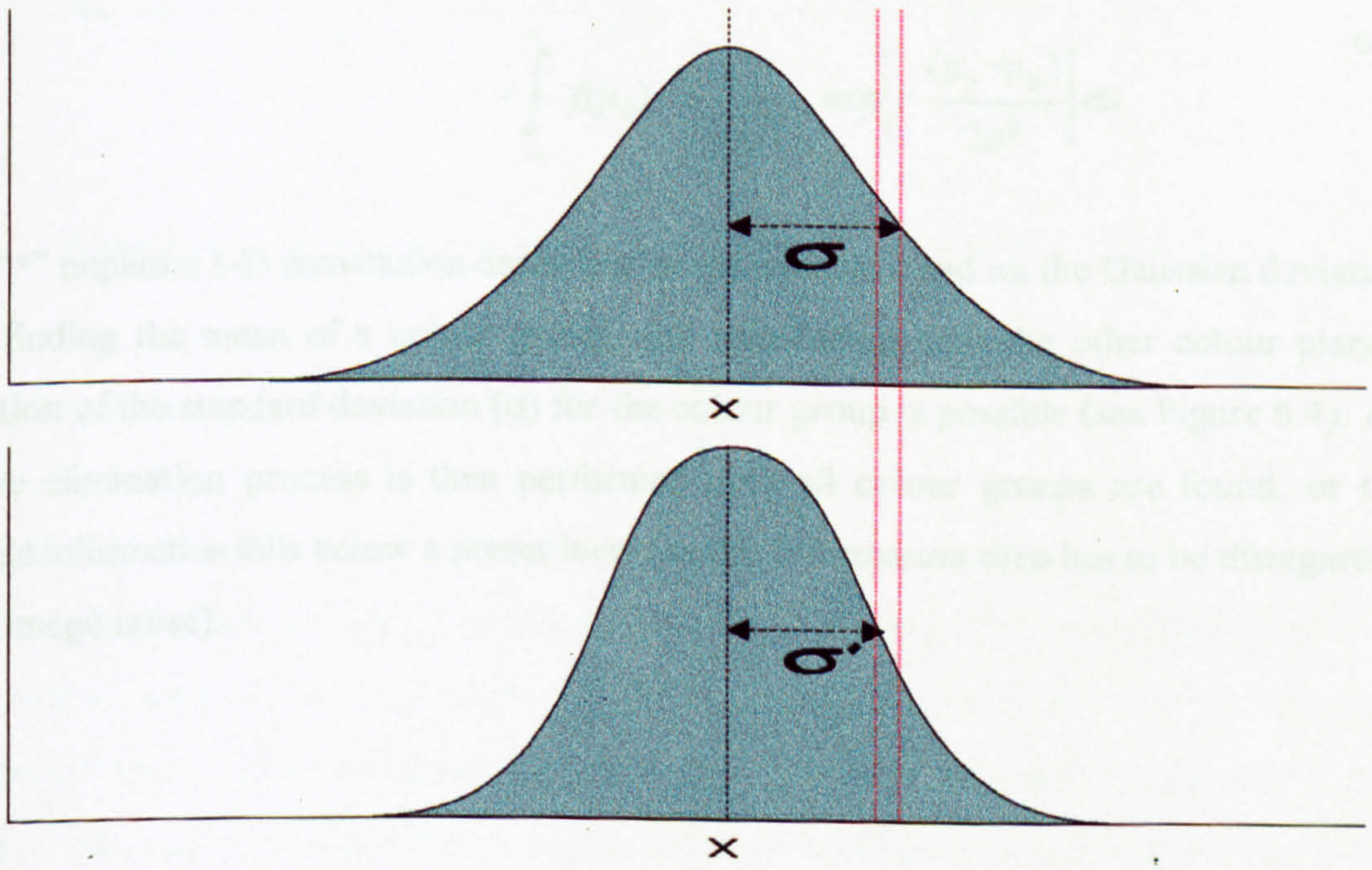

Figure 6.3 : Reduction in Pigment Spread due to Masking

6.3.5 Colour Histogram Acquisition (Stage 5)

Following mask definition, the RGB histogram information for the image is then obtained. Histograms are produced for the red, green, and blue image components, using standard image

processing techniques. From these histograms the first level of segmentation is derived [Crabtree, *et. al.*, 1984].

Assumptions are made concerning the individual histogram's intensity distribution before they are processed. When the investigation looked at RGB colour space distribution, it was observed that the probability distribution of individual pigments approximated to a normal distribution, which can be represented in a Gaussian form (supported by Witkin [1984]). New algorithms were designed by the author using this Gaussian factor (equation 6.5) to smooth and segment the histograms.

$$F(x,\sigma) = f(x)*g(x,\sigma)$$
$$= \int_{-\infty}^{\infty} f(\mu_0)\ \frac{1}{\sqrt{2\pi\sigma^2}}\ .\exp\left[-\frac{(\mu_x-\mu_0)}{2\sigma^2}\right]du \qquad 6.5$$

where "*" implies a 1-D convolution dependent on the variable x and on the Gaussian deviation σ. By finding the mean of a colour group, and referencing with the other colour planes, calculation of the standard deviation (σ) for the colour group is possible (see Figure 6.4). An iterative elimination process is then performed until all colour groups are found, or the threshold information falls below a preset level (as this information then has to be disregarded due to image noise).

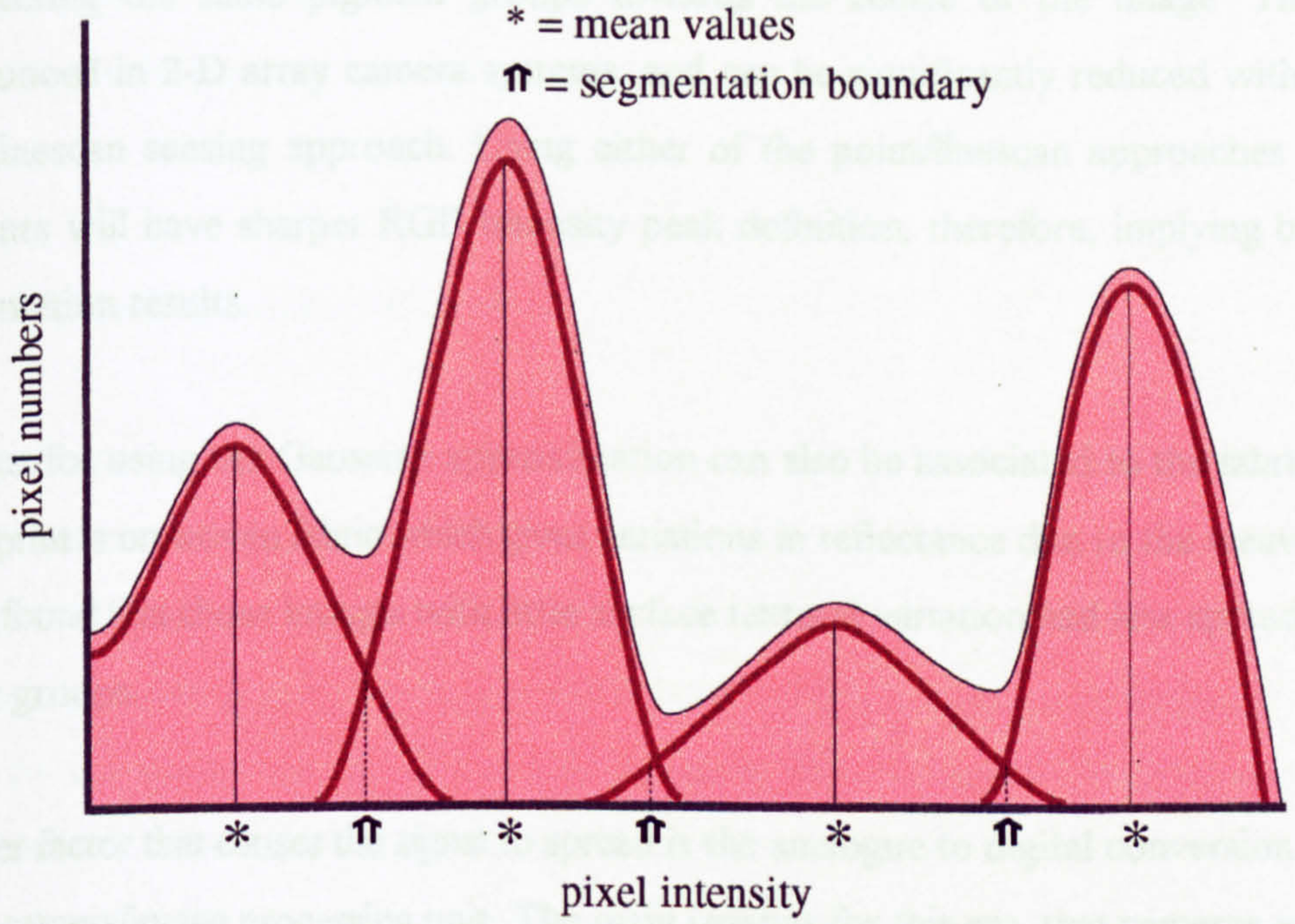

Figure 6.4 : Histogram showing Normalized Distributions of Pigments

6.3.6 First pass segmentation (Stage 6)

The use of this Gaussian-based subtraction process, provides superior segmentation as for speed and accuracy than the other methods investigated (see Chapter 7 for results). The method also proved to be more accurate than the CIE HSI colour cluster method as it did not require conversion from a 3-D to 2-D space (with the implicit loss of information). Also problems induced by rotational searching methods such as Cartesian to Polar conversions, and sensitivity being inversely proportional to distance from origin (similar to the inverse square law) were avoided.

After rigorous testing of the camera and lighting environment it was observed that pigment spread was approximating normalised distribution due to a combination of effects. One of the more noticeable of these is the *Vignetting Effect*, produced by the camera aperture. This is where pixels representing pigment groups on the border of the image appear darker than pixels

representing the same pigment groups towards the centre of the image. This effect is pronounced in 2-D array camera systems, and can be significantly reduced with the colour point/linescan sensing approach. Using either of the point/linescan approaches means that pigments will have sharper RGB intensity peak definition, therefore, implying better image segmentation results.

Reasons for using the Gaussian approximation can also be associated to the fabric structure, as the print is on woven fabric which gives variations in reflectance due to the weave structure. It was found that those images with little surface textural variation had less spread in pigment colour groups.

Another factor that causes the signal to spread is the analogue to digital conversion carried out by the camera/image processing unit. The main reasons for this are, that cameras are generally produced to satisfy human eye-brain expectations, and a large amount of image adaptation is carried out due to this compensation. Cameras are available that give pure digital image information, without any bias towards human visual expectations (logarithmic weighting), but such systems are expensive. Again, a colour point/linescan system is not as biased towards human visual requirements and improved peak definition can be expected.

NB. *It should be noted, however, that the rotary screen printed design is targeted at the human visual system and therefore the use of adaptive camera systems may have some tacit benefit.*

6.3.7 RGB Colour Cube Initialisation (Stage 7)

Using the segmentation information, calculated during the first level of processing, a *regioned* RGB colour space can be defined. A region is an area of the RGB colour space defined by pigment information calculated using the Gaussian methods. The central value of the region is the mean of the distributions for the red, green, and blue values of a pigment, and its boundaries

are defined as $k\sigma$ standard deviations from that mean. (k is taken to be three, giving a 99.7% probability of the pixel falling within the cube.)

6.3.8 Pixel Assignment (Stage 8)

It is rare for the individual pigments to have a separation of more than three standard deviations from the central value, and this causes problems for correct colour group assignment. By using the regioned colour space approach defining RGB colour space's relationship to individual groups is possible (see Figure 6.5). This is done by first assigning the individual raw image pixels to the colour space. The colour space is then inspected for pixel density (P_{DEN}) (Equation 6.6), where each region of the colour space is expressed in terms of the number of pixels it contains (its *mass*, N_p), in relation to its *volume* (expressed in terms of $k\sigma$, where k is a constant). This critical equation was derived by the author as part of the research to produce an optimal colour segmentation algorithm.

$$P_{DEN} = \frac{N_p}{(k\sigma_r \cdot k\sigma_g \cdot k\sigma_b)} \qquad 6.6$$

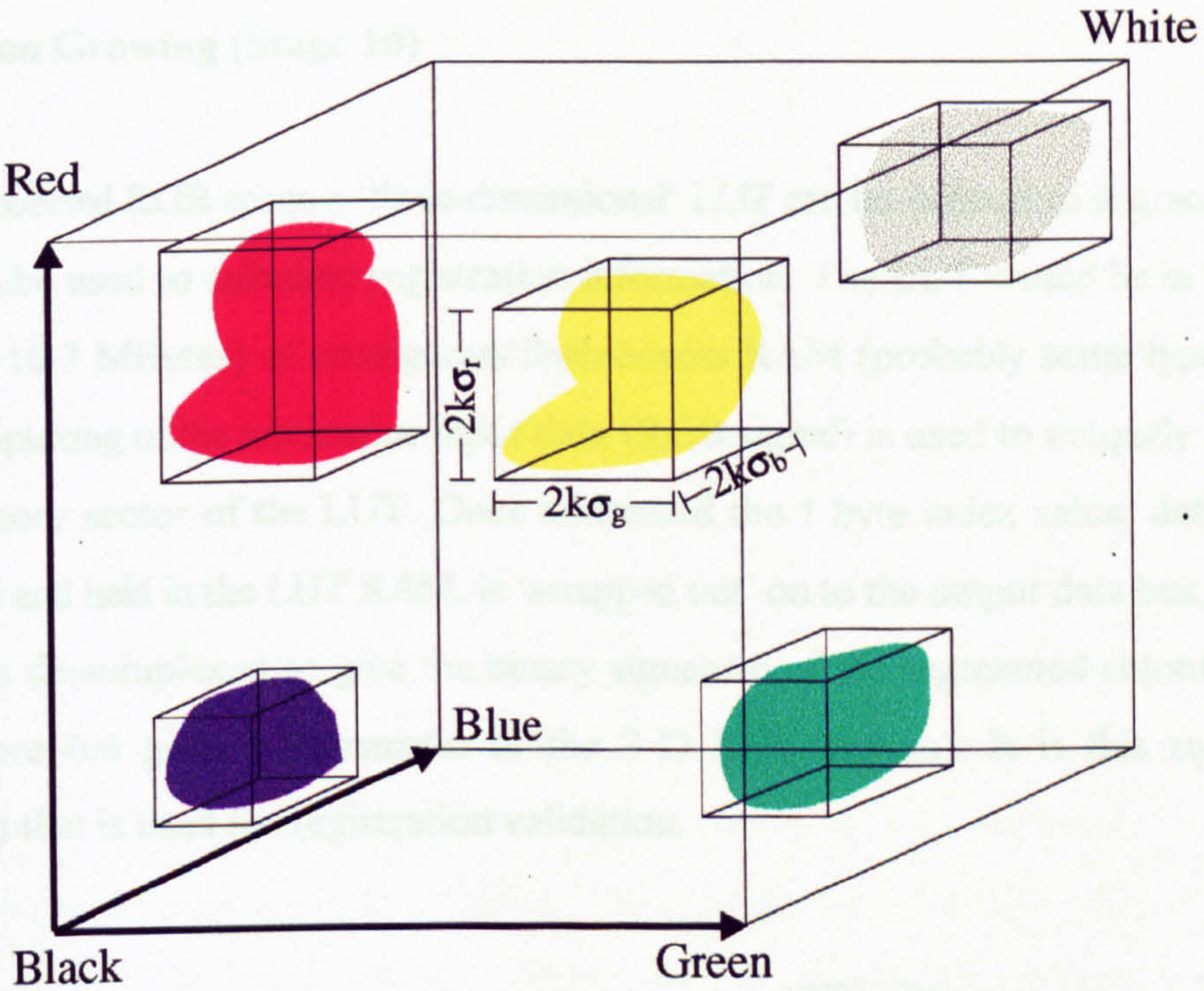

Figure 6.5 : Pigment Bounding in RGB Colour Space

6.3.9 Region Growing (Stage 9)

Each cube, defined in Stage 8, is then grown as a function of its density (cubes with a higher density usually have a smaller spread, and therefore grow at a slower rate than cubes with a low density). When the cubes have reached their maxima, i.e. 'fully grown' (using an *iterative* process) there is no *free* space, boundaries meeting etc., the process has been completed.

6.3.10 Region Growing (Stage 10)

From this processed RGB space a 'three-dimensional' LUT can be defined to segment raw data that can then be used to calculate registration information. The LUT would be in the form of 2^{24} bytes (≈ 16.7 MBytes) of contiguous flash-access RAM (probably some type of bubble RAM). Multiplexing of the tristimulus input data (RGB signal) is used to uniquely address the correct memory sector of the LUT. Once addressed the 1 byte index value, defined by the segmentation and held in the LUT RAM, is 'swapped out' on to the output data bus. This index value is then demultiplexed to give the binary signature of the segmented colour within the image (Figure 6.6 gives a schematic of the 3-D LUT system). It is this signature (or 'fingerprint') that is used for registration validation.

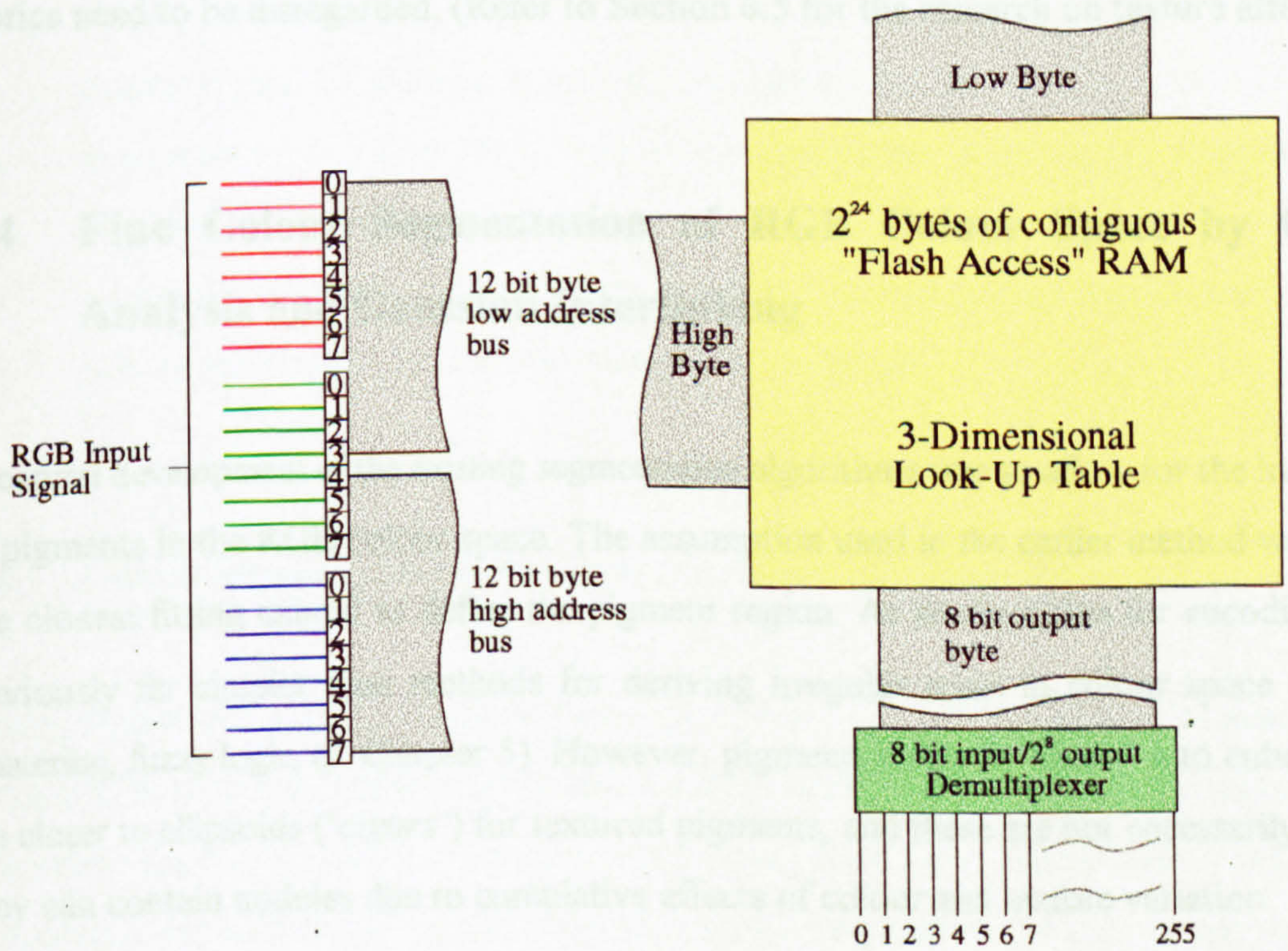

Figure 6.6 : 3-Dimensional LUT System Schematic

6.3.11 Registration Validation (Stage 11)

Once the index values have been assigned to the LUT the colour segmentation preprocessing stage is complete. Tristimulus input to this system renders a series of binarized 'fingerprints' that are used for registration analysis. Chapter 8 shows registration analysis process in a theoretical format that has been simulated in the laboratory.

To satisfy the requirements of 'good' research it is essential that the colour segmentation is quantified. The analysis of segmentation success on a rotary screen printed fabric is complex because it cannot be done in a completely objective manner, some form of subjective analysis is also required (cf. Chapter 5). This is primarily due to the accommodative blending process that existing algorithms are unable to simulate. Also, the effects of texture differences between fabrics need to be disregarded. (Refer to Section 6.5 for the research on texture affects).

6.4 Fine Colour Segmentation of RGB Colour Space by Cluster Analysis and Gaussian Interlinking

A natural development of the existing segmentation algorithms was to allow for the irregularity of pigments in the RGB colour space. The assumption used in the earlier method was that of the closest fitting cuboid to define the pigment region. As an algorithm for encoding this is obviously far simpler than methods for deriving irregular areas in colour space (c-means clustering, fuzzy logic, cf. Chapter 5). However, pigments rarely fit 'nicely' into cuboids, they are closer to ellipsoids ('*cigars*') for textured pigments, and these are not necessarily smooth, they can contain nodules due to cumulative effects of colour and texture variation.

The approach used by the advanced segmentation method is this;

1 – 6. As for the coarse Gaussian-based segmentation method,

7. Initialise RGB colour space to start pigment analysis,

8. Collect pigment information for **all** pigments, remembering that these are not necessarily 'true' colours, but can be texturally varied.

9. Sort pigments according to their density (number of associated pixels in the image).

10. Starting at the least common pigment, associate to densest neighbour (*searches through the list until it finds the proximal neighbour with the most pixel assignments*), and link with reference to Gaussian-based segmentation.

11. Repeat step 10. until all pigments have been inspected and associated.

12. Grow *supra*-pigments according to the pigment density from outlier nodes to centre of mass.

13. Continue until RGB space is defined to preset criterion.

14. Assignment of colour *regions* to three-dimensional RGB LUT, allowing unique identification of colour groups.

15. Registration validation of *real-time* segmented image (repeat step 15 until new print run, as per Step 11 of Gaussian-based segmentation).

6.4.1 Coarse Segmentation using Gaussian Approach (Stage 1-6)

Coarse segmentation of the image (as described in 6.3.1 – 6.3.6), using the Gaussian method, is required to reduce the computational load for the complex fine segmentation stage. It is used to partition the colour space into lower and upper threshold ranges as defined by the Gaussian convolution and its first and second order derivatives. Analysis of the cuboid regions for their associated pixel density (cf. coarse segmentation Stage 8) show that it is possible to estimate the number of colour regions in the colour space. This gives the essential *a priori* information for the colour clustering methodology.

6.4.2 Initialization of RGB Colour Space (Stage 7)

For fast computation the RGB space assignment is controlled by a hashed linked list, with one colour plane at 8 bits (256 levels) and the other two planes at 2 bits (4 levels) resolution. Either the red or green plane can be used as the 8 bit hashing index as it is generally accepted that the blue plane displays less variation in natural scenes [Orchard, *et. al.*, 1991][Goldberg, 1991]. Although the images being analysed are not 'natural' they show greater distributions in the red and green planes. This allows for faster pixel to pigment assignment and gives a better data spread on the first pass.

To initialise the list a one element header is defined, and the hash table values assigned to this header. The header is the anchor point for the dynamic colour space and plays a critical role in the clustering process, as will be seen in the succeeding sections. The structure of the list elements and hash table is shown in Figure 6.7a and is defined by the following pseudo-code algorithm. Figure 6.7b represents the link list and hash table status after initialisation, where the hash table elements have been initialized to point at the list top.

```
DEFINE STRUCTURE PIGMENT
   BEGIN
      POINTER TO PIGMENT  next;
      POINTER TO PIGMENT  previous;
      INTEGER    index;
      INTEGER    density;
   END

DEFINE STRUCTURE HASH TABLE                          "red   g   b"
   BEGIN                                              |    |   |
      DECLARE ARRAY of PIGMENT hash_table[256][4][4];
   END
```

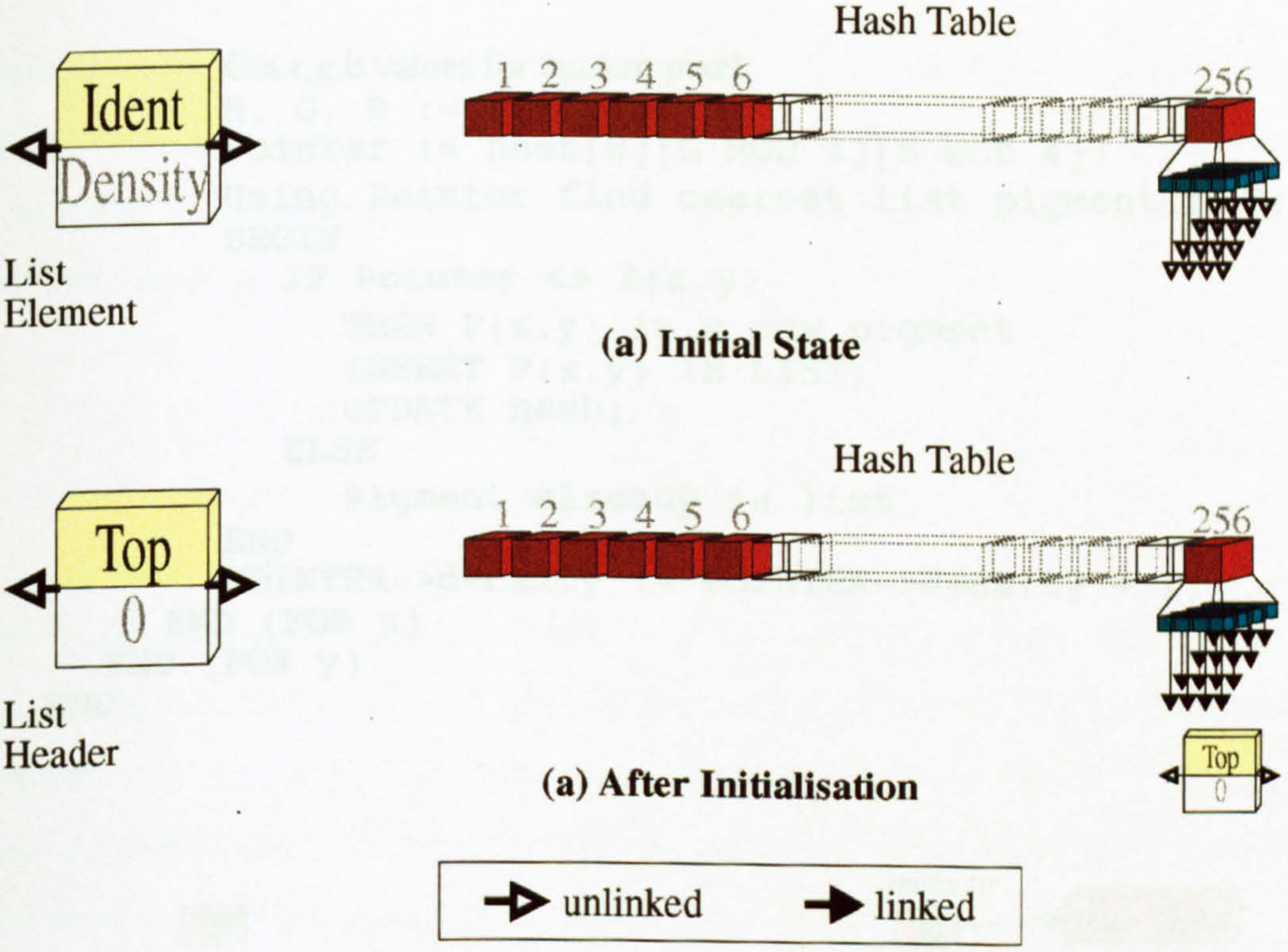

Figure 6. : Structure of List Elements and Hash Table (a) before and (b) after Initialisation

6.4.3 Assignment of Pigments to Dynamic Colour Space (Stage)

Once the dynamic colour cube has been declared the next step is to associate it with the pigment values of the image pixels. The hash table is used to identify the closest list element to the pixel pigment. If the list element has the same pigment value as the pixel its density value is incremented. However, if the pigment is undefined further processing declares a new pigment structure of density 1 that is then inserted, at the correct position, in the list. After insertion of a new pigment the hash table is updated to improve access speed. Figure 6.8 illustrates pixel assignment to the link list in a series of block diagrams, as defined by the following pseudo-code.

```
PIGMENT ASSIGNMENT
BEGIN
   FOR y := 1 TO 512
      FOR x := 1 TO 512
         BEGIN
```

```
Get r,g,b values for current pixel
R, G, B := P(x,y);
Pointer := hash[R][G MOD 4][B MOD 4];
Using Pointer find nearest list pigment to P(x,y)
BEGIN
   IF Pointer <> P(x,y)
      THEN P(x,y) is a new pigment
      INSERT P(x,y) IN LIST;
      UPDATE hash;
   ELSE
         Pigment already in list
      END
      POINTER->density := POINTER->density + 1;
   END (FOR x)
END (FOR y)
END
```

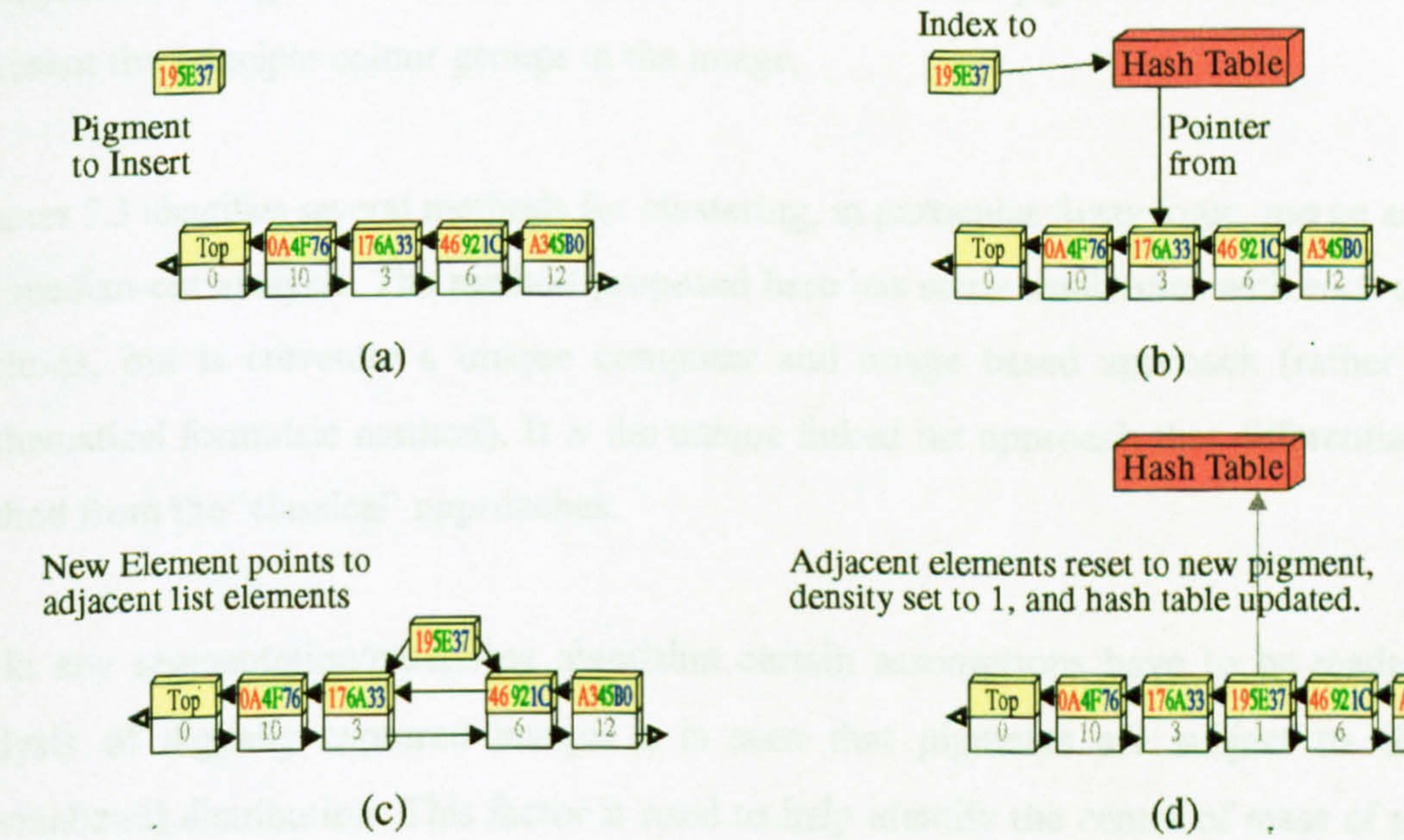

Figure 6. : Block Diagram of Pixel Assignment to Linked List

Assignment continues until all pixel pigment values have been associated with the list pigment values. For a 512×512 by 24 bit image this process takes approximately 20 seconds. This assignment time would be significantly reduced by using parallel processing. For example, using

sixteen processors (a realistic number) in parallel, each processing a separate window of the image, this assignment time could be reduced to less than two seconds. In fact use of parallel processing is desirable throughout the inspection process, as task sharing would greatly improve the inspection systems on-line capabilities.

6.4.4 Pigment Sorting and Grouping (Stages 1 11)

After pixel assignment, pigments are held by the dynamic colour space linked list in sequential order, as defined by their primary hashing element (red or green). The list is unassociated, the pigment order is arbitrary. However, due to the hashing method, related pixels will be nearby. To segment the image it is now necessary to associate individual pigments to super classes that represent the principle colour groups in the image.

Chapter 5.3 identifies several methods for clustering, in particular fuzzy logic, merge and box, and median-cut analysis. The method proposed here has some similarities with each of these methods, but is currently a unique computer and image based approach (rather than a mathematical formulaic method). It is the unique linked list approach that differentiates this method from the 'classical' approaches.

As in any segmentation/clustering algorithm certain assumptions have to be made. From analysis of digitally captured images it is seen that pigments are subject to Gaussian (normalized) distribution. This factor is used to help identify the centre of mass of pigment groups, ie the nearer to the centroid of a pigment group in colour space the denser the pixel assignment. Therefore, the initial parsing of the linked list is a density sort.

The list structure is such that on a forward search the colour space is defined by spatial relationships, with adjacent pigments sharing a narrow bandwidth of the list. However, on reverse search the list is density sorted. This allows fast searching of the dynamic colour space for pigment associations.

Text cut off in original

Pigments are associated by the following criteria: their separation in the colour space (calculated using an Euclidean metric) (cf. Chapter 5); their relative density (pigments of lower density are subsumed by adjacent pigments of higher density). Assignments are regulated by pigment groupings derived from the coarse segmentation, ie pixels that are unclassifiable via coarse segmentation are given probability weightings dependent on their distance from, and the mass of the path to, the nearest supra-pigment groups.

This process is repeated until the association probability falls outside preset tolerance levels. Adjusting these tolerance levels controls the coarseness of the segmentation. The following pseudo-code describes the clustering algorithm.

```
DENSITY SORT
BEGIN
   Perform Bubble Sort on Lists Pigment->Density values,
   Reorder list so reverse parse Pigment->Previous is density orde
END

PIGMENT ASSOCIATE
BEGIN
   With reverse parse density sorted list,
   FOR I := 1 TO NumberOfPigments
      BEGIN
         Find least dense unassociated pigment,
         LIST SEARCH for closest, largest pigment, using pre-define
            BEGIN
            Calculate Euclidean Distance
            Separation := sqrt(|R1-R2|^2 +|G1-G2|^2+|B1-B2|^2);

            END
         Associate selected pigments,
         Remove scanned pigment from search,
         Increment associated pigment density by scanned pigment de
         END (FOR I)
END
```

6.4.5 Pigment Cluster Growing and Assignment (Stages 12, 13, & 14)

The dynamic colour space is now ordered in to *supra*-pigment regions. These regions are defined by the associated link list and have a star topology (Figure 6.9). This star topology provides the skeleton of the pigment cluster. However, because the actual pigment clusters are somewhat nebulous it is important that some form of fuzzy structuring is given to the list-based skeleton.

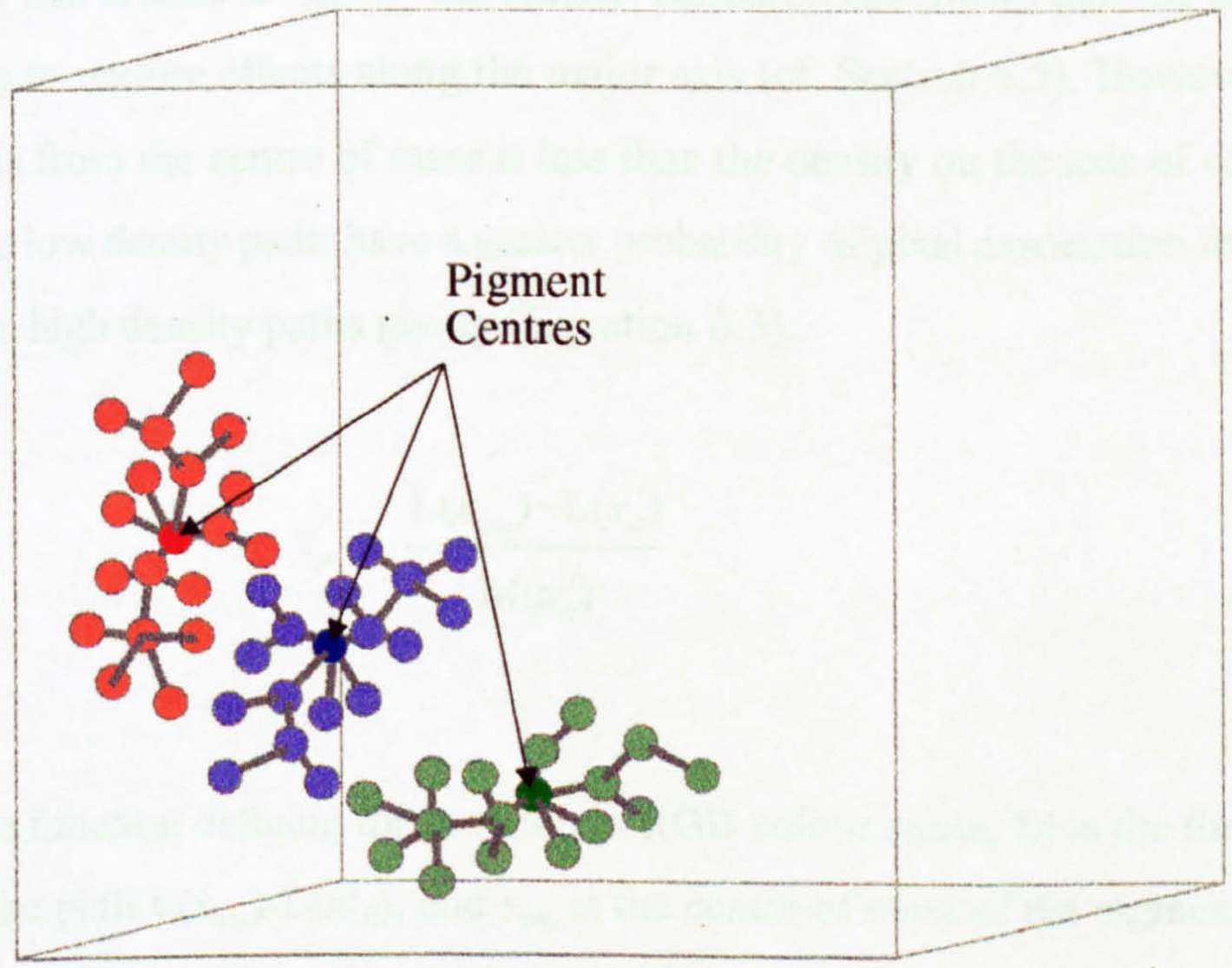

Figure 6.9 : Example of a *Supra*-Pigment's Star Topology

From the associated link list, the structure of the individual pigments is defined as a series of outlier nodes (*sub*-pigment nodes lying on the extremities of the *supra*-pigment). These points define the minimum pigment volume when interconnected. Any pixel with coordinates within the range specified by the outliers is classified as a member of that supra-pigment class.

At this stage pixel classification is strict, in that the cluster is clearly defined by the restricted data set of the original image. Although, this original image can be classified as fully segmented, succeeding images may contain variations in pigment outside the restricted data set. Hence, the need to apply fuzzy structuring.

To achieve a fuzzy data set for each supra-pigment the individual clusters are 'grown'. From the link list the density path of each node to the centre of mass of the supra-pigment is known. It is this factor that is used to 'grow' the cluster. Research has shown that the area of greatest spread is due to texture effects along the major axis (cf. Section 6.5). However, the density along this axis from the centre of mass is less than the density on the axis of variation due to the hue. These low density paths have a greater probability of pixel association further from the mean than the high density paths giving (Equation 6.3);

$$\tau_p' = \frac{L(x_{cm}) - L(x_o')}{M(x_o')} \qquad 6.3$$

where L is the function defining the location in RGB colour space, M is the function defining the mass of the path $L(x_{cm})$-$L(x'_0)$, and x_{cm} is the centre of mass of the pigment, and x'_0 is an outlying node of the pigment, and τ'_p is the rate of expansion of node x'_0 from point x_{cm}. From this it is shown that;

τ is directly proportional to distance from pigment centre,

and

τ is inversely proportional to pixel assignments of associated path.

The requirement for analysis of 24 bit RGB colour space (16 million colours) has involved the development of (the previously discussed) hashing and memory conservation algorithms for algorithm development. In an industrial inspection *engine* hardware-based algorithms would use a Sixteen-MB array for *real-time* LUT development. This array could be used for the initial

computationally expensive processing of the colour data, but once complete 3-D LUTs can be defined leading to *real-time* processing.

6.5 Texture Effects

A major area of interest in textile image processing is the analysis of fabric structure/texture. It is interesting that as a by-product of this research, an approach to texture analysis has been found. The rationale used is as follows; when inspecting a fabric visually (using the human eye-brain mechanism) observation of texture (ie the woven structure of the fabric) is easy. Why is this? The human visual system is far superior to that of computers as it can compartmentalise between colour effects and texture effects. Principally this is because it is very good at pattern recognition, being able to disregard colour while retaining pertinent texture details.

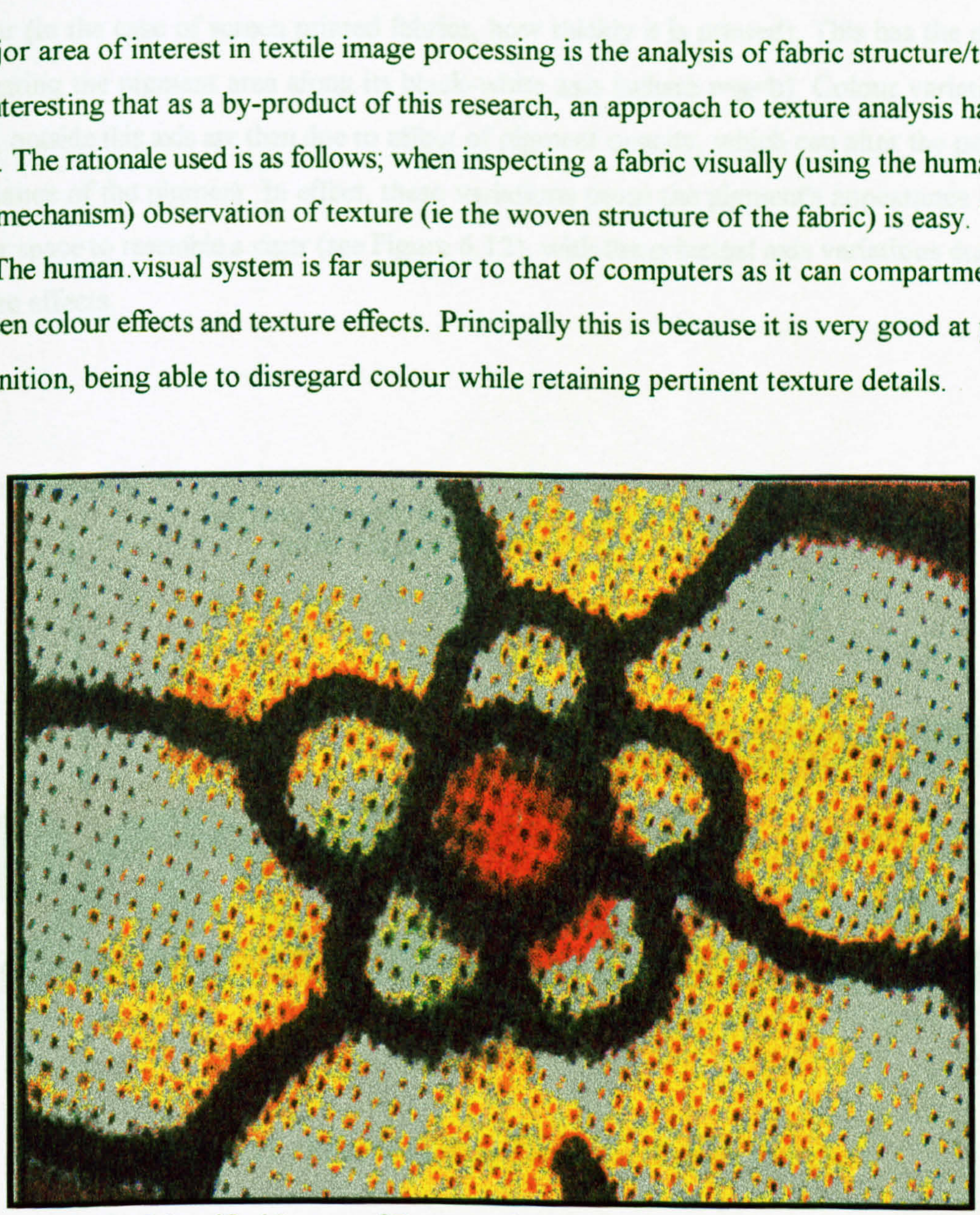

Figure 6.10 : Magnified Image of Pattern, showing Fabric Structure and Background

A fundamental reason that colour segmentation was chosen is that it supplies a method of eliminating texture effects (these effects can cause colour variations). Variation in colour due to texture is a cumulative effect, not only does the structure of the fabric (or textured surface) affect the perceived colour, but also the opacity of the dyestuffs/pigments used. By having an uneven surface, as in fabric printing, colour variations are expected (see Figures 6.10 6.11). It can be shown that the major effect in pigment spreading is due to the saturation shift of the colour (in the case of screen printed fabrics, how thickly it is printed). This has the effect of elongating the pigment area along its black-white axis (where r=g=b). Colour variations, or shifts, outside this axis are then due to effect of pigment opacity, which can alter the perceived luminance of the pigment. In effect, these variations cause the pigment's appearance in RGB colour space to resemble a cigar (see Figure 6.12), with the principal axis variations due to the texture effects.

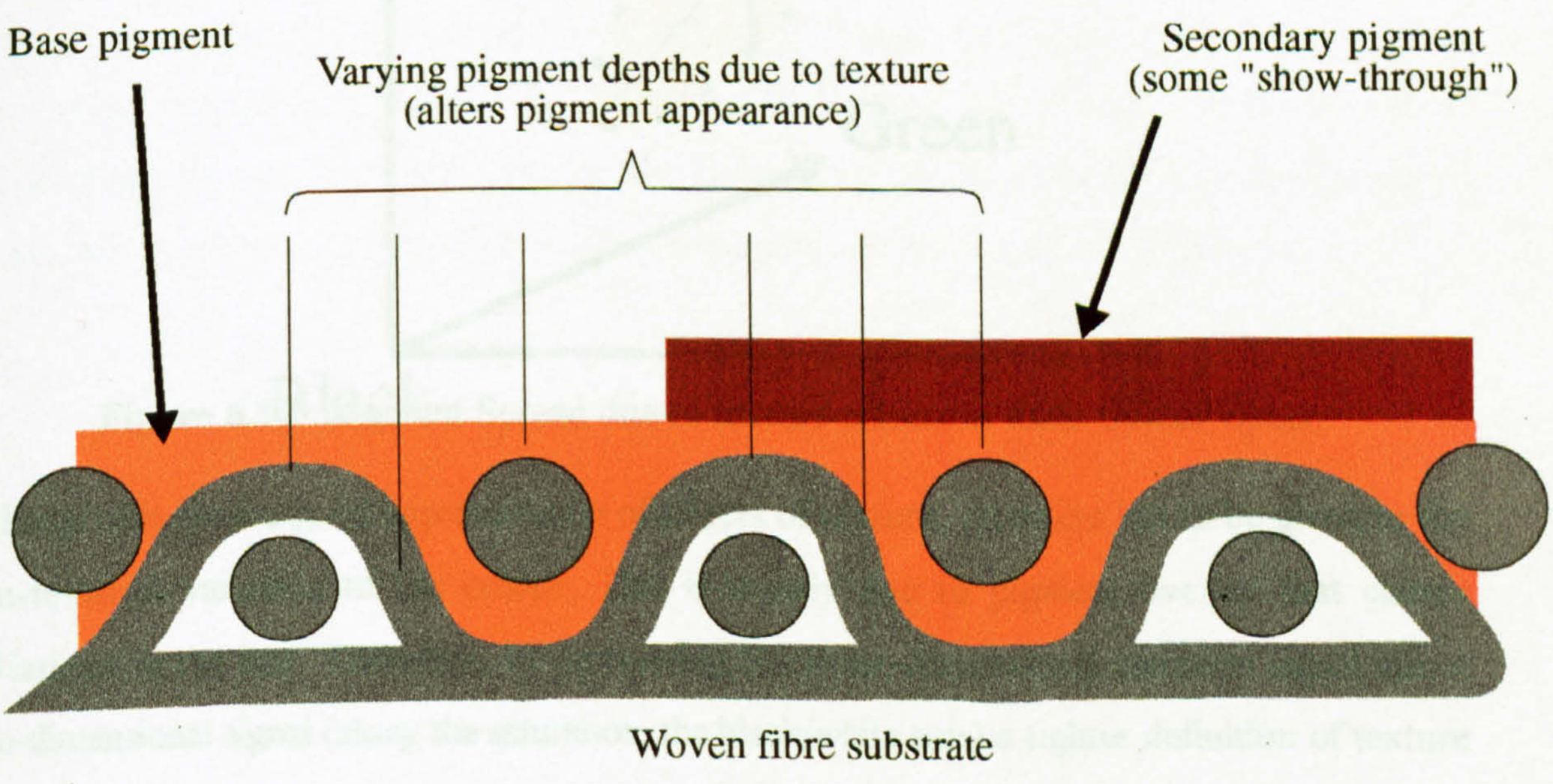

Figure 6.11 : Effect of Fabric Texture on Colour Thickness

What this means in terms of texture analysis is that a simple algorithm can be generated for texture detection. Given an original, textured image, we can see that the colour segmented image has eliminated the texture information, therefore the following axiom holds true;

'original image' - 'colour segmented image' = 'texture information'.

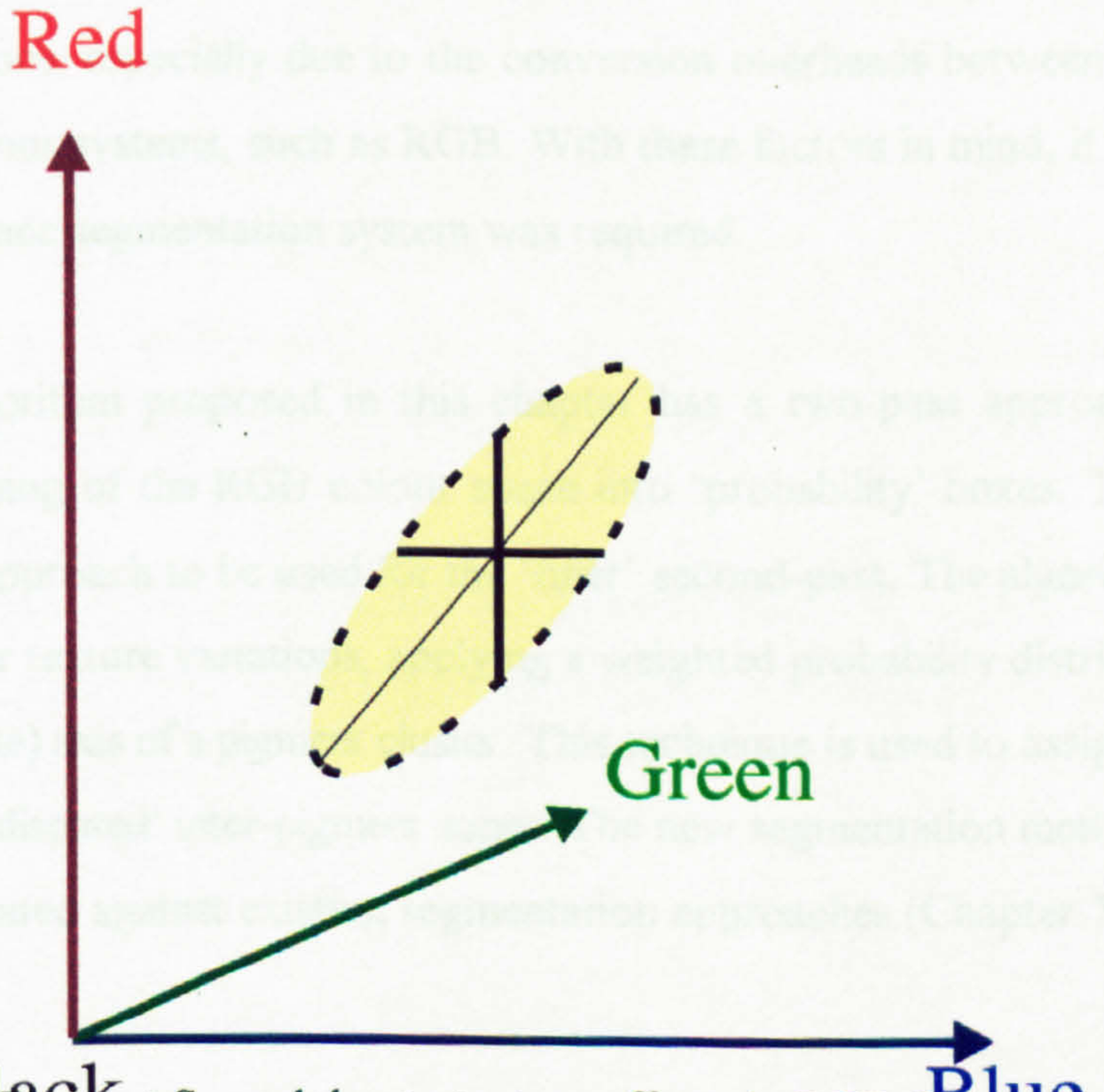

Figure 6.12: Pigment Spread due to texture effects in RGB Colour Space

Although this gives a good approximation of effects of texture, attention has to be given to the non-textural variation of the colour. This is mostly due to pigment overlap that causes variations in the hue. Therefore, by converting the three-dimensional variation signal into a two-dimensional signal (along the saturation, the black/white axis) a tighter definition of texture can be achieved.

6.6 Summary and Conclusions

Although the CIE-HSI based segmentation offers a simple solution to segmentation, via its discarding of the intensity value and its rotational search, it is unsuited to scenes containing many shade variations (ref. Chapter 7). The main reason is that the rotational search method cannot differentiate between distinct pigment groups with small inter-pigment spacing. Also, from Chapter 3, it is seen that the HSI colour space is considered inappropriate for computer based colour applications, especially due to the conversion overheads between it and more standard computer colour systems, such as RGB. With these factors in mind, it was decided that an RGB colour space segmentation system was required.

The segmentation algorithm proposed in this chapter has a two-pass approach allowing preliminary preprocessing of the RGB colour space into 'probability' boxes. This allows a predictive fuzzy logic approach to be used for the 'finer' second-pass. The algorithm is tuned to make allowances for texture variations, applying a weighted probability distribution along the principal (black/white) axis of a pigment cluster. This technique is used to assign pixels that would otherwise be in 'disputed' inter-pigment zones. The new segmentation method performs favourably when evaluated against existing segmentation approaches (Chapter 7).

7 Evaluation of Colour Segmentation Methodologies

7.1 Introduction

Having established new methods for colour segmentation, devised by the author as part of this research, it is necessary to evaluate their success. In Chapter 5, several methods for qualitative analysis of segmented images were proposed. A common factor of these methods is the use of the total squared error (TSE) function to derive an expression of variance of the segmented image from the original image. The inference of this is that the smaller the variance the better the segmentation.

However, TSE only gives a rough result, it is desirable to have a qualitative measure as well. Traditionally, methods for qualitative analysis have been subjective. For the new colour segmentation algorithms, described in Chapter 6, the results of the subjective analysis are excellent, as the segmentation is visually convincing. This is not sufficient for solid research as it is not reproducible.

A method for non-subjective qualitative analysis has been devised. It is discussed in the following section, along with the TSE method, and a method for comparing simulated and real images for Gaussian artifacts.

7.2 Experimental approach to Evaluation

Similar methods for the qualitative analysis of colour segmentation using a TSE approach were proposed by Lim, *et. al.*, [1990], Fletcher [1991], Goldberg [1991], Wu [1992], and Liu, *et. al.*, [1994]. Orchard, *et. al.*, [1991] also used a TSE approach to segmentation analysis, but identified some flaws with the approach (cf. Chapter 5). Bearing this in mind it was decided for this research that the evaluation of colour segmentation would be based on several criteria, not just TSE.

The parameter used to specify the distortion (therefore a function of TSE) between the original (reference) image and the automatically segmented image is defined by quantity D as follows (Equation 7.1);

$$D = \frac{1}{N} \sum_{x=1}^{X_{max}} \sum_{y=1}^{Y_{max}} d_E(I_{x,y}, q(I_{x,y})) \qquad 7.1$$

where $N (= X_{max} \times Y_{max})$ is the number of pixels in the image I, $I_{x,y}$ is the colour of the pixel x, y, $q(X)$ is the quantized colour and d_E is the Euclidean distance measure [Goldberg, 1991]. From this equation a quantitative measure of distortion D (difference) between images is obtained. The smaller the value of D the better the approximation of the quantized image to the original.

To obtain a more realistic measure of segmentation using non-subjective methods requires *a priori* knowledge of the image structure. Without this compositional information realistic assessment is not possible. Therefore fabric images cannot be accurately appraised, even if the design is known, as there is variation between design and realization (due to textural artifacts). However, the parameter's performance can be judged using predefined images.

The images used for the assessment are 512×512 24 bit colour scans of controlled scenes of colour tiles of known areas. As the ratio of the colour tiles within the image is known it is possible to quantify the segmentation. For a 100% segmentation all pixels must be assigned and the ratio of colours within the original and segmented images must be identical.

***Dulux** TRADE* Colour Dimensions© tiles are used for the quantitative evaluation. The colour range is based on a three dimensional system that shows visually every perceivable colour in the relationship between Black, White, Yellow, Red, Blue and Green. The individual colours are expressed by a notation that reflects their relationship to Whiteness/Blackness and Colour Intensity. Therefore a colour with a 30% blackness and 60% colour intensity in the hue area G20Y would have the notation 3060-G20Y (see Figure 7.1).

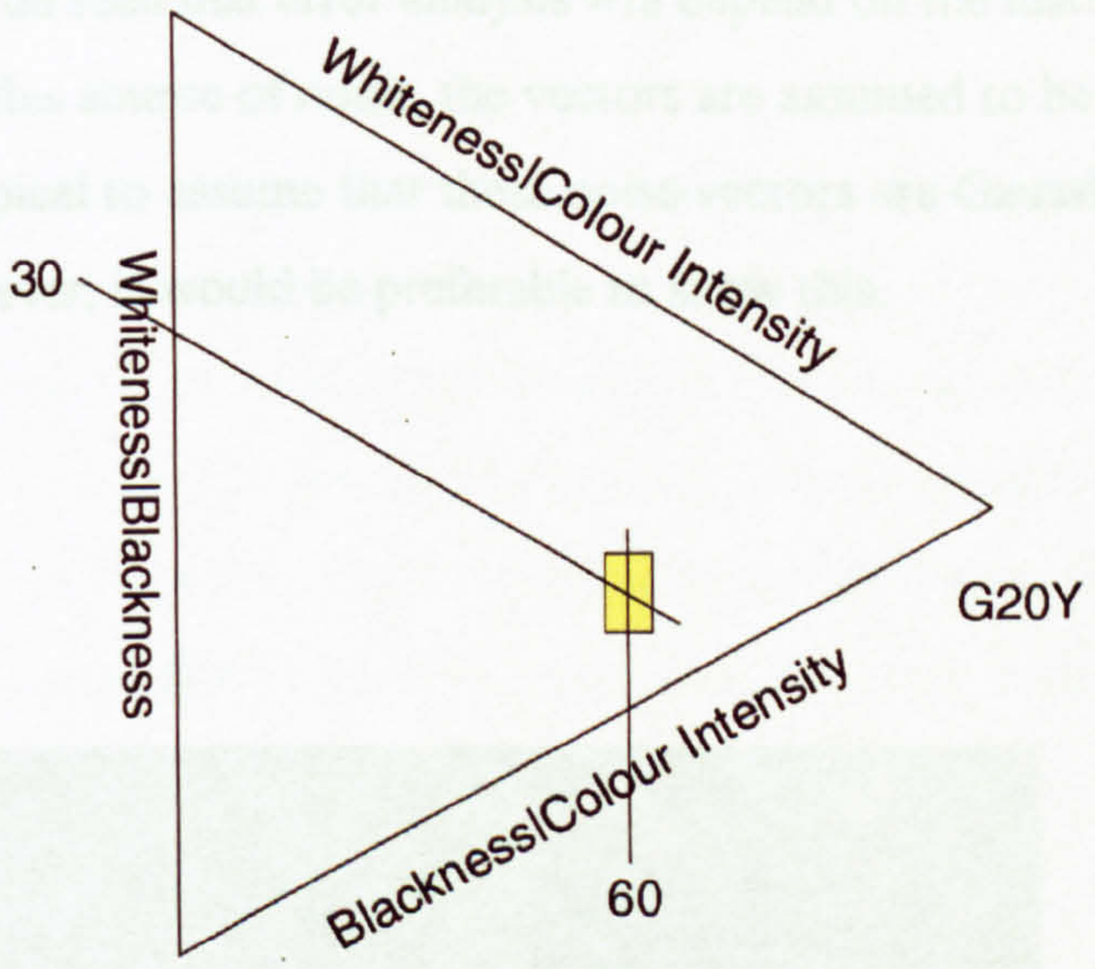

Figure 7.1 : Colour Triangle for 3060-G20Y

The tiles are each 15mm×17mm, giving an area of 255mm^2. This equates to 25500 pixels at the required resolution of 0.1mm/pixel for inspecting rotary screen fabrics. Therefore, one tile represents 9.727% of the total image area, meaning that up to ten colours can be segmented and the results quantified at the correct resolution. However, to test the segmentation algorithm on more than ten colours either the resolution or the tile size has to be reduced. It is easier and more reproducible to alter the resolution. Figure 7.2 shows a typical test image used in the quantitative analysis of the algorithm. NB it is important that the background of the test image is uniform to avoid ambiguities.

An important area of analysis in this research was to confirm that the images were approximating a Gaussian distribution due to noise. The source of this error is measurement noise introduced at the sensor response level [Wandell, 1987]. This problem of sensor noise is relatively straight forward and can be simply expressed (Equation 7.2);

$$\rho^x = \rho_0^x + \eta^x \qquad 7.2$$

where sensor noise is the vector η^x, $\rho^x{}_0$ is the true sensor vector, and ρ^x is the measured sensor vector. From this it can be seen that error analysis will depend on the distribution of the noise vector. Commonly, for this source of noise, the vectors are assumed to be independent across the image. It is also typical to assume that these noise vectors are Gaussian and independent [Wandell, 1987]. However, it would be preferable to show this.

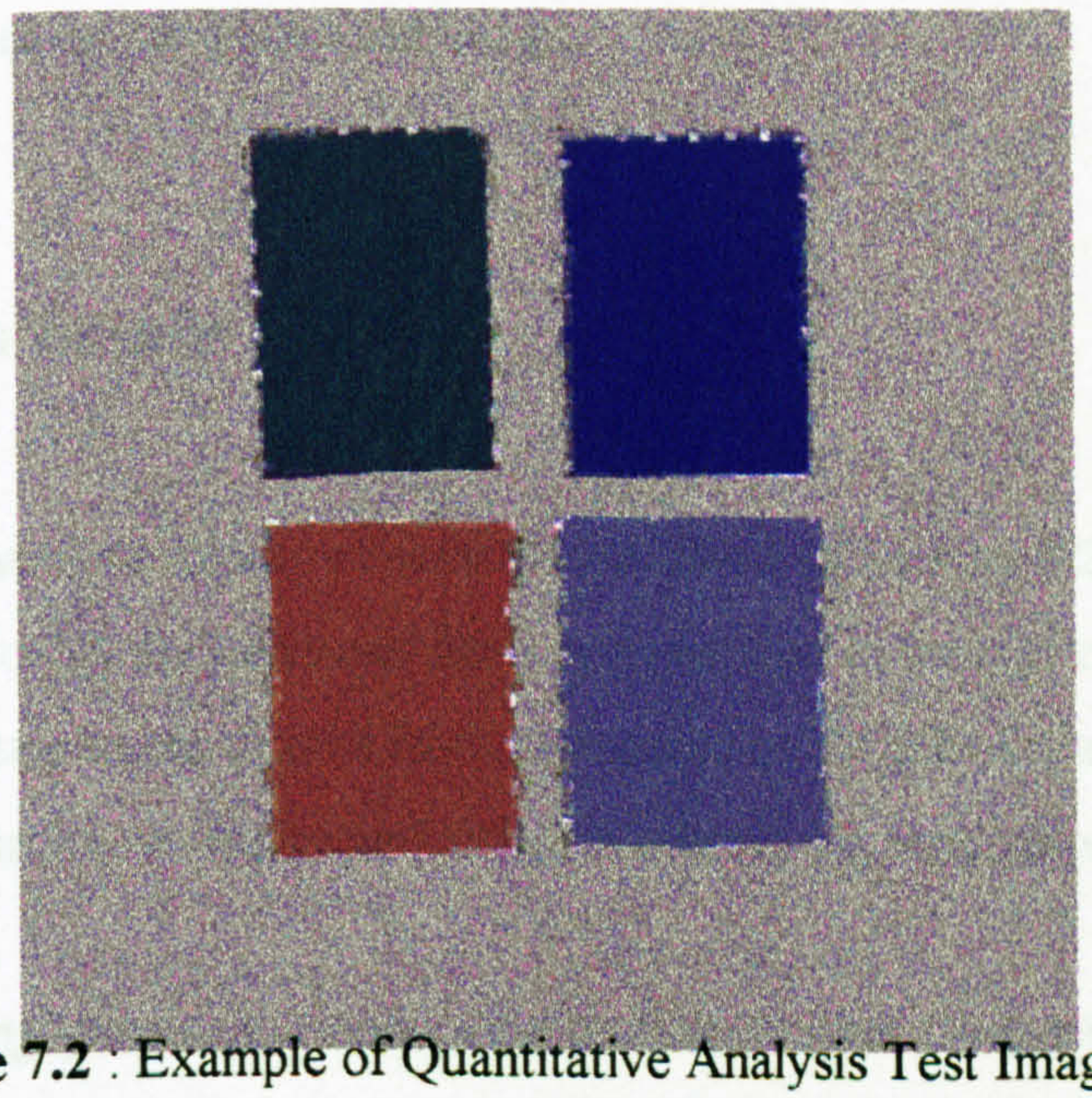

Figure 7.2 : Example of Quantitative Analysis Test Image (Q4)

To test for Gaussian noise distribution in an image generated by the machine vision system used in this research it was necessary to compare real and generated images. The real images were of a single colour (or within a very tight range), that had little or no textural artifacts. Similar to the quantitative analysis of the segmentation process, Colour Dimension tiles were used. The position of each tile in RGB colour space can be derived and therefore simulated. It was necessary to calibrate the system to account for distortion due to lighting. This was a simple statistical process that compared the theoretical colour coordinates against an average of a

series of 'real' images of the colour (cf. Chapter 4, Camera and Lighting Testing). From this data it was possible to adjust for the shift in colour space of the tile due to lighting.

The first stage of processing calculates the standard deviation from the mean for each of the colour planes in the real image. This information is then used to generate an image with a Gaussian distribution with the same standard deviation. The histograms of each colour plane for the real and generated images are then compared, and the variance calculated using a standard statistical package. From the results it is possible to give a measure of 'Gaussian-ness' of the original image. Appendix D describes the algorithm used to generate the random Gaussian noise vectors for the generated image.

7.3 Evaluation Results

The results of the various evaluative methods described in Section 7.2 are presented in this section. Where applicable the measures have been applied to images of fabrics. These are a typical selection of rotary screen printed fabrics produced by DORMA and they have been used throughout this research to evaluate performance criteria (cf. Appendix B).

Evaluation results using generated or controlled images (Colour Dimension tiles) are indicated as such, with the generation/composition information. The intention of these results is to substantiate the research methods; and qualitatively compare them against existing approaches. However, this is not always possible as papers on other methods often fail to present their methods and results in a reproducible manner.

7.3.1 Distortion Measure Results

Table 7.1 and Figure 7.3 show the result of the distortion measure (Equation 7.1) on segmented images of rotary screen fabric using a range of segmentation algorithms (sample images and complete results are given in Appendix E). Ten unique images of each fabric are captured and processed, giving a sample base of 512×512×10 (2,621,440) trivector pixels. The results shown are based on the average distortion measures of the unique images. The Lim-Lee, Khotanzad, Goldberg, and Wu algorithms are described in Chapter 5 and in more detail in the relevant papers [Lim, *et. al.*, 1990][Khotanzad, *et. al.*, 1990][Goldberg, 1991][Wu, 1992]. The HSI algorithm is presented in brief in Chapter 6.2 and in detail in Dodkin [1994]. The two new algorithms are also described in Chapter 6, Section 6.3 and 6.4 respectively.

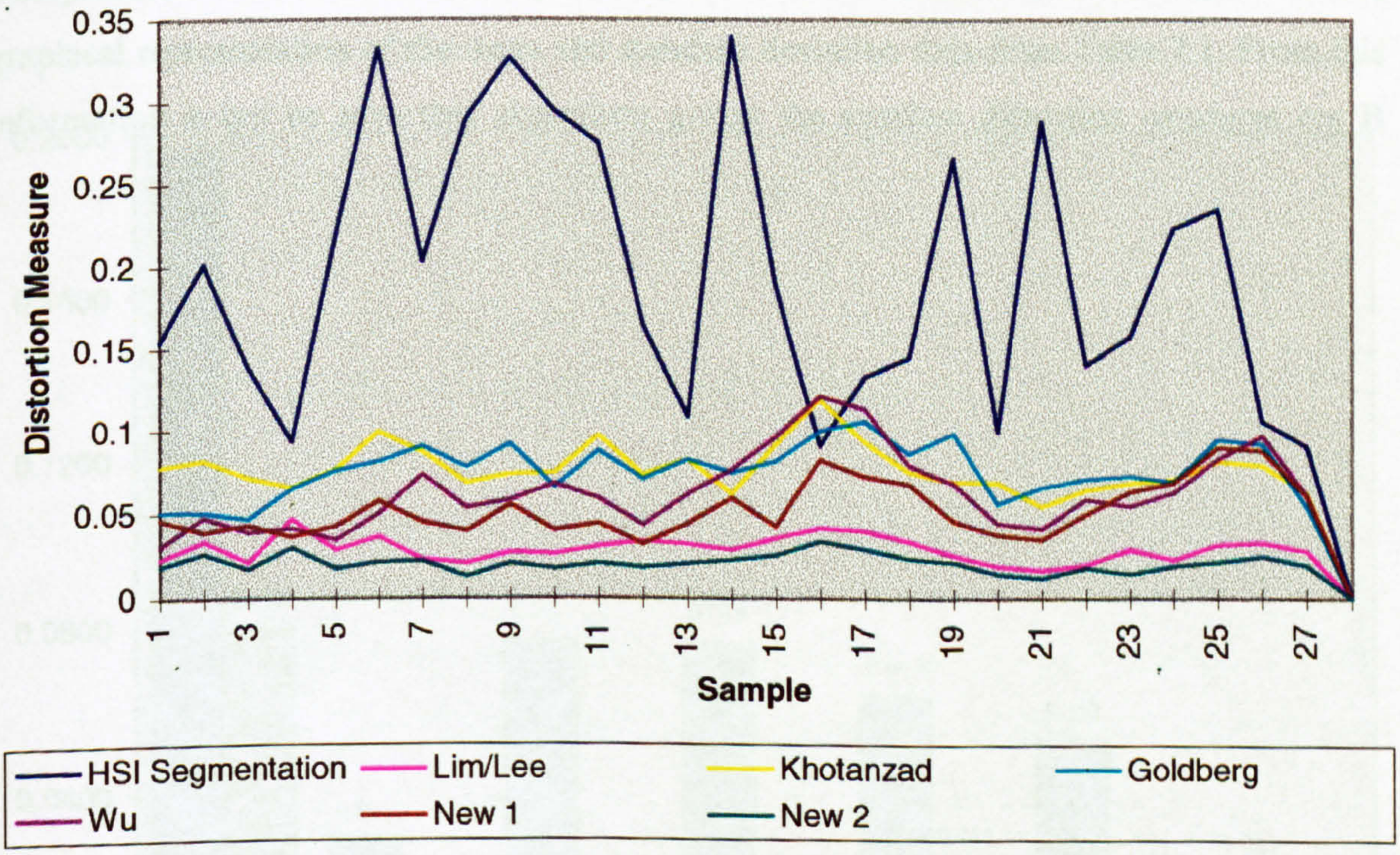

Figure 7.3 : Chart of Distortion Measures for Evaluated Algorithms

Sample Type	#	A	B	C	D	E	F	G
Mean	8.19	0.1967	0.0291	0.0771	0.0762	0.0636	0.0529	0.0209
Standard Dev.		0.0800	0.0071	0.0136	0.0160	0.0228	0.0162	0.0050
Covariance		0.0569	-0.0126	-0.0206	-0.0237	-0.0420	-0.0210	-0.0080
Correlation		0.2437	-0.6053	-0.5198	-0.5078	-0.6330	-0.4380	-0.5310

Table 7.1 : Results of Distortion Measure Testing

Where # represents the number of colours in the sample and the algorithms are denoted as follows: A = HSI method; B = Lim/Lee; C = Khotanzad; D = Goldberg; E = Wu; F = New 1; and G = New 2. The covariance and correlation statistics are the product of two series; colour versus specific algorithm.

Interpretation of these results is subjective, yet certain trends seem obvious. Figure 7.4 is a graphical representation of the mean and standard deviation data from Table 7.1. From this information it can be seen that algorithms giving the smallest distortion measures are B

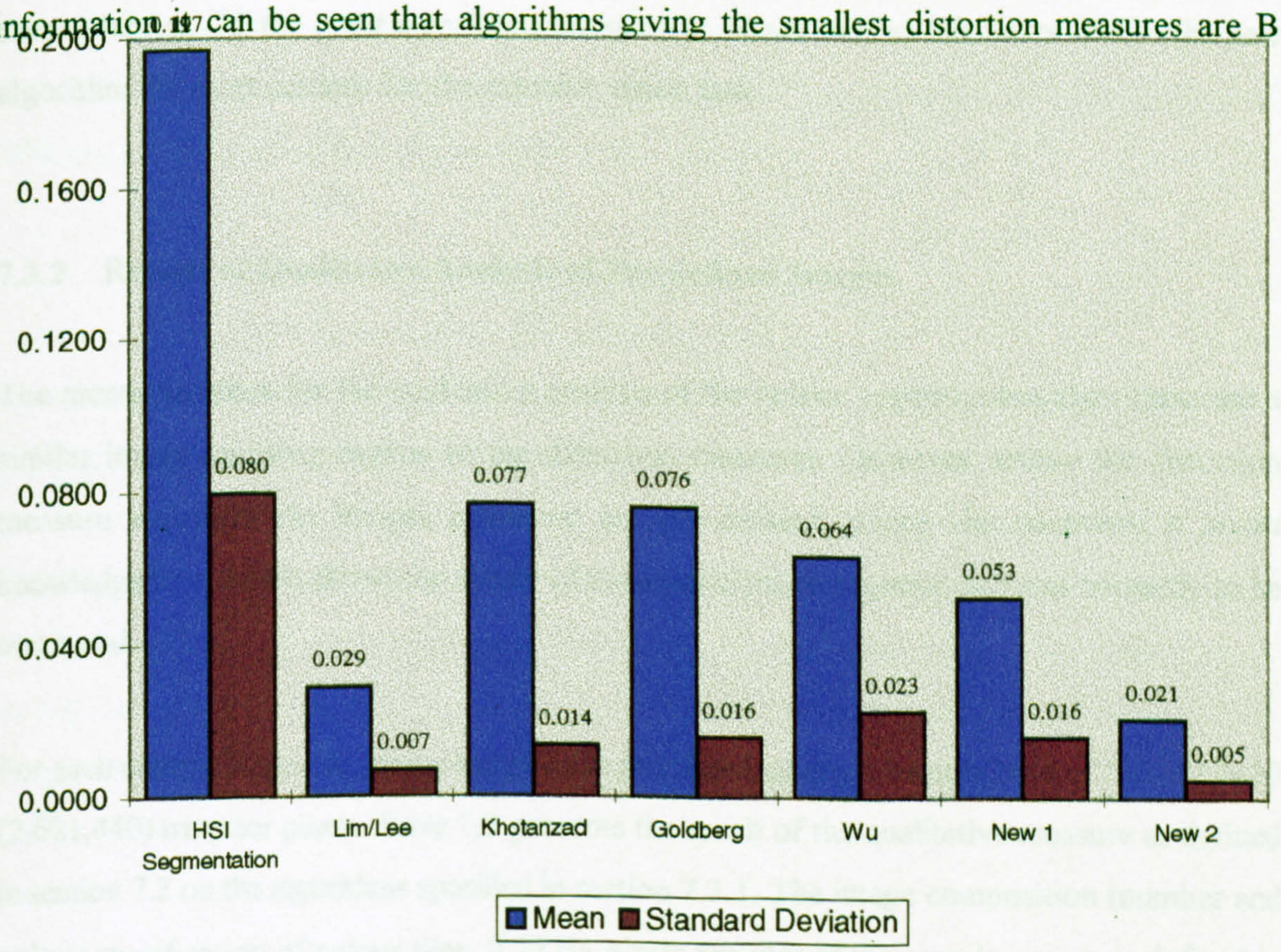

Figure 7.4 : Comparison of Mean and Standard Deviation

(Lim/Lee) and G (New 2). It is apparent from the standard deviation that these two methods also have the smallest deviation from the mean, giving a higher level of consistent segmentation. This is to be expected as they have the smallest data ranges.

Another outcome that can be inferred from the test results is that the algorithm A (HSI method) shows the strongest correlation to the number of colours in the original (reference) images. When cross-referenced with the original images this relationship was found to be true of images with large colour differences. Therefore, the other approaches are better for images with similar colours.

These results suggest that the new algorithm developed by this research is superior to the others (in some cases significantly) and gives the best approximation to the original image. However, this may be due to an increased number of defined colour regions. It is also speculated that the new algorithm performs better than the others as it is 'tuned' to rotary screen fabrics. All the other algorithms are generic. Nevertheless, this factor makes the new algorithm the most suitable for the machine vision task.

7.3.2 Results of Qualitative Analysis of Pre-defined Images

The measures taken for the qualitative analysis of the colour segmentation algorithms use a similar image sampling regime to the distortion measures. However, unlike the distortion measure approach the images inspected are pre-defined, giving the necessary *a priori* knowledge base, which allows the ability of the algorithms to segment patterns correctly to be measured.

For each control image ten unique samples are processed, giving a sample base of 512×512×10 (2,621,440) trivector pixels. Table 7.3 presents the result of the qualitative measure as defined in section 7.2 on the algorithms specified in section 7.3.1. The image composition (number and colour specification of colour tiles, 9.727% pixels per tile) of the sample images is defined in

Table 7.2. From the information in this table and the colour specification of the Dulux Colour Dimension tiles (as described in section 7.2) calculation of the minimum ΔE (colour difference) of each image is possible. This is useful for identifying the performance characteristics of each algorithm in comparison to the colour group separation.

To accurately calculate the ΔE value it is essential to use a uniform colour space, such as CIE*LUV* (see Chapter 3). Therefore, the colour difference is specified as ΔE^*_{uv}, the distance between two points representing colours in the CIE*LUV* space. The first stage for colour difference calculation for the experiment is the conversion from the ***Dulux*** Colour Dimension space (DCD space) to the CIE*LUV* uniform colour space. This is achieved by transforming from the DCD space (which is expressed in terms of hue, intensity and saturation, therefore a form of the CIE*HSI*) to RGB colour space (Equation 7.3), then using the formulas specified in Section 3.3.1 (Colour Space), Equations 3.1, 3.4–3.7 to convert to CIE*LUV*.

From this situation, calculation of ΔE^*_{uv} is possible, assuming the difference between two colours in L^*, u^*, and v^* are denoted by ΔL^*, Δu^*, and Δv^*, respectively, then the total colour difference may be evaluated as (Equation 7.4):

$$\Delta E^*_{uv} = \left[(\Delta L^*)^2+(\Delta u^*)^2+(\Delta v^*)^2\right]^{1/2} \qquad 7.4$$

This is an Euclidean metric giving the separation of two colour points in the three dimensional CIE*LUV* uniform colour space [Hunt, 1992].

NB. The CIE $L^*u^*v^*$ colour space is used here in preference to the CIE $L^*a^*b^*$ (which is the *de facto* standard used by many colour scientist) due to its increasing use in colour measurement in computing and image processing [Poynton, 1995]. Transformation between $L^*u^*v^*$ and $L^*a^*b^*$ colour spaces is computationally simple and well-documented [Hunt, 1992].

Sample	#	Composition (C_1:C_2:....:C_X)	RATIO (C_1:C_2:....:***background***)	Min ΔE
Q1	1	4×0090-Y60R	1 : **1.57**	93.14
Q2	2	2×3050-G20Y, 2×4030-R30B	1 : 1 : **3.14**	30.69
Q3	3	3050-G20Y, 4030-R30B, 0090-Y60R	1: 1: 1: **7.28**	30.69
Q4	4	3030-Y90R, 2020-R90B, 2060-R90B, 3060-B60G	1: 1: 1: 1: **6.28**	26.07
Q5	5	2×0050-Y, 4050-Y40R, 4020-B10G, 4030-R30B, 4010-G10Y	2: 1: 1: 1: 1: **4.28**	20.14
Q6	6	1010-Y30R, 2040-R10B, 2060-R10B, 3060-R10B, 5020-R70B, 3050-G20Y	1: 1: 1: 1: 1: 1: **4.28**	14.29
Q7	7	2×0080-Y80R, 2020-R90B, 0050-Y, 4040-R10B, 0080-G30Y, 7020-R90B, 5020-G10Y	2: 1: 1: 1: 1: 1: 1: **2.28**	26.07
Q8	8	8502-R, 2×8502-G, 0080-G30Y, 4010-G10Y, 0090-Y60R, 2060-R90B, 3020-B70G, 2070-B	1: 2: 1: 1: 1: 1: 1: 1: **1.28**	17.20
Q9	9	4020-B10G, 3050-G20Y, 3010-G70Y, 4040-R90B, 3060-R30B, 7020-R30B, 3070-Y70R, 1060-Y60R, 1020-Y60R	1: 1: 1: 1: 1: 1: 1: 1: 1: **1.28**	15.42
Q10	10	1010-Y30R, 0080-G30Y, 4030-R30B, 1070-G10Y, 0050-Y, 3020-B70G, 2060-R90B, 3050-G20Y, 5020-R70B, 2040-R10B	1: 1: 1: 1: 1: 1: 1: 1: 1: 1: **0.28**	11.56

Table 7.2 : Composition of Test Images for Qualitative Analysis

Sample Type	#	A	B	C	D	E	F	G
Q1	1	99.18	99.97	99.73	99.84	99.33	99.15	99.99
Q2	2	98.74	99.99	99.54	99.43	98.97	98.96	99.99
Q3	3	98.72	99.84	98.97	99.14	98.53	98.91	99.99
Q4	4	95.56	99.81	98.39	98.27	97.67	98.64	99.93
Q5	5	92.33	99.56	98.08	98.03	97.31	98.19	99.75
Q6	6	85.97	99.23	93.66	95.32	95.40	94.55	99.54
Q7	7	89.34	99.46	95.72	95.73	94.71	94.32	99.95
Q8	8	84.14	99.31	92.25	92.61	91.95	92.46	99.37
Q9	9	82.67	99.14	92.97	92.89	91.18	91.89	99.44
Q10	10	79.98	98.96	90.93	91.01	89.74	91.36	99.21
Mean	5.5	90.663	99.527	96.024	96.227	95.479	95.843	99.716
Standard Dev.		6.8832	0.3465	3.1591	3.0287	3.3007	3.0749	0.2846
Covariance		-19.16	-0.954	-8.561	-8.412	-9.227	-8.423	-0.706
Correlation		-0.969	0.986	0.963	0.988	0.993	0.979	0.878
Covar ΔE (see Table 7.2 for minimum ΔE)		35.360	1.711	15.830	14.578	15.160	14.350	1.658

Table 7.3 : Results of Qualitative Analysis Testing (% of correctly assigned pixels)

Where # represents the number of colours in the sample and the algorithms are denoted as follows: A = HSI method; B = Lim/Lee; C = Khotanzad; D = Goldberg; E = Wu; F = New 1; and G = New 2. The covariance and correlation statistics are the product of two series; colour versus specific algorithm.

Figures 7.5 and 7.6 are graphical representations of the result from Table 7.3. The results show that algorithms B and G offer the best segmentation performance (cf. Section 7.3.1). In particular, images with fewer colours and larger ΔE separations are almost perfectly segmented with a false pixel assignment of less than 0.01%. This equates to 1 false assigned pixel per

10,000. It is speculated that these false assignments are due to the image capture rather than the algorithms, due to false colour being introduced at colour boundaries (cf. Chapter 4).

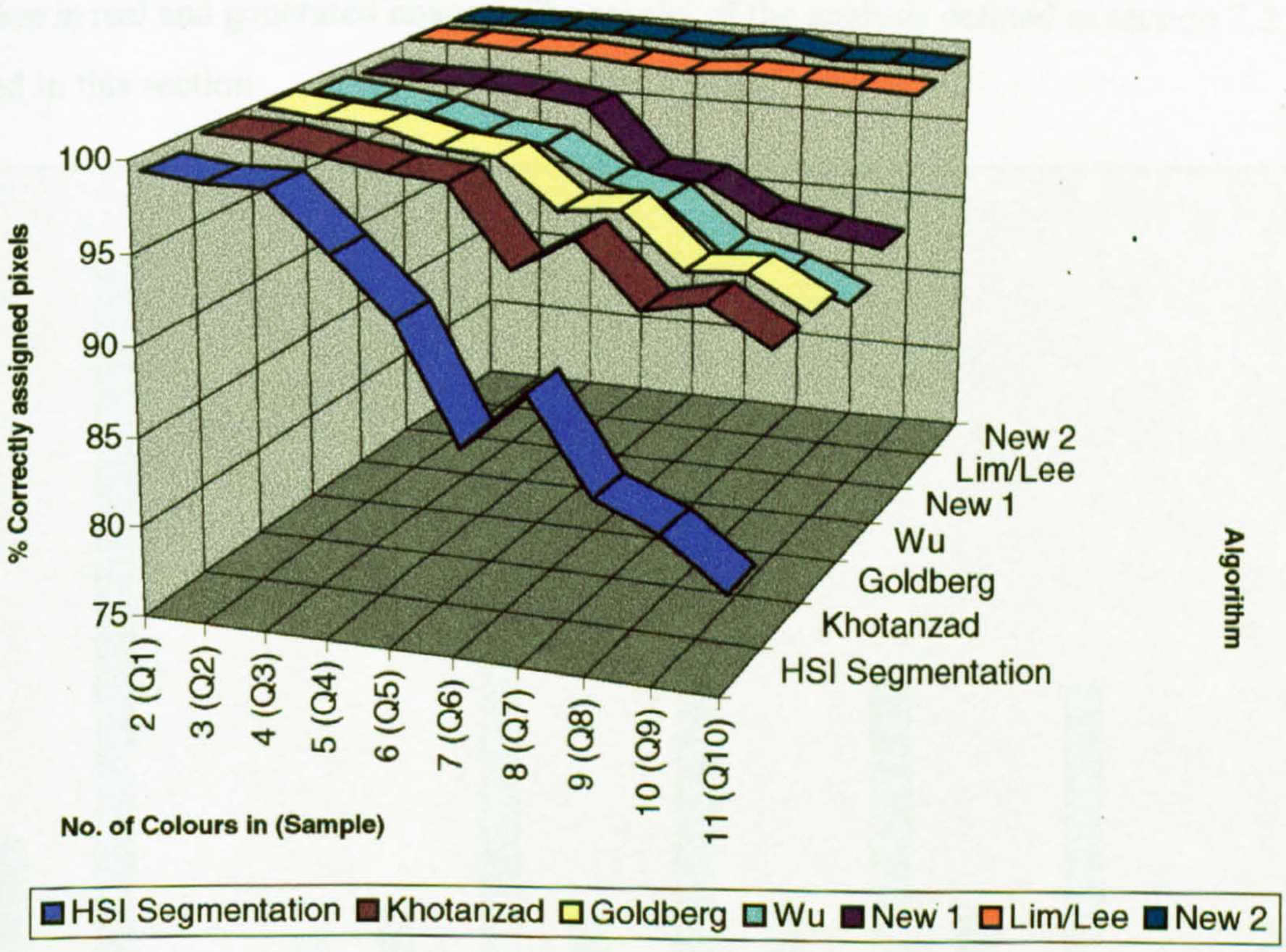

Figure 7.5 : Qualitative Performance of Algorithms

In Q1 there are 2160 boundary pixels of which 28 and 23 are incorrectly assigned by algorithms B and G respectively, this gives an error probability of approximately 1% for boundary pixels. It is seen from the data in Tables 7.2 and 7.3 that the error rate increase in proportion to the number of boundary pixels. A possible way to reduce this problem is to increase the acquisition resolution and use a predictive approach to calculate the boundary position. It is yet to be shown whether this approach is practical.

7.3.3 Inspecting for Gaussian Artifacts

Section 7.2 identifies an important area for analysis, namely the testing for Gaussian noise distribution in real and generated images. The results of the analysis defined in section 7.2 are presented in this section.

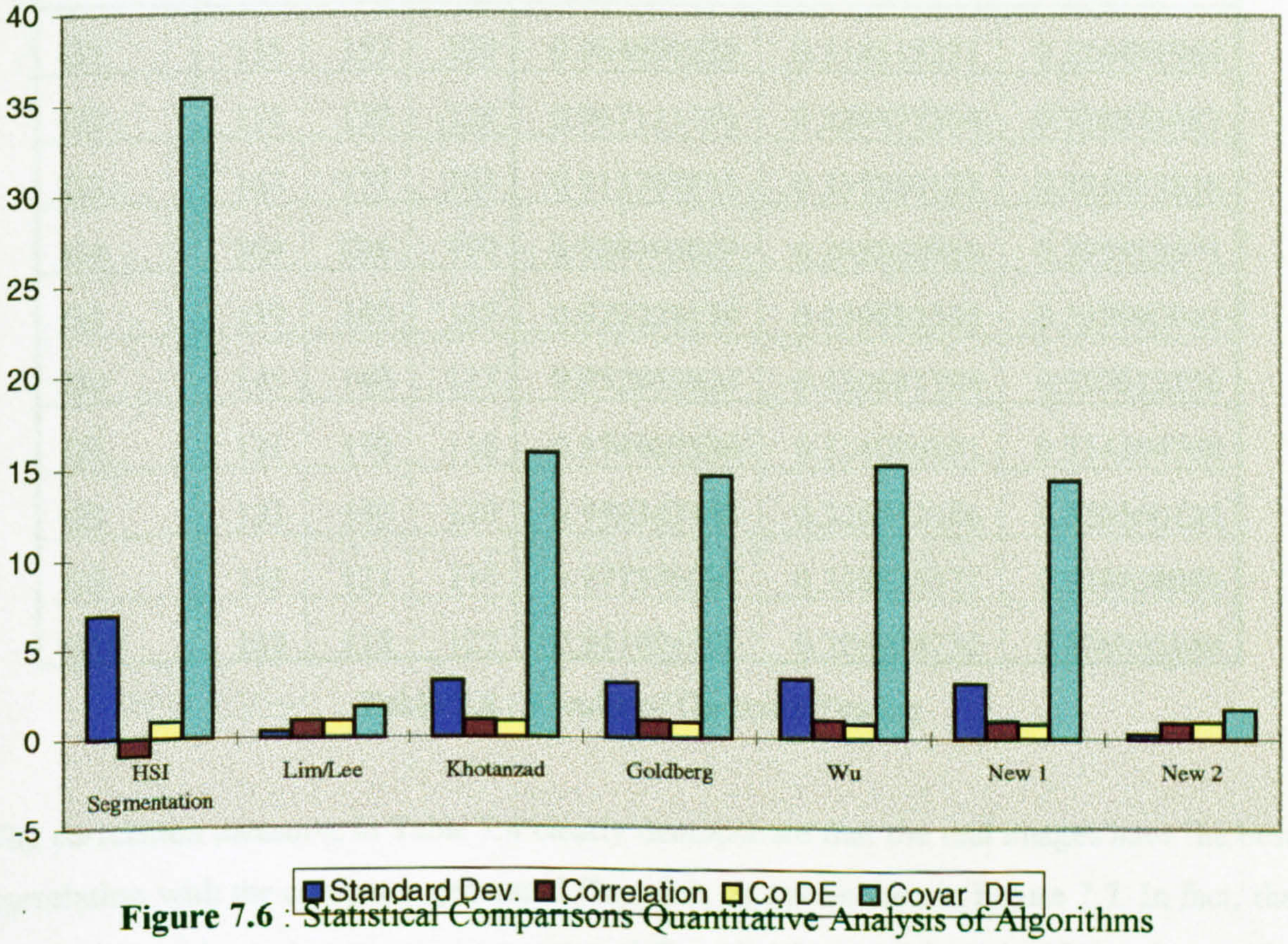

Figure 7.6 : Statistical Comparisons Quantitative Analysis of Algorithms

Table 7.4 shows the results of the mean and standard deviation analysis of the 'real' test images. This data is used to produce a computer generated image with a Gaussian distribution of noise defined by mean and standard deviation of the 'real' image. The RGB histograms of the two images are then compared and an expression of their correlation is given. This correlation value is contrasted with two other correlations: between the 'real' image and a computer generated image with the same mean and a standard deviation of zero; and between the 'real' image and a computer generated image with the same mean, but with additive noise

generated by a Monte Carlo algorithm. It is anticipated that the best correlation will be between the 'real' and computer generated Gaussian images.

Sample	Mode			Correlation		
	R	G	B	Gaussian	Noise	Pure
G1	155	157	129	0.964601228	0.314515331	0.314491969
G2	158	159	129	0.967111196	0.328477504	0.328535487
G3	167	177	163	0.913707415	0.335200173	0.335303318
G4	204	208	170	0.928393629	0.295830939	0.295813671
G5	139	160	135	0.970229139	0.339892535	0.339990942
G6	145	140	117	0.952055926	0.330581794	0.330512256
G7	131	170	118	0.974967536	0.314096101	0.314104768
G8	121	140	120	0.959343148	0.326542186	0.326560132
G9	133	121	114	0.977576087	0.328826571	0.328838988
G10	128	135	127	0.941894393	0.326928732	0.326991084

Table 7.4 : Results of Gaussian Testing

The correlation measures in Table 7.4 clearly demonstrate that the real images have the best correlation with the computer generated Gaussian, as can be seen in Figure 7.7. In fact, the correlation of the real image to the generated Gaussian is approximately 95%, whereas the other correlations are in the low 30%. It is important to note that these histograms are skewed towards zero, this is a function of their acquisition (dark matter on the colour tile, and some dark spikes in the hardware) so is not strictly representative of the colour. This validates the early assumptions about the Gaussian distribution of individual colours in a real image. Appendix E contains the complete results of the Gaussian-fit testing.

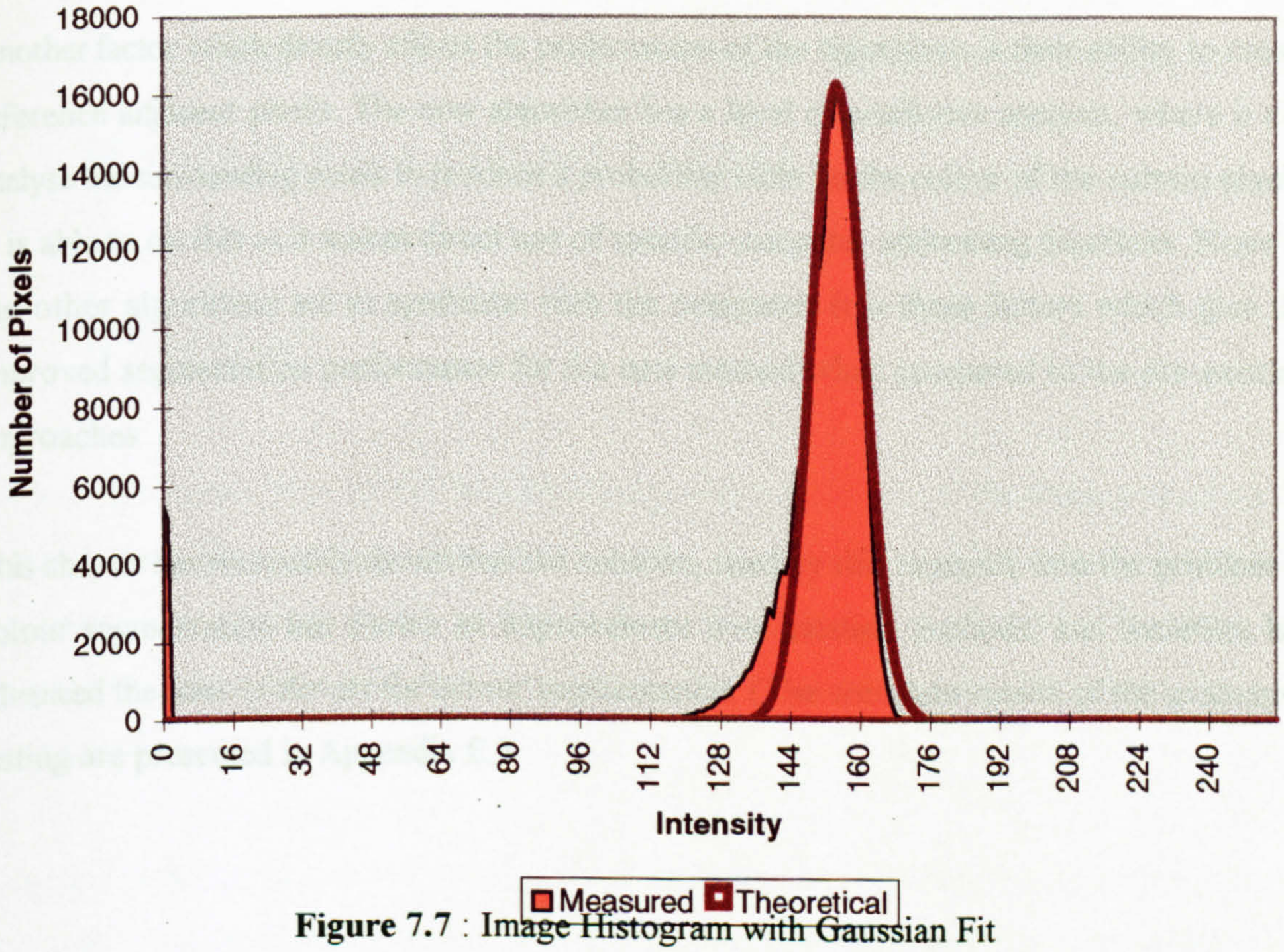

Figure 7.7 : Image Histogram with Gaussian Fit

7.4 Conclusions

The overall conclusion that can be derived from the performance evaluation of the various algorithms examined in this section, is that the new algorithm developed by this research is consistently better than any of the other evaluated algorithms. There are several conjectures for why this is the case. First, and most importantly, the design of the other algorithms is more or less generic, while the new algorithm was designed for a specific application. Most of the more traditional algorithms are optimized to segment natural scenes, where there can be millions of colour variations, and harsh segmentation is not necessarily beneficial. However, the new algorithm is not concerned with the niceties of visually convincing segmentation, but more with the accurate segmentation of distinct colour groups. As such it offers a more flexible approach to the segmentation of screen printed fabrics than the other methods.

Another factor which directly affects the performance of the algorithms is their ability to cross-reference adjacent pixels. The new algorithm has a level of predictive analysis, where it can analyse the surrounding pixels to produce a probability table for the colour of the current pixels. It is able to do this as it makes direct use of specific computer addressing functions. None of the other algorithms are as symbiotic with the computer. It is these factors which give the improved segmentation performance for the new method when compared to the pre-existing approaches.

This chapter has reasonably shown that the solution, used by this research, into the problem of colour segmentation has shown an improvement over existing methods, and therefore has advanced the *state of the art* for colour segmentation. (The complete results of the evaluative testing are presented in Appendix E.)

8 Proposal for an On-line Fault Detection System for Rotary Screen Printed Fabrics

8.1 Introduction

Preceding chapters have established laboratory-based methods for the inspection of rotary screen printed fabrics using colour machine vision. To satisfy the objectives of this research, a proposal for a factory-based, on-line fault detection system is required. Therefore, it is necessary to demonstrate how the laboratory developed methods can be transferred to an on-line system.

Chapter 1 identifies the two main categories of faults that occur during rotary screen printing, systematic and random faults. In the following sections proposals for a systematic fault detection system and a random fault detection system are given. These two systems could then be run in parallel, leading to a 100%, full fabric width, fault detection system. Both systems would use colour line scan cameras (cf. Chapter 4) for fabric data acquisition.

The individual components of the systems that would process the data supplied by the colour line scan camera, have been successfully simulated during this research. For both systematic and random fault detection systems, there is a common life cycle, although the data processing differs. This life cycle is as follows;

1. Initial fabric data acquisition, for colour segmentation and boundary selection (data reduction). This process has been simulated using the area sensor device; image data is processed using the existing colour segmentation algorithms. *For the systematic fault detection system the data can then be defined as a series of mutually exclusive binary signals. A column count is carried out on each of the sensor elements (pixels) to*

identify which bands of the linescan are most 'active' in terms of boundaries. These bands are then selected as the mask for further processing.

2. Data is acquired by the linescan (*with only the relevant band data been used by the systematic system*) to build up the template for the registration analysis. This is then used as the reference to which future rotations must subscribe.

3. On each rotation of the fabric the current data is correlated to these templates using well-established correlation techniques. If the data does not fall within the pre-defined tolerance limits, an error is flagged and further processing is done to decide the error type and signal the appropriate corrective action.

Both systems work on the assumption that at the start of a print-run the fabric print is 'perfect'. It is essential that this is true as all subsequent fault decisions are made with reference to this 'standard'. The following sections will discuss how each system acquires and processes the fabric data.

8.2 Systematic Fault Detection

The on-line inspection system for systematic faults will be based on the software algorithms and hardware used by the laboratory development system. Any modifications, of the system, required for the industrial environment (such as shielded boxes for the electronic components) would be made prior to installation at the factory. The inspection system would be mounted on a rotary screen printing machine, in a position where all the screens have printed, but before the fabric is 'lifted off' the print blanket (ref. Figure 8.1).

It is critical that the system is synchronized to the printing process to enable accurate inspection. This will require some minor modification to the rotary screen printing machine. The use of a Hall sensor and magnet on a screen drive unit should provide a trigger pulse

sufficient to synchronise the inspection system and the print machine (ref. Figure 8.1). A schematic of the proposed system is shown in Figure 8.1.

The proposed system, defined so far, would be the same for systematic and random faults (although, theoretically, the systematic system does not require full-width inspection). Both systems would have a common inspection point and could even utilize the same colour linescan cameras. It could be argued that systematic fault inspection is a subset of random fault inspection, in that to inspect for random faults requires complete fabric coverage, therefore any systematic fault occurrence will also have been acquired. However, inspecting with reduced coverage precludes random faults, and simplifies the inspection process. Section 8.2 will show how the systematic system proposed in the current section can be enhanced to enable random fault detection.

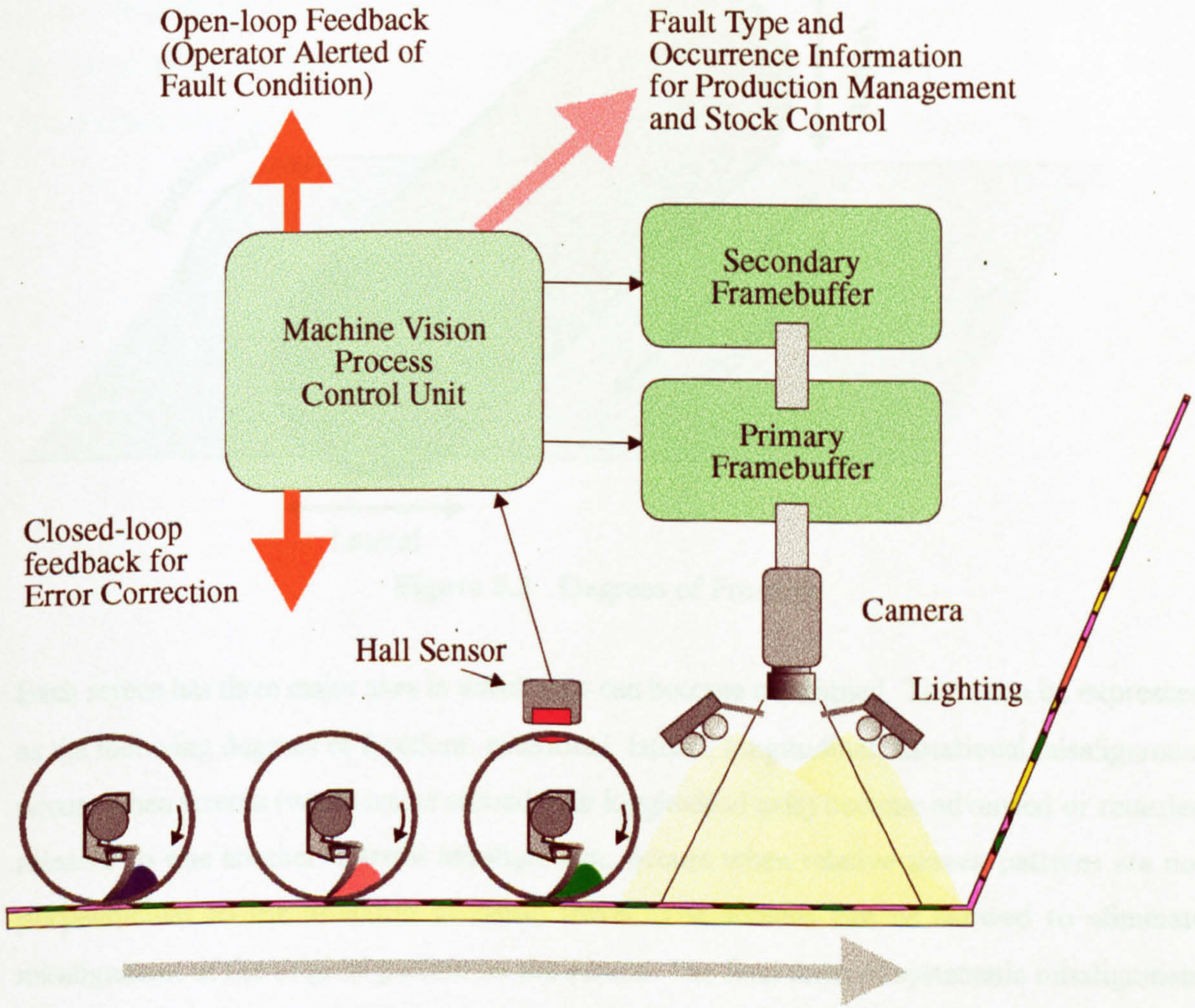

Figure 8.1 : Schematic of proposed Inspection System

Chapter 1 defines systematic faults in detail, but it is useful to reiterate the salient points here. Systematic defects are defects that occur throughout consecutive pattern repeats during the production process. They are almost entirely due to the positioning or motion of the individual rotary print screens. Hence, they can usually be corrected by mechanical adjustment of the screens during production. (Currently, this manual adjustment is gauged by eye, with skilled machine operators, setting up the complex print machinery during a slow speed run-up phase, prior to full-speed production.)

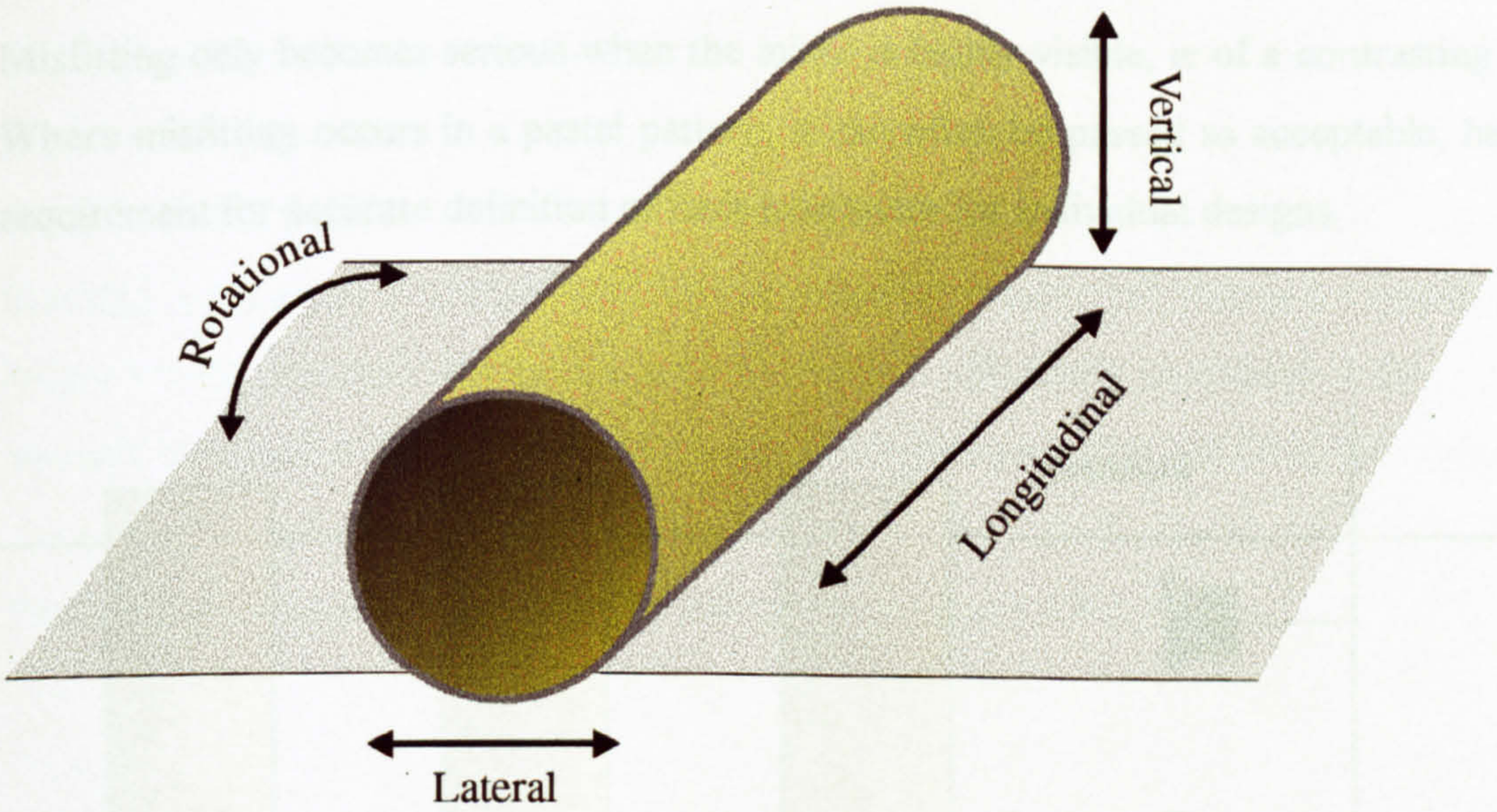

Figure 8.2 : Degrees of Freedom

Each screen has three major axes in which they can become misaligned. These can be expressed as the following degrees of freedom: rotational; lateral; longitudinal. Rotational misalignment occurs when screens (which rotate around their longitudinal axis) become advanced or retarded relative to one another. Lateral misalignment, occurs when relative screen patterns are not perpendicular to the direction of fabric travel. The screens can be skewed to eliminate misalignment of the original pattern on the screen. The final form of systematic misalignment is described as longitudinal. This is occurs when the pattern areas of individual screens are not parallel to one another. (Another degree of freedom is in the vertical axis. However, systematic faults due to vertical misalignment are rare, as they are blatant, causing missing colour and smearing). Figure 8.2 illustrates the possible degrees of freedom that can cause systematic misalignment in rotary screen printing.

Therefore, misfitting occurs when one or more of the rotary screens are incorrectly positioned relative to the others. It is manifested as a gap or border around a section of the printed pattern where two colours that are meant to border each other are now either overlapping or spatially separated by a detectable amount. Overlapping of colours in this case does not produce a completely new shade of colour, due to the opaque nature of the colour paste (cf. Chapter 1), but an overlap at one point in the pattern is likely to be echoed by a gap at some other section.

Misfitting only becomes serious when the misfit is highly visible, ie of a contrasting colour. Where misfitting occurs in a pastel pattern, it can often be passed as acceptable, hence the requirement for accurate definition of fault tolerances for individual designs.

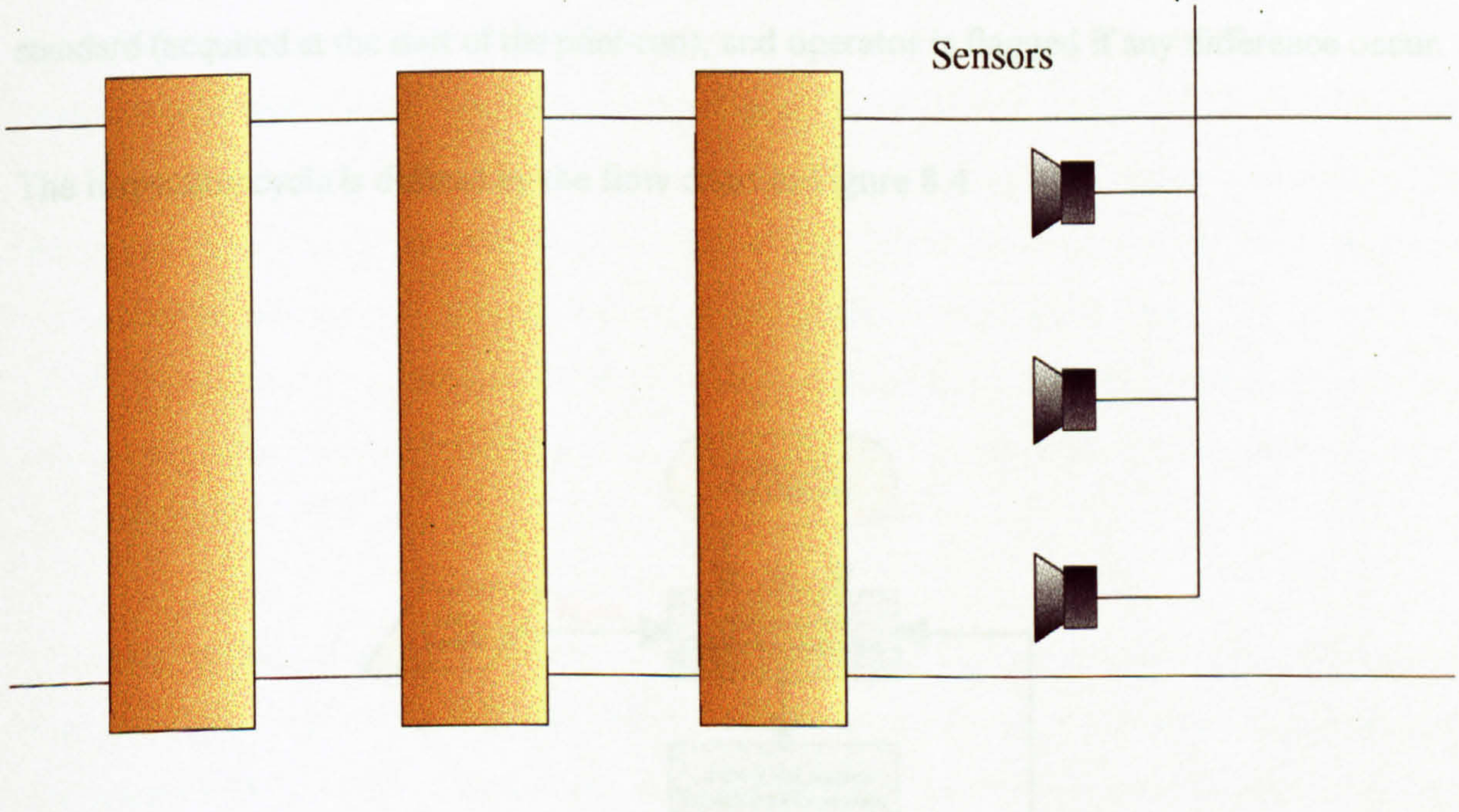

Figure 8.3 : Plan view of Sensor Location

The inspection zone of the fabric would be illuminated by an array of fluorescent tubes, powered by a DC voltage source, helping to prevent AC mains voltage noise from infecting the image data.. Chapter 4 established the requirement for an array of three colour line scan cameras, across the fabric width (perpendicular to the direction of fabric travel), to inspect for systematic faults (Figure 8.3). A minimum inspection system of two sensors, positioned towards either side of the fabric, would allow for the detection of most systematic faults, but a more sophisticated analysis (which would also inspect for bowing faults) requires an additional sensor at the centre of the fabric.

During a print-run image data is constantly acquired by the colour line scan cameras, and passed to an intermediate frame buffer for the colour segmentation preprocessing (cf. Chapter 6). This frame buffer is then flushed to the main processing buffer on each screen repeat. Flushing is triggered by a signal derived from the Hall sensor (ref. Figure 8.1) located on the rotary screen. As each new repeat is produced it is effectively compared with a pre-stored standard (acquired at the start of the print-run), and operator is flagged if any difference occur.

The inspection cycle is defined by the flow chart in Figure 8.4

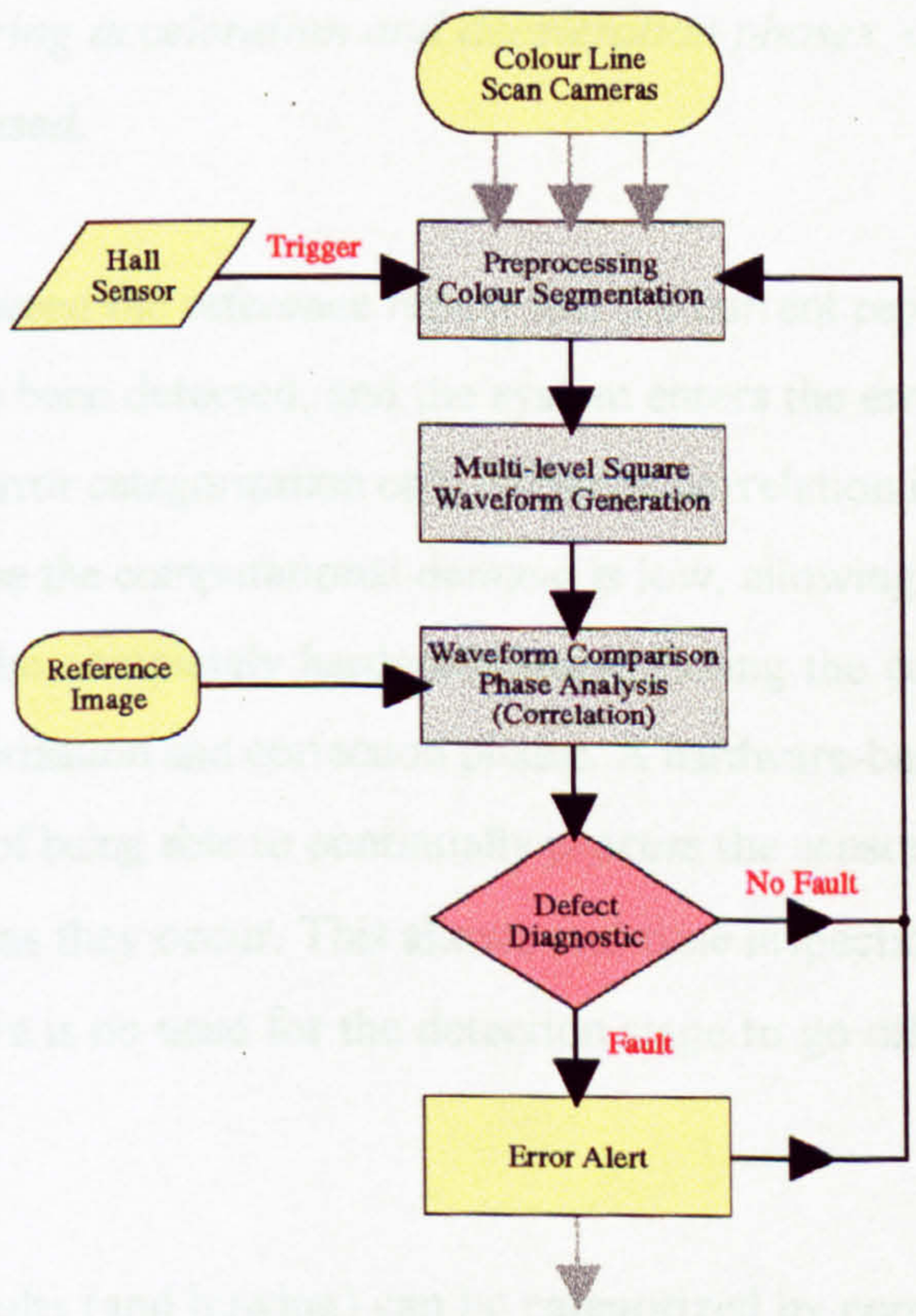

Figure 8.4 : Flow Chart of Systematic Fault Inspection Process

As previously mention in Chapter 6, a multi-level square wave can be generated for any individual cell in the linescan array. This signal can then be either processed immediately or demultiplexed and inspected on an individual binary waveform basis (which simplifies processing for error detection and classification).

Comparison against the pre-stored image (which is also expressed as a series of binary waveforms) uses standard correlation techniques. Each binary wave can be expressed as specific pigment against time and it is apparent that they must have the same time base as the reference waveform. Therefore, careful monitoring of fabric speed, hence screen repeat must be maintained, and the waveform with the higher resolution scaled accordingly. *NB the velocity of the fabric must be constant over the period of a pattern repeat, otherwise scaling errors occur. Therefore during acceleration and deceleration phases, of the print machine, error tolerances are increased.*

If the correlation between the reference repeat and the current repeat falls outside predefined tolerance, an error has been detected, and the system enters the error categorization stage. As the system performs error categorization only when the correlation is outside tolerances during the 'in-tolerance' phase the computational demand is low, allowing fast processing. In fact the detection stage can be completely hardware-based freeing the computer processors for the higher demand categorization and correction phases. A hardware-based detection phase has the additional advantage of being able to continually process the sensor data, queuing faults to the categorization phase as they occur. This allows real-time inspection of the fabric, trapping all detectable faults (there is no need for the detection stage to go off-line, while faults are being categorized).

All the systematic faults (and bowing) can be categorized by comparing the relative position of binary waveforms from the three inspections areas against the ideal waveforms. In the case of a perfect match all three current signals will be in phase with the reference signals. If one of the rotary screens has skewed in relation to the other screens there will be a corresponding

alteration in phase. Figure 8.5(a-f) illustrates how misalignment affects the phase of an idealized signal.

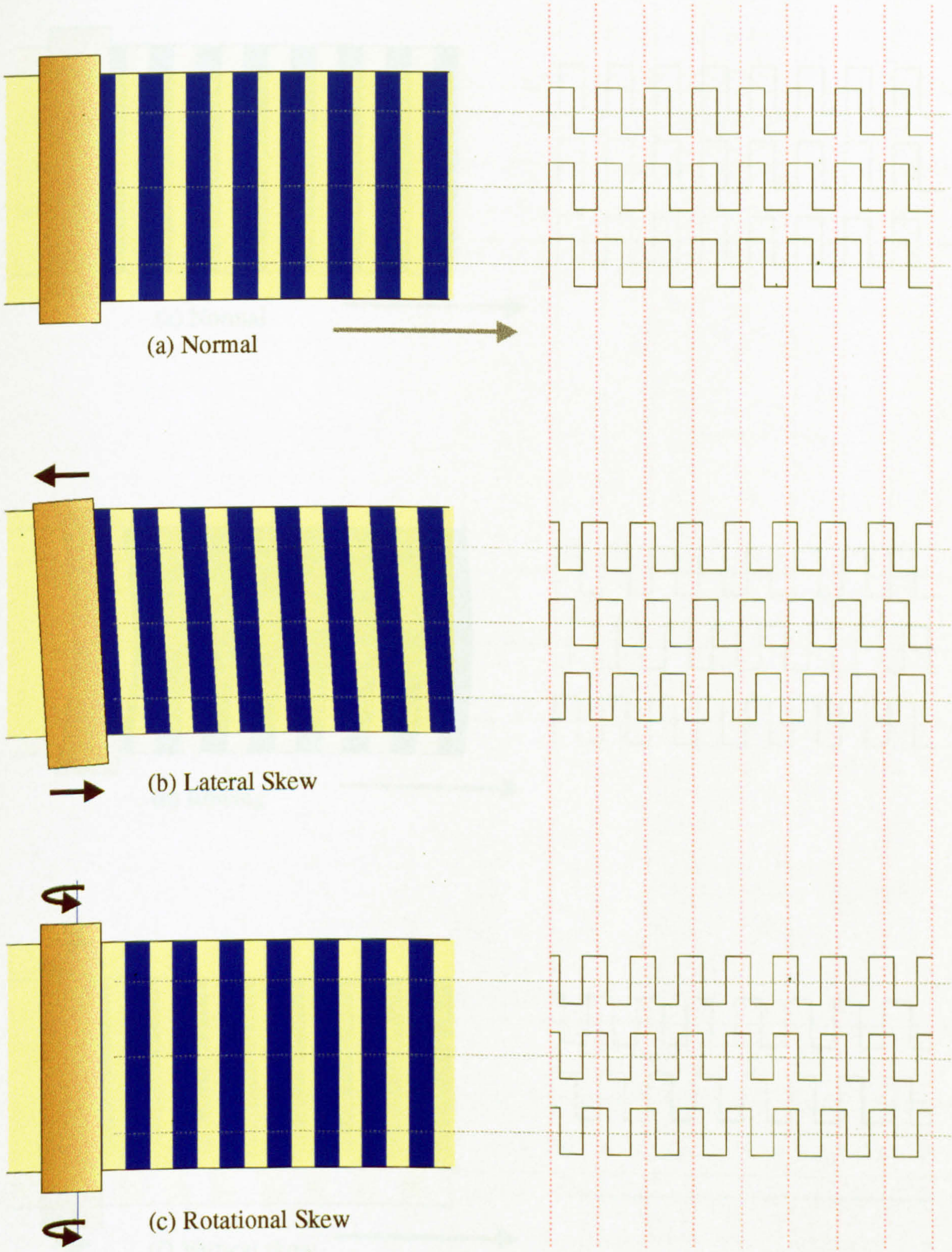

(a) Normal

(b) Lateral Skew

(c) Rotational Skew

Figure 8.5 : Examples of Systematic Errors for Rotary Screen Printing

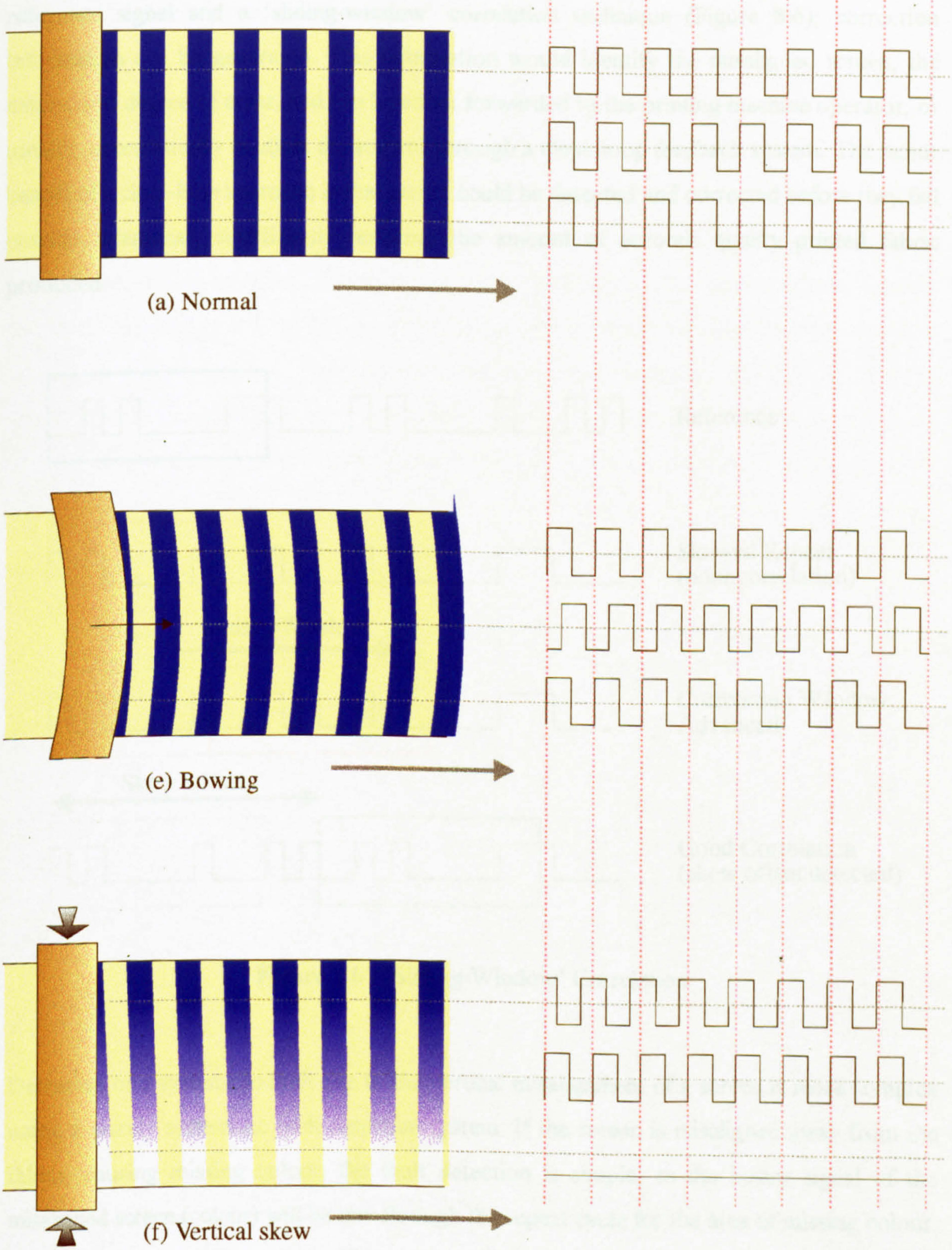

(a) Normal

(e) Bowing

(f) Vertical skew

Figure 8.5 : Examples of Systematic Errors for Rotary Screen Printing

Once the direction and magnitude of misalignment has been detected using a subset of the reference signal and a 'sliding-window' correlation technique (Figure 8.6), correction information can be generated. This information would identify the misaligned screen, the nature, and degree of error, and can be either forwarded to the printing machine operator, or ideally, automatically readjust the screens through a close-loop feedback system. The major benefit of a close-loop approach is that errors could be detected and corrected before they fall outside tolerances, significantly reducing the amount of seconds quality printed fabric produced.

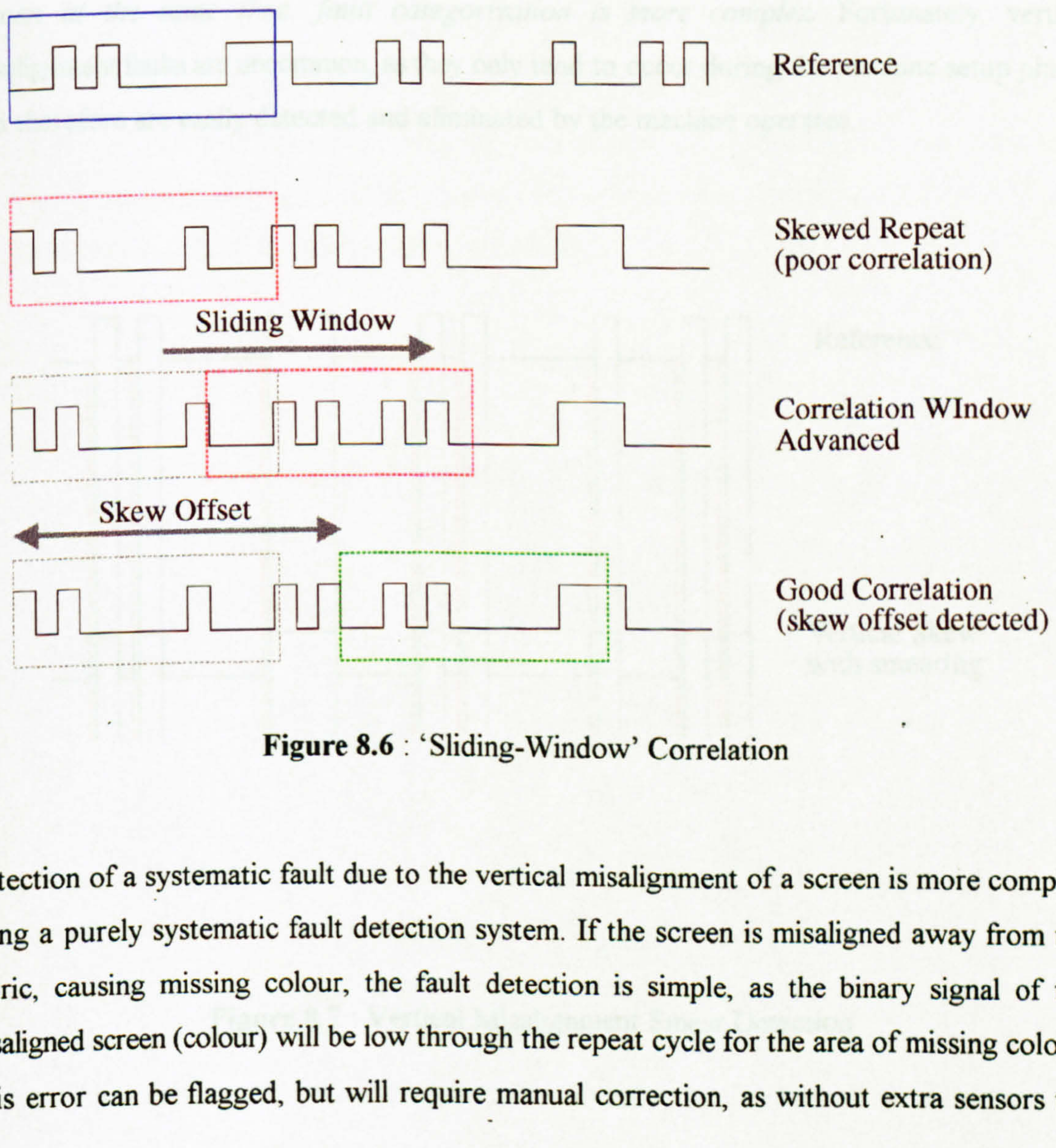

Figure 8.6 : 'Sliding-Window' Correlation

Detection of a systematic fault due to the vertical misalignment of a screen is more complex using a purely systematic fault detection system. If the screen is misaligned away from the fabric, causing missing colour, the fault detection is simple, as the binary signal of the misaligned screen (colour) will be low through the repeat cycle for the area of missing colour. This error can be flagged, but will require manual correction, as without extra sensors the

degree of misalignment is unobtainable. (Missing colour would be apparent as an obvious error on a random fault detection system due to the image subtraction approach, ref. Section 8.3).

The other effect of vertical misalignment (smearing due to too much pressure at the contact point) introduces additional processing difficulties. Detection of the fault is, again, achievable using correlation techniques. However, the fault categorization is different. Usually, the leading edges of the smeared colour areas are in register with the reference signal, but the smearing extends their trailing boundary. Therefore, comparisons of colour area size is needed to identify the fault type (Figure 8.7). *NB if vertical misalignment and skewing both occur on the same screen at the same time, fault categorization is more complex.* Fortunately, vertical misalignment faults are uncommon, as they only tend to occur during the machine setup phase, and therefore are easily detected and eliminated by the machine operator.

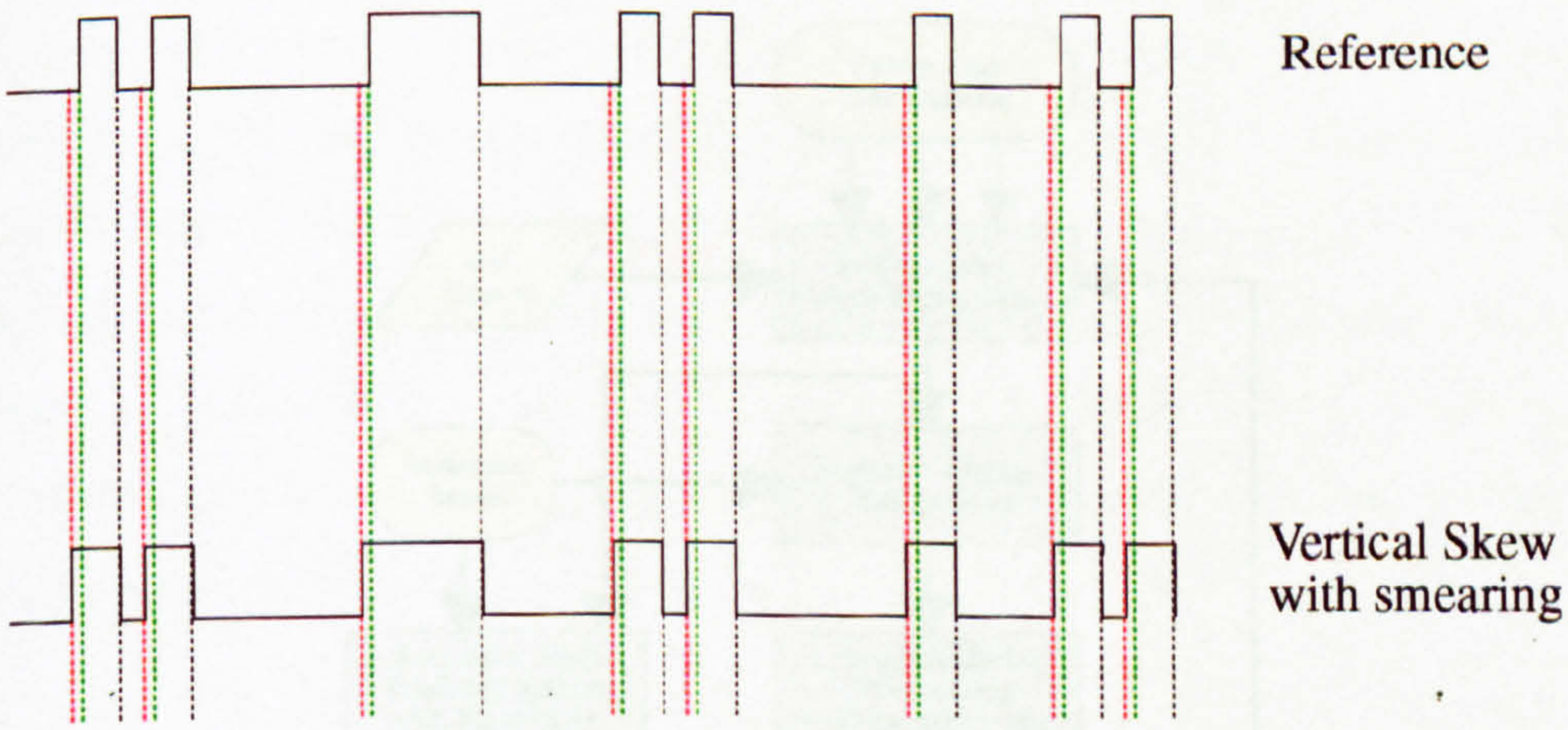

Figure 8.7 : Vertical Misalignment Smear Detection

8.3 Random Fault Detection

Chapter 1 and Section 8.1 highlighted some of the major differences between inspection for random faults and for systematic faults. It was proposed that a systematic fault detection system could be treated as a subset of a random fault detection system. Simply, to provide an additional system for random fault detection requires more hardware, but not significantly more processing. The essential requirement of a random fault inspection system is that it inspects the full-width of the fabric, as a random fault can occur at any position within the print.

As with the systematic design, the Hall sensor triggers the intermediate buffer to be flushed to the process buffer (however, in this case the buffer holds a full-width image of the repeat). Similarly, as each new repeat is produced it is effectively compared with the pre-stored reference image. The flow chart for the random fault inspection cycle (Figure 8.8) is similar to that of the systematic fault system (ref. Figure 8.4).

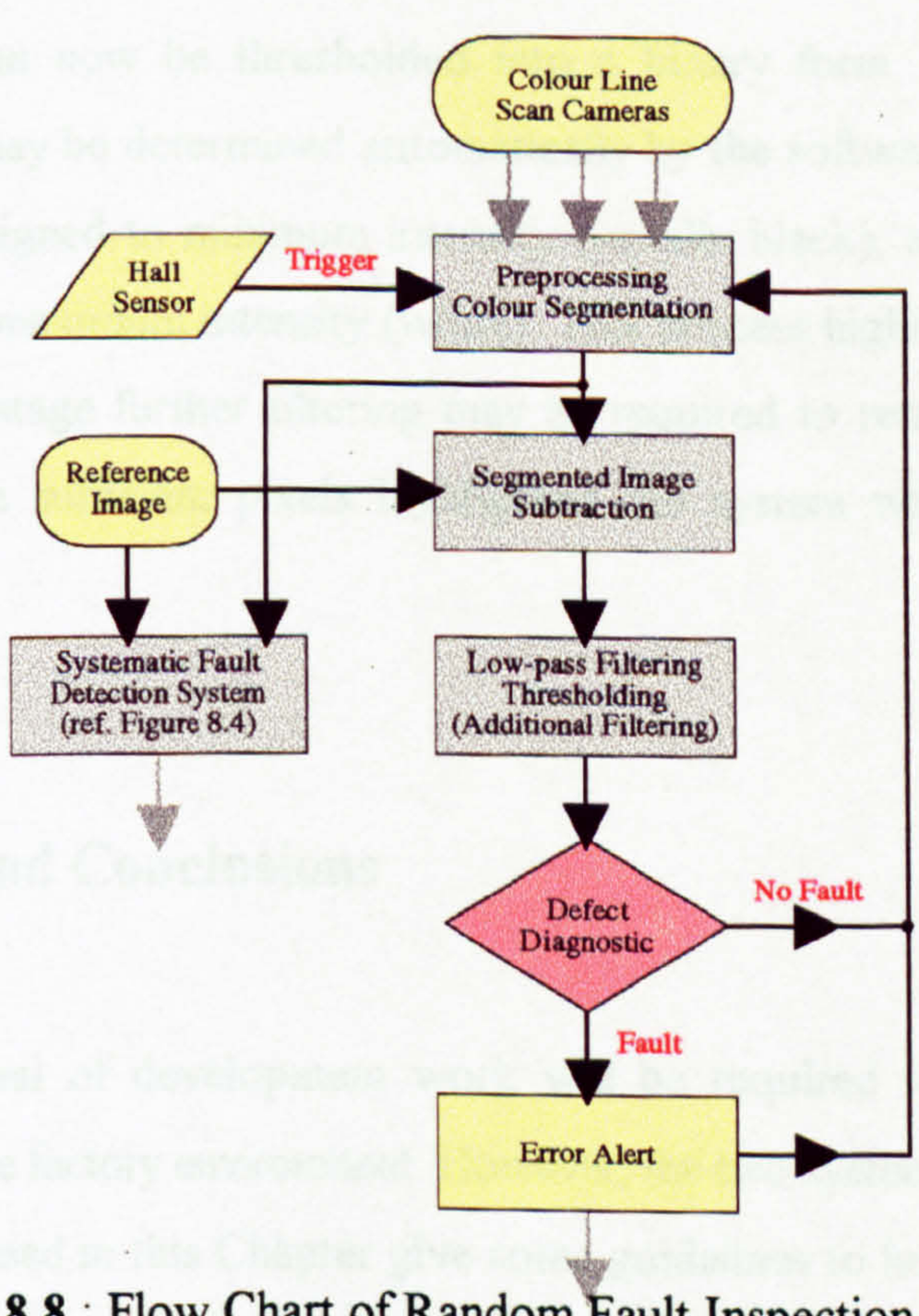

Figure 8.8 : Flow Chart of Random Fault Inspection Process

The segmented image subtraction uses a previously stored segmented image of the pattern as a 'master', subtracting the current repeat pattern from it. Therefore, any differences in the two patterns will be retained, while all areas of similarity will be removed. The process leaves the system with a generally dark image (small differences), with any areas of difference showing up as brighter points (large differences) or areas.

Once subtracted, the resultant image is 'cleaned up' using a low-pass filter. A typical low-pass filter removes unwanted noise by a process of averaging individual points with their immediate neighbours. This process removes individual noise pixels, while leaving genuine clusters of points almost unaffected. However, this form of low-pass filter introduces new pixel intensity values, which may cause complications in the fault categorization and correction stages. A better approach would be to use a median filter to remove noise pixels. A median filter is a non-linear filter widely used for the suppression of impulsive noise, by replacing the central pixel of a moving box with the median value of the pixels within the box.

The filtered image can now be thresholded into a binary form. The threshold may be heuristically set or it may be determined automatically by the software. All points below the threshold will be reassigned to minimum intensity (usually black), and all points above the threshold will be set to maximum intensity (white). This process highlights all the pixel points of difference. At this stage further filtering may be required to remove points below fault tolerance. If there are sufficient pixels highlighted the system will then perform a fault diagnostic procedure.

8.4 Summary and Conclusions

Obviously, a great deal of development work will be required to produce a functional inspection system for the factory environment. However, the two systems (or one complete and one subsystem) proposed in this Chapter give some guidelines to how this can be achieved.

Faults of both random and systematic origin can be detected, and in the case of the systematic system, classified and corrected. Further research is required to develop more complex diagnostic systems to categorize and suggest correction data for random faults. Correction data should include fault location, severity, possible cause, and even a course of remedial action for the operator to take.

9 Conclusions, Further Research

Importantly, the research described in this thesis has contributed **new** knowledge in several areas. First, it has given new knowledge in the field of machine vision and textiles, due to the thorough investigation of the rotary screen inspection problem. Additionally, it has contributed to colour image processing with the development of a colour segmentation methodology that improves on existing, state-of-the-art, colour segmentation algorithms, when applied to 2-D scenes containing only a small number of specific colours, ie less than twenty (eg. images of printed fabrics). This new methodology has an additional benefit of being computationally efficient as it uses computer-based iterative methods for fuzzy logic clustering, and segmentation.

The main achievements of the author during this research are:

- Design and implementation of new methodologies for the segmentation of pigments in RGB colour space.
- Investigation of fabric texture effects on image quality.
- Development of a new qualitative method for evaluation of colour segmentation methods.
- Evaluation and comparison of new and existing colour segmentation methodologies.
- Identification of 'boundary pixels' as principal error originators for segmentation methods.
- Assessment of images for Gaussian-based noise.
- Proposals for on-line inspection systems for systematic and random faults in rotary screen printed fabrics.

The research detailed in this thesis has also shown the feasibility of colour machine vision techniques as a method for detecting (and correcting) faults in rotary screen printed fabrics. Also, the products of the research have implications for a wide range of inspection and processing tasks, especially within the textile industry. During this research project (in common

with all research) several avenues of related research became apparent, these are discussed later in the chapter with other recommendations for further research.

Other important achievements of this research were:

- Specification of the Inspection Task.
- In-depth study of rotary screen printing, through a historical and mechanical perspective.
- A thorough evaluation of rotary screen printing faults, identifying their type, cause, probability, seriousness, and methods for their correction.
- Investigation of Machine Vision and its use in textile applications.
- Identification of colour as a critical aspect of the research, leading to a comprehensive investigation of colour vision systems.
- A thorough evaluation of the various image acquisition and lighting devices.
- Development of a prototype point sensor system.
- Establishment of fundamental Image Processing algorithms, written in C, to allow the development of high-end functions.
- Development and calibration of a laboratory-based machine vision system.
- Comprehensive Literature Survey on relevant areas, in particular, colour segmentation methodologies and colour image processing techniques.
- Simulation of Fault Detection.
- Design and development of other prototyping hardware.
- Presentation of a research paper on colour segmentation at a conference.

In Chapter 1, the problem was first identified and proposals for a solution to the inspection task were made. The proposals suggested two main approaches: a 100% inspection of the fabric; pseudo 100% inspection (ref. Section 1.2.2). It was reasoned that, although desirable, 100% inspection would require too much data processing (90 MBytes per second), therefore either a major amount of data preprocessing, or pseudo 100% inspection was required to reduce the

data processing demand. A pseudo 100% method was developed for the laboratory analysis, but this was designed to be 'up-gradable' to true 100% inspection on-line.

Also in Chapter 1 was an in-depth study of rotary screen printing, first through a historical perspective, and then examined in terms of its physical properties. Having a historical view of the development of rotary screen printing was important as this information allows some projection as to its future development and how this may affect the research. Analysis of the mechanics of rotary screen printing gave an understanding of printing faults and the corrective measures required. A comprehensive study of the types of rotary screen printing faults was also presented in this chapter.

Chapter 2 introduced the fundamental concepts of machine vision systems, and focussed on their suitability for the research. In particular, existing methods for using machine vision systems in textile applications were investigated to identify key areas for research. The information presented in this chapter provides essential supporting material for the research.

When investigating the inspection task, in Chapter 1, it was noted that colour was a critical area of research as it offered the primary method for the data reduction required to produce an on-line inspection system. Therefore, a thorough understanding of colour is essential for some central research issues, particularly for colour segmentation. Chapter 3 examines the issue of colour vision from both a human and computer outlook, focusing on the computer colour systems to select the most appropriate to realize the research goals.

Also identified in Chapter 1, as essential to the research success, was the importance of the data acquisition stage. The results of the research into this area are introduced in Chapter 4. Included in this chapter were the results of the sensor research, which centred on three approaches: point scan; line scan; area scan. Point scan sensors were examined as a possible low cost solution for systematic fault detection and several prototype sensors were developed during this research. The conclusion of the sensor research was that line scan sensors provide the best solution for full on-line inspection.

Another closely scrutinized issue was lighting. Good data acquisition is as dependant on lighting as on sensor quality. The lighting had to be uniform both temporally and spatially, it had to illuminate the printed pattern sufficiently without introducing any additional artifacts due to texture and specular reflection. It was found that this was best achieved by a diffuse front-lighting system. A prototype rig using this specification was developed for the laboratory analysis.

From the sensor and lighting research a proposal for a prototype system was possible. This system was used to simulate an industrial inspection system and its development was an essential part of the research.

As part of the preliminary research analysis an extensive literature survey was undertaken, the outcomes of which are given in Chapter 5. Although many supporting papers were found, few could be directly used by this research. In particular, most of the colour segmentation/quantization algorithms were designed specifically for natural scene analysis and visual display. This is not the best approach for a computer-based printed fabric inspection system because these algorithms are intensely recursive. The lack of directly relevant papers found by the literature survey clearly demonstrated the requirement for this research, as it provides new knowledge to the machine vision and image processing fields.

From the literature survey, in Chapter 5, it was seen that existing colour segmentation methods were unsuited to this research. A new method was required. Chapter 6, presented a new approach to the segmentation of RGB colour space using a computer-based, three-dimensional, fuzzy logic, clustering system. This algorithm also had built-in prediction methods to segment pixels in 'disputed' regions of the colour space. The algorithm was further optimized for screen printed fabrics by a textural weighting function biased towards the black/white axis where pigment group distribution was highest (due to the specular reflection of the textured fabric).

In Chapter 7 the performance of the new colour segmentation algorithm was evaluated, and the results compared against similar measures on existing algorithms surveyed in Chapter 5. These

results showed an improvement (in some case, significant) in segmentation performance, for the new algorithm, over the existing methods. A 28% improvement over the method proposed by Lim and Lee (ref. Chapters 5 and 7), and a 90% enhancement on the CIE HSI space segmentation method.

Also, shown in Chapter 7 was the strong correlation between the distribution of colours within a pigment captured by the image system and a Gaussian distribution. Correlations of above 90% were found when the measured data was compared against a theoretical distribution, whereas when the measured data was compared against an ideal distribution (one point only in the colour space) the correlation was much lower (approx. 30%). This justified the use of Gaussian-based segmentation techniques for the first pass of the colour segmentation algorithm.

Chapter 8 combines the research results, discussed throughout this thesis, to propose a theoretical on-line system for the detection of faults in rotary screen printed fabrics. It is shown that the system for the on-line detection of systematic faults is best expressed as a subset of a complete fault detection system. In other words, the detection systems are interdependent, despite the independent nature of the random and systematic fault sets. It is emphasized that the proposed system is theoretical, but the individual components of the system have been theoretically proven and simulated.

To reiterate, the objective of the research was to investigate the feasibility of a digital colour vision system that would enable the online detection and correction of print faults. Therefore, the requirement of the research was *to develop proposals, and the technology, for a workstation for automated on-line inspection of printed fabric, using opto-electronic sensing and computer signal processing, including machine vision* (ref. Chapter 1). This has been achieved.

9.1 Further Research/Work

There is scope for further work to this research. The research itself can be continued, especially concerning automatic random fault characterization (ref. Chapter 8). The development of a prototype on-line system for fault inspection would introduce its own research difficulties as the hardware issues are complex. There is no immediate theoretical reason that such a fault detection system could not be used on a variety of two-dimensional printed media where registration is an issue (such as paper and carpets). In fact, during the research the developed methodologies were tried on both media and performed well.

It is the colour segmentation algorithm that perhaps offers more opportunities. Currently, it is 'fine-tuned' towards fabric-based colours (particularly pigments), however, the weightings can be easily adjusted. In fact, with a database of weightings for different material, or scene types the algorithm could become general purpose. A general purpose colour segmentation algorithm would be useful for many applications where colour inspection is an issue.

One example, currently in vogue, is that of colour image compression. The recent growth of the Internet has produced a demand for high quality colour images that are not bandwidth intensive. Standard image compression techniques such as GIF and JPEG already exist, but these can have extraction overheads.

A successful colour segmentation algorithm, that can produce visually convincing images is highly desirable, the colour segmentation algorithm developed by the research may be able to offer this. However, it should be noted that the original compression is resource intensive, this might be unacceptable for some applications. Yet, once compressed the image can be transmitted with a palette header (defining the constituent colour groups) and is then independent of the segmentation algorithm. In other words, the segmented images have an inherently smaller data requirement (beneficial for file transfer) and are uncompressed, which allows rapid retrieval. Quantitative comparisons of the image compression techniques against

the colour segmentation method are required before the method's suitability can be fully judged.

10 References

ASANO T., KENWOOD G., MOCHIZUKI J., HATA S., *Colour image recognition using chrominance signals,* IEEE, October 1986.

BEAULIEU J-M., GOLDBERG M., *Hierarchy in picture segmentation: A stepwise optimization approach,* IEEE Trans. on Pattern Analysis and Machine Intelligence, Vol. 11, No. 2, February 1989, pp. 150-163.

BECK H., M^{C}DONALD D., BRZAKOVIC D., *A self-training inspection system for the on-line inspection of printed material,* SPIE, Vol. 1294, Applications of Artificial Neural Networks, 1990, pp. 478-489.

BLOWERS A., DODKIN C., *Automated inspection and control of fabric printing,* Final Review, SERC (ACME), Project No. Gr/G30461, February 1994.

BLOWERS A., DODKIN C., HARWOOD, R., NORTON-WAYNE L., *Automated inspection of printed fabrics – a new method for colour segmentation,* Proc. Image & Vision Computing NZ '93, Industrial Research Limited, 1993, pp. 399-406.

BRADSHAW M., *The automated inspection of textile fabric using machine vision,* PhD Thesis, De Montfort University, 1994.

BRUN-BUISSON A., LATTUATI V., LEMOINE D., *Discrete colorimetric spaces: an application to automatic recognition of colour codes,* Advanced Information Processing in Automatic Control, 1989, pp. 389-394.

CAELLI T., REYE D., *On the classification of image regions by colour, texture and shape,* Pattern Recognition, Vol. 26, No. 4, 1993, pp. 461-470.

CAMPBELL R., *The automated inspection of carpets — inspecting faults in patterned woven axminster carpets*, De Montfort University, Final Report, ESPRC, ACME Project Number GR/H 91008, February, 1995.

CELENK M., *A color clustering technique for image segmentation*, Computer Vision, Graphics, and Image Processing, 52, 1990, pp. 145-170.

CHAMBERLIN G. J., CHAMBERLIN D. G., *Colour: its measurement, computation and application*, Heyden, London, 1982.

CHASSERY J. M., GARBAY C., *An iterative segmentation method based on a contextual color and shape criterion*, IEEE Trans. on Pattern Analysis and Machine Intelligence, Vol. 6, No. 6, November 1984, pp. 794-800.

CONNAH D., FISHBOURNE C., *The use of colour information in industrial scene analysis*, Philips Research Laboratory Papers, 1981, pp. 340-345.

CONNOLLY C., LITTLEWOOD S., KING E., *A method of image segmentation from colour data*, Unpublished, Huddersfield Polytechnic, 1988.

CONVERY S., LUNNEY T., HASHIM A., M^{C}GINNITY M., *Automated fabric inspection*, International Journal of Clothing Science and Technology, Vol. 6, No. 5, 1994, pp. 15-19.

CORMACK B., *Defects in rotary screen printed fabric*, Journal of the Society of Dyers and Colourists, Vol. 109, November 1993, pp. 353-355.

CRABTREE S. J. (Jr), EHRLICH R., PRINCE C., *Evaluation of strategies for segmentation of blue-dyed pores in thin section of reservoir rocks*, Computer Vision, Graphics, and Image Processing, Vol. 28, 1984, pp. 1-18.

DeMARSH L. E., GIORGIANNI E. J., *Color science for imaging systems,* Physics Today, September 1989, pp. 44-52.

de O BARROS A. J. C., *Developments in printing by rotary screen,* Journal of the Society of Dyers and Colourists, Vol. 82, 1966, pp. 3-7.

DODKIN C., *Inspecting printed fabric... automatically,* Journal of the Society of Dyers and Colourists, October 1992, pp. 425-427.

DODKIN C., NORTON-WAYNE L., *The automated inspection of garments using colour machine vision,* De Montfort University, Unpublished, 1993.

DODKIN C., *The automated inspection of garments using colour machine vision,* PhD Thesis, De Montfort University, 1994.

DOWDS B. F., *Variables in textile screen printing,* Journal of the Society of Dyers and Colourists, Vol. 86, 1970, pp. 512-519.

DUSEK Z., *Contactless thread density measurement of woven and knitted fabrics,* Melliand Textilberichte, Vol. 72, No. 11, 1991, pp. 917-920 (E. pp. 366-367).

EQUITZ W. H., *A new vector quantization clustering algorithm,* IEEE Trans. on Acoustics, Speech, and Signal Processing, Vol. 37, No. 10, October 1989, pp. 1568-1575.

FARHOOSH H., SCHRACK G., *CNS-HLS mapping using fuzzy sets,* IEEE CG & A, June 1986, pp. 28-35.

FAUYERAS O. D., LUONG Q.-T., MAYBANK S. J., *Camera self-calibration: theory and experiments,* Proc. ECCV '92, Second European Conference on Computer Vision, Santa Margherita, Ligure, Italy, May 1992, pp. 321-334.

FERBER U., HILDEN J., *Application of printing pastes in rotary screen printing*, Melliand Textilberichte, Vol. 70, 1989, pp. 705-709 (E. pp. 303-305), pp. 775-779 (E. pp. 331-333), pp. 865-874 (E. pp. 372-374).

FLETCHER P., *A SIMD parallel colour quantization algorithm*, Computers and Graphics, Vol. 15, No. 3, 1991, pp. 365-373.

FRECSKA T., *Taming microregistration*, Screen Printing, April 1990, pp. 54-59.

GALBIATI L. J. (Jr.), *Machine vision and digital image processing fundamentals*, Prentice-Hall International Editions, 1990.

GOLDBERG N., *Colour image quantization for high resolution graphics display*, Image and Vision Computing, Vol. 9, No. 5, October 1991, pp. 303-312.

GREMBAN K. D., THORPE C. E., KANADE T., *Geometric camera calibration using systems of linear equations*, Proc. IEEE International Conference on Robotics and Automation, April 1988, pp. 562-567.

GUNAWARDENA C. A., CLARK L. J., DENNIS T. J., *A spot-type defect detection and colour identification system for agricultural produce*, Proc. International Conference on Industrial Electronics, Control and Instrumentation, Kobi, Japan, 1990, pp. 2531-2534.

HAASE C. S., MEYER G. W., *Modelling pigmented materials for realistic image synthesis*, ACM Trans. on Graphics, Vol. 11, No. 4, October 1992, pp. 305-335.

HARMS H., GUNZER U., AUS H. M., *Combined local color and texture analysis of stained cells*, Computer Vision, Graphics, and Image Processing, Vol. 33, 1986, pp. 364-376.

HARWOOD R., NORTON-WAYNE L., *Computer image processing in garment production,* Proc. of Conference on Enhancing Productivity in Clothing Industry for the '90s, 1990.

HAWKYARD C. J., *Textile printing,* (second edition) L. W. C. Miles (ed.), The Society of Dyers and Colourists, 1994, pp. 18-57.

HAWKYARD C. J., MIAH A. S., *The parameters of rotary screen printing,* Journal of the Society of Dyers and Colourists, Vol. 103, January 1987, pp. 27-31.

HEALEY G., *Segmenting images using normalized color,* IEEE Trans. on System, Man, and Cybernetics, Vol. 22, No. 1, 1992, pp. 64-73.

HINZE D., VIERTEL E., *Image sensor technology for the light industry,* Melliand Textilberichte, Vol. 72, No. 11, 1991, pp. 958-962 (E. pp. 385-387).

HINZE D., MEHLHORN H., BURKHARDT S., *Digital image processing by means of a parallel computer system for the testing of fabrics,* Melliand Textilberichte, Vol. 72, No. 12, 1991, p. 993 (E. p. 400).

HOLLINGUM J., *Machine vision — the eyes of automation,* IFS (Publications) Ltd, Springer-Verlag, 1984, pp. 1-24.

HUANG C-L., CHENG T-Y., CHEN C-C., *Color images' segmentation using space filter and Markov random fields,* Pattern Recognition, Vol. 25, No. 10, 1992, pp. 1217-1229.

HUNT R. W. G., *Measuring colour,* (Second Edition). Ellis Horwood, 1992.

ITU-R Recommendation BT.709, *Basic parameter values for the HDTV standard for the studio and for international programme exchange,* [formerly CCIR Rec. 709], ITU, 1211 Geneva 20, Switzerland, 1990.

JOBLOVE G. H., GREENBERG D., *Color spaces for computer graphics,* Program of Computer Graphics, Cornell University, 1978, pp. 20-25.

KAASJAGER A. D. J., *Textile fabric monitoring with image analysis,* Melliand Textilberichte, Vol. 71 No. 1, 1990, pp. 64-66 (E. pp. 33-34).

KASSON J. M., PLOUFFE W., *An analysis of selected computer interchange color spaces,* ACM Trans. on Graphics, Vol. 11, No. 4, October 1992, pp. 373-405.

KHOTANZAD A., BOUARFA A., *Image segmentation by a parallel, non-parametric histogram based clustering algorithm,* Pattern Recognition, Vol. 23, No. 9, 1990, pp. 961-973.

KOOL R. J. M., *Rotary screen printing, alive and kicking,* Journal of the Society of Dyers and Colourists, Vol. 109, October 1993, pp. 318-322.

KREY C., AYACHE A., BIGUET G., BRUEL A., *A color-based system for fruit sorting,* Journal Unknown (photocopy only), 1984, pp. 203-206.

LAI J. Z. C., *On the sensitivity of camera calibration,* Image and Vision Computing, Vol. 11, No. 10, December 1993, pp. 656-663.

LAND E., *The Retinex theory of color vision,* Scientific American, 1977, pp. 108-128.

LIM Y. W., LEE S. U., *On the color image segmentation algorithm based on the thresholding and the fuzzy c-means techniques,* Pattern Recognition, Vol. 23, No. 9, 1990, pp. 935-952.

LIU J., YANG Y-H., *Multiresolution color image segmentation,* IEEE Trans. on Pattern Analysis and Machine Intelligence, Vol. 16, No. 7, July 1994, pp. 689-700.

LOUGHLIN C., *Inspectrum: high speed colour inspection,* 6th AI and PC Conference, Birmingham, April 1982.

LOW A., *Introductory computer vision & image processing,* M°Graw-Hill Book Company, 1991.

M°DONALD L. W., LUO M. R., SCRIVENER S. A. R., *Factors affecting the appearance of coloured images on a video display monitor,* RPS Conference on Quantification of Images, Cambridge, 1989.

MAHDAVIEH Y., STARK J. P. W., TJAHJADI T., *The utilization of colour in machine vision,* UK Patent Application 8229530, 1982.

MASSEN R., VOLK G., *Real-time colour classification for preprocessing photogrammetry images,* SPIE, Vol. 1395, 1990, pp. 283-290.

MEYER G. W., GREENBERG D. P., *Perceptual color spaces for computer graphics,* Association for Computing Machinery Yearbook, 1980, pp. 254-261.

MILES L. W. C., *Textile printing,* (second edition) L. W. C. Miles (ed.), The Society of Dyers and Colourists, 1994, pp. 1-17.

MUNDEN D. L., NORTON-WAYNE L., *Machine vision in textile manufacture,* Textile Asia, October 1988, pp. 85-88.

NICKOLAY B., SCHICKTANZ K., SCHMALFUß H., *Automatic fabric inspection — utopia or reality?* Melliand Textilberichte, Vol. 74, No. 1, 1993, pp. 70-76 (E. pp. 33-37).

NORTON-WAYNE L., *Automated visual inspection for the apparel industry,* Proc. 5th European Conference on Automated Manufacture, Birmingham, UK., May 1989.

NORTON-WAYNE L., BRADSHAW M., SANBY C., *Machine vision for the automatic inspection of web materials,* SPIE Computer Vision for Industry, Vol. 1989, 1993, pp. 2-13.

OHLANDER R., PRICE K. E., REDDY D. R., *Picture segmentation using a recursive region splitting method,* Computer Graphics and Image Processing, 8, 1978, pp. 313-333.

ORCHARD M. T., BOUMAN C. A., *Color quantization of images,* IEEE Trans. on Signal Processing, Vol. 39, No. 12, December 1991, pp. 2677-2690.

PEYSKENS A., *Fine-detail printing,* Screen Printing, February 1991, pp. 70-77.

PIENKOWSKI A. E., DENNIS T. J., *Applications of fuzzy logic to artificial colour vision,* SPIE Computer Vision for Robots, Vol. 595, 1985, pp. 50-55.

PIETIKÄINEN M., HARWOOD D., *Segmentation of colour images using edge-preserving filters,* V. Cappellini, and R. Maconi, (ed.), Advances in Image Processing and Pattern Recognition, Elsevier Science Publishers, 1986, pp. 94-99.

POYNTON C. A., *Frequently asked questions about colour,* Sun Microsystems Computer Corporation, <http://www.inforamp.net/~poynton/Poynton-colour.html>, 1995.

SCHETTINI R., DELLA VENTURA A., ARTESE M. T., *Color specification by visual interaction,* The Visual Computer, No. 9, 1992, pp. 143-150.

SCHICKTANZ K., *What can automatic fabric inspection systems offer us?* Melliand Textilberichte, Vol. 76, No. 4, 1995, (E. pp. 73-74).

SCHICKTANZ K., *Automatic fault detection possibilities on nonwoven fabrics,* Melliand Textilberichte, Vol. 74, No. 4, 1993, pp. 294-295 (E. pp. 136-137).

SMPTE RP 177-1993, *Derivation of basic television color equations,* 1993.

STOREY J., *The Thames & Hudson manual of textile printing,* Thames & Hudson, 1992, pp. 107-152.

SYEDA-MAHMOOD T. F., *Data and model-driven selection using color regions,* Proc. ECCV '92, Second European Conference on Computer Vision, Santa Margherita, Ligure, Italy, May 1992, pp. 115-123.

TSAI I-S., SHENTU K., LIN C-H., LU C-K., *Pattern recognition of fabric representation structure by image processing,* Melliand Textilberichte, Vol. 74, No. 1, 1993, pp. 77-80 (E. pp. 37-38).

UCHIYAMA T., ARBIB M. A., *Color image segmentation using competitive learning,* IEEE Trans. on Pattern Analysis and Machine Intelligence, Vol. 16, No. 12, December 1994, pp. 1197-1206.

van RENESSE R. L., *Automatic quality and ripeness inspection system — AQUARIS,* SPIE Industrial Inspection II, Vol. 1265, 1990, pp. 194-204.

VERNON L. J., *Machine vision — automated visual inspection & robot vision,* Prentice-Hall, 1991.

VETSKOUS A., SHAVIRIN I., STRELKOV O., KORABLIN A., NORTON-WAYNE L., HARWOOD R., *Using linear arrays in an optical sensor for printed fabric inspection,* De Montfort University, Unpublished, 1993.

VINCENT L., SOILLE P., *Watershed in digital spaces: an efficient algorithm based on immersion simulations,* IEEE Trans. on Pattern Analysis and Machine Intelligence, Vol. 13, No. 6, June 1991, pp. 583-598.

WANDELL B. A., *The synthesis and analysis of color images*, IEEE Trans. on Pattern Analysis and Machine Intelligence, Vol. 9, No. 1, January 1987, pp. 2-13.

WITKIN A. P., *Scale-space filtering: a new approach to multi-scale descriptions*, Image Understanding, S. Ullman and W. Richards (eds.), Ablex, New Jersey, 1984, pp. 79-95.

WU X., *Color quantization by dynamic programming and principal analysis*, ACM Trans. on Graphics, Vol. 11, No. 4, October 1992, pp. 384-372.

WYSZECKI G., STILES W. S., *Color science: concepts and methods, quantitative data and formulae*, (Second Edition). John Wiley & Sons, 1982.

YAMABA K., *High performance color sensing systems for flexible automation*, IEEE Papers, 1987, pp. 104-109.

1 Appendices

1.1 Appendix A : Other Colour Interchange Systems

1.1.1 RGB ↔ $Y'P_BP_R$

To encode $Y'P_BP_R$, start with the basic Y', $(B'-Y')$ and $(R'-Y')$ relationships (Equation C.1).

$$\begin{bmatrix} Y'_{601} \\ B'-Y'_{601} \\ R'-Y'_{601} \end{bmatrix} = \begin{bmatrix} 0.299 & 0.587 & 0.144 \\ -0.299 & -0.587 & 0.886 \\ 0.701 & -0.587 & -0.144 \end{bmatrix} \cdot \begin{bmatrix} R' \\ G' \\ B' \end{bmatrix} \qquad \text{C.1}$$

$Y'P_BP_R$ components have a unity excursion, where Y' ranges [0···1] and each of P_B and P_R ranges [-0.5···0.5]. The $(B'-Y')$ and $(R'-Y')$ rows need to be scaled by $^{0.5}/_{0.886}$ and $^{0.5}/_{0.701}$. Equation C.2 shows the matrix transformation to encode from $R'G'B'$ where reference black is 0 and reference white is 1.

$$\begin{bmatrix} Y'_{601} \\ P_B \\ P_R \end{bmatrix} = \begin{bmatrix} 0.299 & 0.587 & 0.144 \\ -0.168736 & -0.331264 & 0.5 \\ 0.5 & -0.418688 & -0.081312 \end{bmatrix} \cdot \begin{bmatrix} R' \\ G' \\ B' \end{bmatrix} \qquad \text{C.2}$$

The first row comprises the luma coefficients; these sum to unity. The second and third rows each sum to zero, this is necessary for colour difference components. The 0.5 entries define the maximum value of P_B and P_R for the blue and red primaries [0,0,1] and [1,0,0] (they cannot exceed 0.5). The inverse, decoding matrix is shown in Equation C.3.

$$\begin{bmatrix} R' \\ G' \\ B' \end{bmatrix} = \begin{bmatrix} 1 & 0 & 0.144 \\ 1 & -0.344136 & -0.714136 \\ 1 & 1.772 & 0 \end{bmatrix} \cdot \begin{bmatrix} Y'_{601} \\ P_B \\ P_R \end{bmatrix} \qquad \text{C.3}$$

1.1.2 RGB ↔ $Y'C_BC_R$

Rec. 601 also specifies an eight-bit coding where Y' has an excursion of 219 and an offset of +16. This coding places black at code 16 and white at code 235, reserving the extremes of the

range for signal processing *headroom* and *footroom*. C_B and C_R have a range of ±112 and offset of +128, for a range of 16 through 240 inclusive.

To compute $Y'C_BC_R$ from $R'G'B'$ in the range [0···1], the rows of the matrix of Equation C.2 must be scaled by the factors 219, 224 and 224, corresponding to the excursions of each component. Equation C.4 shows this.

$$\begin{bmatrix} Y'_{601} \\ C_B \\ C_R \end{bmatrix} = \begin{bmatrix} 16 \\ 128 \\ 128 \end{bmatrix} + \begin{bmatrix} 65.481 & 128.553 & 24.966 \\ -37.797 & -74.203 & 112 \\ 112 & -93.786 & -18.214 \end{bmatrix} \cdot \begin{bmatrix} R' \\ G' \\ B' \end{bmatrix} \qquad \text{C.4}$$

Summing the first row of the matrix yields 219, the luma excursion from black to white. The two entries of 112 reflect the positive C_BC_R extrema of the blue and red primaries. All three components must be rescaled to the range 1 through 254 inclusive, since Rec. 601 reserves codes 0 and 255 for synchronization signals. Equation C.5 uses the inverse of Equation C.4 to recover $R'G'B'$ in the range [0···1] from $Y'C_BC_R$.

$$\begin{bmatrix} R' \\ G' \\ B' \end{bmatrix} = \begin{bmatrix} 0.00456621 & 0 & 0.00625893 \\ 0.00456621 & -0.00153632 & -0.00318811 \\ 0.00456621 & 0.00791071 & 0 \end{bmatrix} \cdot \left(\begin{bmatrix} Y'_{601} \\ C_B \\ C_R \end{bmatrix} - \begin{bmatrix} 16 \\ 128 \\ 128 \end{bmatrix} \right) \qquad \text{C.5}$$

In computing using eight-bit coding with black at code 0 and white at 255 is conventional. Therefore, to encode $Y'C_BC_R$ from $R'G'B'$ in the range [0···255], using eight-bit binary arithmetic, the $Y'C_BC_R$ transform matrix (as shown in Equation C.4) needs to be scaled by $^{256}/_{255}$ (as in Equation C.6). It follows that to decode $R'G'B'$ in the range [0···255] from Rec. 601 $Y'C_BC_R$, using eight-bit binary arithmetic the transform in Equation C.7 is necessary.

$$\begin{bmatrix} Y'_{601} \\ C_B \\ C_R \end{bmatrix} = \begin{bmatrix} 16 \\ 128 \\ 128 \end{bmatrix} + \frac{1}{256} \begin{bmatrix} 65.738 & 129.057 & 25.064 \\ -37.945 & -74.494 & 112.439 \\ 112.439 & -94.154 & -18.285 \end{bmatrix} \cdot \begin{bmatrix} R'_{255} \\ G'_{255} \\ B'_{255} \end{bmatrix} \qquad \text{C.6}$$

$$\begin{bmatrix} R'_{255} \\ G'_{255} \\ B'_{255} \end{bmatrix} = \frac{1}{256}\begin{bmatrix} 298.082 & 0 & 408.583 \\ 298.082 & -100.291 & -208.120 \\ 298.082 & 516.411 & 0 \end{bmatrix} \cdot \left(\begin{bmatrix} Y'_{601} \\ C_B \\ C_R \end{bmatrix} - \begin{bmatrix} 16 \\ 128 \\ 128 \end{bmatrix} \right) \quad \text{C.7}$$

The multiplications by $^1/_{256}$ can be accomplished by logical bitwise shifting. Yet, some coefficients, when scaled by $^1/_{256}$, are larger than unity. Therefore, these coefficients will need more than eight multiplier bits. In computational terms doing the transformation using floating-point variables is easier, then convert back to eight-bits after processing. However, for implementation in binary arithmetic the matrix coefficients have to be rounded, and therefore preserving the row sums of is critical, for instance, [1,0,0].

The matrix of Equation C.7 will decode standard $Y'C_BC_R$ components to RGB components in the range [0···255]. NB. This of course is subject to roundoff error. Care must be taken to avoid overflows due to roundoff error. Principally, because studio video signals use the extremes of the coding range to handle the signal overshoot and undershoot, and therefore any overflow will require clipping[1] when decoded to an RGB range that has no headroom or footroom.

Using studio standards is common in machine vision. Mainly, this is due to the video camera specification used by machine vision systems. Typically, the high-fidelity camera systems used in laboratory simulations are preset with studio standards. Studio $R'G'B'$ signals use the same 219 extrema as the luma component of $Y'C_BC_R$. To encode $Y'C_BC_R$ from $R'G'B'$ in the range [0···219], using eight-bit binary arithmetic, the $Y'C_BC_R$ encoding matrix as shown in Equation C.4 must be scaled $^{256}/_{219}$. Equation C.8 shows the encoding transform for studio video. To decode $R'G'B'$ in the range [0···219] from $Y'C_BC_R$, using eight-bit binary arithmetic the inverse transform of Equation C.8 is used, as shown by Equation C.9.

$$\begin{bmatrix} Y'_{601} \\ C_B \\ C_R \end{bmatrix} = \begin{bmatrix} 16 \\ 128 \\ 128 \end{bmatrix} + \frac{1}{256}\begin{bmatrix} 76.544 & 150.272 & 29.184 \\ -44.182 & -86.740 & 130.922 \\ 130.922 & -109.631 & -21.291 \end{bmatrix} \begin{bmatrix} R'_{219} \\ G'_{219} \\ B'_{219} \end{bmatrix} \quad \text{C.8}$$

---

1 *Clipping is used when a signal over- or under-flows, when this happens the signal is reset to the maxima or minima (respectively) of the scale range.*

$$\begin{bmatrix} R'_{219} \\ G'_{219} \\ B'_{219} \end{bmatrix} = \frac{1}{256} \begin{bmatrix} 256 & 0 & 350.901 \\ 256 & -86.132 & -178.738 \\ 256 & 443.506 & 0 \end{bmatrix} \cdot \left(\begin{bmatrix} Y'_{601} \\ C_B \\ C_R \end{bmatrix} - \begin{bmatrix} 16 \\ 128 \\ 128 \end{bmatrix} \right) \qquad \text{C.9}$$

The entries of 256 in the matrix expressed by Equation C.9 show that the corresponding component can simply be added so a multiplication operation is not needed. As before, this equation will need to use floating-point conversion for computational calculations.

The matrices in this section conform to Rec. 601 and apply directly to conventional 525/59.94 and 625/50 video. However, it is uncertain whether the standards for the emerging HDTV will use the same matrices. If they do not, this will introduce extra concerns when encoding and decoding image data.

In digital video, Rec. 601 standardizes sub-sampling denoted by 4:2:2, where the C_B and C_R components are sub-sampled horizontally by a factor of two with respect to luma. Commonly used computer image formats (in particular JPEG and MPEG) conventionally sub-sample by a factor of two in the vertical dimension as well, denoted as 4:2:0. (Colour difference coding is also standardized in Rec. 601.)

When using transforms verifying the encoding and decoding to ensure that the colours are handled correctly is important. The standard way to do this is to use a colour bar signal. A colour bar signal comprises a binary RGB sequence ordered for decreasing luma: white, yellow, cyan, green, magenta, red, blue and black (Table C.1 shows the tristimulus values needed for colour bar generation). To ensure that the scale factors used by the transforms are correct and that there is no clipping a colour bar sequence having 75%-amplitude bars instead of 100% is required.

	White	Yellow	Cyan	Green	Magenta	Red	Blue	Black
G	1	1	1	1	0	0	0	0
R	1	1	0	0	1	1	0	0
B	1	0	1	0	1	0	1	0

Table C.1: Binary Pattern for Colour bar Generation

1.2 Appendix B : Point Sensors per Design

Investigation was made to identify the minimum number of point sensors required to inspect all possible colour boundaries on typical DORMA designs. The following table gives the results of the investigation on a range of samples that represent the DORMA range.

Sample Type	Number of Colours	Number of Sensors Required
Floral #1	11	6
Geometrical #1	3	3
Floral #2	11	6
Floral #3	11	9
Floral #4	8	6
Floral #5	9	6
Geometrical #2	6	3
Pastel #1	6	3
Geometrical #3	5	3
Floral #6	4	3
Floral #7	11	6
Geo/Floral #1	9	6
Geometrical #4	2	3(awkward setup)
Floral #8	10	6
Geo/Floral #2	10	6
Floral #9	10	6
Geo/Floral #3	10	6
Floral #11	10	6
Geometrical #5	2	3
Geometrical #6	9	6
Floral #10	10	9
Paisley #1	10	6

Geo/Floral #4	10	9
Paisley #2	11	9
Floral #12	10	6
Paisley #3	4	3
Paisley #4	9	3

Average numbers of colours per design (8.185) = more than 8.

Average numbers of point sensors (5.444) = at least six.

From these figures it is shown that the number of point sensors required is design dependent. In reality this means that there must be enough point sensors to cope with the more complicated designs — this means nine point sensors in the minimum system. Each point sensor will require precise positioning for each design (difficult on a three metre wide print table), and will be extremely vibration sensitive due to the high resolution required for fault detection.

1.3 Appendix C : Camera & Lighting Test Results

Gain	Mag.	Aperture	Mean Green	Standard Deviation Green	Mean Red	Standard Deviation Red	Mean Blue	Standard Deviation Blue
0	15	16.0	41	4.959888	23	7.713953	29	5.607186
0	15	11.0	61	6.606017	50	7.333932	52	6.147730
0	15	8.0	88	6.840621	82	7.028469	84	6.781089
0	15	5.6	105	0.585308	97	2.114828	103	3.070630
0	15	4.0	111	1.711146	102	1.600441	109	2.153617
0	15	2.8	110	1.072266	101	0.982089	108	2.012513
0	15	2.0	109	0.917277	101	0.903171	107	1.929753
0	15	1.4	109	0.971007	101	1.050509	107	1.932115
0	30	16.0	44	3.240511	24	6.149885	29	3.635404
0	30	11.0	69	4.738611	56	5.479975	57	4.031354
0	30	8.0	91	4.795857	82	4.713653	82	4.051856
0	30	5.6	111	0.482987	102	0.181290	106	2.265728
0	30	4.0	114	1.957213	104	2.172356	109	2.104285
0	30	2.8	113	1.851757	103	1.941826	108	2.060094
0	30	2.0	112	1.810033	102	2.346755	107	2.057805
0	30	1.4	112	1.783006	102	1.525320	107	1.965330
0	30	16.0	37	2.981368	15	5.185360	22	4.462093
0	60	11.0	67	4.431963	58	4.032388	60	4.059870
0	60	8.0	96	3.750892	88	2.712739	88	4.527929
0	60	5.6	111	2.029520	103	1.615383	107	3.451234
0	60	4.0	113	1.898419	104	0.516356	109	3.102495
0	60	2.8	113	1.766419	103	1.570900	108	2.606068
0	60	2.0	112	1.765625	103	0.177313	108	2.659221
0	60	1.4	112	1.768956	102	1.195559	107	2.785104

Gain	Mag.	Aperture	Mean Green	Standard Deviation Green	Mean Red	Standard Deviation Red	Mean Blue	Standard Deviation Blue
0	90	16.0	46	2.758212	29	3.602619	33	3.877732
0	90	11.0	64	3.704510	51	3.402952	53	3.709880
0	90	8.0	93	3.482278	84	2.912634	85	3.379100
0	90	5.6	112	2.237828	103	0.785616	107	2.530141
0	90	4.0	113	1.717442	104	1.632307	109	2.670540
0	90	2.8	111	0.910405	102	1.503827	108	3.025612
0	90	2.0	110	0.796649	102	1.470568	108	3.110088
0	90	1.4	110	0.958657	101	1.229451	107	3.091795
3	15	16.0	51	5.505563	44	6.049553	44	6.579944
3	15	11.0	74	7.886249	68	8.011612	69	8.306765
3	15	8.0	98	8.928134	91	6.658509	97	8.060164
3	15	5.6	111	1.807418	103	1.541359	109	3.065571
3	15	4.0	111	1.670292	102	1.812739	108	3.052185
3	15	2.8	109	1.641221	102	1.642844	107	3.277672
3	15	2.0	110	1.703435	101	1.516803	107	3.120936
3	15	1.4	109	1.782717	101	1.555799	106	3.025337
3	30	16.0	51	3.305518	43	3.621496	44	2.943830
3	30	11.0	78	4.295053	72	4.381932	72	3.229531
3	30	8.0	105	2.454194	97	0.879917	103	2.026921
3	30	5.6	113	1.874476	104	0.906488	110	1.745131
3	30	4.0	111	1.838115	103	0.871565	109	1.811853
3	30	2.8	110	1.703726	102	2.308879	108	1.630048
3	30	2.0	109	3.779774	101	3.082199	106	3.496681
3	30	1.4	110	1.631559	101	1.324355	107	1.603910
3	60	16.0	54	3.031118	46	2.871650	47	2.530299

Gain	Mag.	Aperture	Mean Green	Standard Deviation Green	Mean Red	Standard Deviation Red	Mean Blue	Standard Deviation Blue
3	60	11.0	78	3.679481	72	3.169021	73	3.026293
3	60	8.0	101	3.473218	93	3.336241	99	4.116773
3	60	5.6	112	2.705647	103	1.560881	110	2.397569
3	60	4.0	110	1.462258	102	0.715733	108	1.639825
3	60	2.8	109	1.386527	102	1.187482	107	1.643110
3	60	2.0	109	1.374946	101	0.798635	107	1.505623
3	60	1.4	109	1.369677	101	1.010911	107	1.520161
3	90	16.0	49	2.777272	41	2.472501	42	2.406255
3	90	11.0	75	3.649531	70	2.963899	71	2.844733
3	90	8.0	99	3.419284	93	1.289229	98	2.321966
3	90	5.6	111	1.529676	103	0.788488	110	1.576608
3	90	4.0	110	1.381541	102	0.344091	108	1.620396
3	90	2.8	109	1.351038	102	0.761599	107	1.554222
3	90	2.0	109	1.328557	101	0.748346	107	1.595843
3	90	1.4	109	1.336671	101	1.206730	107	1.578471
9	15	16.0	68	7.393682	58	7.945883	62	6.823863
9	15	11.0	97	6.659616	91	4.527391	96	5.493224
9	15	8.0	110	4.138338	102	3.184453	108	3.733921
9	15	5.6	110	1.436714	103	1.329067	109	1.448344
9	15	4.0	109	1.262179	101	1.290319	108	1.384190
9	15	2.8	109	1.273030	101	1.169947	107	1.360640
9	15	2.0	108	1.259942	101	0.837546	107	1.307122
9	15	1.4	108	1.256268	100	1.248509	107	1.362892
9	30	16.0	74	5.018370	65	5.625025	69	4.462495
9	30	11.0	100	3.579308	93	2.057096	98	2.483252

Gain	Mag.	Aperture	Mean Green	Standard Deviation Green	Mean Red	Standard Deviation Red	Mean Blue	Standard Deviation Blue
9	30	8.0	110	1.650614	103	1.833727	110	1.188836
9	30	5.6	110	1.281837	102	1.252831	109	1.368163
9	30	4.0	109	1.282666	101	1.252374	108	1.281869
9	30	2.8	109	1.266916	101	1.249459	107	1.212842
9	30	2.0	108	1.269256	101	1.221062	107	1.224426
9	30	1.4	108	1.267778	100	1.238879	107	1.181641
9	60	16.0	72	4.457464	62	4.280007	66	4.084921
9	60	11.0	100	2.910303	93	1.645152	99	1.969805
9	60	8.0	110	1.660950	103	1.499958	110	1.522113
9	60	5.6	110	1.278371	102	0.985096	109	1.535371
9	60	4.0	109	1.274654	101	0.925743	108	1.599232
9	60	2.8	109	1.267624	101	0.781784	107	1.419802
9	60	2.0	108	1.273718	101	0.542953	107	1.491233
9	60	1.4	108	1.249130	100	1.243762	107	1.481590
9	90	16.0	73	4.311969	63	3.873135	67	3.720272
9	90	11.0	100	0.879027	93	1.247880	99	1.991555
9	90	8.0	110	1.382485	103	1.238471	110	1.519426
9	90	5.6	110	1.270294	102	1.368537	109	1.557971
9	90	4.0	109	1.278970	101	0.521893	108	1.483707
9	90	2.8	108	1.266751	101	1.205142	107	1.398793
9	90	2.0	108	1.263116	101	1.198931	107	1.474322
9	90	1.4	108	1.261550	101	0.959570	107	1.356707
12	15	16.0	70	7.505914	61	8.274251	60	7.459381
12	15	11.0	114	3.087491	106	2.212024	110	2.771534
12	15	8.0	115	0.590415	107	1.417036	110	1.966850

Gain	Mag.	Aperture	Mean Green	Standard Deviation Green	Mean Red	Standard Deviation Red	Mean Blue	Standard Deviation Blue
12	15	5.6	114	2.558908	105	1.704950	109	2.674830
12	15	4.0	113	1.610078	105	1.050300	108	1.760940
12	15	2.8	112	1.368609	104	0.430363	108	1.874053
12	15	2.0	112	1.655706	104	1.178400	107	1.809779
12	15	1.4	111	1.047459	103	1.358058	107	1.673144
12	30	16.0	92	5.704621	86	5.366151	87	4.831285
12	30	11.0	112	1.403234	104	0.690358	110	1.523420
12	30	8.0	113	0.977627	105	1.224267	111	1.653631
12	30	5.6	112	1.338343	104	1.356375	110	1.634180
12	30	4.0	111	1.256459	104	0.707094	109	1.662981
12	30	2.8	111	1.472269	103	0.985202	108	1.627196
12	30	2.0	110	0.439054	103	1.391412	108	1.641925
12	30	1.4	110	1.420099	103	1.095384	107	1.637650
12	60	16.0	90	4.656596	85	3.851890	86	4.421095
12	60	11.0	109	1.480568	101	0.637505	106	2.124419
12	60	8.0	113	1.584168	105	0.965046	110	2.208184
12	60	5.6	112	1.323276	104	0.503958	109	2.098994
12	60	4.0	111	2.488131	103	2.004759	108	2.820510
12	60	2.8	110	1.371442	103	0.423390	107	2.024309
12	60	2.0	110	1.378359	103	1.372338	107	2.024178
12	60	1.4	110	0.555169	102	1.098572	107	2.019506
12	90	16.0	84	4.516892	78	3.598072	79	4.074553
12	90	11.0	110	2.369926	103	1.720241	108	2.048293
12	90	8.0	112	1.394229	105	1.497984	110	2.097448
12	90	5.6	111	1.581190	104	1.500228	109	2.074201

Gain	Mag.	Aperture	Mean Green	Standard Deviation Green	Mean Red	Standard Deviation Red	Mean Blue	Standard Deviation Blue
12	90	4.0	110	1.202542	103	1.428416	108	2.155575
12	90	2.8	109	1.530761	102	0.450100	108	1.907637
12	90	2.0	109	1.400841	102	1.333353	108	2.073638
12	90	1.4	109	1.431814	102	1.527172	107	2.096562
18	15	16.0	104	3.674652	97	3.551586	103	3.801267
18	15	11.0	111	1.464147	104	0.715866	111	2.070710
18	15	8.0	110	1.342201	103	1.152198	110	2.229974
18	15	5.6	110	1.268528	103	1.460345	109	2.098781
18	15	4.0	110	1.238371	102	0.577552	109	2.341451
18	15	2.8	109	1.223871	102	1.258593	109	2.466475
18	15	2.0	109	1.233999	102	1.441908	108	2.322279
18	15	1.4	109	1.239174	102	0.967261	108	2.293813
18	30	16.0	109	1.789289	102	0.621485	109	2.229780
18	30	11.0	111	1.550856	104	1.669465	110	1.819596
18	30	8.0	111	1.356945	103	1.537651	110	2.404428
18	30	5.6	110	1.278320	103	0.676066	109	2.372345
18	30	4.0	110	1.237808	102	1.475168	109	2.357020
18	30	2.8	109	1.231487	102	1.342160	108	2.374702
18	30	2.0	109	1.218609	102	1.371005	108	1.712254
18	30	1.4	109	1.230815	102	0.552752	108	2.236461
18	60	16.0	106	1.619242	99	0.168329	105	2.577468
18	60	11.0	111	1.517161	104	0.862715	111	2.634621
18	60	8.0	110	1.376241	103	0.273384	110	2.557926
18	60	5.6	110	1.275673	103	1.285078	109	2.240544
18	60	4.0	110	1.240478	102	1.393118	109	2.268991

Gain	Mag.	Aperture	Mean Green	Standard Deviation Green	Mean Red	Standard Deviation Red	Mean Blue	Standard Deviation Blue
18	60	2.8	109	1.249133	102	0.826822	108	2.294500
18	60	2.0	109	1.237478	102	1.347310	108	2.233228
18	60	1.4	109	1.220278	102	1.256313	108	2.148603
18	90	16.0	105	1.601681	98	1.059888	105	2.630192
18	90	11.0	111	1.252098	104	1.151420	111	2.258708
18	90	8.0	110	1.354333	103	0.802957	110	2.457221
18	90	5.6	110	1.271784	103	0.795007	109	2.246910
18	90	4.0	110	1.232707	102	0.444830	109	2.274185
18	90	2.8	109	1.237574	102	1.409878	108	2.241039
18	90	2.0	109	1.231878	102	1.102743	108	2.221560
18	90	1.4	109	1.245268	102	1.430135	108	2.219521

Mean Green
Magnification 15

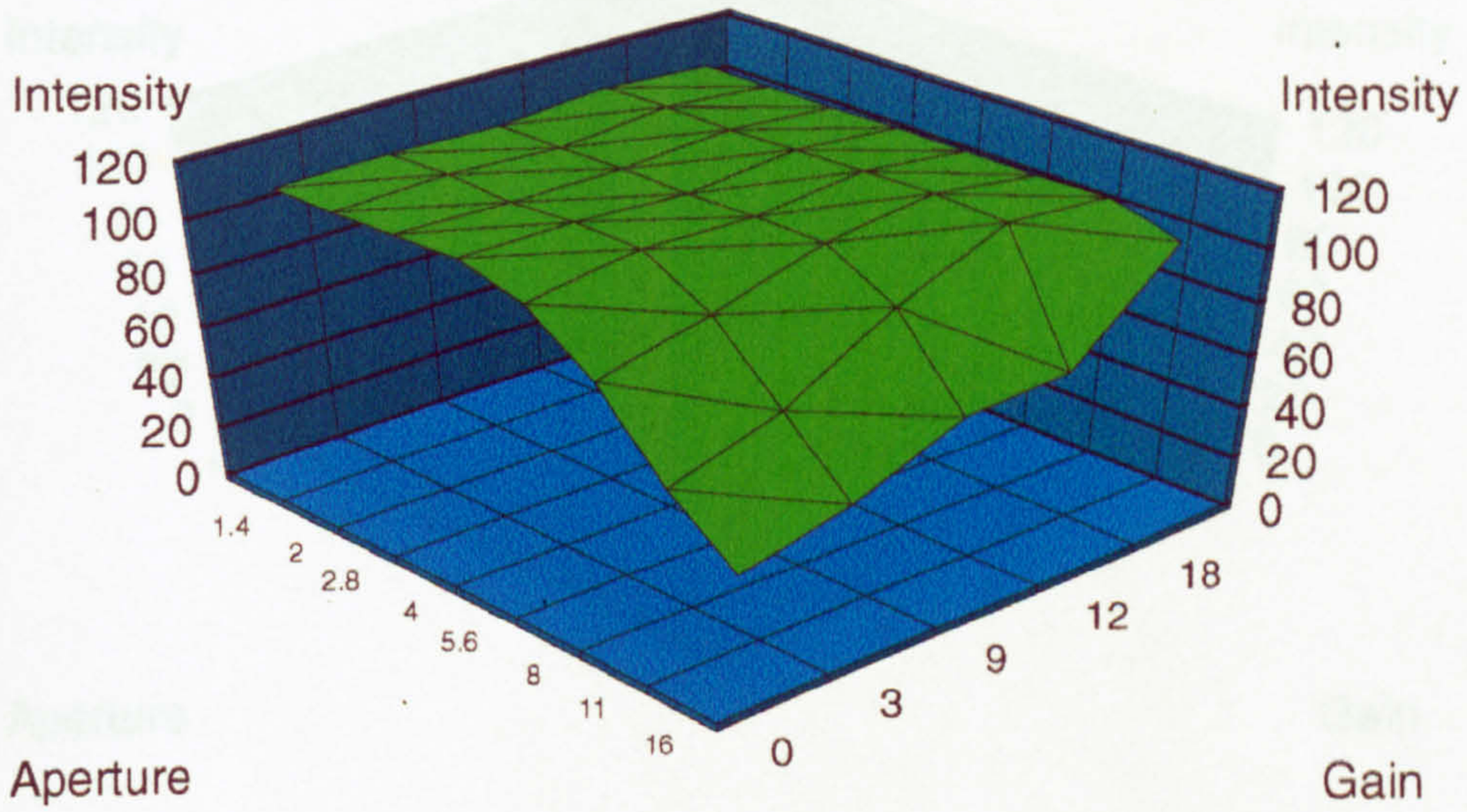

Standard Deviation Green
Magnification 15

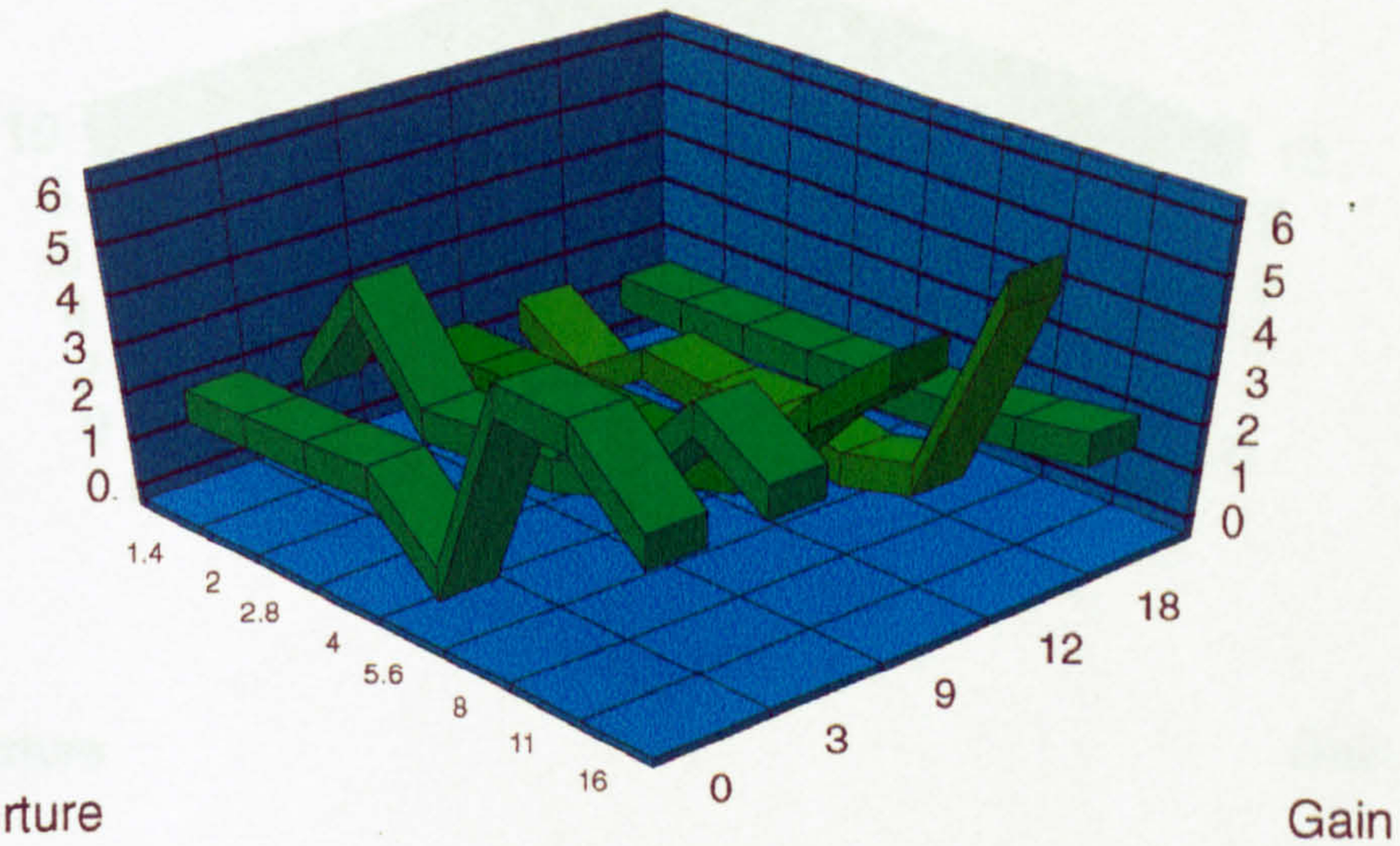

Mean Red
Magnification 15

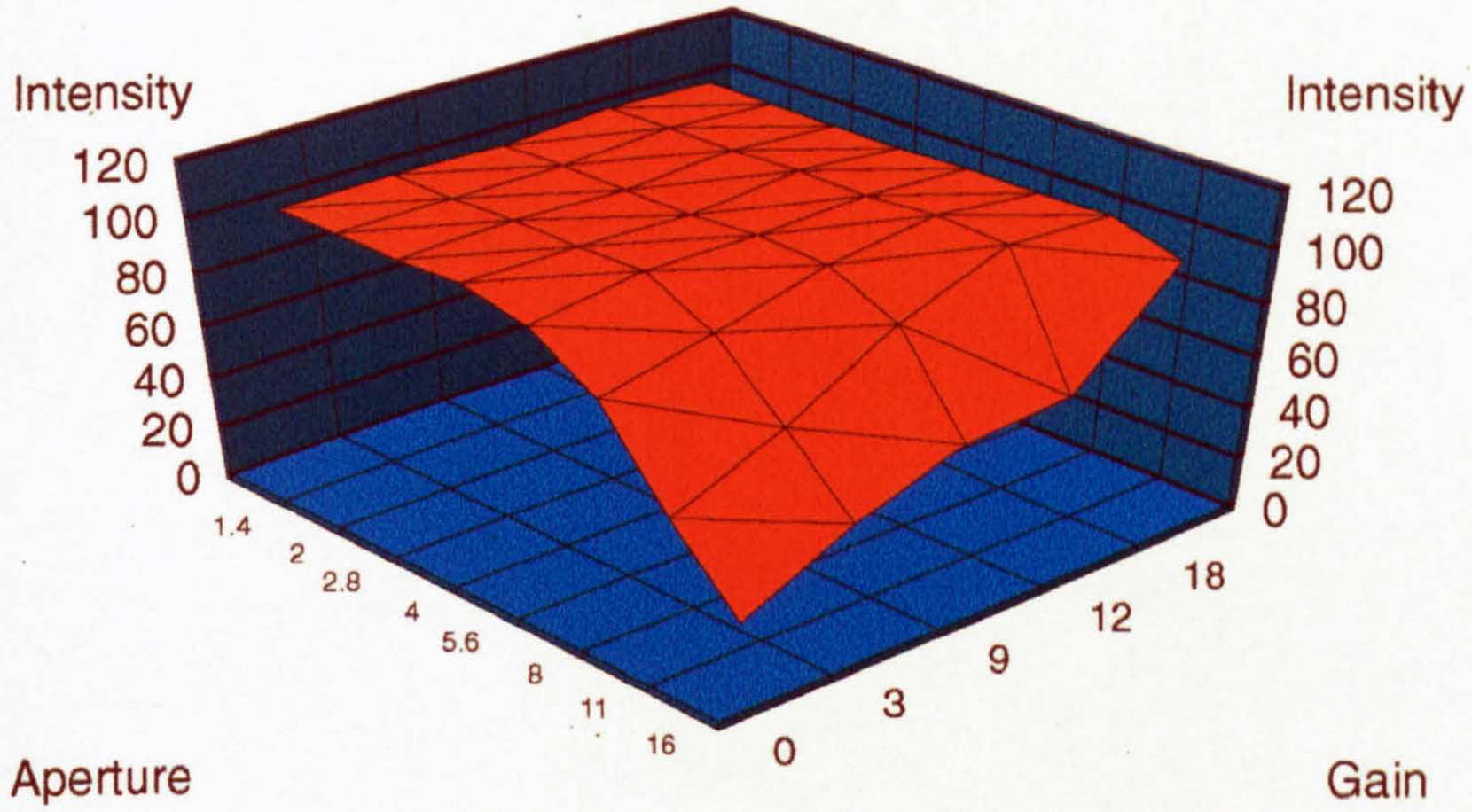

Standard Deviation Red
Magnification 15

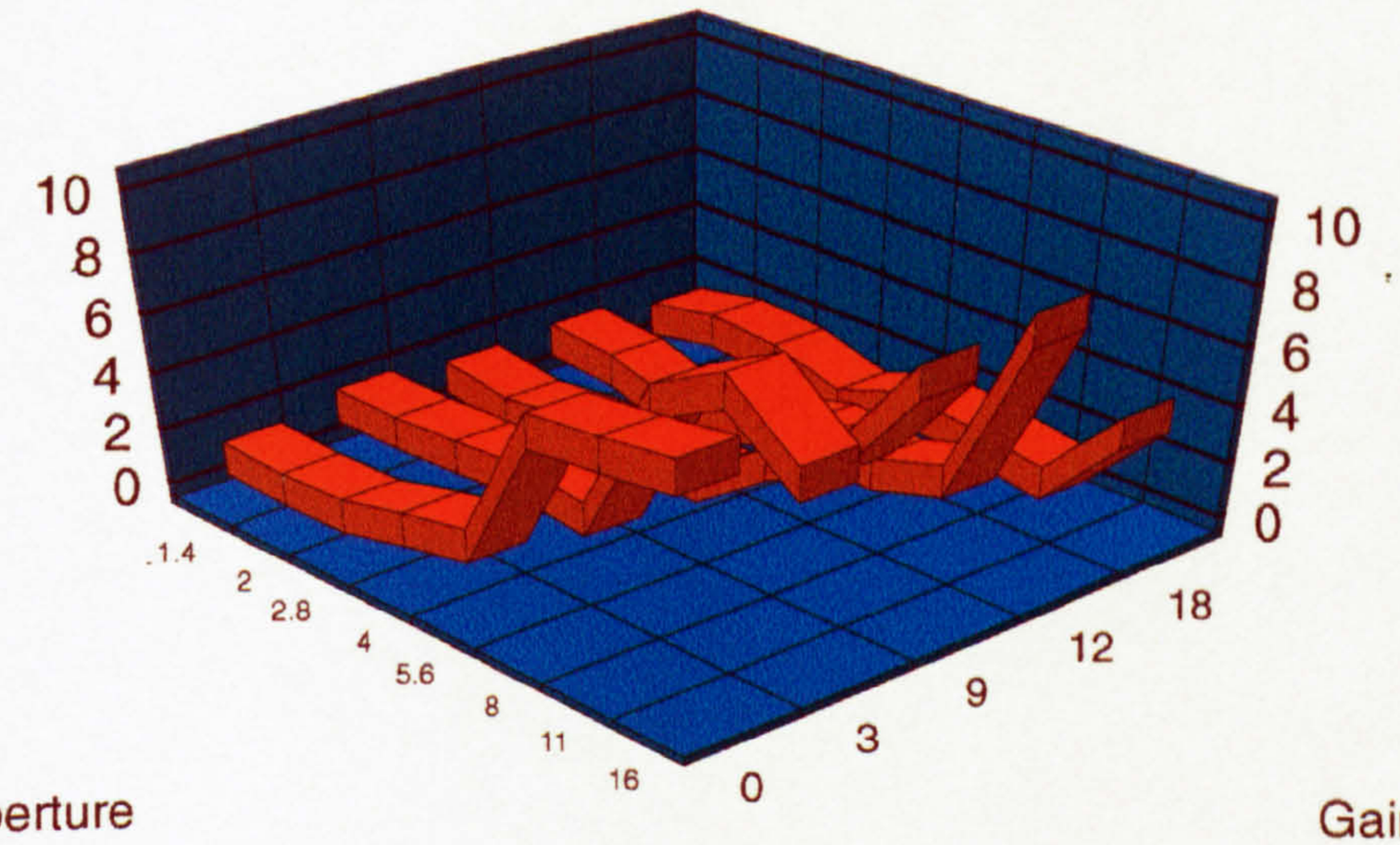

Mean Blue
Magnification 15

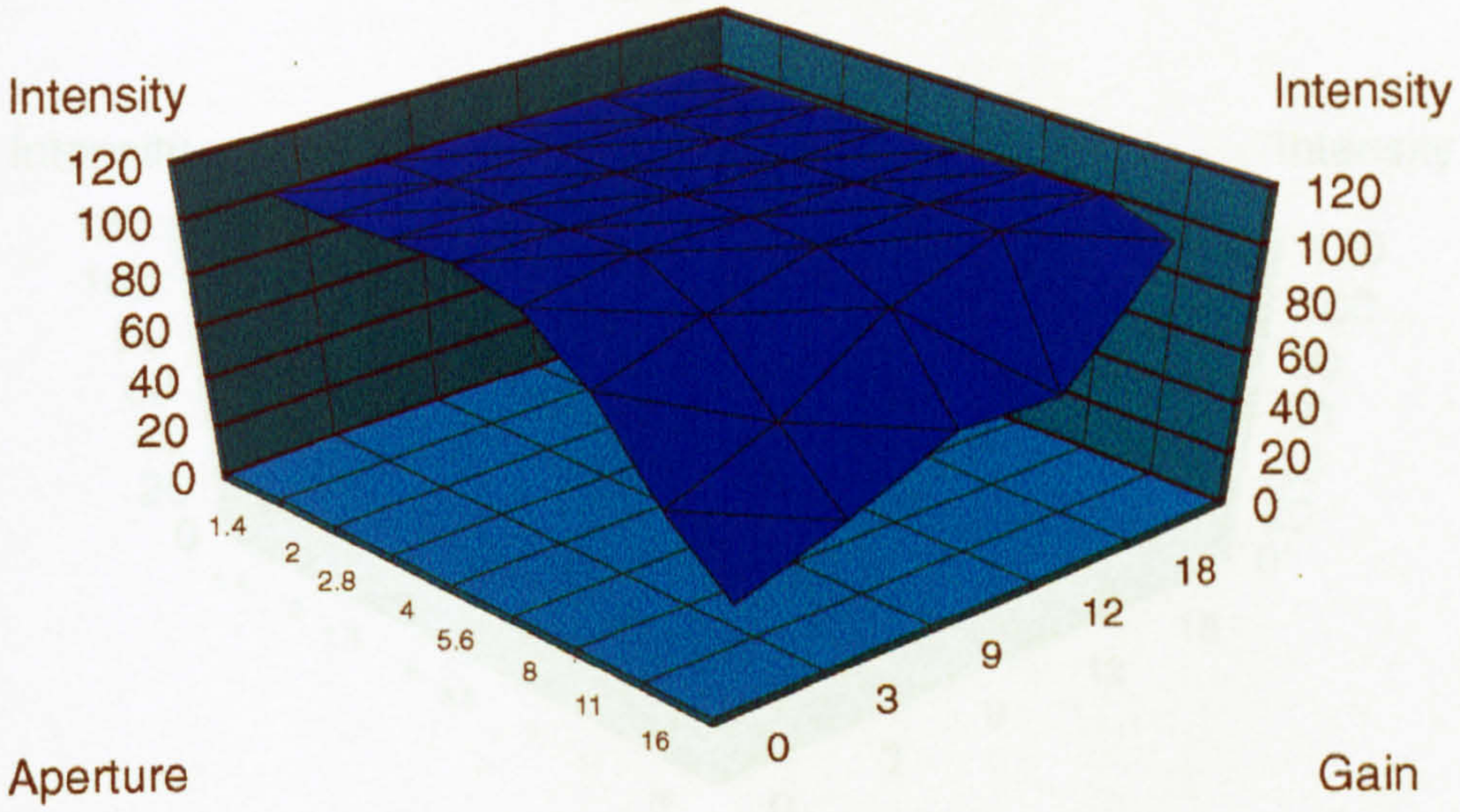

Standard Deviation Blue
Magnification 15

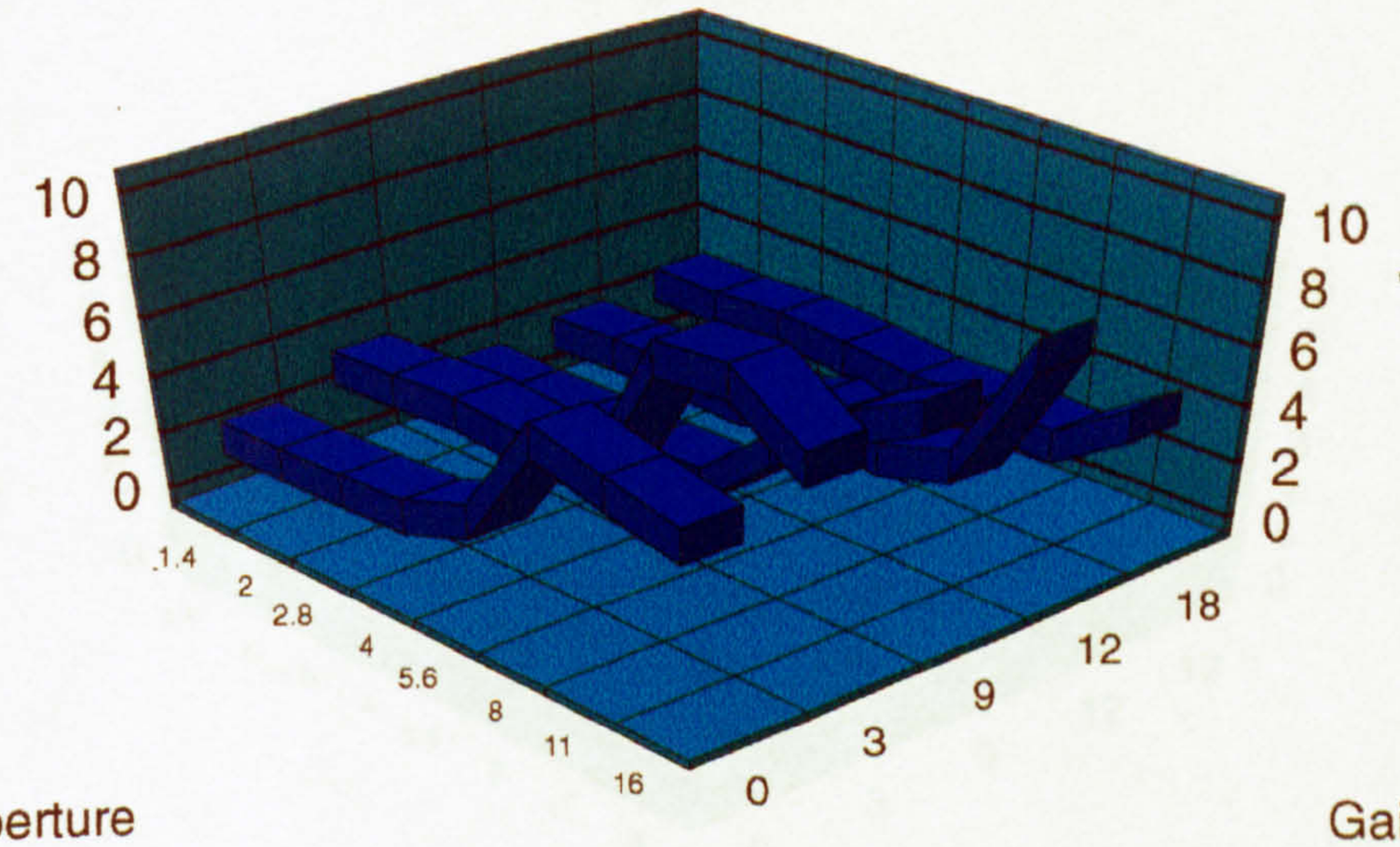

Mean Red

Magnification 30

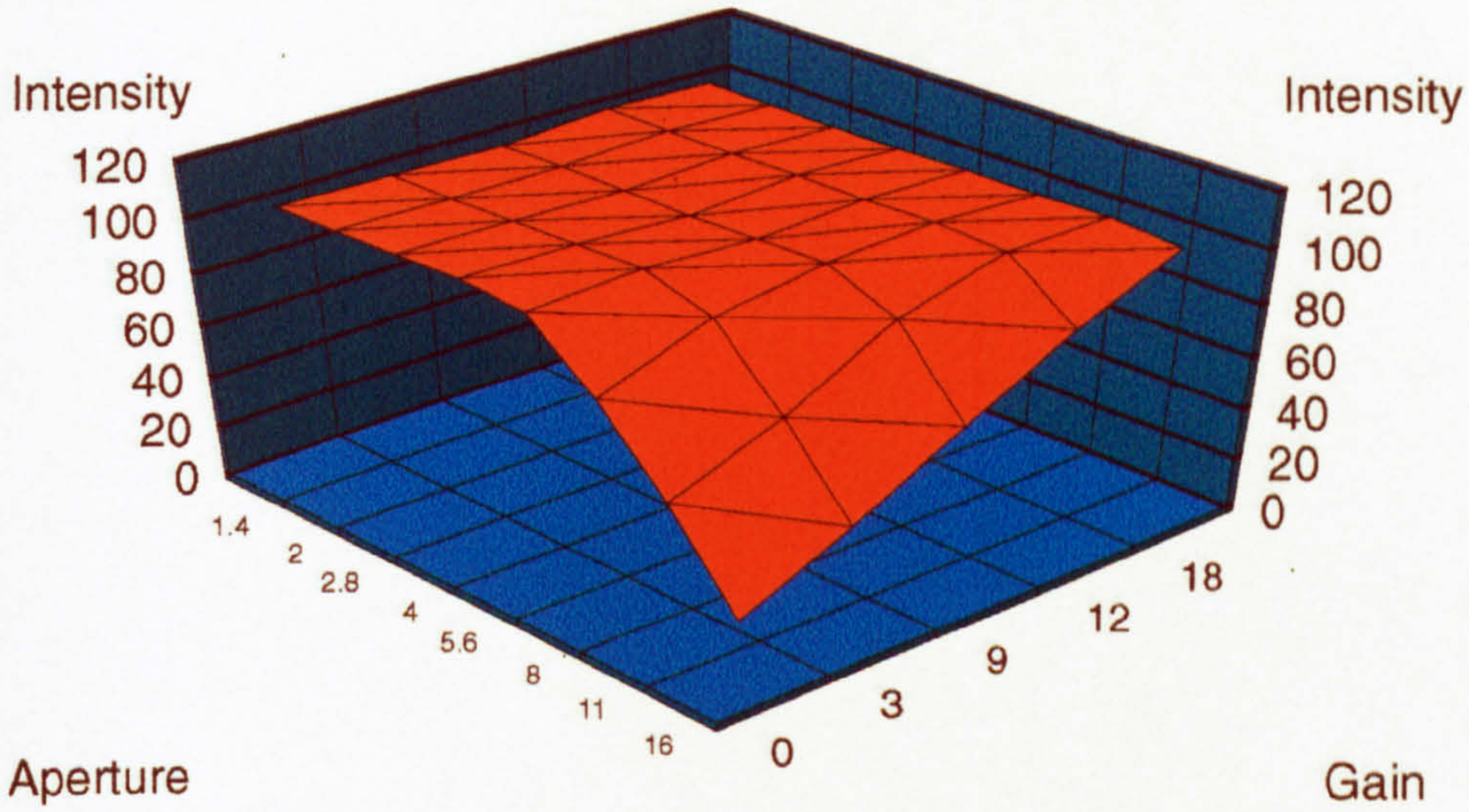

Standard Deviation Red

Magnification 30

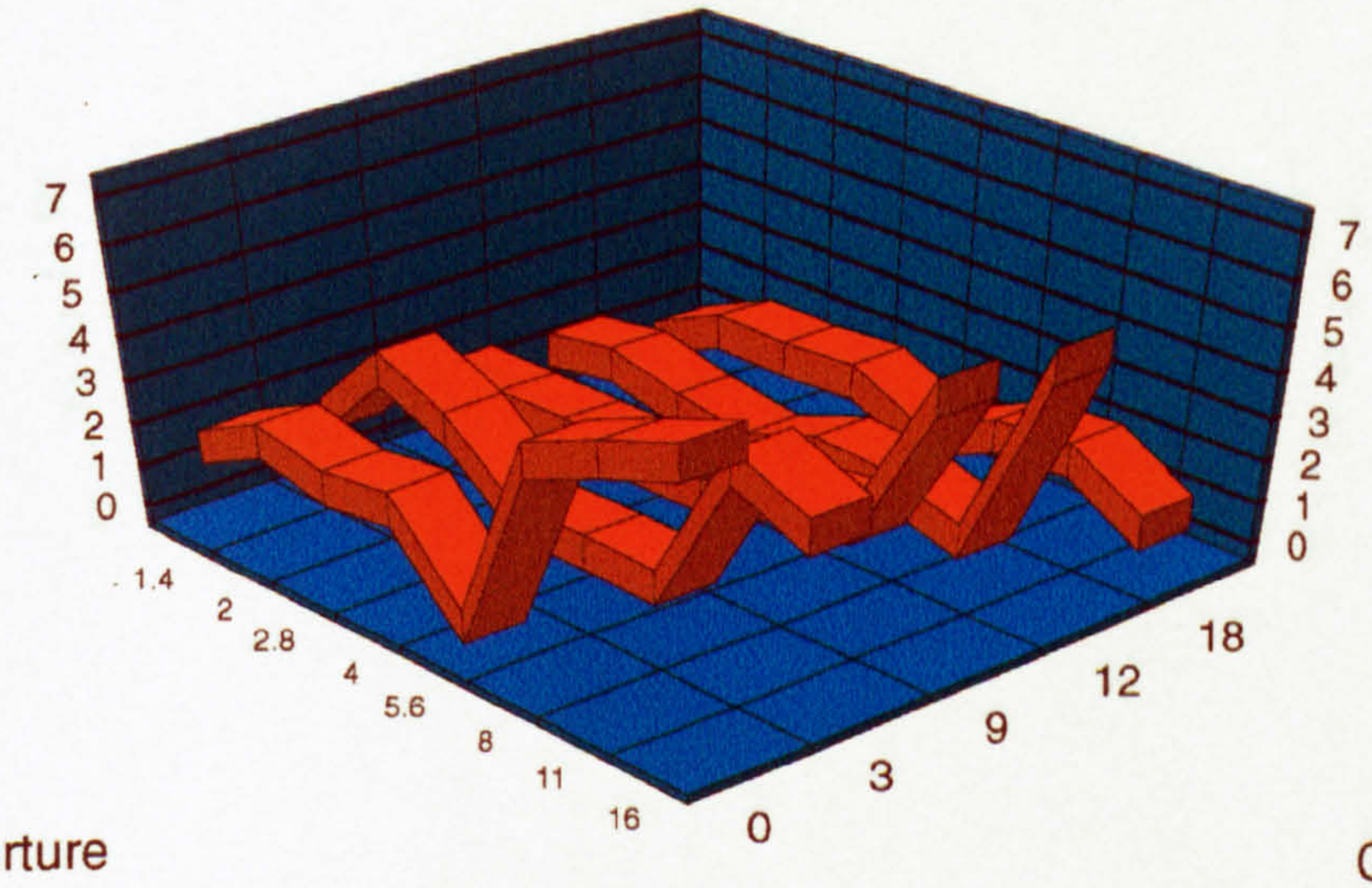

Mean Blue

Magnification 30

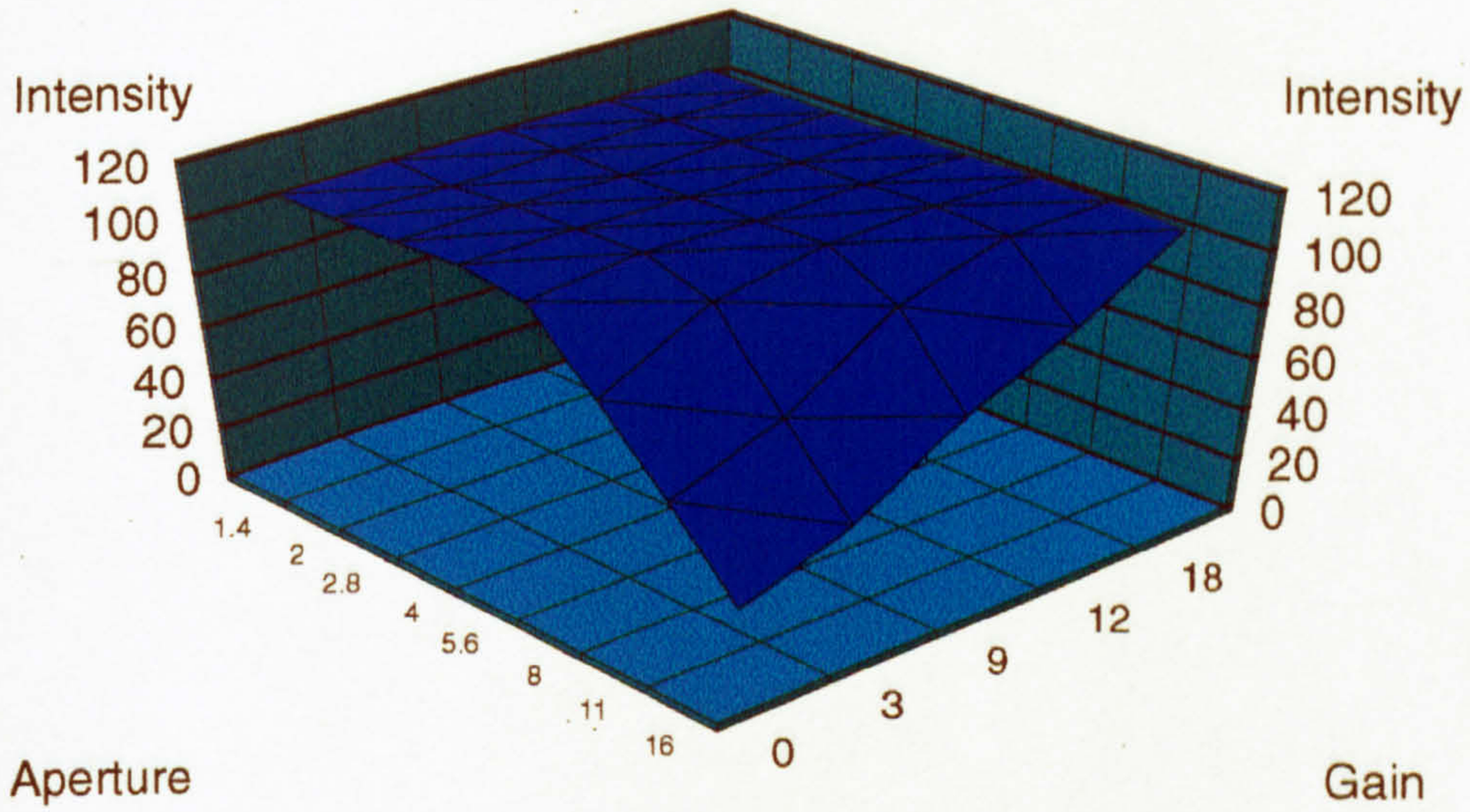

Standard Deviation Blue

Magnification 30

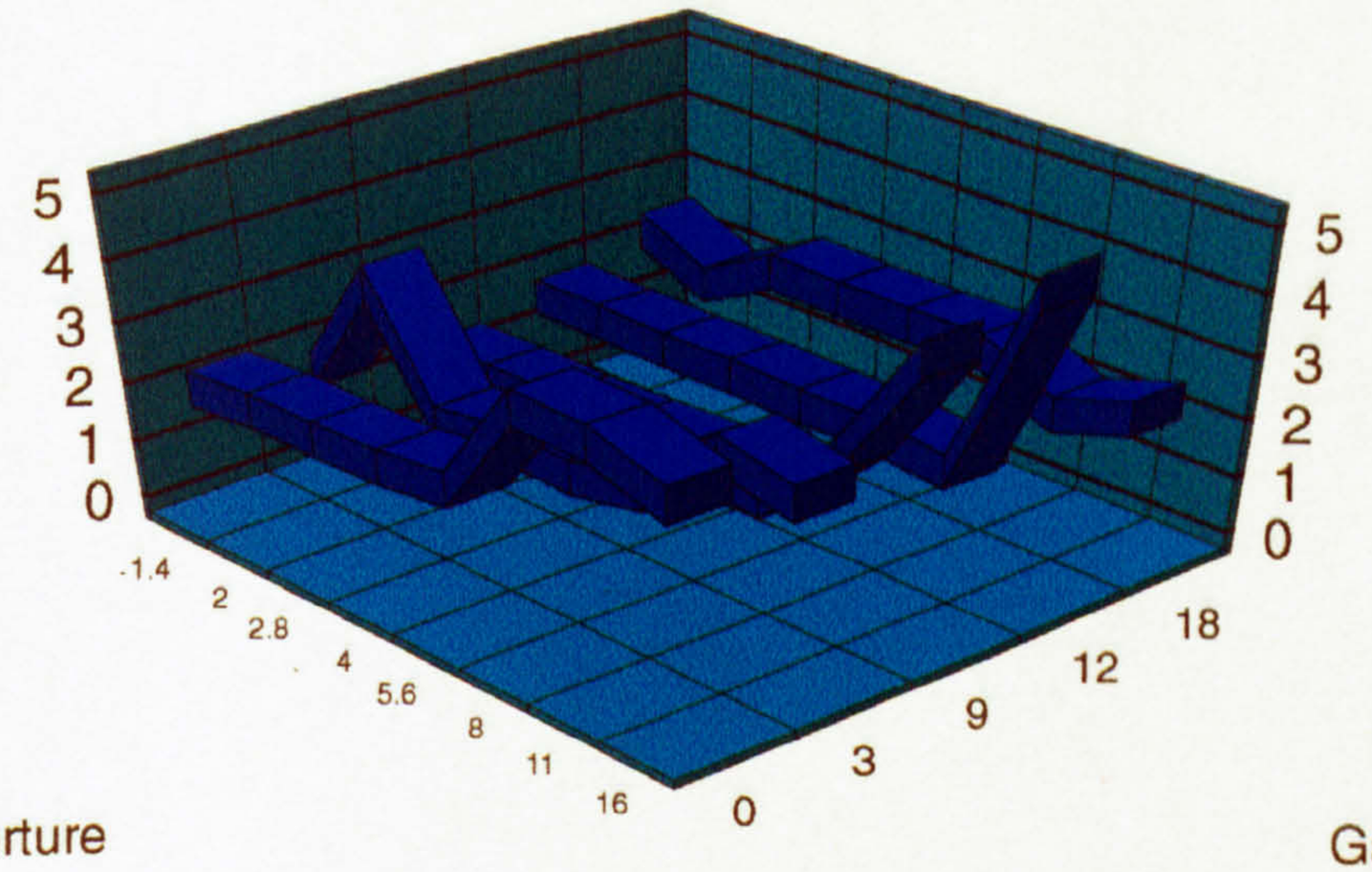

Mean Green
Magnification 60

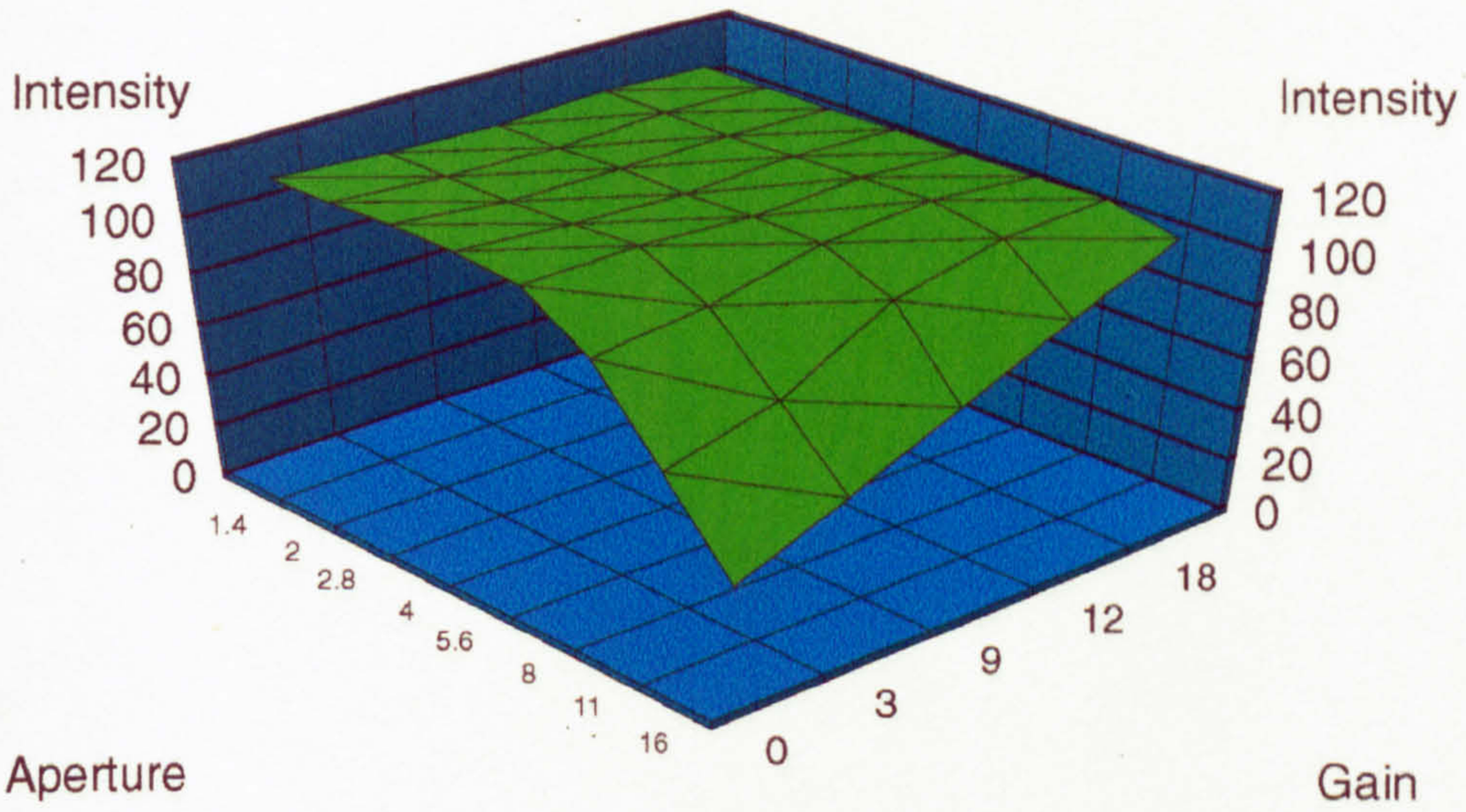

Standard Deviation Green
Magnification 60

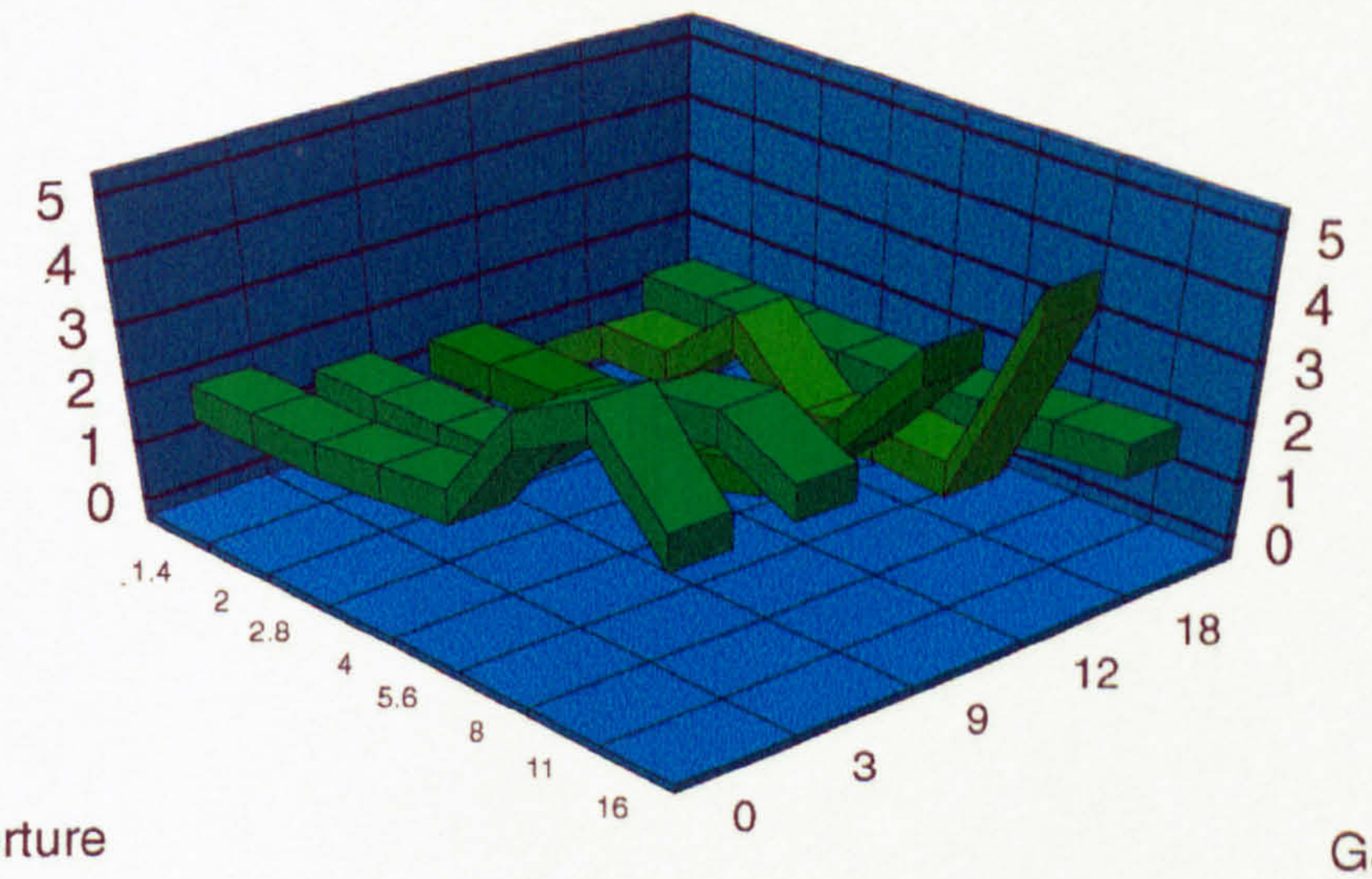

Mean Red

Magnification 60

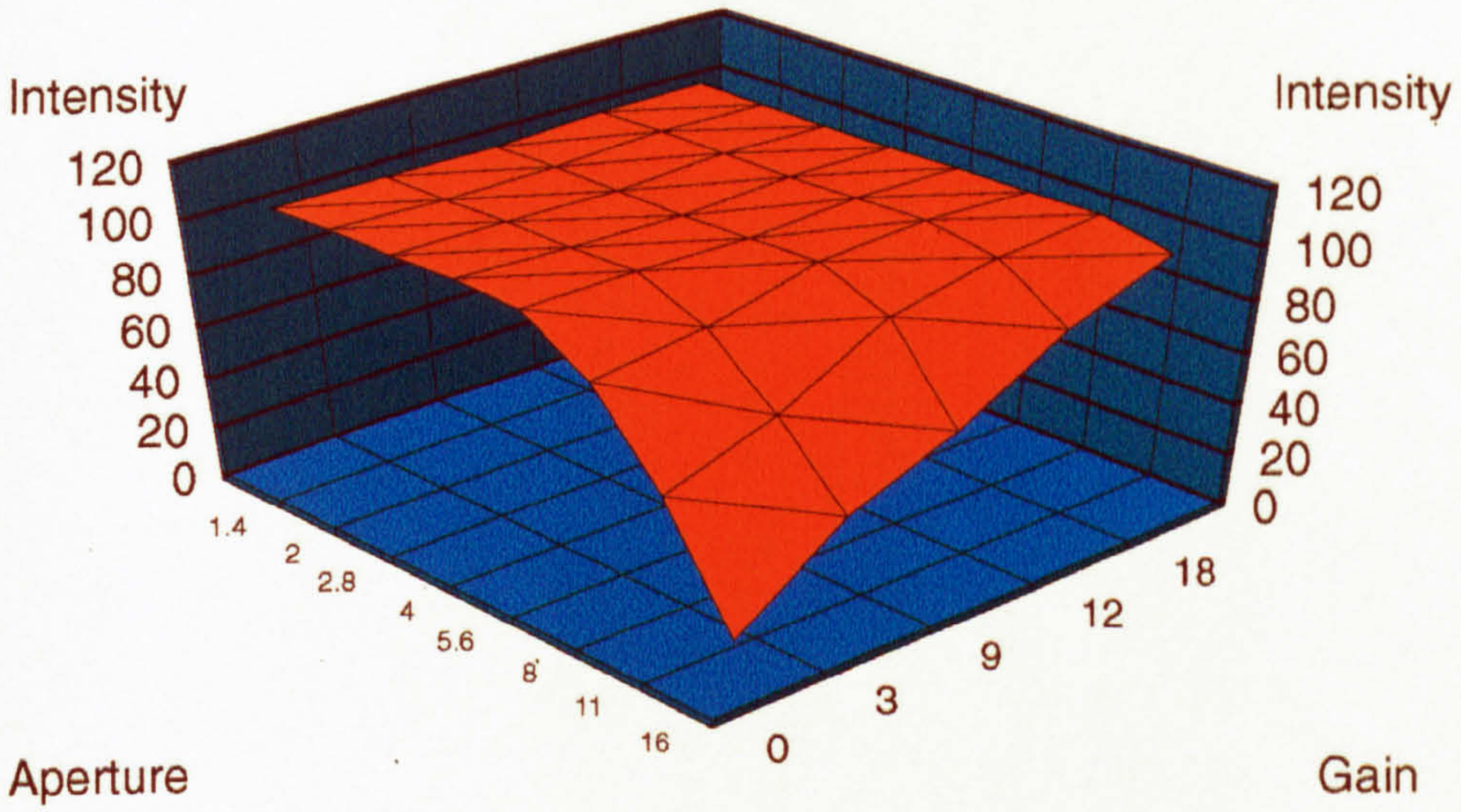

Standard Deviation Red

Magnification 60

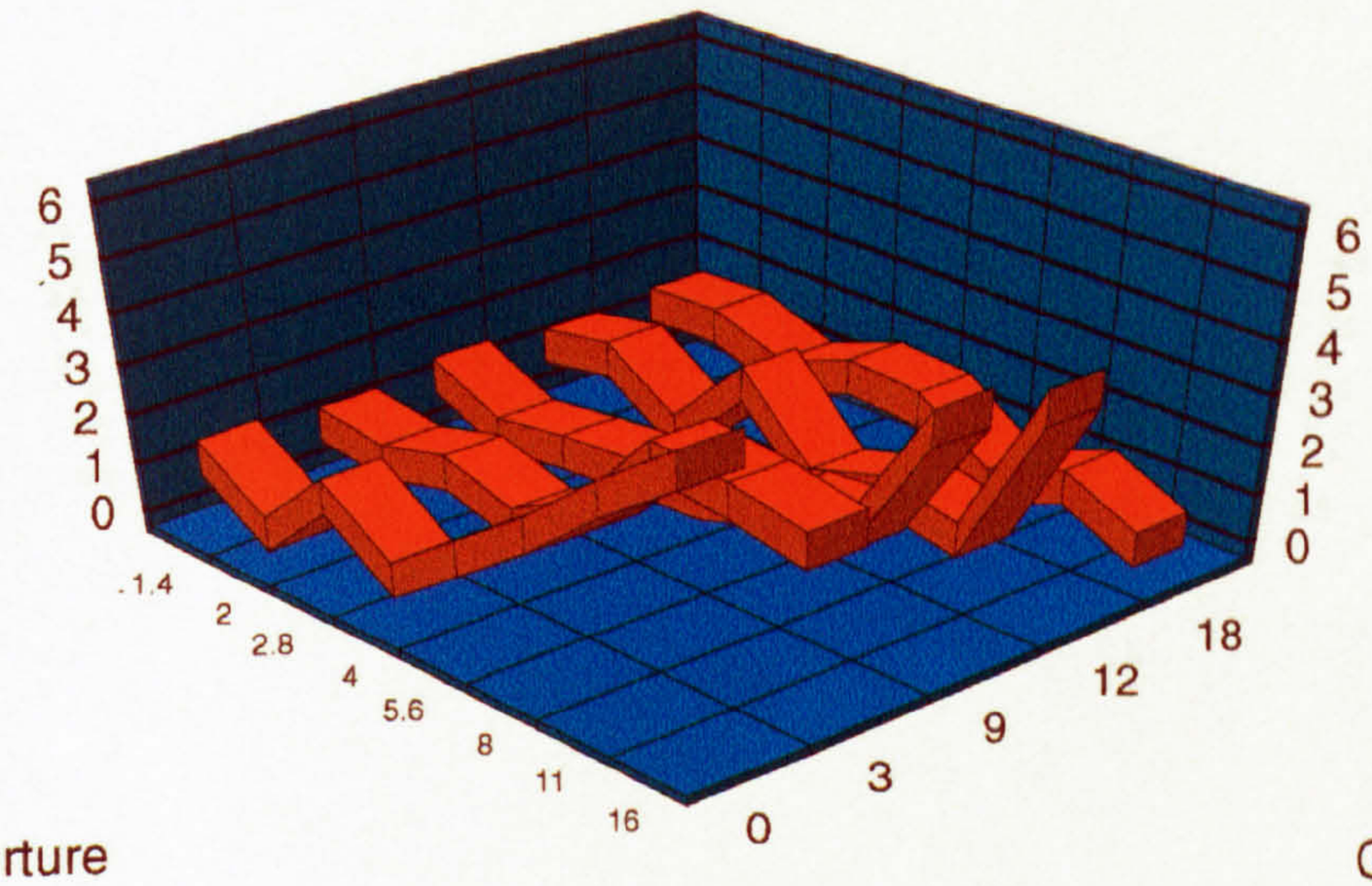

Mean Blue

Magnification 60

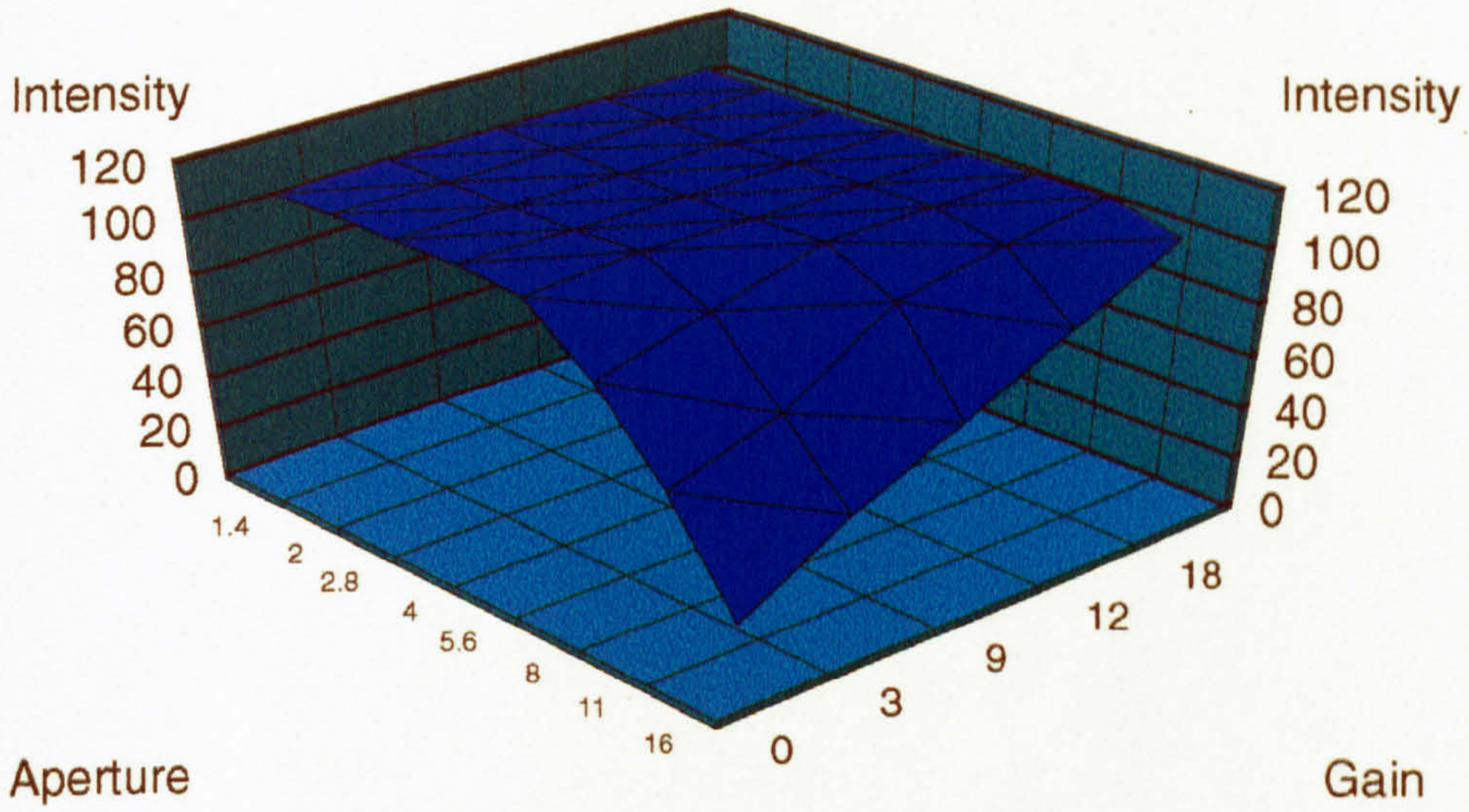

Standard Deviation Blue

Magnification 60

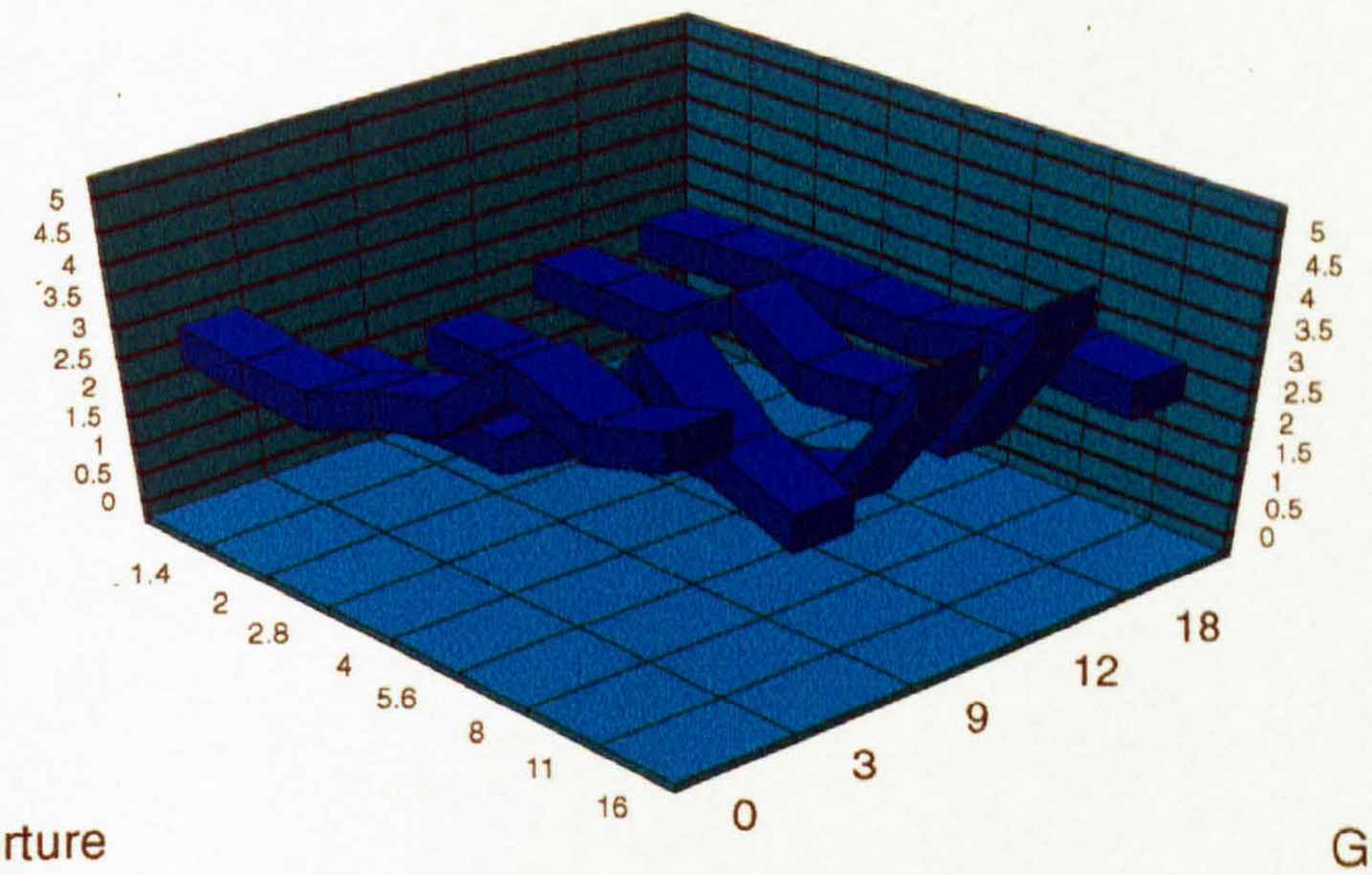

Mean Green

Magnification 90

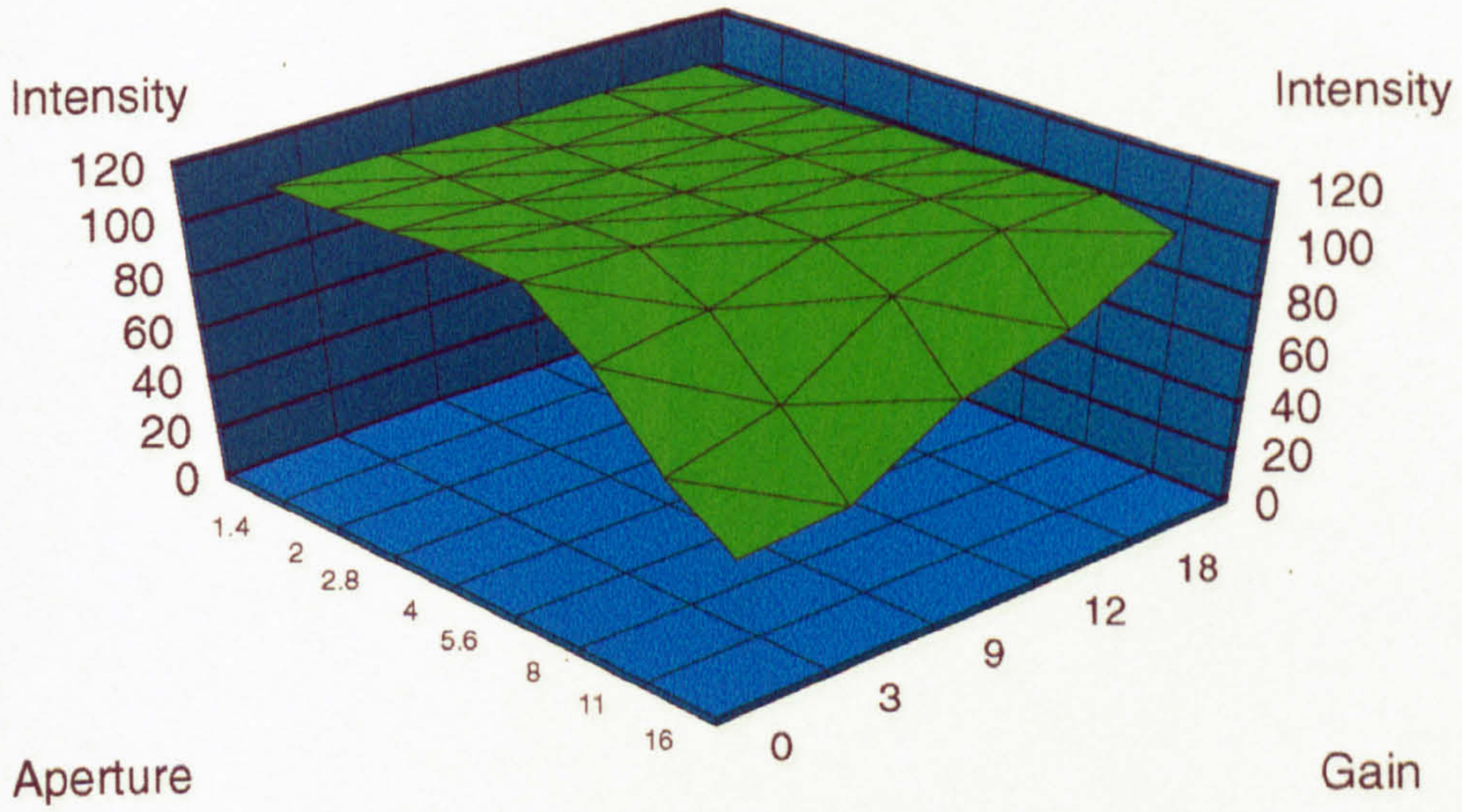

Standard Deviation Green

Magnification 90

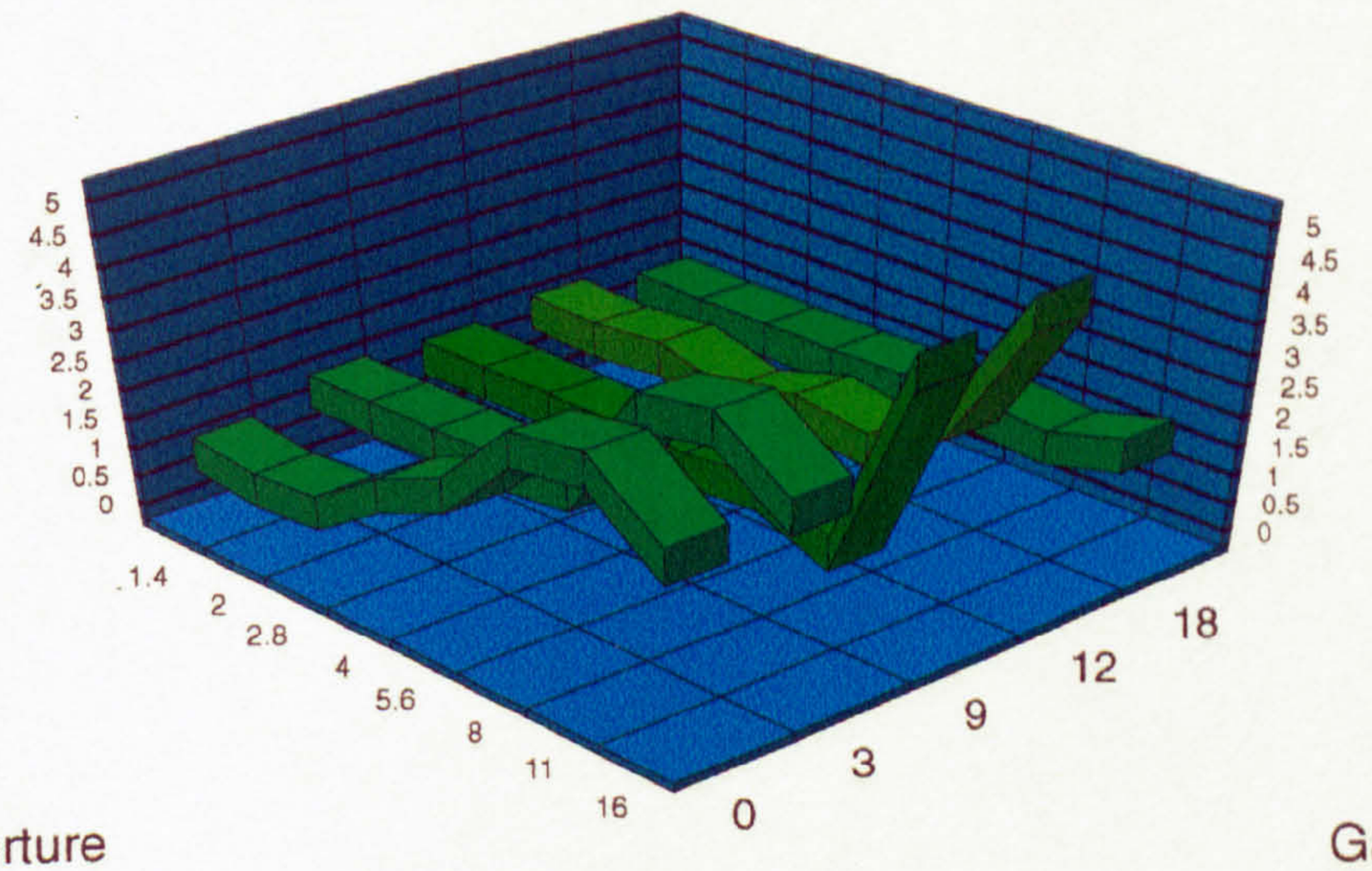

Mean Red

Magnification 90

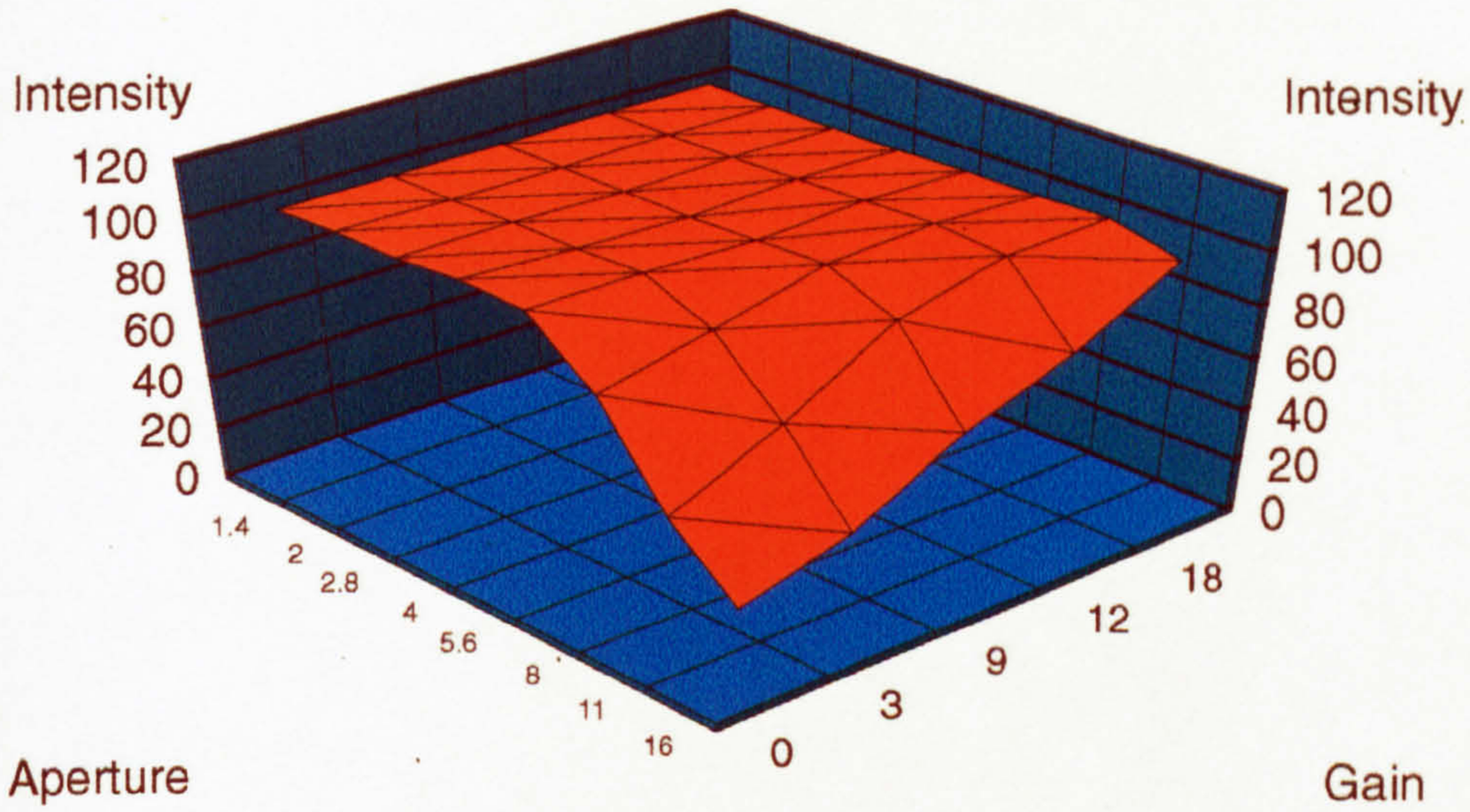

Standard Deviation Red

Magnification 90

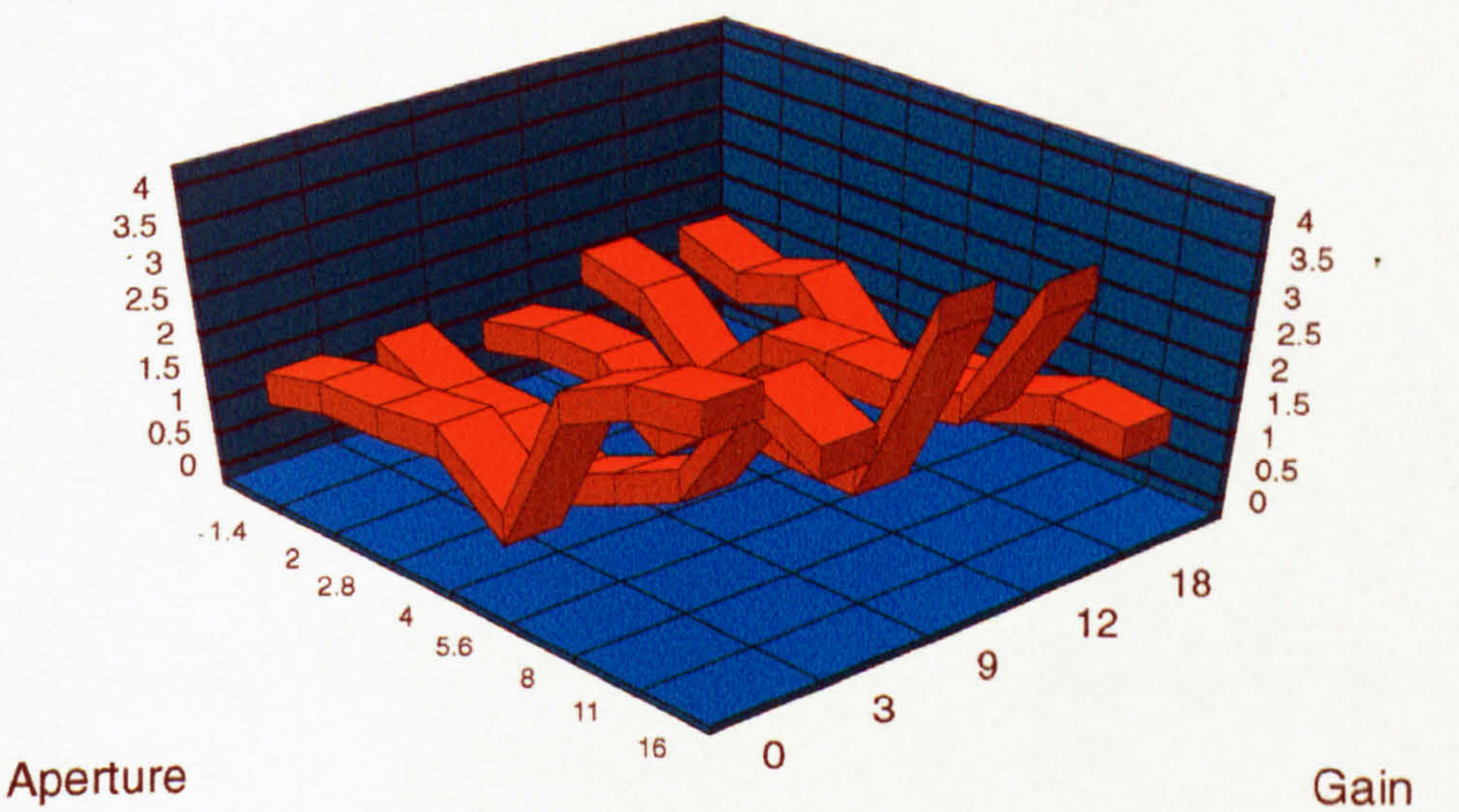

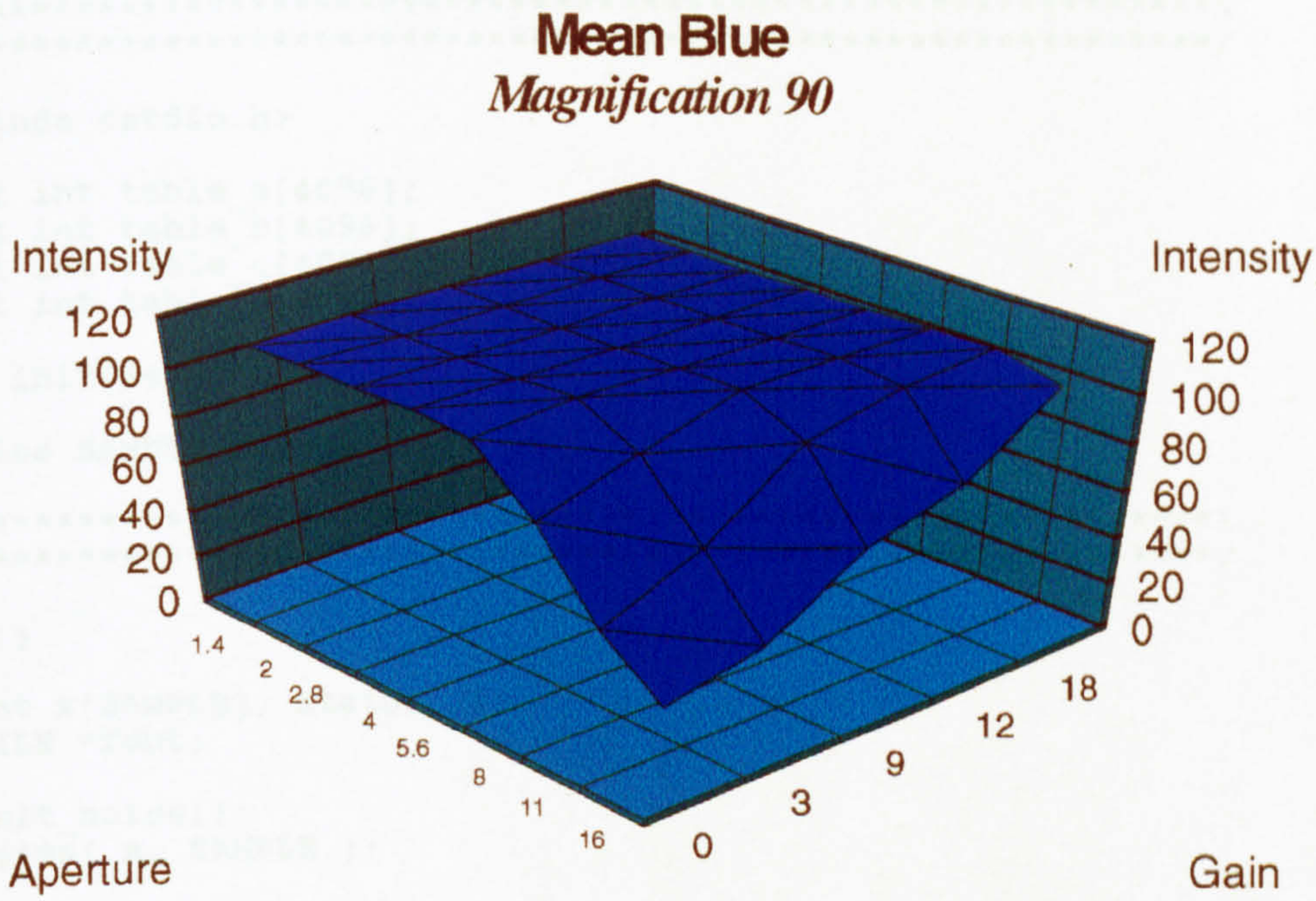
Mean Blue
Magnification 90
Intensity
120
100
80
60
40
20
0
1.4
2
2.8
4
5.6
8
11
16
Aperture
0
3
9
12
18
Gain
Intensity

1.4 Appendix D : Fast Gaussian Noise Generator

```
/*************************************************************\
\*************************************************************/

#include <stdio.h>

short int table_a[4096];
short int table_b[4096];
short int table_c[4096];
short int table_d[4096];

long init[64];

#define SAMPLE 262144

/*************************************************************\
\*************************************************************/

main()
{
   int x[SAMPLE], status, I;
   FILE *fout;

   init_noise();
   noise( x, SAMPLE );

   printf(" Done \n");

   fout = fopen( "result.dat", "wb" );
   status = fwrite( (char *)x, 2, SAMPLE, fout );
   printf("No. words written was %d\n", status );
   fclose( fout );
}

/*************************************************************\
\*************************************************************/

int init_noise()
{
   long  status, ind;
   FILE  *fp;

   for( ind = 0; ind < 64; ++ind )
      init[ind] = 0x80000000 + ind*0x13e22c1;

   fp = fopen( "table.dat", "rb" );

   status = fread( table_a, 2, 4096, fp );
   status = fread( table_b, 2, 4096, fp );
   status = fread( table_c, 2, 4096, fp );
   status = fread( table_d, 2, 4096, fp );

   fclose( fp );
}

/*************************************************************\
\*************************************************************/

int noise( int x[], int length )
{
   int vlaue, il;
```

```
register long ind, ind_lo, ind_hi, j;
long circular[64];
float   fdumb;
long status, jump_index, table_index, threshold, count, i, k;

ind = 0;
for( i = 0; i < 64; ++i )
   circular[i] = init[i];

for( i = 0; i < length; i++ )
{
   ++ind;
ind_lo = ind - 1;
ind = ind&0x3f;
circular[ind] += circular[ind_lo];
if(( circular[ind]&0x8000000 ) != 0 )
   ++circular[ind];
j = circular[ind];
table_index = j&0xfff;
jump_index = (j>>12)&0x7f;
if( jump_index != 0 )
{
   x[i] = table_a[table_index];
   goto FINISHED;
}

++ind;
ind_lo = ind - 1;
ind = ind&0x3f;
circular[ind] += circular[ind_lo];
if(( circular[ind]&0x8000000 ) != 0 )
   ++circular[ind];
j = circular[ind];
table_index = j&0xfff;
jump_index = (j>>12)&0x7f;
if( jump_index != 0 )
{
   x[i] = table_b[table_index];
   goto FINISHED;
}

++ind;
ind_lo = ind - 1;
ind = ind&0x3f;
circular[ind] += circular[ind_lo];
if(( circular[ind]&0x8000000 ) != 0 )
   ++circular[ind];
j = circular[ind];
table_index = j&0xfff;
jump_index = (j>>12)&0x7f;
if( jump_index != 0 )
{
   x[i] = table_c[table_index];
   goto FINISHED;
}

++ind;
ind_lo = ind - 1;
ind = ind&0x3f;
circular[ind] += circular[ind_lo];
if(( circular[ind]&0x8000000 ) != 0 )
   ++circular[ind];
j = circular[ind];
```

```
        table_index = j&0xfff;
        jump_index = (j>>12)&0x7f;
        x[i] = table_a[table_index];

FINISHED: ;
        if(( j&0x10000000 ) == 0) x[i] = -x[i];
    }

    for( i=0; i<64; ++i)
        init[i] = circular[i];
}
```

```
/*************************************************************\
   table.c
\*************************************************************/

#include <stdio.h>
#include <math.h>

/*************************************************************\
\*************************************************************/

short int table[16384];
double recp_tpi, errf[6000];

#define PI  3.1415926

/*************************************************************\
\*************************************************************/
```

```
main( )
{
    double  prob_seg, range, upper_tail, prob_dens();
    int     status, i, j, k, jstart, kstart, index;
    FILE  *fp;

    recp_tpi = 1.0 / sqrt( 2*PI );

    create_erf( errf );

    range = 0.5;
    i = 1, kstart = 0, table[0] = 0;

    for( index = 0; index < 4; ++index )
    {
        prob_seg = ( range - ( range/128.0 )) / 4096.0;
        upper_tail = range;

        if( index == 0 )
    jstart = 1;
else
    jstart = 0;

for( j = jstart; j < 4096; ++j )
{
    for( k = kstart; k < 6000; ++k )
    {
        if( errf[k] <= upper_tail )
            break;
    }

    table[i] = (int)( ( (float)( k + kstart ) / 2.0 ) + 0.5 );
```

```
            kstart = k;
            upper_tail -= prob_seg;
            ++i;
        }


        range = range / 128.0;
    }

    fp = fopen( "table.dat", "wb" );
    status = fwrite( (char *)table, 2, 16384, fp );
    printf("No. words written was %d\n", status );
    fclose( fp );
}

/*****************************************************************\
\*****************************************************************/

double   prob_dens( double x )
{
    return( recp_tpi * exp( -(x*x)/2.0 ) );
}


/*****************************************************************\
\*****************************************************************/

create_erf( double errf[] )
{
    int    i;
    double  integral_inc, prob_dens(), old, mid;

    errf[0] = 0.5;
    old = 0.5;

/*  For standard deviation < 3 use dumb integration to find the function */

    for( i = 1; i < 30000; ++i )
    {
        if( (i % 10) == 0 )
            errf[i/10] = old;

        mid = ((float)(i-1) + 0.5 ) / 10000.0;
        integral_inc = 0.0001 * prob_dens( mid );
        old = old-integral_inc;
    }

/*  For standard deviation > 3 use close form approximation */

    for( i = 3000; i < 6000; ++i )
    {
        mid = ( (float)(i-1) + 0.5 ) / 1000.0;
        errf[i] = recp_tpi * ( exp( -(mid*mid)/2.0 ) / mid );
    }
}

/*****************************************************************\
\*****************************************************************/
```

1.5 Appendix E : Evaluation Results

1.5.1 Samples of Fabric Images used for Evaluation

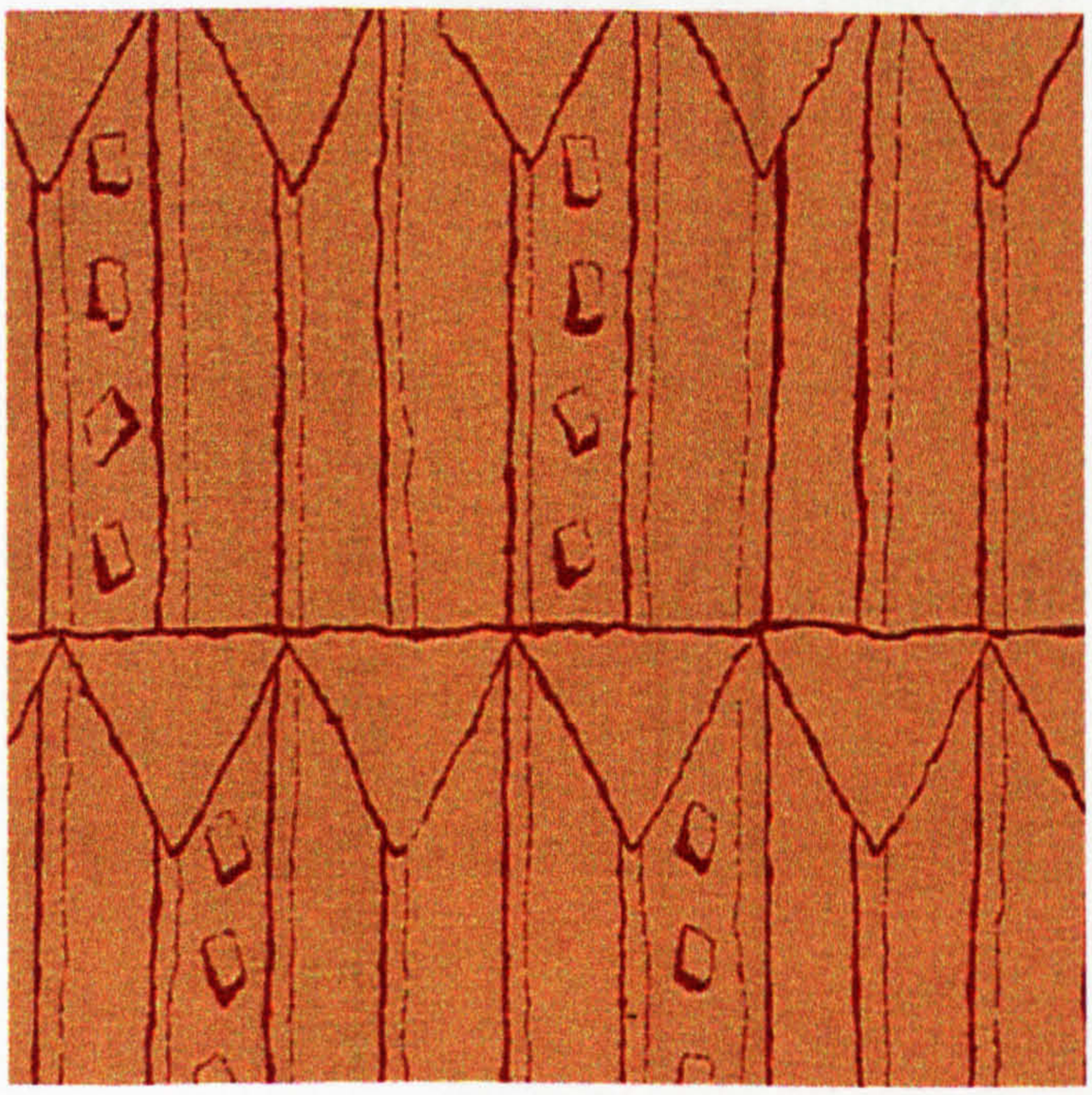

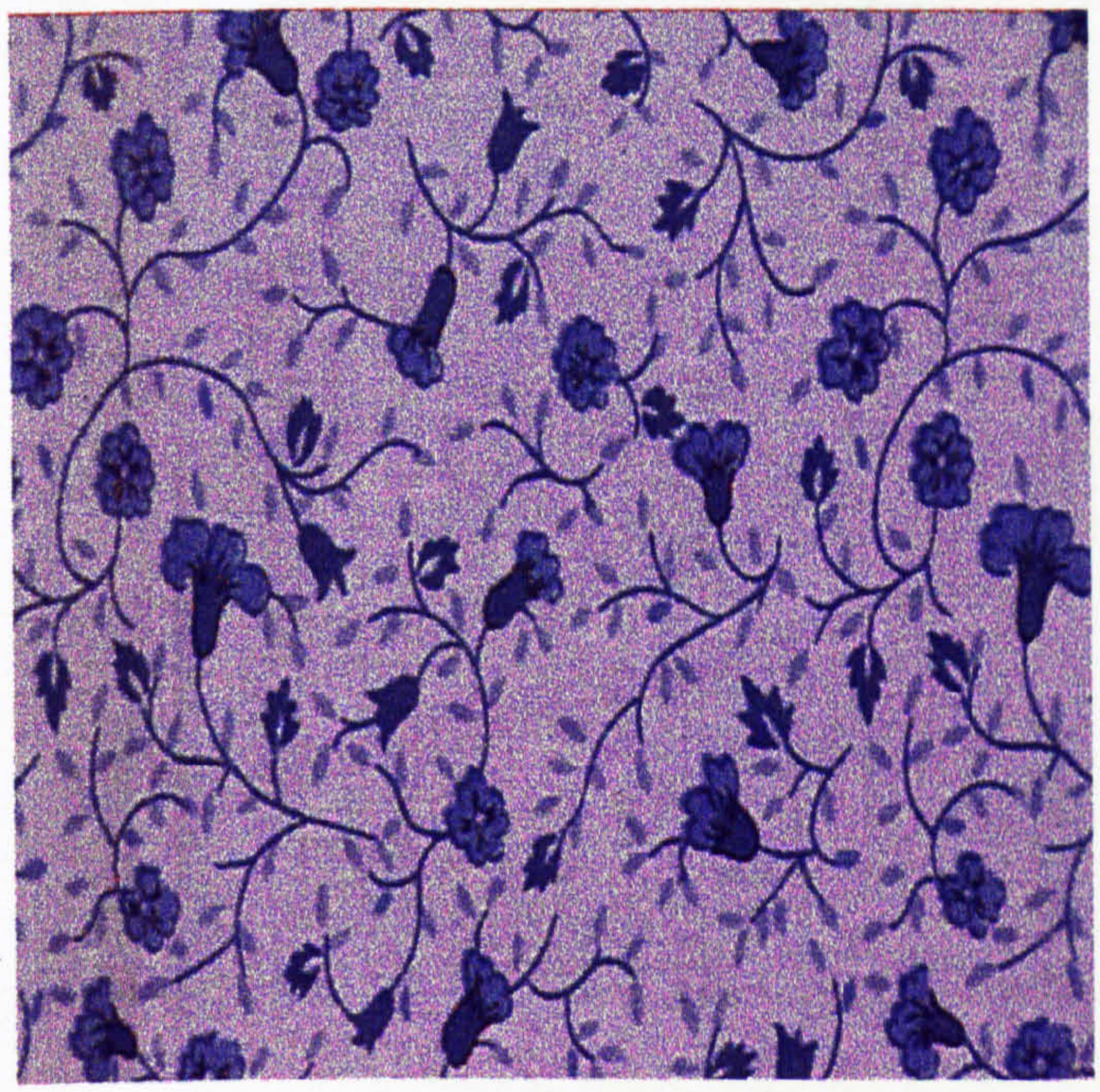

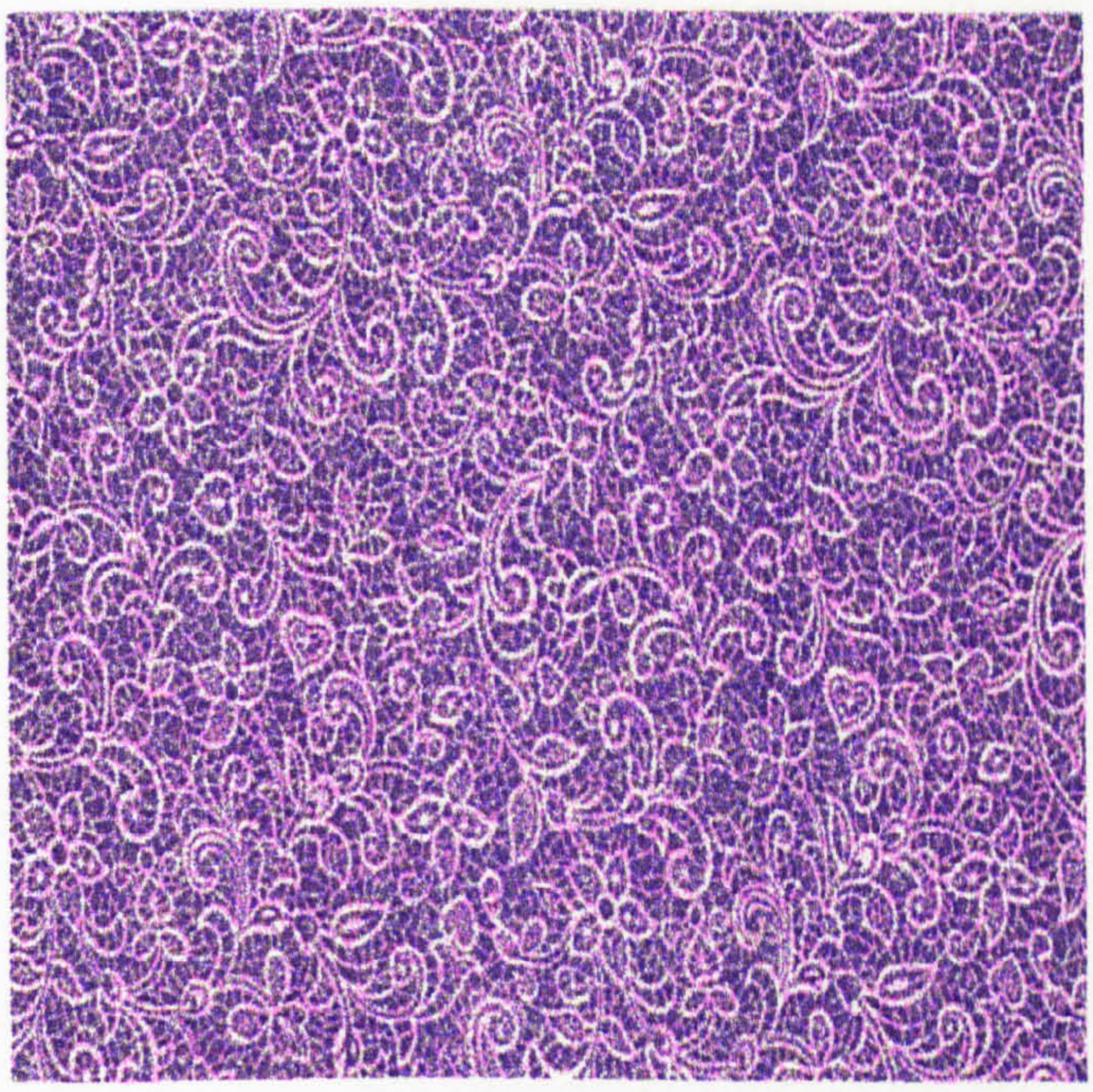

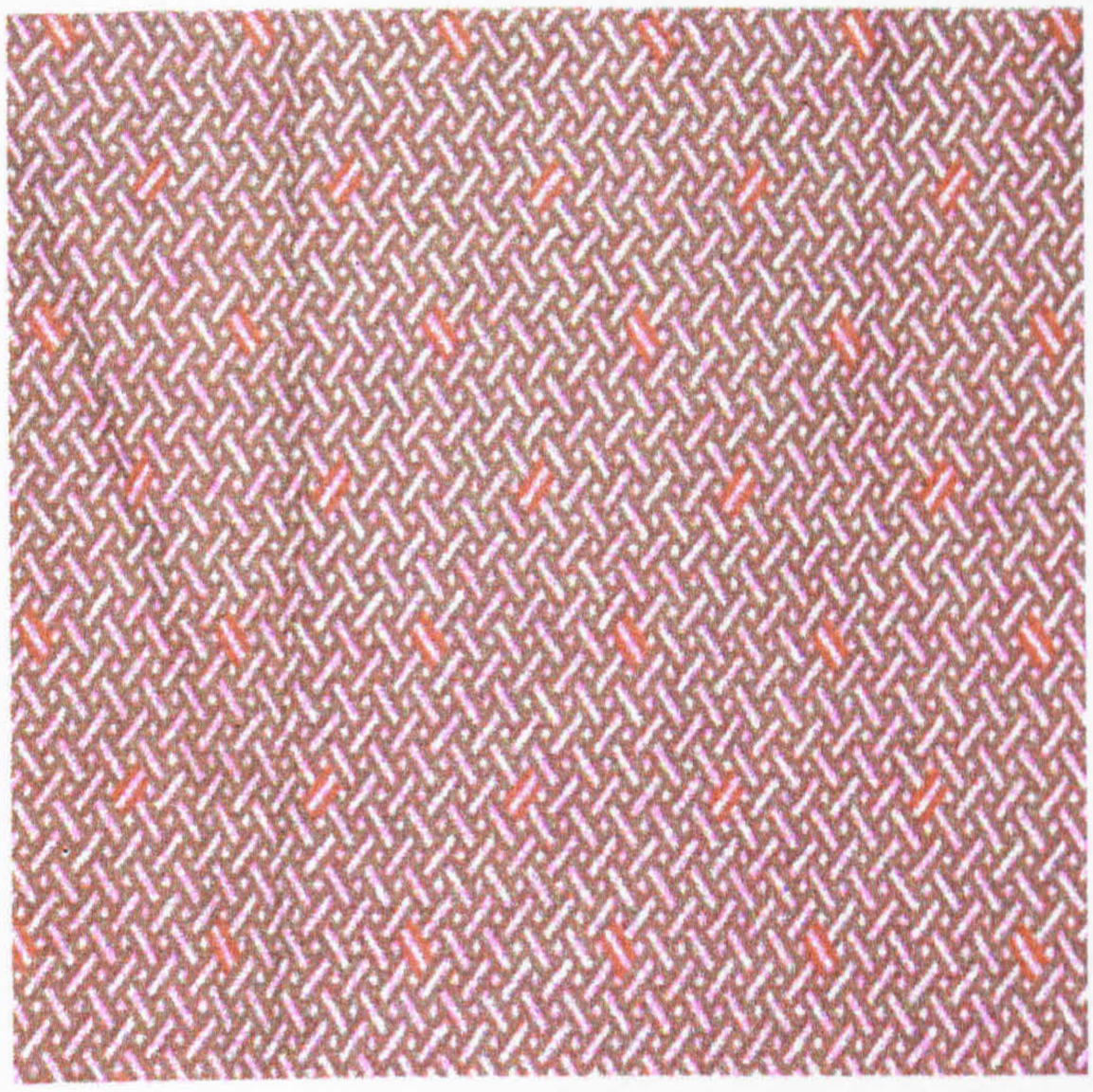

1.5.2 Results of Distortion Measure Tests on Fabric Images

Sample Type	#	A	B	C	D	E	F	G
Floral #1	11	0.1544	0.0233	0.0780	0.0510	0.0311	0.0463	0.0192
Floral #2	11	0.2010	0.0339	0.0814	0.0504	0.0477	0.0390	0.0262
Floral #3	11	0.1387	0.0214	0.0711	0.0468	0.0392	0.0433	0.0175
Floral #4	8	0.0935	0.0470	0.0649	0.0645	0.0413	0.0364	0.0301
Floral #5	9	0.2179	0.0287	0.0760	0.0754	0.0348	0.0427	0.0178
Floral #6	4	0.3333	0.0364	0.0987	0.0809	0.0502	0.0574	0.0212
Floral #7	11	0.2029	0.0228	0.0864	0.0899	0.0729	0.0452	0.0219
Floral #8	10	0.2899	0.0206	0.0676	0.0774	0.0532	0.0397	0.0128
Floral #9	10	0.3274	0.0268	0.0726	0.0917	0.0579	0.0551	0.0206
Floral #10	10	0.2951	0.0261	0.0736	0.0655	0.0675	0.0401	0.0171
Floral #11	10	0.2753	0.0306	0.0966	0.0874	0.0587	0.0440	0.0206
Floral #12	10	0.1648	0.0336	0.0728	0.0706	0.0431	0.0319	0.0184
Geometrical #1	3	0.1082	0.0317	0.0824	0.0823	0.0613	0.0442	0.0206
Geometrical #2	6	0.3399	0.0285	0.0613	0.0746	0.0766	0.0593	0.0227
Geometrical #3	5	0.1889	0.0355	0.0915	0.0813	0.0965	0.0423	0.0254
Geometrical #4	2	0.0912	0.0415	0.1191	0.1001	0.1216	0.0824	0.0335
Geometrical #5	2	0.1332	0.0395	0.0931	0.1062	0.1138	0.0724	0.0291
Geometrical #6	9	0.1453	0.0336	0.0749	0.0864	0.0793	0.0679	0.0236
Geo/Floral #1	9	0.2664	0.0254	0.0691	0.0986	0.0683	0.0455	0.0215
Geo/Floral #2	10	0.1001	0.0193	0.0685	0.0558	0.0441	0.0373	0.0147
Geo/Floral #3	10	0.2891	0.0168	0.0541	0.0658	0.0408	0.0346	0.0122
Geo/Floral #4	10	0.1407	0.0201	0.0644	0.0708	0.0589	0.0498	0.0182
Pastel #1	6	0.1579	0.0286	0.0681	0.0727	0.0547	0.0631	0.0144
Paisley #1	10	0.2235	0.0228	0.0706	0.0691	0.0629	0.0685	0.0189
Paisley #2	11	0.2349	0.0314	0.0815	0.0951	0.0835	0.0901	0.0215
Paisley #3	4	0.1063	0.0327	0.0792	0.0922	0.0972	0.0884	0.0244

Sample Type	#	A	B	C	D	E	F	G
Paisley #4	9	0.0910	0.0278	0.0629	0.0544	0.0614	0.0609	0.0197

Where # represents the number of colours in the sample and the algorithms are denoted as follows: A = HSI method; B = Lim/Lee; C = Khotanzad; D = Goldberg; E = Wu; F = New 1; and G = New 2. The covariance and correlation statistics are the product of two series; colour versus specific algorithm.

Sample Type	#	A	B	C	D	E	F	G
Mean	8.19	0.1967	0.0291	0.0771	0.0762	0.0636	0.0529	0.0209
Standard Dev.		0.0800	0.0071	0.0136	0.0160	0.0228	0.0162	0.0050
Covariance		0.0569	-0.0126	-0.0206	-0.0237	-0.0420	-0.0210	-0.0080
Correlation		0.2437	-0.6053	-0.5198	-0.5078	-0.6330	-0.4380	-0.5310

1.5.3 Images used for Qualitative Evaluation

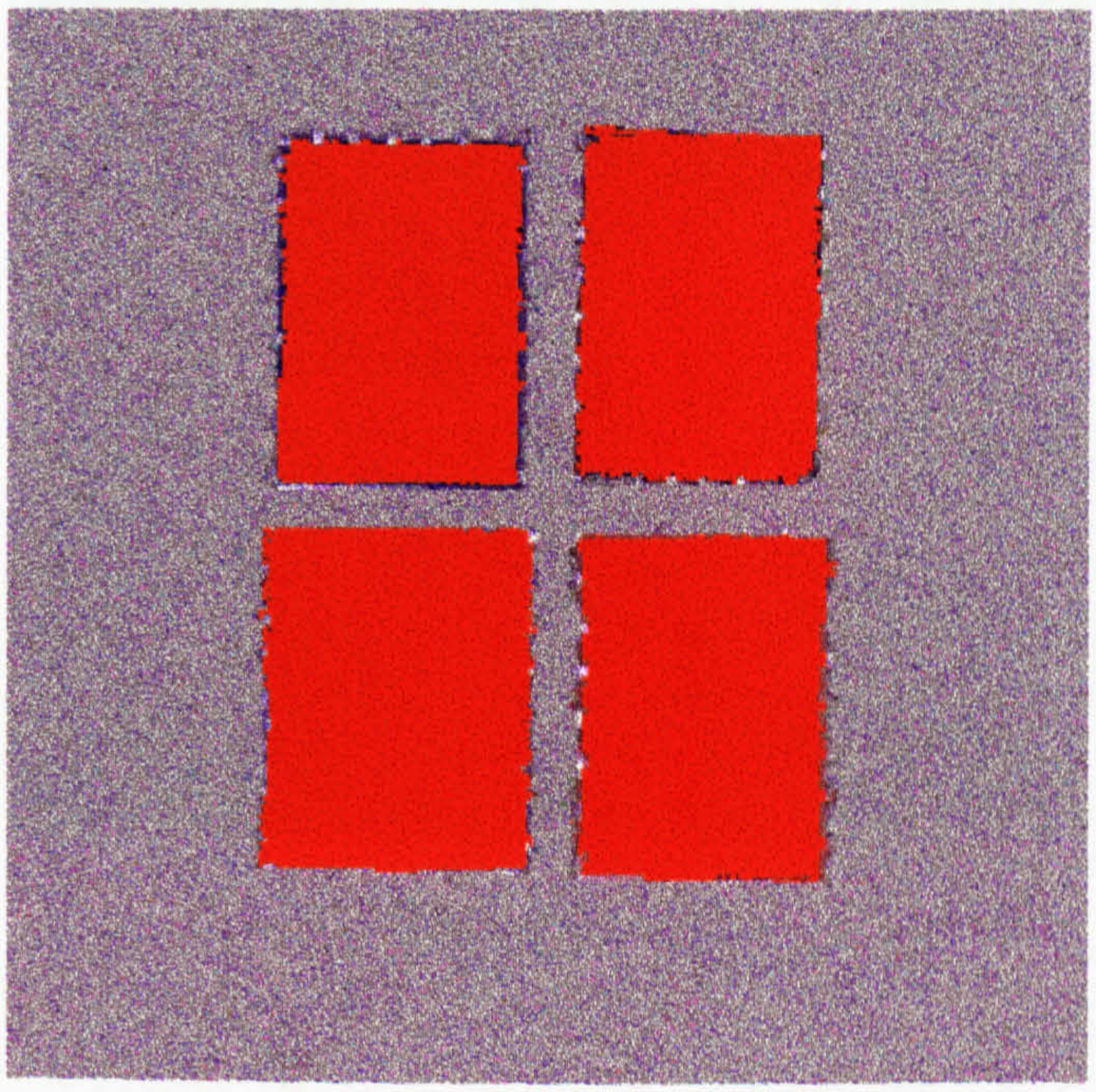

Test Image - Q1

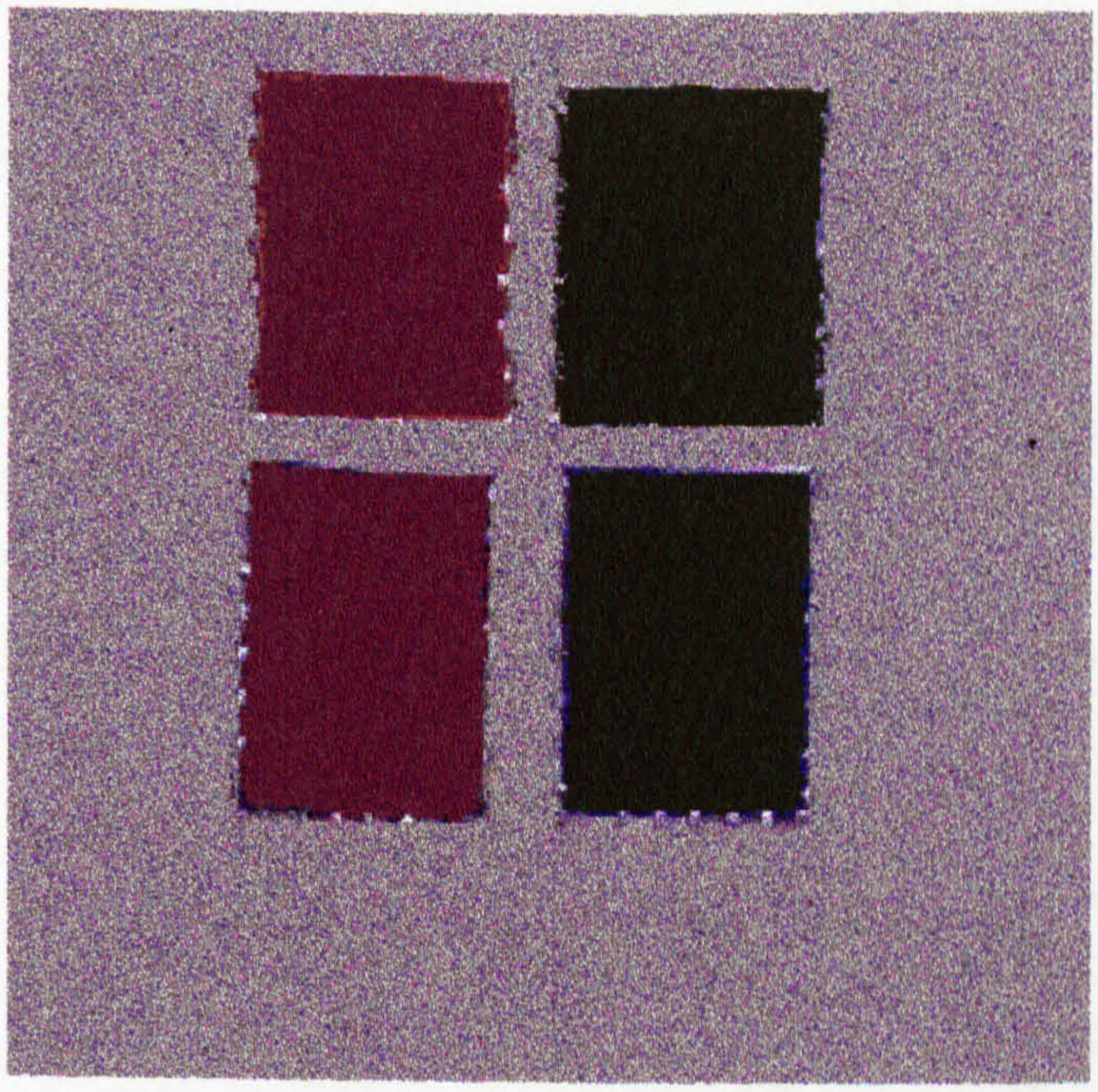

Test Image - Q2

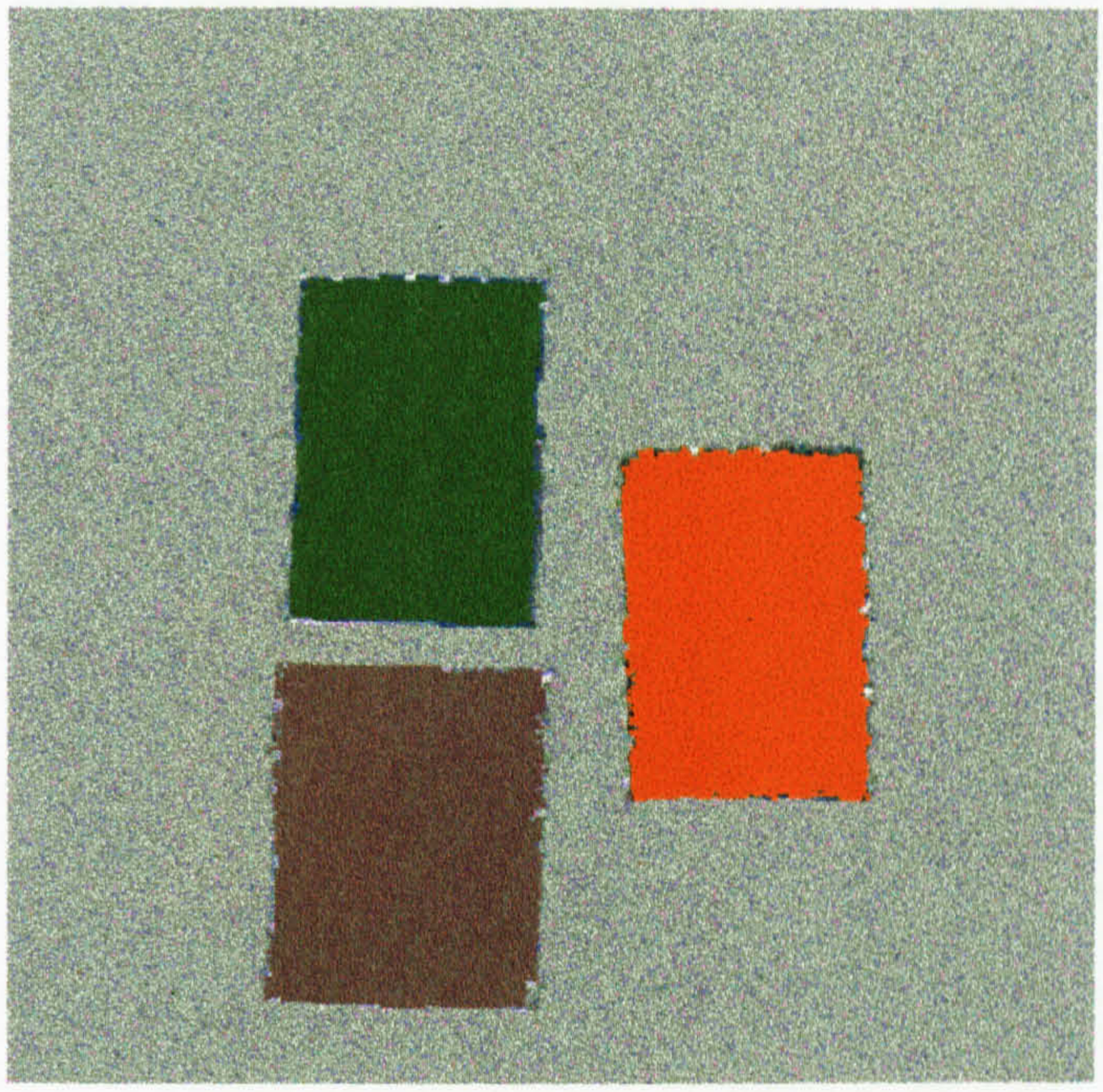

Test Image - Q3

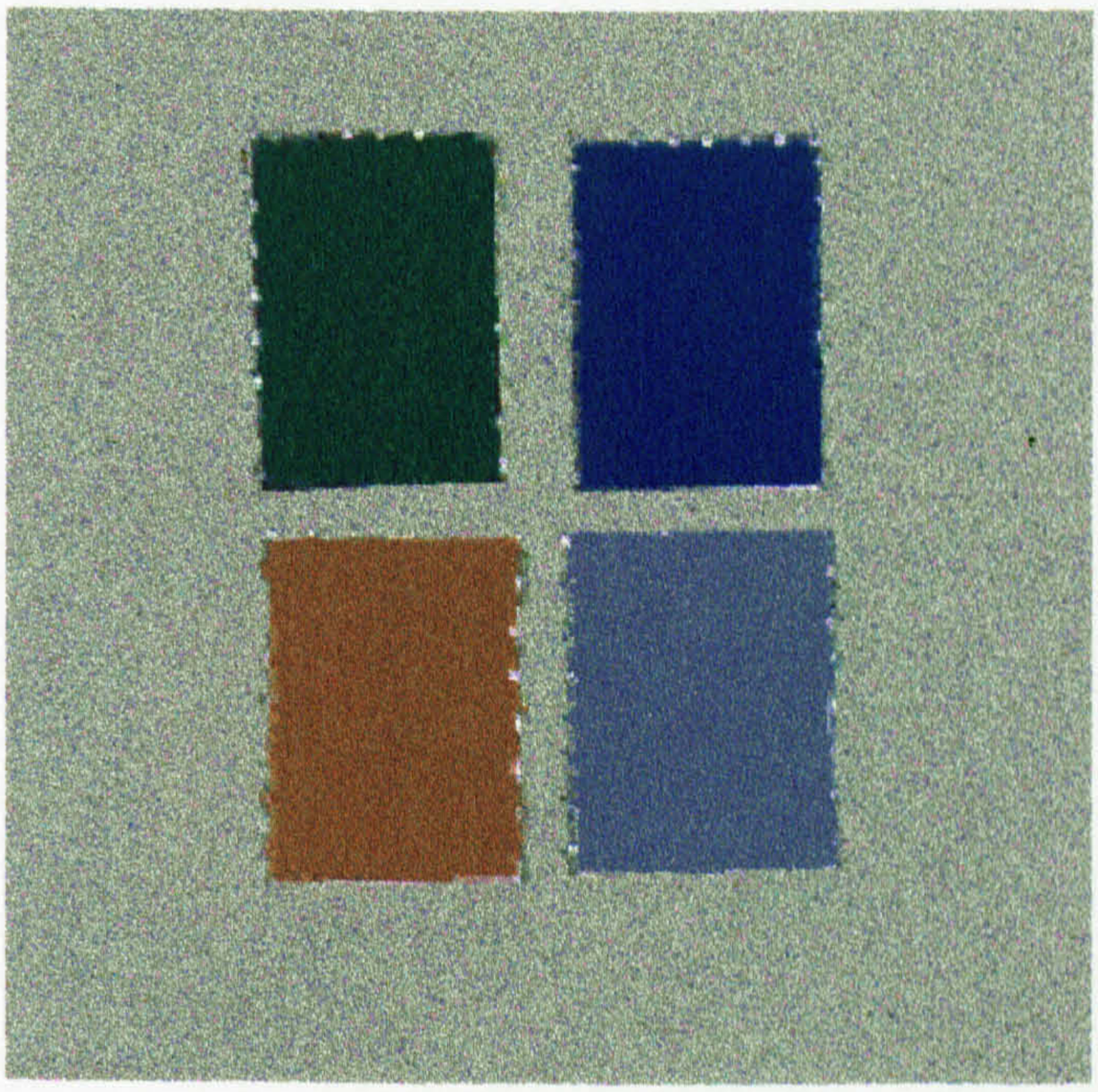

Test Image - Q4

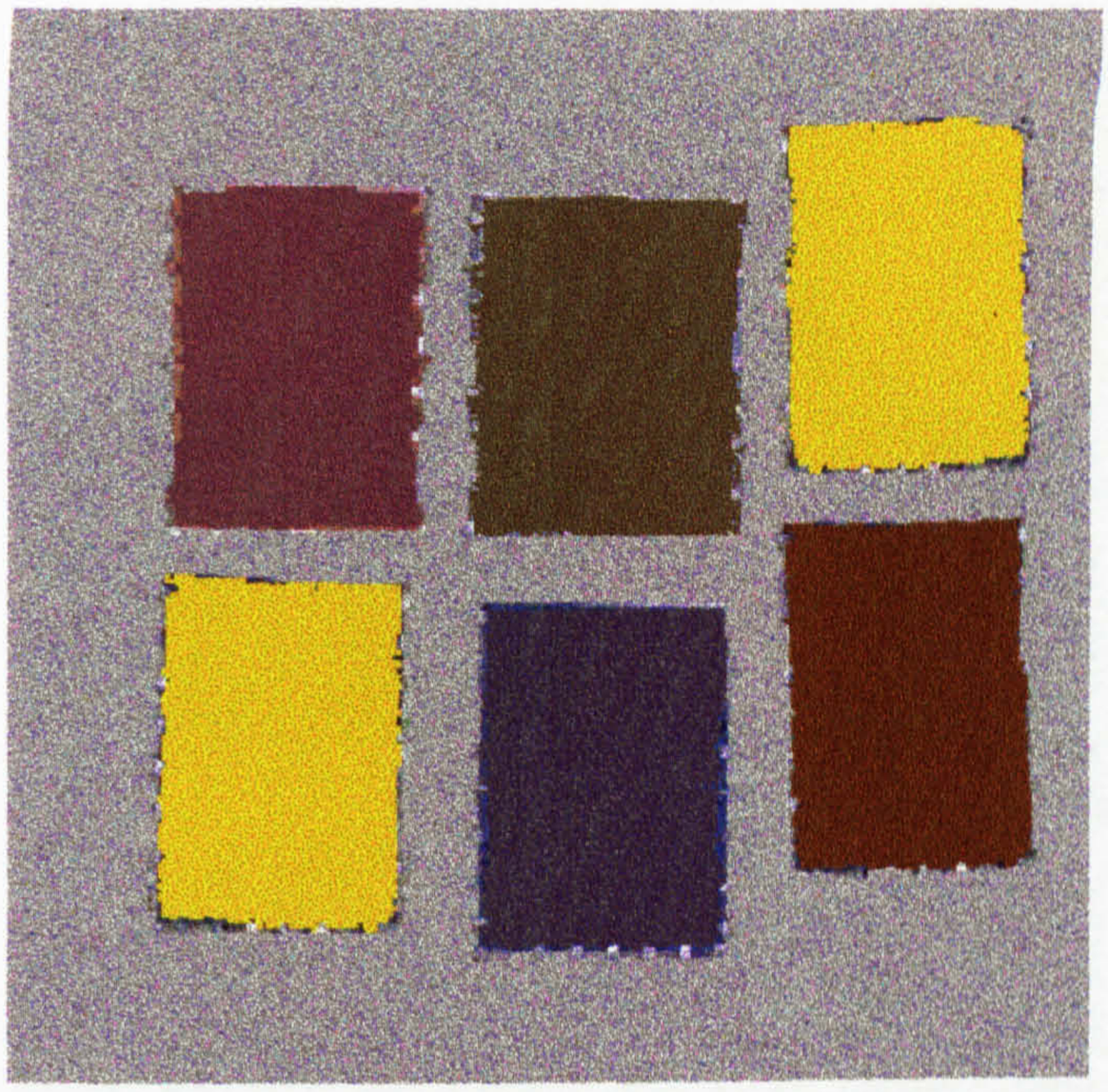

Test Image - Q5

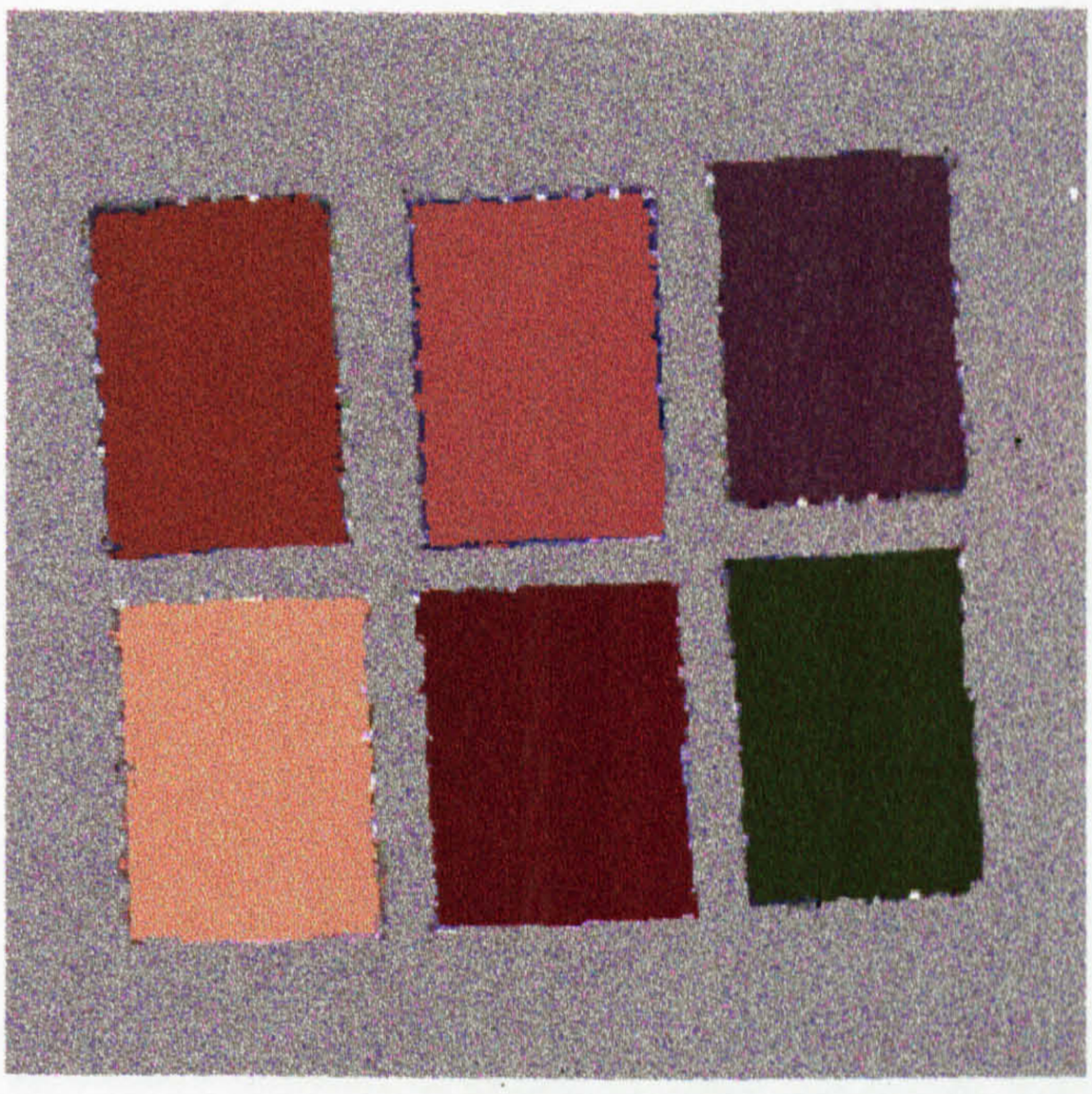

Test Image - Q6

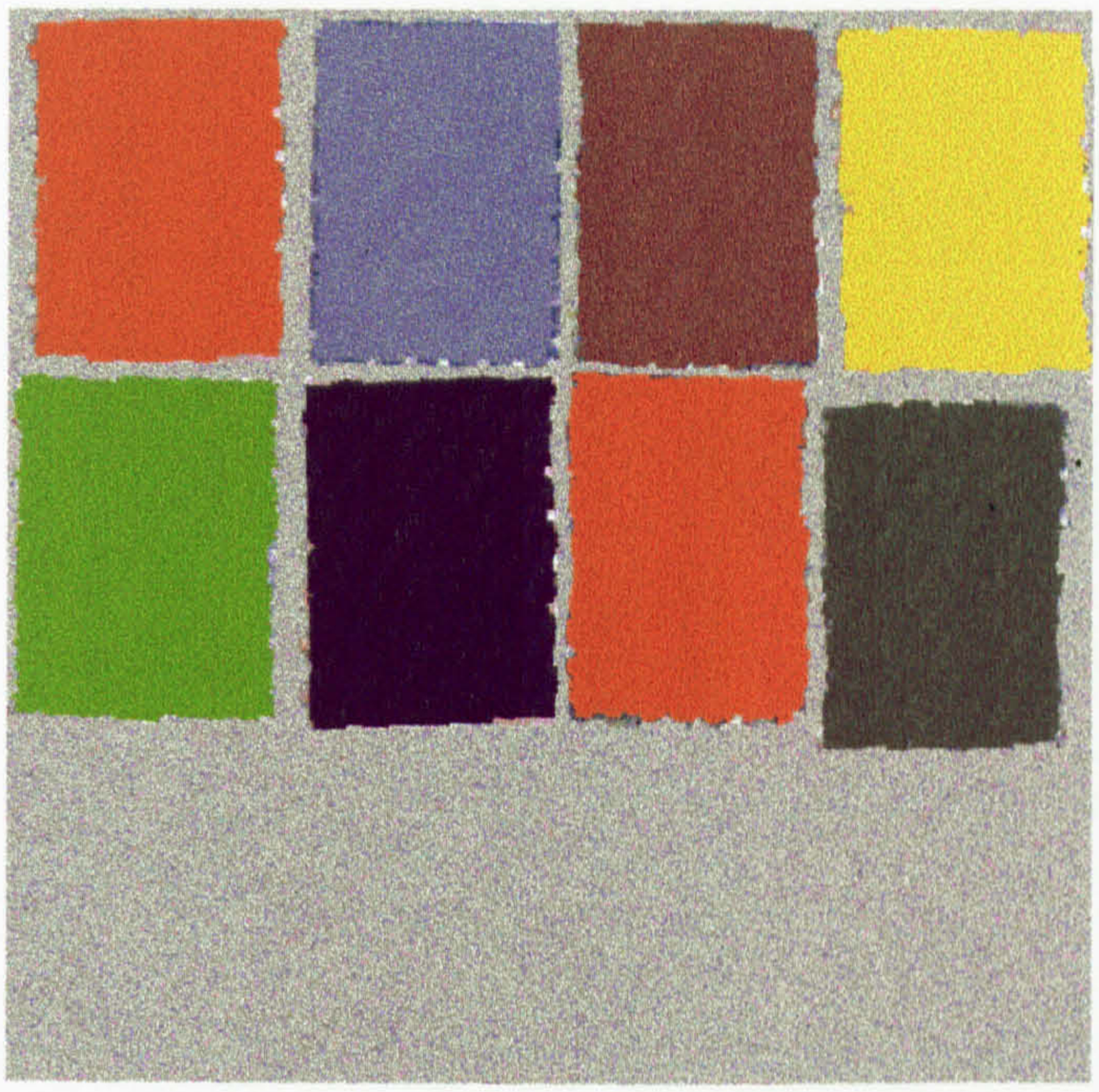

Test Image - Q7

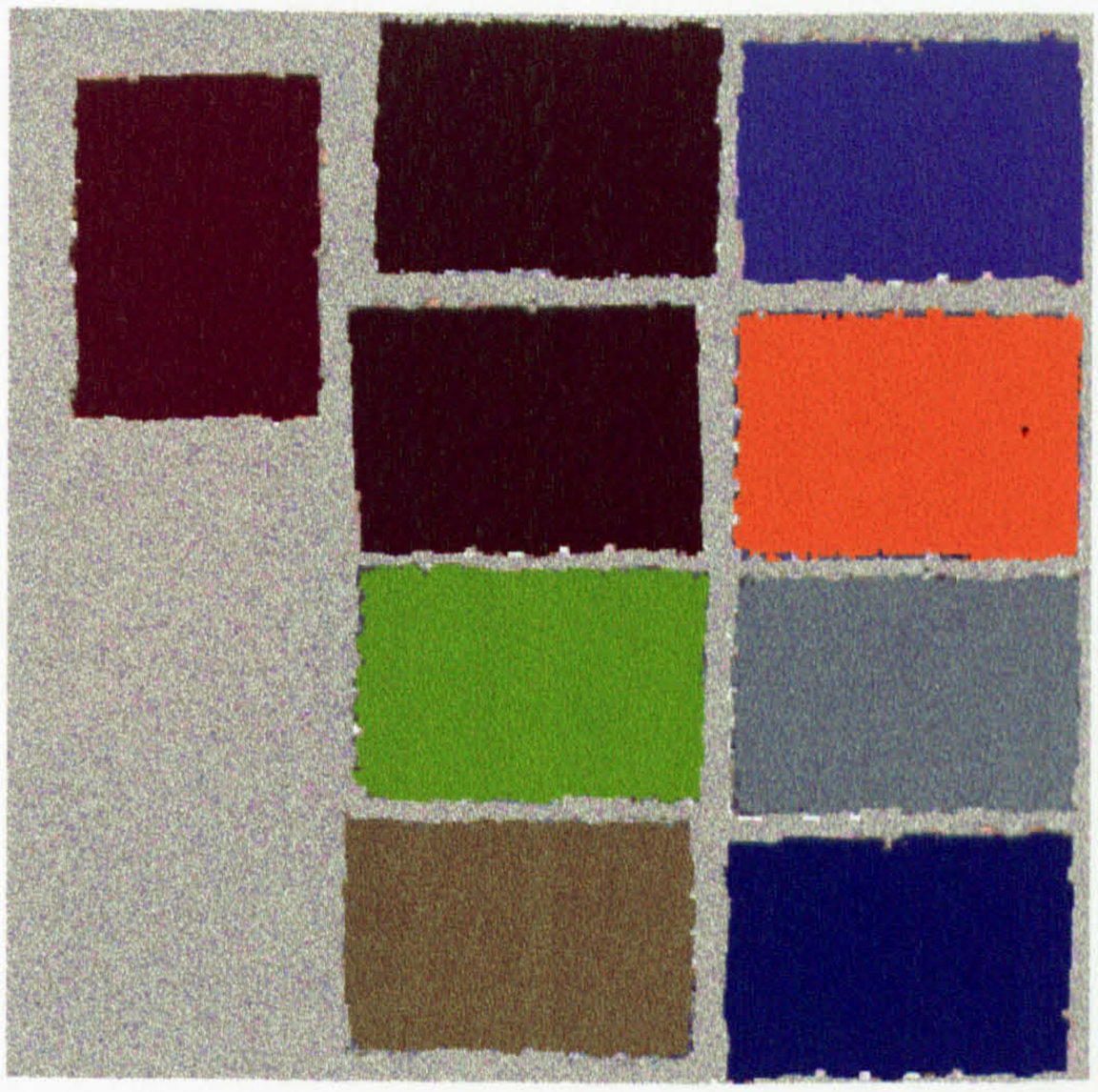

Test Image - Q8

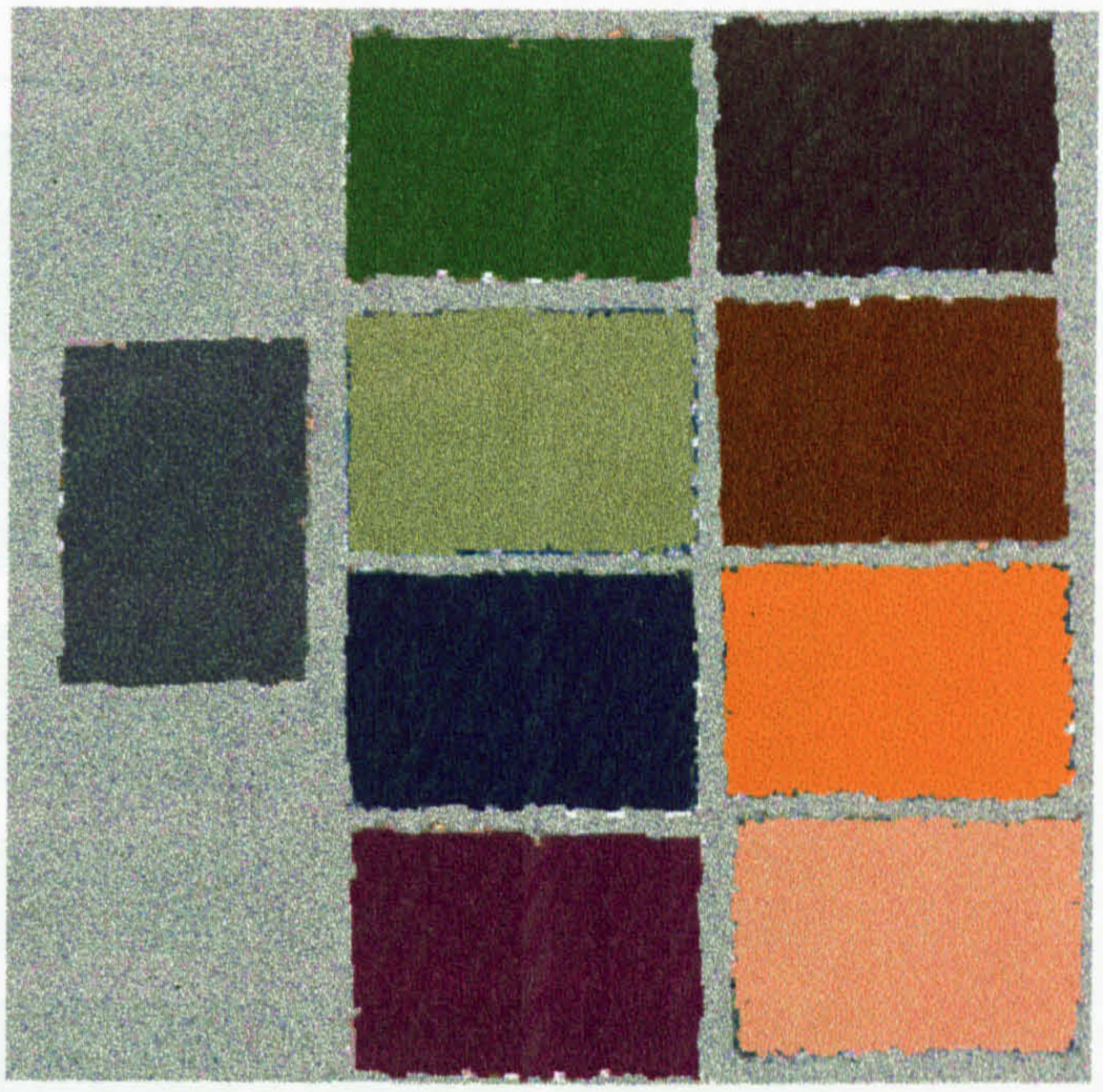

Test Image - Q9

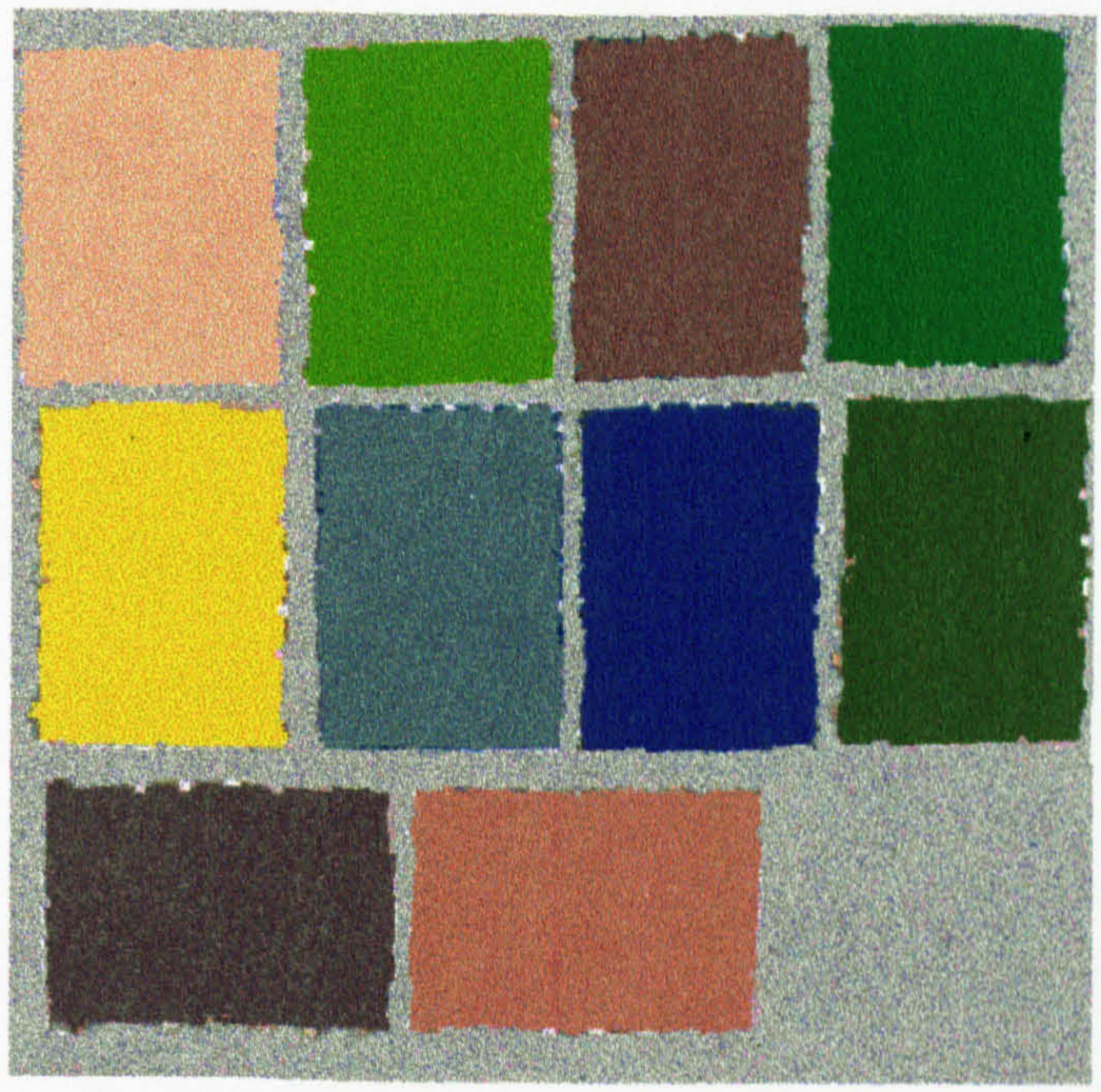

Test Image - Q10

1.5.4 Qualitative Test Results

	Background	1
Dulux Code	2500-N	0090-Y60R
Red	175	248
Green	175	72
Blue	175	31
Red	0.68359375	0.96875
Green	0.68359375	0.28125
Blue	0.68359375	0.12109375
X	0.649725781	0.521981316
Y	0.683599902	0.415905527
Z	0.74426543	0.167319395
u'	0.197838012	0.287493125
v'	0.468343126	0.515406292
L*	86.18613817	70.58770322
u*	3.120738063	84.82706062
v*	7.117165736	49.01611308

	Background	1	2
Dulux Code	2500-N	3050-G20Y	4030-R30B
Red	175	71	123
Green	175	104	78
Blue	175	63	105
Red	0.68359375	0.27734375	0.48046875
Green	0.68359375	0.40625	0.3046875
Blue	0.68359375	0.24609375	0.41015625
X	0.649725781	0.304059109	0.381122555
Y	0.683599902	0.367280719	0.349685391
Z	0.74426543	0.287629246	0.435347543
u'	0.197838012	0.182176112	0.219906539
v'	0.468343126	0.49512409	0.453976633
L*	86.18613817	67.07251633	65.72416376
u*	3.120738063	-11.22763257	21.23548604
v*	7.117165736	28.89024822	-6.84749782

	Background	1	2	3
Dulux Code	2500-N	3050-G20Y	4030-R30B	0090-Y60R
Red	175	71	123	248
Green	175	104	78	72
Blue	175	63	105	31
`Red	0.68359375	0.27734375	0.48046875	0.96875
`Green	0.68359375	0.40625	0.3046875	0.28125
`Blue	0.68359375	0.24609375	0.41015625	0.12109375
X	0.649725781	0.304059109	0.381122555	0.521981316
Y	0.683599902	0.367280719	0.349685391	0.415905527
Z	0.74426543	0.287629246	0.435347543	0.167319395
u'	0.197838012	0.182176112	0.219906539	0.287493125
v'	0.468343126	0.49512409	0.453976633	0.515406292
L*	86.18613817	67.07251633	65.72416376	70.58770322
u*	3.120738063	-11.22763257	21.23548604	84.82706062
v*	7.117165736	28.89024822	-6.84749782	49.01611308

	Background	1	2	3	4
Dulux Code	2500-N	3030-Y90R	2020-R90B	2060-R90B	3060-B60G
Red	175	148	124	58	45
Green	175	89	134	68	96
Blue	175	100	182	174	102
Red	0.68359375	0.578125	0.484375	0.2265625	0.17578125
Green	0.68359375	0.34765625	0.5234375	0.265625	0.375
Blue	0.68359375	0.390625	0.7109375	0.6796875	0.3984375
X	0.649725781	0.433242047	0.51522218	0.311059828	0.278481293
Y	0.683599902	0.39977441	0.528666438	0.287202406	0.334326785
Z	0.74426543	0.423798082	0.747307	0.681898414	0.426702
u'	0.197838012	0.225024202	0.192838193	0.186688417	0.169457218
v'	0.468343126	0.4671928	0.445207797	0.387832356	0.45773881
L*	86.18613817	69.4534602	77.79619825	60.53392985	64.50973181
u*	3.120738063	27.0611343	-2.239625512	-6.582184543	-21.4650354
v*	7.117165736	4.696774265	-16.97359552	-58.35840124	-3.565910451

	Background	1	2	3	4
Dulux Code	2500-N	0050-Y	4050-Y40R	4020-B10G	4030-R30B
Red	175	238	107	89	123
Green	175	232	65	89	78
Blue	175	54	32	114	105
Red	0.68359375	0.9296875	0.41796875	0.34765625	0.48046875
Green	0.68359375	0.90625	0.25390625	0.34765625	0.3046875
Blue	0.68359375	0.2109375	0.125	0.4453125	0.41015625
X	0.649725781	0.74556725	0.285737137	0.348051402	0.381122555
Y	0.683599902	0.861062625	0.279496836	0.354707133	0.349685391
Z	0.74426543	0.326431742	0.15712323	0.471307738	0.435347543
u'	0.197838012	0.203695742	0.230919252	0.196567535	0.219906539
v'	0.468343126	0.529312787	0.508221306	0.450734544	0.453976633
L*	86.18613817	94.35776646	59.84325342	66.11351247	65.72416376
u*	3.120738063	10.60201692	27.90283832	1.301978535	21.23548604
v*	7.117165736	82.58046392	35.96551675	-9.674558782	-6.84749782

	5
Dulux Code	4010-G10Y
Red	104
Green	102
Blue	73
Red	0.40625
Green	0.3984375
Blue	0.28515625
X	0.361481059
Y	0.391927184
Z	0.326308566
u'	0.20028553
v'	0.48859828
L*	68.8906355
u*	4.686424152
v*	23.82899607

	Background	1	2	3	4
Dulux Code	2500-N	1010-Y30R	2040-R10B	2060-R10B	3060-R10B
Red	175	228	184	151	104
Green	175	198	112	71	32
Blue	175	171	132	89	60
`Red	0.68359375	0.890625	0.71875	0.58984375	0.40625
`Green	0.68359375	0.7734375	0.4375	0.27734375	0.125
`Blue	0.68359375	0.66796875	0.515625	0.34765625	0.234375
X	0.649725781	0.76442366	0.545922453	0.405180586	0.254543172
Y	0.683599902	0.79075527	0.502955859	0.348880316	0.192708328
Z	0.74426543	0.744129621	0.556004047	0.374813828	0.245463016
u`	0.197838012	0.205792536	0.223778319	0.239651611	0.262310369
v`	0.468343126	0.478983014	0.463873369	0.464291476	0.446824532
L*	86.18613817	91.26845384	76.25033386	65.66139822	51.00257349
u*	3.120738063	12.74272769	28.47441131	38.06956391	44.59409622
v*	7.117165736	20.160978	1.866011302	1.96377269	-10.05580558
	5	6			
Dulux Code	5020-R70B	3050-G20Y			
Red	99	71			
Green	80	104			
Blue	105	63			
`Red	0.38671875	0.27734375			
`Green	0.3125	0.40625			
`Blue	0.41015625	0.24609375			
X	0.34524868	0.304059109			
Y	0.335334742	0.367280719			
Z	0.434466176	0.287629246			
u`	0.206776957	0.182176112			
v`	0.451888389	0.49512409			
L*	64.59055985	67.07251633			
u*	9.8446068	-11.22763257			
v*	-8.48284383	28.89024822			

	Background	1	2	3	4
Dulux Code	2500-N	0080-Y80R	2020-R90B	0050-Y	4040-R10B
Red	175	213	124	238	104
Green	175	51	134	232	53
Blue	175	41	182	54	64
Red	0.68359375	0.83203125	0.484375	0.9296875	0.40625
Green	0.68359375	0.19921875	0.5234375	0.90625	0.20703125
Blue	0.68359375	0.16015625	0.7109375	0.2109375	0.25
X	0.649725781	0.443306297	0.51522218	0.74556725	0.286695016
Y	0.683599902	0.330982309	0.528666438	0.861062625	0.252502176
Z	0.74426543	0.192016766	0.747307	0.326431742	0.270087863
u'	0.197838012	0.296323221	0.192838193	0.203695742	0.234779838
v'	0.468343126	0.497793343	0.445207797	0.529312787	0.465252054
L*	86.18613817	64.24036881	77.79619825	94.35776646	57.31840875
u*	3.120738063	84.57353746	-2.239625512	10.60201692	29.602265
v*	7.117165736	29.89951296	-16.97359552	82.58046392	2.430018082
	5	6	7		
Dulux Code	0080-G30Y	7020-R90B	5020-G10Y		
Red	116	23	56		
Green	188	23	80		
Blue	34	49	68		
Red	0.453125	0.08984375	0.21875		
Green	0.734375	0.08984375	0.3125		
Blue	0.1328125	0.19140625	0.265625		
X	0.473453008	0.103716742	0.249892703		
Y	0.631153727	0.097174223	0.289181984		
Z	0.222495102	0.194325172	0.293881172		
u'	0.178522665	0.193473808	0.182761419		
v'	0.535468776	0.407856047	0.475866024		
L*	83.50304536	37.33042127	60.70936725		
u*	-17.9439886	-0.76622107	-9.700533147		
v*	79.76314907	-26.27139671	10.9505546		

	Background	1	2	3	4
Dulux Code	2500-N	8502-R	8502-G	0080-G30Y	4010-G10Y
Red	175	30	21	116	104
Green	175	21	29	188	102
Blue	175	21	21	34	73
Red	0.68359375	0.1171875	0.08203125	0.453125	0.40625
Green	0.68359375	0.08203125	0.11328125	0.734375	0.3984375
Blue	0.68359375	0.08203125	0.08203125	0.1328125	0.28515625
X	0.649725781	0.092467395	0.089141469	0.473453008	0.361481059
Y	0.683599902	0.089508703	0.10438102	0.631153727	0.391927184
Z	0.74426543	0.089991563	0.093036633	0.222495102	0.326308566
u'	0.197838012	0.216923063	0.184370228	0.178522665	0.20028553
v'	0.468343126	0.472459832	0.485752518	0.535468776	0.48859828
L*	86.18613817	35.88953085	38.6175021	83.50304536	68.8906355
u*	3.120738063	10.20393003	-5.362886236	-17.94398859	4.686424152
v*	7.117165736	4.884428474	11.92898939	79.76314907	23.82899607
	5	6	7	8	
Dulux Code	0090-Y60R	2060-R90B	3020-B70G	2070-B	
Red	248	58	108	13	
Green	72	68	136	58	
Blue	31	174	149	129	
Red	0.96875	0.2265625	0.421875	0.05078125	
Green	0.28125	0.265625	0.53125	0.2265625	
Blue	0.12109375	0.6796875	0.58203125	0.50390625	
X	0.521981316	0.311059828	0.468979809	0.192875375	
Y	0.415905527	0.287202406	0.511658723	0.209196586	
Z	0.167319395	0.681898414	0.624539621	0.506811793	
u'	0.287493125	0.186688417	0.187264594	0.159031174	
v'	0.515406292	0.387832356	0.459689336	0.388099061	
L*	70.58770322	60.53392985	76.77937658	52.86145372	
u*	84.82706062	-6.582184543	-7.773539977	-24.75394138	
v*	49.01611308	-58.35840124	-2.297258931	-50.77838646	

	Background	1	2	3	4
Dulux Code	2500-N	4020-B10G	3050-G20Y	3010-G70Y	4040-R90B
Red	175	89	71	152	51
Green	175	89	104	152	57
Blue	175	114	63	121	101
`Red	0.68359375	0.34765625	0.27734375	0.59375	0.19921875
`Green	0.68359375	0.34765625	0.40625	0.59375	0.22265625
`Blue	0.68359375	0.4453125	0.24609375	0.47265625	0.39453125
X	0.649725781	0.348051402	0.304059109	0.542485152	0.232968305
Y	0.683599902	0.354707133	0.367280719	0.585016129	0.230077824
Z	0.74426543	0.471307738	0.287629246	0.531381137	0.405285008
u'	0.197838012	0.196567535	0.182176112	0.198860554	0.190178569
v'	0.468343126	0.450734544	0.49512409	0.482515364	0.422592725
L*	86.18613817	66.11351247	67.07251633	81.01687224	55.08035309
u*	3.120738063	1.301978535	-11.22763257	4.010523109	-3.490082832
v*	7.117165736	-9.674558782	28.89024822	21.61676795	-28.21084615
	5	6	7	8	9
Dulux Code	3060-R30B	7020-R30B	3070-Y70R	1060-Y60R	1020-Y60R
Red	101	64	108	247	233
Green	9	44	33	132	174
Blue	94	66	21	74	159
Red	0.39453125	0.25	0.421875	0.96484375	0.91015625
`Green	0.03515625	0.171875	0.12890625	0.515625	0.6796875
Blue	0.3671875	0.2578125	0.08203125	0.2890625	0.62109375
X	0.24154584	0.211087617	0.23489823	0.63448341	0.73049893
Y	0.13554757	0.194693492	0.187830445	0.594814652	0.724478984
Z	0.360729723	0.270300195	0.101469563	0.354788172	0.688791004
u'	0.287815956	0.214172201	0.279910364	0.238952779	0.213845403
v'	0.36340388	0.444461651	0.503602342	0.50402954	0.477187046
L*	43.58750961	51.23186122	50.43240655	81.55552609	88.18373428
u*	52.56316062	12.73387036	55.63450214	46.54384002	21.54375941
v*	-55.8631116	-11.67472476	27.28135048	44.57029004	17.42069443

	Background	1	2	3	4	5
Dulux Code	2500-N	1010-Y30R	0080-G30Y	4030-R30B	1070-G10Y	0050-Y
Red	175	228	116	123	47	238
Green	175	198	188	78	141	232
Blue	175	171	34	105	67	54
'Red	0.68359375	0.890625	0.453125	0.48046875	0.18359375	0.9296875
'Green	0.68359375	0.7734375	0.734375	0.3046875	0.55078125	0.90625
'Blue	0.68359375	0.66796875	0.1328125	0.41015625	0.26171875	0.2109375
X(D65)	0.649725781	0.76442366	0.473453008	0.381122555	0.319892234	0.74556725
Y(D65)	0.683599902	0.79075527	0.631153727	0.349685391	0.451834723	0.861062625
Z(D65)	0.74426543	0.744129621	0.222495102	0.435347543	0.317891094	0.326431742
u'	0.197838012	0.205792536	0.178522665	0.219906539	0.158931215	0.203695742
v'	0.468343126	0.478983014	0.535468776	0.453976633	0.505088671	0.529312787
L*	86.18613817	91.26845384	83.50304536	65.72416376	73.01253921	94.35776646
u*	3.120738063	12.74272769	-17.94398859	21.23548604	-34.28516118	10.60201692
v*	7.117165736	20.160978	79.76314907	-6.84749782	40.90681498	82.58046392
	6	7	8	9	10	
Dulux Code	3020-B70G	2060-R90B	3050-G20Y	5020-R70B	2040-R10B	
Red	108	58	71	99	184	
Green	136	68	104	80	112	
Blue	149	174	63	105	132	
'Red	0.421875	0.2265625	0.27734375	0.38671875	0.71875	
'Green	0.53125	0.265625	0.40625	0.3125	0.4375	
'Blue	0.58203125	0.6796875	0.24609375	0.41015625	0.515625	
X(D65)	0.468979809	0.311059828	0.304059109	0.34524868	0.545922453	
Y(D65)	0.511658723	0.287202406	0.367280719	0.335334742	0.502955859	
Z(D65)	0.624539621	0.681898414	0.287629246	0.434466176	0.556004047	
u'	0.187264594	0.186688417	0.182176112	0.206776957	0.223778319	
v'	0.459689336	0.387832356	0.49512409	0.451888389	0.463873369	
L*	76.77937658	60.53392985	67.07251633	64.59055985	76.25033386	
u*	-7.773539977	-6.582184543	-11.22763257	9.8446068	28.47441131	
v*	-2.297258931	-58.35840124	28.89024822	-8.482843834	1.866011302	

1.5.5 Measured ΔE Colour Separation of Tested Dulux Tiles

	2500-N	0050-Y	0080-Y80R	0080-G30Y	0090-Y60R	1010-Y30R
L*	86.19	94.36	64.24	83.50	70.59	91.27
u*	3.12	10.60	84.57	-17.94	84.83	12.74
v*	7.12	82.58	29.90	79.76	49.02	20.16
*E						
	2500-N	0050-Y	0080-Y80R	0080-G30Y	0090-Y60R	1010-Y30R
2500-N		76.27	87.38	75.69	93.14	16.99
0050-Y	76.27		95.68	30.67	84.86	62.53
0080-Y80R	87.38	95.68		115.62	20.14	77.36
0080-G30Y	75.69	30.67	115.62		108.05	67.49
0090-Y60R	93.14	84.86	20.14	108.05		80.35
1010-Y30R	16.99	62.53	77.36	67.49	80.35	
1020-Y60R	21.20	66.36	68.57	73.94	72.89	9.72
1060-Y60R	57.53	53.86	44.29	73.49	40.07	42.81
1070-G10Y	52.10	64.86	119.69	43.44	119.41	54.55
2020-R90B	26.07	101.74	99.59	98.17	109.49	42.25
2040-R10B	27.73	84.63	63.85	90.97	73.69	28.42
2060-R10B	40.86	89.87	54.27	97.51	66.52	40.35
2060-R90B	70.99	145.96	126.94	140.48	141.37	86.51
2070-B	72.38	144.07	136.35	134.26	149.27	88.96
3010-G70Y	15.42	62.75	82.71	62.20	85.97	13.54
3020-B70G	17.20	88.61	98.60	82.96	106.05	33.69
3030-Y90R	29.31	83.41	63.01	88.64	72.82	30.33
3050-G20Y	32.33	64.06	95.85	53.88	98.20	35.16
3060-R10B	57.03	107.78	58.05	114.17	74.11	59.57
3060-R30B	90.70	153.31	93.84	157.98	113.00	98.18
3060-B60G	34.47	96.65	111.19	85.54	118.74	49.49
3070-Y70R	66.65	83.76	32.17	96.24	41.60	59.65
4010-G10Y	24.10	64.31	80.25	62.08	84.02	24.07
4020-B10G	26.23	96.93	92.22	93.12	102.18	40.67
4030-R30B	30.69	94.50	73.24	96.71	84.78	38.13
4040-R10B	39.45	90.32	61.84	94.48	73.46	41.85
4040-R90B	47.53	118.39	105.91	112.58	118.34	62.55
4050-Y40R	46.26	60.53	57.16	67.68	59.38	38.30
5020-G10Y	28.78	81.70	96.22	72.96	102.38	39.02
5020-R70B	27.48	95.81	84.01	94.43	94.68	39.25
7020-R30B	40.83	103.67	84.02	101.70	96.21	51.15
7020-R90B	59.30	123.41	105.65	116.92	118.75	72.44
8502-R	50.84	97.24	83.43	93.09	93.38	57.50
8502-G	48.56	91.40	95.23	82.31	102.62	56.28

	1020-Y60R	1060-Y60R	1070-G10Y	2020-R90B	2040-R10B	2060-R10B
L*	88.18	81.56	73.01	77.80	76.25	65.66
a*	21.54	46.54	-34.29	-2.24	28.47	38.07
b*	17.42	44.57	40.91	-16.97	1.87	1.96
ΔE						
	1020-Y60R	1060-Y60R	1070-G10Y	2020-R90B	2040-R10B	2060-R10B
2500-N	21.20	57.53	52.10	26.07	27.73	40.86
0050-Y	66.36	53.86	64.86	101.74	84.63	89.87
0080-Y80R	68.57	44.29	119.69	99.59	63.85	54.27
0080-G30Y	73.94	73.49	43.44	98.17	90.97	97.51
0090-Y60R	72.89	40.07	119.41	109.49	73.69	66.52
1010-Y30R	9.72	42.81	54.55	42.25	28.42	40.35
1020-Y60R		37.50	62.44	43.09	20.79	31.93
1060-Y60R	37.50		81.36	78.62	46.67	46.26
1070-G10Y	62.44	81.36		66.33	73.98	82.50
2020-R90B	43.09	78.62	66.33		36.06	46.16
2040-R10B	20.79	46.67	73.98	36.06		14.29
2060-R10B	31.93	46.26	82.50	46.16	14.29	
2060-R90B	85.43	117.72	103.81	45.05	71.43	75.23
2070-B	89.68	122.47	94.36	47.66	78.43	83.02
3010-G70Y	19.40	48.33	43.62	39.23	31.80	42.21
3020-B70G	37.13	71.90	50.83	15.72	36.49	47.36
3030-Y90R	23.31	46.00	71.32	37.39	7.50	11.96
3050-G20Y	40.63	61.59	26.67	47.95	48.90	56.19
3060-R10B	51.66	62.62	96.45	54.40	32.24	20.05
3060-R30B	91.22	107.54	133.31	75.41	70.57	63.57
3060-B60G	53.39	85.05	47.06	26.94	51.59	59.80
3070-Y70R	51.81	36.75	93.71	77.82	45.28	34.37
4010-G10Y	26.41	48.40	42.75	42.33	33.20	40.04
4020-B10G	40.39	72.30	62.23	14.22	31.21	38.57
4030-R30B	33.07	59.46	73.59	28.27	15.46	19.00
4040-R10B	35.25	51.48	76.21	42.54	18.97	11.90
4040-R90B	61.68	92.20	77.76	25.37	48.73	52.44
4050-Y40R	34.46	29.88	63.76	63.51	37.85	35.96
5020-G10Y	42.11	68.76	40.66	33.58	42.21	48.86
5020-R70B	36.94	66.70	66.77	19.81	24.29	30.12
7020-R30B	47.85	72.29	73.82	30.95	32.51	32.19
7020-R90B	70.66	95.98	83.12	41.55	56.23	55.75
8502-R	54.96	70.58	68.23	48.88	44.41	40.88
8502-G	56.67	74.86	53.47	48.79	51.60	52.13

	2060-R90B	2070-B	3010-G70Y	3020-B70G	3030-Y90R	3050-G20Y
L*	60.53	52.86	81.02	76.78	69.45	67.07
u*	-6.58	-24.75	4.01	-7.77	27.06	-11.23
v*	-58.36	-50.78	21.62	-2.30	4.70	28.89
ΔE						
	2060-R90B	2070-B	3010-G70Y	3020-B70G	3030-Y90R	3050-G20Y
2500-N	70.99	72.38	15.42	17.20	29.31	32.33
0050-Y	145.96	144.07	62.75	88.61	83.41	64.06
0080-Y80R	126.94	136.35	82.71	98.60	63.01	95.85
0080-G30Y	140.48	134.26	62.20	82.96	88.64	53.88
0090-Y60R	141.37	149.27	85.97	106.05	72.82	98.20
1010-Y30R	86.51	88.96	13.54	33.69	30.33	35.16
1020-Y60R	85.43	89.68	19.40	37.13	23.31	40.63
1060-Y60R	117.72	122.47	48.33	71.90	46.00	61.59
1070-G10Y	103.81	94.36	43.62	50.83	71.32	26.67
2020-R90B	45.05	47.66	39.23	15.72	37.39	47.95
2040-R10B	71.43	78.43	31.80	36.49	7.50	48.90
2060-R10B	75.23	83.02	42.21	47.36	11.96	56.19
2060-R90B		21.13	83.23	58.38	72.02	87.62
2070-B	21.13		82.83	56.66	77.70	82.05
3010-G70Y	83.23	82.83		26.99	30.84	21.90
3020-B70G	58.38	56.66	26.99		36.28	32.85
3030-Y90R	72.02	77.70	30.84	36.28		45.35
3050-G20Y	87.62	82.05	21.90	32.85	45.35	
3060-R10B	71.01	80.44	59.59	58.88	29.42	69.94
3060-R30B	61.58	78.04	98.80	87.24	70.62	108.65
3060-B60G	56.92	48.74	39.44	18.43	49.47	34.13
3070-Y70R	106.33	112.08	60.27	74.76	41.09	68.92
4010-G10Y	83.38	81.79	12.34	30.00	29.44	16.80
4020-B10G	49.63	50.44	34.76	15.83	29.69	40.56
4030-R30B	58.77	64.89	36.62	31.38	13.46	48.30
4040-R10B	70.82	76.19	39.81	42.40	12.60	49.62
4040-R90B	30.79	31.09	56.67	34.07	47.15	58.86
4050-Y40R	100.43	101.72	35.00	54.99	32.72	40.42
5020-G10Y	69.38	64.02	26.72	20.92	38.30	19.10
5020-R70B	52.67	55.89	34.78	22.30	22.22	42.98
7020-R30B	51.37	54.19	45.51	34.08	28.38	49.71
7020-R90B	40.02	37.65	65.00	46.69	52.59	63.54
8502-R	69.92	67.89	48.53	45.24	37.56	44.81
8502-G	73.64	67.16	44.49	40.80	45.33	33.64

	3060-R10B	3060-R30B	3060-B60G	3070-Y70R	4010-G10Y	4020-B10G
L*	51.00	43.59	64.51	50.43	68.89	66.11
u*	44.59	52.56	-21.47	55.63	4.69	1.30
v*	-10.06	-55.86	-3.57	27.28	23.83	-9.67
ΔE						

	3060-R10B	3060-R30B	3060-B60G	3070-Y70R	4010-G10Y	4020-B10G
2500-N	57.03	90.70	34.47	66.65	24.10	26.23
0050-Y	107.78	153.31	96.65	83.76	64.31	96.93
0080-Y80R	58.05	93.84	111.19	32.17	80.25	92.22
0080-G30Y	114.17	157.98	85.54	96.24	62.08	93.12
0090-Y60R	74.11	113.00	118.74	41.60	84.02	102.18
1010-Y30R	59.57	98.18	49.49	59.65	24.07	40.67
1020-Y60R	51.66	91.22	53.39	51.81	26.41	40.39
1060-Y60R	62.62	107.54	85.05	36.75	48.40	72.30
1070-G10Y	96.45	133.31	47.06	93.71	42.75	62.23
2020-R90B	54.40	75.41	26.94	77.82	42.33	14.22
2040-R10B	32.24	70.57	51.59	45.28	33.20	31.21
2060-R10B	20.05	63.57	59.80	34.37	40.04	38.57
2060-R90B	71.01	61.58	56.92	106.33	83.38	49.63
2070-B	80.44	78.04	48.74	112.08	81.79	50.44
3010-G70Y	59.59	98.80	39.44	60.27	12.34	34.76
3020-B70G	58.88	87.24	18.43	74.76	30.00	15.83
3030-Y90R	29.42	70.62	49.47	41.09	29.44	29.69
3050-G20Y	69.94	108.65	34.13	68.92	16.80	40.56
3060-R10B		47.08	67.74	38.94	55.32	45.86
3060-R30B	47.08		93.02	83.48	96.35	72.58
3060-B60G	67.74	93.02		84.23	38.13	23.63
3070-Y70R	38.94	83.48	84.23		54.30	67.55
4010-G10Y	55.32	96.35	38.13	54.30		33.79
4020-B10G	45.86	72.58	23.63	67.55	33.79	
4030-R30B	27.80	62.24	42.84	50.81	35.00	20.14
4040-R10B	20.51	64.14	51.92	36.64	34.82	32.01
4040-R90B	51.56	63.55	31.93	81.22	54.46	22.10
4050-Y40R	49.75	96.46	63.42	30.55	27.72	53.20
5020-G10Y	59.02	92.92	19.07	68.12	20.97	23.99
5020-R70B	37.34	67.16	31.69	59.80	33.00	8.76
7020-R30B	31.90	59.98	37.57	57.95	40.46	18.87
7020-R90B	50.07	61.31	41.02	78.87	59.46	33.29
8502-R	40.43	74.46	43.51	52.70	38.45	34.71
8502-G	55.97	89.31	34.20	64.00	34.04	35.60

	4030-R30B	4040-R10B	4040-R90B	4050-Y40R	5020-G10Y	5020-R70B
L*	65.72	57.32	55.08	59.84	60.71	64.59
a*	21.24	29.60	-3.49	27.90	-9.70	9.84
b*	-6.85	2.43	-28.21	35.97	10.95	-8.48
ΔE						

	4030-R30B	4040-R10B	4040-R90B	4050-Y40R	5020-G10Y	5020-R70B
2500-N	30.69	39.45	47.53	46.26	28.78	27.48
0050-Y	94.50	90.32	118.39	60.53	81.70	95.81
0080-Y80R	73.24	61.84	105.91	57.16	96.22	84.01
0080-G30Y	96.71	94.48	112.58	67.68	72.96	94.43
0090-Y60R	84.78	73.46	118.34	59.38	102.38	94.68
1010-Y30R	38.13	41.85	62.55	38.30	39.02	39.25
1020-Y60R	33.07	35.25	61.68	34.46	42.11	36.94
1060-Y60R	59.46	51.48	92.20	29.88	68.76	66.70
1070-G10Y	73.59	76.21	77.76	63.76	40.66	66.77
2020-R90B	28.27	42.54	25.37	63.51	33.58	19.81
2040-R10B	15.46	18.97	48.73	37.85	42.21	24.29
2060-R10B	19.00	11.90	52.44	35.96	48.86	30.12
2060-R90B	58.77	70.82	30.79	100.43	69.38	52.67
2070-B	64.89	76.19	31.09	101.72	64.02	55.89
3010-G70Y	36.62	39.81	56.67	35.00	26.72	34.78
3020-B70G	31.38	42.40	34.07	54.99	20.92	22.30
3030-Y90R	13.46	12.60	47.15	32.72	38.30	22.22
3050-G20Y	48.30	49.62	58.86	40.42	19.10	42.98
3060-R10B	27.80	20.51	51.56	49.75	59.02	37.34
3060-R30B	62.24	64.14	63.55	96.46	92.92	67.16
3060-B60G	42.84	51.92	31.93	63.42	19.07	31.69
3070-Y70R	50.81	36.64	81.22	30.55	68.12	59.80
4010-G10Y	35.00	34.82	54.46	27.72	20.97	33.00
4020-B10G	20.14	32.01	22.10	53.20	23.99	8.76
4030-R30B		15.06	34.37	43.73	36.04	11.56
4040-R10B	15.06		45.16	33.67	40.36	23.71
4040-R90B	34.37	45.16		71.60	40.05	25.64
4050-Y40R	43.73	33.67	71.60		45.17	48.21
5020-G10Y	36.04	40.36	40.05	45.17		27.83
5020-R70B	11.56	23.71	25.64	48.21	27.83	
7020-R30B	17.48	22.82	23.48	50.73	33.24	14.04
7020-R90B	40.84	46.32	18.06	72.13	44.85	34.24
8502-R	33.90	29.01	40.63	43.05	32.39	31.66
8502-G	42.37	40.77	43.43	46.20	22.53	36.37

	7020-R30B	7020-R90B	8502-R	8502-G
L*	51.23	37.33	35.89	38.62
u*	12.73	-0.77	10.20	-5.36
v*	-11.67	-26.27	4.88	11.93
ΔE				

	7020-R30B	7020-R90B	8502-R	8502-G
2500-N	40.83	59.30	50.84	48.56
0050-Y	103.67	123.41	97.24	91.40
0080-Y80R	84.02	105.65	83.43	95.23
0080-G30Y	101.70	116.92	93.09	82.31
0090-Y60R	96.21	118.75	93.38	102.62
1010-Y30R	51.15	72.44	57.50	56.28
1020-Y60R	47.85	70.66	54.96	56.67
1060-Y60R	72.29	95.98	70.58	74.86
1070-G10Y	73.82	83.12	68.23	53.47
2020-R90B	30.95	41.55	48.88	48.79
2040-R10B	32.51	56.23	44.41	51.60
2060-R10B	32.19	55.75	40.88	52.13
2060-R90B	51.37	40.02	69.92	73.64
2070-B	54.19	37.65	67.89	67.16
3010-G70Y	45.51	65.00	48.53	44.49
3020-B70G	34.08	46.69	45.24	40.80
3030-Y90R	28.38	52.59	37.56	45.33
3050-G20Y	49.71	63.54	44.81	33.64
3060-R10B	31.90	50.07	40.43	55.97
3060-R30B	59.98	61.31	74.46	89.31
3060-B60G	37.57	41.02	43.51	34.20
3070-Y70R	57.95	78.87	52.70	64.00
4010-G10Y	40.46	59.46	38.45	34.04
4020-B10G	18.87	33.29	34.71	35.60
4030-R30B	17.48	40.84	33.90	42.37
4040-R10B	22.82	46.32	29.01	40.77
4040-R90B	23.48	18.06	40.63	43.43
4050-Y40R	50.73	72.13	43.05	46.20
5020-G10Y	33.24	44.85	32.39	22.53
5020-R70B	14.04	34.24	31.66	36.37
7020-R30B		24.26	22.72	32.31
7020-R90B	24.26		33.06	38.50
8502-R	22.72	33.06		17.30
8502-G	32.31	38.50	17.30	

1.5.6 Statistical Results of Qualitative Testing

Sample Type	Colours	HSI Segmentation	Lim/Lee	Khotanzad	Goldberg
Q1	2 (Q1)	99.18	99.97	99.73	99.84
Q2	3 (Q2)	98.74	99.99	99.54	99.43
Q3	4 (Q3)	98.72	99.84	98.97	99.14
Q4	5 (Q4)	95.56	99.81	98.39	98.27
Q5	6 (Q5)	92.33	99.56	98.08	98.03
Q6	7 (Q6)	85.97	99.23	93.66	95.32
Q7	8 (Q7)	89.34	99.46	95.72	95.73
Q8	9 (Q8)	84.14	99.31	92.25	92.61
Q9	10 (Q9)	82.67	99.14	92.97	92.89
Q10	11 (Q10)	79.98	98.96	90.93	91.01
Mean		90.663	99.527	96.024	96.227
Standard Dev.		6.883244947	0.346527055	3.159120764	3.028666538
Covariance		-19.1605	-0.9535	-8.561	-8.4115
Correlation		-0.969140268	0.986231268	0.962877462	0.987532159
Co ϕE		0.93105916	0.940237398	0.892687726	0.859392138
Covar ϕE		35.3597125	1.710775	15.8304	14.578125
Sample Type	Colours	Wu	New 1	New 2	
Q1	2 (Q1)	99.33	99.15	99.99	
Q2	3 (Q2)	98.97	98.96	99.99	
Q3	4 (Q3)	98.53	98.91	99.99	
Q4	5 (Q4)	97.67	98.64	99.93	
Q5	6 (Q5)	97.31	98.19	99.75	
Q6	7 (Q6)	95.4	94.55	99.54	
Q7	8 (Q7)	94.71	94.32	99.95	
Q8	9 (Q8)	91.95	92.46	99.37	
Q9	10 (Q9)	91.18	91.89	99.44	
Q10	11 (Q10)	89.74	91.36	99.21	
Mean		95.479	95.843	99.716	
Standard Dev.		3.300725526	3.074892031	0.284576879	
Covariance		-9.2265	-8.4225	-0.706	
Correlation		0.992965752	0.978715771	0.877673263	
Co ϕE		0.825834785	0.815359151	0.943958692	
Covar ϕE		15.1604375	14.350125	1.6575375	

1.5.7 Test Data for Gaussian Correlation Evaluation between Measured and Theoretical Distributions

1010-Y30R	RED				GREEN				BLUE			
	Measured	Theoretica	Noise	Pure	Measured	Theoretica	Noise	Pure	Measured	Theoretica	Noise	Pure
0	5516	0	32	0	9801	0	96	0	10687	0	75	0
1	5181	0	42	0	889	0	42	0	6	0	32	0
2	11	0	39	0	4	0	97	0	6	0	86	0
3	5	0	76	0	3	0	91	0	5	0	82	0
4	3	0	95	0	3	0	91	0	5	0	83	0
5	3	0	48	0	5	0	75	0	5	0	96	0
6	3	0	58	0	3	0	12	0	4	0	27	0
7	2	0	99	0	6	0	65	0	7	0	21	0
8	0	0	79	0	4	0	87	0	2	0	11	0
9	5	0	69	0	1	0	44	0	7	0	44	0
10	6	0	22	0	1	0	77	0	3	0	86	0
11	2	0	75	0	1	0	23	0	7	0	32	0
12	2	0	6	0	1	0	5	0	2	0	48	0
13	3	0	99	0	2	0	39	0	5	0	61	0
14	3	0	59	0	1	0	41	0	5	0	5	0
15	6	0	32	0	2	0	86	0	2	0	62	0
16	2	0	21	0	3	0	23	0	4	0	91	0
17	4	0	71	0	0	0	2	0	1	0	24	0
18	3	0	0	0	0	0	29	0	3	0	42	0
19	4	0	98	0	3	0	75	0	3	0	29	0
20	1	0	27	0	0	0	4	0	2	0	29	0
21	3	0	42	0	2	0	15	0	3	0	52	0
22	0	0	90	0	1	0	23	0	6	0	17	0
23	2	0	35	0	1	0	42	0	4	0	79	0
24	2	0	94	0	2	0	13	0	5	0	20	0
25	2	0	98	0	0	0	41	0	4	0	90	0
26	2	0	58	0	1	0	1	0	2	0	23	0
27	2	0	43	0	0	0	54	0	1	0	4	0
28	10	0	41	0	2	0	53	0	9	0	36	0
29	6	0	70	0	1	0	25	0	3	0	19	0
30	3	0	38	0	0	0	40	0	3	0	30	0
31	2	0	94	0	1	0	29	0	4	0	36	0
32	2	0	66	0	5	0	13	0	6	0	30	0
33	10	0	34	0	2	0	22	0	2	0	53	0
34	0	0	35	0	0	0	2	0	4	0	66	0
35	2	0	72	0	2	0	70	0	5	0	11	0
36	5	0	76	0	1	0	6	0	3	0	53	0
37	2	0	34	0	2	0	63	0	1	0	16	0
38	6	0	16	0	2	0	25	0	4	0	10	0
39	3	0	67	0	5	0	1	0	1	0	42	0
40	4	0	38	0	1	0	42	0	4	0	34	0
41	0	0	83	0	4	0	68	0	3	0	70	0
42	6	0	15	0	1	0	48	0	3	0	80	0
43	0	0	53	0	3	0	40	0	1	0	17	0
44	2	0	79	0	0	0	17	0	3	0	22	0
45	3	0	16	0	2	0	89	0	2	0	57	0
46	3	0	3	0	1	0	68	0	3	0	56	0
47	3	0	70	0	3	0	68	0	2	0	82	0
48	2	0	80	0	4	0	89	0	2	0	96	0
49	2	0	21	0	1	0	32	0	3	0	26	0
50	6	0	20	0	1	0	23	0	6	0	8	0
51	1	0	5	0	1	0	38	0	2	0	6	0
52	2	0	82	0	0	0	72	0	5	0	42	0
53	1	0	78	0	2	0	45	0	0	0	40	0
54	1	0	7	0	3	0	7	0	0	0	55	0
55	0	0	14	0	2	0	22	0	1	0	45	0
56	7	0	40	0	3	0	99	0	1	0	77	0
57	3	0	50	0	2	0	80	0	2	0	86	0
58	1	0	8	0	2	0	41	0	3	0	32	0
59	1	0	89	0	5	0	67	0	1	0	44	0
60	4	0	74	0	4	0	69	0	3	0	40	0
61	0	0	93	0	7	0	82	0	1	0	32	0
62	2	0	59	0	2	0	14	0	2	0	3	0
63	0	0	47	0	1	0	88	0	1	0	39	0
64	2	0	5	0	2	0	44	0	0	0	5	0
65	0	0	20	0	6	0	93	0	6	0	48	0
66	4	0	44	0	4	0	31	0	0	0	99	0
67	2	0	20	0	2	0	93	0	6	0	82	0
68	0	0	71	0	4	0	58	0	1	0	3	0
69	1	0	37	0	0	0	72	0	1	0	28	0
70	2	0	70	0	4	0	38	0	3	0	81	0
71	2	0	98	0	2	0	14	0	2	0	58	0
72	0	0	20	0	6	0	44	0	3	0	38	0
73	4	0	36	0	2	0	29	0	2	0	8	0
74	2	0	26	0	2	0	65	0	1	0	90	0
75	3	0	29	0	2	0	29	0	6	0	46	0
76	3	0	10	0	3	0	90	0	4	0	51	0

1G10-Y30R	RED				GREEN				BLUE			
	Measured	Theoretica	Noise	Pure	Measured	Theoretica	Noise	Pure	Measured	Theoretica	Noise	Pure
77	1	0	22	0	2	0	84	0	4	0	69	0
78	2	0	87	0	1	0	8	0	4	0	22	0
79	2	0	26	0	1	0	85	0	1	0	89	0
80	2	0	8	0	2	0	20	0	3	0	45	0
81	4	0	3	0	3	0	83	0	5	0	15	0
82	1	0	18	0	2	0	26	0	8	0	52	0
83	4	0	45	0	2	0	97	0	6	0	42	0
84	1	0	23	0	2	0	33	0	6	0	64	0
85	3	0	15	0	4	0	10	0	3	0	15	0
86	3	0	0	0	1	0	51	0	3	0	41	0
87	2	0	1	0	0	0	38	0	6	0	22	0
88	4	0	30	0	3	0	74	0	9	0	91	0
89	1	0	43	0	1	0	96	0	5	0	54	0
90	3	0	63	0	3	0	67	0	5	0	26	0
91	8	0	31	0	2	0	20	0	4	0	87	0
92	7	0	28	0	4	0	70	0	14	0	34	0
93	3	0	34	0	2	0	48	0	6	0	68	0
94	4	0	42	0	2	0	57	0	12	0	1	0
95	2	0	4	0	2	0	18	0	17	0	83	0
96	1	0	60	0	2	0	8	0	7	0	35	0
97	3	0	60	0	2	0	36	0	19	0	1	0
98	3	0	39	0	1	0	42	0	10	0	12	0
99	1	0	33	0	2	0	92	0	15	0	35	0
100	3	0	81	0	1	0	52	0	28	0	59	0
101	4	0	90	0	1	0	4	0	31	0	47	0
102	8	0	85	0	0	0	48	0	46	0	95	0
103	1	0	47	0	1	0	64	0	44	0	53	0
104	4	0	30	0	4	0	49	0	82	0	96	0
105	8	0	96	0	1	0	5	0	90	0	43	0
106	7	0	48	0	2	0	74	0	141	0	80	0
107	8	0	59	0	0	0	62	0	191	0	5	0
108	2	0	61	0	4	0	9	0	242	0	88	0
109	15	0	29	0	0	0	99	0	333	0	20	0
110	2	0	97	0	0	0	55	0	475	0	74	0
111	6	0	20	0	2	0	45	0	591	0	97	0
112	22	0	27	0	4	0	41	0	759	0	0	0
113	16	0	94	0	2	0	97	0	1021	0	94	0
114	32	0	80	0	5	0	65	0	1559	0	59	0
115	41	0	38	0	3	0	54	0	1740	88	27	0
116	37	0	30	0	1	0	28	0	2281	187	87	0
117	62	0	78	0	0	0	6	0	3163	374	1	0
118	62	0	39	0	2	0	59	0	3983	707	57	0
119	83	0	34	0	6	0	90	0	4717	1267	86	0
120	89	0	38	0	6	0	42	0	6467	2146	12	0
121	134	0	12	0	16	0	59	0	7379	3439	91	0
122	158	0	95	0	24	0	84	0	8761	5213	99	0
123	223	0	19	0	24	0	38	0	10706	7476	66	0
124	227	0	61	0	32	0	0	0	13482	10142	58	0
125	293	0	88	0	56	0	59	0	14359	13018	2	0
126	336	0	93	0	62	0	66	0	15512	15807	20	0
127	451	0	8	0	61	0	40	0	18724	18157	9	0
128	550	0	90	0	114	0	54	0	16482	19733	249009	261632
129	586	0	85	0	139	0	40	0	20288	20288	41	0
130	669	0	61	0	178	0	85	0	17159	19733	50	0
131	834	0	6	0	246	0	21	0	17407	18157	17	0
132	931	0	43	0	296	0	38	0	14075	15807	81	0
133	1061	0	35	0	426	0	56	0	14560	13018	77	0
134	1249	0	11	0	513	0	88	0	9272	10142	48	0
135	1351	0	33	0	596	0	40	0	9202	7476	25	0
136	1691	98	43	0	749	0	61	0	5491	5213	71	0
137	1987	166	26	0	897	0	48	0	3957	3439	45	0
138	2333	272	36	0	1322	0	6	0	2563	2146	94	0
139	2881	434	30	0	1312	0	53	0	1583	1267	75	0
140	2645	674	35	0	1841	0	67	0	837	707	53	0
141	3399	1016	84	0	2046	0	47	0	429	374	51	0
142	3818	1488	4	0	2451	0	49	0	181	187	60	0
143	3760	2120	17	0	2700	89	89	0	85	88	95	0
144	4182	2935	38	0	2977	190	19	0	39	0	61	0
145	5592	3951	25	0	3656	380	44	0	10	0	88	0
146	6376	5170	27	0	4174	720	28	0	2	0	12	0
147	6873	6575	58	0	4331	1289	78	0	1	0	91	0
148	7934	8130	54	0	4835	2183	25	0	0	0	92	0
149	9361	9772	13	0	6442	3498	40	0	0	0	28	0
150	11470	11418	38	0	6430	5303	55	0	0	0	32	0
151	11553	12968	85	0	7831	7604	0	0	0	0	20	0
152	12510	14318	47	0	8989	10317	48	0	0	0	60	0
153	15115	15368	73	0	11447	13242	97	0	0	0	93	0

10:0:Y30R	RED				GREEN				BLUE			
	Measured	Theoretica	Noise	Pure	Measured	Theoretica	Noise	Pure	Measured	Theoretica	Noise	Pure
154	15191	16034	88	0	13267	16079	44	0	0	0	27	0
155	16263	16262	249530	261632	15612	18470	32	0	0	0	60	0
156	16075	16034	74	0	16352	20072	26	0	0	0	79	0
157	15580	15368	63	0	20637	20636	249288	261632	0	0	99	0
158	15433	14318	43	0	19199	20072	97	0	0	0	32	0
159	12931	12968	5	0	19669	18470	52	0	0	0	76	0
160	9935	11418	1	0	18240	16079	34	0	0	0	69	0
161	8698	9772	21	0	15832	13242	92	0	0	0	23	0
162	6679	8130	60	0	12200	10317	95	0	0	0	89	0
163	4531	6575	20	0	9292	7604	82	0	0	0	28	0
164	2826	5170	49	0	5863	5303	2	0	0	0	50	0
165	1686	3951	41	0	3743	3498	42	0	0	0	37	0
166	1020	2935	41	0	2016	2183	65	0	0	0	43	0
167	496	2120	40	0	957	1289	28	0	0	0	2	0
168	167	1488	53	0	401	720	44	0	0	0	1	0
169	66	1016	60	0	141	380	44	0	0	0	70	0
170	26	674	27	0	43	190	56	0	0	0	0	0
171	9	434	23	0	7	89	32	0	0	0	37	0
172	1	272	50	0	0	0	64	0	0	0	10	0
173	1	166	32	0	0	0	51	0	0	0	90	0
174	0	98	89	0	0	0	17	0	0	0	85	0
175	0	0	55	0	0	0	52	0	0	0	68	0
176	0	0	78	0	0	0	0	0	0	0	15	0
177	0	0	25	0	0	0	78	0	0	0	79	0
178	0	0	6	0	0	0	72	0	0	0	81	0
179	0	0	43	0	0	0	38	0	0	0	66	0
180	0	0	22	0	0	0	38	0	0	0	11	0
181	0	0	89	0	0	0	41	0	0	0	19	0
182	0	0	45	0	0	0	91	0	0	0	25	0
183	0	0	39	0	0	0	68	0	0	0	70	0
184	0	0	41	0	0	0	45	0	0	0	25	0
185	0	0	46	0	0	0	27	0	0	0	72	0
186	0	0	31	0	0	0	22	0	0	0	72	0
187	0	0	16	0	0	0	81	0	0	0	2	0
188	0	0	35	0	0	0	38	0	0	0	49	0
189	0	0	27	0	0	0	37	0	0	0	45	0
190	0	0	61	0	0	0	15	0	0	0	41	0
191	0	0	1	0	0	0	36	0	0	0	87	0
192	0	0	0	0	0	0	10	0	0	0	83	0
193	0	0	11	0	0	0	46	0	0	0	72	0
194	0	0	81	0	0	0	41	0	0	0	63	0
195	0	0	18	0	0	0	12	0	0	0	27	0
196	0	0	89	0	0	0	61	0	0	0	45	0
197	0	0	92	0	0	0	60	0	0	0	52	0
198	0	0	45	0	0	0	5	0	0	0	76	0
199	0	0	54	0	0	0	88	0	0	0	81	0
200	0	0	78	0	0	0	36	0	0	0	87	0
201	0	0	6	0	0	0	55	0	0	0	44	0
202	0	0	38	0	0	0	77	0	0	0	31	0
203	0	0	41	0	0	0	70	0	0	0	60	0
204	0	0	98	0	0	0	98	0	0	0	54	0
205	0	0	85	0	0	0	72	0	0	0	28	0
206	0	0	56	0	0	0	53	0	0	0	62	0
207	0	0	70	0	0	0	56	0	0	0	1	0
208	0	0	60	0	0	0	86	0	0	0	36	0
209	0	0	30	0	0	0	96	0	0	0	82	0
210	0	0	12	0	0	0	85	0	0	0	7	0
211	0	0	86	0	0	0	30	0	0	0	38	0
212	0	0	92	0	0	0	91	0	0	0	66	0
213	0	0	67	0	0	0	7	0	0	0	21	0
214	0	0	40	0	0	0	98	0	0	0	11	0
215	0	0	60	0	0	0	41	0	0	0	73	0
216	0	0	54	0	0	0	65	0	0	0	94	0
217	0	0	80	0	0	0	77	0	0	0	32	0
218	0	0	83	0	0	0	79	0	0	0	7	0
219	0	0	67	0	0	0	41	0	0	0	85	0
220	0	0	31	0	0	0	7	0	0	0	81	0
221	0	0	44	0	0	0	28	0	0	0	12	0
222	0	0	41	0	0	0	95	0	0	0	2	0
223	0	0	34	0	0	0	10	0	0	0	37	0
224	0	0	73	0	0	0	88	0	0	0	58	0
225	0	0	62	0	0	0	18	0	0	0	79	0
226	0	0	36	0	0	0	22	0	0	0	76	0
227	0	0	37	0	0	0	18	0	0	0	43	0
228	0	0	42	0	0	0	85	0	0	0	47	0
229	0	0	85	0	0	0	14	0	0	0	96	0
230	0	0	0	0	0	0	47	0	0	0	57	0

1010-Y30R	RED				GREEN				BLUE			
	Measured	Theoretica	Noise	Pure	Measured	Theoretica	Noise	Pure	Measured	Theoretica	Noise	Pure
231	0	0	23	0	0	0	8	0	0	0	24	0
232	0	0	73	0	0	0	72	0	0	0	24	0
233	0	0	97	0	0	0	11	0	0	0	82	0
234	0	0	20	0	0	0	21	0	0	0	37	0
235	0	0	40	0	0	0	0	0	0	0	84	0
236	0	0	0	0	0	0	43	0	0	0	88	0
237	0	0	1	0	0	0	20	0	0	0	99	0
238	0	0	79	0	0	0	10	0	0	0	55	0
239	0	0	76	0	0	0	6	0	0	0	85	0
240	0	0	80	0	0	0	55	0	0	0	49	0
241	0	0	46	0	0	0	73	0	0	0	11	0
242	0	0	27	0	0	0	29	0	0	0	65	0
243	0	0	40	0	0	0	17	0	0	0	52	0
244	0	0	80	0	0	0	56	0	0	0	8	0
245	0	0	69	0	0	0	37	0	0	0	4	0
246	0	0	24	0	0	0	16	0	0	0	60	0
247	0	0	40	0	0	0	83	0	0	0	9	0
248	0	0	65	0	0	0	61	0	0	0	79	0
249	0	0	83	0	0	0	92	0	0	0	14	0
250	0	0	57	0	0	0	58	0	0	0	14	0
251	0	0	77	0	0	0	82	0	0	0	88	0
252	0	0	54	0	0	0	31	0	0	0	80	0
253	0	0	27	0	0	0	91	0	0	0	92	0
254	0	0	32	0	0	0	33	0	0	0	32	0
255	0	0	25	0	0	0	10	0	0	0	81	0
mode:	155				157				129			
mean:	145.9121				148.855736				122.2055			
std dev:	5.944798				4.246285				4.246285			
Correlation		0.972167	0.308106	0.308135		0.962252	0.356911	0.356772		0.959385	0.278529	0.278569

1020-Y60R	RED				GREEN				BLUE			
	Measured	Theoretica	Noise	Pure	Measured	Theoretica	Noise	Pure	Measured	Theoretica	Noise	Pure
0	5477	0	99	0	9673	0	34	0	10585	0	5	0
1	5140	0	82	0	960	0	23	0	18	0	93	0
2	6	0	21	0	8	0	20	0	14	0	23	0
3	5	0	11	0	6	0	11	0	13	0	52	0
4	6	0	60	0	5	0	73	0	3	0	47	0
5	8	0	51	0	3	0	8	0	4	0	89	0
6	6	0	45	0	0	0	56	0	5	0	90	0
7	6	0	77	0	3	0	73	0	4	0	70	0
8	3	0	71	0	1	0	43	0	5	0	33	0
9	5	0	2	0	3	0	69	0	7	0	87	0
10	4	0	5	0	1	0	8	0	4	0	14	0
11	4	0	92	0	1	0	87	0	3	0	67	0
12	5	0	0	0	1	0	53	0	3	0	16	0
13	3	0	10	0	1	0	11	0	4	0	56	0
14	3	0	23	0	3	0	67	0	1	0	59	0
15	0	0	71	0	3	0	16	0	2	0	20	0
16	2	0	43	0	2	0	90	0	2	0	63	0
17	0	0	58	0	1	0	88	0	5	0	57	0
18	2	0	80	0	2	0	55	0	1	0	83	0
19	2	0	50	0	4	0	46	0	2	0	98	0
20	1	0	42	0	2	0	97	0	2	0	49	0
21	2	0	92	0	3	0	65	0	1	0	29	0
22	1	0	44	0	3	0	33	0	1	0	10	0
23	1	0	15	0	3	0	73	0	1	0	86	0
24	2	0	97	0	2	0	28	0	1	0	51	0
25	2	0	11	0	3	0	65	0	1	0	76	0
26	3	0	85	0	2	0	53	0	3	0	27	0
27	1	0	37	0	3	0	6	0	3	0	26	0
28	1	0	29	0	0	0	46	0	2	0	23	0
29	0	0	13	0	1	0	2	0	2	0	19	0
30	0	0	3	0	2	0	83	0	2	0	21	0
31	2	0	91	0	2	0	43	0	1	0	23	0
32	1	0	57	0	3	0	30	0	1	0	21	0
33	1	0	62	0	4	0	42	0	2	0	21	0
34	1	0	2	0	1	0	2	0	2	0	22	0
35	5	0	15	0	3	0	52	0	1	0	89	0
36	2	0	89	0	0	0	92	0	0	0	32	0
37	2	0	33	0	0	0	59	0	3	0	17	0
38	2	0	5	0	2	0	53	0	0	0	64	0
39	3	0	36	0	2	0	91	0	1	0	30	0
40	0	0	70	0	0	0	13	0	7	0	74	0
41	5	0	5	0	0	0	21	0	3	0	16	0
42	0	0	61	0	1	0	60	0	2	0	53	0
43	1	0	39	0	0	0	4	0	5	0	53	0
44	0	0	89	0	1	0	25	0	3	0	14	0
45	4	0	15	0	2	0	39	0	1	0	52	0
46	2	0	81	0	0	0	34	0	0	0	32	0
47	2	0	34	0	1	0	31	0	5	0	74	0
48	4	0	15	0	0	0	84	0	1	0	50	0
49	4	0	32	0	1	0	27	0	3	0	66	0
50	0	0	30	0	0	0	93	0	3	0	49	0
51	1	0	98	0	0	0	48	0	2	0	65	0
52	0	0	5	0	0	0	69	0	3	0	36	0
53	0	0	19	0	1	0	29	0	1	0	18	0
54	3	0	95	0	2	0	24	0	0	0	52	0
55	2	0	44	0	1	0	6	0	2	0	64	0
56	0	0	28	0	1	0	95	0	0	0	32	0
57	3	0	93	0	2	0	60	0	1	0	47	0
58	0	0	53	0	0	0	13	0	1	0	93	0
59	3	0	20	0	0	0	59	0	2	0	57	0
60	0	0	82	0	1	0	47	0	0	0	48	0
61	3	0	32	0	0	0	54	0	0	0	39	0
62	2	0	33	0	2	0	31	0	1	0	82	0
63	1	0	18	0	0	0	96	0	1	0	9	0
64	2	0	34	0	0	0	14	0	1	0	80	0
65	0	0	78	0	0	0	69	0	3	0	90	0
66	0	0	91	0	3	0	28	0	2	0	35	0
67	1	0	68	0	2	0	59	0	1	0	58	0
68	1	0	95	0	1	0	62	0	0	0	97	0
69	1	0	83	0	1	0	21	0	0	0	1	0
70	0	0	87	0	1	0	82	0	3	0	15	0
71	0	0	61	0	2	0	21	0	2	0	35	0
72	0	0	68	0	1	0	64	0	0	0	12	0
73	1	0	44	0	2	0	93	0	1	0	6	0
74	4	0	18	0	0	0	87	0	3	0	61	0
75	0	0	74	0	4	0	52	0	1	0	27	0
76	0	0	43	0	1	0	70	0	0	0	84	0

1020-Y60R	RED				GREEN				BLUE			
	Measured	Theretica	Noise	Pure	Measured	Theoretica	Noise	Pure	Measured	Theoretica	Noise	Pure
77	2	0	94	0	1	0	73	0	2	0	88	0
78	0	0	20	0	1	0	43	0	2	0	13	0
79	0	0	76	0	2	0	52	0	0	0	66	0
80	3	0	71	0	2	0	12	0	1	0	12	0
81	0	0	23	0	0	0	72	0	2	0	14	0
82	2	0	11	0	3	0	95	0	0	0	19	0
83	0	0	18	0	1	0	0	0	2	0	93	0
84	0	0	38	0	4	0	47	0	4	0	94	0
85	1	0	15	0	2	0	34	0	3	0	24	0
86	1	0	7	0	8	0	95	0	1	0	31	0
87	2	0	46	0	1	0	40	0	2	0	31	0
88	2	0	71	0	4	0	41	0	4	0	90	0
89	2	0	5	0	0	0	25	0	2	0	68	0
90	1	0	18	0	0	0	63	0	2	0	32	0
91	1	0	89	0	1	0	94	0	4	0	19	0
92	2	0	59	0	3	0	38	0	4	0	99	0
93	0	0	4	0	0	0	23	0	2	0	96	0
94	3	0	92	0	1	0	99	0	0	0	36	0
95	2	0	67	0	4	0	56	0	5	0	39	0
96	3	0	53	0	0	0	1	0	3	0	43	0
97	2	0	80	0	2	0	12	0	3	0	29	0
98	1	0	50	0	0	0	53	0	5	0	93	0
99	4	0	72	0	1	0	6	0	15	0	93	0
100	0	0	42	0	0	0	66	0	13	0	69	0
101	5	0	25	0	2	0	81	0	31	0	5	0
102	7	0	8	0	0	0	90	0	41	0	89	0
103	3	0	80	0	0	0	12	0	33	0	10	0
104	5	0	67	0	0	0	3	0	62	0	51	0
105	4	0	8	0	3	0	75	0	105	0	25	0
106	1	0	53	0	0	0	27	0	111	0	77	0
107	5	0	55	0	0	0	45	0	144	0	95	0
108	2	0	25	0	0	0	55	0	205	0	80	0
109	2	0	65	0	2	0	98	0	249	0	60	0
110	3	0	2	0	0	0	21	0	418	118	4	0
111	5	0	82	0	0	0	98	0	518	199	52	0
112	4	0	75	0	1	0	6	0	646	327	47	0
113	10	0	85	0	1	0	83	0	865	522	19	0
114	10	0	19	0	1	0	57	0	1244	809	43	0
115	24	0	25	0	4	0	5	0	1398	1220	24	0
116	14	0	38	0	0	0	63	0	1895	1787	77	0
117	22	0	87	0	0	0	33	0	2572	2546	93	0
118	39	0	83	0	1	0	92	0	3408	3525	23	0
119	45	0	15	0	2	0	16	0	3999	4745	50	0
120	49	0	47	0	1	0	78	0	5623	6208	61	0
121	51	0	63	0	6	0	20	0	6612	7896	18	0
122	76	0	88	0	6	0	5	0	8037	9763	58	0
123	120	0	5	0	14	0	80	0	9852	11734	71	0
124	110	0	27	0	9	0	14	0	12184	13711	57	0
125	150	0	50	0	24	0	49	0	13317	15572	41	0
126	201	0	49	0	39	0	9	0	14500	17194	39	0
127	229	0	95	0	28	0	88	0	17750	18454	12	0
128	316	0	82	0	57	0	37	0	15887	19254	10	0
129	399	0	67	0	89	0	79	0	19529	19528	249054	261632
130	464	0	54	0	112	0	92	0	17349	19254	11	0
131	517	0	7	0	156	0	33	0	18225	18454	86	0
132	539	0	40	0	137	0	79	0	15240	17194	78	0
133	635	0	2	0	243	0	66	0	16111	15572	1	0
134	702	0	23	0	293	0	54	0	10929	13711	80	0
135	771	0	76	0	387	0	90	0	11133	11734	3	0
136	991	0	49	0	502	0	77	0	6862	9763	98	0
137	1152	0	41	0	606	0	75	0	5255	7896	6	0
138	1333	0	48	0	851	0	19	0	3735	6208	78	0
139	1699	0	68	0	987	0	70	0	2238	4745	64	0
140	1778	0	28	0	1297	0	12	0	1210	3525	25	0
141	2337	0	72	0	1571	0	10	0	669	2546	7	0
142	2518	118	87	0	2005	0	15	0	338	1787	73	0
143	2644	215	72	0	2340	0	13	0	151	1220	48	0
144	2871	376	44	0	2519	0	5	0	60	809	80	0
145	3887	632	82	0	3280	85	12	0	21	522	49	0
146	4164	1024	44	0	3647	180	32	0	7	327	76	0
147	4406	1595	41	0	3813	361	28	0	3	199	65	0
148	4968	2390	51	0	4391	683	77	0	1	118	69	0
149	5522	3446	55	0	5855	1223	25	0	0	0	44	0
150	7130	4780	40	0	5858	2072	6	0	0	0	28	0
151	7238	6381	41	0	6747	3320	87	0	0	0	77	0
152	8087	8197	80	0	7574	5033	61	0	0	0	18	0
153	9879	10131	42	0	10024	7218	53	0	0	0	17	0

1020-Y60R	RED				GREEN				BLUE			
	Measured	Theoretica	Noise	Pure	Measured	Theoretica	Noise	Pure	Measured	Theoretica	Noise	Pure
154	10769	12048	32	0	11310	9793	49	0	0	0	47	0
155	12155	13786	21	0	13588	12569	68	0	0	0	38	0
156	13009	15180	34	0	14543	15262	31	0	0	0	8	0
157	14475	16083	42	0	18590	17532	50	0	0	0	43	0
158	16396	16396	249305	261632	18015	19053	2	0	0	0	24	0
159	16238	16083	39	0	19589	19589	249781	261632	0	0	68	0
160	14501	15180	70	0	19463	19053	81	0	0	0	4	0
161	15557	13786	90	0	18213	17532	5	0	0	0	13	0
162	15063	12048	92	0	15314	15262	82	0	0	0	42	0
163	12736	10131	35	0	12870	12569	12	0	0	0	96	0
164	9832	8197	42	0	9305	9793	4	0	0	0	4	0
165	7494	6381	43	0	6353	7218	71	0	0	0	58	0
166	5882	4780	49	0	4124	5033	10	0	0	0	84	0
167	4134	3446	8	0	2221	3320	75	0	0	0	29	0
168	2024	2390	47	0	1114	2072	36	0	0	0	92	0
169	1287	1595	84	0	495	1223	24	0	0	0	5	0
170	608	1024	16	0	173	683	95	0	0	0	78	0
171	321	632	7	0	45	361	99	0	0	0	20	0
172	127	376	87	0	11	180	17	0	0	0	6	0
173	47	215	22	0	10	85	38	0	0	0	36	0
174	25	118	88	0	3	0	62	0	0	0	90	0
175	4	0	77	0	1	0	30	0	0	0	88	0
176	1	0	32	0	0	0	16	0	0	0	49	0
177	0	0	7	0	0	0	5	0	0	0	78	0
178	0	0	25	0	0	0	28	0	0	0	96	0
179	0	0	44	0	0	0	62	0	0	0	31	0
180	0	0	83	0	0	0	4	0	0	0	81	0
181	0	0	50	0	0	0	49	0	0	0	52	0
182	0	0	73	0	0	0	21	0	0	0	76	0
183	0	0	18	0	0	0	52	0	0	0	3	0
184	0	0	56	0	0	0	33	0	0	0	64	0
185	0	0	2	0	0	0	3	0	0	0	59	0
186	0	0	24	0	0	0	69	0	0	0	98	0
187	0	0	49	0	0	0	63	0	0	0	62	0
188	0	0	24	0	0	0	79	0	0	0	74	0
189	0	0	55	0	0	0	80	0	0	0	60	0
190	0	0	94	0	0	0	6	0	0	0	17	0
191	0	0	38	0	0	0	61	0	0	0	24	0
192	0	0	48	0	0	0	92	0	0	0	34	0
193	0	0	4	0	0	0	77	0	0	0	29	0
194	0	0	69	0	0	0	66	0	0	0	67	0
195	0	0	34	0	0	0	35	0	0	0	43	0
196	0	0	1	0	0	0	34	0	0	0	53	0
197	0	0	32	0	0	0	67	0	0	0	87	0
198	0	0	48	0	0	0	87	0	0	0	92	0
199	0	0	12	0	0	0	28	0	0	0	33	0
200	0	0	11	0	0	0	30	0	0	0	56	0
201	0	0	6	0	0	0	95	0	0	0	33	0
202	0	0	5	0	0	0	40	0	0	0	56	0
203	0	0	52	0	0	0	78	0	0	0	99	0
204	0	0	69	0	0	0	70	0	0	0	20	0
205	0	0	3	0	0	0	63	0	0	0	88	0
206	0	0	87	0	0	0	76	0	0	0	1	0
207	0	0	23	0	0	0	37	0	0	0	5	0
208	0	0	88	0	0	0	2	0	0	0	20	0
209	0	0	76	0	0	0	58	0	0	0	90	0
210	0	0	98	0	0	0	1	0	0	0	71	0
211	0	0	89	0	0	0	28	0	0	0	13	0
212	0	0	30	0	0	0	52	0	0	0	90	0
213	0	0	69	0	0	0	19	0	0	0	70	0
214	0	0	32	0	0	0	60	0	0	0	14	0
215	0	0	70	0	0	0	5	0	0	0	74	0
216	0	0	58	0	0	0	98	0	0	0	53	0
217	0	0	59	0	0	0	9	0	0	0	32	0
218	0	0	65	0	0	0	91	0	0	0	79	0
219	0	0	35	0	0	0	31	0	0	0	92	0
220	0	0	69	0	0	0	68	0	0	0	94	0
221	0	0	68	0	0	0	0	0	0	0	41	0
222	0	0	70	0	0	0	29	0	0	0	18	0
223	0	0	57	0	0	0	3	0	0	0	95	0
224	0	0	40	0	0	0	11	0	0	0	75	0
225	0	0	5	0	0	0	30	0	0	0	96	0
226	0	0	30	0	0	0	32	0	0	0	72	0
227	0	0	90	0	0	0	87	0	0	0	99	0
228	0	0	4	0	0	0	44	0	0	0	38	0
229	0	0	40	0	0	0	77	0	0	0	85	0
230	0	0	49	0	0	0	89	0	0	0	59	0

1020-Y60R	RED				GREEN				BLUE			
	Measured	Theoretica	Noise	Pure	Measured	Theoretica	Noise	Pure	Measured	Theoretica	Noise	Pure
231	0	0	13	0	0	0	13	0	0	0	11	0
232	0	0	71	0	0	0	38	0	0	0	92	0
233	0	0	65	0	0	0	61	0	0	0	27	0
234	0	0	41	0	0	0	2	0	0	0	71	0
235	0	0	62	0	0	0	45	0	0	0	28	0
236	0	0	22	0	0	0	6	0	0	0	10	0
237	0	0	94	0	0	0	10	0	0	0	49	0
238	0	0	42	0	0	0	30	0	0	0	45	0
239	0	0	22	0	0	0	80	0	0	0	17	0
240	0	0	21	0	0	0	4	0	0	0	86	0
241	0	0	65	0	0	0	6	0	0	0	0	0
242	0	0	74	0	0	0	51	0	0	0	27	0
243	0	0	69	0	0	0	80	0	0	0	78	0
244	0	0	75	0	0	0	74	0	0	0	79	0
245	0	0	34	0	0	0	92	0	0	0	55	0
246	0	0	19	0	0	0	58	0	0	0	68	0
247	0	0	91	0	0	0	70	0	0	0	79	0
248	0	0	94	0	0	0	4	0	0	0	86	0
249	0	0	93	0	0	0	55	0	0	0	60	0
250	0	0	0	0	0	0	21	0	0	0	94	0
251	0	0	40	0	0	0	63	0	0	0	15	0
252	0	0	70	0	0	0	21	0	0	0	18	0
253	0	0	26	0	0	0	65	0	0	0	3	0
254	0	0	37	0	0	0	30	0	0	0	11	0
255	0	0	71	0	0	0	21	0	0	0	4	0
mode:	158				159				129			
mean:	149.3642				150.017207				122.9194			
std dev:	5.095541				4.246285				5.944798			
Correlation		0.965495	0.312624	0.312535		0.961667	0.338498	0.338601		0.974171	0.334311	0.33447

2020-R908	RED				GREEN				BLUE			
	Measured	Theoretica	Noise	Pure	Measured	Theoretica	Noise	Pure	Measured	Theoretica	Noise	Pure
0	5579	0	64	0	9886	0	32	0	10733	0	33	0
1	5161	0	72	0	826	0	57	0	11	0	65	0
2	8	0	46	0	5	0	97	0	6	0	25	0
3	8	0	57	0	6	0	56	0	9	0	21	0
4	3	0	87	0	3	0	47	0	5	0	33	0
5	5	0	28	0	2	0	32	0	4	0	31	0
6	4	0	28	0	0	0	65	0	8	0	46	0
7	4	0	22	0	3	0	28	0	3	0	10	0
8	8	0	28	0	4	0	10	0	2	0	84	0
9	1	0	21	0	0	0	65	0	9	0	32	0
10	4	0	98	0	1	0	96	0	2	0	8	0
11	7	0	33	0	1	0	70	0	5	0	77	0
12	4	0	62	0	3	0	9	0	2	0	35	0
13	2	0	74	0	1	0	11	0	5	0	98	0
14	5	0	64	0	1	0	78	0	5	0	71	0
15	1	0	34	0	2	0	11	0	5	0	75	0
16	3	0	24	0	2	0	98	0	2	0	21	0
17	4	0	75	0	4	0	46	0	2	0	55	0
18	6	0	93	0	4	0	93	0	2	0	13	0
19	1	0	8	0	5	0	11	0	1	0	51	0
20	3	0	31	0	2	0	6	0	4	0	42	0
21	1	0	2	0	2	0	76	0	1	0	5	0
22	1	0	17	0	5	0	68	0	2	0	99	0
23	3	0	20	0	3	0	86	0	1	0	89	0
24	1	0	53	0	3	0	39	0	4	0	95	0
25	2	0	70	0	3	0	85	0	4	0	89	0
26	2	0	25	0	3	0	35	0	4	0	2	0
27	1	0	56	0	3	0	13	0	1	0	64	0
28	10	0	58	0	4	0	48	0	7	0	80	0
29	0	0	27	0	2	0	64	0	6	0	32	0
30	4	0	98	0	4	0	16	0	5	0	98	0
31	6	0	57	0	4	0	17	0	3	0	27	0
32	3	0	97	0	2	0	11	0	3	0	35	0
33	7	0	37	0	0	0	70	0	3	0	92	0
34	2	0	13	0	3	0	8	0	3	0	65	0
35	5	0	72	0	3	0	52	0	5	0	1	0
36	2	0	95	0	6	0	26	0	5	0	76	0
37	1	0	16	0	4	0	95	0	0	0	78	0
38	10	0	78	0	0	0	40	0	6	0	13	0
39	5	0	25	0	3	0	82	0	2	0	57	0
40	4	0	95	0	1	0	27	0	2	0	44	0
41	3	0	71	0	3	0	41	0	4	0	18	0
42	6	0	92	0	3	0	78	0	3	0	25	0
43	1	0	96	0	2	0	26	0	4	0	7	0
44	2	0	5	0	4	0	6	0	1	0	55	0
45	7	0	5	0	2	0	50	0	4	0	44	0
46	2	0	46	0	2	0	67	0	6	0	91	0
47	2	0	40	0	3	0	97	0	8	0	38	0
48	6	0	80	0	2	0	72	0	4	0	93	0
49	7	0	84	0	4	0	69	0	5	0	50	0
50	5	0	83	0	0	0	51	0	5	0	2	0
51	2	0	23	0	0	0	45	0	2	0	16	0
52	4	0	20	0	3	0	40	0	0	0	44	0
53	3	0	87	0	1	0	20	0	8	0	63	0
54	0	0	87	0	3	0	14	0	6	0	16	0
55	3	0	77	0	1	0	32	0	5	0	43	0
56	9	0	56	0	2	0	55	0	6	0	64	0
57	4	0	18	0	0	0	98	0	5	0	18	0
58	4	0	26	0	0	0	99	0	19	0	25	0
59	15	0	13	0	1	0	66	0	2	0	45	0
60	12	0	26	0	7	0	99	0	18	0	22	0
61	9	0	32	0	3	0	97	0	8	0	22	0
62	14	0	95	0	2	0	44	0	20	0	77	0
63	1	0	73	0	0	0	64	0	3	0	68	0
64	5	0	57	0	1	0	5	0	1	0	65	0
65	16	0	74	0	6	0	89	0	14	0	25	0
66	10	0	13	0	2	0	4	0	4	0	94	0
67	14	0	15	0	3	0	37	0	11	0	0	0
68	4	0	97	0	3	0	10	0	2	0	31	0
69	9	0	82	0	0	0	60	0	6	0	89	0
70	7	0	25	0	5	0	4	0	7	0	52	0
71	8	0	29	0	1	0	53	0	9	0	14	0
72	3	0	55	0	3	0	6	0	6	0	29	0
73	7	0	16	0	4	0	63	0	12	0	51	0
74	12	0	55	0	0	0	47	0	2	0	73	0
75	6	0	61	0	5	0	86	0	11	0	24	0
76	8	0	49	0	1	0	32	0	9	0	50	0

2020-R90B	RED				GREEN				BLUE			
	Measured	Theoretica	Noise	Pure	Measured	Theoretica	Noise	Pure	Measured	Theoretica	Noise	Pure
77	2	0	26	0	5	0	97	0	9	0	28	0
78	1	0	48	0	2	0	29	0	13	0	86	0
79	12	0	21	0	0	0	74	0	2	0	94	0
80	12	0	48	0	4	0	18	0	3	0	44	0
81	5	0	50	0	1	0	50	0	10	0	56	0
82	14	0	19	0	1	0	13	0	2	0	8	0
83	4	0	9	0	3	0	10	0	5	0	95	0
84	1	0	74	0	3	0	91	0	7	0	34	0
85	4	0	15	0	1	0	49	0	4	0	70	0
86	10	0	42	0	4	0	4	0	4	0	53	0
87	2	0	13	0	3	0	44	0	6	0	45	0
88	3	0	9	0	2	0	12	0	5	0	51	0
89	4	0	16	0	0	0	65	0	2	0	21	0
90	0	0	78	0	3	0	96	0	3	0	37	0
91	8	0	24	0	7	0	88	0	2	0	94	0
92	4	0	89	0	6	0	38	0	10	0	82	0
93	5	0	77	0	2	0	45	0	5	0	80	0
94	4	0	48	0	3	0	44	0	2	0	48	0
95	5	0	68	0	1	0	50	0	1	0	87	0
96	2	0	58	0	2	0	64	0	0	0	46	0
97	3	0	43	0	3	0	68	0	3	0	80	0
98	2	0	99	0	5	0	4	0	2	0	3	0
99	0	0	5	0	2	0	61	0	1	0	40	0
100	1	0	73	0	1	0	10	0	1	0	99	0
101	1	0	27	0	1	0	75	0	1	0	63	0
102	3	0	93	0	9	0	19	0	0	0	53	0
103	2	0	52	0	19	0	93	0	0	0	97	0
104	0	0	53	0	12	0	38	0	1	0	67	0
105	1	0	90	0	9	0	86	0	2	0	17	0
106	0	0	48	0	12	0	80	0	1	0	47	0
107	1	0	77	0	1	0	59	0	0	0	64	0
108	1	0	53	0	14	0	99	0	0	0	3	0
109	1	0	34	0	15	0	46	0	0	0	13	0
110	0	0	61	0	0	0	30	0	0	0	43	0
111	0	0	88	0	11	0	62	0	1	0	47	0
112	0	0	80	0	6	0	19	0	1	0	60	0
113	2	0	70	0	8	0	62	0	0	0	2	0
114	0	0	95	0	8	0	88	0	0	0	93	0
115	0	0	61	0	8	0	84	0	0	0	92	0
116	0	0	9	0	10	0	55	0	0	0	68	0
117	0	0	28	0	14	0	95	0	0	0	31	0
118	0	0	90	0	8	0	58	0	0	0	97	0
119	0	0	87	0	7	0	80	0	0	0	62	0
120	0	0	90	0	0	0	52	0	0	0	35	0
121	0	0	95	0	8	0	46	0	0	0	45	0
122	0	0	92	0	13	0	64	0	1	0	29	0
123	1	0	22	0	6	0	25	0	0	0	10	0
124	0	0	59	0	8	0	1	0	0	0	95	0
125	3	0	86	0	11	0	75	0	2	0	2	0
126	1	0	92	0	0	0	56	0	2	0	60	0
127	3	0	21	0	3	0	28	0	1	0	45	0
128	9	0	28	0	18	0	16	0	6	0	37	0
129	12	0	69	0	3	0	33	0	10	0	37	0
130	19	0	53	0	2	0	69	0	11	0	60	0
131	18	0	53	0	5	0	42	0	9	0	58	0
132	40	0	17	0	5	0	89	0	8	0	58	0
133	54	0	52	0	8	0	86	0	29	0	17	0
134	66	0	9	0	3	0	68	0	29	0	92	0
135	94	0	35	0	13	0	0	0	60	0	94	0
136	133	0	9	0	5	0	60	0	64	0	70	0
137	162	0	45	0	4	0	30	0	95	0	6	0
138	201	0	86	0	7	0	33	0	113	0	33	0
139	308	0	83	0	9	0	16	0	152	0	31	0
140	290	0	77	0	18	0	93	0	190	0	96	0
141	445	0	32	0	15	0	87	0	291	0	74	0
142	559	0	87	0	14	0	42	0	344	0	87	0
143	620	0	16	0	24	0	75	0	523	0	41	0
144	836	0	92	0	48	0	70	0	579	105	70	0
145	1187	0	33	0	43	0	15	0	688	178	57	0
146	1554	0	83	0	44	0	1	0	979	293	76	0
147	1729	0	4	0	84	0	65	0	1238	467	77	0
148	2072	0	52	0	103	0	98	0	1474	725	44	0
149	2555	0	21	0	169	0	47	0	2122	1093	66	0
150	3169	0	9	0	191	0	8	0	2365	1602	8	0
151	3352	0	7	0	239	0	94	0	2998	2282	54	0
152	3651	0	54	0	274	0	28	0	3725	3160	2	0
153	4622	0	33	0	389	0	68	0	4888	4253	42	0

2020-R908	RED				GREEN				BLUE			
	Measured	Theoretica	Noise	Pure	Measured	Theoretica	Noise	Pure	Measured	Theoretica	Noise	Pure
154	5088	0	47	0	462	0	45	0	6195	5565	61	0
155	6068	0	47	0	652	0	52	0	7108	7078	39	0
156	6681	96	74	0	737	0	97	0	8370	8752	67	0
157	7779	240	41	0	1077	0	88	0	11688	10519	99	0
158	9548	548	4	0	1193	0	28	0	10976	12290	66	0
159	10284	1145	24	0	1536	0	66	0	14706	13959	43	0
160	10212	2193	16	0	1987	0	16	0	14530	15413	60	0
161	12236	3853	82	0	2512	0	22	0	17179	16542	27	0
162	14152	6205	88	0	2994	0	46	0	17388	17260	89	0
163	14978	9165	9	0	3655	0	91	0	17506	17505	249568	261632
164	14834	12413	67	0	3953	0	92	0	15936	17260	22	0
165	15497	15415	1	0	4819	0	42	0	17475	16542	17	0
166	16695	17555	29	0	5533	111	53	0	15648	15413	68	0
167	18333	18332	249301	261632	6379	275	42	0	14153	13959	34	0
168	13704	17555	98	0	7291	628	74	0	10915	12290	95	0
169	13244	15415	57	0	9102	1313	25	0	9486	10519	9	0
170	10582	12413	21	0	10487	2515	20	0	6273	8752	50	0
171	8304	9165	40	0	11769	4417	99	0	5073	7078	23	0
172	5761	6205	1	0	13285	7114	39	0	2889	5565	61	0
173	3816	3853	80	0	15679	10507	83	0	1974	4253	39	0
174	2349	2193	11	0	17156	14231	16	0	912	3160	53	0
175	1207	1145	26	0	17801	17673	14	0	596	2282	11	0
176	645	548	97	0	19101	20126	15	0	228	1602	85	0
177	368	240	29	0	21018	21018	249851	261632	108	1093	79	0
178	144	96	77	0	18033	20126	31	0	57	725	97	0
179	82	0	90	0	15994	17673	70	0	14	467	8	0
180	12	0	57	0	12841	14231	29	0	3	293	20	0
181	12	0	98	0	9315	10507	13	0	2	178	95	0
182	1	0	91	0	5734	7114	75	0	0	105	67	0
183	3	0	59	0	3547	4417	28	0	2	0	36	0
184	1	0	4	0	1751	2515	27	0	0	0	29	0
185	1	0	97	0	880	1313	87	0	4	0	82	0
186	3	0	55	0	274	628	38	0	0	0	4	0
187	0	0	32	0	117	275	40	0	0	0	55	0
188	0	0	62	0	23	111	23	0	1	0	95	0
189	0	0	2	0	5	0	90	0	0	0	43	0
190	1	0	0	0	2	0	94	0	0	0	50	0
191	1	0	46	0	4	0	42	0	0	0	99	0
192	0	0	0	0	2	0	21	0	0	0	61	0
193	0	0	27	0	3	0	10	0	0	0	66	0
194	0	0	14	0	0	0	12	0	0	0	98	0
195	0	0	33	0	0	0	40	0	0	0	35	0
196	0	0	31	0	0	0	32	0	0	0	63	0
197	0	0	11	0	2	0	99	0	0	0	69	0
198	0	0	82	0	2	0	61	0	0	0	57	0
199	0	0	91	0	0	0	77	0	0	0	34	0
200	0	0	18	0	1	0	10	0	0	0	74	0
201	0	0	27	0	0	0	78	0	0	0	65	0
202	0	0	77	0	0	0	7	0	0	0	59	0
203	0	0	78	0	0	0	40	0	0	0	37	0
204	0	0	51	0	1	0	96	0	0	0	28	0
205	0	0	12	0	0	0	30	0	0	0	57	0
206	0	0	16	0	0	0	38	0	0	0	70	0
207	0	0	94	0	0	0	28	0	0	0	44	0
208	0	0	5	0	0	0	59	0	0	0	1	0
209	0	0	36	0	0	0	99	0	0	0	11	0
210	0	0	68	0	0	0	63	0	0	0	44	0
211	0	0	45	0	0	0	85	0	0	0	78	0
212	0	0	11	0	0	0	65	0	0	0	67	0
213	0	0	70	0	0	0	1	0	0	0	3	0
214	0	0	5	0	0	0	16	0	0	0	74	0
215	0	0	4	0	0	0	44	0	0	0	38	0
216	0	0	72	0	0	0	42	0	0	0	47	0
217	0	0	81	0	0	0	81	0	0	0	84	0
218	0	0	86	0	0	0	54	0	0	0	15	0
219	0	0	52	0	0	0	93	0	0	0	11	0
220	0	0	38	0	0	0	30	0	0	0	26	0
221	0	0	18	0	0	0	86	0	0	0	31	0
222	0	0	33	0	0	0	60	0	0	0	86	0
223	0	0	83	0	0	0	38	0	0	0	92	0
224	0	0	93	0	0	0	60	0	0	0	76	0
225	0	0	58	0	0	0	66	0	0	0	76	0
226	0	0	37	0	0	0	12	0	0	0	16	0
227	0	0	11	0	0	0	27	0	0	0	9	0
228	0	0	2	0	0	0	36	0	0	0	42	0
229	0	0	66	0	0	0	99	0	0	0	78	0
230	0	0	71	0	0	0	32	0	0	0	91	0

2020-R908	RED				GREEN				BLUE			
	Measured	Theoretica	Noise	Pure	Measured	Theoretica	Noise	Pure	Measured	Theoretica	Noise	Pure
231	0	0	42	0	0	0	91	0	0	0	77	0
232	0	0	92	0	0	0	0	0	0	0	69	0
233	0	0	62	0	0	0	94	0	0	0	2	0
234	0	0	61	0	0	0	95	0	0	0	9	0
235	0	0	54	0	0	0	4	0	0	0	50	0
236	0	0	90	0	0	0	29	0	0	0	68	0
237	0	0	37	0	0	0	41	0	0	0	31	0
238	0	0	69	0	0	0	64	0	0	0	20	0
239	0	0	28	0	0	0	42	0	0	0	21	0
240	0	0	54	0	0	0	99	0	0	0	83	0
241	0	0	48	0	0	0	29	0	0	0	76	0
242	0	0	78	0	0	0	1	0	0	0	94	0
243	0	0	22	0	0	0	15	0	0	0	99	0
244	0	0	43	0	0	0	51	0	0	0	81	0
245	0	0	96	0	0	0	97	0	0	0	38	0
246	0	0	40	0	0	0	64	0	0	0	38	0
247	0	0	84	0	0	0	42	0	0	0	53	0
248	0	0	75	0	0	0	88	0	0	0	14	0
249	0	0	36	0	0	0	17	0	0	0	92	0
250	0	0	42	0	0	0	93	0	0	0	85	0
251	0	0	4	0	0	0	86	0	0	0	61	0
252	0	0	83	0	0	0	24	0	0	0	72	0
253	0	0	65	0	0	0	57	0	0	0	25	0
254	0	0	30	0	0	0	26	0	0	0	8	0
255	0	0	38	0	0	0	28	0	0	0	77	0
mode:	167				177				163			
mean:	155.6004				166.205036				154.786			
std dev:	3.397028				3.397028				5.944798			
Correlation:		0.858596	0.341102	0.341231		0.910571	0.360456	0.360603		0.971954	0.304042	0.304076

3010-C70Y	RED				GREEN				BLUE			
	Measured	Theoretica	Noise	Pure	Measured	Theoretica	Noise	Pure	Measured	Theoretica	Noise	Pure
0	9696	0	15	0	9704	0	23	0	9698	0	54	0
1	2	0	85	0	0	0	13	0	2	0	3	0
2	2	0	71	0	1	0	75	0	1	0	87	0
3	1	0	68	0	1	0	30	0	1	0	13	0
4	6	0	20	0	0	0	75	0	1	0	79	0
5	0	0	58	0	0	0	56	0	2	0	78	0
6	2	0	40	0	0	0	85	0	2	0	69	0
7	1	0	90	0	0	0	75	0	1	0	3	0
8	1	0	98	0	0	0	14	0	6	0	53	0
9	0	0	8	0	2	0	6	0	2	0	96	0
10	2	0	60	0	0	0	20	0	1	0	40	0
11	0	0	65	0	0	0	10	0	1	0	72	0
12	2	0	83	0	0	0	58	0	2	0	72	0
13	2	0	64	0	1	0	65	0	1	0	97	0
14	3	0	68	0	0	0	22	0	1	0	63	0
15	0	0	90	0	0	0	39	0	0	0	35	0
16	2	0	64	0	0	0	65	0	1	0	10	0
17	0	0	1	0	0	0	6	0	1	0	31	0
18	1	0	2	0	0	0	95	0	1	0	42	0
19	0	0	81	0	0	0	31	0	2	0	2	0
20	0	0	22	0	0	0	11	0	0	0	40	0
21	1	0	49	0	0	0	64	0	1	0	94	0
22	1	0	14	0	1	0	37	0	1	0	70	0
23	1	0	13	0	0	0	22	0	0	0	66	0
24	3	0	34	0	0	0	99	0	0	0	81	0
25	0	0	27	0	0	0	50	0	0	0	35	0
26	1	0	73	0	0	0	37	0	0	0	17	0
27	0	0	37	0	1	0	43	0	1	0	59	0
28	1	0	99	0	2	0	69	0	1	0	39	0
29	0	0	26	0	0	0	73	0	2	0	71	0
30	0	0	60	0	1	0	80	0	2	0	35	0
31	0	0	0	0	0	0	13	0	3	0	7	0
32	0	0	97	0	1	0	63	0	0	0	52	0
33	1	0	7	0	0	0	29	0	1	0	14	0
34	2	0	58	0	0	0	29	0	1	0	66	0
35	2	0	1	0	0	0	13	0	0	0	80	0
36	1	0	49	0	0	0	95	0	0	0	73	0
37	1	0	5	0	0	0	96	0	0	0	23	0
38	2	0	48	0	2	0	51	0	0	0	62	0
39	1	0	2	0	0	0	43	0	0	0	14	0
40	0	0	50	0	0	0	58	0	1	0	22	0
41	0	0	30	0	1	0	50	0	1	0	40	0
42	0	0	7	0	1	0	93	0	0	0	53	0
43	0	0	0	0	2	0	29	0	0	0	43	0
44	0	0	82	0	1	0	32	0	1	0	81	0
45	0	0	37	0	2	0	92	0	0	0	96	0
46	0	0	59	0	1	0	51	0	0	0	74	0
47	1	0	60	0	0	0	59	0	2	0	93	0
48	0	0	6	0	0	0	52	0	3	0	2	0
49	0	0	33	0	0	0	99	0	1	0	96	0
50	1	0	95	0	0	0	95	0	0	0	3	0
51	0	0	31	0	0	0	30	0	0	0	75	0
52	0	0	79	0	0	0	67	0	0	0	84	0
53	1	0	27	0	2	0	23	0	0	0	18	0
54	3	0	6	0	0	0	14	0	0	0	62	0
55	1	0	18	0	0	0	42	0	1	0	8	0
56	1	0	11	0	0	0	0	0	0	0	32	0
57	0	0	86	0	1	0	99	0	1	0	94	0
58	0	0	13	0	0	0	85	0	2	0	54	0
59	0	0	84	0	2	0	5	0	1	0	26	0
60	0	0	38	0	0	0	66	0	0	0	31	0
61	0	0	62	0	1	0	97	0	0	0	99	0
62	1	0	8	0	0	0	31	0	0	0	45	0
63	1	0	23	0	0	0	60	0	0	0	71	0
64	0	0	6	0	1	0	5	0	0	0	46	0
65	0	0	34	0	0	0	11	0	0	0	93	0
66	2	0	97	0	0	0	34	0	0	0	89	0
67	0	0	31	0	0	0	12	0	0	0	88	0
68	0	0	12	0	0	0	89	0	0	0	16	0
69	1	0	89	0	0	0	59	0	3	0	13	0
70	0	0	27	0	0	0	50	0	1	0	50	0
71	0	0	5	0	0	0	65	0	0	0	97	0
72	0	0	27	0	1	0	58	0	0	0	87	0
73	0	0	56	0	1	0	53	0	1	0	29	0
74	0	0	42	0	1	0	95	0	1	0	12	0
75	2	0	38	0	0	0	8	0	0	0	44	0
76	1	0	67	0	0	0	38	0	0	0	80	0

3010-G70Y	RED				GREEN				BLUE			
	Measured	Theoretica	Noise	Pure	Measured	Theoretica	Noise	Pure	Measured	Theoretica	Noise	Pure
77	0	0	38	0	1	0	53	0	0	0	77	0
78	0	0	88	0	1	0	71	0	0	0	70	0
79	0	0	23	0	0	0	82	0	0	0	55	0
80	1	0	70	0	1	0	95	0	2	0	75	0
81	0	0	53	0	2	0	19	0	2	0	12	0
82	0	0	83	0	0	0	93	0	0	0	60	0
83	0	0	49	0	1	0	73	0	0	0	18	0
84	0	0	3	0	0	0	52	0	0	0	19	0
85	1	0	74	0	0	0	88	0	1	0	50	0
86	1	0	87	0	0	0	28	0	0	0	91	0
87	0	0	80	0	0	0	74	0	2	0	3	0
88	0	0	54	0	0	0	39	0	1	0	44	0
89	0	0	84	0	0	0	76	0	4	0	31	0
90	0	0	93	0	0	0	77	0	0	0	30	0
91	1	0	0	0	0	0	27	0	0	0	86	0
92	2	0	8	0	0	0	46	0	0	0	1	0
93	1	0	71	0	0	0	81	0	0	0	88	0
94	0	0	38	0	0	0	57	0	1	0	47	0
95	0	0	82	0	1	0	26	0	0	0	95	0
96	0	0	19	0	0	0	97	0	1	0	46	0
97	0	0	93	0	0	0	85	0	0	0	9	0
98	1	0	66	0	0	0	97	0	1	0	41	0
99	1	0	31	0	0	0	26	0	1	0	52	0
100	0	0	86	0	0	0	44	0	1	0	98	0
101	2	0	54	0	2	0	3	0	1	0	90	0
102	3	0	70	0	1	0	7	0	0	0	70	0
103	1	0	24	0	1	0	80	0	1	0	12	0
104	0	0	33	0	1	0	60	0	0	0	68	0
105	0	0	14	0	2	0	36	0	2	0	30	0
106	0	0	97	0	0	0	2	0	0	0	26	0
107	1	0	4	0	0	0	45	0	2	0	59	0
108	0	0	33	0	0	0	14	0	0	0	16	0
109	0	0	25	0	0	0	4	0	0	0	1	0
110	1	0	45	0	0	0	2	0	2	0	54	0
111	0	0	10	0	0	0	50	0	0	0	30	0
112	1	0	12	0	0	0	35	0	1	0	87	0
113	2	0	92	0	1	0	87	0	2	0	51	0
114	0	0	72	0	0	0	21	0	1	0	13	0
115	1	0	64	0	1	0	98	0	0	0	13	0
116	0	0	77	0	2	0	75	0	1	0	45	0
117	1	0	82	0	0	0	52	0	1	0	52	0
118	0	0	60	0	1	0	24	0	0	0	68	0
119	1	0	22	0	0	0	91	0	1	0	89	0
120	0	0	91	0	0	0	63	0	0	0	63	0
121	0	0	97	0	0	0	68	0	1	0	12	0
122	0	0	33	0	0	0	38	0	0	0	66	0
123	0	0	75	0	1	0	91	0	1	0	27	0
124	1	0	14	0	0	0	77	0	2	0	7	0
125	1	0	67	0	1	0	78	0	2	0	82	0
126	2	0	48	0	2	0	41	0	2	0	70	0
127	1	0	66	0	0	0	16	0	1	0	59	0
128	0	0	81	0	0	0	37	0	3	0	41	0
129	0	0	54	0	0	0	85	0	2	0	53	0
130	1	0	0	0	2	0	82	0	2	0	54	0
131	0	0	31	0	0	0	0	0	1	0	99	0
132	4	0	54	0	1	0	9	0	1	0	66	0
133	0	0	28	0	0	0	1	0	1	0	56	0
134	1	0	38	0	2	0	63	0	2	0	90	0
135	0	0	90	0	1	0	12	0	2	0	61	0
136	1	0	92	0	2	0	63	0	0	0	55	0
137	0	0	67	0	1	0	7	0	2	0	17	0
138	1	0	25	0	3	0	4	0	1	0	42	0
139	0	0	68	0	1	0	53	0	2	0	78	0
140	0	0	23	0	2	0	91	0	5	0	83	0
141	0	0	79	0	2	0	75	0	2	0	40	0
142	1	0	23	0	5	0	3	0	5	0	78	0
143	0	0	36	0	4	0	16	0	13	0	56	0
144	1	0	31	0	10	0	4	0	16	0	57	0
145	2	0	5	0	3	0	24	0	30	0	59	0
146	0	0	74	0	10	0	23	0	51	0	92	0
147	0	0	20	0	10	0	60	0	60	0	48	0
148	3	0	61	0	7	0	68	0	119	0	34	0
149	0	0	25	0	8	0	85	0	185	0	64	0
150	2	0	62	0	6	0	9	0	274	0	88	0
151	1	0	90	0	11	0	20	0	370	0	22	0
152	2	0	81	0	7	0	80	0	558	0	42	0
153	2	0	9	0	8	0	21	0	843	0	82	0

3010-G70Y	RED				GREEN				BLUE			
	Measured	Theoretica	Noise	Pure	Measured	Theoretica	Noise	Pure	Measured	Theoretica	Noise	Pure
154	1	0	56	0	19	0	68	0	1304	0	84	0
155	1	0	28	0	12	0	69	0	1469	0	98	0
156	4	0	8	0	11	0	68	0	2384	78	50	0
157	6	0	62	0	8	0	25	0	2831	166	50	0
158	5	0	69	0	7	0	62	0	4294	333	16	0
159	17	0	86	0	8	0	18	0	5262	631	81	0
160	12	0	76	0	11	0	54	0	7353	1130	89	0
161	25	0	41	0	10	0	35	0	8250	1913	74	0
162	26	0	83	0	14	0	86	0	10335	3066	35	0
163	36	0	13	0	13	0	17	0	11030	4648	85	0
164	38	0	58	0	24	0	5	0	12866	6665	95	0
165	43	0	25	0	11	0	28	0	15220	9043	10	0
166	84	0	42	0	14	0	46	0	16549	11607	67	0
167	92	0	40	0	17	0	81	0	17363	14093	45	0
168	97	0	71	0	15	0	22	0	17519	16189	84	0
169	125	0	19	0	12	0	90	0	17272	17594	22	0
170	171	0	28	0	19	0	51	0	18089	18089	249338	261632
171	222	0	88	0	14	0	34	0	15419	17594	78	0
172	277	0	42	0	11	0	83	0	13915	16189	66	0
173	317	0	96	0	19	0	74	0	12255	14093	79	0
174	426	0	18	0	16	0	53	0	11369	11607	58	0
175	438	0	46	0	30	0	22	0	6940	9043	4	0
176	559	0	62	0	32	0	65	0	6038	6665	22	0
177	704	0	34	0	37	0	91	0	4818	4648	45	0
178	921	0	55	0	67	0	93	0	3648	3066	6	0
179	1017	0	7	0	80	0	50	0	2342	1913	0	0
180	1114	0	44	0	136	0	82	0	1413	1130	47	0
181	1533	0	73	0	182	0	65	0	703	631	22	0
182	1434	0	48	0	227	0	21	0	441	333	81	0
183	1856	0	21	0	299	0	18	0	255	166	90	0
184	2132	0	82	0	436	0	49	0	167	78	14	0
185	2441	79	1	0	494	0	10	0	82	0	58	0
186	2993	133	94	0	664	0	38	0	42	0	10	0
187	3623	219	0	0	813	0	40	0	19	0	91	0
188	4318	349	36	0	1045	0	29	0	8	0	65	0
189	4840	541	5	0	1160	98	70	0	4	0	0	0
190	5430	816	78	0	1741	166	80	0	2	0	82	0
191	5653	1196	62	0	1927	273	63	0	7	0	87	0
192	7195	1704	18	0	2705	435	71	0	1	0	68	0
193	7679	2359	53	0	2601	675	87	0	0	0	31	0
194	8550	3176	47	0	3796	1018	33	0	2	0	15	0
195	8971	4155	9	0	3860	1492	63	0	1	0	36	0
196	9741	5285	30	0	5305	2126	61	0	0	0	65	0
197	9610	6535	69	0	5284	2943	4	0	0	0	34	0
198	11510	7854	81	0	7311	3962	77	0	0	0	42	0
199	11849	9177	85	0	6226	5184	60	0	0	0	45	0
200	12537	10423	42	0	9658	6594	84	0	0	0	56	0
201	12126	11509	33	0	8480	8153	83	0	0	0	23	0
202	11301	12352	16	0	10995	9799	13	0	0	0	87	0
203	12282	12888	18	0	9661	11449	20	0	0	0	77	0
204	13072	13072	249845	261632	13629	13004	60	0	0	0	28	0
205	11829	12888	57	0	11435	14358	93	0	0	0	88	0
206	11360	12352	33	0	14899	15410	82	0	0	0	69	0
207	9873	11509	51	0	12773	16078	22	0	0	0	14	0
208	9138	10423	50	0	16308	16308	249455	261632	0	0	37	0
209	7850	9177	29	0	13203	16078	40	0	0	0	89	0
210	6775	7854	97	0	16254	15410	86	0	0	0	43	0
211	5053	6535	11	0	12418	14358	23	0	0	0	21	0
212	3984	5285	79	0	13750	13004	64	0	0	0	97	0
213	2662	4155	72	0	10350	11449	53	0	0	0	85	0
214	1634	3176	92	0	9659	9799	76	0	0	0	49	0
215	1057	2359	31	0	6500	8153	64	0	0	0	38	0
216	646	1704	1	0	6221	6594	2	0	0	0	91	0
217	285	1196	49	0	3185	5184	6	0	0	0	55	0
218	143	816	26	0	2788	3962	61	0	0	0	42	0
219	51	541	59	0	1323	2943	39	0	0	0	9	0
220	18	349	77	0	858	2126	91	0	0	0	87	0
221	7	219	80	0	391	1492	46	0	0	0	64	0
222	5	133	99	0	188	1018	61	0	0	0	92	0
223	1	79	65	0	60	675	63	0	0	0	99	0
224	0	0	75	0	26	435	36	0	0	0	60	0
225	0	0	67	0	8	273	67	0	0	0	8	0
226	0	0	65	0	4	166	15	0	0	0	77	0
227	0	0	44	0	0	98	40	0	0	0	75	0
228	0	0	91	0	1	0	32	0	0	0	54	0
229	0	0	20	0	0	0	79	0	0	0	75	0
230	0	0	38	0	0	0	68	0	0	0	12	0

3020-B70G	RED				GREEN				BLUE			
	Measured	Theoretica	Noise	Pure	Measured	Theoretica	Noise	Pure	Measured	Theoretica	Noise	Pure
0	5528	0	40	0	9661	0	21	0	10724	0	65	0
1	5207	0	38	0	1048	0	87	0	7	0	12	0
2	4	0	98	0	11	0	22	0	7	0	64	0
3	3	0	51	0	3	0	28	0	6	0	38	0
4	4	0	42	0	1	0	7	0	8	0	2	0
5	6	0	12	0	3	0	26	0	2	0	91	0
6	5	0	71	0	2	0	41	0	4	0	3	0
7	6	0	99	0	2	0	6	0	6	0	39	0
8	3	0	33	0	1	0	25	0	6	0	93	0
9	4	0	0	0	0	0	22	0	1	0	36	0
10	4	0	5	0	1	0	74	0	4	0	48	0
11	1	0	86	0	1	0	46	0	3	0	92	0
12	0	0	71	0	4	0	93	0	3	0	58	0
13	2	0	91	0	2	0	88	0	6	0	9	0
14	4	0	48	0	1	0	54	0	6	0	18	0
15	1	0	75	0	4	0	87	0	4	0	57	0
16	7	0	33	0	1	0	58	0	10	0	2	0
17	4	0	2	0	2	0	16	0	5	0	37	0
18	9	0	43	0	1	0	84	0	4	0	26	0
19	9	0	63	0	1	0	39	0	3	0	63	0
20	4	0	80	0	2	0	36	0	5	0	50	0
21	5	0	76	0	1	0	86	0	3	0	93	0
22	3	0	79	0	1	0	67	0	4	0	60	0
23	3	0	14	0	1	0	24	0	1	0	89	0
24	2	0	45	0	3	0	5	0	8	0	46	0
25	5	0	97	0	1	0	17	0	3	0	64	0
26	3	0	3	0	4	0	90	0	7	0	2	0
27	1	0	18	0	3	0	69	0	0	0	23	0
28	11	0	68	0	3	0	13	0	9	0	96	0
29	6	0	91	0	4	0	25	0	1	0	76	0
30	3	0	21	0	4	0	93	0	4	0	12	0
31	6	0	53	0	5	0	97	0	5	0	18	0
32	1	0	6	0	2	0	37	0	4	0	60	0
33	8	0	77	0	3	0	93	0	2	0	65	0
34	1	0	72	0	1	0	5	0	5	0	81	0
35	3	0	19	0	3	0	92	0	6	0	92	0
36	5	0	88	0	2	0	56	0	5	0	60	0
37	0	0	80	0	2	0	74	0	3	0	14	0
38	10	0	4	0	3	0	28	0	7	0	12	0
39	5	0	65	0	1	0	83	0	3	0	25	0
40	8	0	20	0	2	0	32	0	3	0	27	0
41	1	0	54	0	2	0	33	0	5	0	84	0
42	6	0	91	0	2	0	54	0	4	0	76	0
43	5	0	87	0	4	0	25	0	7	0	97	0
44	1	0	4	0	8	0	4	0	2	0	88	0
45	5	0	82	0	3	0	96	0	2	0	7	0
46	4	0	97	0	3	0	35	0	1	0	21	0
47	2	0	4	0	4	0	83	0	6	0	1	0
48	3	0	45	0	6	0	0	0	6	0	24	0
49	9	0	44	0	6	0	40	0	5	0	71	0
50	5	0	15	0	2	0	86	0	8	0	21	0
51	2	0	71	0	2	0	13	0	8	0	13	0
52	5	0	33	0	1	0	35	0	5	0	83	0
53	6	0	90	0	3	0	69	0	3	0	33	0
54	6	0	97	0	4	0	42	0	3	0	42	0
55	5	0	83	0	1	0	74	0	9	0	19	0
56	9	0	48	0	0	0	12	0	12	0	92	0
57	4	0	52	0	2	0	61	0	3	0	82	0
58	2	0	82	0	2	0	40	0	9	0	87	0
59	10	0	4	0	2	0	0	0	6	0	6	0
60	14	0	42	0	3	0	57	0	19	0	4	0
61	4	0	70	0	6	0	23	0	9	0	28	0
62	14	0	85	0	3	0	54	0	13	0	20	0
63	1	0	91	0	1	0	41	0	5	0	69	0
64	11	0	49	0	4	0	24	0	2	0	90	0
65	17	0	50	0	4	0	38	0	13	0	22	0
66	5	0	96	0	0	0	78	0	4	0	82	0
67	8	0	45	0	4	0	21	0	10	0	41	0
68	5	0	44	0	2	0	41	0	3	0	84	0
69	8	0	75	0	0	0	87	0	4	0	69	0
70	6	0	11	0	5	0	47	0	16	0	35	0
71	13	0	50	0	2	0	23	0	7	0	29	0
72	4	0	25	0	2	0	98	0	12	0	52	0
73	14	0	92	0	3	0	82	0	15	0	22	0
74	15	0	54	0	2	0	94	0	4	0	69	0
75	3	0	85	0	2	0	81	0	6	0	26	0
76	7	0	31	0	6	0	37	0	2	0	32	0

3020-B70C	RED				GREEN				BLUE			
	Measured	Theoretica	Noise	Pure	Measured	Theoretica	Noise	Pure	Measured	Theoretica	Noise	Pure
77	3	0	96	0	5	0	5	0	11	0	19	0
78	0	0	42	0	2	0	34	0	7	0	27	0
79	6	0	27	0	1	0	87	0	0	0	40	0
80	10	0	23	0	4	0	82	0	4	0	45	0
81	5	0	30	0	3	0	92	0	1	0	14	0
82	5	0	87	0	1	0	87	0	6	0	80	0
83	3	0	39	0	3	0	71	0	5	0	73	0
84	2	0	30	0	7	0	3	0	7	0	89	0
85	3	0	31	0	1	0	68	0	7	0	76	0
86	10	0	9	0	6	0	27	0	4	0	2	0
87	2	0	17	0	2	0	97	0	6	0	80	0
88	1	0	28	0	2	0	24	0	6	0	10	0
89	5	0	43	0	0	0	95	0	1	0	84	0
90	1	0	42	0	4	0	58	0	2	0	94	0
91	12	0	75	0	0	0	8	0	0	0	39	0
92	5	0	50	0	7	0	55	0	3	0	75	0
93	5	0	94	0	5	0	43	0	5	0	33	0
94	2	0	82	0	4	0	82	0	1	0	72	0
95	2	0	89	0	6	0	51	0	1	0	17	0
96	0	0	29	0	1	0	78	0	1	0	66	0
97	2	0	6	0	7	0	73	0	1	0	22	0
98	4	0	3	0	3	0	70	0	0	0	44	0
99	0	0	3	0	3	0	15	0	2	0	35	0
100	2	0	48	0	7	0	36	0	3	0	37	0
101	2	0	62	0	2	0	68	0	3	0	0	0
102	5	0	24	0	11	0	83	0	4	0	80	0
103	6	0	68	0	10	0	4	0	8	0	12	0
104	12	0	56	0	8	0	26	0	12	0	28	0
105	16	0	88	0	8	0	48	0	20	0	89	0
106	20	0	28	0	11	0	15	0	20	0	72	0
107	33	0	92	0	5	0	84	0	36	0	34	0
108	50	0	50	0	18	0	94	0	51	0	2	0
109	61	0	90	0	8	0	45	0	91	0	10	0
110	100	0	81	0	0	0	26	0	122	0	61	0
111	131	0	6	0	13	0	92	0	143	0	99	0
112	185	0	37	0	8	0	95	0	173	0	21	0
113	210	0	74	0	11	0	63	0	216	0	93	0
114	269	0	37	0	13	0	44	0	322	0	92	0
115	331	0	69	0	18	0	31	0	390	0	57	0
116	468	0	43	0	13	0	3	0	527	0	57	0
117	618	0	62	0	21	0	67	0	726	0	42	0
118	712	0	2	0	14	0	25	0	975	0	88	0
119	870	0	36	0	14	0	2	0	1165	146	14	0
120	998	0	26	0	17	0	66	0	1554	266	42	0
121	1406	0	35	0	21	0	5	0	1950	466	82	0
122	1546	0	94	0	33	0	68	0	2432	783	31	0
123	2345	132	34	0	25	0	23	0	3076	1268	58	0
124	2419	241	40	0	33	0	44	0	4086	1975	24	0
125	3216	421	23	0	75	0	79	0	4822	2960	89	0
126	3569	708	37	0	59	0	92	0	5990	4267	86	0
127	4042	1147	48	0	74	0	29	0	7997	5920	18	0
128	5405	1786	54	0	99	0	70	0	7970	7903	64	0
129	5920	2677	48	0	130	0	89	0	11147	10151	39	0
130	6519	3859	10	0	118	0	36	0	11418	12547	83	0
131	7787	5354	3	0	157	0	78	0	13926	14921	98	0
132	8798	7148	95	0	150	0	38	0	13652	17074	5	0
133	10352	9181	99	0	227	0	6	0	18298	18800	30	0
134	10902	11347	23	0	236	0	39	0	15360	19918	66	0
135	11903	13495	84	0	311	0	64	0	20306	20306	249713	261632
136	14159	15442	22	0	386	0	78	0	16629	19918	39	0
137	15623	17003	94	0	478	0	0	0	16904	18800	24	0
138	16207	18014	12	0	656	0	10	0	15991	17074	30	0
139	18365	18364	249749	261632	680	0	32	0	14408	14921	10	0
140	16027	18014	37	0	953	0	23	0	11156	12547	16	0
141	17601	17003	54	0	1055	0	10	0	8957	10151	77	0
142	15977	15442	71	0	1367	0	1	0	6330	7903	9	0
143	12629	13495	93	0	1572	0	47	0	4900	5920	23	0
144	10168	11347	87	0	1907	138	70	0	2763	4267	47	0
145	9101	9181	0	0	2398	251	86	0	1639	2960	93	0
146	5979	7148	31	0	2941	440	27	0	923	1975	50	0
147	3354	5354	36	0	3040	740	58	0	465	1268	63	0
148	2103	3859	56	0	3474	1198	81	0	200	783	65	0
149	1024	2677	86	0	4625	1865	92	0	89	466	40	0
150	521	1786	14	0	4569	2795	70	0	30	266	10	0
151	205	1147	53	0	5319	4031	14	0	11	146	16	0
152	83	708	50	0	6134	5592	26	0	4	0	73	0
153	30	421	65	0	7849	7465	35	0	2	0	56	0

3020-B70C	RED				GREEN				BLUE			
	Measured	Theoretica	Noise	Pure	Measured	Theoretica	Noise	Pure	Measured	Theoretica	Noise	Pure
154	9	241	80	0	9094	9588	28	0	0	0	35	0
155	5	132	65	0	10686	11851	10	0	2	0	1	0
156	0	0	36	0	11692	14094	96	0	0	0	23	0
157	0	0	92	0	15250	16127	30	0	1	0	61	0
158	1	0	61	0	15225	17758	30	0	1	0	14	0
159	1	0	15	0	17584	18814	25	0	0	0	3	0
160	0	0	46	0	19180	19180	249457	261632	0	0	15	0
161	0	0	84	0	19178	18814	0	0	0	0	41	0
162	0	0	17	0	18354	17758	44	0	0	0	37	0
163	1	0	96	0	17379	16127	8	0	0	0	43	0
164	0	0	50	0	14050	14094	10	0	0	0	66	0
165	0	0	80	0	11122	11851	76	0	0	0	74	0
166	0	0	83	0	8187	9588	4	0	0	0	1	0
167	0	0	88	0	5597	7465	67	0	0	0	66	0
168	0	0	6	0	3266	5592	6	0	0	0	50	0
169	0	0	95	0	1903	4031	38	0	0	0	11	0
170	0	0	40	0	882	2795	21	0	0	0	99	0
171	0	0	1	0	381	1865	67	0	0	0	98	0
172	0	0	19	0	165	1198	58	0	0	0	86	0
173	0	0	87	0	54	740	64	0	0	0	30	0
174	0	0	36	0	21	440	69	0	0	0	45	0
175	0	0	43	0	9	251	15	0	0	0	36	0
176	0	0	10	0	4	138	31	0	0	0	51	0
177	0	0	96	0	0	0	15	0	0	0	5	0
178	0	0	65	0	0	0	41	0	0	0	95	0
179	0	0	88	0	2	0	50	0	0	0	31	0
180	0	0	29	0	0	0	16	0	0	0	97	0
181	0	0	36	0	0	0	22	0	0	0	70	0
182	0	0	66	0	1	0	2	0	0	0	78	0
183	0	0	50	0	0	0	30	0	0	0	74	0
184	0	0	6	0	1	0	2	0	0	0	78	0
185	0	0	46	0	0	0	44	0	0	0	16	0
186	0	0	85	0	0	0	95	0	0	0	91	0
187	0	0	49	0	0	0	35	0	0	0	82	0
188	0	0	30	0	0	0	4	0	0	0	87	0
189	0	0	61	0	0	0	19	0	0	0	22	0
190	0	0	0	0	0	0	2	0	0	0	90	0
191	0	0	72	0	0	0	98	0	0	0	45	0
192	0	0	63	0	0	0	52	0	0	0	27	0
193	0	0	83	0	0	0	6	0	0	0	47	0
194	0	0	1	0	0	0	74	0	0	0	52	0
195	0	0	19	0	0	0	88	0	0	0	9	0
196	0	0	50	0	0	0	9	0	0	0	26	0
197	0	0	60	0	0	0	70	0	0	0	99	0
198	0	0	1	0	0	0	0	0	0	0	53	0
199	0	0	38	0	0	0	86	0	0	0	40	0
200	0	0	26	0	0	0	70	0	0	0	70	0
201	0	0	29	0	0	0	57	0	0	0	25	0
202	0	0	32	0	0	0	73	0	0	0	51	0
203	0	0	54	0	0	0	5	0	0	0	34	0
204	0	0	69	0	0	0	51	0	0	0	5	0
205	0	0	26	0	0	0	39	0	0	0	63	0
206	0	0	37	0	0	0	2	0	0	0	8	0
207	0	0	41	0	0	0	24	0	0	0	84	0
208	0	0	13	0	0	0	30	0	0	0	46	0
209	0	0	69	0	0	0	97	0	0	0	7	0
210	0	0	94	0	0	0	25	0	0	0	65	0
211	0	0	63	0	0	0	11	0	0	0	79	0
212	0	0	39	0	0	0	85	0	0	0	89	0
213	0	0	9	0	0	0	14	0	0	0	78	0
214	0	0	5	0	0	0	70	0	0	0	92	0
215	0	0	34	0	0	0	5	0	0	0	10	0
216	0	0	86	0	0	0	34	0	0	0	21	0
217	0	0	86	0	0	0	9	0	0	0	61	0
218	0	0	41	0	0	0	15	0	0	0	39	0
219	0	0	11	0	0	0	75	0	0	0	83	0
220	0	0	46	0	0	0	46	0	0	0	61	0
221	0	0	54	0	0	0	60	0	0	0	63	0
222	0	0	42	0	0	0	20	0	0	0	49	0
223	0	0	38	0	0	0	90	0	0	0	87	0
224	0	0	24	0	0	0	42	0	0	0	41	0
225	0	0	51	0	0	0	63	0	0	0	35	0
226	0	0	47	0	0	0	31	0	0	0	19	0
227	0	0	82	0	0	0	41	0	0	0	19	0
228	0	0	89	0	0	0	21	0	0	0	17	0
229	0	0	49	0	0	0	74	0	0	0	29	0
230	0	0	50	0	0	0	51	0	0	0	68	0

3020-B70G	RED				GREEN				BLUE			
	Measured	Theoretica	Noise	Pure	Measured	Theoretica	Noise	Pure	Measured	Theoretica	Noise	Pure
231	0	0	99	0	0	0	0	0	0	0	2	0
232	0	0	61	0	0	0	43	0	0	0	96	0
233	0	0	9	0	0	0	70	0	0	0	66	0
234	0	0	56	0	0	0	53	0	0	0	58	0
235	0	0	49	0	0	0	0	0	0	0	55	0
236	0	0	90	0	0	0	19	0	0	0	96	0
237	0	0	19	0	0	0	0	0	0	0	2	0
238	0	0	28	0	0	0	65	0	0	0	76	0
239	0	0	80	0	0	0	10	0	0	0	65	0
240	0	0	59	0	0	0	59	0	0	0	30	0
241	0	0	39	0	0	0	15	0	0	0	39	0
242	0	0	36	0	0	0	85	0	0	0	92	0
243	0	0	82	0	0	0	7	0	0	0	7	0
244	0	0	42	0	0	0	18	0	0	0	76	0
245	0	0	95	0	0	0	85	0	0	0	88	0
246	0	0	45	0	0	0	62	0	0	0	37	0
247	0	0	46	0	0	0	18	0	0	0	61	0
248	0	0	12	0	0	0	62	0	0	0	81	0
249	0	0	48	0	0	0	65	0	0	0	22	0
250	0	0	9	0	0	0	38	0	0	0	68	0
251	0	0	81	0	0	0	85	0	0	0	13	0
252	0	0	23	0	0	0	94	0	0	0	5	0
253	0	0	31	0	0	0	33	0	0	0	99	0
254	0	0	54	0	0	0	8	0	0	0	98	0
255	0	0	. 0	0	0	0	62	0	0	0	67	0
mode:	139				160				135			
mean:	130.9675				151.357777				127.9892			
std dev:	5.095541				5.095541				5.095541			
Correlation:		0.970023	0.332842	0.332822		0.970413	0.334148	0.334374		0.970252	0.352688	0.352778

3030-Y90R	RED				GREEN				BLUE			
	Measured	Theoretica	Noise	Pure	Measured	Theoretica	Noise	Pure	Measured	Theoretica	Noise	Pure
0	5435	0	69	0	9388	0	19	0	10620	0	67	0
1	5203	0	71	0	1267	0	1	0	16	0	29	0
2	8	0	38	0	2	0	20	0	6	0	39	0
3	11	0	40	0	8	0	8	0	5	0	87	0
4	11	0	27	0	5	0	73	0	3	0	26	0
5	6	0	26	0	0	0	46	0	3	0	93	0
6	2	0	62	0	4	0	74	0	6	0	90	0
7	1	0	76	0	2	0	4	0	5	0	20	0
8	2	0	42	0	5	0	68	0	4	0	98	0
9	2	0	78	0	2	0	78	0	5	0	50	0
10	3	0	87	0	3	0	30	0	7	0	11	0
11	2	0	13	0	1	0	54	0	3	0	11	0
12	1	0	20	0	3	0	46	0	2	0	66	0
13	2	0	84	0	4	0	76	0	1	0	81	0
14	5	0	28	0	4	0	26	0	2	0	36	0
15	2	0	55	0	0	0	48	0	3	0	40	0
16	0	0	50	0	1	0	15	0	4	0	61	0
17	3	0	7	0	1	0	81	0	7	0	11	0
18	0	0	92	0	1	0	74	0	1	0	43	0
19	1	0	87	0	4	0	10	0	5	0	9	0
20	4	0	17	0	2	0	54	0	4	0	91	0
21	7	0	39	0	3	0	84	0	3	0	73	0
22	1	0	14	0	2	0	45	0	3	0	60	0
23	2	0	98	0	3	0	52	0	2	0	19	0
24	4	0	69	0	0	0	26	0	2	0	21	0
25	5	0	44	0	2	0	68	0	4	0	87	0
26	2	0	30	0	0	0	35	0	3	0	29	0
27	3	0	90	0	2	0	9	0	1	0	75	0
28	5	0	42	0	1	0	24	0	4	0	60	0
29	3	0	46	0	0	0	30	0	1	0	16	0
30	2	0	85	0	0	0	68	0	3	0	55	0
31	2	0	24	0	1	0	52	0	3	0	6	0
32	1	0	45	0	0	0	3	0	3	0	58	0
33	4	0	13	0	1	0	1	0	3	0	93	0
34	1	0	12	0	1	0	60	0	2	0	21	0
35	2	0	78	0	1	0	89	0	2	0	8	0
36	3	0	17	0	2	0	64	0	1	0	9	0
37	0	0	33	0	3	0	83	0	2	0	69	0
38	2	0	47	0	1	0	34	0	2	0	52	0
39	4	0	34	0	0	0	11	0	3	0	27	0
40	2	0	66	0	0	0	30	0	3	0	20	0
41	1	0	92	0	1	0	1	0	3	0	75	0
42	1	0	93	0	1	0	17	0	3	0	24	0
43	4	0	77	0	1	0	54	0	0	0	68	0
44	2	0	45	0	1	0	22	0	2	0	70	0
45	2	0	46	0	3	0	7	0	2	0	54	0
46	4	0	51	0	4	0	7	0	1	0	46	0
47	1	0	44	0	2	0	57	0	2	0	23	0
48	2	0	67	0	1	0	20	0	5	0	54	0
49	1	0	55	0	4	0	98	0	3	0	78	0
50	1	0	23	0	1	0	81	0	2	0	47	0
51	4	0	42	0	0	0	69	0	4	0	77	0
52	1	0	74	0	6	0	81	0	1	0	13	0
53	2	0	31	0	1	0	87	0	2	0	23	0
54	3	0	65	0	2	0	57	0	3	0	98	0
55	1	0	58	0	1	0	39	0	1	0	24	0
56	2	0	18	0	1	0	89	0	1	0	72	0
57	2	0	36	0	3	0	89	0	4	0	64	0
58	1	0	88	0	0	0	43	0	3	0	70	0
59	1	0	76	0	2	0	17	0	1	0	65	0
60	2	0	15	0	2	0	94	0	2	0	60	0
61	3	0	83	0	2	0	89	0	2	0	76	0
62	0	0	9	0	0	0	68	0	2	0	70	0
63	1	0	46	0	0	0	20	0	1	0	2	0
64	0	0	68	0	3	0	96	0	0	0	91	0
65	3	0	48	0	1	0	27	0	2	0	50	0
66	1	0	69	0	2	0	58	0	0	0	4	0
67	2	0	21	0	0	0	29	0	0	0	25	0
68	1	0	43	0	2	0	50	0	1	0	86	0
69	0	0	74	0	0	0	79	0	3	0	32	0
70	1	0	31	0	1	0	21	0	1	0	49	0
71	1	0	28	0	2	0	61	0	2	0	63	0
72	2	0	38	0	2	0	29	0	3	0	96	0
73	1	0	51	0	1	0	2	0	1	0	39	0
74	2	0	78	0	1	0	97	0	0	0	62	0
75	0	0	11	0	1	0	18	0	4	0	92	0
76	0	0	40	0	4	0	91	0	1	0	48	0

3030-Y90R	RED				GREEN				BLUE			
	Measured	Theoretica	Noise	Pure	Measured	Theoretica	Noise	Pure	Measured	Theoretica	Noise	Pure
77	1	0	28	0	0	0	3	0	0	0	50	0
78	1	0	36	0	2	0	3	0	3	0	3	0
79	2	0	4	0	2	0	50	0	1	0	5	0
80	0	0	10	0	2	0	54	0	2	0	93	0
81	1	0	99	0	2	0	21	0	3	0	51	0
82	1	0	30	0	0	0	39	0	3	0	58	0
83	0	0	6	0	3	0	84	0	6	0	4	0
84	1	0	17	0	1	0	59	0	2	0	74	0
85	0	0	74	0	3	0	78	0	2	0	79	0
86	3	0	76	0	1	0	60	0	0	0	46	0
87	2	0	41	0	4	0	48	0	1	0	47	0
88	1	0	94	0	2	0	46	0	2	0	66	0
89	1	0	50	0	0	0	13	0	5	0	5	0
90	1	0	51	0	0	0	60	0	3	0	54	0
91	3	0	54	0	3	0	93	0	14	0	17	0
92	4	0	70	0	2	0	63	0	16	0	97	0
93	4	0	63	0	1	0	53	0	21	0	73	0
94	1	0	13	0	3	0	40	0	40	0	13	0
95	0	0	99	0	1	0	75	0	72	0	36	0
96	0	0	89	0	1	0	56	0	100	0	9	0
97	2	0	95	0	1	0	39	0	196	0	35	0
98	3	0	92	0	1	0	94	0	254	0	54	0
99	1	0	61	0	0	0	26	0	357	0	85	0
100	1	0	82	0	1	0	31	0	547	0	83	0
101	4	0	20	0	1	0	46	0	745	135	19	0
102	6	0	18	0	1	0	22	0	1131	246	62	0
103	2	0	89	0	5	0	11	0	1392	430	37	0
104	6	0	86	0	0	0	21	0	2080	724	15	0
105	13	0	3	0	2	0	51	0	2706	1172	74	0
106	21	0	76	0	0	0	3	0	3558	1825	20	0
107	22	0	65	0	0	0	64	0	4770	2735	83	0
108	32	0	77	0	4	0	87	0	5770	3943	5	0
109	34	0	81	0	2	0	36	0	7227	5470	96	0
110	48	0	44	0	2	0	24	0	9569	7303	90	0
111	67	0	4	0	4	0	39	0	11367	9380	79	0
112	91	0	50	0	16	0	87	0	12473	11593	86	0
113	131	0	12	0	19	0	48	0	14000	13787	48	0
114	131	0	62	0	40	0	76	0	17056	15777	45	0
115	210	0	25	0	47	0	31	0	16367	17371	14	0
116	283	0	96	0	83	0	83	0	17522	18405	36	0
117	379	0	9	0	168	0	86	0	18763	18762	249453	261632
118	471	0	68	0	185	0	80	0	17897	18405	35	0
119	528	0	61	0	296	0	60	0	16052	17371	79	0
120	576	0	71	0	385	0	75	0	15713	15777	6	0
121	780	0	32	0	542	0	10	0	12916	13787	86	0
122	854	0	65	0	716	0	87	0	10607	11593	11	0
123	1213	0	50	0	1013	0	59	0	8768	9380	70	0
124	1168	0	61	0	1257	144	89	0	6764	7303	72	0
125	1514	0	60	0	1836	262	38	0	4717	5470	18	0
126	1744	0	13	0	2013	459	41	0	3367	3943	68	0
127	2063	0	51	0	2593	772	88	0	2375	2735	2	0
128	2727	0	27	0	3172	1250	9	0	1308	1825	7	0
129	3164	0	50	0	4442	1947	19	0	933	1172	80	0
130	3555	0	38	0	4799	2917	66	0	474	724	9	0
131	4244	75	38	0	6623	4206	11	0	271	430	25	0
132	5068	158	1	0	7147	5835	83	0	115	246	64	0
133	5957	317	93	0	9456	7789	7	0	73	135	83	0
134	6527	601	93	0	10498	10005	18	0	28	0	42	0
135	7255	1076	40	0	12006	12366	26	0	32	0	41	0
136	8742	1822	92	0	13786	14706	19	0	14	0	7	0
137	9700	2920	67	0	14310	16829	86	0	4	0	48	0
138	10690	4427	63	0	17809	18530	74	0	6	0	20	0
139	12552	6348	38	0	17014	19632	85	0	8	0	48	0
140	11546	8613	35	0	20014	20014	249589	261632	3	0	59	0
141	14682	11054	92	0	17998	19632	29	0	5	0	33	0
142	15524	13422	3	0	17845	18530	65	0	8	0	37	0
143	14584	15419	91	0	15698	16829	96	0	7	0	27	0
144	14417	16756	33	0	13005	14706	16	0	12	0	0	0
145	17228	17228	249437	261632	11651	12366	84	0	7	0	4	0
146	15425	16756	53	0	8612	10005	90	0	10	0	38	0
147	13529	15419	62	0	5368	7789	91	0	11	0	7	0
148	11589	13422	62	0	3571	5835	81	0	4	0	76	0
149	9315	11054	77	0	2449	4206	24	0	13	0	80	0
150	7734	8613	25	0	1064	2917	90	0	7	0	33	0
151	4860	6348	52	0	597	1947	40	0	11	0	67	0
152	3196	4427	37	0	256	1250	85	0	18	0	26	0
153	2297	2920	20	0	140	772	53	0	6	0	92	0

3030-Y90R	RED				GREEN				BLUE			
	Measured	Theoretica	Noise	Pure	Measured	Theoretica	Noise	Pure	Measured	Theoretica	Noise	Pure
154	1132	1822	6	0	34	459	79	0	12	0	39	0
155	604	1076	85	0	22	262	28	0	11	0	36	0
156	284	601	52	0	20	144	32	0	9	0	3	0
157	125	317	38	0	15	0	27	0	10	0	21	0
158	52	158	80	0	7	0	98	0	5	0	91	0
159	23	75	33	0	12	0	50	0	9	0	9	0
160	9	0	21	0	12	0	45	0	3	0	4	0
161	10	0	12	0	12	0	2	0	6	0	52	0
162	8	0	4	0	13	0	90	0	5	0	48	0
163	3	0	9	0	10	0	94	0	1	0	39	0
164	2	0	63	0	9	0	94	0	2	0	37	0
165	3	0	78	0	10	0	32	0	3	0	73	0
166	1	0	79	0	10	0	36	0	1	0	44	0
167	0	0	2	0	4	0	53	0	2	0	62	0
168	3	0	14	0	13	0	16	0	1	0	53	0
169	2	0	19	0	7	0	10	0	1	0	58	0
170	0	0	39	0	8	0	58	0	2	0	91	0
171	2	0	26	0	3	0	25	0	0	0	15	0
172	2	0	88	0	1	0	40	0	0	0	93	0
173	0	0	59	0	3	0	21	0	1	0	46	0
174	0	0	64	0	2	0	31	0	1	0	28	0
175	0	0	68	0	1	0	93	0	1	0	56	0
176	1	0	13	0	1	0	26	0	0	0	70	0
177	0	0	4	0	0	0	61	0	1	0	96	0
178	0	0	75	0	2	0	28	0	0	0	49	0
179	2	0	29	0	1	0	37	0	0	0	30	0
180	0	0	25	0	1	0	95	0	2	0	36	0
181	1	0	73	0	1	0	53	0	0	0	30	0
182	2	0	38	0	0	0	40	0	0	0	85	0
183	0	0	34	0	0	0	10	0	1	0	65	0
184	0	0	38	0	1	0	50	0	0	0	51	0
185	1	0	56	0	0	0	82	0	0	0	18	0
186	0	0	56	0	1	0	22	0	0	0	16	0
187	0	0	47	0	1	0	2	0	0	0	50	0
188	1	0	22	0	0	0	31	0	0	0	90	0
189	0	0	66	0	0	0	3	0	0	0	82	0
190	1	0	75	0	0	0	59	0	0	0	79	0
191	0	0	9	0	1	0	13	0	0	0	37	0
192	1	0	61	0	1	0	33	0	0	0	61	0
193	0	0	27	0	0	0	71	0	1	0	11	0
194	0	0	63	0	0	0	19	0	0	0	51	0
195	2	0	94	0	0	0	8	0	0	0	81	0
196	0	0	21	0	1	0	41	0	0	0	26	0
197	0	0	50	0	1	0	50	0	0	0	39	0
198	1	0	56	0	0	0	97	0	0	0	71	0
199	0	0	26	0	0	0	79	0	0	0	58	0
200	0	0	39	0	0	0	21	0	0	0	98	0
201	2	0	29	0	1	0	93	0	0	0	84	0
202	1	0	30	0	1	0	75	0	0	0	51	0
203	1	0	84	0	1	0	3	0	0	0	36	0
204	1	0	44	0	0	0	22	0	0	0	56	0
205	0	0	42	0	0	0	11	0	0	0	86	0
206	0	0	54	0	1	0	98	0	1	0	84	0
207	0	0	75	0	0	0	22	0	0	0	85	0
208	0	0	13	0	0	0	96	0	0	0	9	0
209	0	0	77	0	0	0	2	0	0	0	68	0
210	0	0	92	0	0	0	49	0	0	0	72	0
211	0	0	41	0	0	0	19	0	0	0	6	0
212	0	0	36	0	0	0	60	0	0	0	17	0
213	0	0	5	0	0	0	18	0	0	0	17	0
214	0	0	81	0	0	0	50	0	0	0	69	0
215	0	0	96	0	1	0	60	0	0	0	98	0
216	0	0	74	0	0	0	1	0	0	0	16	0
217	1	0	50	0	0	0	78	0	0	0	57	0
218	0	0	28	0	0	0	94	0	0	0	35	0
219	0	0	66	0	0	0	33	0	0	0	96	0
220	0	0	84	0	0	0	47	0	0	0	14	0
221	0	0	0	0	0	0	6	0	0	0	35	0
222	0	0	86	0	0	0	54	0	0	0	65	0
223	0	0	24	0	0	0	80	0	0	0	51	0
224	0	0	6	0	0	0	10	0	0	0	49	0
225	1	0	30	0	0	0	82	0	0	0	50	0
226	0	0	55	0	1	0	0	0	0	0	19	0
227	0	0	45	0	0	0	47	0	0	0	39	0
228	0	0	29	0	0	0	40	0	0	0	83	0
229	0	0	62	0	0	0	55	0	0	0	46	0
230	0	0	16	0	0	0	56	0	0	0	32	0

3036SY90R	RED				GREEN				BLUE			
	Measured	Theoretica	Noise	Pure	Measured	Theoretica	Noise	Pure	Measured	Theoretica	Noise	Pure
231	0	0	52	0	0	0	7	0	0	0	88	0
232	0	0	93	0	0	0	2	0	0	0	90	0
233	0	0	99	0	0	0	86	0	0	0	7	0
234	0	0	86	0	0	0	58	0	0	0	71	0
235	0	0	34	0	0	0	19	0	0	0	94	0
236	0	0	83	0	0	0	72	0	0	0	11	0
237	0	0	20	0	0	0	40	0	0	0	87	0
238	0	0	5	0	0	0	43	0	0	0	99	0
239	0	0	29	0	0	0	87	0	0	0	88	0
240	0	0	78	0	0	0	11	0	0	0	28	0
241	0	0	98	0	0	0	51	0	0	0	34	0
242	0	0	14	0	0	0	49	0	0	0	95	0
243	0	0	36	0	0	0	16	0	0	0	4	0
244	0	0	34	0	0	0	25	0	0	0	72	0
245	0	0	1	0	0	0	23	0	0	0	59	0
246	0	0	79	0	0	0	96	0	0	0	94	0
247	0	0	91	0	0	0	65	0	0	0	77	0
248	0	0	5	0	0	0	6	0	0	0	80	0
249	0	0	36	0	0	0	59	0	0	0	61	0
250	0	0	76	0	0	0	18	0	0	0	30	0
251	0	0	97	0	0	0	97	0	0	0	32	0
252	0	0	43	0	0	0	21	0	0	0	57	0
253	0	0	43	0	0	0	84	0	0	0	49	0
254	0	0	70	0	0	0	47	0	0	0	40	0
255	0	0	55	0	0	0	72	0	0	0	19	0
mode:	145				140				117			
mean:	135.0853				132.749041				111.2272			
std dev:	4.246285				5.095541				5.095541			
Correlation		0.906605	0.324793	0.324696		0.974546	0.344622	0.344521		0.975017	0.32233	0.322319

3050-G20Y	RED				GREEN				BLUE			
	Measured	Theoretica	Noise	Pure	Measured	Theoretica	Noise	Pure	Measured	Theoretica	Noise	Pure
0	5335	0	31	0	8864	0	7	0	10255	0	56	0
1	5034	0	52	0	1374	0	98	0	43	0	92	0
2	59	0	72	0	90	0	56	0	49	0	88	0
3	36	0	91	0	98	0	66	0	42	0	46	0
4	20	0	21	0	62	0	71	0	21	0	60	0
5	12	0	15	0	35	0	40	0	35	0	67	0
6	9	0	83	0	19	0	85	0	17	0	35	0
7	9	0	45	0	13	0	87	0	16	0	6	0
8	1	0	65	0	4	0	59	0	8	0	54	0
9	6	0	97	0	4	0	79	0	7	0	80	0
10	6	0	23	0	6	0	25	0	8	0	44	0
11	11	0	27	0	4	0	40	0	4	0	37	0
12	7	0	69	0	8	0	81	0	11	0	36	0
13	3	0	90	0	9	0	25	0	8	0	67	0
14	4	0	77	0	7	0	17	0	5	0	31	0
15	6	0	32	0	3	0	25	0	7	0	76	0
16	2	0	85	0	5	0	34	0	7	0	54	0
17	5	0	43	0	3	0	58	0	13	0	12	0
18	3	0	89	0	1	0	64	0	4	0	1	0
19	4	0	78	0	3	0	0	0	3	0	75	0
20	2	0	4	0	1	0	99	0	2	0	30	0
21	3	0	2	0	3	0	56	0	4	0	46	0
22	4	0	2	0	3	0	95	0	3	0	27	0
23	3	0	34	0	2	0	16	0	3	0	49	0
24	4	0	47	0	2	0	88	0	1	0	88	0
25	4	0	53	0	3	0	7	0	3	0	27	0
26	6	0	12	0	0	0	15	0	0	0	18	0
27	9	0	75	0	1	0	60	0	3	0	38	0
28	0	0	78	0	1	0	93	0	0	0	68	0
29	0	0	40	0	3	0	81	0	5	0	79	0
30	5	0	65	0	1	0	66	0	0	0	42	0
31	2	0	9	0	2	0	96	0	2	0	22	0
32	2	0	99	0	1	0	17	0	3	0	21	0
33	0	0	97	0	1	0	22	0	6	0	92	0
34	2	0	90	0	1	0	47	0	7	0	55	0
35	4	0	63	0	2	0	98	0	5	0	28	0
36	0	0	55	0	2	0	98	0	4	0	29	0
37	5	0	65	0	1	0	11	0	3	0	96	0
38	0	0	1	0	0	0	18	0	1	0	84	0
39	0	0	22	0	0	0	34	0	2	0	39	0
40	2	0	23	0	4	0	19	0	2	0	68	0
41	2	0	9	0	2	0	30	0	3	0	16	0
42	1	0	68	0	1	0	46	0	2	0	51	0
43	2	0	61	0	6	0	46	0	2	0	74	0
44	3	0	54	0	1	0	91	0	1	0	77	0
45	0	0	39	0	3	0	9	0	1	0	6	0
46	0	0	48	0	1	0	69	0	2	0	13	0
47	4	0	8	0	1	0	33	0	3	0	9	0
48	2	0	33	0	3	0	57	0	2	0	56	0
49	2	0	87	0	4	0	45	0	0	0	67	0
50	2	0	19	0	1	0	41	0	1	0	5	0
51	0	0	8	0	2	0	5	0	3	0	33	0
52	0	0	11	0	4	0	59	0	1	0	85	0
53	1	0	64	0	0	0	8	0	3	0	30	0
54	1	0	42	0	2	0	48	0	2	0	6	0
55	3	0	49	0	3	0	40	0	2	0	76	0
56	1	0	55	0	0	0	43	0	0	0	70	0
57	2	0	89	0	1	0	13	0	2	0	12	0
58	1	0	75	0	1	0	63	0	0	0	53	0
59	1	0	20	0	2	0	8	0	1	0	69	0
60	0	0	99	0	2	0	68	0	2	0	18	0
61	1	0	85	0	2	0	39	0	2	0	92	0
62	2	0	98	0	2	0	97	0	0	0	36	0
63	1	0	98	0	1	0	79	0	2	0	53	0
64	2	0	79	0	0	0	3	0	2	0	61	0
65	0	0	12	0	2	0	71	0	2	0	4	0
66	2	0	40	0	4	0	86	0	1	0	6	0
67	2	0	67	0	4	0	61	0	3	0	46	0
68	0	0	0	0	1	0	95	0	2	0	97	0
69	0	0	3	0	1	0	62	0	0	0	69	0
70	1	0	32	0	0	0	45	0	0	0	57	0
71	1	0	41	0	0	0	70	0	2	0	3	0
72	3	0	92	0	2	0	42	0	2	0	48	0
73	3	0	84	0	3	0	96	0	1	0	54	0
74	2	0	71	0	1	0	99	0	3	0	22	0
75	1	0	75	0	2	0	83	0	3	0	88	0
76	2	0	60	0	0	0	7	0	2	0	64	0

3050-C20Y	RED				GREEN				BLUE			
	Measured	Theoretica	Noise	Pure	Measured	Theoretica	Noise	Pure	Measured	Theoretica	Noise	Pure
77	3	0	94	0	0	0	71	0	2	0	76	0
78	4	0	93	0	1	0	42	0	1	0	99	0
79	0	0	98	0	3	0	29	0	3	0	85	0
80	0	0	71	0	2	0	92	0	2	0	86	0
81	1	0	22	0	2	0	9	0	3	0	76	0
82	2	0	58	0	2	0	29	0	1	0	57	0
83	0	0	13	0	1	0	61	0	0	0	46	0
84	2	0	79	0	0	0	35	0	7	0	46	0
85	5	0	81	0	1	0	39	0	2	0	81	0
86	0	0	87	0	1	0	92	0	3	0	9	0
87	1	0	15	0	1	0	85	0	5	0	45	0
88	3	0	92	0	0	0	18	0	4	0	15	0
89	2	0	42	0	1	0	41	0	1	0	60	0
90	1	0	12	0	0	0	47	0	4	0	41	0
91	2	0	76	0	2	0	88	0	8	0	25	0
92	4	0	47	0	0	0	89	0	12	0	68	0
93	5	0	71	0	0	0	45	0	19	0	84	0
94	3	0	50	0	0	0	9	0	37	0	3	0
95	4	0	43	0	1	0	47	0	53	0	14	0
96	4	0	55	0	0	0	37	0	67	0	87	0
97	5	0	4	0	1	0	67	0	122	0	65	0
98	4	0	8	0	1	0	6	0	181	0	43	0
99	11	0	53	0	0	0	36	0	254	111	65	0
100	15	0	25	0	0	0	18	0	379	188	52	0
101	17	0	97	0	2	0	19	0	579	308	3	0
102	28	0	75	0	1	0	67	0	777	492	4	0
103	37	0	5	0	0	0	7	0	1066	763	3	0
104	41	0	81	0	1	0	60	0	1549	1150	25	0
105	80	0	46	0	0	0	91	0	2034	1685	60	0
106	112	0	71	0	3	0	49	0	2509	2400	5	0
107	162	0	98	0	0	0	57	0	3555	3324	91	0
108	212	0	65	0	1	0	79	0	4348	4474	96	0
109	301	0	70	0	0	0	46	0	5452	5853	88	0
110	375	0	73	0	2	0	39	0	7250	7445	82	0
111	615	0	10	0	2	0	76	0	8749	9206	74	0
112	700	0	77	0	1	0	86	0	10049	11064	24	0
113	1001	0	2	0	1	0	7	0	11463	12928	47	0
114	1238	0	90	0	1	0	31	0	14787	14683	15	0
115	1696	123	49	0	2	0	65	0	14857	16212	28	0
116	2084	224	85	0	2	0	19	0	16090	17400	41	0
117	2795	391	96	0	0	0	20	0	18195	18155	49	0
118	3321	658	5	0	2	0	43	0	18414	18414	249433	261632
119	3957	1066	71	0	3	0	27	0	17265	18155	62	0
120	4441	1660	23	0	2	0	58	0	17756	17400	49	0
121	6051	2487	74	0	3	0	11	0	15140	16212	49	0
122	6477	3586	59	0	2	0	7	0	13203	14683	48	0
123	8911	4975	44	0	3	0	48	0	11451	12928	1	0
124	8597	6642	14	0	2	0	81	0	9848	11064	81	0
125	10936	8531	14	0	17	0	43	0	7136	9206	85	0
126	11746	10544	6	0	23	0	88	0	5203	7445	3	0
127	13008	12539	87	0	21	0	66	0	3977	5853	39	0
128	15622	14349	43	0	33	0	45	0	2322	4474	53	0
129	16155	15799	83	0	43	0	15	0	1875	3324	82	0
130	15899	16739	50	0	42	0	65	0	999	2400	83	0
131	17065	17064	249399	261632	61	0	42	0	698	1685	64	0
132	16727	16739	24	0	60	0	78	0	388	1150	76	0
133	16220	15799	67	0	86	0	16	0	281	763	16	0
134	14131	14349	74	0	95	0	73	0	123	492	31	0
135	12459	12539	74	0	92	0	12	0	123	308	64	0
136	10972	10544	9	0	144	0	18	0	74	188	45	0
137	8498	8531	70	0	139	0	49	0	42	111	2	0
138	6212	6642	32	0	175	0	13	0	37	0	21	0
139	4712	4975	3	0	199	0	5	0	26	0	35	0
140	2693	3586	65	0	271	0	28	0	12	0	87	0
141	2064	2487	63	0	267	0	48	0	14	0	3	0
142	1162	1660	47	0	283	0	76	0	12	0	78	0
143	572	1066	80	0	367	0	57	0	6	0	56	0
144	327	658	0	0	377	0	48	0	4	0	9	0
145	205	391	51	0	477	0	25	0	5	0	20	0
146	84	224	58	0	516	0	32	0	4	0	36	0
147	35	123	37	0	592	0	48	0	3	0	37	0
148	24	0	71	0	722	0	61	0	3	0	34	0
149	13	0	53	0	953	0	39	0	4	0	8	0
150	9	0	77	0	958	0	28	0	3	0	51	0
151	5	0	8	0	1120	0	18	0	2	0	15	0
152	7	0	63	0	1391	0	53	0	3	0	10	0
153	7	0	70	0	1701	0	95	0	1	0	14	0

3050-G20Y	RED				GREEN				BLUE			
	Measured	Theoretica	Noise	Pure	Measured	Theoretica	Noise	Pure	Measured	Theoretica	Noise	Pure
154	4	0	56	0	1896	124	31	0	1	0	72	0
155	3	0	61	0	2327	226	68	0	0	0	99	0
156	6	0	23	0	2540	395	18	0	0	0	86	0
157	3	0	93	0	3273	664	62	0	0	0	9	0
158	2	0	67	0	3316	1075	88	0	1	0	30	0
159	2	0	90	0	4021	1675	46	0	1	0	99	0
160	3	0	61	0	4611	2510	30	0	0	0	96	0
161	5	0	80	0	5455	3619	59	0	1	0	71	0
162	3	0	68	0	6073	5021	78	0	2	0	41	0
163	2	0	85	0	7455	6703	72	0	0	0	29	0
164	3	0	97	0	8201	8610	11	0	0	0	34	0
165	1	0	47	0	9762	10642	2	0	0	0	68	0
166	0	0	64	0	11336	12656	94	0	0	0	14	0
167	0	0	66	0	12930	14482	98	0	0	0	45	0
168	2	0	26	0	14023	15946	42	0	1	0	94	0
169	0	0	47	0	16438	16894	93	0	0	0	40	0
170	0	0	70	0	17223	17222	249455	261632	1	0	91	0
171	2	0	71	0	16943	16894	75	0	0	0	90	0
172	0	0	51	0	16499	15946	30	0	1	0	67	0
173	2	0	0	0	16698	14482	44	0	1	0	89	0
174	0	0	73	0	14062	12656	63	0	0	0	79	0
175	1	0	11	0	11899	10642	34	0	3	0	71	0
176	0	0	84	0	10030	8610	7	0	0	0	3	0
177	0	0	49	0	8381	6703	75	0	0	0	95	0
178	0	0	78	0	5504	5021	88	0	0	0	71	0
179	2	0	65	0	3747	3619	7	0	1	0	13	0
180	0	0	71	0	2308	2510	2	0	0	0	19	0
181	3	0	9	0	1302	1675	47	0	0	0	54	0
182	0	0	53	0	657	1075	81	0	0	0	79	0
183	2	0	63	0	390	664	50	0	0	0	41	0
184	0	0	76	0	145	395	72	0	0	0	31	0
185	0	0	14	0	75	226	67	0	0	0	96	0
186	0	0	24	0	23	124	4	0	0	0	26	0
187	1	0	24	0	18	0	28	0	0	0	78	0
188	0	0	68	0	7	0	50	0	0	0	47	0
189	0	0	15	0	14	0	14	0	0	0	77	0
190	0	0	31	0	5	0	31	0	0	0	15	0
191	0	0	68	0	5	0	42	0	0	0	98	0
192	1	0	37	0	5	0	96	0	0	0	11	0
193	0	0	87	0	1	0	50	0	0	0	64	0
194	0	0	97	0	3	0	13	0	0	0	20	0
195	0	0	13	0	5	0	60	0	0	0	35	0
196	0	0	75	0	3	0	16	0	0	0	11	0
197	0	0	67	0	2	0	86	0	0	0	26	0
198	0	0	81	0	1	0	82	0	0	0	87	0
199	0	0	71	0	2	0	20	0	0	0	47	0
200	0	0	2	0	2	0	91	0	0	0	22	0
201	0	0	52	0	3	0	31	0	0	0	34	0
202	0	0	14	0	3	0	25	0	0	0	36	0
203	0	0	89	0	2	0	58	0	0	0	80	0
204	0	0	14	0	0	0	56	0	0	0	17	0
205	0	0	93	0	2	0	92	0	0	0	37	0
206	0	0	32	0	0	0	10	0	0	0	56	0
207	0	0	1	0	2	0	85	0	0	0	30	0
208	0	0	68	0	0	0	28	0	0	0	90	0
209	0	0	66	0	0	0	50	0	0	0	52	0
210	0	0	42	0	2	0	41	0	0	0	29	0
211	0	0	78	0	0	0	43	0	0	0	94	0
212	0	0	8	0	0	0	23	0	0	0	38	0
213	0	0	88	0	1	0	44	0	0	0	97	0
214	0	0	17	0	3	0	46	0	0	0	36	0
215	0	0	33	0	0	0	61	0	0	0	90	0
216	0	0	44	0	0	0	42	0	0	0	95	0
217	0	0	35	0	0	0	62	0	0	0	10	0
218	0	0	20	0	1	0	46	0	0	0	6	0
219	0	0	62	0	1	0	64	0	0	0	53	0
220	0	0	48	0	0	0	47	0	0	0	3	0
221	0	0	97	0	0	0	23	0	0	0	0	0
222	0	0	23	0	2	0	29	0	0	0	30	0
223	0	0	3	0	1	0	61	0	0	0	9	0
224	0	0	91	0	0	0	91	0	0	0	19	0
225	0	0	47	0	0	0	47	0	0	0	41	0
226	0	0	60	0	0	0	74	0	0	0	95	0
227	0	0	36	0	0	0	33	0	0	0	84	0
228	0	0	70	0	0	0	60	0	0	0	82	0
229	0	0	65	0	0	0	49	0	0	0	46	0
230	0	0	82	0	0	0	80	0	0	0	35	0

3050-G20Y	RED				GREEN				BLUE			
	Measured	Theoretica	Noise	Pure	Measured	Theoretica	Noise	Pure	Measured	Theoretica	Noise	Pure
231	0	0	50	0	0	0	57	0	0	0	23	0
232	0	0	5	0	0	0	48	0	0	0	27	0
233	0	0	10	0	1	0	91	0	0	0	78	0
234	0	0	26	0	0	0	32	0	0	0	11	0
235	0	0	87	0	0	0	17	0	0	0	88	0
236	0	0	60	0	0	0	79	0	0	0	16	0
237	0	0	72	0	0	0	72	0	0	0	4	0
238	0	0	13	0	0	0	99	0	0	0	40	0
239	0	0	68	0	0	0	30	0	0	0	26	0
240	0	0	74	0	0	0	96	0	0	0	10	0
241	0	0	88	0	0	0	23	0	0	0	76	0
242	0	0	67	0	0	0	64	0	0	0	97	0
243	0	0	22	0	0	0	79	0	0	0	81	0
244	0	0	86	0	0	0	9	0	0	0	84	0
245	0	0	26	0	0	0	30	0	0	0	18	0
246	0	0	90	0	0	0	39	0	0	0	66	0
247	0	0	63	0	0	0	51	0	0	0	20	0
248	0	0	12	0	0	0	76	0	0	0	8	0
249	0	0	88	0	0	0	38	0	0	0	59	0
250	0	0	49	0	0	0	93	0	0	0	59	0
251	0	0	6	0	0	0	63	0	0	0	18	0
252	0	0	62	0	0	0	64	0	0	0	74	0
253	0	0	8	0	0	0	49	0	0	0	1	0
254	0	0	72	0	0	0	97	0	0	0	58	0
255	0	0	0	0	0	0	57	0	0	0	67	0
mode:	131				170				118			
mean:	123.9617				161.389108				112.5088			
std dev:	5.095541				5.095541				5.944798			
Correlation		0.974823	0.307931	0.307998		0.972001	0.315871	0.315821		0.978079	0.318487	0.318495

4020-B10C	RED				GREEN				BLUE			
	Measured	Theoretica	Noise	Pure	Measured	Theoretica	Noise	Pure	Measured	Theoretica	Noise	Pure
0	5492	0	80	0	9698	0	44	0	10651	0	26	0
1	5181	0	76	0	979	0	63	0	16	0	93	0
2	8	0	10	0	4	0	70	0	9	0	68	0
3	7	0	67	0	4	0	21	0	3	0	89	0
4	5	0	85	0	7	0	60	0	6	0	34	0
5	3	0	59	0	1	0	60	0	3	0	17	0
6	5	0	97	0	2	0	59	0	5	0	59	0
7	2	0	32	0	7	0	20	0	6	0	79	0
8	3	0	36	0	7	0	31	0	4	0	58	0
9	5	0	1	0	3	0	37	0	4	0	44	0
10	2	0	35	0	0	0	69	0	7	0	82	0
11	3	0	2	0	2	0	59	0	1	0	74	0
12	7	0	26	0	1	0	40	0	5	0	32	0
13	3	0	64	0	2	0	66	0	3	0	46	0
14	3	0	79	0	1	0	36	0	3	0	11	0
15	3	0	2	0	2	0	87	0	5	0	35	0
16	3	0	10	0	0	0	93	0	5	0	79	0
17	1	0	15	0	1	0	7	0	7	0	97	0
18	10	0	93	0	0	0	7	0	2	0	16	0
19	2	0	12	0	3	0	15	0	2	0	43	0
20	2	0	70	0	0	0	39	0	4	0	74	0
21	5	0	77	0	0	0	26	0	2	0	64	0
22	2	0	1	0	5	0	26	0	5	0	28	0
23	4	0	39	0	0	0	54	0	4	0	83	0
24	1	0	19	0	1	0	27	0	1	0	89	0
25	6	0	45	0	1	0	8	0	4	0	39	0
26	1	0	83	0	0	0	41	0	7	0	87	0
27	4	0	95	0	1	0	51	0	1	0	46	0
28	4	0	4	0	1	0	76	0	2	0	31	0
29	3	0	81	0	5	0	73	0	3	0	51	0
30	4	0	55	0	1	0	44	0	4	0	86	0
31	1	0	56	0	1	0	91	0	3	0	98	0
32	2	0	66	0	0	0	60	0	2	0	8	0
33	5	0	54	0	1	0	0	0	3	0	26	0
34	1	0	21	0	3	0	39	0	2	0	7	0
35	3	0	52	0	3	0	80	0	1	0	10	0
36	1	0	50	0	0	0	66	0	3	0	47	0
37	2	0	84	0	0	0	11	0	2	0	75	0
38	4	0	78	0	2	0	14	0	5	0	20	0
39	2	0	51	0	4	0	6	0	2	0	28	0
40	5	0	57	0	1	0	47	0	4	0	26	0
41	2	0	45	0	2	0	96	0	3	0	88	0
42	3	0	64	0	1	0	62	0	2	0	21	0
43	1	0	14	0	2	0	2	0	2	0	3	0
44	4	0	52	0	3	0	40	0	2	0	46	0
45	4	0	8	0	0	0	55	0	3	0	86	0
46	3	0	14	0	6	0	41	0	3	0	16	0
47	0	0	43	0	1	0	32	0	2	0	23	0
48	2	0	13	0	3	0	37	0	2	0	76	0
49	1	0	31	0	2	0	1	0	1	0	75	0
50	3	0	97	0	1	0	57	0	2	0	60	0
51	0	0	36	0	4	0	65	0	3	0	96	0
52	2	0	12	0	0	0	70	0	0	0	68	0
53	2	0	14	0	2	0	60	0	0	0	70	0
54	1	0	85	0	1	0	61	0	1	0	2	0
55	0	0	7	0	3	0	84	0	1	0	43	0
56	1	0	96	0	2	0	39	0	2	0	72	0
57	0	0	26	0	5	0	1	0	3	0	0	0
58	1	0	21	0	0	0	55	0	3	0	14	0
59	6	0	43	0	4	0	88	0	0	0	11	0
60	2	0	41	0	2	0	5	0	3	0	89	0
61	2	0	67	0	2	0	12	0	1	0	26	0
62	1	0	46	0	2	0	96	0	5	0	5	0
63	0	0	0	0	1	0	96	0	0	0	69	0
64	1	0	20	0	1	0	30	0	0	0	4	0
65	4	0	9	0	3	0	0	0	5	0	85	0
66	4	0	70	0	3	0	6	0	0	0	84	0
67	1	0	11	0	5	0	93	0	2	0	14	0
68	2	0	49	0	2	0	53	0	1	0	71	0
69	0	0	78	0	1	0	95	0	1	0	44	0
70	1	0	71	0	3	0	2	0	2	0	96	0
71	3	0	71	0	1	0	72	0	2	0	24	0
72	0	0	36	0	2	0	42	0	3	0	41	0
73	5	0	22	0	2	0	19	0	3	0	22	0
74	4	0	72	0	3	0	30	0	4	0	31	0
75	3	0	48	0	2	0	26	0	2	0	42	0
76	4	0	9	0	4	0	55	0	3	0	8	0

4020-B10C	RED				GREEN				BLUE			
	Measured	Theoretica	Noise	Pure	Measured	Theoretica	Noise	Pure	Measured	Theoretica	Noise	Pure
77	1	0	27	0	4	0	94	0	5	0	3	0
78	2	0	87	0	1	0	29	0	2	0	36	0
79	2	0	84	0	1	0	61	0	0	0	50	0
80	5	0	45	0	1	0	3	0	2	0	13	0
81	0	0	55	0	3	0	66	0	3	0	52	0
82	4	0	55	0	1	0	43	0	6	0	66	0
83	5	0	88	0	5	0	9	0	4	0	89	0
84	4	0	29	0	2	0	83	0	5	0	35	0
85	7	0	35	0	1	0	99	0	5	0	2	0
86	8	0	45	0	2	0	52	0	6	0	43	0
87	5	0	97	0	0	0	92	0	4	0	70	0
88	4	0	64	0	1	0	74	0	7	0	33	0
89	3	0	81	0	0	0	75	0	1	0	84	0
90	8	0	65	0	3	0	5	0	20	0	45	0
91	17	0	60	0	0	0	29	0	7	0	33	0
92	23	0	84	0	0	0	18	0	18	0	91	0
93	31	0	3	0	0	0	66	0	29	0	52	0
94	56	0	92	0	0	0	43	0	27	0	72	0
95	77	0	28	0	2	0	13	0	44	0	6	0
96	115	0	32	0	5	0	7	0	56	0	38	0
97	173	0	0	0	1	0	75	0	99	0	31	0
98	219	0	1	0	0	0	98	0	128	0	53	0
99	336	0	60	0	1	0	19	0	220	0	24	0
100	472	0	19	0	3	0	7	0	289	0	22	0
101	664	0	85	0	0	0	39	0	373	102	37	0
102	974	0	49	0	6	0	75	0	521	172	46	0
103	1263	0	64	0	5	0	69	0	673	283	89	0
104	1444	0	79	0	15	0	55	0	1001	451	39	0
105	2250	131	99	0	15	0	46	0	1327	699	7	0
106	2385	238	15	0	26	0	52	0	1623	1055	51	0
107	3166	417	92	0	27	0	42	0	2050	1545	82	0
108	4051	702	38	0	47	0	65	0	2560	2201	86	0
109	4739	1136	21	0	63	0	10	0	3118	3048	34	0
110	5216	1770	15	0	66	0	90	0	4254	4103	51	0
111	6449	2652	41	0	107	0	79	0	5165	5368	46	0
112	7504	3824	50	0	148	0	42	0	6024	6828	9	0
113	8733	5305	2	0	190	0	38	0	7083	8443	47	0
114	9446	7081	38	0	265	0	58	0	9313	10147	89	0
115	11422	9096	91	0	318	0	47	0	9696	11856	64	0
116	12042	11242	59	0	456	0	97	0	11256	13466	68	0
117	14363	13370	83	0	556	0	10	0	13517	14868	20	0
118	14764	15299	96	0	694	0	43	0	14399	15958	49	0
119	15862	16846	41	0	829	0	34	0	14828	16650	89	0
120	15704	17847	31	0	1038	0	27	0	16888	16888	249422	261632
121	18195	18195	249420	261632	1321	0	96	0	16460	16650	6	0
122	16147	17847	36	0	1638	0	8	0	16194	15958	96	0
123	17890	16846	85	0	1999	0	65	0	16226	14868	10	0
124	12962	15299	45	0	2376	0	78	0	16142	13466	15	0
125	12528	13370	50	0	2952	0	43	0	13809	11856	1	0
126	9688	11242	44	0	3131	87	81	0	11684	10147	24	0
127	6624	9096	66	0	3622	185	54	0	10512	8443	85	0
128	5435	7081	15	0	4434	370	50	0	6859	6828	43	0
129	3220	5305	80	0	5512	701	87	0	6265	5368	83	0
130	1914	3824	38	0	5874	1256	22	0	3726	4103	13	0
131	1052	2652	43	0	7357	2127	8	0	2624	3048	51	0
132	586	1770	67	0	8047	3409	93	0	1516	2201	26	0
133	284	1136	23	0	10207	5167	86	0	1105	1545	23	0
134	106	702	28	0	10901	7410	56	0	433	1055	94	0
135	51	417	46	0	12751	10053	9	0	326	699	24	0
136	24	238	47	0	14482	12903	45	0	121	451	6	0
137	12	131	20	0	15111	15667	46	0	47	283	55	0
138	6	0	8	0	18698	17997	3	0	20	172	54	0
139	0	0	42	0	17624	19559	18	0	12	102	48	0
140	1	0	19	0	20109	20109	249498	261632	3	0	93	0
141	1	0	4	0	17424	19559	42	0	3	0	44	0
142	1	0	68	0	16482	17997	47	0	0	0	97	0
143	1	0	69	0	13566	15667	20	0	0	0	92	0
144	1	0	80	0	10150	12903	80	0	1	0	58	0
145	0	0	0	0	8287	10053	25	0	2	0	79	0
146	1	0	14	0	5516	7410	44	0	0	0	56	0
147	0	0	69	0	2989	5167	7	0	0	0	89	0
148	0	0	49	0	1648	3409	67	0	0	0	18	0
149	1	0	97	0	1000	2127	66	0	1	0	47	0
150	0	0	11	0	400	1256	17	0	1	0	73	0
151	0	0	93	0	173	701	10	0	0	0	28	0
152	0	0	1	0	59	370	57	0	0	0	73	0
153	0	0	0	0	23	185	45	0	0	0	47	0

4020-E10C	RED				GREEN				BLUE			
	Measured	Theoretica	Noise	Pure	Measured	Theoretica	Noise	Pure	Measured	Theoretica	Noise	Pure
154	0	0	32	0	8	87	43	0	1	0	39	0
155	0	0	60	0	3	0	39	0	0	0	17	0
156	0	0	69	0	7	0	7	0	0	0	64	0
157	0	0	7	0	1	0	78	0	0	0	21	0
158	0	0	86	0	0	0	48	0	0	0	27	0
159	0	0	57	0	1	0	94	0	0	0	47	0
160	0	0	43	0	1	0	28	0	0	0	92	0
161	0	0	80	0	1	0	54	0	0	0	60	0
162	0	0	7	0	0	0	82	0	0	0	97	0
163	0	0	20	0	1	0	27	0	0	0	18	0
164	0	0	57	0	1	0	16	0	0	0	88	0
165	0	0	26	0	0	0	36	0	0	0	68	0
166	0	0	34	0	0	0	98	0	0	0	69	0
167	0	0	30	0	0	0	64	0	0	0	21	0
168	0	0	16	0	1	0	67	0	0	0	40	0
169	0	0	40	0	0	0	58	0	0	0	46	0
170	0	0	25	0	1	0	75	0	0	0	45	0
171	0	0	21	0	0	0	36	0	0	0	98	0
172	0	0	95	0	0	0	20	0	0	0	38	0
173	0	0	41	0	0	0	59	0	0	0	34	0
174	0	0	58	0	0	0	4	0	0	0	73	0
175	0	0	46	0	0	0	31	0	0	0	0	0
176	0	0	39	0	0	0	95	0	0	0	5	0
177	0	0	40	0	0	0	79	0	0	0	23	0
178	0	0	67	0	0	0	6	0	0	0	80	0
179	0	0	67	0	0	0	34	0	0	0	52	0
180	0	0	96	0	0	0	64	0	0	0	14	0
181	0	0	87	0	0	0	0	0	0	0	3	0
182	0	0	38	0	0	0	59	0	0	0	75	0
183	0	0	34	0	0	0	59	0	0	0	57	0
184	0	0	52	0	0	0	67	0	0	0	21	0
185	0	0	66	0	0	0	31	0	0	0	3	0
186	0	0	92	0	0	0	17	0	0	0	56	0
187	0	0	93	0	0	0	25	0	0	0	14	0
188	0	0	35	0	0	0	89	0	0	0	15	0
189	0	0	35	0	0	0	74	0	0	0	12	0
190	0	0	1	0	0	0	90	0	0	0	28	0
191	0	0	30	0	0	0	20	0	0	0	77	0
192	0	0	23	0	0	0	11	0	0	0	68	0
193	0	0	46	0	0	0	8	0	0	0	71	0
194	0	0	29	0	0	0	38	0	0	0	14	0
195	0	0	54	0	0	0	2	0	0	0	52	0
196	0	0	58	0	0	0	80	0	0	0	45	0
197	0	0	1	0	0	0	8	0	0	0	66	0
198	0	0	48	0	0	0	95	0	0	0	62	0
199	0	0	82	0	0	0	51	0	0	0	83	0
200	0	0	68	0	0	0	38	0	0	0	4	0
201	0	0	58	0	0	0	90	0	0	0	16	0
202	0	0	70	0	0	0	8	0	0	0	97	0
203	0	0	10	0	0	0	78	0	0	0	97	0
204	0	0	34	0	0	0	66	0	0	0	39	0
205	0	0	45	0	0	0	2	0	0	0	63	0
206	0	0	8	0	0	0	31	0	0	0	35	0
207	0	0	6	0	0	0	19	0	0	0	29	0
208	0	0	22	0	0	0	1	0	0	0	31	0
209	0	0	94	0	0	0	16	0	0	0	10	0
210	0	0	63	0	0	0	63	0	0	0	71	0
211	0	0	51	0	0	0	54	0	0	0	94	0
212	0	0	30	0	0	0	5	0	0	0	45	0
213	0	0	37	0	0	0	27	0	0	0	58	0
214	0	0	1	0	0	0	78	0	0	0	3	0
215	0	0	70	0	0	0	30	0	0	0	77	0
216	0	0	98	0	0	0	42	0	0	0	67	0
217	0	0	83	0	0	0	85	0	0	0	75	0
218	0	0	81	0	0	0	42	0	0	0	66	0
219	0	0	75	0	0	0	87	0	0	0	40	0
220	0	0	28	0	0	0	99	0	0	0	24	0
221	0	0	16	0	0	0	2	0	0	0	93	0
222	0	0	39	0	0	0	82	0	0	0	90	0
223	0	0	61	0	0	0	91	0	0	0	21	0
224	0	0	86	0	0	0	63	0	0	0	79	0
225	0	0	40	0	0	0	37	0	0	0	41	0
226	0	0	76	0	0	0	66	0	0	0	40	0
227	0	0	43	0	0	0	66	0	0	0	53	0
228	0	0	16	0	0	0	16	0	0	0	16	0
229	0	0	68	0	0	0	30	0	0	0	41	0
230	0	0	91	0	0	0	92	0	0	0	80	0

4020-B10C	RED				GREEN				BLUE			
	Measured	Theoretica	Noise	Pure	Measured	Theoretica	Noise	Pure	Measured	Theoretica	Noise	Pure
231	0	0	84	0	0	0	86	0	0	0	31	0
232	0	0	3	0	0	0	62	0	0	0	74	0
233	0	0	93	0	0	0	32	0	0	0	9	0
234	0	0	87	0	0	0	17	0	0	0	47	0
236	0	0	87	0	0	0	64	0	0	0	32	0
238	0	0	31	0	0	0	79	0	0	0	39	0
237	0	0	88	0	0	0	23	0	0	0	77	0
238	0	0	98	0	0	0	55	0	0	0	41	0
239	0	0	70	0	0	0	92	0	0	0	70	0
240	0	0	13	0	0	0	66	0	0	0	8	0
241	0	0	37	0	0	0	1	0	0	0	11	0
242	0	0	11	0	0	0	89	0	0	0	74	0
243	0	0	40	0	0	0	94	0	0	0	3	0
244	0	0	19	0	0	0	15	0	0	0	44	0
245	0	0	43	0	0	0	66	0	0	0	67	0
246	0	0	97	0	0	0	35	0	0	0	5	0
247	0	0	22	0	0	0	7	0	0	0	68	0
248	0	0	99	0	0	0	36	0	0	0	37	0
249	0	0	8	0	0	0	65	0	0	0	82	0
250	0	0	27	0	0	0	27	0	0	0	17	0
251	0	0	32	0	0	0	0	0	0	0	61	0
252	0	0	9	0	0	0	27	0	0	0	59	0
253	0	0	58	0	0	0	20	0	0	0	90	0
254	0	0	12	0	0	0	47	0	0	0	96	0
255	0	0	38	0	0	0	23	0	0	0	85	0
mode:	121				140				120			
mean:	113.6754				131.2396				114.9516			
std dev:	5.095541				4.246285				5.944798			
Correlation		0.96308	0.327478	0.327346		0.94316	0.352467	0.352569		0.971789	0.299682	0.299765

4030-R308	RED				GREEN				BLUE			
	Measured	Theoretica	Noise	Pure	Measured	Theoretica	Noise	Pure	Measured	Theoretica	Noise	Pure
0	5497	0	25	0	9741	0	18	0	10717	0	56	0
1	5224	0	39	0	980	0	4	0	8	0	78	0
2	6	0	11	0	1	0	76	0	7	0	26	0
3	7	0	46	0	1	0	46	0	3	0	77	0
4	3	0	35	0	1	0	14	0	3	0	16	0
5	6	0	66	0	3	0	1	0	2	0	75	0
6	1	0	83	0	0	0	47	0	5	0	83	0
7	2	0	0	0	0	0	58	0	6	0	85	0
8	4	0	51	0	2	0	71	0	9	0	53	0
9	2	0	16	0	3	0	68	0	4	0	59	0
10	5	0	3	0	1	0	70	0	5	0	54	0
11	2	0	11	0	0	0	73	0	6	0	15	0
12	8	0	54	0	4	0	53	0	2	0	23	0
13	3	0	32	0	0	0	90	0	4	0	0	0
14	4	0	99	0	1	0	37	0	2	0	66	0
15	3	0	70	0	0	0	14	0	1	0	14	0
16	5	0	59	0	2	0	13	0	2	0	49	0
17	3	0	51	0	2	0	83	0	3	0	67	0
18	1	0	40	0	5	0	39	0	4	0	85	0
19	1	0	73	0	2	0	91	0	3	0	46	0
20	4	0	73	0	1	0	11	0	6	0	69	0
21	2	0	24	0	1	0	97	0	4	0	72	0
22	4	0	16	0	3	0	61	0	5	0	89	0
23	3	0	63	0	0	0	89	0	7	0	85	0
24	1	0	67	0	2	0	22	0	5	0	10	0
25	5	0	32	0	1	0	39	0	3	0	83	0
26	8	0	15	0	2	0	48	0	7	0	63	0
27	4	0	10	0	4	0	19	0	4	0	51	0
28	11	0	60	0	3	0	66	0	9	0	39	0
29	4	0	27	0	5	0	97	0	4	0	86	0
30	3	0	16	0	3	0	44	0	6	0	90	0
31	5	0	64	0	1	0	10	0	1	0	7	0
32	4	0	80	0	3	0	64	0	11	0	37	0
33	9	0	71	0	3	0	70	0	4	0	88	0
34	2	0	64	0	1	0	87	0	3	0	48	0
35	2	0	59	0	1	0	88	0	5	0	86	0
36	6	0	71	0	3	0	54	0	6	0	11	0
37	2	0	4	0	3	0	39	0	2	0	65	0
38	10	0	21	0	2	0	59	0	8	0	33	0
39	4	0	36	0	2	0	83	0	4	0	0	0
40	8	0	98	0	3	0	30	0	3	0	32	0
41	2	0	80	0	1	0	52	0	5	0	2	0
42	7	0	65	0	4	0	39	0	7	0	56	0
43	0	0	34	0	1	0	25	0	7	0	21	0
44	5	0	17	0	4	0	46	0	2	0	37	0
45	2	0	14	0	2	0	21	0	5	0	18	0
46	6	0	58	0	0	0	18	0	6	0	28	0
47	1	0	13	0	5	0	96	0	3	0	57	0
48	5	0	75	0	6	0	90	0	6	0	97	0
49	7	0	20	0	6	0	76	0	8	0	17	0
50	8	0	10	0	1	0	21	0	6	0	64	0
51	6	0	70	0	2	0	66	0	2	0	81	0
52	2	0	41	0	8	0	70	0	6	0	20	0
53	5	0	80	0	5	0	60	0	4	0	48	0
54	4	0	4	0	0	0	6	0	6	0	16	0
55	2	0	72	0	5	0	87	0	2	0	79	0
56	4	0	22	0	2	0	37	0	5	0	22	0
57	3	0	28	0	5	0	47	0	2	0	19	0
58	1	0	16	0	3	0	32	0	15	0	6	0
59	7	0	98	0	9	0	59	0	3	0	21	0
60	9	0	73	0	3	0	75	0	11	0	9	0
61	2	0	22	0	6	0	43	0	7	0	41	0
62	6	0	68	0	6	0	80	0	18	0	90	0
63	0	0	36	0	4	0	0	0	3	0	94	0
64	2	0	41	0	4	0	57	0	1	0	91	0
65	12	0	47	0	6	0	86	0	21	0	69	0
66	5	0	7	0	2	0	88	0	4	0	29	0
67	8	0	28	0	6	0	16	0	9	0	49	0
68	8	0	78	0	4	0	45	0	3	0	95	0
69	5	0	7	0	0	0	19	0	2	0	4	0
70	5	0	53	0	9	0	95	0	17	0	12	0
71	13	0	37	0	4	0	54	0	9	0	62	0
72	10	0	37	0	5	0	43	0	12	0	38	0
73	10	0	65	0	10	0	58	0	9	0	24	0
74	11	0	36	0	4	0	84	0	6	0	77	0
75	7	0	54	0	6	0	47	0	12	0	98	0
76	5	0	44	0	4	0	49	0	7	0	17	0

4030-R30B	RED				GREEN				BLUE			
	Measured	Theoretica	Noise	Pure	Measured	Theoretica	Noise	Pure	Measured	Theoretica	Noise	Pure
77	1	0	98	0	8	0	70	0	9	0	30	0
78	2	0	96	0	9	0	55	0	8	0	96	0
79	10	0	72	0	0	0	46	0	1	0	97	0
80	8	0	29	0	6	0	26	0	10	0	42	0
81	6	0	33	0	7	0	32	0	5	0	17	0
82	6	0	67	0	1	0	97	0	5	0	34	0
83	13	0	79	0	10	0	20	0	10	0	95	0
84	5	0	70	0	10	0	0	0	12	0	35	0
85	7	0	31	0	5	0	64	0	4	0	52	0
86	15	0	68	0	10	0	81	0	3	0	56	0
87	6	0	21	0	10	0	49	0	3	0	58	0
88	4	0	77	0	12	0	49	0	6	0	18	0
89	7	0	89	0	4	0	71	0	6	0	45	0
90	1	0	55	0	15	0	1	0	17	0	24	0
91	9	0	57	0	13	0	86	0	15	0	78	0
92	7	0	44	0	16	0	88	0	27	0	65	0
93	4	0	3	0	15	0	36	0	44	0	79	0
94	3	0	11	0	15	0	9	0	86	0	52	0
95	6	0	82	0	11	0	40	0	101	0	35	0
96	3	0	3	0	16	0	51	0	162	0	88	0
97	10	0	2	0	21	0	99	0	308	0	0	0
98	7	0	4	0	14	0	5	0	457	133	86	0
99	2	0	95	0	12	0	58	0	634	242	66	0
100	7	0	65	0	31	0	21	0	948	424	86	0
101	10	0	83	0	55	0	69	0	1372	713	89	0
102	22	0	17	0	81	0	88	0	2041	1154	90	0
103	33	0	12	0	148	0	89	0	2530	1797	68	0
104	37	0	72	0	183	0	56	0	3597	2693	67	0
105	54	0	27	0	310	0	4	0	4358	3883	39	0
106	51	0	21	0	498	0	67	0	5723	5387	46	0
107	93	0	23	0	784	93	41	0	7256	7192	87	0
108	102	0	90	0	1260	198	4	0	8304	9238	37	0
109	149	0	28	0	1872	397	4	0	9805	11417	17	0
110	153	0	45	0	2372	752	71	0	12610	13578	75	0
111	228	0	0	0	3382	1346	94	0	13964	15537	36	0
112	303	0	1	0	5420	2280	47	0	14839	17108	45	0
113	428	0	63	0	6472	3653	93	0	15974	18125	45	0
114	558	109	19	0	9037	5538	25	0	18478	18478	249437	261632
115	693	185	34	0	10412	7942	44	0	17072	18125	58	0
116	815	304	96	0	13046	10775	13	0	17195	17108	17	0
117	1292	485	41	0	16542	13829	24	0	17918	15537	64	0
118	1453	752	45	0	17504	16792	85	0	15961	13578	16	0
119	1840	1133	59	0	19727	19290	94	0	13173	11417	56	0
120	2105	1660	66	0	19326	20963	50	0	12318	9238	45	0
121	3142	2365	13	0	21553	21552	249379	261632	9312	7192	11	0
122	3529	3275	41	0	20175	20963	11	0	7292	5387	85	0
123	5161	4408	44	0	19341	19290	75	0	5658	3883	33	0
124	5244	5768	9	0	16218	16792	17	0	4050	2693	3	0
125	6999	7336	21	0	14261	13829	24	0	2654	1797	29	0
126	8249	9071	33	0	9568	10775	65	0	1576	1154	8	0
127	9215	10902	81	0	6892	7942	64	0	1043	713	86	0
128	12270	12738	28	0	5158	5538	93	0	591	424	54	0
129	13222	14468	62	0	3708	3653	25	0	415	242	47	0
130	14121	15974	8	0	2029	2280	0	0	165	133	52	0
131	15761	17145	95	0	1295	1346	87	0	105	0	9	0
132	17048	17889	69	0	691	752	71	0	66	0	71	0
133	18144	18144	249432	261632	466	397	60	0	32	0	71	0
134	17172	17889	86	0	207	198	35	0	12	0	12	0
135	16428	17145	27	0	123	93	97	0	19	0	42	0
136	16382	15974	5	0	83	0	51	0	12	0	61	0
137	14375	14468	85	0	39	0	76	0	7	0	1	0
138	11957	12738	87	0	24	0	61	0	8	0	70	0
139	10216	10902	89	0	19	0	88	0	9	0	50	0
140	6665	9071	43	0	15	0	53	0	4	0	57	0
141	5662	7336	84	0	7	0	30	0	6	0	6	0
142	3813	5768	70	0	13	0	8	0	2	0	62	0
143	2062	4408	16	0	7	0	11	0	4	0	62	0
144	1275	3275	34	0	2	0	89	0	8	0	78	0
145	908	2365	53	0	5	0	20	0	5	0	46	0
146	458	1660	3	0	8	0	41	0	3	0	39	0
147	205	1133	9	0	6	0	74	0	3	0	21	0
148	89	752	41	0	4	0	14	0	4	0	6	0
149	46	485	98	0	7	0	59	0	4	0	25	0
150	26	304	77	0	3	0	43	0	5	0	8	0
151	12	185	29	0	1	0	88	0	2	0	52	0
152	13	109	84	0	3	0	70	0	4	0	79	0
153	7	0	8	0	6	0	96	0	3	0	95	0

4030-R306	RED				GREEN				BLUE			
	Measured	Theoretica	Noise	Pure	Measured	Theoretica	Noise	Pure	Measured	Theoretica	Noise	Pure
154	9	0	0	0	7	0	86	0	0	0	9	0
155	7	0	13	0	2	0	29	0	1	0	78	0
156	5	0	28	0	4	0	25	0	1	0	52	0
157	3	0	16	0	1	0	49	0	3	0	82	0
158	7	0	16	0	2	0	33	0	2	0	64	0
159	5	0	95	0	2	0	31	0	1	0	29	0
160	5	0	41	0	1	0	57	0	2	0	51	0
161	5	0	59	0	2	0	69	0	1	0	25	0
162	6	0	50	0	0	0	32	0	1	0	12	0
163	5	0	25	0	1	0	62	0	0	0	61	0
164	2	0	24	0	2	0	43	0	0	0	33	0
165	3	0	61	0	2	0	24	0	1	0	32	0
166	1	0	62	0	1	0	51	0	0	0	26	0
167	7	0	98	0	1	0	94	0	2	0	60	0
168	3	0	54	0	1	0	98	0	0	0	59	0
169	4	0	34	0	1	0	89	0	0	0	72	0
170	1	0	12	0	2	0	56	0	2	0	40	0
171	0	0	93	0	1	0	58	0	1	0	97	0
172	0	0	88	0	0	0	25	0	1	0	36	0
173	3	0	5	0	1	0	47	0	2	0	69	0
174	2	0	36	0	0	0	77	0	1	0	69	0
175	1	0	95	0	2	0	28	0	0	0	56	0
176	0	0	44	0	1	0	74	0	0	0	2	0
177	1	0	29	0	0	0	63	0	0	0	14	0
178	0	0	46	0	2	0	41	0	0	0	91	0
179	4	0	73	0	1	0	90	0	0	0	73	0
180	0	0	91	0	1	0	1	0	1	0	1	0
181	2	0	49	0	0	0	88	0	0	0	83	0
182	0	0	92	0	0	0	67	0	0	0	91	0
183	2	0	78	0	0	0	2	0	1	0	35	0
184	2	0	87	0	0	0	75	0	0	0	69	0
185	1	0	0	0	0	0	19	0	1	0	35	0
186	0	0	48	0	1	0	42	0	0	0	82	0
187	2	0	81	0	0	0	62	0	0	0	85	0
188	1	0	2	0	0	0	33	0	0	0	66	0
189	1	0	51	0	0	0	49	0	0	0	10	0
190	1	0	37	0	0	0	37	0	0	0	49	0
191	0	0	12	0	0	0	39	0	0	0	6	0
192	0	0	9	0	1	0	38	0	0	0	37	0
193	0	0	74	0	1	0	59	0	0	0	16	0
194	0	0	2	0	0	0	25	0	0	0	39	0
195	0	0	33	0	0	0	77	0	0	0	28	0
196	0	0	87	0	0	0	73	0	0	0	66	0
197	0	0	0	0	0	0	61	0	0	0	44	0
198	0	0	87	0	0	0	8	0	1	0	95	0
199	0	0	32	0	0	0	83	0	0	0	23	0
200	0	0	67	0	0	0	4	0	0	0	43	0
201	1	0	45	0	1	0	4	0	0	0	41	0
202	1	0	46	0	0	0	57	0	0	0	69	0
203	1	0	41	0	0	0	31	0	0	0	6	0
204	0	0	44	0	0	0	14	0	0	0	72	0
205	0	0	12	0	0	0	84	0	0	0	29	0
206	0	0	14	0	0	0	40	0	0	0	77	0
207	0	0	29	0	0	0	33	0	0	0	80	0
208	0	0	65	0	0	0	19	0	0	0	66	0
209	0	0	49	0	0	0	93	0	0	0	56	0
210	0	0	78	0	0	0	73	0	0	0	65	0
211	0	0	76	0	0	0	37	0	0	0	36	0
212	0	0	18	0	0	0	43	0	0	0	29	0
213	0	0	81	0	0	0	14	0	0	0	51	0
214	0	0	25	0	0	0	41	0	0	0	9	0
215	1	0	81	0	0	0	14	0	0	0	92	0
216	0	0	14	0	0	0	10	0	0	0	25	0
217	0	0	51	0	0	0	15	0	0	0	62	0
218	0	0	16	0	0	0	63	0	0	0	36	0
219	0	0	41	0	0	0	42	0	0	0	84	0
220	0	0	94	0	0	0	91	0	0	0	53	0
221	0	0	8	0	0	0	18	0	0	0	52	0
222	0	0	58	0	0	0	0	0	0	0	96	0
223	0	0	69	0	0	0	33	0	0	0	79	0
224	0	0	48	0	0	0	95	0	0	0	52	0
225	0	0	85	0	0	0	95	0	0	0	38	0
226	0	0	38	0	0	0	43	0	0	0	58	0
227	0	0	87	0	0	0	97	0	0	0	27	0
228	0	0	45	0	0	0	25	0	0	0	70	0
229	0	0	16	0	0	0	45	0	0	0	92	0
230	0	0	43	0	0	0	95	0	0	0	28	0

4030+R308	RED				GREEN				BLUE			
	Measured	Theoretica	Noise	Pure	Measured	Theoretica	Noise	Pure	Measured	Theoretica	Noise	Pure
231	0	0	85	0	0	0	3	0	0	0	59	0
232	0	0	85	0	0	0	23	0	0	0	60	0
233	0	0	81	0	0	0	26	0	0	0	25	0
234	0	0	10	0	0	0	85	0	0	0	64	0
235	0	0	73	0	0	0	19	0	0	0	75	0
236	0	0	55	0	0	0	55	0	0	0	22	0
237	0	0	75	0	0	0	65	0	0	0	20	0
238	0	0	3	0	0	0	91	0	0	0	68	0
239	0	0	44	0	0	0	92	0	0	0	24	0
240	0	0	58	0	0	0	40	0	0	0	73	0
241	0	0	54	0	0	0	88	0	0	0	64	0
242	0	0	65	0	0	0	77	0	0	0	45	0
243	0	0	67	0	0	0	6	0	0	0	19	0
244	0	0	21	0	0	0	43	0	0	0	8	0
245	0	0	8	0	0	0	37	0	0	0	3	0
246	0	0	28	0	0	0	79	0	0	0	47	0
247	0	0	59	0	0	0	91	0	0	0	46	0
248	0	0	68	0	0	0	92	0	0	0	6	0
249	0	0	67	0	0	0	22	0	0	0	32	0
250	0	0	80	0	0	0	95	0	0	0	97	0
251	0	0	42	0	0	0	79	0	0	0	66	0
252	0	0	85	0	0	0	95	0	0	0	44	0
253	0	0	84	0	0	0	42	0	0	0	56	0
254	0	0	90	0	0	0	31	0	0	0	49	0
255	0	0	65	0	0	0	47	0	0	0	6	0
mode:	133				121				114			
mean:	126.4461				115.093849				109.5392			
std dev:	5.944798				4.246285				5.095541			
Correlation		0.984444	0.32088	0.320785		0.977285	0.346472	0.346538		0.970999	0.319127	0.319194

5020-R708	RED				GREEN				BLUE			
	Measured	Theoretica	Noise	Pure	Measured	Theoretica	Noise	Pure	Measured	Theoretica	Noise	Pure
0	5378	0	2	0	9070	0	75	0	10450	0	39	0
1	5136	0	21	0	1441	0	63	0	39	0	36	0
2	24	0	35	0	39	0	81	0	22	0	89	0
3	9	0	55	0	23	0	36	0	17	0	97	0
4	5	0	64	0	13	0	77	0	9	0	93	0
5	6	0	54	0	10	0	5	0	7	0	63	0
6	4	0	92	0	7	0	45	0	8	0	83	0
7	9	0	15	0	8	0	72	0	3	0	76	0
8	3	0	33	0	3	0	82	0	3	0	40	0
9	6	0	42	0	7	0	31	0	5	0	97	0
10	5	0	66	0	1	0	15	0	5	0	85	0
11	3	0	32	0	4	0	99	0	10	0	98	0
12	8	0	76	0	2	0	99	0	5	0	70	0
13	9	0	89	0	8	0	14	0	6	0	49	0
14	4	0	89	0	3	0	50	0	2	0	71	0
15	4	0	9	0	2	0	34	0	4	0	26	0
16	5	0	60	0	2	0	70	0	5	0	86	0
17	1	0	71	0	4	0	85	0	7	0	99	0
18	4	0	89	0	0	0	81	0	6	0	41	0
19	7	0	30	0	4	0	90	0	3	0	94	0
20	3	0	19	0	0	0	46	0	3	0	81	0
21	4	0	30	0	1	0	23	0	2	0	35	0
22	3	0	39	0	0	0	6	0	6	0	41	0
23	1	0	57	0	2	0	61	0	3	0	84	0
24	4	0	21	0	2	0	82	0	3	0	79	0
25	1	0	94	0	3	0	77	0	5	0	5	0
26	1	0	49	0	2	0	54	0	2	0	25	0
27	7	0	50	0	2	0	72	0	3	0	93	0
28	1	0	34	0	1	0	88	0	0	0	5	0
29	0	0	63	0	2	0	84	0	4	0	43	0
30	1	0	79	0	3	0	66	0	0	0	12	0
31	4	0	18	0	1	0	29	0	2	0	46	0
32	2	0	29	0	1	0	31	0	5	0	95	0
33	1	0	9	0	6	0	37	0	3	0	83	0
34	1	0	24	0	1	0	1	0	2	0	25	0
35	0	0	16	0	3	0	45	0	2	0	13	0
36	3	0	54	0	3	0	23	0	1	0	38	0
37	1	0	75	0	2	0	52	0	1	0	95	0
38	0	0	90	0	3	0	86	0	0	0	37	0
39	3	0	90	0	3	0	44	0	2	0	65	0
40	0	0	85	0	1	0	41	0	4	0	17	0
41	2	0	74	0	3	0	2	0	2	0	98	0
42	2	0	50	0	1	0	69	0	4	0	41	0
43	3	0	80	0	1	0	67	0	2	0	29	0
44	0	0	27	0	2	0	77	0	1	0	82	0
45	1	0	19	0	1	0	20	0	1	0	85	0
46	1	0	35	0	3	0	10	0	1	0	4	0
47	6	0	53	0	1	0	59	0	2	0	1	0
48	0	0	65	0	1	0	71	0	4	0	12	0
49	1	0	15	0	2	0	96	0	0	0	3	0
50	0	0	32	0	0	0	98	0	1	0	69	0
51	1	0	95	0	3	0	3	0	1	0	76	0
52	1	0	93	0	2	0	32	0	1	0	93	0
53	2	0	40	0	1	0	53	0	2	0	54	0
54	1	0	35	0	1	0	88	0	2	0	59	0
55	4	0	54	0	4	0	47	0	1	0	16	0
56	1	0	33	0	0	0	66	0	1	0	82	0
57	1	0	47	0	1	0	90	0	4	0	27	0
58	4	0	32	0	1	0	3	0	1	0	79	0
59	4	0	16	0	1	0	81	0	3	0	16	0
60	0	0	90	0	0	0	55	0	1	0	60	0
61	1	0	2	0	0	0	85	0	3	0	61	0
62	1	0	98	0	2	0	45	0	1	0	45	0
63	4	0	34	0	2	0	80	0	5	0	98	0
64	2	0	45	0	2	0	24	0	2	0	71	0
65	1	0	59	0	0	0	55	0	1	0	77	0
66	2	0	79	0	1	0	40	0	3	0	71	0
67	1	0	50	0	1	0	11	0	1	0	41	0
68	2	0	0	0	0	0	9	0	1	0	73	0
69	2	0	92	0	1	0	40	0	3	0	44	0
70	2	0	27	0	2	0	81	0	2	0	9	0
71	2	0	9	0	0	0	26	0	2	0	14	0
72	4	0	54	0	0	0	69	0	3	0	96	0
73	3	0	86	0	0	0	51	0	4	0	49	0
74	2	0	22	0	0	0	44	0	1	0	29	0
75	2	0	25	0	1	0	32	0	2	0	91	0
76	2	0	77	0	3	0	15	0	2	0	7	0

5020-R708	RED				GREEN				BLUE			
	Measured	Theoretica	Noise	Pure	Measured	Theoretica	Noise	Pure	Measured	Theoretica	Noise	Pure
77	2	0	40	0	4	0	32	0	4	0	63	0
78	3	0	93	0	1	0	33	0	2	0	14	0
79	2	0	21	0	3	0	13	0	1	0	75	0
80	2	0	41	0	0	0	81	0	2	0	86	0
81	0	0	51	0	0	0	64	0	2	0	24	0
82	3	0	74	0	0	0	31	0	2	0	74	0
83	1	0	23	0	0	0	52	0	0	0	67	0
84	0	0	36	0	4	0	96	0	1	0	72	0
85	4	0	71	0	1	0	21	0	1	0	57	0
86	1	0	19	0	1	0	29	0	1	0	25	0
87	0	0	31	0	2	0	84	0	4	0	39	0
88	3	0	44	0	0	0	70	0	1	0	78	0
89	3	0	37	0	1	0	89	0	1	0	13	0
90	2	0	31	0	2	0	97	0	6	0	66	0
91	5	0	11	0	2	0	86	0	5	0	9	0
92	6	0	2	0	2	0	46	0	15	0	97	0
93	8	0	57	0	1	0	16	0	12	0	72	0
94	9	0	73	0	2	0	67	0	9	0	89	0
95	24	0	72	0	0	0	50	0	34	0	50	0
96	37	0	20	0	1	0	20	0	31	0	50	0
97	60	0	84	0	0	0	51	0	59	0	48	0
98	65	0	51	0	2	0	95	0	78	0	41	0
99	106	0	97	0	2	0	4	0	105	0	72	0
100	119	0	56	0	1	0	42	0	140	0	7	0
101	169	0	89	0	2	0	33	0	162	0	69	0
102	244	0	40	0	2	0	48	0	223	0	48	0
103	313	0	79	0	4	0	18	0	262	0	20	0
104	413	0	91	0	3	0	3	0	373	0	48	0
105	608	0	59	0	17	0	15	0	421	0	8	0
106	708	0	28	0	22	0	56	0	590	0	99	0
107	821	0	89	0	39	0	64	0	762	0	10	0
108	1152	0	9	0	60	0	17	0	995	0	5	0
109	1411	0	23	0	68	0	77	0	1228	0	78	0
110	1662	0	63	0	102	0	56	0	1643	0	80	0
111	2034	0	59	0	185	0	29	0	2076	0	29	0
112	2401	0	7	0	261	0	60	0	2408	0	81	0
113	2811	0	14	0	269	0	64	0	3007	75	74	0
114	3149	81	94	0	446	0	57	0	4271	159	73	0
115	3958	172	24	0	581	0	26	0	4612	318	30	0
116	4430	345	59	0	758	0	9	0	5810	603	45	0
117	5574	654	10	0	1067	0	46	0	7535	1080	16	0
118	6159	1170	33	0	1347	0	85	0	8847	1829	27	0
119	7472	1983	69	0	1741	142	83	0	9571	2931	91	0
120	7891	3177	55	0	2059	258	99	0	12035	4443	4	0
121	10164	4816	88	0	2719	451	60	0	12734	6372	66	0
122	10712	6907	20	0	3131	759	15	0	13971	8645	91	0
123	13912	9370	35	0	4002	1228	29	0	15348	11096	47	0
124	12450	12026	3	0	4676	1913	4	0	17259	13473	61	0
125	15300	14603	89	0	5828	2867	61	0	16592	15477	51	0
126	16148	16775	49	0	6176	4133	53	0	16373	16820	78	0
127	16175	18230	2	0	7174	5734	22	0	17293	17292	249491	261632
128	18743	18743	249528	261632	8683	7655	74	0	13970	16820	21	0
129	17141	18230	49	0	11002	9832	27	0	15202	15477	38	0
130	15421	16775	54	0	11434	12152	44	0	11416	13473	52	0
131	13830	14603	93	0	14707	14452	40	0	10305	11096	6	0
132	11828	12026	41	0	15134	16538	3	0	7267	8645	87	0
133	9241	9370	33	0	18489	18209	59	0	6300	6372	49	0
134	6308	6907	31	0	18560	19292	57	0	3485	4443	65	0
135	4112	4816	83	0	19668	19667	249403	261632	2964	2931	48	0
136	2738	3177	21	0	19251	19292	47	0	1331	1829	75	0
137	1487	1983	25	0	17264	18209	49	0	829	1080	62	0
138	681	1170	94	0	16977	16538	35	0	447	603	75	0
139	351	654	33	0	11864	14452	8	0	208	318	11	0
140	133	345	29	0	10123	12152	62	0	108	159	31	0
141	81	172	19	0	6181	9832	36	0	57	75	67	0
142	24	81	96	0	4080	7655	77	0	24	0	63	0
143	7	0	11	0	2310	5734	81	0	11	0	18	0
144	14	0	11	0	1166	4133	50	0	7	0	23	0
145	6	0	7	0	676	2867	72	0	6	0	27	0
146	5	0	28	0	284	1913	5	0	4	0	25	0
147	1	0	0	0	116	1228	84	0	1	0	5	0
148	4	0	29	0	49	759	88	0	2	0	37	0
149	2	0	74	0	36	451	82	0	3	0	98	0
150	3	0	25	0	14	258	18	0	3	0	44	0
151	3	0	10	0	5	142	3	0	5	0	53	0
152	0	0	31	0	6	0	94	0	2	0	15	0
153	0	0	89	0	8	0	29	0	4	0	69	0

5020-R708	RED				GREEN				BLUE			
	Measured	Theoretica	Noise	Pure	Measured	Theoretica	Noise	Pure	Measured	Theoretica	Noise	Pure
154	1	0	36	0	2	0	74	0	2	0	61	0
155	4	0	32	0	1	0	82	0	0	0	38	0
156	2	0	89	0	4	0	92	0	0	0	88	0
157	1	0	43	0	3	0	54	0	1	0	85	0
158	1	0	62	0	2	0	54	0	0	0	6	0
159	3	0	35	0	2	0	58	0	1	0	93	0
160	1	0	42	0	2	0	23	0	1	0	38	0
161	2	0	3	0	2	0	24	0	2	0	0	0
162	1	0	22	0	3	0	77	0	1	0	91	0
163	0	0	51	0	0	0	42	0	0	0	0	0
164	0	0	74	0	2	0	52	0	0	0	29	0
165	0	0	18	0	1	0	33	0	0	0	93	0
166	0	0	24	0	2	0	65	0	1	0	58	0
167	1	0	88	0	1	0	76	0	0	0	28	0
168	2	0	39	0	1	0	61	0	2	0	75	0
169	0	0	38	0	2	0	82	0	0	0	77	0
170	1	0	53	0	0	0	41	0	1	0	44	0
171	1	0	24	0	1	0	11	0	0	0	11	0
172	0	0	92	0	0	0	11	0	0	0	21	0
173	0	0	14	0	1	0	44	0	0	0	10	0
174	0	0	94	0	0	0	7	0	0	0	11	0
175	0	0	30	0	0	0	65	0	1	0	50	0
176	0	0	93	0	0	0	85	0	0	0	62	0
177	0	0	5	0	0	0	93	0	0	0	63	0
178	0	0	61	0	2	0	67	0	0	0	61	0
179	0	0	27	0	1	0	71	0	0	0	98	0
180	0	0	47	0	0	0	1	0	0	0	11	0
181	1	0	68	0	1	0	57	0	0	0	43	0
182	0	0	22	0	0	0	62	0	0	0	98	0
183	0	0	1	0	0	0	98	0	0	0	80	0
184	0	0	90	0	0	0	83	0	0	0	4	0
185	0	0	6	0	0	0	78	0	0	0	6	0
186	0	0	69	0	0	0	80	0	0	0	7	0
187	0	0	62	0	0	0	89	0	0	0	38	0
188	0	0	31	0	0	0	21	0	0	0	71	0
189	0	0	77	0	0	0	76	0	0	0	69	0
190	0	0	19	0	0	0	80	0	0	0	41	0
191	0	0	19	0	0	0	24	0	0	0	32	0
192	1	0	88	0	0	0	33	0	1	0	60	0
193	0	0	35	0	0	0	1	0	0	0	88	0
194	0	0	7	0	0	0	44	0	0	0	73	0
195	0	0	54	0	0	0	2	0	0	0	48	0
196	0	0	77	0	0	0	36	0	0	0	20	0
197	0	0	29	0	0	0	9	0	0	0	66	0
198	0	0	3	0	1	0	57	0	0	0	71	0
199	0	0	39	0	0	0	73	0	0	0	18	0
200	0	0	51	0	0	0	89	0	0	0	67	0
201	0	0	79	0	0	0	5	0	0	0	16	0
202	0	0	42	0	0	0	54	0	0	0	41	0
203	0	0	3	0	0	0	23	0	0	0	84	0
204	0	0	39	0	0	0	64	0	0	0	99	0
205	0	0	40	0	0	0	28	0	0	0	4	0
206	0	0	61	0	0	0	64	0	0	0	40	0
207	0	0	2	0	0	0	93	0	0	0	32	0
208	0	0	35	0	0	0	39	0	0	0	92	0
209	0	0	36	0	0	0	85	0	0	0	76	0
210	0	0	98	0	0	0	90	0	0	0	56	0
211	0	0	87	0	0	0	71	0	0	0	9	0
212	0	0	88	0	0	0	17	0	0	0	68	0
213	0	0	15	0	0	0	74	0	0	0	92	0
214	0	0	80	0	0	0	52	0	0	0	93	0
215	0	0	46	0	0	0	55	0	0	0	47	0
216	0	0	4	0	0	0	96	0	0	0	90	0
217	0	0	50	0	0	0	99	0	0	0	96	0
218	0	0	51	0	0	0	60	0	0	0	18	0
219	0	0	23	0	0	0	83	0	0	0	80	0
220	0	0	58	0	0	0	65	0	0	0	6	0
221	0	0	11	0	0	0	64	0	0	0	46	0
222	0	0	6	0	0	0	52	0	0	0	44	0
223	0	0	37	0	0	0	8	0	0	0	49	0
224	0	0	12	0	0	0	10	0	0	0	41	0
225	0	0	49	0	0	0	75	0	0	0	40	0
226	0	0	62	0	0	0	5	0	0	0	40	0
227	0	0	14	0	0	0	9	0	0	0	70	0
228	0	0	61	0	0	0	65	0	0	0	79	0
229	0	0	62	0	0	0	94	0	0	0	42	0
230	0	0	46	0	0	0	6	0	0	0	15	0

5020-R706	RED				GREEN				BLUE			
	Measured	Theoretica	Noise	Pure	Measured	Theoretica	Noise	Pure	Measured	Theoretica	Noise	Pure
231	0	0	79	0	0	0	66	0	0	0	89	0
232	0	0	1	0	0	0	70	0	0	0	10	0
233	0	0	39	0	0	0	17	0	0	0	38	0
234	0	0	27	0	0	0	93	0	0	0	88	0
235	0	0	73	0	0	0	55	0	0	0	40	0
236	0	0	10	0	0	0	89	0	0	0	88	0
237	0	0	55	0	0	0	54	0	0	0	5	0
238	0	0	63	0	0	0	21	0	0	0	52	0
239	0	0	71	0	0	0	88	0	0	0	95	0
240	0	0	86	0	0	0	34	0	0	0	66	0
241	0	0	65	0	0	0	87	0	0	0	25	0
242	0	0	75	0	0	0	15	0	0	0	78	0
243	0	0	68	0	0	0	32	0	0	0	38	0
244	0	0	59	0	0	0	83	0	0	0	65	0
245	0	0	60	0	0	0	32	0	0	0	29	0
246	0	0	47	0	0	0	30	0	0	0	71	0
247	0	0	4	0	0	0	22	0	0	0	0	0
248	0	0	22	0	0	0	41	0	0	0	31	0
249	0	0	47	0	0	0	74	0	0	0	79	0
250	0	0	7	0	0	0	45	0	0	0	17	0
251	0	0	30	0	0	0	51	0	0	0	8	0
252	0	0	22	0	0	0	61	0	0	0	85	0
253	0	0	18	0	0	0	77	0	0	0	3	0
254	0	0	40	0	0	0	66	0	0	0	82	0
255	0	0	47	0	0	0	33	0	0	0	94	0
mode:	128				135				127			
mean:	119.9776				127.402187				118.8197			
std dev:	4.246285				5.095541				4.246285			
Correlation		0.947041	0.339451	0.339476		0.967416	0.334609	0.33474		0.911225	0.306725	0.306757

1.5.8 Gaussian Test Data Histograms

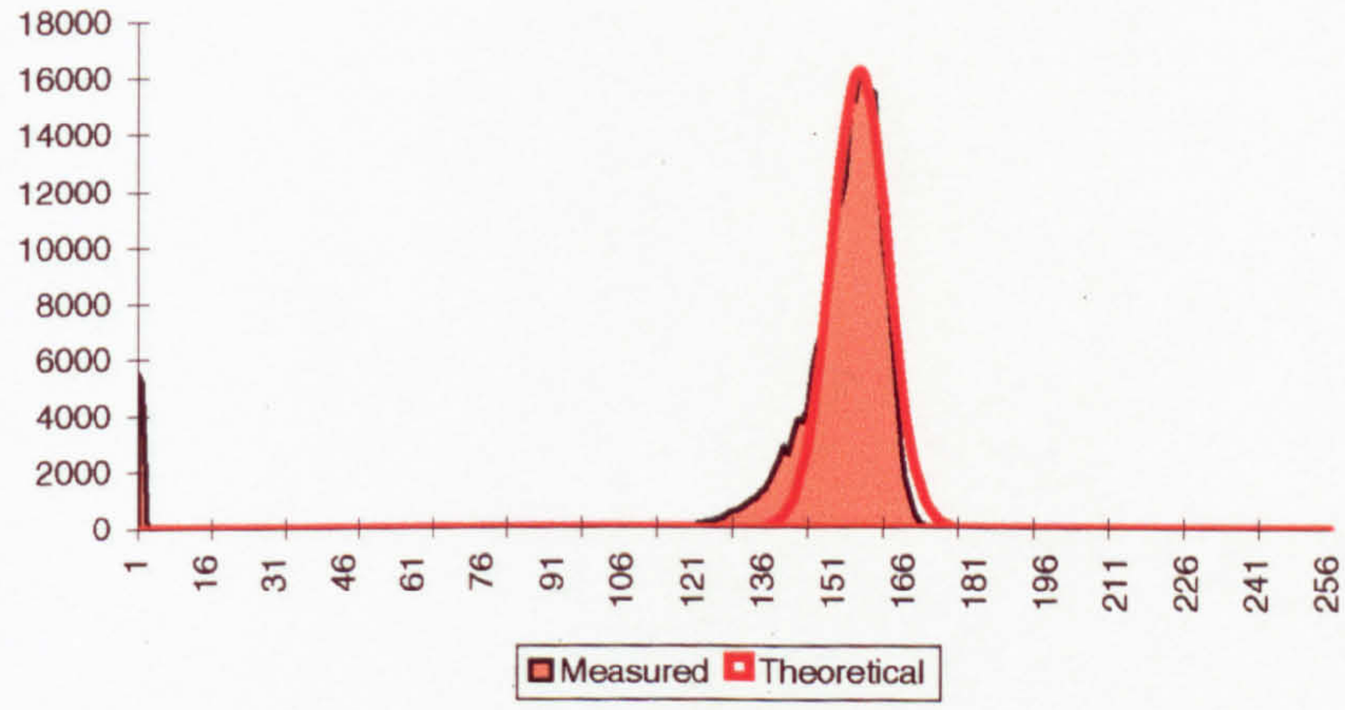

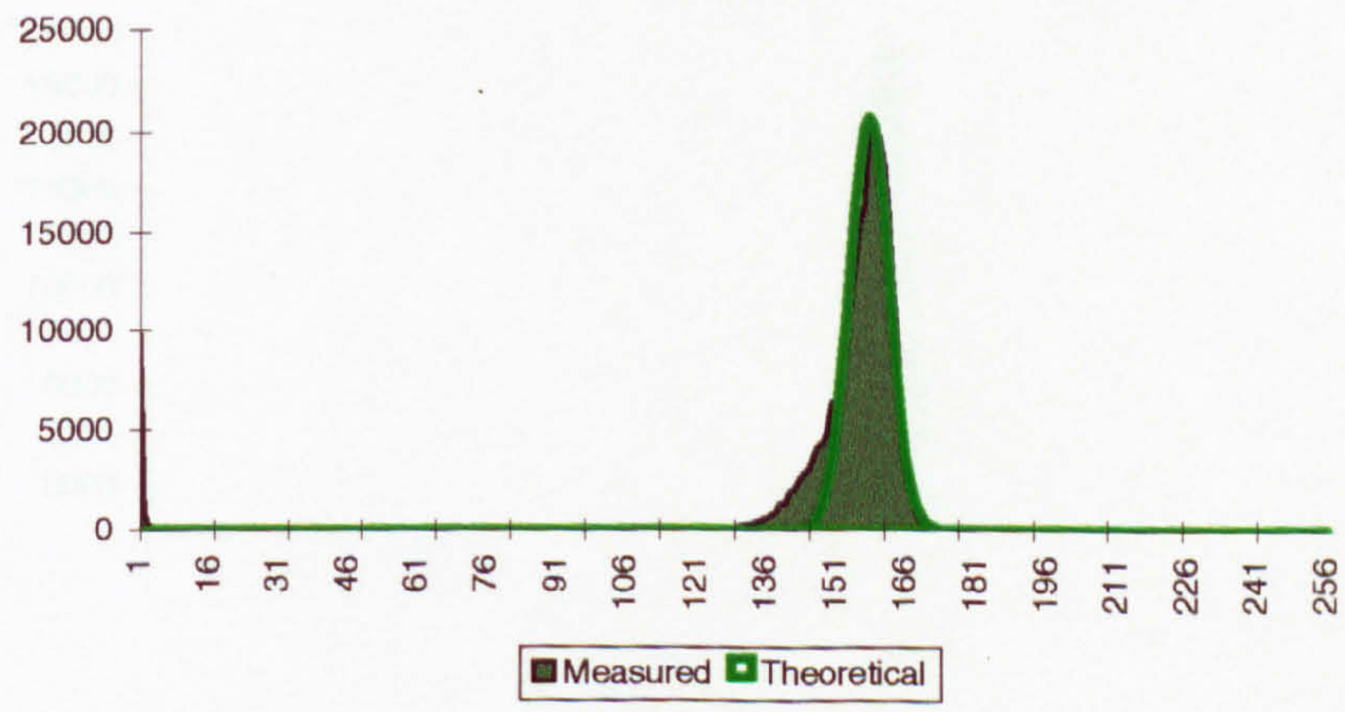

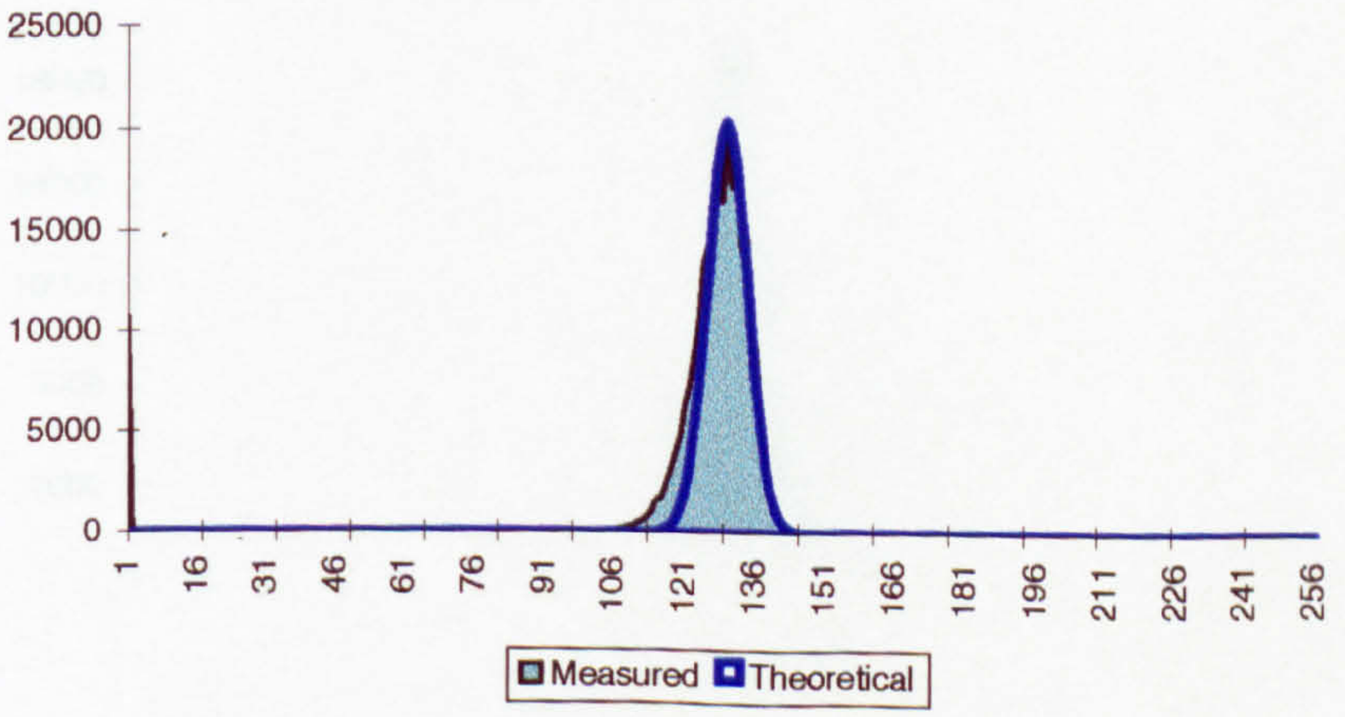

G1 Histograms

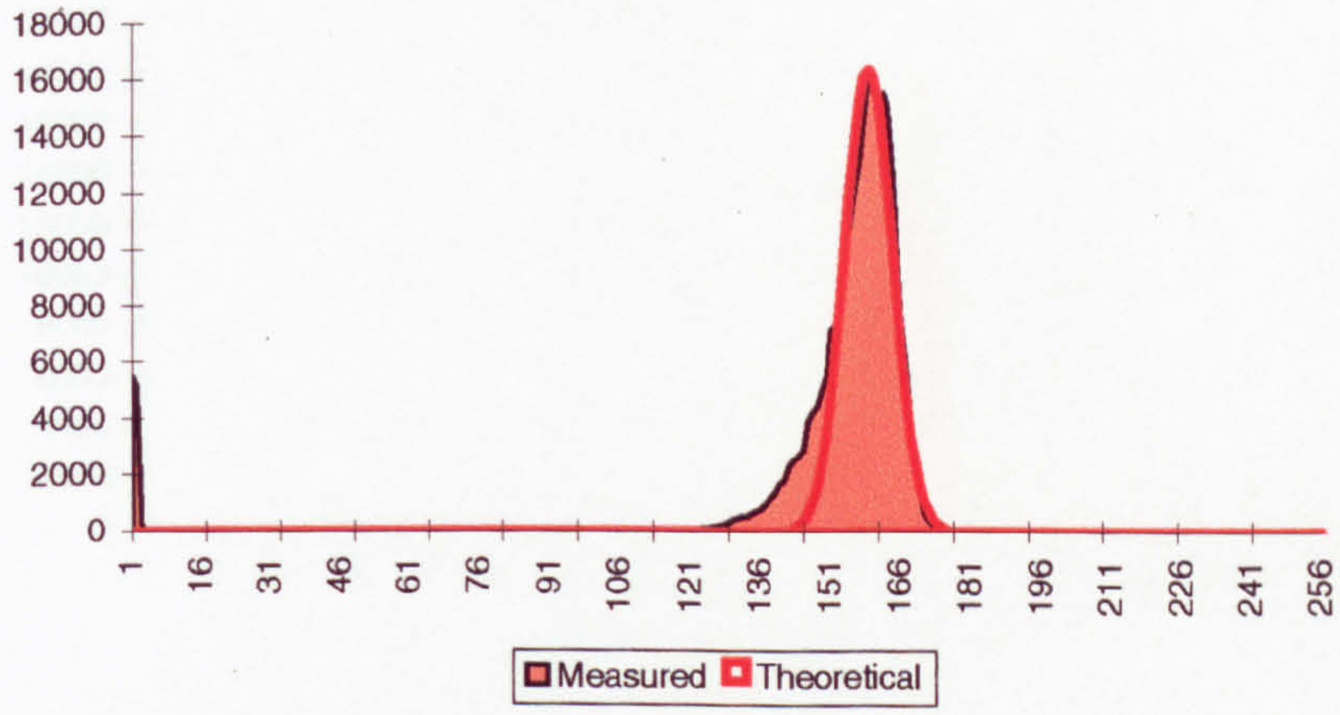

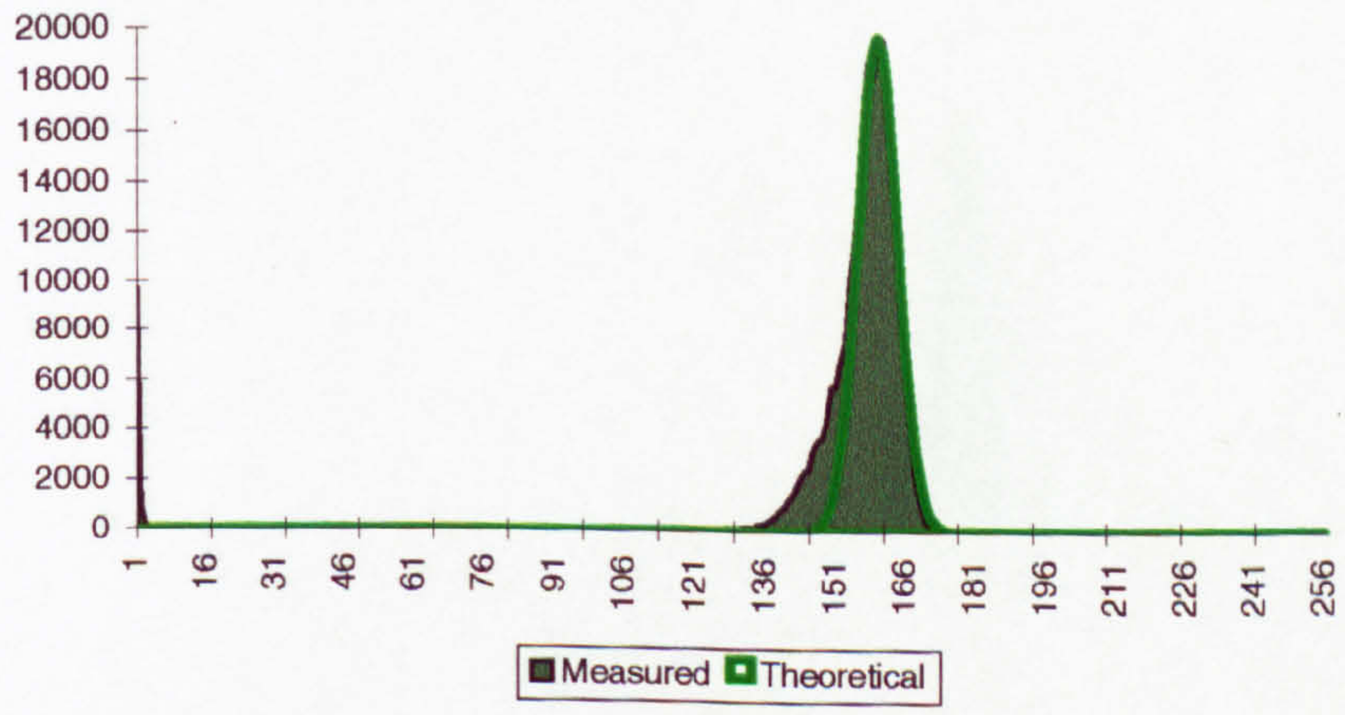

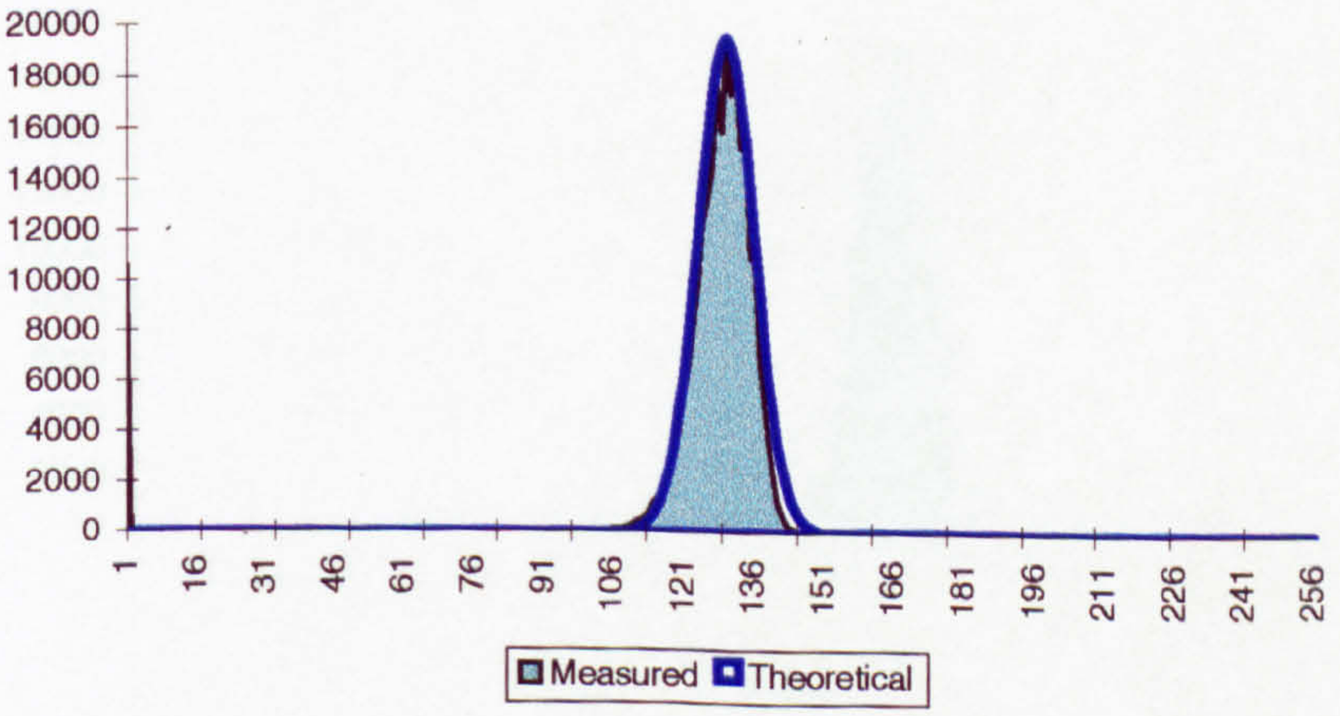

G2 Histograms

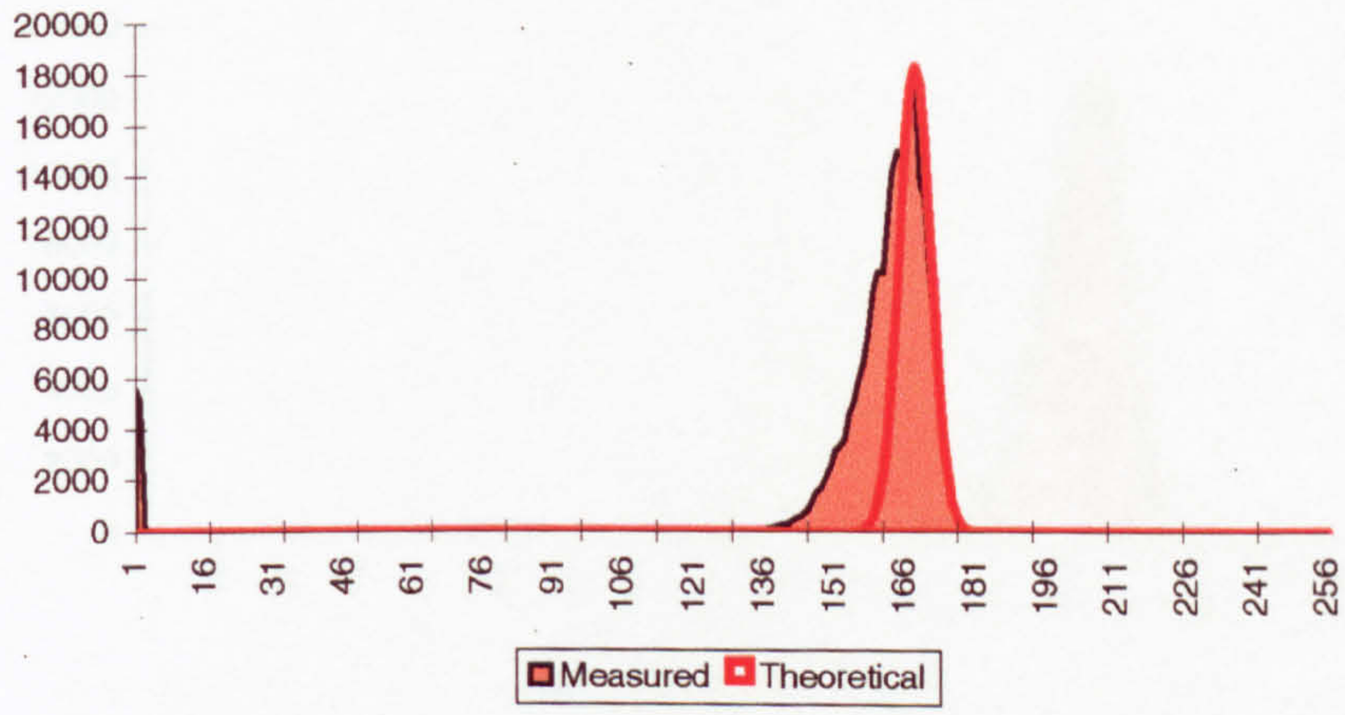

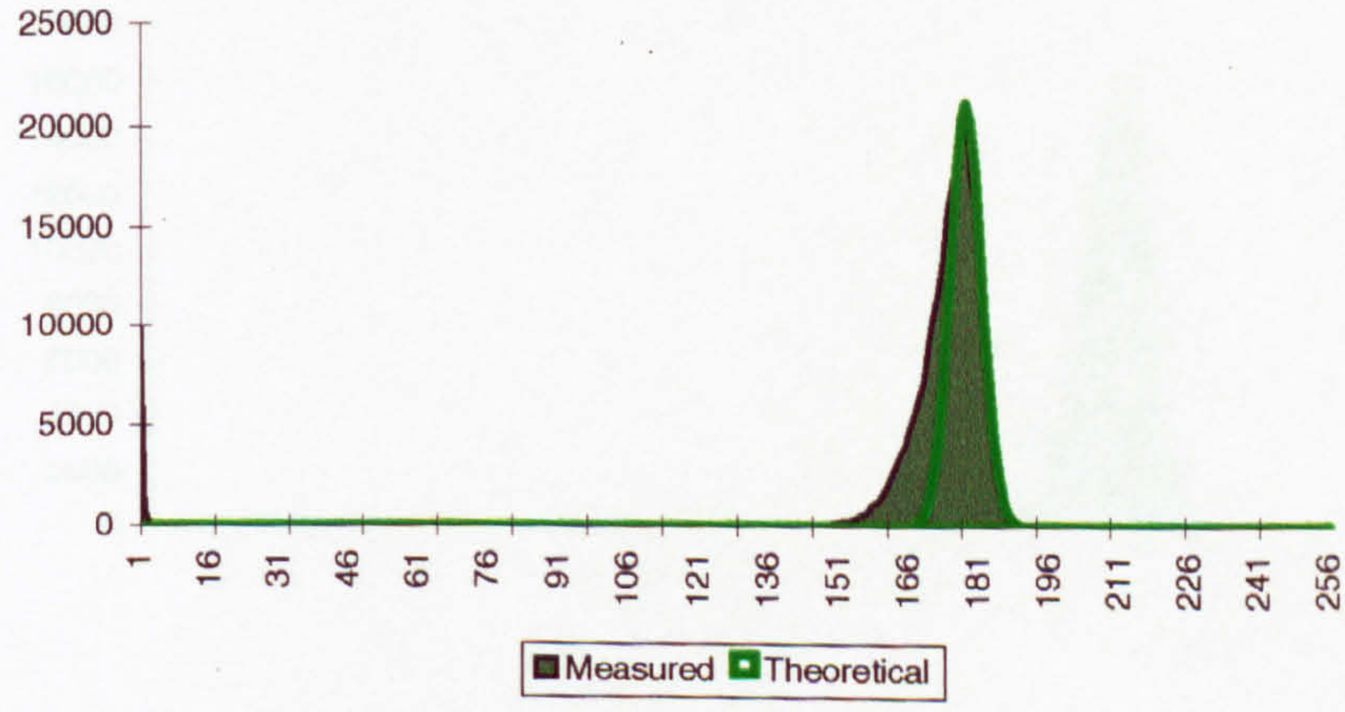

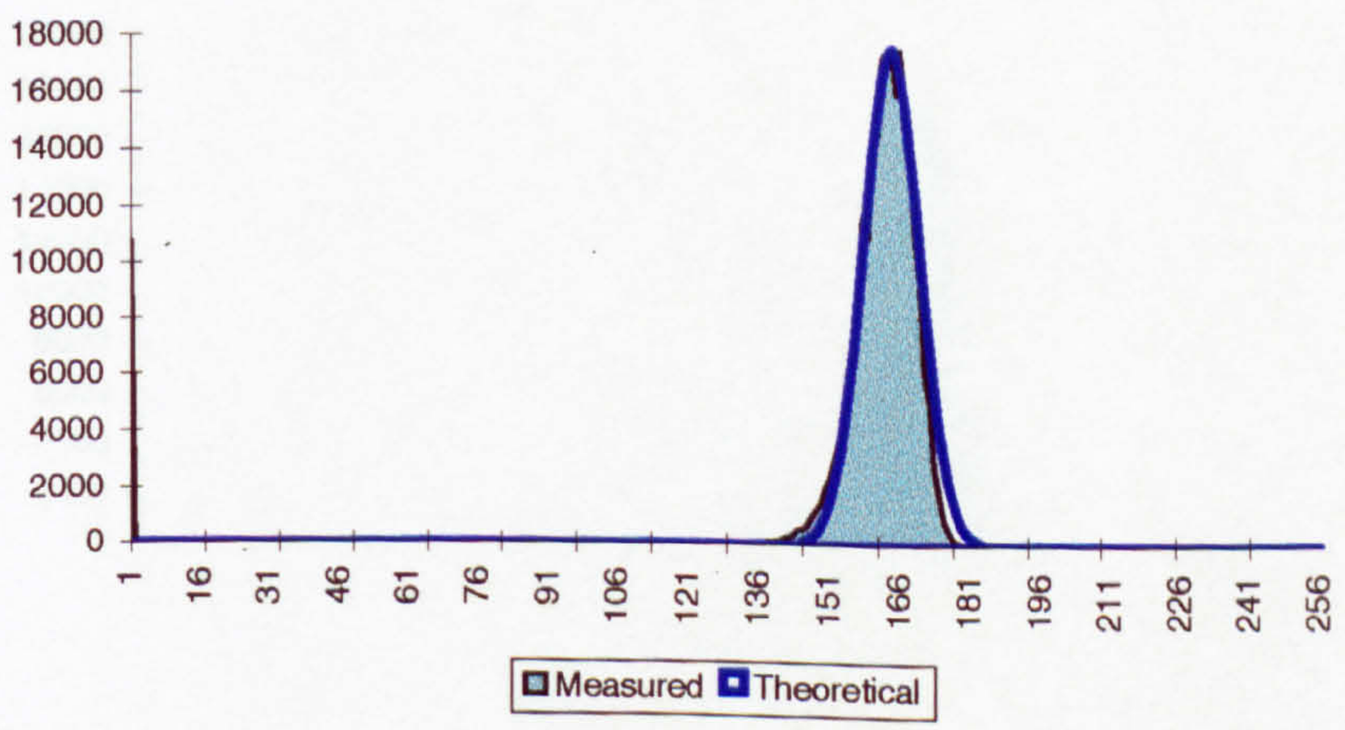

G3 Histograms

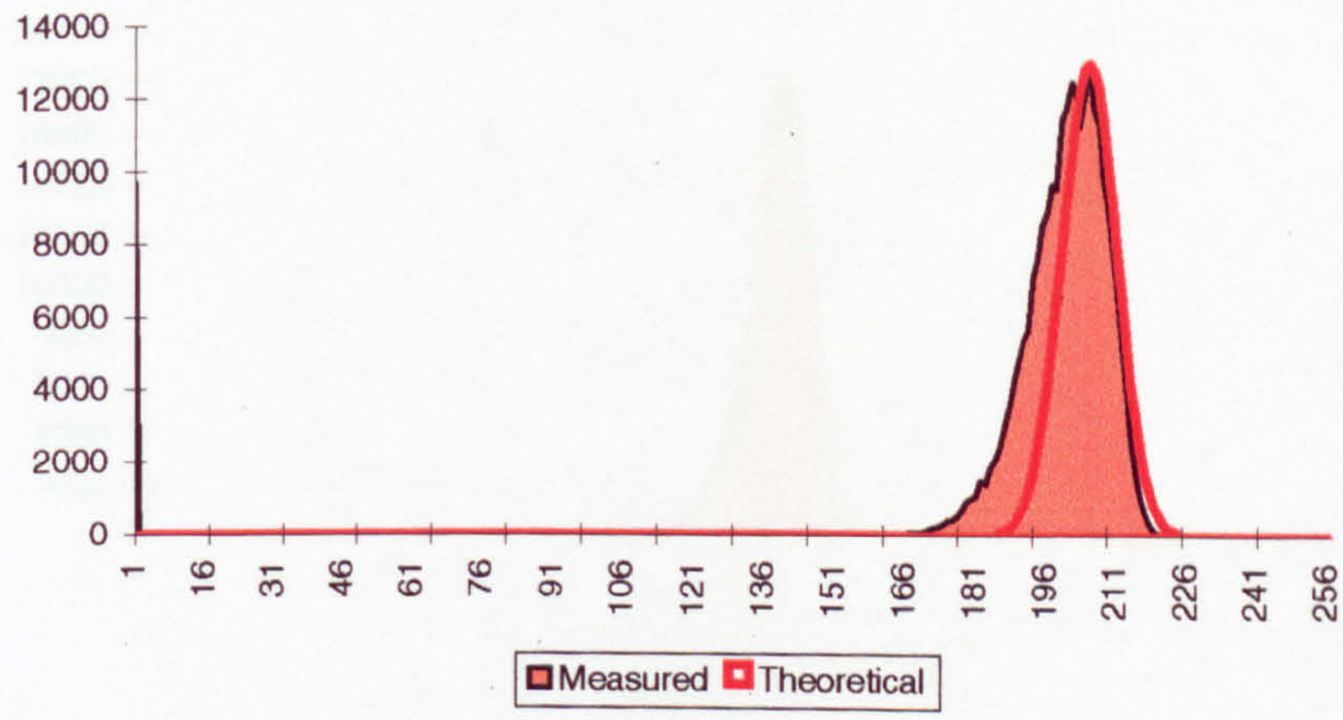

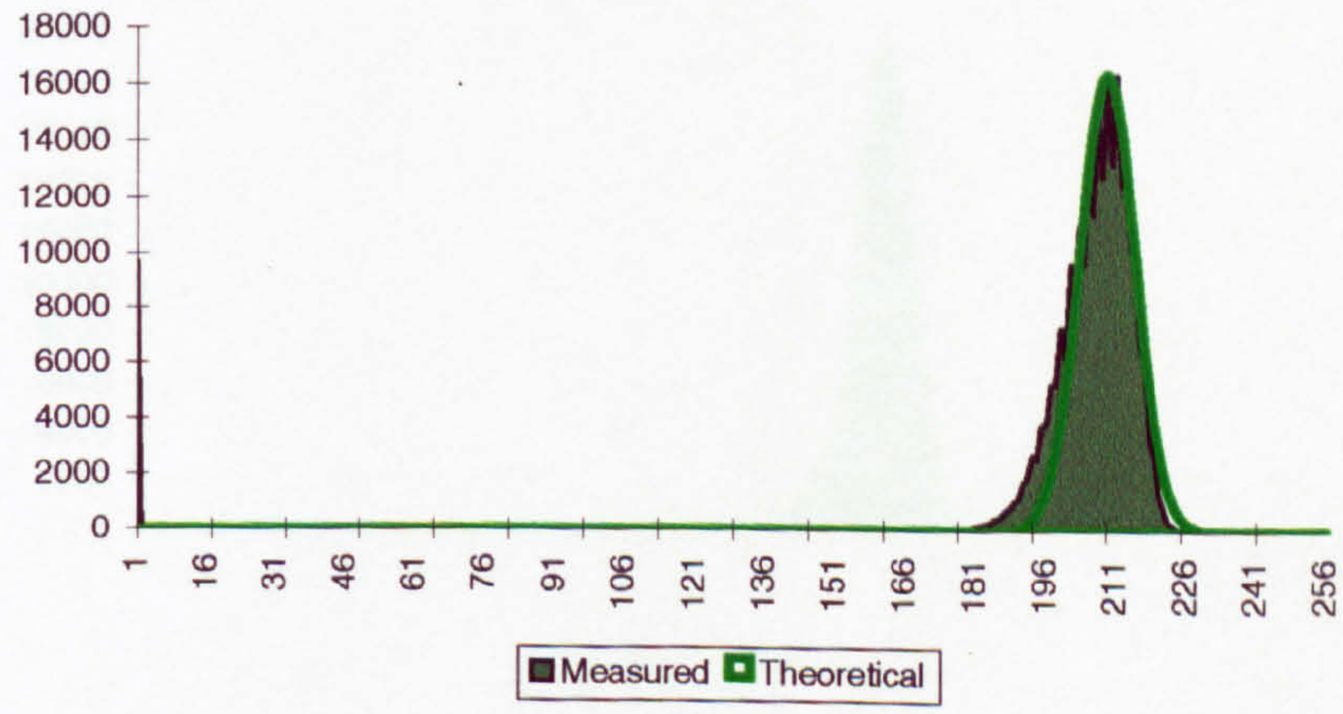

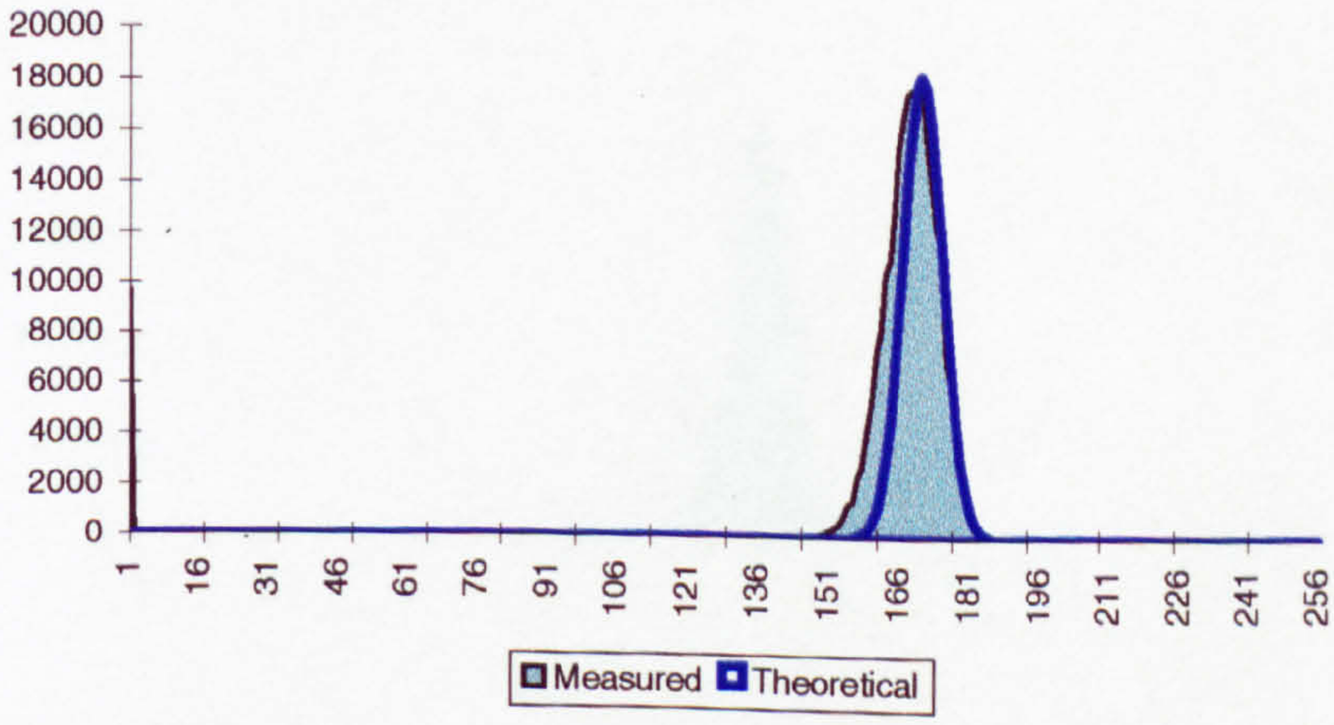

G4 Histograms

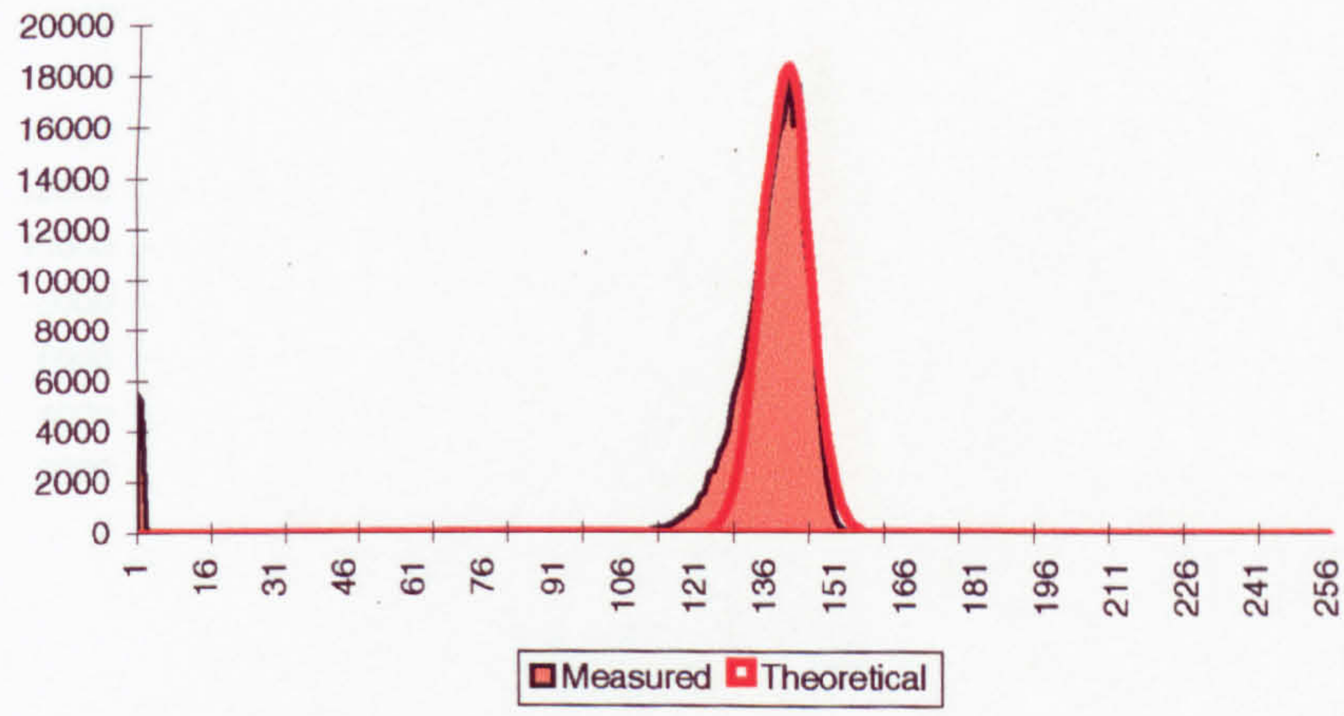

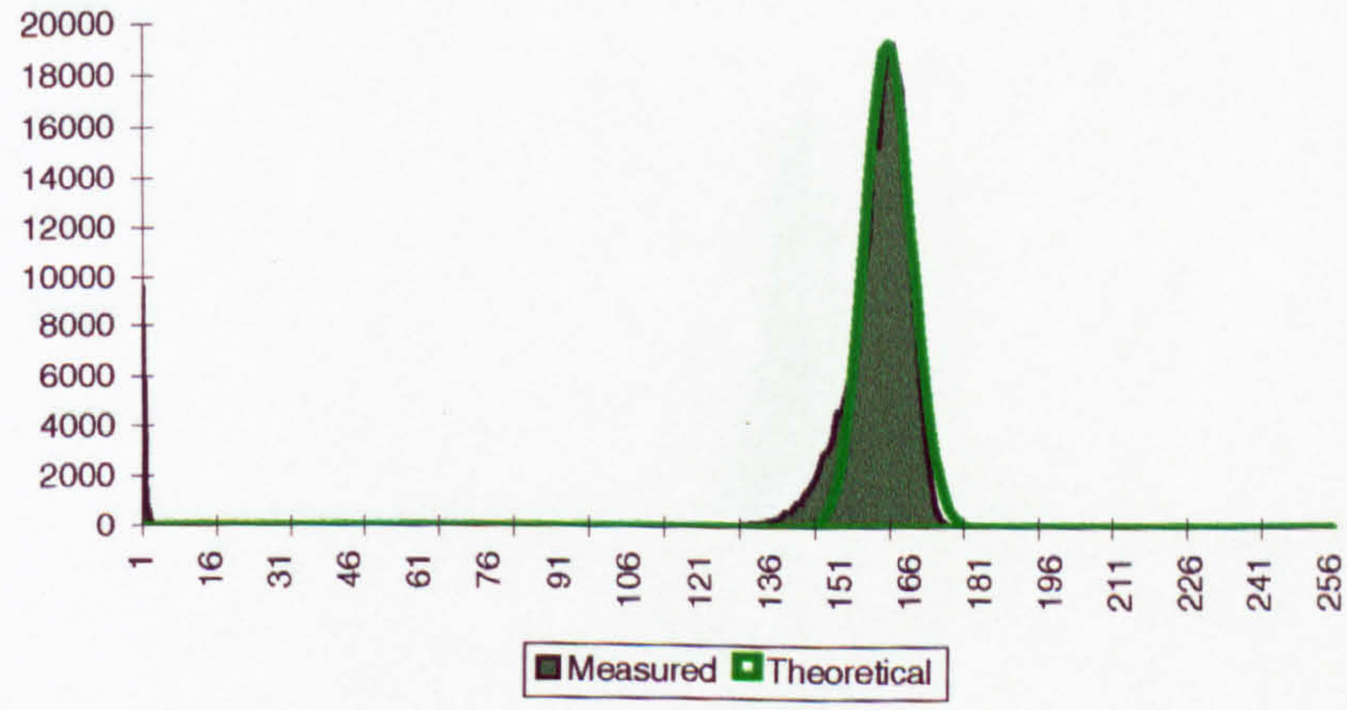

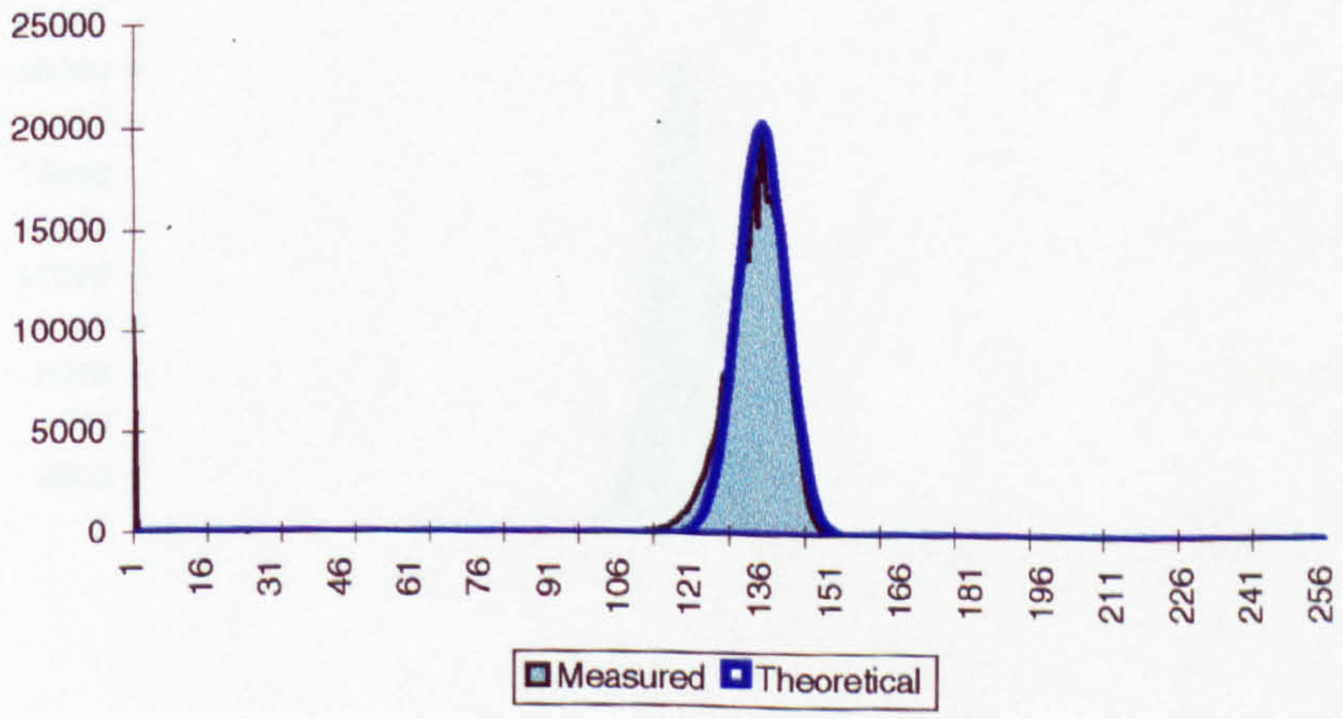

G5 Histograms

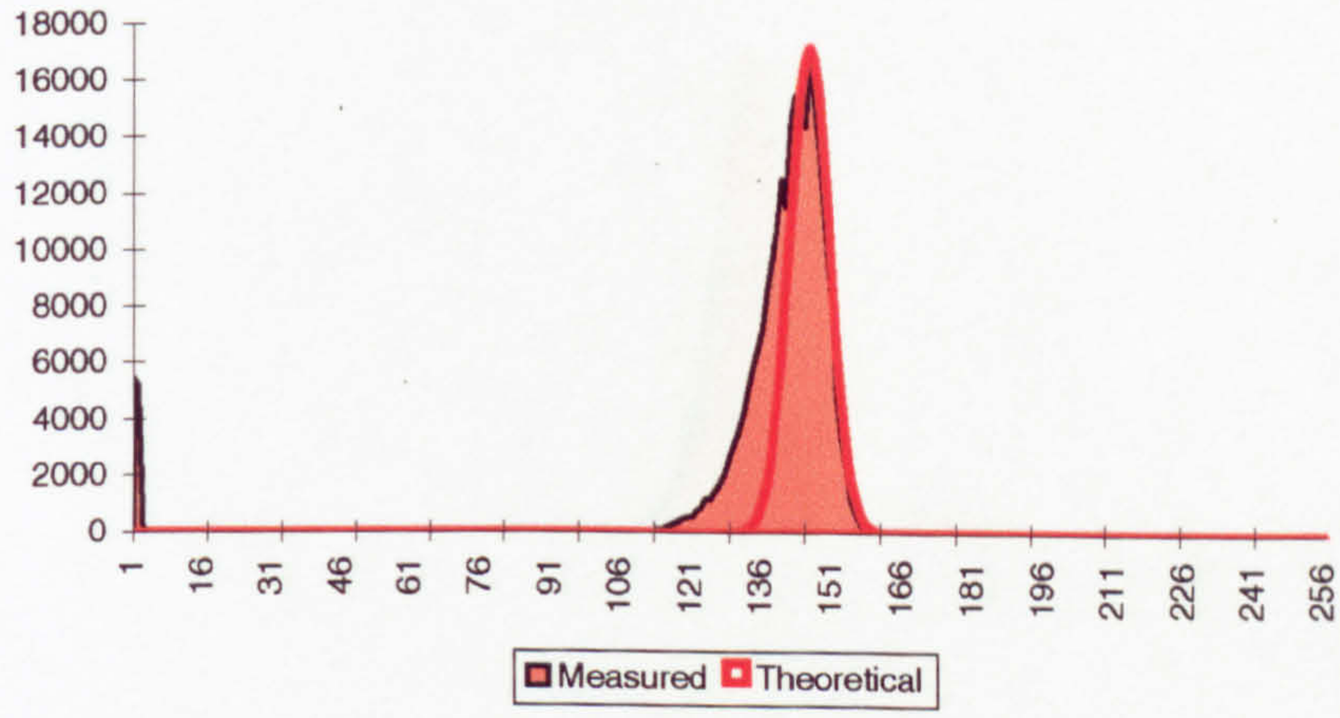

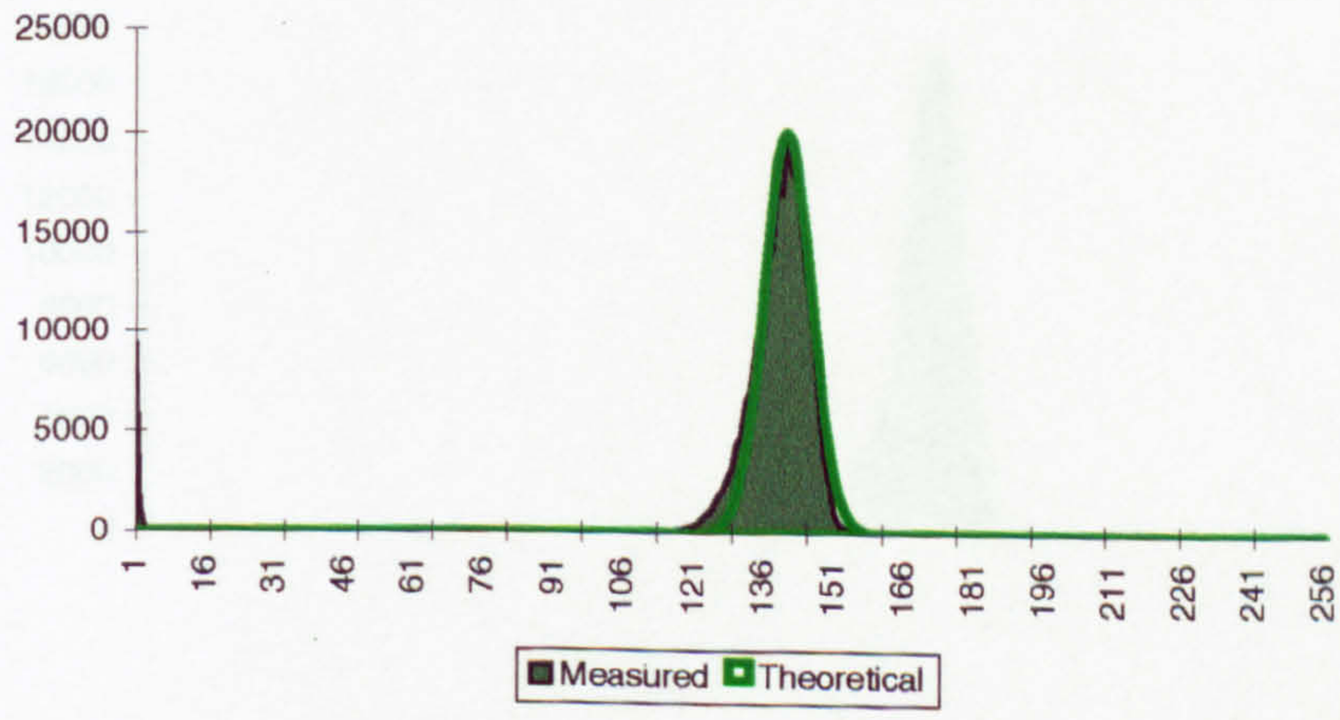

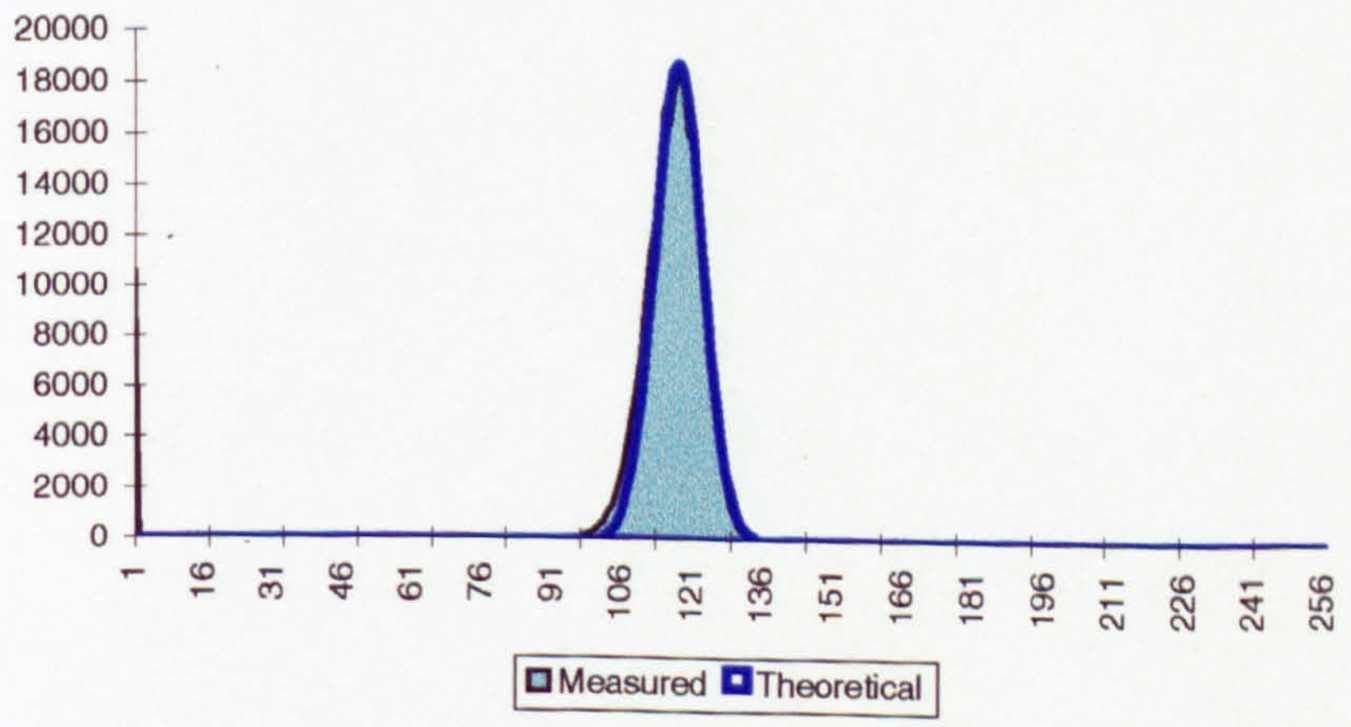

G6 Histograms

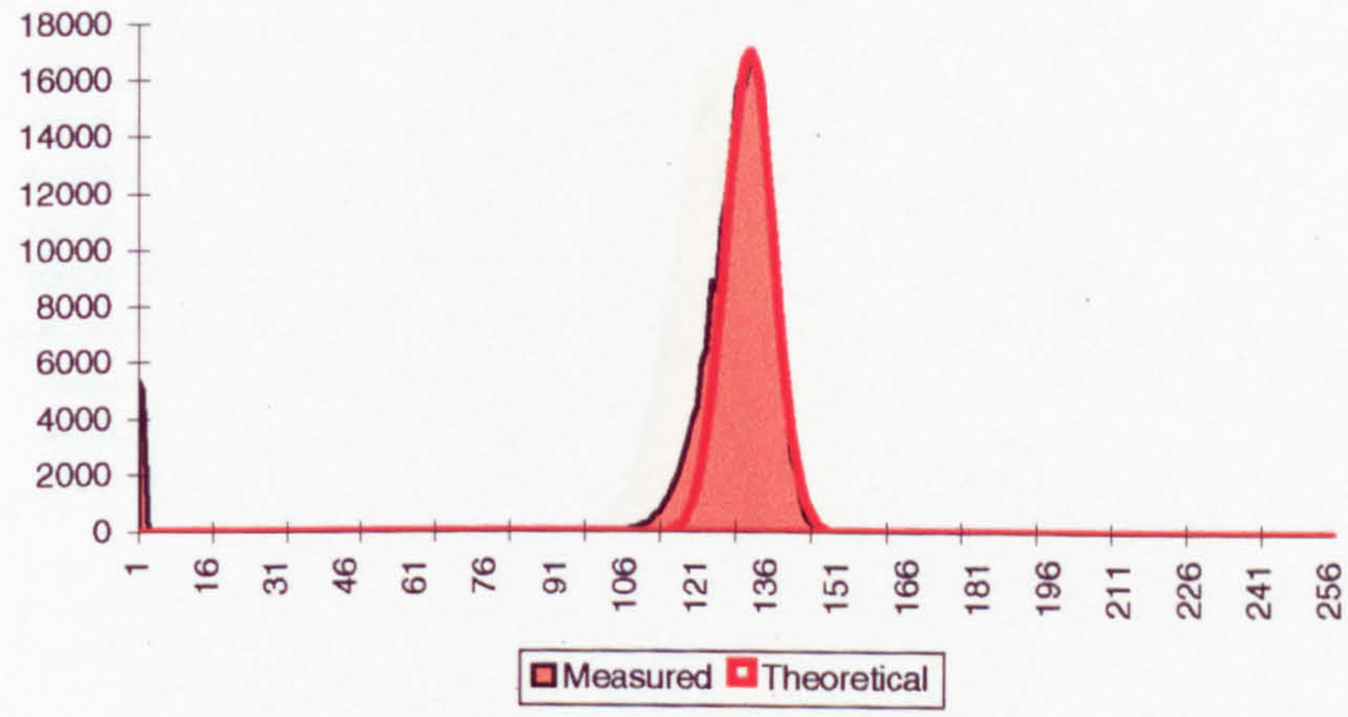

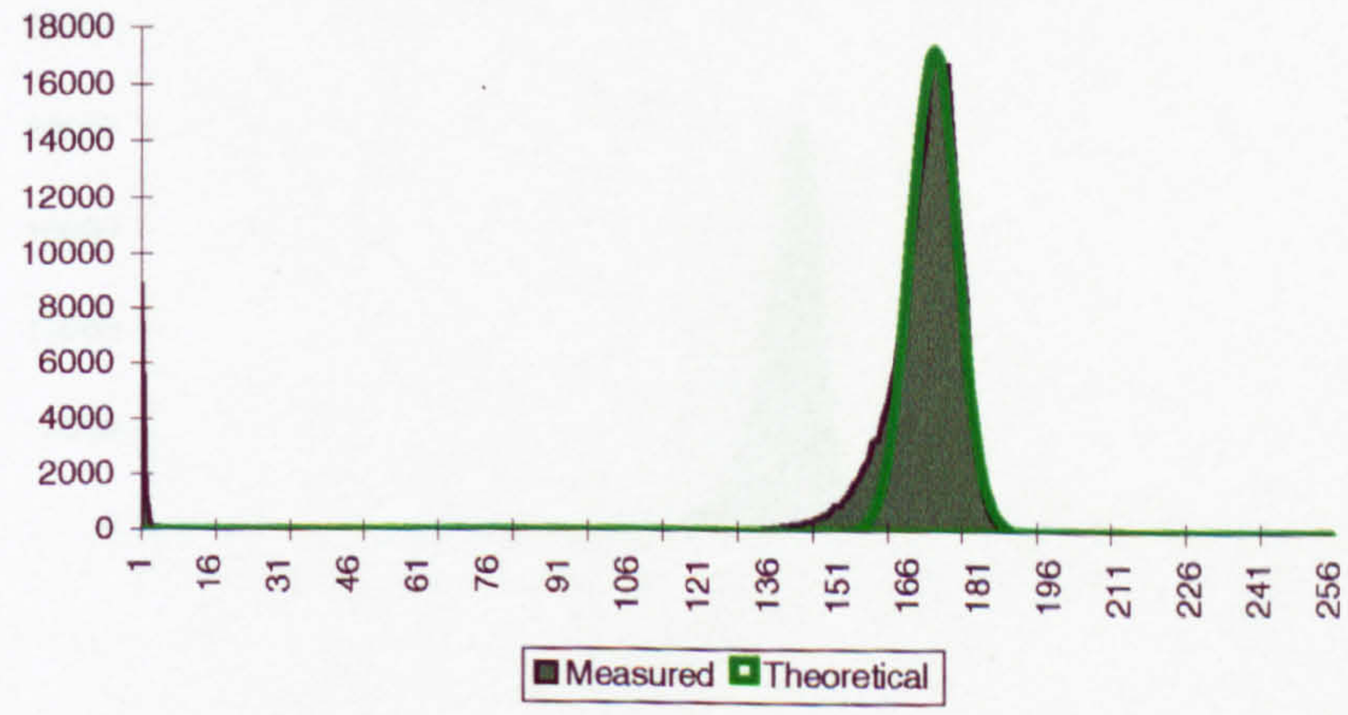

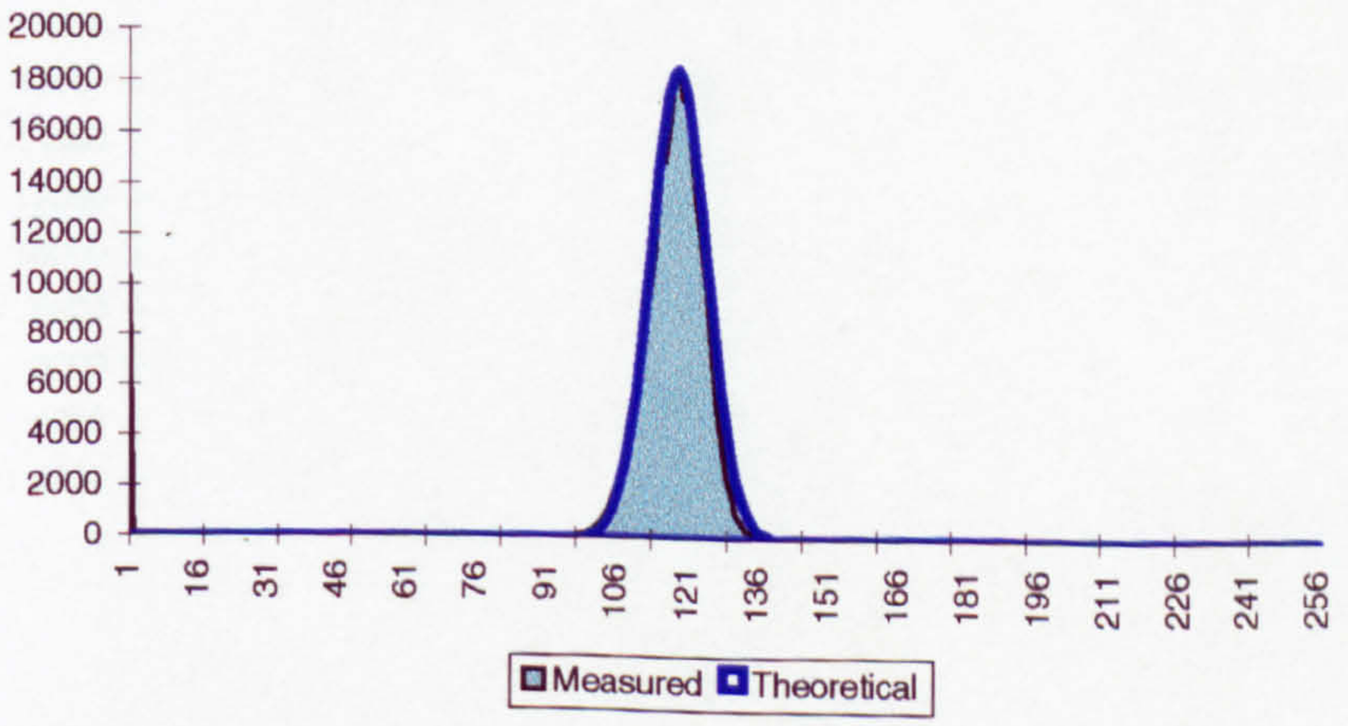

G7 Histograms

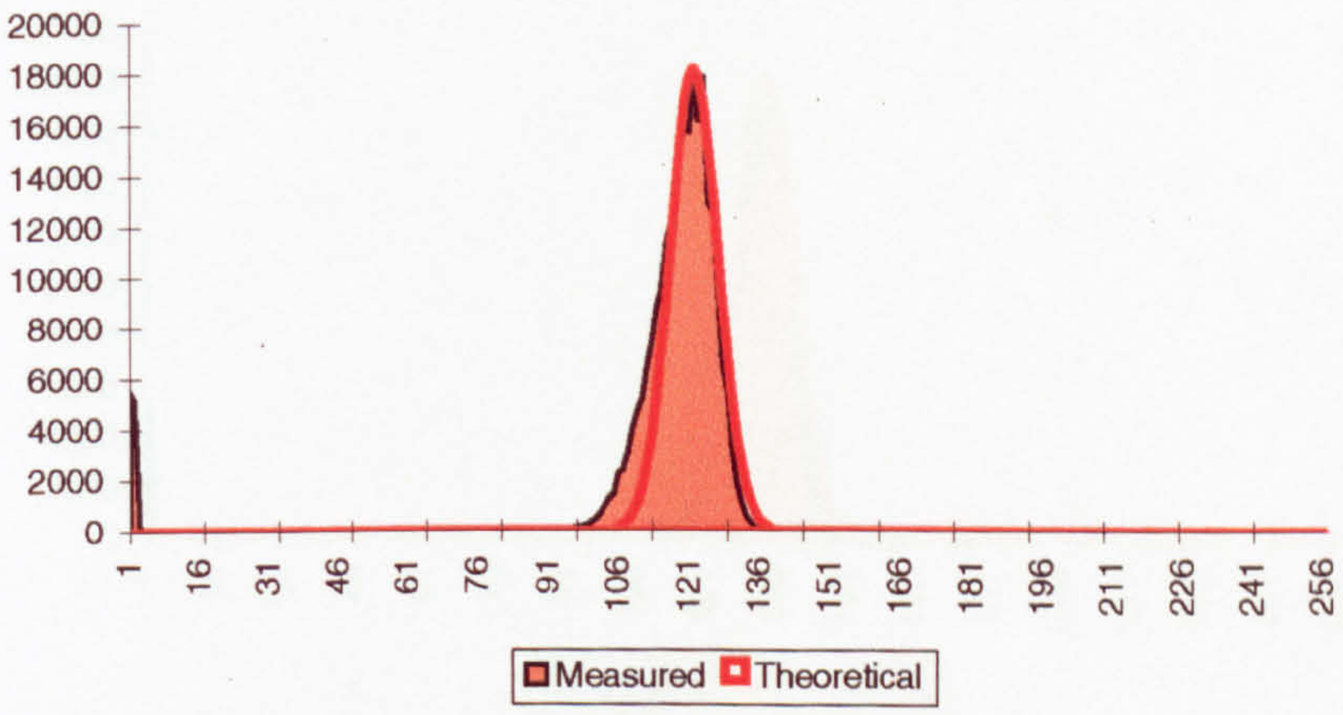

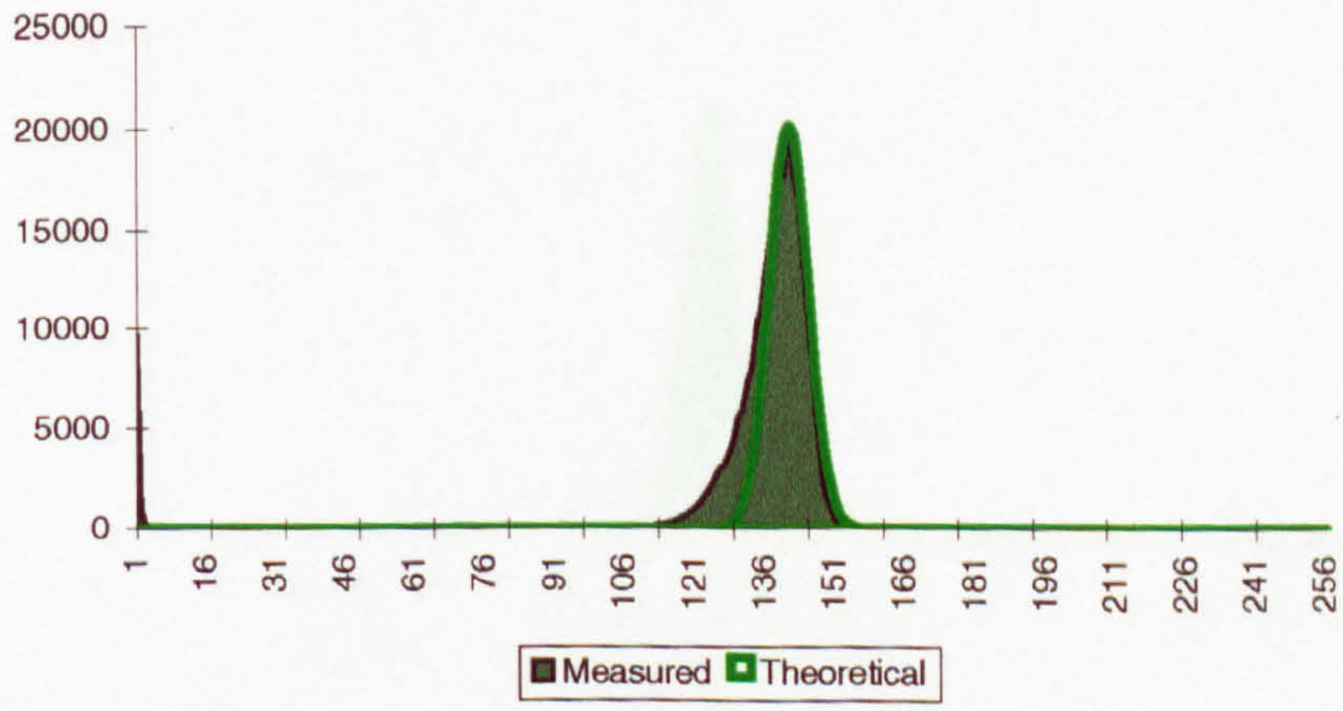

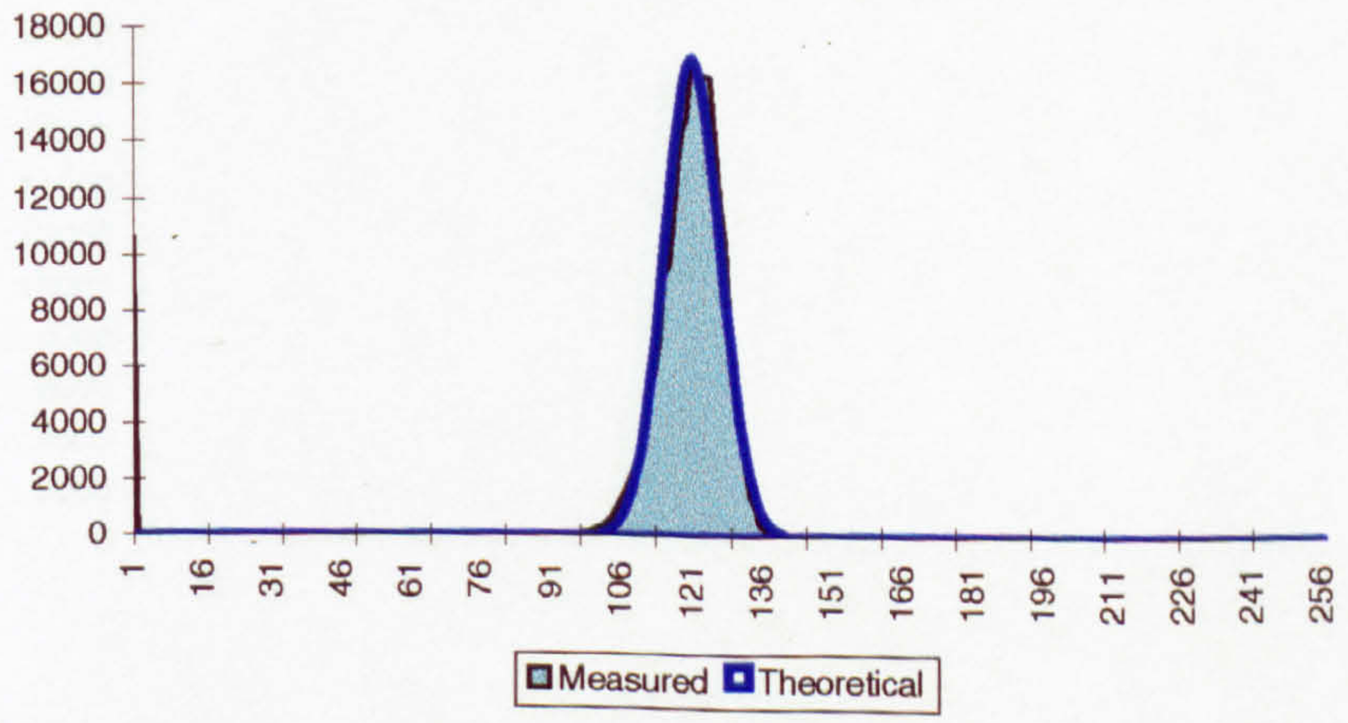

G8 Histograms

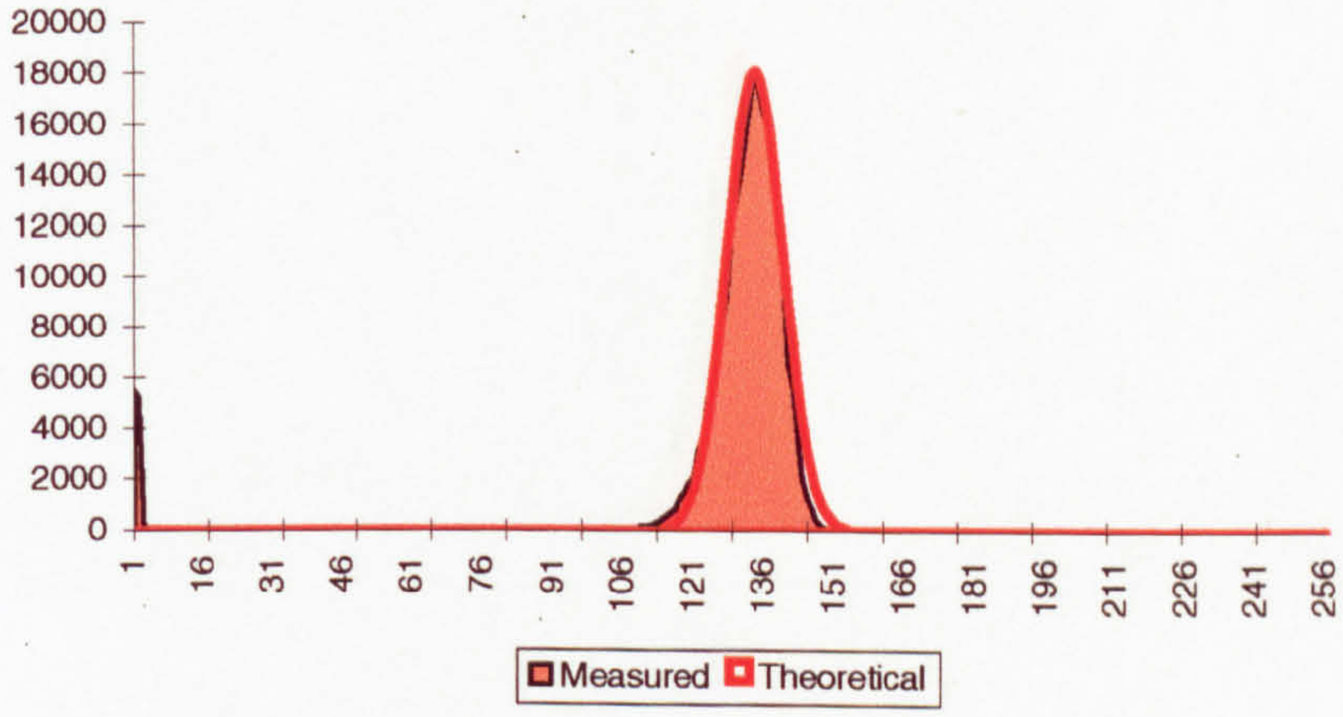

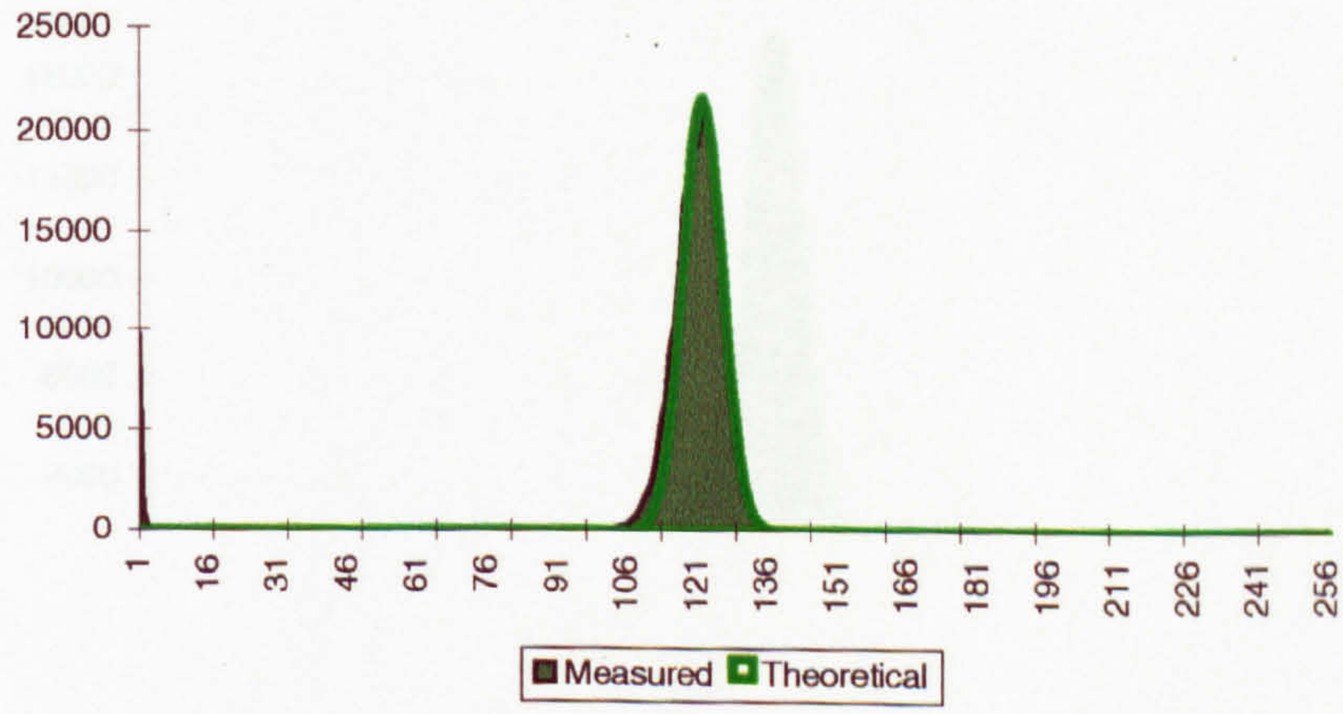

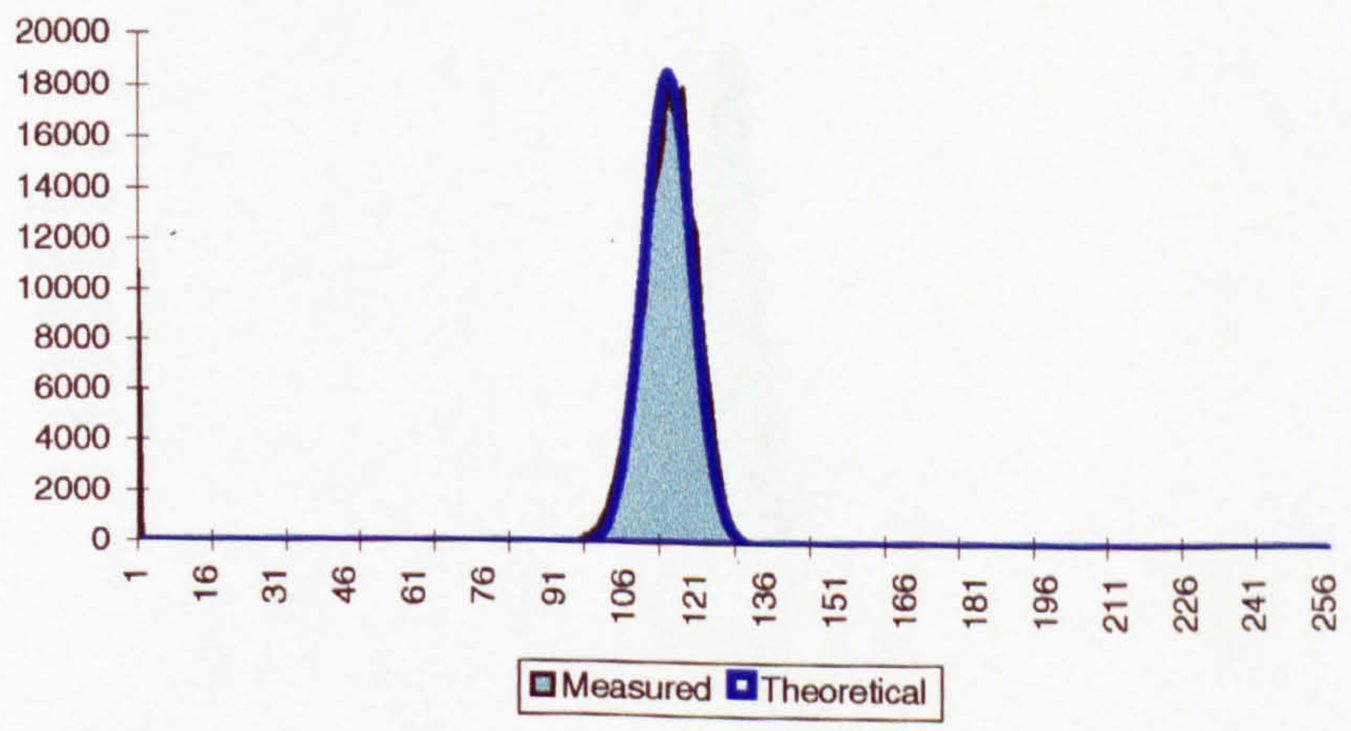

G9 Histograms

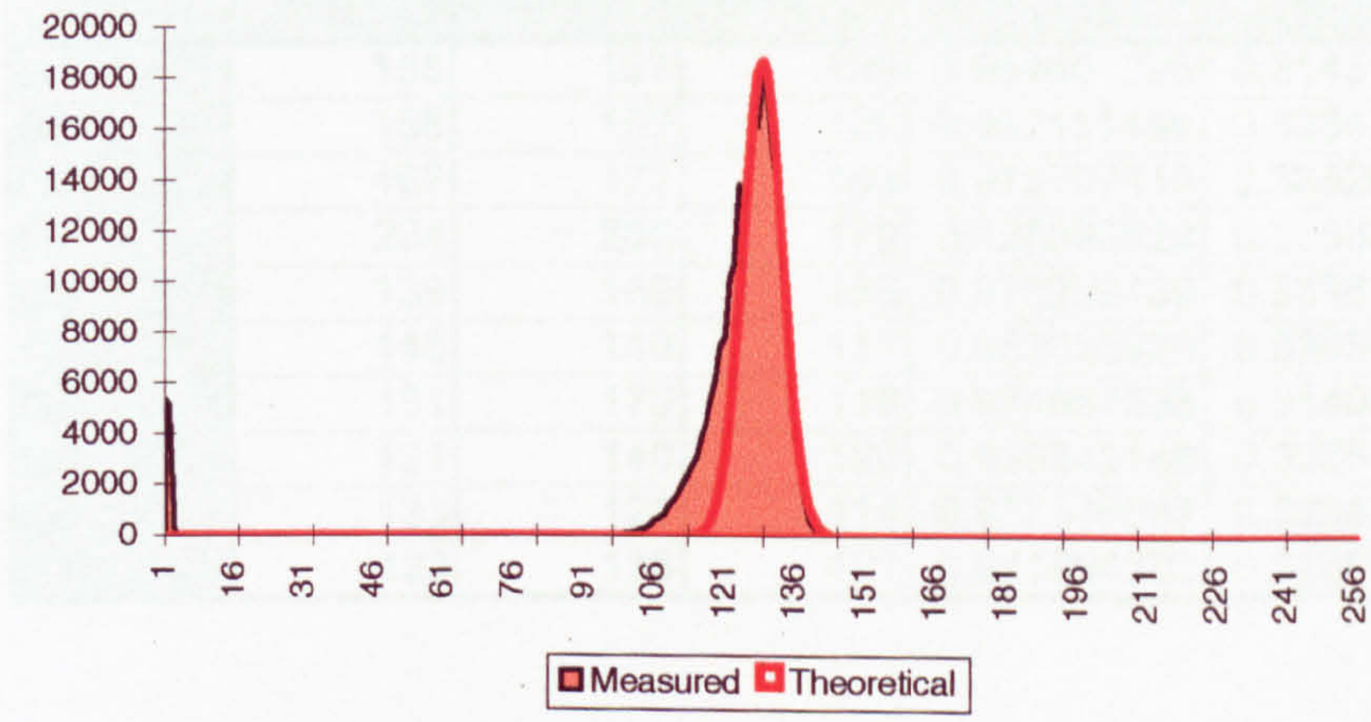

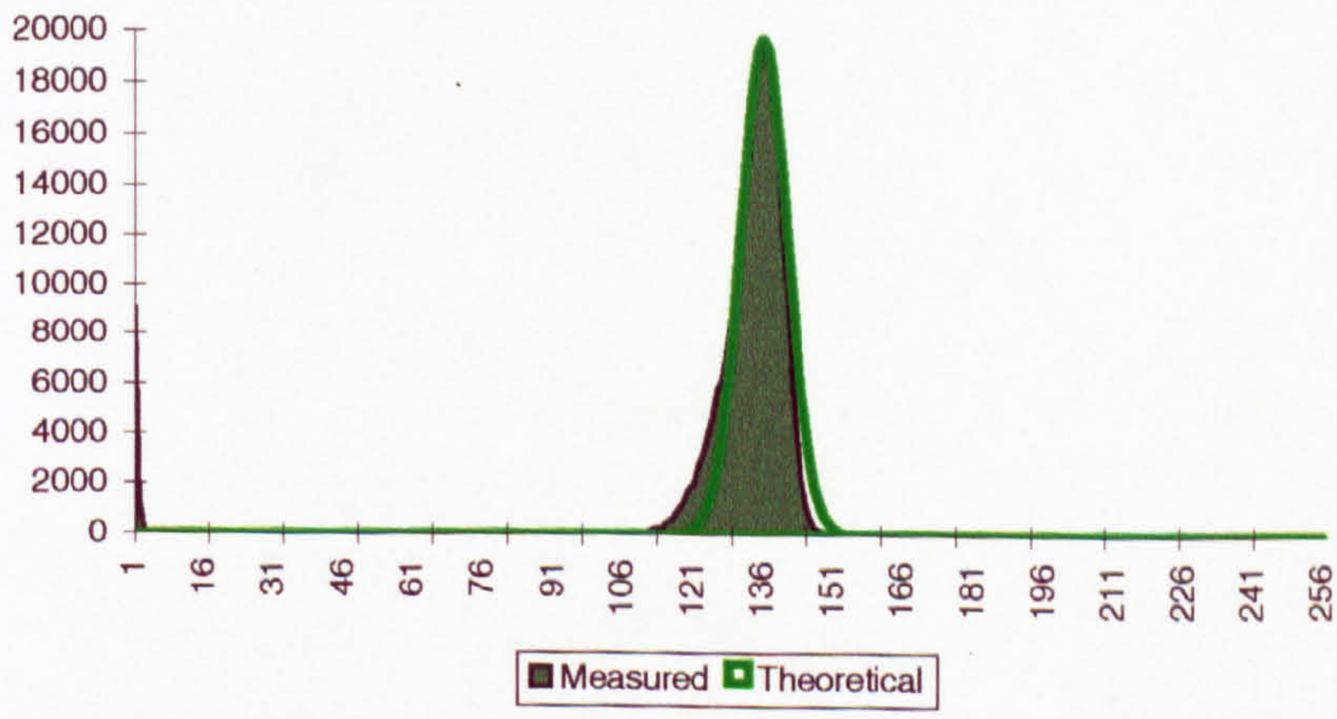

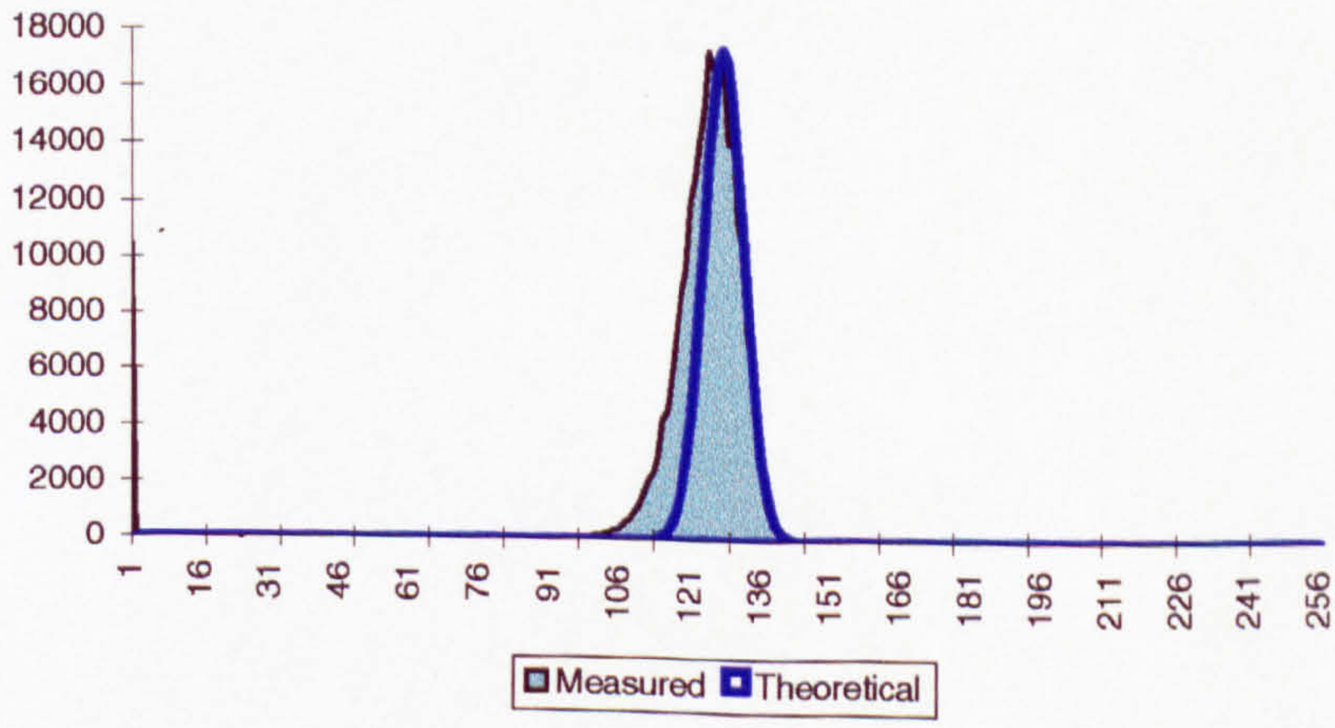

G10 Histograms

1.5.9 Gaussian Correlation Test Results

Sample	Mode			Correlation		
	R	G	B	Gauss	Noise	Pure
G1	155	157	129	0.964601228	0.314515331	0.314491969
G2	158	159	129	0.967111196	0.328477504	0.328535487
G3	167	177	163	0.913707415	0.335200173	0.335303318
G4	204	208	170	0.928393629	0.295830939	0.295813671
G5	139	160	135	0.970229139	0.339892535	0.339990942
G6	145	140	117	0.952055926	0.330581794	0.330512256
G7	131	170	118	0.974967536	0.314096101	0.314104768
G8	121	140	120	0.959343148	0.326542186	0.326560132
G9	133	121	114	0.977576087	0.328826571	0.328838988
G10	128	135	127	0.941894393	0.326928732	0.326991084